Compositional Structure in the Asteroid Belt: Results of a Spectroscopic Survey

by

Schelte John Bus

B. S., Geology, California Institute of Technology (1979)

Submitted to the Department of Earth, Atmospheric, and Planetary Sciences in partial fulfillment of the requirements for the degree of

Doctor of Philosophy

at the

MASSACHUSETTS INSTITUTE OF TECHNOLOGY

April 1999

© Massachusetts Institute of Technology, 1999. All Rights Reserved.

Author .....
Department of Earth, Atmospheric, and Planetary Sciences
April 1999

Certified by .....
Professor Richard P. Binzel
Department of Earth, Atmospheric, and Planetary Sciences
Thesis Supervisor

Accepted by .....
Professor Ronald G. Prinn
Chairman
Department of Earth, Atmospheric, and Planetary Sciences

MASSACHUSETTS INSTITUTE OF TECHNOLOGY
JUN 01 1999
LIBRARIES

ARCHIVES

Compositional Structure in the Asteroid Belt: Results of a Spectroscopic Survey

by
Schelte John Bus

Submitted to the Department of Earth, Atmospheric, and
Planetary Sciences on April 14, 1999
in partial fulfillment of the requirements for the degree of
Doctor of Philosophy

Abstract

Visible wavelength spectra have been obtained for 1189 main-belt asteroids during the second phase of the Small Main-belt Asteroid Spectroscopic Survey. These telescopic measurements were made using charge-coupled device (CCD) detectors, allowing for the targeting of smaller asteroids. A majority of the asteroids sampled have estimated diameters of 30 km or less. The SMASSII survey provides the largest internally-consistent sample of asteroid spectra ever obtained, and reveals a greater range of spectral diversity among asteroids than has been previously shown. This diversity may arise from a broad range of surface ages, where smaller (collisionally younger) asteroids may have less evolved or processed surfaces than do larger asteroids. Processes that affect the development of a regolith, and the distribution of regolith particle sizes may produce the observed variations in spectral features.

The larger sample size, greater spectral resolution, and greater photometric precision of the SMASSII survey, compared with the most extensive previous survey, provide a basis for developing a new "feature-based" taxonomic classification system for asteroids. This new taxonomy builds on the robust, large-scale structure of existing taxonomies, and relies on the presence or absence of specific spectral features to define new class boundaries. The SMASSII measurements reveal that many of the previous taxonomic classes that appeared to be distinctly separate, are instead spanned by a

nearly continuous transition of spectral properties. This continuum may be evidence of sampling a more complete range of mineralogies. This newly found continuum makes it difficult to define a unique taxonomic structure using classical multivariate techniques, requiring that subjective boundaries be defined in some cases. The scale-length in spectral variance observed in many dynamical asteroid families was used as a metric for constraining the class sizes in this new taxonomy. The resulting new taxonomy consists of twenty-six spectral classes. Members of the previously defined X-class (which could be subdivided only using albedo information) display sufficient variation in spectral features to allow subgroups to be distinguished without the use of albedo.

A subset of 465 SMASSII asteroids were specifically targeted to test the genetic reality of small dynamical "families." These families likely result from the collisional disruption of larger parent asteroids, and are identified as clusters of objects having similar orbital parameters. The targeted region, encompassing the heliocentric distance range of 2.690 to 2.815 AU, contains 14 families that had been previously identified, based on numerous analyses of orbital distributions in this region of the main belt. A newly developed multivariate technique that analyzes the combination of spectral characteristics and orbital parameters reveals that all 14 of these previously proposed families are distinct from the "background" population of asteroids. This result implies that each of these families is likely to have been truly formed by a collisional event, providing strong evidence for an extensive collisional history within the asteroid belt. C- and S-type asteroids appear equally capable of forming families. Each family is found to be relatively homogeneous in its spectral characteristics, allowing the boundaries of the families, and potential interlopers, to be more precisely identified than was possible in previous dynamical analyses. The relative spectral homogeneity within each of these families provides little evidence for any to have been formed from a differentiated parent body. It remains a mystery as to why there is no clear evidence of a major family containing members from different geologic units, derived from a differentiated parent asteroid. In addition to the 14 previously identified dynamical families, our analysis has revealed five additional associations of spectrally similar asteroids in this same small heliocentric range. These spectral clusters may represent the dispersed fragments of older collisionally derived families.

Thesis Supervisor: Professor Richard P. Binzel
Department of Earth, Atmospheric, and Planetary Sciences

Acknowledgments

I am grateful to everyone in the Planetary Science group at MIT, the faculty, staff, and students, who have helped make the last seven years a very rewarding and memorable experience for me.

Foremost, I want to thank Rick Binzel for being the ideal advisor. You provided me with academic guidance, financial support, ample telescope time, and even the occasional home-cooked meal (thanks, Michelle). But most importantly, you gave me the freedom to explore on my own, and room to stretch my wings. On those many occasions I started to flounder, you were always there to help get me back on course. I couldn't have asked for anything more. I look forward to our continuing collaboration, and to a very long-lasting friendship.

To Chuck Counselman, Tim Dowling, Jim Elliot, and Jack Wisdom, I learned many things from each of you, both inside and outside of the classroom. Jim, I especially want to thank you for all of your help and support during my first years as a graduate student. Our work together on occultations provided experiences I will always remember. I am also very grateful for the regular trips back to Flagstaff. Those visits helped make my transition to Boston, and to graduate school much easier.

I want to thank my thesis committee, Rick, Jim, Chuck, and Clark Chapman for their valuable comments and suggestions.

I also want to thank all of the other graduate students in our group, both past and present, for helping me get through this. In particular, Shui Xu, Amanda Bosh, Leslie Young, and Cathy Olkin each showed me that it could be done, and provided me with much needed encouragement along the way. And to Jeff Foust and Tom Burbine, thanks for putting up with all my craziness, especially over the last year.

Finally, I want to thank Steve McDonald, Rich Meserole, Ginny Siggia, and Allison Cocuzzo for always answering my questions, and for taking care of all the little things that make our group run so smoothly.

To put it mildly, this thesis project was observationally intensive. It would have never been possible without the telescopes and instrumentation of the MDM Observatory. I am greatly indebted to Bob Barr, Paul Hartmann, and Tony Negrete, who, through their dedication and hard work, make the MDM Observatory a joy to observe at. I'm going to miss all of you.

I want to acknowledge all of my friends at Lowell Observatory. The years that I worked at Lowell were very important in helping me prepare for graduate school. In particular, I want to thank Ted Bowell, Marc Buie, Bob Millis, and Dave Schleicher for providing me with many different research opportunities while I was there. Lowell Observatory will always have a special place in my heart, and no matter where I eventually end up, I'll always consider Flagstaff to be home.

To Carolyn, Fred, Linda, Stefani, and all the rest of the Shoemaker family, your friendship and encouragement has meant so much to me over the years. I think that Gene would be proud of what I've accomplished, and relieved that I'm finally done.

To my Mom and Dad, and to my sister, Judy, this thesis would have never been possible without your constant love and support. I know you may not always understand what I'm doing, or why, but you've always encouraged me to follow my dreams.

And finally, to Rigel, the best four-legged friend a guy could ever have. I wish you could have been around a while longer. I'll never forget you.

Dedicated to the memory of

Eugene M. Shoemaker
(1928-1997)

Advisor, mentor, and friend

Table of Contents

Chapter 1

Introduction

1.1 Discovery of the asteroids

The origin of asteroid studies can be traced back to the end of the 16th century. It was then that the German mathematician and astronomer, Johannes Kepler (1571-1630) found that the distances of the known planets from the sun could be described by six concentric spheres, whose sizes were determined by the nesting of five "perfect" geometrical solids. This simple analogy led Kepler to realize that the distance separating Mars and Jupiter was not proportional to those distances between the other planets, and that there must be another, as yet undiscovered planet, occupying this part of the solar system: *"Inter Jovem et Martem interposui planetam"* (Between Jupiter and Mars I placed a planet) (Kepler 1596).

Efforts to further understand the relative distances of the planets from the sun laid dormant for 170 years until 1766, when the German physicist and mathematician Johann Daniel Titius von Wittenberg (1729-1796) found an empirical relationship for describing planetary distances. This relationship is based on the series of numbers given by:

$$y = 0.4, 0.4 + (0.3 \times 2^{n})$$

where $n = 0, 1, 2, 3, \ldots$. The resulting values of 0.4, 0.7, 1.0, 1.6,... give the approximate heliocentric distances for the major planets in astronomical units (AU). This rule was popularized by the young astronomer, Johann Elert Bode (1747-1826), and soon became known as "Bode's Law". The accidental discovery of a seventh planet, Uranus,

by Sir William Herschel in 1781, added even more weight to the Titius-Bode relationship. With an orbital semimajor axis of 19.2 AU, the average distance of Uranus from the sun closely matches the predicted distance of 19.6 AU. While we now know that the relationship between planetary distances and the numerical sequence described by Titius and Bode is purely coincidental, Bode's Law did prompt the search for, and discovery of several previously unknown objects orbiting the sun. In particular, this law predicts that, at a distance of 2.8 AU, there should be a planet located between Mars and Jupiter, just as Kepler had surmised.

One of the strongest supporters of Bode's Law was Baron Xavier von Zach (1754-1832). Inspired by the discovery of Uranus, von Zach began a dedicated search for the missing planet between Mars and Jupiter in 1783, going so far as predicting its orbit and position in the sky in 1785. However, it was the Sicilian monk, Father Giuseppe Piazzi (1746-1826), director of the Palermo Observatory, who discovered a moving star in the constellation of Taurus on January 1, 1801. While initially believing that he had discovered a comet, Piazzi continued to follow the object for over a month. Upon learning of Piazzi's discovery, Bode concluded that the missing planet had been found. This new planet was named Ceres, after the Roman goddess of corn and harvests.

By the time that the discovery of Ceres was made public, the new planet had moved into conjunction with the sun, temporarily making observations impossible. Once Ceres had moved clear of the sun by the summer of 1801, several attempts were made for its recovery, but were all unsuccessful. The short orbital arc that had been recorded by Piazzi made it impossible to accurately predict the future track of Ceres using the techniques that were presently available. In October, this problem caught the attention of the German mathematician, Karl Friedrich Gauss (1777-1855). Gauss quickly perfected the method of least-squares, and derived a technique of orbit determination, the basis of which is still used for calculating orbits today. Based on Gauss' orbit, Ceres was recovered on the morning of January 1, 1802, exactly one year after its discovery, by both Baron von Zach, and by the German doctor, Heinrich Wilhelm Olbers (1758-1840), the latter normally being credited for the recovery.

Olbers continued to observe Ceres, providing Gauss with additional positions so that its orbit could be improved. On the night of March 28, 1802, Olbers unexpectedly found a second moving planet in the vicinity of Ceres. Initial orbit computations showed

that this new object was also in a heliocentric orbit, located between Mars and Jupiter. Named Pallas, after the goddess of wisdom, this new planet posed a problem, since now there were two planets where Bode's Law had predicted only one. Observations by Herschel showed that the sizes of both Ceres and Pallas were much smaller than any of the other planets, and he proposed a new class of objects which he called "asteroids" because of their star-like appearance. Olbers (1803) developed the first theory for the origin of asteroids by suggesting that Ceres and Pallas were actually fragments of a planet that had been broken to pieces and that additional fragments might be found. As predicted, a third asteroid, named Juno, was discovered by Karl Harding on September 1, 1804, and Olbers himself discovered the fourth asteroid, Vesta, on March 29, 1807.

Even with this seemingly rapid succession of discoveries, an understanding of the true nature of the region of asteroids, called the "asteroid belt" was slow to emerge. The fifth asteroid, Astraea, was not discovered until 1845. By 1850, ten asteroids were known, and it was generally assumed among astronomers that few asteroids remained yet to be found. However, after 1850, the rate of asteroid discoveries began to accelerate, due in large part to the efforts of amateur astronomers, who were armed with increasingly better star charts, and would visually scour the sky for moving objects. By the end of 1890, over 300 asteroids were known. In 1891, a major revolution occurred when Max Wolf (1863-1932) of the Königstuhl Observatory in Heidelberg introduced the photographic process as a way of searching for asteroids. By taking photograpns of the night sky, not only was the search for new objects made much more efficient, but the accuracy and reliability of positional measurements were also greatly improved. By this time, however, the astronomical community was beginning to lose interest in asteroids. The introduction of photography had opened up numerous avenues of study of much more distant and exotic parts of the universe. Techniques of photographic photometry and spectroscopy were focused on stars and galaxies, and asteroids were commonly relegated to the level of "vermin of the skies". Thanks to the hard work of a dedicated handful of observers, the rate of asteroid discoveries has continued to grow over much of the 20th century, with improvements in photographic emulsions and astronomical cameras leading the way for greater numbers of fainter objects to be found. Since the introduction of computers, the calculation of orbital elements has also become routine, and strategies have been established for handling the "bookkeeping" that is associated with monitoring thousands of objects. Today, over 10,000 asteroids have been

observed sufficiently well that they have received a permanent catalog number, and several hundred are being added to this catalog every year. A current view of the inner solar system is shown in Figure 1.1, where the positions of all numbered asteroids up to 10,257 have been plotted.

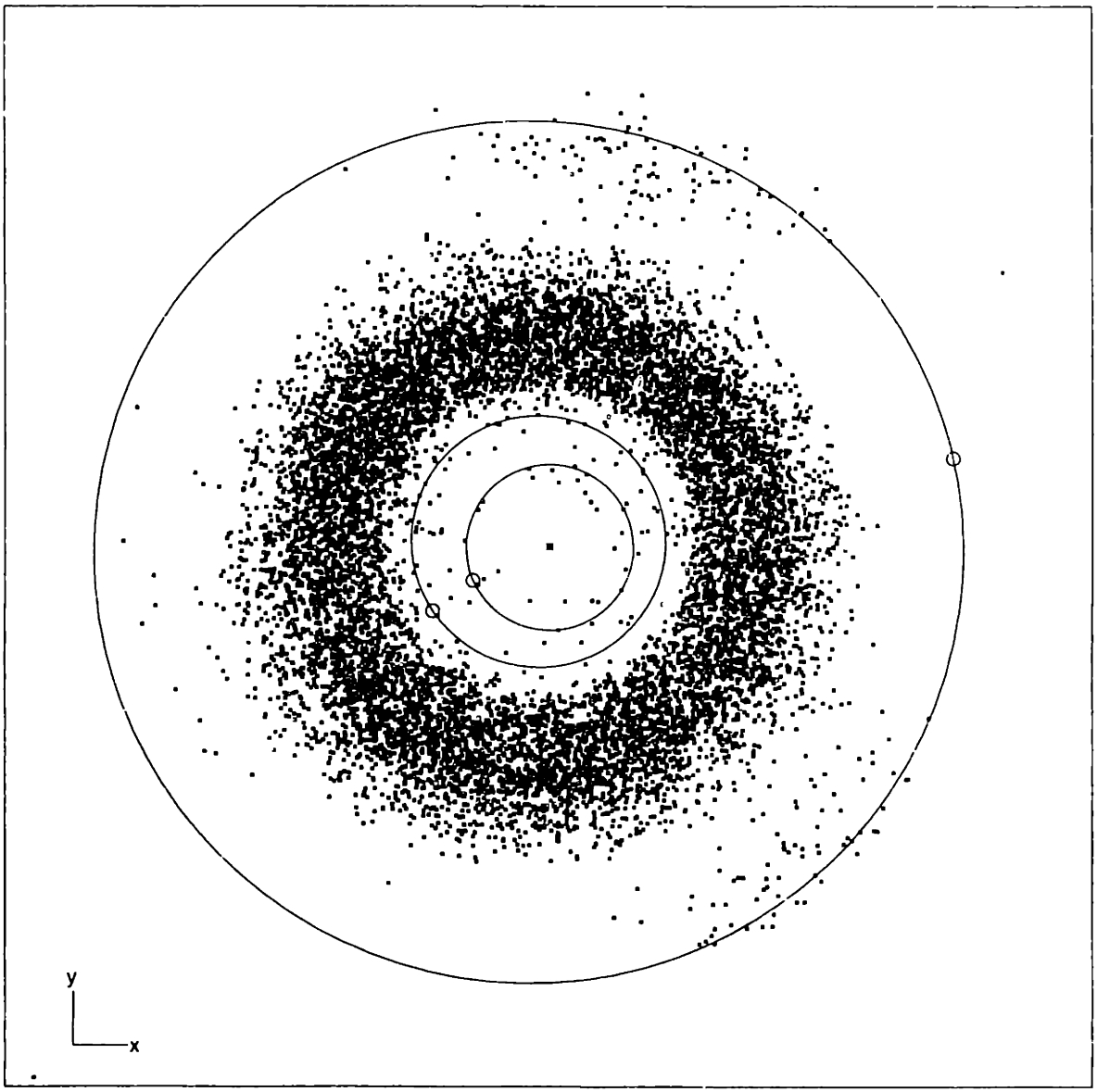

Figure 1.1: Planar view of inner solar system, showing the positions of approximately 10,257 asteroids on 14 April 1999 19:00 UT (2:00 EST). Large circles show the orbits of the Earth (inner-most), Mars, and Jupiter. The locations of these planets are marked by small circles. Planet-crossing asteroids are seen inside of the orbit of Mars, while the two clouds of objects preceding and following Jupiter in its orbit are the Trojan asteroids.

1.2 The physical nature of asteroids

Asteroids (also called "minor planets") are generally described as being small bodies that are in orbit about the sun, and which have no atmosphere or detectable outflow of gases or dust. Asteroids do not represent the most pristine material in the solar system (this distinction is usually given to the comets and Kuiper Belt Objects). Many asteroids have undergone various degrees of geological processing such as melting, differentiation and metamorphism, while others have tended to retain their original, primitive mineralogical forms. However, asteroids have not undergone the extensive processing associated with large planet formation, and thus still hold a significant amount of information about the conditions in the early solar system. Rather than being the disrupted fragments of one large planet, as was suggested by Olbers, the currently accepted explanation for the formation of the asteroids is that they are remnant planetesimals that never fully accreted into a major planet. In the early stages of planetary accretion, it is believed that Jupiter formed rapidly. As Jupiter grew, the extent of its gravitational influence also expanded, perturbing the orbits of those planetesimals in the present asteroid belt, and increasing their relative orbital velocities so that, when mutual collisions occurred, they were more likely to be destructive (leading to the break-up of the objects) than constructive (the accretional agglomeration of objects).

Collisions have played a significant role throughout the formation and evolution of the solar system. They are central to the later stages of the planetary accretion, and continue today, with the surface of essentially every terrestrial planet and satellite showing some evidence of recent impacts. The mutual collisions between asteroids play a major role in the evolution of objects within the main belt. During the recent spacecraft flybys of the asteroids 951 Gaspra, 243 Ida, 253 Mathilde, and 433 Eros, the irregular shapes and cratered surfaces of these objects were clearly revealed. Besides altering the asteroid's topography, mutual collisions also result in a dynamical evolution of the asteroids. A collision can instantaneously change the rotational characteristics of an asteroid, altering the period of rotation, and inducing a precession of the rotational pole. Fragments that are formed during a collision will likely take on orbital characteristics that are similar to that of the original parent asteroid. The resulting groups of fragments in orbital element space are called families. If a fragment resulting from a mutual collision is injected into one of the chaotic resonance regions within the main belt, the orbit of that object may evolve dramatically in response to planetary perturbations. If the fragment

becomes Mars-crossing, it may eventually experience a close gravitational encounter with Mars, and become Earth-crossing. This combination of collisional production, resonance transport and planetary encounters is believed to be a primary mechanism for resupplying the meteoroid and near-Earth asteroid population that we see today.

There are strong lines of cosmochemical and dynamical evidence that a majority of the meteorites found on the Earth originated in the asteroid belt. From these meteorites, we have learned much about the early conditions of the solar nebula. We can place constraints on the physical environment, the temperatures and pressures, under which accretion took place. The meteorites also record a long history of thermal and collisional processing that has occurred throughout the history of the asteroid belt. In all, the meteorites provide some of the most fundamental details about the origin and formation of the solar system, and give us hands-on examples of what the asteroids are like. The only problem is, we don't know exactly where they came from. To form a complete picture of the asteroid belt, the source bodies of the meteorites must be known.

The best observational evidence currently available for linking meteorites and asteroids is through their spectral reflectance properties. The way in which light is reflected from the surfaces of meteorites and asteroids depends strongly on the specific minerals that are present. The comparison of spectral properties between the asteroids and meteorites should be straightforward, and has led to some reliable matches. However, in several cases, the spectral comparisons do not match. There are systematic differences between the spectral reflectance properties of asteroids and meteorites that are difficult to explain, and have led to significant debates between asteroid and meteorite scientists. For example, one of the most common types of meteorites, the ordinary chondrites, have few spectral analogs among the observed asteroid population. A solution to this dilemma may be on the horizon, however, with the observations of very small, near-Earth asteroids, where a spectral link between the ordinary chondrites, and the S-type asteroids (one of the most common asteroid spectral types) is beginning to emerge. This apparent connection between the near-Earth S-type asteroids and the ordinary chondrites provides further evidence to a growing consensus that surface alteration processes on the asteroids (possibly the development and aging of loose material, called a "regolith") can significantly alter the spectral properties of asteroids. The effects of these weathering processes must be understood if a solid connection between the meteorites and asteroids is to be made.

1.3 Structure in the asteroid belt

Even in the snapshot of the inner solar system seen in Figure 1.1, the distribution of the asteroids is not completely random. In this two-dimensional view, the primary concentration of asteroids (the main belt), forms an annulus, with inner and outer boundaries that are defined by the gravitational influences of Mars and Jupiter, respectively. There are a number of asteroids located inside of the orbit of Mars. These asteroids are planet-crossing (including the near-Earth asteroids), and are much more transient in nature, having relatively short dynamical lifetimes. There are two clouds of asteroids located roughly 60° either side of Jupiter that are known as the Trojan asteroids. The Trojan asteroids are locked into stable orbits by the 1:1 resonance with Jupiter, so that their orbital period around the sun is essentially the same as that of Jupiter. The positions of these asteroids, with respect to Jupiter, slowly change over time as they "librate" or oscillate around the L_4 and L_5 stability points in the sun-Jupiter system.

More detailed structures are identified when examining the distributions of the orbital elements. In Figure 1.2, the distribution of semimajor axes is plotted for the numbered asteroids up to and including number 8980. This distribution is not smooth, but instead, there are concentrations of asteroids at some values of semimajor axis, while at other values of semimajor axis, there are distinct gaps where no asteroids are found. These gaps were first identified by Daniel Kirkwood (1867) as coinciding with mean-motion resonances with Jupiter. These resonances occur when the orbital period of an asteroid is a low-order multiple of Jupiter's period, such that Jupiter and the asteroid make regular close approaches at the same points in their orbits. The resulting gravitational tugs by Jupiter have the effect of increasing the asteroid's orbital eccentricity. However, the exact means by which asteroids are cleared from these gaps has been debated.

Statistically significant groupings in the orbital elements of asteroids were first recognized by Hirayama (1918). Hirayama called these clusters "families", and suggested that the members of a family shared a common origin, such as the break-up of a larger, parent body. To recognize these families, the effects of long-term, or "secular" perturbations on the orbital elements must first be accounted for. These secular perturbations are the results of fundamental oscillations in the orbits of the major

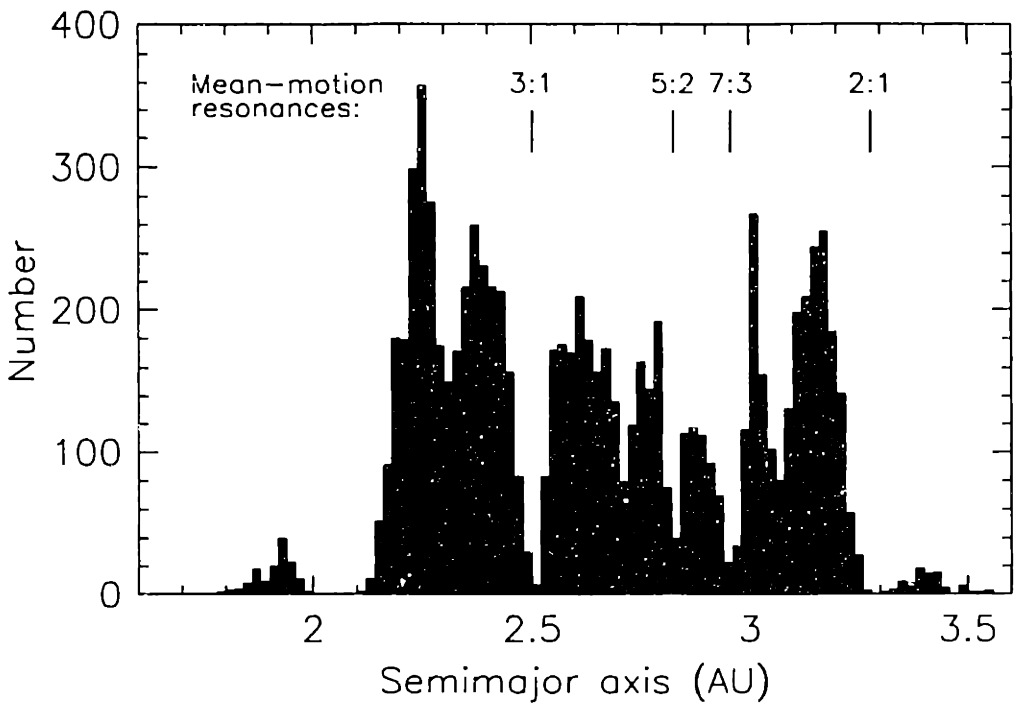

Figure 1.2: Plot of the distribution of semimajor axes for over 8000 asteroids in the main belt. Four prominent mean-motion resonances are marked. At the locations of these resonances, the numbers of asteroids are depleted. These depleted zones are called the Kirkwood Gaps.

planets, and affect all of the asteroids. Thus, if an asteroid family is formed from single parent, the orbits of the individual fragments will become dispersed over time due to these perturbations. The effects of secular perturbations can be removed by calculating a set of elements called "proper elements".

In the remainder of Hirayama's work (1923, 1928, 1933), a total of nine clusters of asteroids were identified, though only five of these were significant enough to be considered as the "classical" Hirayama families. Many advances have occurred since Hirayama's time, including the methods used for calculating proper elements, and the statistical techniques used to search of asteroid groupings. The significant increase in the number of known asteroids since 1918 has also helped in the search for dynamical families. Brouwer (1951) was the first to confirm Hirayama's results. More recently, searches by Williams (1971, 1979, 1989, 1992), Kozai (1979), Lindblad (1994), Bendjoya (1993), and Zappalà *et al.* (1990, 1994, 1995) have added varying numbers of families. In the latest work of Zappalà *et al.* (1995), two different clustering techniques

were used to search of asteroid clusters. In this search, roughly 30 statistically significant families were identified, and an equal number of groupings were recognized that are classified as being less significant. The set of proper elements used by Zappalà *et al.* are plotted in Figure 1.3, where many clusters of asteroids can be seen of various sizes.

Another trend that is observed among the asteroids is that asteroids with different mineralogical compositions tend to be found at different distances from the sun. These gradations in composition are probably a reflection of the chemical and physical conditions in the early solar nebula. In particular, the temperature in different regions of the solar nebula would control what mineral grains would condense out first. Condensation models for the early solar system predict that higher temperature minerals, such as silicates, will tend to dominate the inner part of the asteroid belt, while lower temperature carbonaceous materials will more likely be found in the outer regions of the belt. These trends are observed in the distributions of spectral classes, as seen in Figures 1.4 and 1.5, where the distribution of silicate-rich S-type asteroids peaks in the inner part of the belt, while the carbon- and volatile-rich C-types tend to dominate the outer part of the main belt.

1.4 The "reality" of dynamical families

One of the major questions surrounding the dynamical asteroid families is: "Are they real?" When Hirayama (1918) first identified clusters of asteroids, he hypothesized that the members of each family were genetically related - that is, coming from a common parent. However, the mechanism he proposed for the formation of these families was the internal, spontaneous disruption of the parent, much like the splitting that had been observed in various cometary nuclei. Kuiper (1950) dismissed this theory because there appeared to be no suitable mechanism. Instead, he proposed that these families resulted from the mutual collisions between asteroids.

If these families are the result of collisions, then they represent natural collisional experiments at sizes and energies many orders of magnitude greater than is possible to reproduce in laboratory experiments, and could provide considerable insight into the collisional processes that have occurred throughout the history of the asteroid belt. From the study of these families, there are many important questions that might be addressed

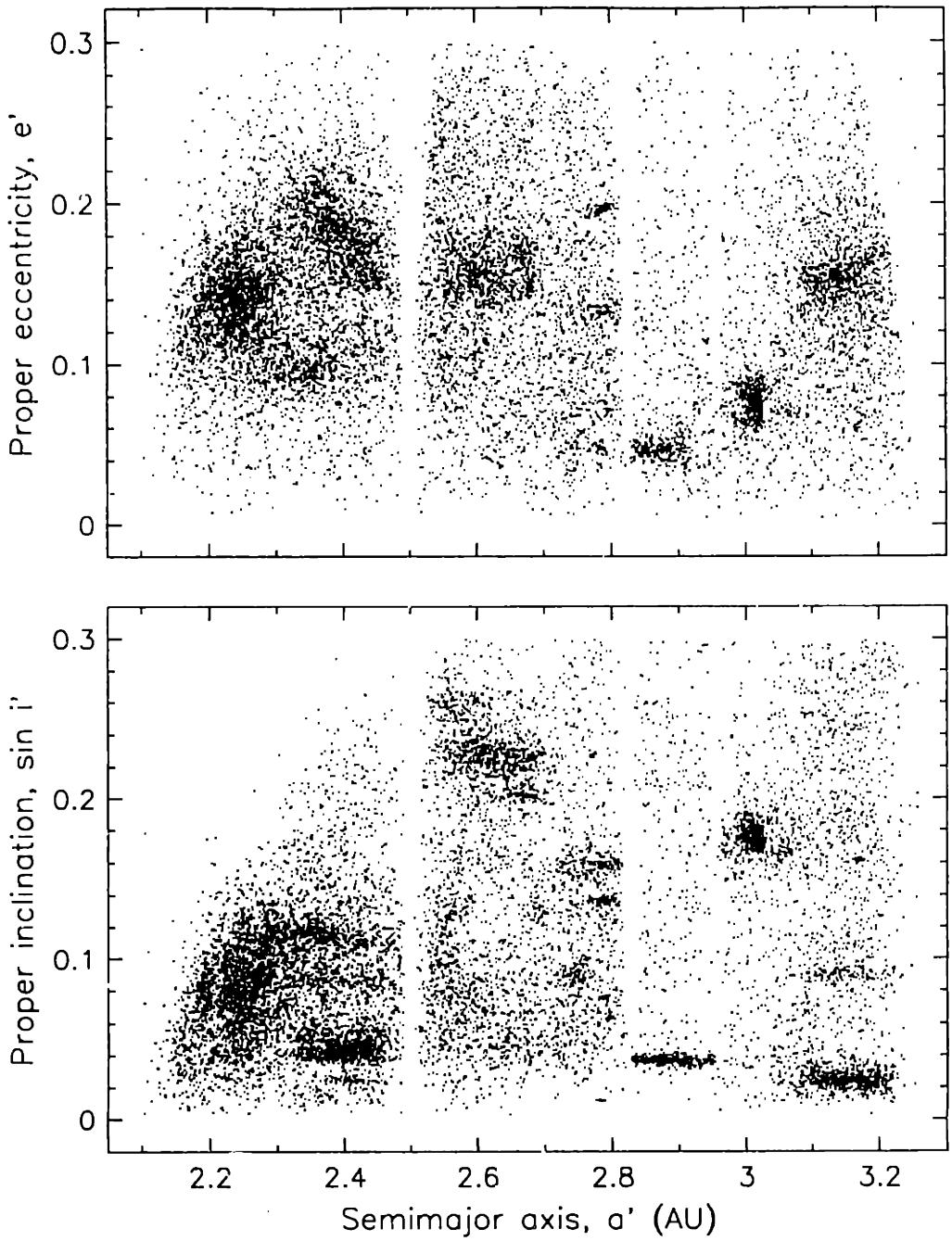

Figure 1.3: Plots showing the distribution of proper elements for 12,437 asteroids. The upper plot shows the distribution in eccentricity (plotted again semimajor axis) while the lower panel shows the distribution in inclination versus semimajor axis. The Kirkwood Gaps are visible as depleted zones, such as that located at the semimajor axis distance of 2.5 AU. Many clusters of asteroids, referred to as dynamical families, are also visible in both plots. Approximately 30 significant clusters have been identified in this dataset by Zappalà *et al.* (1995).

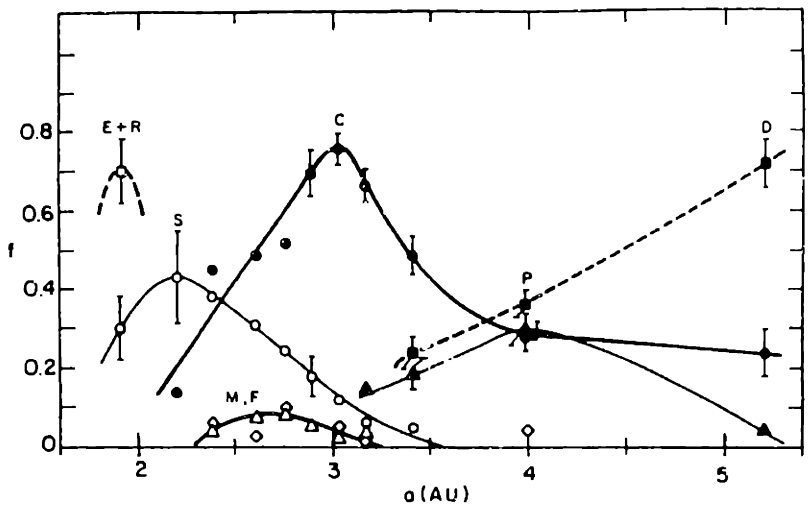

Figure 1.4: Plot showing the relative (not fully bias-corrected) distributions of spectral classes for asteroids as determined by Gradie and Tedesco (1982). The number of silicate-rich (higher-temperature) S-types peaks at about 2.2 AU, while the more primitive, lower-temperature C-types are most numerous around 3 AU. Reproduced from Gradie *et al.* (1989).

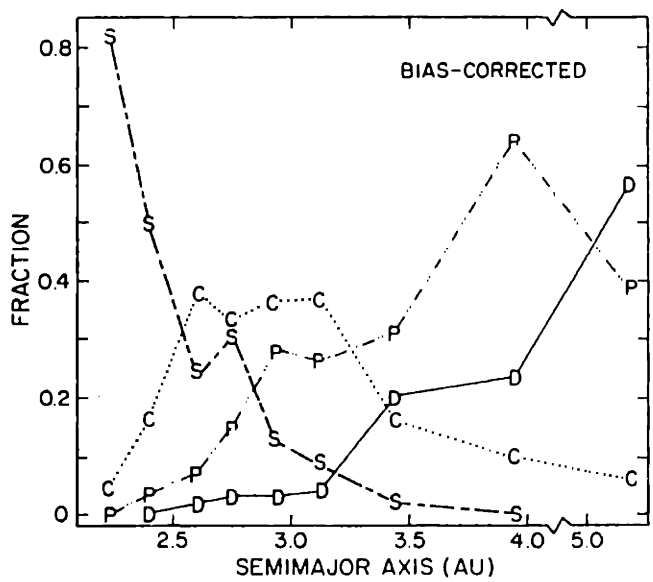

Figure 1.5: Similar to Figure 1.4, but showing the distribution of classes defined by Chapman (1987). Note the relative difference in the distributions of C- and S-types in this plot, as compared to those shown in Figure 1.4. Also reproduced from Gradie *et al.* (1989).

about the physics of collisions, such as the partitioning of kinetic and rotational energies among the fragments. The sizes and shapes of the family members could be used to determine how the parent body fragmented. True, genetic families also provide the unique opportunity to examine the exposed interiors of once, much larger planetary bodies.

By measuring the spectral reflectance properties of the asteroids in a dynamical family, it is possible to address the question of whether the family makes "cosmochemical sense". If the spectral properties of the family members are very similar, this provides strong evidence that the family results from the disruption of a homogeneous parent. On the other hand, if the family results from the break-up of a differentiated body, we might expect to see different spectral types among the family members, related to the different mineralogical layers of the parent. If the members of a purported family appear to have originated from both differentiated (high-temperature) and undifferentiated (low-temperature) sources, then it is unlikely that this group of asteroids resulted from the breakup of a single body.

Some of the previous investigations into the reality of asteroid families (Gradie and Zellner 1977, Gradie *et al.* 1979, Chapman 1987, Bell 1989) have produced mixed results. Each of these studies was conducted by examining the distribution of taxonomic types among the family members. It was generally found that the largest of the dynamical families were real, with the majority of members from each of these families belonging to the same taxonomic class. However, Bell found that most of the small dynamical families were not made up of genetically related members, while Chapman showed that many of the small families were likely real. More recent spectroscopic studies have focused on asteroids in the larger families (Binzel *et al.* 1993a, Doressoundiram *et al.* 1998, Florczak *et al.* 1999). In each case, the members of a family have been found to be spectrally similar, suggesting a relatively homogeneous parent body. The question still remains about the reality of smaller asteroid families.

1.5 Motivation for the SMASSII survey

Some of the fundamental problems currently confronting asteroid scientists may stem from the fact that we have substantial knowledge about the physical properties of the larger asteroids, but know very little about the smaller ones. Those fundamental

questions that deal with compositional interpretations, and the comparison to meteorite evidence, may be particularly prone to this bias towards larger objects. Smaller asteroids are more susceptible to collisional disruptions, so that their surfaces may be much younger than those of larger asteroids. Similarly, the ability to form and retain a regolith will be significantly reduced on smaller asteroids, due to their weaker gravitational potential.

In the 1980s, the introduction of charge-coupled devices (CCDs) to astronomy marked a major milestone in the physical studies of asteroids. The increased sensitivity of CCDs, and the 2-dimensional format, provided new and more efficient ways of observing asteroids. In particular, the development of CCD spectrographs in the late 1980s made it possible to obtain spectra of significantly fainter asteroids, and at much higher spectral resolution than had been previously possible with filter photometry.

Between 1991 and 1993, the first phase of the Small Main-belt Asteroid Spectroscopic Survey (denoted SMASSI) produced CCD spectra for 316 asteroids, covering the visible wavelength region from 0.4 to 1.0 μm (Xu *et al.* 1995). The goal of the SMASSI survey was to sample a significant number of smaller asteroids to address some of the major problems relating to the connection between meteorites and asteroids. In particular, SMASSI tried to address the apparent shortages of ordinary chondrite-like asteroids, and olivine-rich asteroids within the main belt. The apparent link that has been found between the small, S-type near-Earth asteroids and the ordinary chondrites was mentioned above. However, the missing olivine still remains a puzzle. One of the major results of the SMASSI survey was the identification of over 20 asteroids with spectra similar to the basaltic achondrite meteorites (Binzel and Xu 1993). This spectral signature is quite distinctive, and had previously only been observed for the asteroid Vesta. All of these new asteroids have orbits similar to that of Vesta, confirming the previous predictions of a dynamical family associated with Vesta. The distribution of these Vesta-like asteroids extends to the 3:1 Jovian resonance which establishes a viable dynamical link for Vesta as the source of the basaltic achondrite meteorites.

The second phase of this spectroscopic survey (SMASSII), builds on what was learned during the first phase while focusing on the detailed study of small dynamical families. Most significantly, the approach we have taken in studying dynamical families focuses on understanding the compositional characteristics of an entire region where a

number of small dynamical families have been proposed. In this region, concentrated effort is made to sample not only the members of these proposed families, but also the background population. The goals of this concentrated surveying are:

- to determine if these small dynamical families are real genetic associations;
- to determine an accurate list of members for each family and define the family boundaries in orbital space;
- to determine the taxonomic makeup of each family, and establish whether the parent was homogeneous or differentiated;
- to search for new families that have not been identified based on previous searches of orbital elements.

As described above, resolving these questions with regard to the validity of small asteroid families provides an important step for understanding the collisional history of the asteroid belt.

1.6 Outline for this work

This work presents the results of the SMASSII survey as it relates to the compositional nature and distribution of asteroids in the main belt. Chapter 2 details the manner in which this survey was conducted, the data reduction procedures, and the basic observational results. All of the final spectra are displayed in Appendix B. While the study of dynamical families is the main objective of this work, the tremendous bulk of the SMASSII survey (in terms of spectral resolution and the number of objects surveyed) posed an additional challenge. The current system of asteroid taxonomy, developed by Tholen (1984), was based on broad-band spectrophotometry. Our CCD data reveal significantly more detail about the spectral characteristics of asteroids than do the broad-band colors, and as a result, the Tholen taxonomy could not adequately address the richness of information within the SMASSII data set. Thus a significant component of this work is the development of a new feature-based taxonomy that takes fuller advantage of the CCD data. The principles of asteroid classification are discussed in Chapter 3, and this new feature-based taxonomic system is developed and described in Chapter 4. Armed with this new taxonomy, Chapter 5 presents a combined spectroscopic and orbital analysis designed to accomplish goals for investigating asteroid families, as specified above. Chapter 6 summarizes the conclusions.

Chapter 2

SMASSII: The Small Main-belt Asteroid Spectroscopic Survey - Phase II

Since their introduction in the late-1970s, charge-coupled devices (CCDs) have revolutionized many aspects of optical astronomy. Due to their high quantum efficiency, large dynamic range, and the dimensional stability of CCDs, these solid-state detectors have virtually replaced photographic emulsions and photomultiplier tubes in most astronomical applications (Janesick and Elliott 1992). Use of CCDs has thus lead to substantial improvements in the light-collecting efficiency for telescopes of all aperture sizes, and correspondingly, in the efficient use of the available observing time. Ground-based observations of asteroids have greatly benefited from CCD technology. In direct imaging mode, CCDs are now routinely used to discover new asteroids, and to provide the astrometric measurements needed to accurately calculate their orbits (Gehrels 1991, Rabinowitz 1991). Multiple images of an asteroid can be used to measure changes in its brightness over time, leading to a estimation of that asteroid's shape and its rotational properties (Wisniewski and McMillan 1987, French and Binzel 1989). With the increasing availability of low-resolution CCD spectrographs, more observers are using this technique to measure the spectral reflectance properties of asteroids (e.g. Vilas and Gaffey 1989, Luu and Jewitt 1990, Sawyer 1991, Vilas *et al.* 1993, Xu *et al.* 1995, Doressoundiram *et al.* 1998).

The first reported use of CCDs in asteroid spectroscopy was by Vilas and Smith (1985). The procedures for taking and reducing asteroid spectra have been fairly well established by Vilas and Smith (1985), Sawyer (1991), and Xu *et al.* (1995), as well as others. Central to the calibration process is the division of the recorded asteroid

spectrum by that of a solar-like star, revealing a signature of how the asteroid's surface reflects sunlight as a function of wavelength. While this method for determining a reflectance spectrum is straightforward, it works only if the data are taken and reduced in a way that preserves the relative spectrophotometric integrity of both the asteroid spectrum and that of the solar-like star. Besides the improved quantum efficiency of the detector, which allows for the observations of fainter targets, the principal advantage of a two-dimensional CCD array within a long-slit spectrograph is the ability to measure the spectrum of an asteroid and that of the background sky simultaneously, over a large wavelength interval. This avoids many of the complications encountered by filter photometry techniques that arise due to temporal variations in sky conditions, as well as possible photometric variability of the asteroid due to its inherent rotation.

Between 1991 and 1993, the first phase of the Small Main-belt Asteroid Spectroscopic Survey (hereafter referred to as SMASSI) was carried out, resulting in spectral measurements for 316 different asteroids (Xu *et al.* 1995). The goal of SMASSI was to survey the spectral properties for a large sample of small- to medium-sized asteroids, primarily focusing on those objects located in the inner main-belt. Among the accomplishments of SMASSI was the identification of the first main-belt asteroid whose reflectance properties resemble that of ordinary chondrite meteorites (Binzel *et al.* 1993b), and the spectral verification of a delivery method for basaltic achondrite (HED) meteorites from Vesta to the Earth (Binzel and Xu 1993).

Building on the experiences of SMASSI, our goal in carrying out phase two of the Small Main-belt Asteroid Spectroscopic Survey (SMASSII) has been to produce a spectral dataset that is internally consistent, where the observations and reductions are carried out in the most uniform manner possible. The procedures used in SMASSII roughly parallel those used during SMASSI (Xu *et al.*. 1995), though a number of modifications were made, especially in how the data were reduced. The primary observational objectives of SMASSII were the sampling of planet-crossing asteroids (both Near-Earth Asteroids and Mars-crossing asteroids), and the continued study of dynamical families, with particular emphasis on the Vesta family, and an in-depth study of several dynamical families located in the middle of the main asteroid belt, between 2.7 and 2.8 AU.

2.1 Observations

All SMASSII observations were carried out between August 1993 and May 1997, using either the 2.4 m (f/7.5) Hiltner or 1.3 m (f/7.6) McGraw-Hill reflecting telescopes. These telescopes are operated by the MDM Observatory (formerly known as the Michigan-Dartmouth-MIT Observatory) and are located on the southwest ridge of Kitt Peak in Arizona. The data were obtained using the Mark III long-slit CCD spectrograph, along with one of two CCD cameras, all facility instruments of the MDM Observatory. The camera that was primarily used contains a SITE 1024x1024 thinned, backside illuminated CCD with 24 μm square pixels, and is nicknamed "Charlotte". The second camera, called "Wilbur", was used only when Charlotte was not available, and contains a Loral 2048x2048 thick, front-side illuminated CCD with 15 μm pixels. The spectrograph is equipped with a low-resolution grism (150 lines per mm, blazed at 0.73 μm) that gives a dispersion of roughly 0.001 μm per unbinned CCD pixel. A slit, oriented in the north-south direction on the sky, and measuring 4.5 arcseconds wide and approximately five arcminutes long, was used for all of the observations. We chose this moderately large slit width to ensure that most of the light from the asteroid or standard star passed through the slit, allowing for uncertainties in guiding and variations in seeing. The spectral resolution, as defined by the width of this slit, was about 0.007 μm. Since the unbinned pixel sizes for both Charlotte and Wilbur are small compared with this spectral resolution, and with the spatial image scale projected by the spectrograph, Charlotte's pixels were binned 2 by 2 during readout, while Wilbur's pixels were binned 3 by 3. This avoided greatly oversampling the 2-D spectral images and helped improve the signal-to-noise ratio for faint targets. A Wratten 22 gelatin filter was always placed directly over the long-wavelength half of the dewar window, positioned to block the second-order spectral image that would otherwise be superimposed on the red half of the first-order spectrum. This procedure allowed the entire 0.4 to 1.0 μm wavelength range of the first-order spectrum to be recorded in a single exposure.

For each asteroid, a set of 2 to 5 spectral images were usually taken, with exposure times ranging from a few seconds, up to 900 seconds for the faintest objects. Longer exposures were avoided in order to limit the number of cosmic ray strikes that accumulate on the detector. Whenever possible, objects were observed within ±1 hr of crossing the meridian, when the airmass for the object was near its minimum value. The median airmass for all of the SMASSII observations was about 1.12. Observing near the

meridian has the added benefit that any dispersion of the image, due to differential refraction, would be roughly parallel to the north-south orientation of the slit. This reduced the chance of variations in the color or slope of a spectrum due to light being refracted outside of the slit. In order to calibrate the relative reflectance of each asteroid, observations were also taken every night of selected solar analog stars. To minimize the spectral uncertainties that might be introduced by using different solar analogs, only four stars were used in the final reduction of the SMASSII data. The two primary stars, 16 Cyg B (HD186427, M_V = 6.2, spectral type G5V) and Hyades 64 (HD28099, M_V = 8.1, G8V), are both widely accepted as good solar analogs (Hardorp 1978), and were used for the calibration whenever possible. When neither of these two stars could be observed, HR4486 (HD101177, M_V = 6.4, G0V) was used (Hoffleit 1982). On two nights in May 1995, a fourth star, HR5384 (HD126053, M_V = 6.3, G1V) (Hoffleit) was observed and ultimately used in the calibration of nine asteroid spectra. During each observing run, a series of bias frames was taken that would be used in processing the CCD images. For wavelength calibration, we also regularly obtained a set of Hg-, Ar-, and Xe-spectral line images that was produced using lamp sources contained within the Mark III spectrograph. During each observing run, as the CCD images were taken, they were closely examined for quality. In particular, as each asteroid was observed, a quick-look reduction was performed on at least one of the CCD frames, in which a 1-D spectrum for the asteroid was extracted and divided by the spectrum of a solar analog. This real-time examination allowed us to quickly estimate the quality of the CCD data, and determine if an object should be reobserved on another night.

2.2 Data Reduction

The data reduction was performed using the Image Reduction and Analysis Facility (*IRAF*), developed and maintained by the National Optical Astronomy Observatories (NOAO) (Tody 1993). Preprocessing of the CCD images involved a two-step bias subtraction. First, the mean bias level was determined from the unexposed overscan region in each CCD image, and subtracted. Then, any higher-order residual variations in the bias were removed, using a bias structure image constructed from the bias frames taken at the telescope. The spectral images span the entire dynamic range of the CCD, with peak data numbers being recorded around 0.7 μm where the quantum efficiency of the CCD is highest. As was found in SMASSI (Xu *et al.* 1995), this large range in data

values makes flat fielding of the images difficult without considerably increasing the noise level at the extreme blue and red ends of the spectrum. Rather than attempting to flat field the images, we relied on the inherently flat characteristics of both Charlotte and Wilbur. Based on flat fields obtained of the twilight sky in a direct imaging mode, we know the average pixel to pixel variations for both of these detectors to be considerably less than 1%. To ensure that the lack of flat fielding did not affect our final spectra, great care was taken to center the object during each observation along a prescribed CCD column, so that any variations in pixel sensitivity would be divided out during calibration by the solar analog.

Extraction of a 1-D spectrum from the 2-D image was carried out using the *apall* task within *IRAF*. This extraction procedure involves several operations: locating and tracing the spectral image and defining the boundaries of an aperture, summing the pixels within that aperture, and subtracting a background level that is determined from a row by row fit to sky regions outside of the aperture. After many tests and a careful selection of parameter values used in *apall*, the extraction of the SMASSII data was carried out in a semi-automatic mode. The width of the extraction aperture was determined entirely by the peak data number recorded in the spectrum, and ranged from 9 arcseconds for the faintest asteroids to 24 arcseconds for the brightest targets, such as the solar analog stars. The background sky level was determined for each row in the image using a 4th-order polynomial fit to two sky regions, 45 arcseconds wide, and located just to either side of the extraction aperture. Along with the extracted 1-D spectrum, *apall* produces a record of the 1σ uncertainty at each point in the spectrum, based on a Poisson noise model that includes the gain and readnoise of the detector. These uncertainties were propagated through the rest of the calibration process, so that meaningful error bars could be attached to the final spectra. A wavelength correction was applied to each spectrum, using a dispersion model based on measured lines in the Hg-Ar-Xe lamp images. When this correction was applied, the pixels making up the 1-D spectra were rebinned to a dispersion of 0.0025 μm, providing a uniform database from which different spectra could be easily compared and combined. A correction for atmospheric extinction was applied to the data, using the airmass of the observation, and a mean extinction model developed for Kitt Peak (based on Hayes and Latham 1975). By keeping the airmass of the observations low, any differences between this model and the true extinction would be largely corrected for in the division by the solar

analog. Finally, a nightly spectrum of the solar analog was produced by averaging the individual star observations after each was examined for bad pixels and for any inconsistencies in spectral slope. Each asteroid spectrum was then divided by this average solar analog and normalized to unity at 0.55 μm.

After the reduction and calibration of the asteroid spectra was complete, each spectrum was visually inspected for discrepant pixels. This process of defining which pixels are "bad" is rather subjective, but flagging and deleting pixels from the data ultimately had little effect on the final combined spectrum, its analysis or interpretation. We found discrepant pixels to be either the random spikes that are due to cosmic ray events, or systematic absorption or emission features in the spectra that can usually be linked to the incomplete removal of terrestrial atmospheric bands during the division by the solar analog spectrum. Locations of the major atmospheric oxygen and H_2O bands between 0.5 and 1.0 μm are shown in Figure 2.1. There is one systematic feature that cannot be matched to an atmospheric band, but which appears in many spectra between 0.515 and 0.535 μm. This feature was seen only in observations taken in bright moonlight, where the background sky level in the spectral image was particularly high, and always appeared as a drop in flux (an absorption feature) in the final asteroid spectrum. A possible explanation for this feature is the presence of the Wratten 22

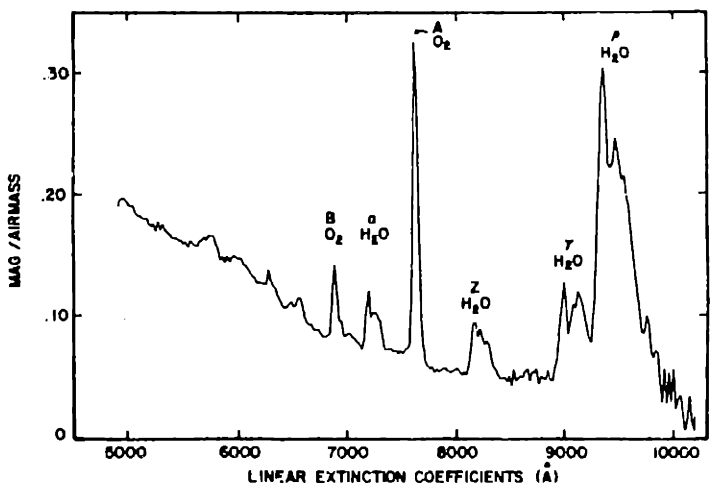

Figure 2.1: Atmospheric extinction in magnitudes per airmass as a function of wavelength, showing the major absorption bands due to telluric H_2O and O_2 molecules (from Cochran and Barnes 1981).

blocking filter. The transmission of the Wratten 22 is essentially zero shortward of 0.55 μm, and increases to over 80% by 0.58 μm. While this strong gradient in filter transmission is offset in wavelength from the observed spectral feature, we think a combination of scattered moonlight, location of the edge of the gelatin filter over the dewar window, and reflections from the surfaces of that window may lead to a background sky pattern whose value was consistently overestimated by the background fitting function we used, producing the observed artifact in many of the reduced spectra.

During the observing runs and throughout the reduction process, the SMASSII data were evaluated for overall quality and internal consistency. As might be expected, the quality of these data is closely tied to the sky conditions when the observations were made. In trying to make efficient use of the telescope time that was available, many observations were made under sky conditions that might be considered marginal, and as a result, some data were taken that later had to be rejected. Observations made through high-level cirrus were usually free of large systematic effects, though these spectra generally showed an overall increase in their level of random noise. The presence of cirrus usually meant that observations had to be limited to the brighter asteroids, especially when moonlight was present. More significant, systematic effects were seen in spectra that were taken through mid- to low-level clouds, high humidity or when the seeing was bad. Spectra taken under these conditions often contained substantial residual water bands, and sometimes showed large changes in the overall spectral slope between consecutive exposures. If the water bands or slope changes in the spectra were too extreme (differences in average spectral slope that are typically >0.03, using the definition of slope, γ, given in Chapter 3), the observations were usually rejected, and the asteroid would be reobserved on another night.

Probably the most arguable aspect of the observation and reduction process used was our decision to rely on a mean extinction model for Kitt Peak, rather than independently determine nightly extinction coefficients. This course was followed primarily as a matter of observing efficiency, with our goal being to survey the largest number of asteroids possible without dedicating excessive amounts of observing time for the purpose of calibration. Because of temporal, as well as spatial (different quadrants of the sky) variations in extinction, there is a limit to the accuracy with which a nightly extinction function can be determined. Based on long-term records of both nightly and seasonal variations in extinction for Flagstaff, Arizona (Lockwood and Thompson 1986)

(a continental observing site, having weather patterns and sky conditions similar to that experienced on Kitt Peak), I tried to estimate the uncertainties introduced into the final spectra based on the use of a mean extinction function. Since our observations were targeted close to the time of meridian crossing, differences in airmass were kept to a minimum, thus minimizing the effects of differences in the extinction coefficients. Overall, uncertainties in the average spectral slope (related to the use of a mean extinction model) should be less than ±0.02 for those objects observed at the highest values of airmass, and considerably less than this for most of the asteroids observed during SMASSII. Since the magnitude of extinction coefficients rise sharply at short wavelengths, we expect any difficulties tied to the extinction model to be most pronounced in the violet end of our spectra.

The source of the larger, more sporadic changes in the average spectral slope, with variations of up to ±0.05 or even higher, is unknown, though a preferential loss of either blue or red light through the spectrograph slit is implied. This effect is primarily seen to occur in observations taken through cloudy skies, suggesting that clouds may not behave like a completely neutral filter. The other possible explanation for the slope variations is that the slit size we used was not sufficient to collect all the light when poor seeing is combined with the effects of differential refraction (Filippenko 1982). Whatever the cause, a random offset in the slope of an asteroid spectrum may not be detected without observations on multiple dates. As spectral observations become more common, and asteroids are reobserved by different observers, we suggest that offsets in the overall slopes of spectra may be routinely seen, and that care must be taken to separate these random effects from potentially real variations in the spectra due to actual surface effects, such as phase reddening (Miner and Young 1975, Poutanen *et al.* 1985), or compositional differences on the asteroid (e.g. Howell 1995, Gaffey 1997).

A listing of observational circumstances for the 1189 asteroids presented in this paper is given in Appendix A. For each asteroid, we identify the telescope and detector used, and note the presence of clouds, high humidity or moonlight during the observations. Also listed is the solar analog star used for the reflectance calibration. This information can be useful in evaluating the quality and reliability of a spectrum. Only those observations that were retained through the analysis process and included in the final dataset are listed. If an asteroid was observed on more than one night, multiple lines in the table give the observational circumstances for each night. Along with the

asteroid number and name, this table also gives spectral parameters and a taxonomic classification determined during the analysis of these data.

For each asteroid, a final reflectance spectrum was produced by combining the individual spectra of the object using a weighted mean. Only those spectra that were of acceptable quality were included, and any pixel values that were flagged as bad were omitted from this calculation. Likewise, a formal set of errors, based on Poisson statistics, was calculated using the uncertainties associated with the individual spectra. The magnitude of these errors was compared with the actual scatter of the data making up the mean, confirming that these errors are consistent with the level of random noise contained in the final reflectance spectrum. Although the spectrograph/CCD combination gives a wavelength coverage from roughly 0.4 to 1.0 μm, the final spectra presented in this paper cover the interval from 0.435 to 0.925 μm. The spectra were trimmed to this length to produce a uniform dataset, independent of the detector used, the brightness of the asteroid, or the conditions in which the observations were made. The quantum efficiency of Wilbur falls off rapidly shortward of 0.435 μm, affecting the spectra of even bright asteroids. This provided a natural limit for our spectra at the blue end, while at the red end, the limit is defined by the sharp band head of the telluric ρH_2O band, located at about 0.93 μm (Cochran and Barnes 1981). The final spectra, along with error bars, are shown in Appendix B.

Chapter 3

Parameterization and classification of the SMASSII asteroid spectra

3.1 Some thoughts on classification

Whenever several individual members of a large population are studied in detail, there is a natural desire to arrange those individuals into groups based on similarities in their observed characteristics. This process of intercomparing and classifying members of a population is common in many branches of research, especially in the biological sciences. The basic concept of classifying a population and applying a set of labels (called a taxonomy) to the resulting groups should be straightforward, but controversies exist to the point that many books have been devoted to the competing philosophies of classification (e.g. Abbott *et al.* 1985, Ridley 1986). These controversies develop from the single fact that different groupings or taxonomies result when different characteristics of the population are used in defining the classification process.

The goal of any taxonomy should be to represent a population in a way that reflects the natural similarities among (or differences between) its individual members. The choice of characteristics used in defining the classes should be driven by a theoretical principle, or by some observable or measurable property of nature. In biology, taxonomic systems are usually developed as hierarchical structures, designed to reflect the theoretical pathways of evolution. The lowest level in this hierarchical structure, the level of species, is commonly defined by the ability for members of the same species to interbreed (Ridley 1986).

Classification techniques are also widely used in other physical sciences. For example, in astronomy, the classification of stars is based on a continuous taxonomic system that, while derived from measurements of absorption lines in a star's visible spectrum, is ultimately tied to one fundamental property of stars: their temperature (Kaler 1989). Since this classification system is rooted in some fundamental property of nature, it is referred to as "natural" or "objective" taxonomy (Ridley 1986). Besides helping to simplify or generalize the broad aspects of a population, the development of a natural taxonomy can often help reveal new relationships that exist among members of the population, and can lead to a better understanding of secondary processes that give rise to more subtle differences between its members.

A population can be classified even when the underlying process responsible for the differences among its members is not known. In this case, the taxonomy is usually referred to as being "artificial" or "subjective" (Ridley), and is often more susceptible to controversy among researchers. If such a taxonomy is based on characteristics of the population that are superficial, or is steered by incorrect assumptions about the physical nature and evolution of the population, it can actually lead to increased confusion. While taxonomic classification is usually a necessary step in understanding the gross properties of a population, its value should not be overestimated. Adopting a taxonomy should never mask the importance of the actual observed (and measured) characteristics of the individual members of the population. Finally, it is important that a taxonomy is allowed to evolve over time, and that we confine its status to be a tool of research, rather than allowing it to become a force the controls the direction of scientific efforts.

3.2 Previous asteroid taxonomies

Prior to the first close flyby of an asteroid (951 Gaspra) by the Galileo spacecraft in October 1991 (Belton *et al.* 1992), our knowledge of the physical properties of asteroids was limited to two sources: those disk-averaged characteristics that can be measured from the Earth's surface (or from satellites in Earth orbit), and measurements of meteorite samples that have been delivered to Earth via collisional and dynamical processes in the asteroid belt (Binzel 1989). While meteorites can be carefully studied in the laboratory and provide important constraints on the bulk properties of the asteroid belt (Lipschutz *et al.* 1989), these samples have not so far been linked to individual

parent asteroids, and therefore, do not provide a reliable foundation on which asteroid taxonomy can be defined. Instead, asteroids have traditionally been grouped and classified based on similarities in their observed reflectance properties. The way in which an asteroid reflects incident sunlight is the most reliable indicator we have of its surface mineralogy, and (presumably) its bulk composition.

Subtle differences in the color of asteroids were first reported by Bobrovnikoff (1929), based on microphotometric measurements obtained from photographic spectra. However, due to limitations of the photographic technique, very little progress was made in the study of asteroid colors over the two decades that followed. In the mid-1950's, standard UBV photometry was first used to systematically investigate the broad-band colors of a large sample of asteroids. These observations led Wood and Kuiper (1963), Chapman *et al.* (1971), as well as others to describe two distinct groups of objects, based on their reflectance properties. Zellner (1973) was one of the first to recognize a bimodal distribution in albedos, leading him to also suggest that asteroids could be divided into two groups: dark "carbonaceous" types and brighter "stony" types. The basis for a more rigorous taxonomy was finally developed in the mid-1970s, after numerous programs were initiated to measure the physical properties of asteroids. Combining narrow-band spectrophotometry with polarimetric and radiometric albedo measurements, Chapman *et al.* (1975) applied the first taxonomy based on a system of single letters: C representing the dark carbonaceous objects, S for the stony or "silicaceous" objects, and U for those asteroids not fitting into those two main categories, and thus considered "unusual" or "unclassifiable". In the years that have followed, improvements in instrumentation and observing techniques, a substantial growth in the size of asteroid databases, and the availability of different classification algorithms have all helped inspire many researchers to try to improve on the way asteroids are classified. While this evolution in asteroid taxonomy has helped reveal some important aspects, as well as important questions, about the compositional and physical nature of these objects, it has also led to a rather complex and sometimes confusing use of nearly every letter in the alphabet. The early history of asteroid taxonomy has been thoroughly reviewed, first by Bowell *et al.* (1978), and more recently by Tholen and Barucci (1989).

The most widely used of the various asteroid taxonomies is the one proposed by Tholen (1984). The classification system developed by Tholen was a logical extension of previous taxonomies (Chapman *et al.* 1975, Bowell *et al.* 1978), and was developed

primarily using broad-band spectrophotometric colors obtained during the Eight Color Asteroid Survey (ECAS, Zellner *et al.* 1985), though measurements of albedo were also included in defining some of the class boundaries. The resulting taxonomy is comprised of 14 classes, each denoted by a single letter. In addition to the two classical, and most densely populated spectral classes, the C- and S-types, Tholen identified six other spectrally distinct groups of objects, labelling them A, B, D, F, G, and T. Another three groups, designated by the letters E, M, and P, are spectrally featureless at the resolution of the ECAS data, and could only be separated based on their albedos. When albedo information was not available, the E-, M-, and P-types were lumped into a generic "X" class. Finally, three classes, denoted by Q, R, and V, were created for three spectrally unusual objects: 1862 Apollo (Q-type), 349 Dembowska (R-type) and 4 Vesta (V-type). Most of the ECAS asteroids were uniquely classified, and grouped into one of these 14 taxonomic classes, though when the classification was uncertain, multiple letter designations were assigned. The wide acceptance of the Tholen taxonomy has been due, in part, to the simple way the spectral classes have been described, as shown in Fig. 3.1 and Table 3.1.

Subsequent attempts have been made to improve, or expand on the Tholen taxonomy. The taxonomy proposed by Chapman (1987) was intended to extend Tholen's taxonomy to less thoroughly observed asteroids. Barucci *et al.* (1987) and Tedesco *et al.* (1989) each combined the ECAS data with IRAS (Infrared Astronomical Satellite) albedo measurements (Veeder *et al.* 1989) before applying different classification algorithms to define their taxonomic classes. Howell *et al.* (1994) combined data from the 52-color asteroid survey (Bell *et al.* 1988) with the ECAS measurements, and used an artificial neural network as a way of identifying the natural boundaries between spectral groups. In each of these attempts to revisit the problem of asteroid classification, the general structure of the Tholen classes was reproduced, verifying the robust nature of this taxonomy. Over time, new classes have been added to the Tholen system, based on spectral observations of particular objects. Bell (1988) proposed the addition of a K-class to represent the unusual spectral properties observed among asteroids belonging to the Eos family. The unique and possibly ordinary chondrite-like spectrum of 3628 Božněmcová prompted Binzel *et al.* (1993b) to define the O-class. Similarly, the Z-class was proposed by Mueller *et al.* (1992) to account for the extreme red color of the distant asteroid (Centaur) 5145 Pholus. In analyzing the

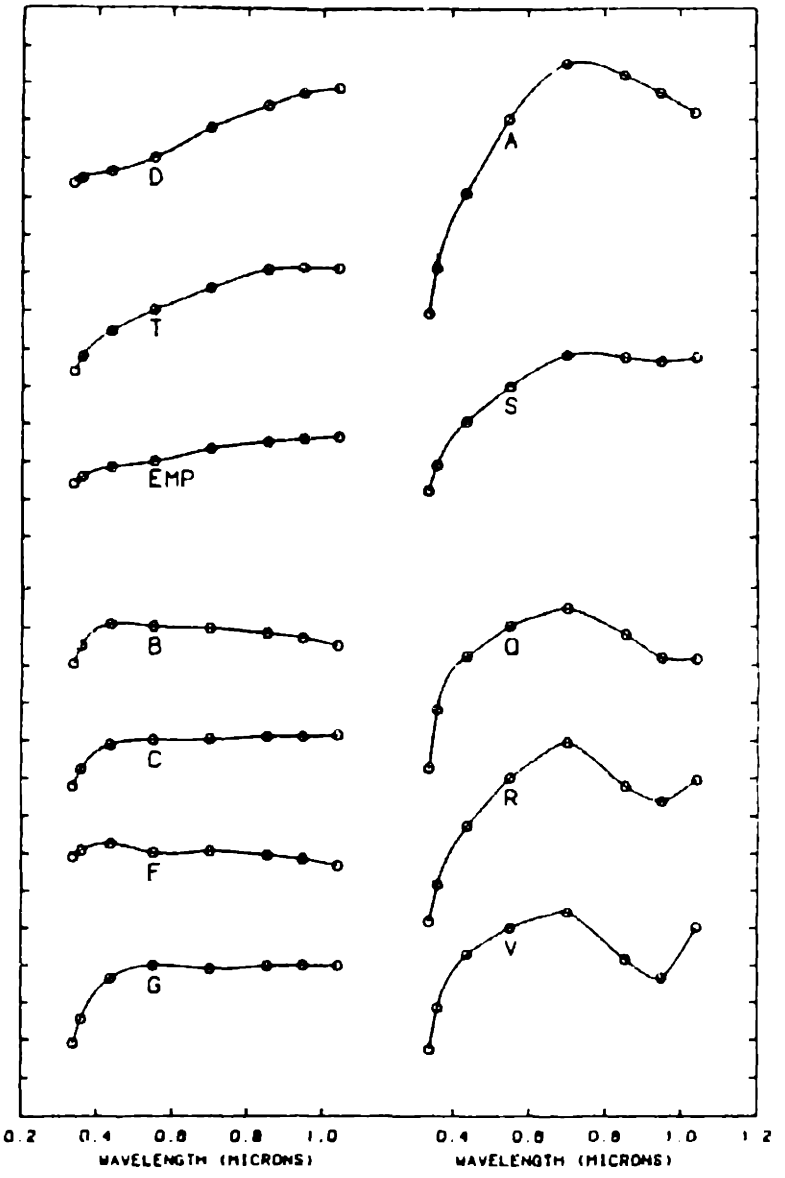

Figure 3.1: Mean reflectance spectra for the Tholen taxonomic classes. From Tholen and Barucci (1989).

spectra of a large number of Vesta family asteroids, Binzel and Xu (1993) proposed splitting the V-type spectral class into two parts by introducing a new J-class to represent those objects with particularly deep spectral absorption features.

Table 3.1: Description of Asteroid Classes

Letter Designation	Albedo	Spectrum
A	moderately high	extremely reddish shortward of 0.7 μm; strong absorption feature longward of 0.7 μm, centered near the 1.05 μm filter
B	moderately low	higher albedo variant of the C class with a tendency toward lower reflectivities at the red end of the spectrum (subclass of the C class)
C	low	ultraviolet absorption feature shortward of 0.4 μm, generally flat to slightly reddish longward of 0.4 μm
D	low	generally featureless spectrum; neutral to slightly reddish shortward of 0.55 μm, very red longward of 0.55 μm; some objects' spectra tend to flatten longward of 0.95 μm
E	high	featureless spectrum; flat to slightly reddish over entire 0.3 to 1.1 μm wavelength range; differs from the spectrally identical M and P classes in albedo only
F	low	featureless spectrum; flat to slightly bluish over entire 0.3 to 1.1 μm wavelength range; differs from the C class in the weakness of the ultraviolet absorption feature (subclass of the C class)
G	low	very strong ultraviolet absorption feature shortward of 0.4 μm, flat longward of 0.4 μm; differs from the C class in the strength of the ultraviolet absorption feature (subclass of the C class)
M	moderate	featureless spectrum; flat to slightly reddish over entire 0.3 to 1.1 μm wavelength range; differs from the spectrally identical E and P classes in albedo only
P	low	featureless spectrum; flat to slightly reddish over entire 0.3 to 1.1 μm wavelength range; differs from the spectrally identical E and M classes in albedo only; spectra are intermediate between C and D classes
Q	moderately high	strong absorption features shortward and longward of 0.7 μm; band center between those of A and V classes (1862 Apollo is the type example)
R	moderately high	strong absorption features shortward and longward of 0.7 μm; band center between those of A and V classes (349 Dembowska is the type example)
S	moderate	moderate to strong absorption feature shortward of 0.7 μm, and moderate to nonexistent absorption feature longward of 0.7 μm

Letter Designation	Albedo	Spectrum
T	low	moderate absorption feature shortward of 0.85 μm, and generally flat longward of 0.85 μm
V	moderately high	strong absorption feature shortward of 0.7 μm and strong feature longward of 0.7 μm, centered near the 0.95 μm filter
other letters and symbols used in the classifications		
I		used for inconsistent data (e.g. a low albedo but an A-type spectrum); such a designation would be used only in the case of unconfirmed data; should high-quality data confirm such a combination, then a new asteroid class should be introduced
K		this letter has been reserved to represent a class of objects similar to 221 Eos; at this time, no formal definition for this class exists in the taxonomic system described above
U		appended to the classifications of those objects that fall far from the cluster center, indicating an unusual spectrum for that class
X		in the absence of albedo information, the E, M, and P classes are spectrally degenerate; X is used to represent the spectrum shared by these three classes and should be replaced by E, M, or P once a high-quality albedo becomes available
:		indicates noisy data and a classification of lower quality
::		indicates extremely noisy data and a classification of dubious quality
---		indicates that physical data do exist but are useless for classification purposes due to excessive noise

The descriptions listed in this table are from Table I, Tholen and Barucci (1989)

3.3 Parameterization of the SMASSII data

Before analysis of the SMASSII spectral data was begun, we constructed a uniform dataset, consisting of a fixed number of evenly spaced data values for each spectrum. In SMASSI, this was accomplished by fitting each spectrum with a moderately high (7th to 9th)-order polynomial. While these polynomials were sufficient to follow the features along much of the spectrum's length, the fits were essentially unconstrained outside of the observed data interval. For SMASSII, we decided to use a smoothing spline algorithm (Reinsch 1967, adapted by D. G. Schleicher). This is a cubic spline routine in which the strict rules for interpolation have been modified to allow for variable amounts

of smoothing. It makes use of a user-defined scaling factor that controls the level of smoothing by scaling the uncertainty of each point in the spectrum. For consistency, the value of this scaling factor was independently determined for each spectrum based on the total uncertainty and number of data points contained in the spectrum. Output from the spline fit consisted of 49 points, or "channels", covering the interval from 0.44 to 0.92 μm at steps of 0.01 μm. The normalization of each fitted spectrum was then re-calculated to ensure that the reflectance at 0.55 μm was 1.00. Since this normalization makes the 0.55 μm channel redundant, each fitted spectrum is completely described by the remaining 48 channels.

Due to the very broad, and often shallow profiles of mineral absorption bands, adjacent channels in the spline-fitted asteroid spectra are highly correlated. This can be seen in Table 3.2, where a representative section of the SMASSII correlation matrix, centered on the diagonal from 0.80 to 0.88 μm, is listed. Due to the potential presence of strong pyroxene and olivine absorption features within this interval, it might be expected that the variance between adjacent channels in this interval would be greatest. By comparison, a broad sampling of this same correlation matrix is shown in Table 3.3, where values at every 0.06 μm are listed. It is clear that the correlation between channels becomes weaker as their separation in wavelength increases. This is consistent with the fact that the number of characteristic features contained in an

Table 3.2: SMASSII correlation matrix (detail from 0.80 to 0.88μm)

μm	0.80	0.81	0.82	0.83	0.84	0.85	0.86	0.87	0.88
0.80	1.00	0.99	0.98	0.95	0.92	0.88	0.83	0.79	0.75
0.81	0.99	1.00	0.99	0.98	0.95	0.92	0.88	0.84	0.80
0.82	0.98	0.99	1.00	0.99	0.98	0.95	0.92	0.89	0.86
0.83	0.95	0.98	0.99	1.00	0.99	0.98	0.96	0.93	0.90
0.84	0.92	0.95	0.98	0.99	1.00	0.99	0.98	0.96	0.94
0.85	0.88	0.92	0.95	0.98	0.99	1.00	1.00	0.98	0.97
0.86	0.83	0.88	0.92	0.96	0.98	1.00	1.00	1.00	0.99
0.87	0.79	0.84	0.89	0.93	0.96	0.98	1.00	1.00	1.00
0.88	0.75	0.80	0.86	0.90	0.94	0.97	0.99	1.00	1.00

Table 3.3: SMASSII correlation matrix (overview, 0.06μm resolution)

μm	0.44	0.50	0.56	0.62	0.68	0.74	0.80	0.86	0.92
0.44	1.00	0.97	-0.91	-0.91	-0.90	-0.89	-0.80	-0.45	-0.24
0.50	0.97	1.00	-0.95	-0.94	-0.94	-0.93	-0.83	-0.47	-0.25
0.56	-0.91	-0.95	1.00	0.97	0.96	0.94	0.86	0.53	0.33
0.62	-0.91	-0.94	0.97	1.00	0.99	0.98	0.91	0.58	0.36
0.68	-0.90	-0.94	0.96	0.99	1.00	0.99	0.92	0.58	0.35
0.74	-0.89	-0.93	0.94	0.98	0.99	1.00	0.94	0.61	0.39
0.80	-0.80	-0.83	0.86	0.91	0.92	0.94	1.00	0.83	0.65
0.86	-0.45	-0.47	0.53	0.58	0.58	0.61	0.83	1.00	0.94
0.92	-0.24	-0.25	0.33	0.36	0.35	0.39	0.65	0.94	1.00

asteroid spectrum is small compared to the 48 channels we use to define that spectrum. It is therefore useful to parameterize the important characteristics or features in a spectrum, reducing the number of variables needed to describe them, and simplifying the comparison of these particular features with those in other spectra.

The parameterization of spectral data can be achieved in different ways, though the choice of rules by which the data are parametrized can have a substantial effect on how the results are interpreted. One way to parameterize asteroid spectra is to identify and measure specific features in the spectrum. This could include measuring the center, depth or area of one or more specific absorption bands, or measuring the spectral slope over a defined wavelength interval. This was the approach of Chapman *et al.* (1975), who chose the parameters R/B, BEND, DEPTH and IR, defined by McCord and Chapman (1975). These parameters provided a way of quantifying the presence or absence of a UV slope and 1 μm absorption feature in each spectrum, allowing the C- and S-type asteroids to be easily separated. More recently, Gaffey *et al.* (1993a) combined visible and near-infrared spectrophotometry and measured the depths and positions of absorption bands at both 1 and 2 μm as a means of dividing the S-types into 7 subclasses. In both cases, the rules for parameterization are carefully chosen, based on prior knowledge of mineralogy, and assumptions about how this knowledge should be applied to the problems of asteroid composition.

Parameterization can also be achieved using various techniques in the field of multivariate analysis. An example of this is Principal Component Analysis (PCA), used by Tholen (1984) to visualize the distribution of taxonomic classes he had assigned to the ECAS asteroids. The results of Tholen are reproduced in Fig 3.2, where the first two principal components calculated from the ECAS dataset are shown, labeled by spectral class. The allure of PCA, and similar multivariate techniques, is that parameterization is based on the overall variance of the spectral data, without *a priori* knowledge of what characteristics of the spectra are important.

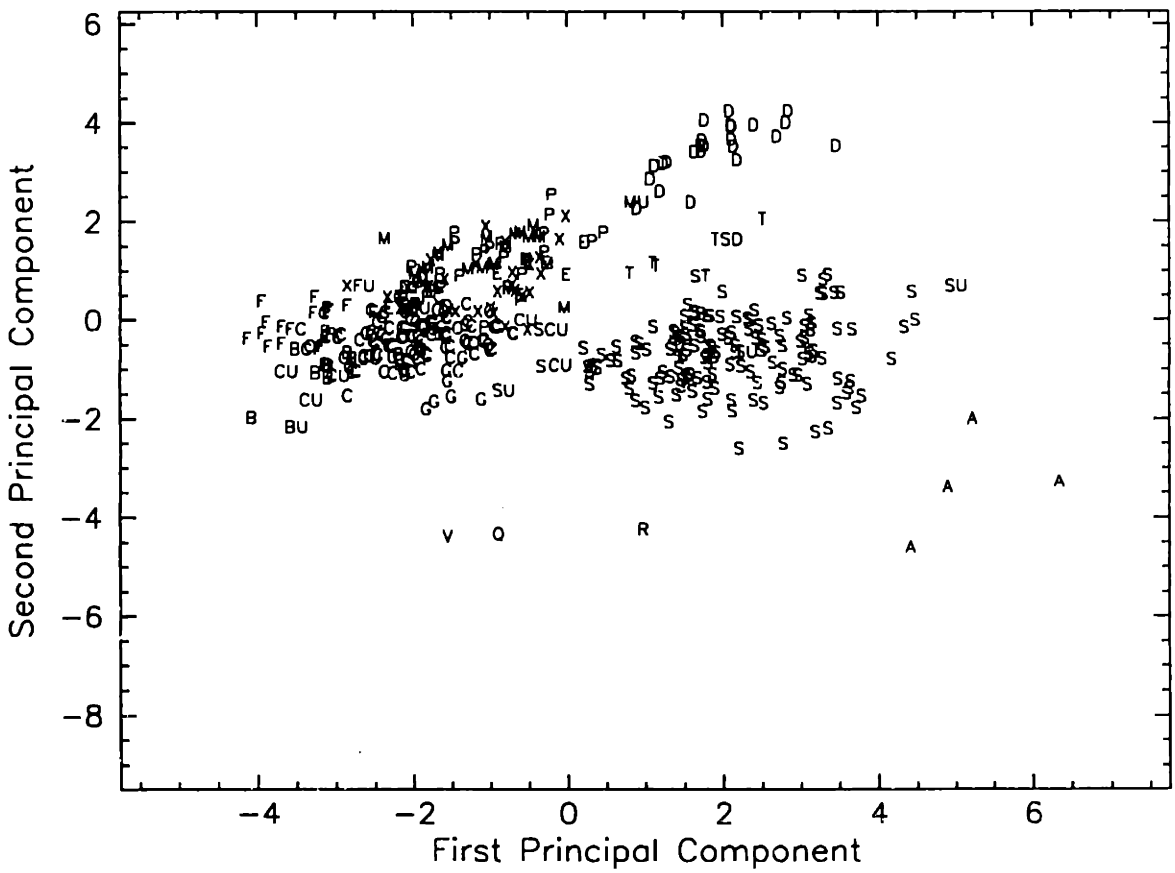

Figure 3.2: Principal component plot showing the 405 ECAS asteroids used by Tholen in defining his taxonomy (labeled with the Tholen class designation).

3.4 The use of multivariate techniques

As a first step in the analysis of the SMASSII data, we used PCA to examine the overall variations in spectral reflectance. For this, and all further studies of the SMASSII spectra, we relied heavily on statistical analysis routines contained in *S-Plus*, a program environment developed by *AT&T*'s Bell Laboratories (Venables and Ripley 1994). PCA is one of the most basic techniques of multivariate analysis, and one that is regularly applied in problems related to taxonomy. Often referred to as an "ordination" technique (Abbott *et al.* 1985), PCA effectively remaps the original data into a new space whose axes are oriented in a way that best represents the data's total variance. Applying PCA involves a series of linear transformations of the data, using weighting values, called "loadings" that are determined from the eigenvectors of the correlation (or covariance) matrix for the original data. These transformations result in a series of orthogonal rotations of the data in *n*-space, so that the largest amount of variance in the data is described by the smallest number of uncorrelated variables, with the largest possible fraction of the variance being accounted for by the first variable, or principal component (PC1). The second principal component (PC2) represents the next largest fraction of the variance, and so on. Using the eigenvectors derived from the correlation matrix results in a scaling of the variance in each spectral channel by its standard deviation, giving each channel equal weighting in the calculation of the principal components. The first two principal components calculated by this method, based on the SMASSII data, are plotted in Fig. 3.3. The overall appearance of this SMASSII principal component space is very similar to that of the ECAS component plot in Fig. 3.2, with the primary difference being that some of the major gaps separating spectral classes in the ECAS plot are much less apparent in the SMASSII data. Also, there is the addition of objects in the lower portion of the SMASSII principal component space (known to be V-type asteroids, Binzel and Xu 1993) that, due to their small sizes, were not sampled during the ECAS observations.

Instead of using the scaled variances to determine the loadings, use of the covariance matrix (unscaled variances) might be more appropriate for spectral data. This should be considered, since all channels in the spectrum are measured in the same units of relative reflectance, and differences in the true variance from channel to channel could be significant in helping to differentiate between spectral types. To test this, the principal components for the SMASSII data were recalculated, based on the unscaled

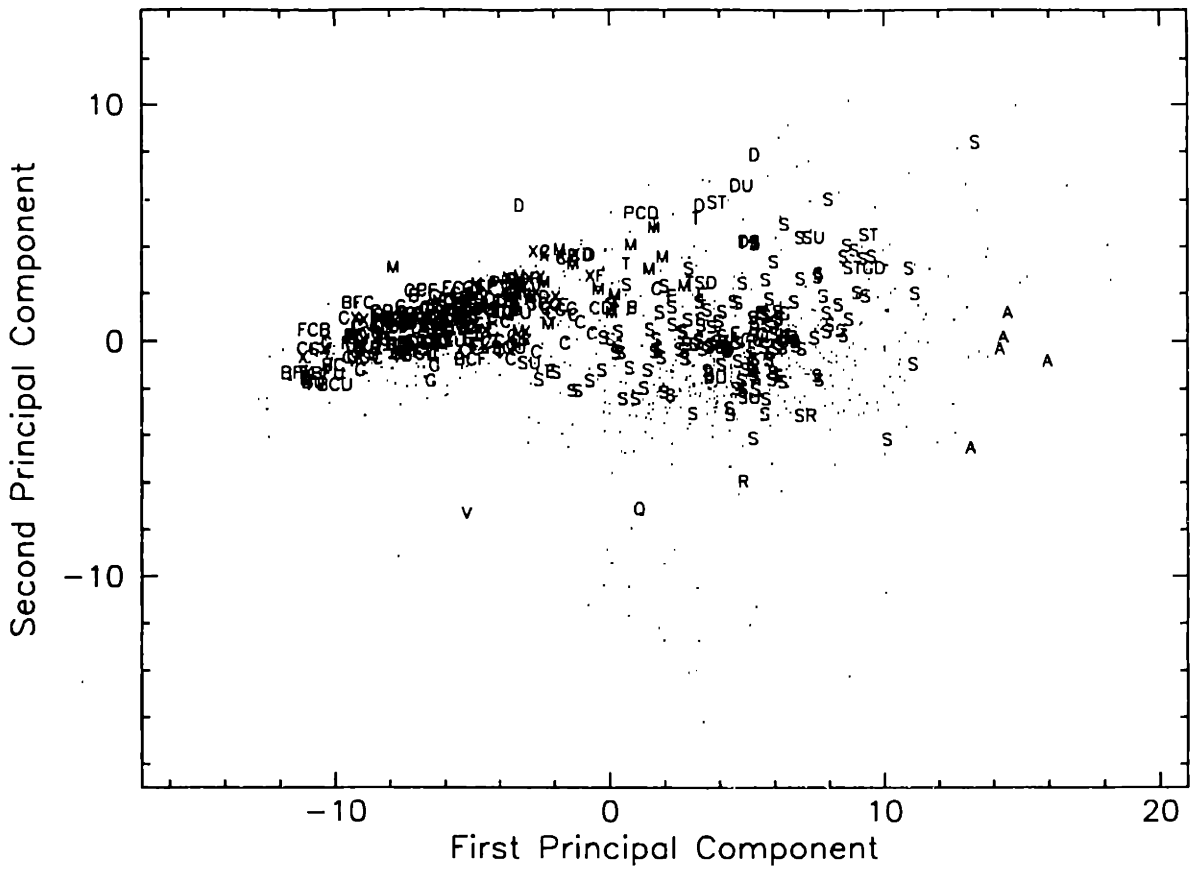

Figure 3.3: Plot of the first two principal components for 1190 SMASSII asteroids, calculated using eigenvectors of the correlation matrix (each channel is given equal weight). Asteroids observed as part of the Eight Color Asteroid Survey are labeled with the Tholen class, while objects newly observed as part of SMASSII are shown as dots.

variances. The first two components from this solution are plotted in Fig. 3.4. Higher numbered principal components are usually not very diagnostic in separating asteroid spectra, as is seen in Fig. 3.5, where PC2 is plotted against PC3. While there are subtle differences between Figs. 3.3 and 3.4, the fundamental structure of the space defined by the first two components remains the same, independent of the matrix used in defining the transformation. One way to quantitatively determine which parameterization is more representative of the original data is with the percentage-of-variance criterion (Dillon and Goldstein 1984), defined as:

$$s = \left(\sum_{i=1}^{k} l_i \right) \Big/ \left(\sum_{i=1}^{p} l_i \right) \tag{3.1}$$

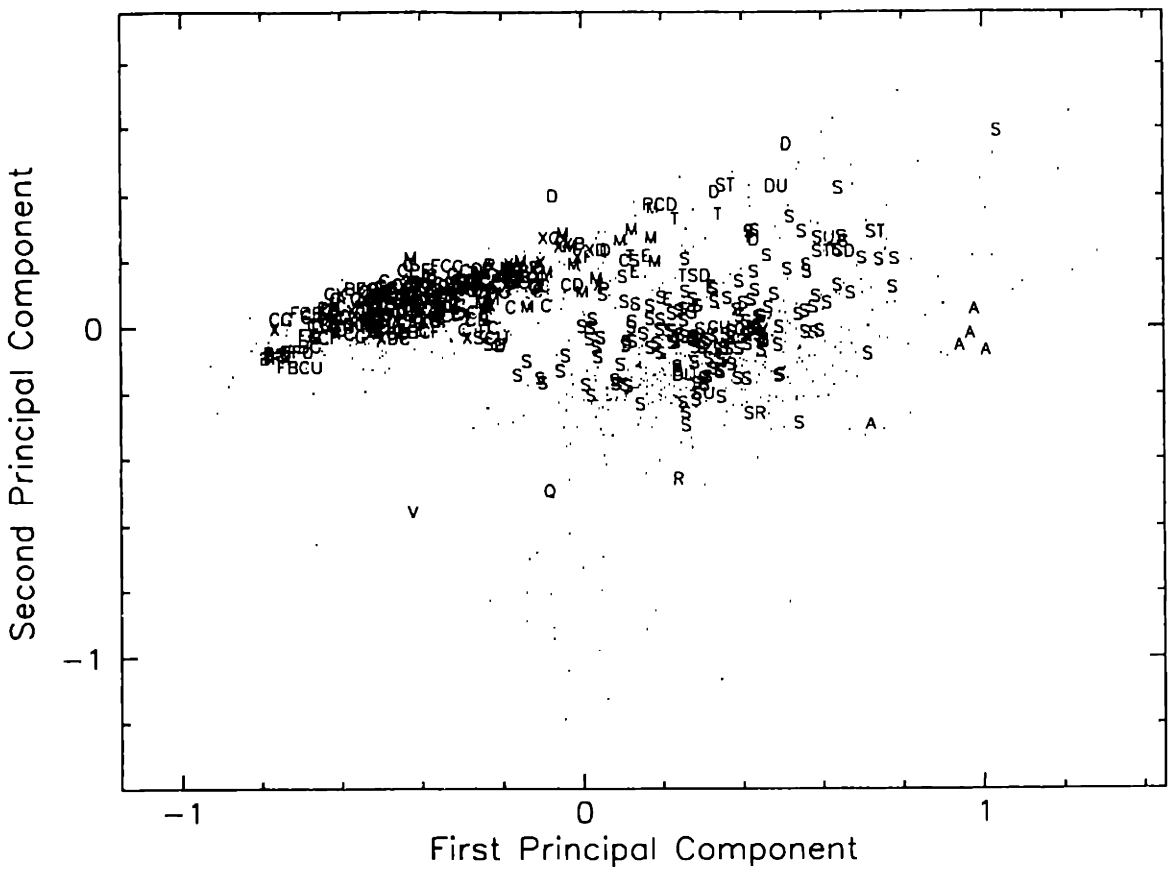

Figure 3.4: Plot of the first two principal components for 1190 SMASSII asteroids, calculated using eigenvectors of the covariance matrix (unscaled variances). Asteroids observed as part of the Eight Color Asteroid Survey are labeled with the Tholen class designation, while those objects newly observed as part of SMASSII are shown as dots.

where l_i is the i-th eigenvalue, p is the number of variables, or channels in the spectrum, and k is the number of principal components being considered. Using $k = 2$, we find values for the percentage-of-variance of $s = 0.970$ based on eigenvalues from the correlation matrix, and $s = 0.979$ from the covariance matrix. While this difference in values for the percentage-of-variance is small, and the choice of matrix used in PCA appears to have little effect on the interpretation of the results, I have adopted the use of the covariance matrix (the unscaled variances) for all of the following investigations of the SMASSII spectra. By comparison, in the analysis of the SMASSI asteroid data (Xu *et al.* 1995), classification closely followed the Tholen taxonomy, with the assignment of spectral types being based primarily on principal component scores determined by using scaled variances (the correlation matrix).

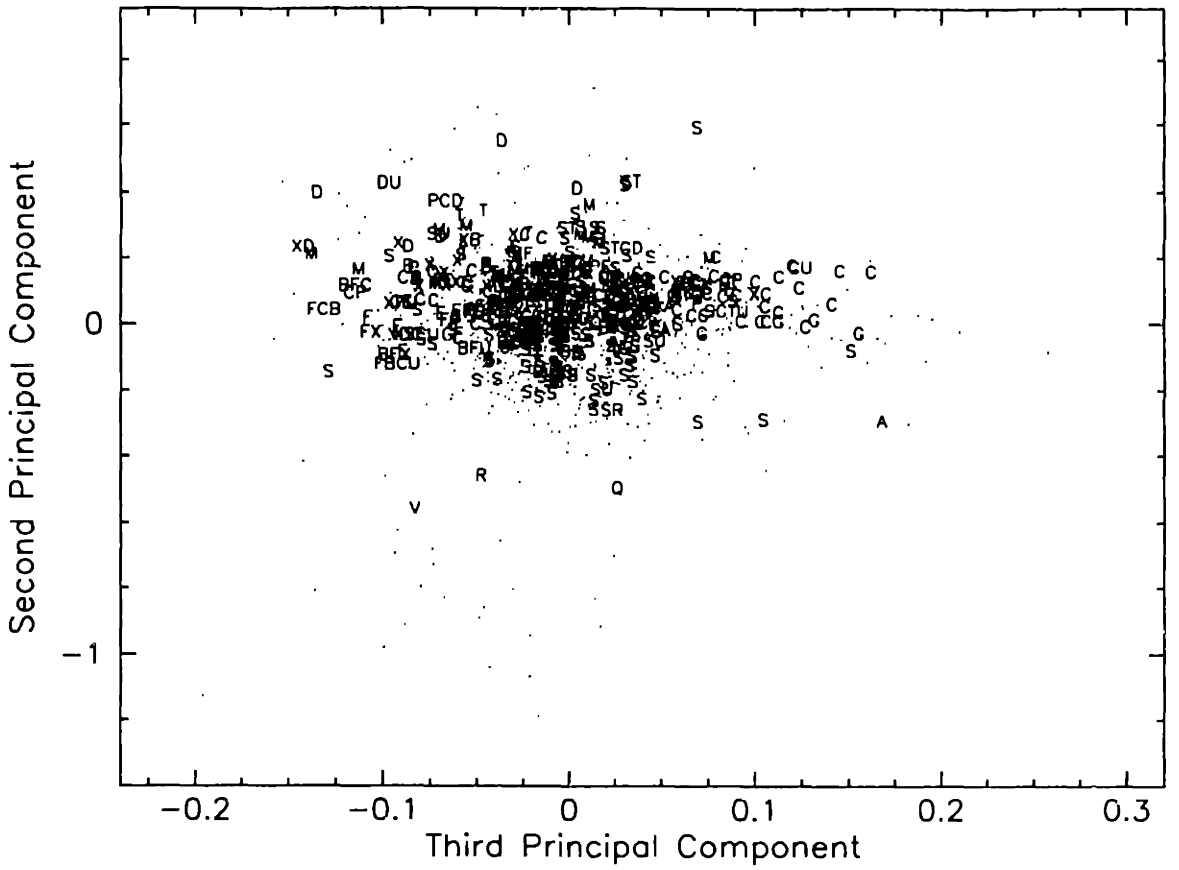

Figure 3.5: Same as Fig. 3.4, except plotting the second and third principal components.

While Tholen (1984) used PCA as a way to visualize the distribution of the ECAS spectral classes, his classification scheme was actually defined using another multivariate technique, the minimum-spanning tree (MST). MST uses a measure of the distance, often referred to as "dissimilarity", separating pairs of spectra. A spectrum can be represented as a point in *n*-dimensional space, with the dissimilarity between two spectra being the measured distance between the two respective points. This distance is measured using a specific rule or formula, called a metric. The most common metric, and probably most applicable to spectral data, is the ordinary Euclidean distance,

$$d_{ij} = \left\{ \sum_{n=1}^{p} (X_{in} - X_{jn})^2 \right\}^{1/2} \qquad (3.2)$$

where d_{ij} is the distance, or dissimilarity between the i-th and j-th spectrum, and X represents the individual channels of the spectrum, where the total number of channels is p. A number of multivariate techniques, especially clustering algorithms, utilize this measure of dissimilarity, and are collectively referred to as "distance" methods. In the minimum-spanning tree algorithm, each object in a dataset (where that dataset contains a total number of objects, m) is represented by a point in n-dimensional space, and all m points are connected, using the minimum number of m -1 segments, called branches. The points are connected in such a way that the total length of all branches is minimized, with the MST solution for any specific dataset being unique. In defining his taxonomy, Tholen used the minimum tree solution for 405 ECAS objects for which high-quality data were available. The taxonomic clusters were then identified by cutting the longest branches of the tree, where a branch was considered long when compared to the lengths of shorter, neighboring branches. The decision of how many branches to cut was arbitrary (Tholen and Barucci 1989).

Our original goal in classifying the SMASSII asteroids was to accurately assign a spectral type to each object, based on the Tholen taxonomy. To properly classify a new asteroid in the Tholen system, it is necessary to find the three asteroids in the ECAS dataset that are spectrally most similar (nearest neighbors) to the new object. The new asteroid is then assigned the spectral class of its nearest neighbor, with the class designations of the second and third nearest neighbors being added, in succession, if these are different from the first designation (Tholen and Barucci 1989). However, there are significant differences between the SMASSII and ECAS datasets. In particular, the SMASSII spectra cover a narrower wavelength interval than that sampled by the ECAS observations, with only 4 of the 8 ECAS filter bandpasses falling within the SMASSII spectral interval from 0.44 to 0.92 μm. As a result, we cannot classify the SMASSII asteroids using all of the ECAS colors in the way that Tholen had intended. This raises important questions about how to best classify asteroids based on CCD spectroscopy. If the spectral characteristics that are necessary to differentiate the Tholen classes are present over the wavelength interval covered by the CCD spectra, then it should be possible to tie the Tholen taxonomy to those spectra by obtaining CCD observations of enough representative ECAS asteroids. On the other hand, the higher resolution of CCD spectra reveals subtle details, such as shallow absorption features (e.g. Vilas *et al.* 1993, Hiroi *et al.* 1996), which cannot be identified in the broadband ECAS

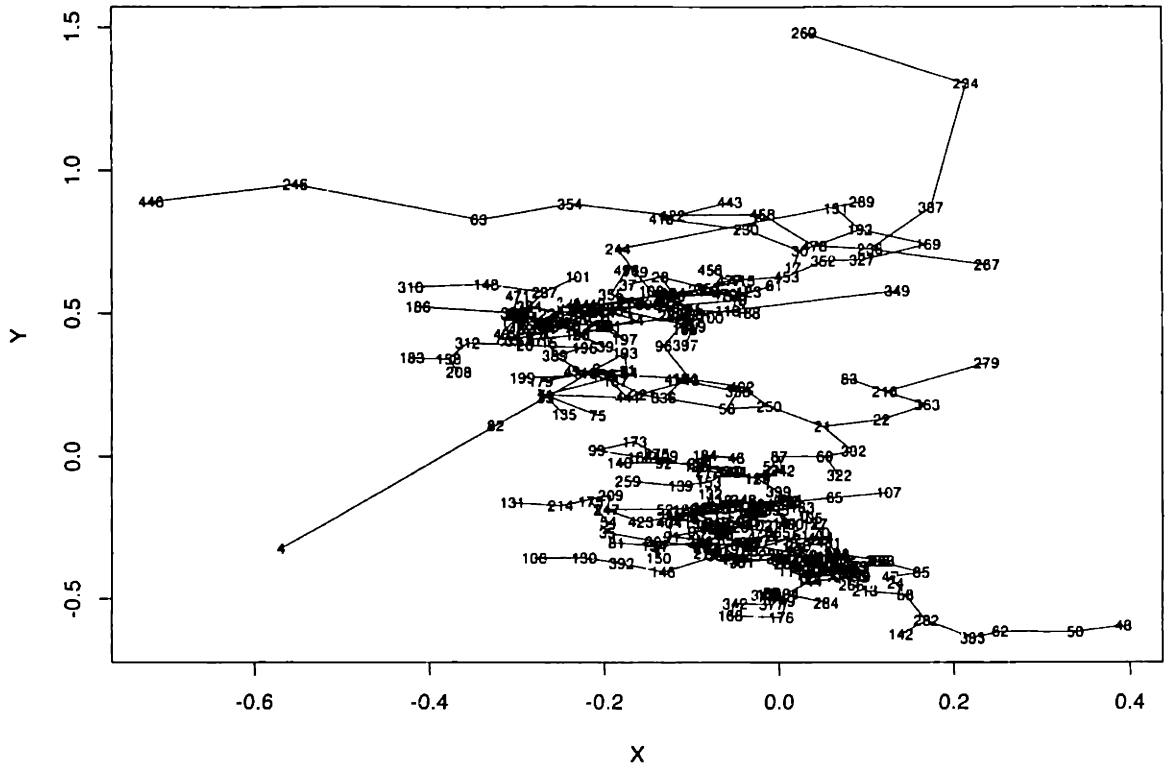

Figure 3.6: Minimum-spanning tree solution based on the 300 lowest numbered asteroids observed during SMASSII (includes up to asteroid number 503). Two distinct clusters are seen: S-types clustering near the middle of this plot, while the C- and X-type asteroids cluster together to the lower-right of center..

measurements. Therefore, we decided it would be more prudent to revise the way asteroids are classified, based on spectral reflectance properties, in a way that takes fuller advantage of the information contained in CCD spectra.

Considerable effort was expended in determining which multivariate technique (or combination of techniques) would be most applicable in defining a classification structure from the SMASSII spectra. The argument made by Tholen in his decision to use the MST algorithm for the ECAS data was based on the fact that the solution for any particular dataset is unique. While the uniqueness of a solution is an important consideration, other similar clustering methods, such as the different variations of hierarchical clustering, may be more appropriate for this analysis, depending on the particular rules used in determining the order that objects (or clusters) are linked. The results from any of these clustering techniques are challenging to represent in two dimensions, and plotting can become very unwieldy when the number of objects being

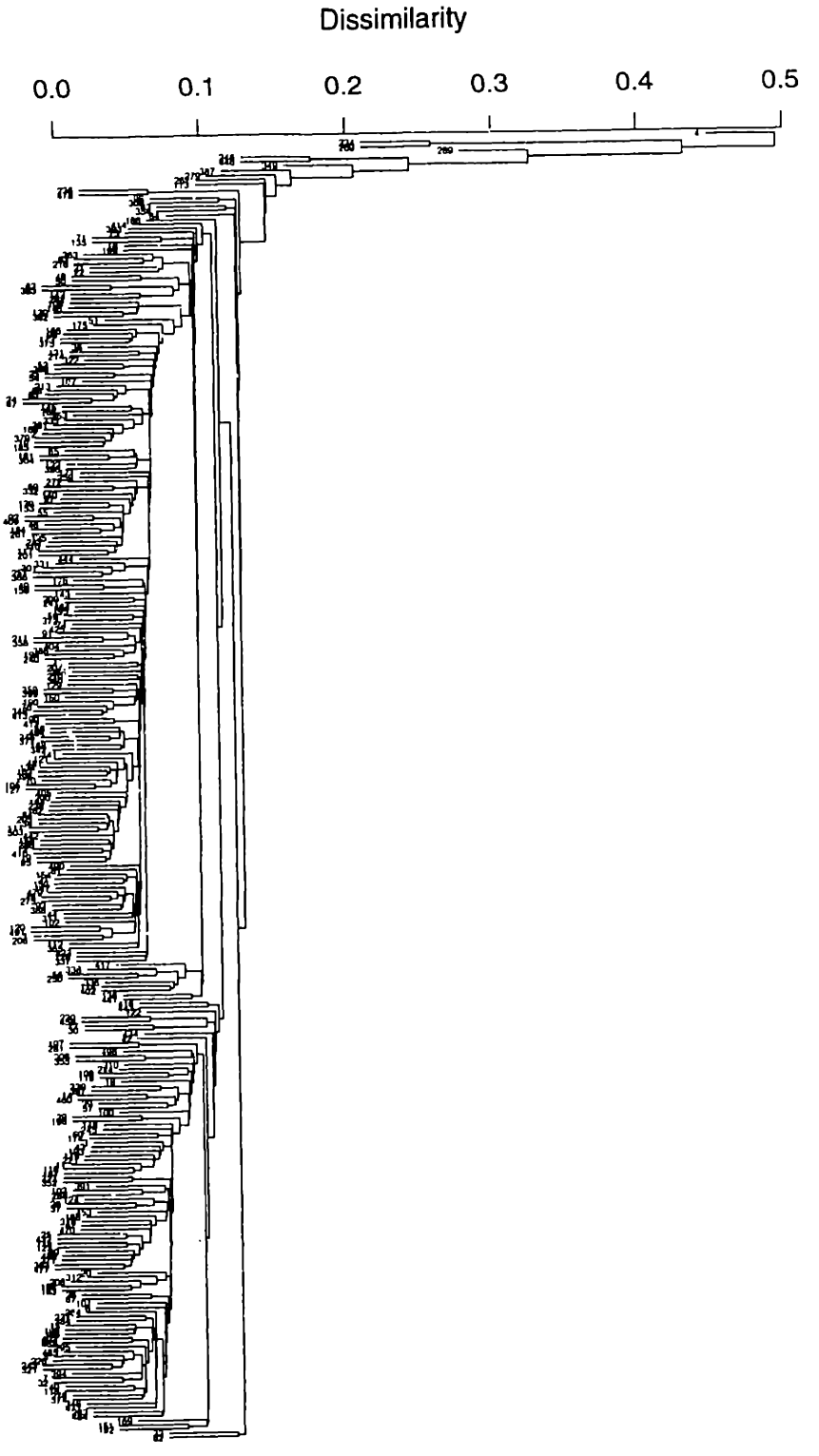

Figure 3.7: Dendrogram showing the hierarchical clustering solution (using the single-linkage algorithm), based on the same set of 300 asteroids as used in creating Figure 3.6.

classified is large. The solution determined from a minimum-spanning tree can be represented in two dimensions using the Friedman-Rafsky algorithm (Venables and Ripley 1994). An example of this is shown in Fig 3.6. By comparison, hierarchical clustering has the advantage that results can be represented in a somewhat more orderly fashion as a dendrogram, as seen in Fig 3.7.

A major disadvantage of using any of the distance techniques in defining a taxonomy is that, while a clustering solution based on a specific dataset and clustering algorithm may be unique, only the large-scale structure of the solution can really be considered robust. In reality, a change in the clustering algorithm used, or more importantly, a small change in the initial dataset (the addition or omission of even just a couple of objects) can result in a very different clustering solution at the level that individual objects are linked together. This is especially true when the characteristics used to differentiate members of a population vary continuously throughout the population, as seems to be the case with the spectral features seen in the SMASSII data. Using a distance algorithm as the sole basis for defining class boundaries among the SMASSII spectra would likely lead to a taxonomy that is subjective, and hard to defend. Instead, we have decided to rely on PCA as the major tool in classifying the SMASSII asteroids. Because PCA maps objects into a complete space, the overall solution is robust, even though the relationship between individual objects, and thus the identification of clusters, cannot be quantified in the same manner as when distance algorithms are used. The fact that PCA is so robust is clearly seen when comparing the similarities in the principal component solution for the ECAS dataset and that for the SMASSII spectra (Figs 3.2 and 3.4, respectively).

3.5 Discussion of the spectral slope and albedo

The average, or overall slope is one of the most fundamental, and more controversial characteristics of an asteroid spectrum. This spectral slope, or color, can range from slightly bluish or neutral, as in the spectrum of the asteroid 2 Pallas, to very red, with 5145 Pholus (Binzel 1992) as an extreme example. In PCA, this average spectral slope is highly correlated with the first principal component, though inspection of the eigenvector that defines this principal component indicates that some fraction of the short-wavelength wing of the 1 μm absorption feature is also represented by PC1. While most of the absorption features found in asteroid spectra can be linked to the presence

of particular minerals, and are thus indicative of the asteroid's composition, the average slopes measured from these spectra are not as easy to interpret. The spectral slope is certainly dependent, to some extent, on the composition of the asteroid. However, there are a number of processes, often collectively referred to as "space weathering", that have been proposed as ways of altering the optical properties of asteroid surfaces. Recent evidence from both laboratory experiments (Moroz 1996) and spacecraft observations (Chapman 1996) suggest that these surface alteration processes can result in an increase, or reddening of the spectral slope, as well as an associated decrease in the relative depths and band areas of the other mineral absorption features contained in the spectrum. Observing asteroids at high phase angles can also result in an artificial increase in the spectral slope, called phase-reddening, though not enough asteroids have been observed over a sufficiently large range of phase angles to fully understand the effect. Added to this are the observational uncertainties, discussed in the Chapter 2 that, to some extent, impact our confidence in the accuracy of the spectral slope measurements. Based on these considerations, we decided to calculate, and remove the average slope from each spectrum in the SMASSII dataset before proceeding with any multivariate analyses. For each spectrum, we found the least-squares fit to the equation:

$$r = 1.0 + \gamma(\lambda - 0.55) \tag{3.3}$$

where r is the relative reflectance at each channel, λ is the wavelength of the channel in microns, and γ is the slope of the fitted line, forced to have the value of unity at 0.55 μm. Dividing each spectrum by this best-fit line resulted in a residual spectrum whose value at 0.55 μm is still 1.00, and whose mean value over all channels is approximately 1. The value of the slope, γ, is recorded as a major spectral parameter, corresponding mostly to the first principal component (PC1), that describes the spectrum. A similar process of removing the background slope, by fitting a straight line over the entire spectrum, was used by Vilas *et al.* (1993) to study weak absorption bands in the reflectance spectra of low albedo asteroids.

After the average slope of each spectrum was fitted and a residual spectrum had been constructed, all of residual spectra were parameterized using PCA. It was anticipated that, by first removing the average spectral slopes, the application of PCA to the residual spectra would be more efficient at separating objects based predominantly

on differences in their spectral absorption features. With the introduction of this newest set of principal components, there is the potential for confusion about which component system is being used in describing the spectral data. To help minimize confusion, we make the following distinctions: Slope, PC2', and PC3' refer to this new set of spectral components, where the slope was independently fitted and removed before PCA was applied, while the variables PC1, PC2, and PC3 refer to the more traditional principal components that were determined initially, based on the unscaled variances of the original spectra, and which are plotted in Figs 3.4 and 3.5. In Appendix A, it is the newer set of spectral components, Slope, PC2', and PC3' that are listed for each SMASSII asteroid.

The spectral components listed in Appendix A are recorded to four decimal places, corresponding to the precision with which these components have been plotted in various figures (such as Figures 3.8 and 3.9). However, these spectral components should be considered accurate to only the second decimal place. As described in Chapter 2, there is an inherent uncertainty (less than ±0.02) in the average spectral slope that arises from the use of a mean extinction model in the calibration process. In addition, sporadic variations in spectral slope (±0.05 or higher) were occasionally noted in successive measurements of the same asteroid obtained under poor sky conditions, though these observations were usually rejected from the final SMASSII dataset. Even under good observing conditions, however, spectra obtained of an asteroid on multiple nights sometimes showed variations that are difficult to explain. While these variations are most noticeable in the average spectral slope, differences are also seen in the shapes and depths of various absorption features within the asteroid spectra.

During the SMASSII survey, 131 different asteroids were observed on multiple nights. This number includes asteroids that were measured on different nights of the same observing run, as well as objects that were reobserved during different runs, with the observations being separated in time by months, or even years. By comparing these multiple observations, it is found that spectra taken on different nights of the same observing run are usually similar in form, with typical variations in the Slope component (for ~80% of the cases) being ±0.03 or less. In those cases where an asteroid was measured during different observing runs, however, the resulting spectra sometimes show greater variations, with differences in the Slope component being typically less than ±0.07 (again, for ~80% of the cases), but in the worst case, is found to be as large

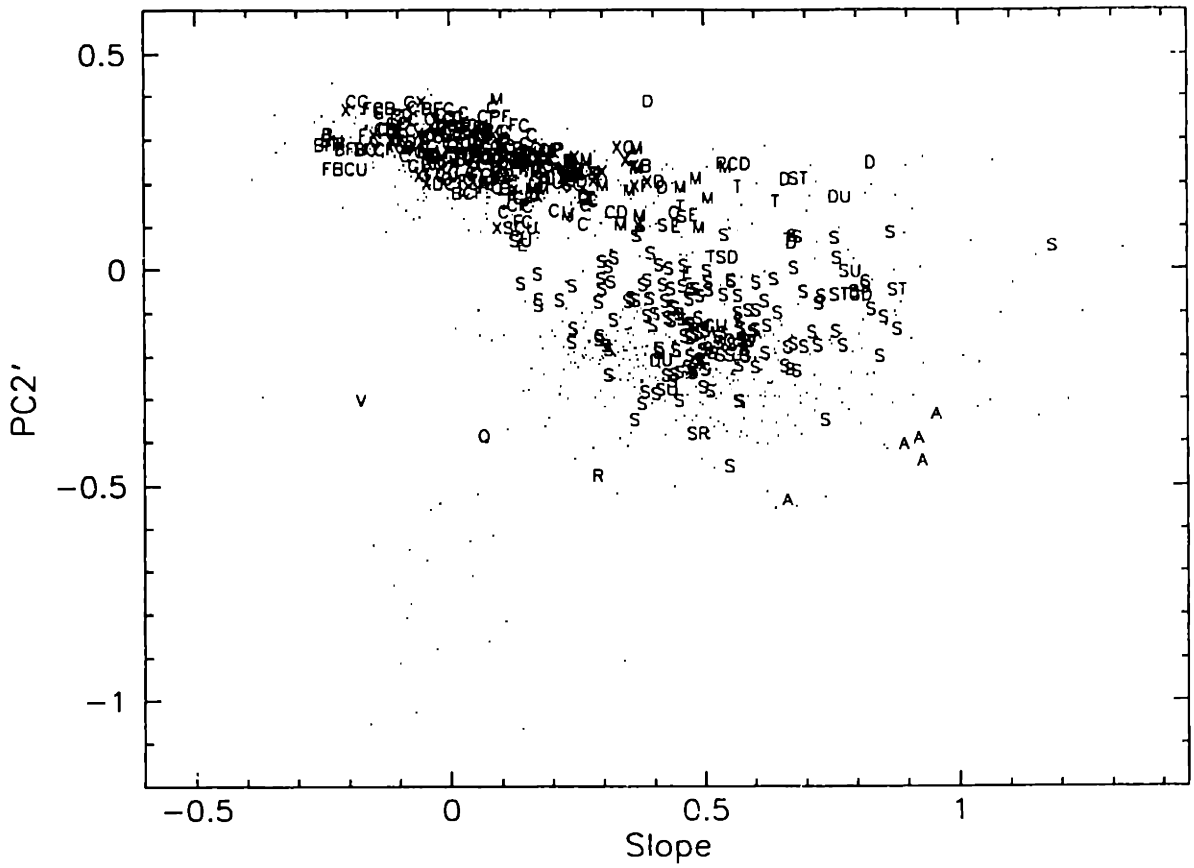

Figure 3.8: Plot of the fir. two spectral components (Slope and PC2') for 1190 SMASSII asteroids. Objects that were observed as part of the Eight Color Asteroid Survey are labeled with their Tholen taxonomic class, while asteroids newly observed during SMASSII are shown as dots.

as ±0.15. Because the run-to-run variations are generally larger than the night-to-night differences, I suggest that compositional heterogeneity (revealed by the asteroid's rotation) is not the primary source for the observed spectral differences. These run-to-run variations might be instrumental in nature, though every attempt was made to minimize differences between observing runs by following the same observing procedures throughout the entire SMASSII survey. It is also possible that these variations arise from differences in observing geometry, such as phase-angle effects (phase-reddening, e.g. Miner and Young 1976) or temperature-related variations in spectral properties that occur with changes in the asteroid's neliocentric distance (Lucey and Keil 1998, Lucey *et al.* 1998). While the photometric precision of the SMASSII observations is typically high, and by itself, would lead to relatively small formal uncertainties in the calculated spectral components (less than ±0.01), the variations in

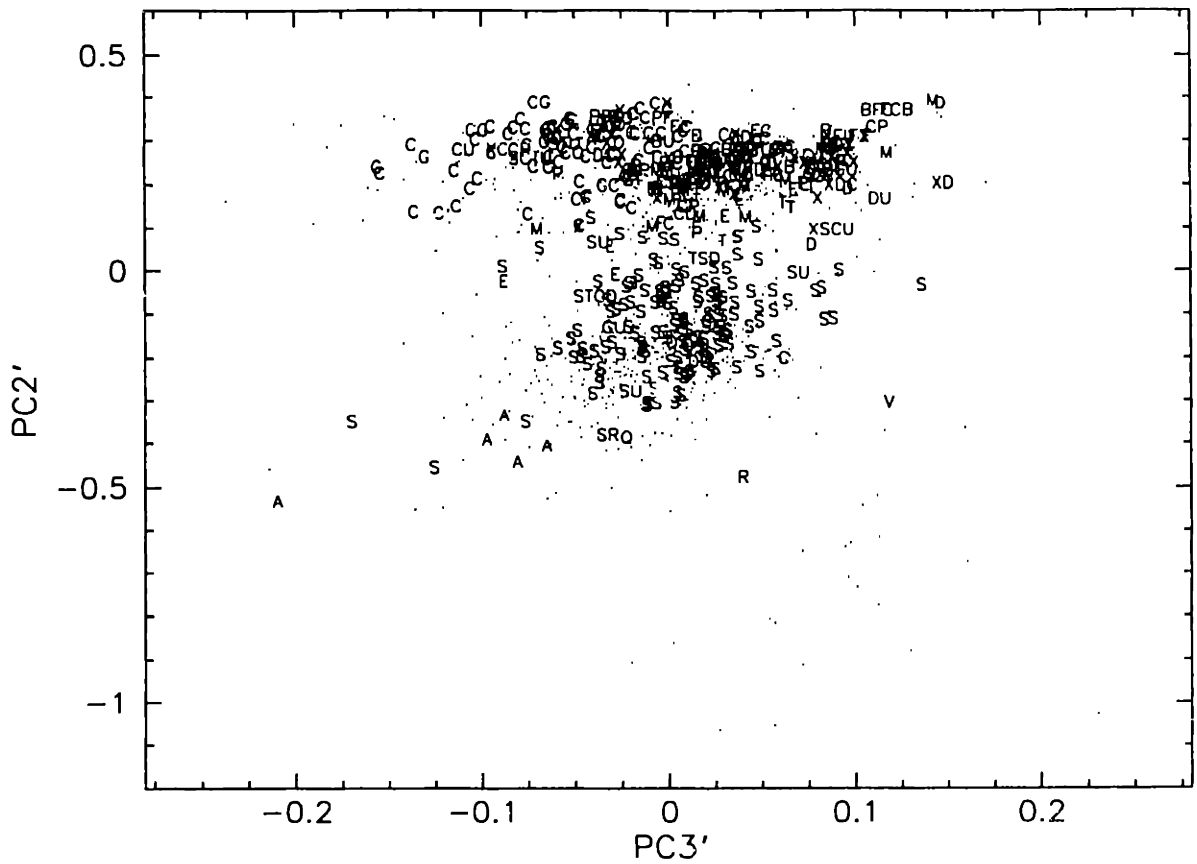

Figure 3.9: Same as in Fig. 3.8, except showing the spectral component plane defined by components PC3' and PC2'. Compare the structure seen in this plot with that of Fig. 3.5.

spectral properties that have been observed for some asteroids at different epochs lead to larger estimated uncertainties in the spectral components listed in Appendix A. Based on the repeatability of spectra in our final analysis, we estimate the 1σ uncertainty in Slope to be ±0.05, while the uncertainty in PC2' is ±0.025 and the uncertainty in PC3' is ±0.02 for any asteroid that was observed only during one observing run.

The 3-D parameter space defined by Slope, PC2', and PC3' is best examined along the two planes shown in Figures 3.8 and 3.9. Except for an apparent clockwise rotation in the plane, the overall appearance and relative locations of the spectral groups seen in Fig 3.8 are very similar to those found in Fig 3.4. However, plotting PC3' against PC2' (Fig 3.9) reveals significantly more structure in the data than is seen in the comparable plot of PC3 vs. PC2 (Fig 3.5). A direct comparison of the two principal component systems is shown in Fig. 3.10, where corresponding components from the

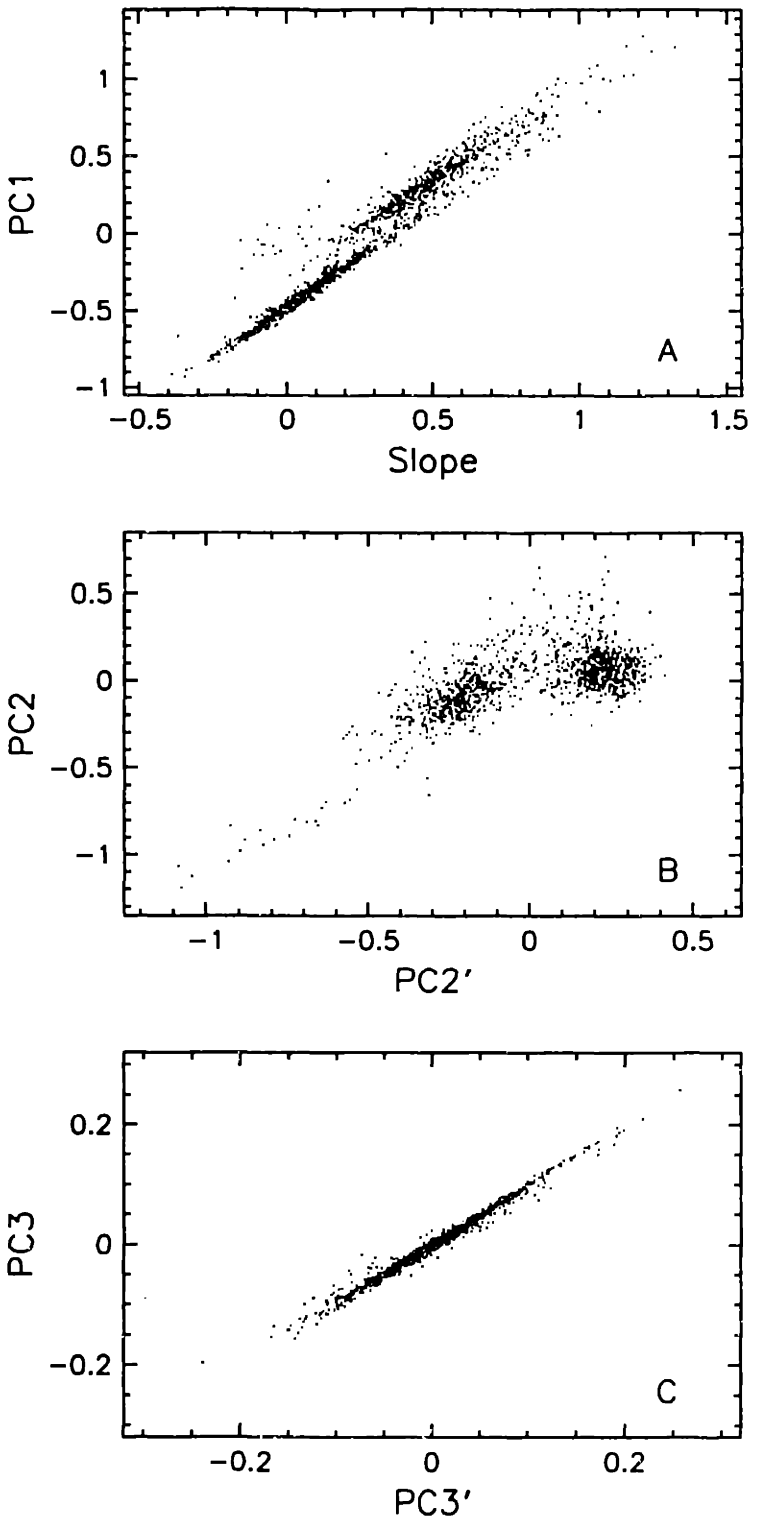

Figure 3.10: Comparison of the first three spectral components (Slope, PC2', and PC3') with the corresponding principal components (PC1, PC2, and PC3).

Table 3.4: Percentage of variance accounted for by spectral components

Component	ECAS (Tholen 1984)	SMASSI (Xu *et al.* 1995)	SMASSII (normal PCA)	SMASSII (fitted slope)
PC1	67.7%	58.7%	53.3%	45.6% (slope)
PC2	26.8%	28.6%	24.4%	31.3% (PC2')
PC3	2.6%	7.4%	6.7%	7.0% (PC3')
PC4	1.7%	3.7%	3.7%	3.7% (PC4')
Total:	98.8%	98.4%	88.1%	87.6%

two systems are plotted against each other. Frame B of this figure shows that the difference between components PC2' and PC2 is particularly large, suggesting that the increased structure revealed in Fig. 3.9 is primarily a result of the spectral detail that is preserved in component PC2'. Another way of comparing these different sets of parameters is to determine what percentage of the variance in the original spectral data is accounted for by each of the principal (or spectral) components. In Table 3.4, the percentages for the first four components from each system are listed, with the results from the ECAS principal component solution (Tholen 1984) and that of SMASSI (Xu *et al.* 1995) being included for comparison. As expected, the percentage of the total variance accounted for by the Slope parameter is noticeably less than the maximum possible that is accounted for by component PC1. What is interesting is that this difference in the percentage between the Slope component and PC1 is almost entirely accounted for by next spectral component, PC2'. It is also important to note that the total variance accounted for by the first four components describing the SMASSII data is substantially less than that accounted for by the first four components describing either the ECAS or SMASSI datasets (88%, as compared to 98%). This can be attributed to the significantly larger size of the SMASSII dataset, and to the correspondingly greater trend towards a continuum in the variation of spectral features.

Another characteristic describing how an asteroid's surface reflects sunlight is its albedo. Ever since the early-1970s, when photopolarimetric and radiometric albedo measurements first became available (e.g. Zellner 1973, Morrison 1974), these measurements have been included as a major component in the classification schemes of asteroids. In the Tholen taxonomy, spectral classes were initially identified using the

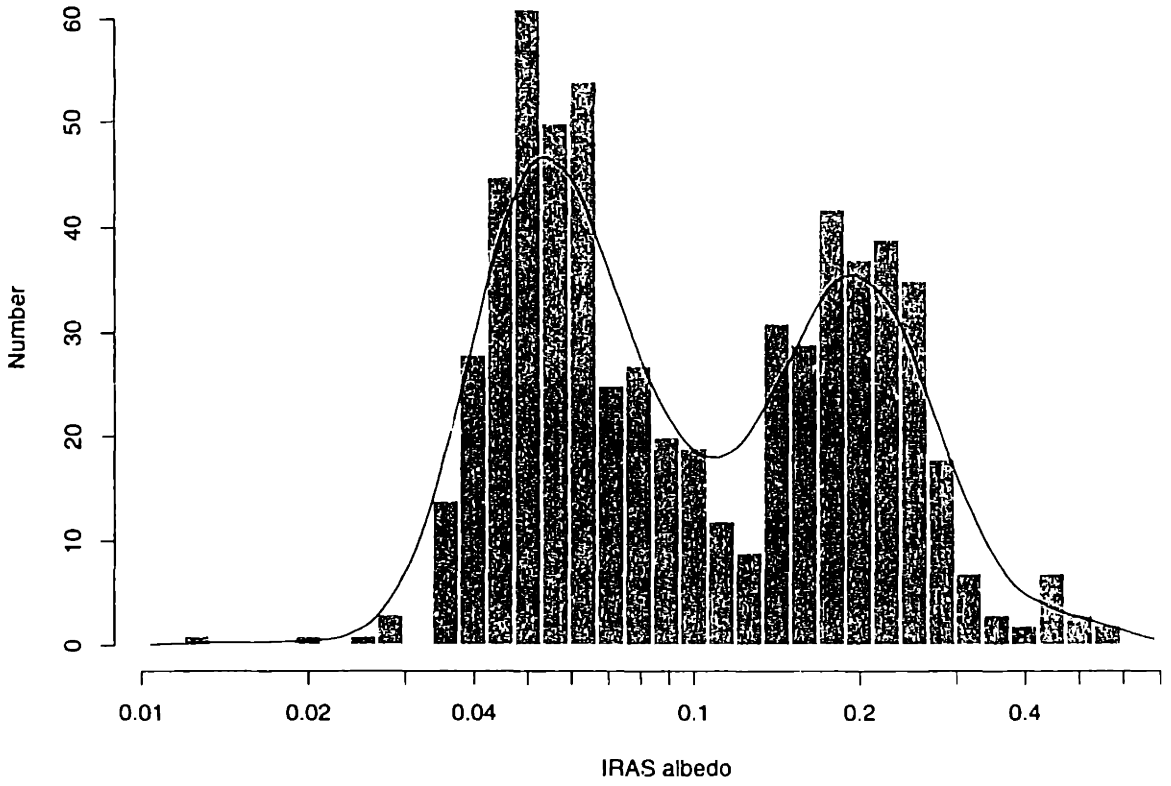

Figure 3.11: Histogram of IRAS albedos for 625 asteroids that were also observed as part of SMASSII. The overplotted curve shows the frequency estimate resulting from an average shifted histogram. The saddle point separating the two modes of the distribution occurs at an albedo of approximately 0.11.

ECAS broad-band colors, but albedos were subsequently used to subdivide the spectrally degenerate X-class into the low-, medium-, and high-albedo P-, M-, and E-types. Albedos were also used to test the significance of other class divisions, such as the B- and F-types. Introduction of the IRAS asteroid measurements prompted Tedesco *et al.* (1989) and Barucci *et al.* (1987) to include the IRAS albedo as a principal characteristic when defining their taxonomic classes.

A gross relationship between albedo and spectral features has long been recognized, and can be clearly seen in Figs. 3.11 and 3.12, where the 625 SMASSII asteroids that also have IRAS albedo measurements have been plotted. Even with this relationship, however, the classification of asteroids based on measurements of albedo should be done with hesitation, especially when that classification ultimately leads to interpretations about the bulk composition of asteroids. An important example of the

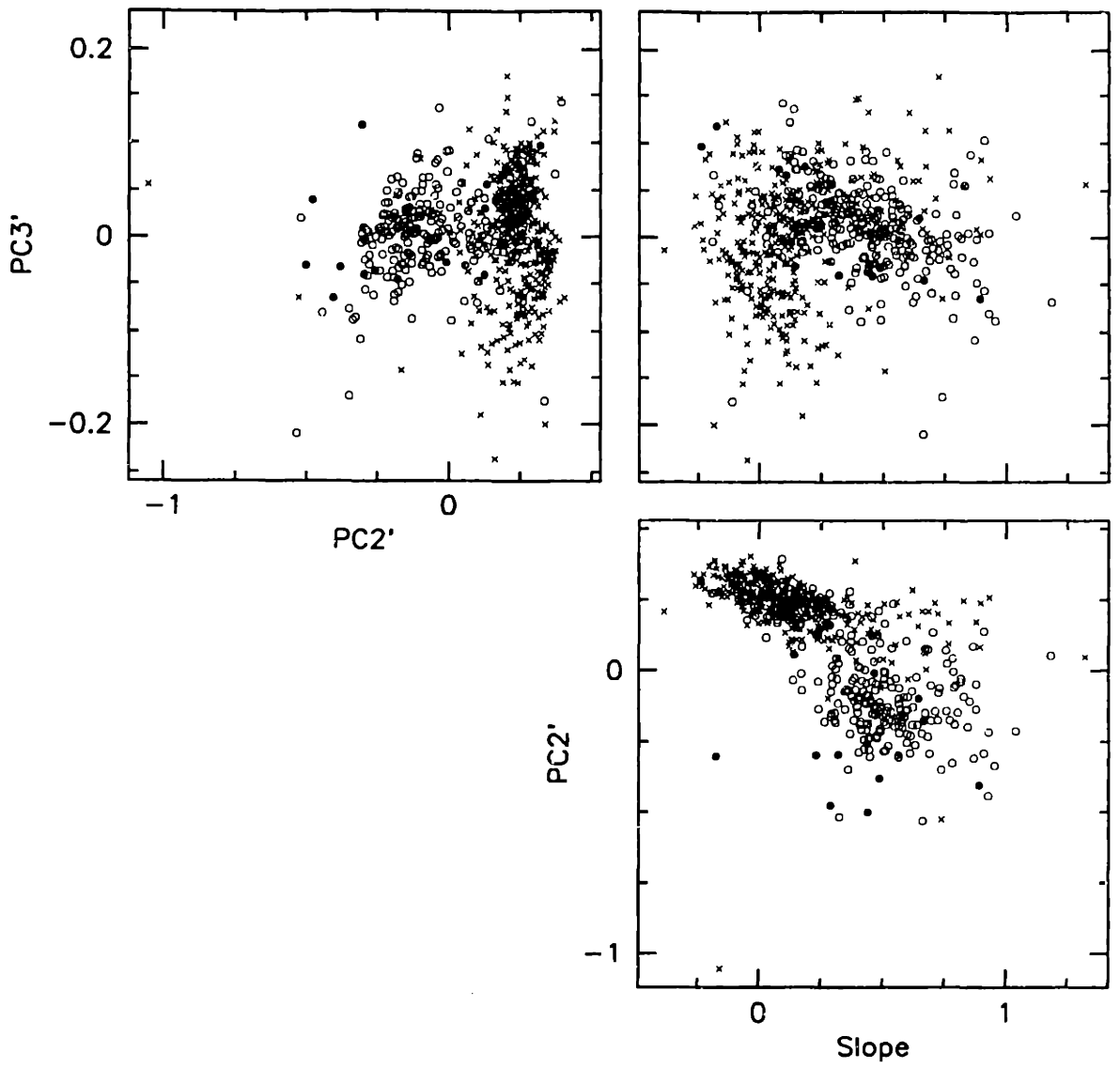

Figure 3.12: The three primary planes of spectral component space. Plotted are the 625 SMASSII asteroids for which IRAS albedos are available. Those asteroids for which the IRAS albedo is less than 0.11 are shown as Xs. Asteroids with albedos ≥ 0.11 and < 0.3 are plotted as open circles. Filled circles represent those asteroids with albedos ≥ 0.3. The separation between low- and high-albedo asteroids is most correlated with component PC2'.

contradictions that arise, due to interpretations based on albedo, is found within Tholen's M-class, which includes asteroids with moderately high albedos, ranging from 0.1 to 0.3. Based primarily on measurements of their albedo, members of this class have long been presumed to have a metallic NiFe composition, and to be the source bodies for iron meteorites. However, polarimetric (Lupishko and Belskaya 1989), radar (Ostro *et al.*

1985), and near-IR (Jones *et al.* 1990, Rivkin *et al.* 1995) observations of M-types have shown several of these asteroids to have properties that are inconsistent with a metallic iron composition. As with the spectral slope, an asteroid's albedo might be modified by space weathering processes. In the laboratory, simulations of repeated shock melting and recrystallization have been shown to darken both meteorite samples, and selected minerals that are thought to be common on asteroid surfaces. This reduction in reflectivity is most evident in silicate minerals, and is often seen in conjunction with an increase, or reddening of the spectral slope (Moroz 1996). Along with true compositional differences between asteroids, surface alteration processes might help explain the wide range of albedos measured in some spectral classes.

3.6 Fundamentals of developing a feature-based taxonomy

The decision to reexamine (and revise) the structure of asteroid taxonomy was made very cautiously. When the SMASSII survey was initiated, we had no intention of changing the way asteroids are classified. The taxonomic system developed by Tholen has been in use for over a decade, and is generally well accepted by the asteroid science community. It was only as the analysis of the SMASSII data progressed that it became apparent just how difficult it would be to reconcile the SMASSII spectral results with the Tholen taxonomy. While it would have been possible to force the SMASSII data to fit within the general structure of this taxonomy, doing so would have been a disservice to the information contained in the SMASSII spectra, and to asteroid science in general by propagating a classification system that will eventually have to evolve to meet the needs of the higher-resolution asteroid spectroscopy available today.

Before proceeding with the definition of a new asteroid taxonomy, it is important to define a set of goals, or fundamentals, that can direct how the classification is carried out, and how the taxonomy should be structured. Because we do not yet know the true underlying composition or surface properties of individual asteroids, the taxonomy we develop will necessarily be artificial, and will thus be open to considerable debate. However, by providing these fundamental guidelines, it is hoped that the reasoning behind certain decisions (which, at times, are subjective) might be clearer. Some of the points listed here were raised in the previous discussions, but because of their importance, they are repeated here.

• This new classification system should be built on the robust structure of the Tholen taxonomy. Our goal is to maintain the overall structure, and spirit of the present asteroid taxonomy that has evolved over time through the works of Tholen and others. The commonly used definitions of the primary asteroid classes should be maintained in order to help preserve continuity between past and future research efforts.

• This new classification system should be based only on spectral (absorption) features. Spectral features provide the best indicator of an asteroid's underlying composition. For this purpose, the average slope of the spectrum is considered a spectral feature, though its importance should be carefully weighed against that of the other absorption features contained in the spectrum. Albedo is not included in this classification system, because its diagnostic power is not as great as that of spectral features. Rather, albedo should be considered as a separate, quantitative parameter in conjunction with the spectral class. Whatever their cause (compositional heterogeneity, phase effects, temperature effects, etc.), some degree of variation in the features (including slope) of an asteroid's spectrum should be expected over time.

• This new classification system must account for the apparent continuum between spectral classes. While the primary concentrations of C- and S-type asteroids are well defined in principal component space, the regions surrounding them, and the boundaries separating minor spectral classes are growing more vague as the number of objects is increased (and as the average size of the asteroids observed decreases). The taxonomy should be structured in a way that reflects the fact that boundaries between classes are not distinct. Tholen identified several spectral endmembers, such as the A-, B-, D-, Q-, and R-types, which continue to define the limits of spectral variation. However, as significantly smaller asteroids are measured, especially among the NEAs, unusual spectral types are likely to emerge, and so any classification system must not only be flexible in allowing for the continuum between the known classes, but it must be expandable to accommodate future outliers.

• The scale length for taxonomic classes should be comparable to the spectral variance seen in many of the dynamical families. For the asteroid families we have sampled, we generally find the members of any particular family to be spectrally similar. The range of spectral variance that is observed within these families can be used as a guide in judging the average extent of the taxonomic classes. In some cases, a

particular dynamical family is used to define a specific spectral class (for example, the V-types are defined by the Vesta family, while the K-types are defined by the Eos family). This strategy provides for an optimum number of spectral classes. This number of classes needs to be great enough to make efficient use of the information contained in the spectra, but should not be so numerous that the classification system promotes overinterpretation of the results.

• This new classification system should be defined based on an intelligent use of multivariate analysis techniques. Whatever techniques are chosen, they should be used as tools, in combination with other numerical methods, and should involve some level of intervention by the "human neural net". The information contained in an asteroid spectrum is complex. Not all features in the spectrum can (or should) be weighed equally, nor can any one numerical technique properly parameterize all of the information contained in each of the various spectral features. Thus, visual inspection of the data, and the ability to make human judgments about the classification of objects, based on specific rules, must be allowed. While this implies a certain level of subjectivity, it protects against having to blindly accept the results of clustering techniques that may not be sensitive to subtle details in the spectra. Ultimately, the classification system might be best refined using a supervised, regression algorithm, such as an artificial neural network (Howell *et al.* 1994). To properly apply such an algorithm, though, the initial classification scheme should first be well established.

• This classification system is based only on visible wavelength spectra. For observations of asteroids at different wavelengths (UV, near-IR, etc.), similar, parallel classification systems should be developed such that the characteristics of any asteroid can be judged on the merits of each type of observation, rather than attempting to consolidate all of our knowledge into a single letter designation. Ultimately, this may lead to a hierarchical structure of asteroid classification.

• Once defined, this new classification scheme should be easily usable and applicable by others. The visual inspection of a CCD spectrum, to identify the presence of pertinent features, and a straightforward quantitative comparison of relative reflectances with those defining a taxonomic class, should be all that is needed to assign an asteroid to that class.

Chapter 4

Derivation of a Feature-based Asteroid Taxonomy

The development of this feature-based taxonomy takes advantage of several strengths inherent in the SMASSII observations. The most significant aspect of the SMASSII survey is its size. The spectra of 1190 individual asteroids are included in this investigation, nearly three times the number that was used by Tholen in the formulation of his taxonomy (405 asteroids with high quality spectrophotometry, Tholen 1984). This total of 1190 objects arises from the 1189 asteroids discussed in Chapter 2 (and presented in both Appendices A and B, all having perihelion distances of $q > 1.3$ AU), plus the Earth-crossing asteroid 1862 Apollo, which is included as a taxonomic benchmark for the Q-class. While there are 74 other near-Earth asteroids that were observed during the SMASSII survey, apart from 1862 Apollo and its historical definition of the Q-class, the taxonomy developed here is based only on those asteroids having perihelion distances greater than 1.3 AU. The rationale for this is primarily based on our interest in revealing the maximum spectral diversity within the main belt as it pertains to the study of asteroid families. Because of their small sizes, and likely younger surfaces, NEAs tend to have an even broader diversity of spectral characteristics that could skew this taxonomy away from its primary emphasis. The near-Earth objects observed during SMASSII are being treated in a separate study by Binzel *et al.* (1999b).

Another important aspect of the SMASSII data is its internal consistency. By closely following the same observing strategy and data reduction procedures throughout the SMASSII survey, we have tried to limit the number of variables that might affect the final spectra. This leaves the primary source of uncertainty in our results to be those factors that were, for the most part, outside of our control, such as an asteroid's apparent

brightness, or variations in sky conditions at the time of the observations. In general, as fainter objects are observed, or if the sky conditions are less than perfect, a decrease in the overall signal-to-noise of the resulting spectrum should be expected. Under certain conditions, however, systematic features (or artifacts) also appear in these spectra, usually resulting from the incomplete subtraction of telluric sky lines (as described in Chapter 2). A serious attempt has been made to identify and remove any artifacts from the final spectra, but residual traces of these features may still be present. Special care was taken to ensure that the presence of such artifacts did not influence the development of this taxonomy, nor the scientific interpretation of the spectra (Chapter 5).

The primary limitations of the SMASSII survey are associated with its relatively narrow wavelength coverage (0.44 to 0.92 μm). While the high spectral resolution of the SMASSII data provides a detailed mapping of several different absorption features regularly found in asteroid spectra, this wavelength interval is not usually considered sufficient to provide meaningful interpretations of the underlying mineralogy. The most diagnostic absorption features readily identified in asteroid spectra are those of silicates, with two major bands being located between 0.7 and 2.5 μm (with band centers near 1 and 2 μm, Cloutis *et al.* 1986). With the addition of observations in the near-infrared (e.g. 52-color, Bell *et al.* 1988, and SMASSIR, Burbine *et al.* 1997), a quantitative analysis of these silicate bands is possible (Gaffey *et al.* 1993a, Sunshine and Pieters 1993), and can lead to the relatively unambiguous identification of olivines ($(Mg,Fe)_2SiO_4$), orthopyroxenes ($(Mg,Fe)SiO_3$), and/or clinopyroxenes ($(Ca,Mg,Fe)_2Si_2O_6$) on asteroid surfaces. However, since this new feature-based taxonomy is not dependent on considerations of mineralogy or cosmochemistry, this limitation in wavelength coverage does not affect our classification results. Accordingly, I will not dwell on details of mineralogy in the discussions of taxonomy that follow, nor will I attempt to be complete in reviewing all previous works on asteroid compositions, their thermal histories, or on the comparisons between asteroids and meteorites. Instead, thorough reviews of these topics can be found in the literature (Gaffey *et al.* 1989, Gaffey *et al.* 1993b, Pieters and McFadden 1994).

In trying to preserve the general taxonomic structure for asteroids that has evolved since the early works of Chapman *et al.* (1975) and Bowell *et al.* (1978), and which was refined by Tholen (1984), we adopt the well-defined separation between C- and S-type

asteroids, as well as the somewhat vague division that separates the C- and X-types in forming the basis of our taxonomy. We also retain many endmember classes that have been previously recognized, such as the B-, D-, A-, R-, and Q-types, which help define the nominal range of variation observed among asteroid spectra. The primary difference in comparing our feature-based taxonomy with the Tholen taxonomy is how intermediate classes are defined. Tholen concatenated different class designations (letters) to describe those ECAS asteroids lying near the boundaries separating distinct spectral classes. In contrast, we try to reinforce the idea of a continuum between asteroid types by increasing the total number of classes, so that the typical scale length in parameter space of these classes is consistent with the variance in spectral properties observed in most of the dynamical families that we have sampled. The use of asteroid families to provide a scale length is based on the assumption that families are collisional in origin, and that members of each family are composed of inherently similar material. Because we do not rely on any one quantitative method to define all of the spectral classes, there is no simple means for distinguishing those objects that lie near the boundaries separating classes from those near the center of a class. For now, we accept the fact that there will be some level of uncertainty in the taxonomic classification of asteroids, especially for those objects that may straddle class boundaries.

4.1 Overview of the classification process

In the following six sections I describe the philosophy, as well as the specific techniques, used in establishing the SMASSII taxonomic system. In particular, many decisions were made affecting the resulting taxonomy that need to be explained and defended. A general discussion in section 4.7 describes the application of this taxonomy to future datasets in terms of quantifiable spectral features and characteristics.

The approach used in defining our taxonomic classes is divisive; that is, the process begins by considering the entire set of SMASSII asteroids as a single cluster. At each step in the classification process, this cluster is subdivided into an increasing number of smaller clusters, with the boundaries between these groups being defined by the presence or absence of specific features in the asteroid spectrum, or by the parameterization of particular spectral characteristics. This is the basis for describing this work as a feature-based taxonomy. At first, boundaries are drawn that divide the entire population into the most basic associations: the classical C-, S-, and X-types.

These associations, or "complexes", are very large, and each, in turn, is subdivided to form the final taxonomic classes. As asteroids are assigned to these final classes, they are excluded from further consideration in the classification process. A brief summary of the steps making up this decision tree is given here, with a thorough discussion of the classification process following in subsequent sections.

The first decisions made in this classification process dealt with initial parameterization of the entire SMASSII dataset. This included the calculation of average spectral slopes, and construction of the residual spectra, as well as the decision to use PCA as the primary parameterization tool. Each of these preliminary procedures were discussed in detail in Chapter 3. Once the SMASSII data were represented in the spectral component space of Slope, PC2', and PC3', the next major step involved identifying the three primary spectral domains (the C-complex, the S-complex and the X-complex), defining the boundaries that separate these complexes, and identifying those outlying asteroid types that should not be included in any one of the three complexes. While seemingly straightforward, this step is undoubtedly the most critical in determining how the final taxonomy is structured. Defining the exact boundaries between the major complexes was necessarily subjective, but relied as much as possible on the previous classification results of Tholen (1984), Barucci *et al.* (1987) and Howell *et al.* (1994).

In the next step, those asteroids not included in the three major complexes were assigned to one of five final taxonomic classes. For the most part, this involved using the existing definitions for the D-, T-, O-, and V-classes, although a new Ld-class was introduced to describe a spectral type that had not been well observed, or noted as being significantly different, prior to the SMASSII survey.

This was followed by a rather long, though straightforward treatment of the S-complex. First, five classes that make up the periphery of the S-complex were defined. This included the well-established A-, Q-, and R-classes, the K-class that was first proposed by Bell (1988) based on observations of asteroids in the Eos family, and finally, a new L-class that we have introduced to represent a spectral type that was previously noted as being unusual (Burbine *et al.* 1992), but which had not been separately classified. The assignment of asteroids to these five classes relied heavily on the visual identification of certain spectral features: specifically the unusual widths and shapes of both the reflectance maximum near 0.7 μm and the short-wavelength end of

the 1 μm absorption band. After the A-, K-, L-, Q-, and R-types had been identified and removed from consideration, the remaining members of the S-complex were subdivided analytically. This involved first calculating the mean of all remaining S-complex asteroids using the original spectra, as well as finding the mean spectrum for each of the A-, K-, L-, Q-, and R-classes. Based on their dissimilarity with respect to each of these mean spectra, the remaining S-complex asteroids were assigned to one of six classes: the S-, Sa-, Sk-, Sl-, Sq-, and Sr-types.

The next steps in the decision tree involved subdividing the C-complex. First, the spectral component plane of PC2' versus PC3' was used to identify those members of the C-complex whose spectra either contain a broad 0.7 μm absorption feature (identified as Ch-types) or exhibit an excessive UV reflectance drop-off (classified as Cg-types). The class designation of Cgh was reserved for those objects showing both a 0.7 μm feature and a strong UV absorption. After the Cg-, Ch-, and Cgh-types were removed from consideration, the remaining asteroids in the C-complex were subdivided into the C-, B-, and Cb-classes, based on a combination of spectral slope, and the presence or absence of a slight to moderate UV reflectance drop-off.

The final steps used in defining this taxonomy were reserved for the X-complex. The X-types, as defined by Tholen, were considered spectrally featureless, and were only separable into the E-, M-, and P-classes when albedo measurements were included. Based on the SMASSII observations, we find that many members of the X-complex are not totally featureless, and that subtle differences in the spectra are sufficient to subdivide this group. The first step is to identify those members of the X-complex whose spectra contain a unique set of features, similar to those seen in the spectrum of 64 Angelina and which are described in detail below, and to assign these asteroids to the Xe-class. The remaining members of the X-complex are then subdivided into three additional classes. The first of these classes, the X-class (also referred to as "X-types", not to be confused with the X-complex) is reserved for those asteroids whose spectra are relatively linear (featureless), except for the occasional presence of two minor absorption features: a small, curved UV drop-off shortward of 0.50 μm, and a shallow absorption feature centered near 0.9 μm. The Xc- and Xk-types are distinguished from members of the X-class by a distinct bend in their spectra around 0.7 μm (a decrease in spectral slope longward of 0.7 μm), and are separated based on their average spectral slope, with the Xk-types being redder than the Xc-types.

4.2 Separation of the three spectral complexes

As was demonstrated several times in Chapter 3, the use of multivariate analysis to represent the diversity of asteroid spectra regularly results in the identification of two distinct groupings. This bimodal distribution in reflectance properties has long been known from measurements of both broad-band colors (Chapman *et al.* 1971) and albedos (Zellner 1973, Morrison 1974), and led to the initial taxonomic assignments for C- and S-type asteroids. With the introduction of narrow-band spectrophotometry, and now CCD spectroscopy, our understanding of the spectral reflectance characteristics that underlie this bimodal distribution is becoming more refined. Over the visible wavelength interval from 0.4 to 1.0 μm, the spectra of "S-type" asteroids are generally described as having a moderate to strong UV slope shortward of 0.7 μm and range from being flat to having a deep silicate absorption feature longward of 0.7 μm (the minimum of that absorption band being centered at roughly 1 μm). By comparison, the "C-type" asteroids have spectra that tend to be more neutral in color, and have absorption features that are relatively shallow, if present at all. Because the spectral properties of these two asteroid types are sufficiently different, and because these two types dominate the observed asteroid population, they are represented as two distinctly separate concentrations in spectral component space.

Introduction of the E- and M-classes by Bowell *et al.* (1978) provided the basis for a third major spectral grouping of asteroids that, today, are generically referred to as X-types (Tholen 1984). These asteroids have spectra that range from slightly to moderately red in color, and any absorption features that may be present are usually very subtle. In spectral component space, the X-types plot approximately between the C- and S-types. However, while the division between the X- and S-types is well defined in this component space, a natural boundary separating the C- and X-type asteroids is essentially nonexistent. The difficulty in separating the C- and X-types occurs because there is no significant variation in the number density of objects along the line connecting these two groups in component space. The transition between C's and X's, based primarily on the gradual increase in the average spectral slope, appears to be truly continuous, and makes any clear definition of the boundary separating these two groups problematic.

I have adopted these classical definitions for S-, C-, and X-types as the foundation of this feature-based taxonomy. The number of SMASSII asteroids contained in each of these groups is quite large, and correspondingly, the spectral variance among the members of each group is large. These three major groupings, from here on referred to as "complexes", are not, in themselves, the final product of this taxonomy, but rather define the basis on which further divisions in the classification process are made. Because of this, however, the separation of these three complexes is a critical step in the development of this taxonomy. Thanks to the intermediate location of the X-complex bridging the gap between the C- and S-complexes in spectral component space, the approach used in defining the boundaries dividing these three complexes is actually straightforward. The primary question that needed to be addressed is "What is the extent of the X-types (and thus, of the X-complex)?". By defining, at this point in the process, what spectral properties constituted membership in the X-complex, the memberships of both the S- and C-complexes would also, as a result, be determined. To ensure a good level of consistency with earlier taxonomies, we relied on those asteroids observed during the SMASSII survey that had been previously classified by Tholen (1984), Barucci *et al.* (1987) or Howell *et al.* (1994). In particular, there are 98 SMASSII asteroids that were at least partially identified as X-types in one or more of these previous taxonomies (this includes any asteroid for which the class assignment of X, E, M, or P was used as either a single, or in a multiple designation). Based on these asteroids, we determined those spectral characteristics that are most consistent with X-types (described in detail in a following section), and identified all of the SMASSII asteroids that share those particular characteristics. By establishing this range for the X-complex, boundaries were automatically drawn that separate the C-, X-, and S-complexes.

These boundaries separating the C-, X-, and S-complexes can be approximated as planar surfaces in the 3-dimensional spectral component space. In Figure 4.1, the three primary planes representing this space have been plotted (showing all pairwise combinations of the components Slope, PC2', and PC3'). All 1190 asteroids are shown, and lines have been added to each plot to represent the two surfaces dividing the spectral complexes, as projected onto these primary component planes. These plots are then repeated in Figure 4.2, where the boundaries have been reproduced for reference, but only members of the S-complex have been replotted. It is clear from this

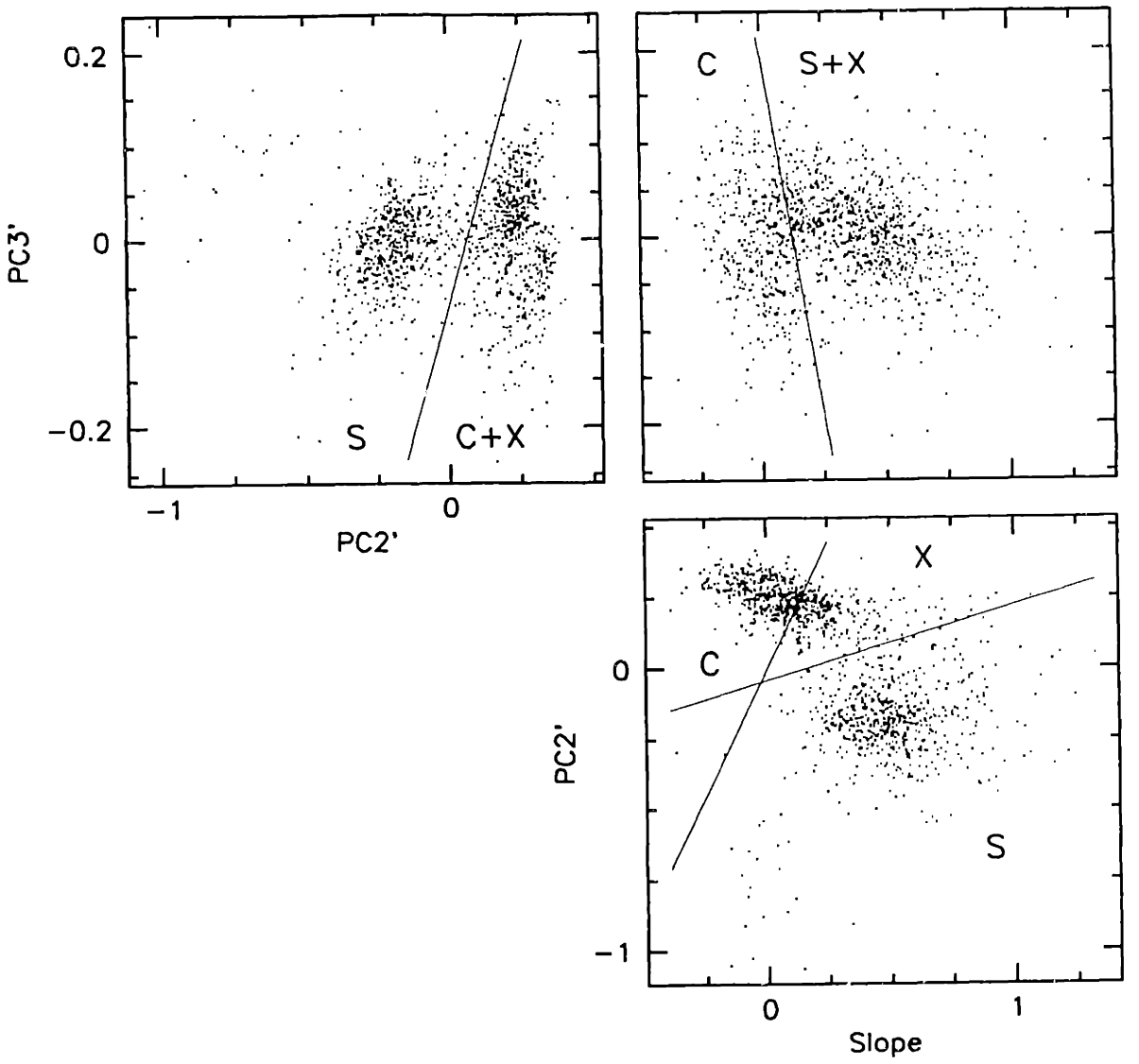

Figure 4.1: The three principal planes of spectral component space. Plotted are all 1190 asteroids used in defining this feature-based taxonomy. The lines drawn on each plot represent the approximate boundaries separating the C-, X-, and S-complexes.

figure that the lines shown do not represent solid boundaries separating the spectral complexes, but are rather to be used as guides. The three spectral components plotted here can account for a majority of the variance due to features in the asteroid spectra, but not all of it. For asteroids making up the S-complex, the first three spectral components mainly account for the slope of the spectrum, and the shape and depth of the 1 μm silicate band. Higher order variations in these spectra simply contribute to scatter in the location of points in this space. This is a limitation of PCA, and must be

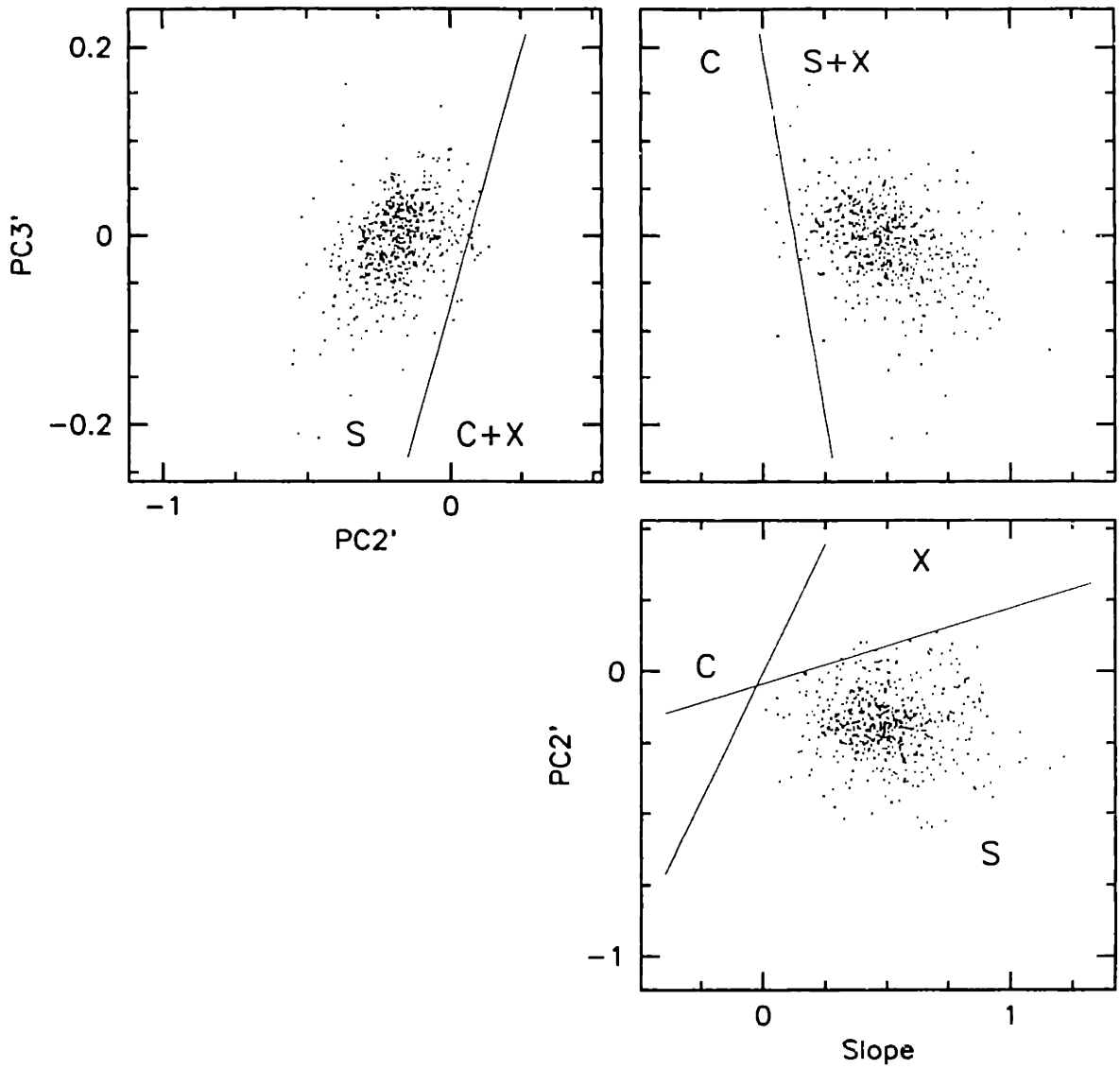

Figure 4.2: Same as Figure 4.1, but showing only the 553 SMASSII asteroids belonging to the S-complex.

acknowledged throughout the classification process discussed below. It is important, therefore, that any asteroid lying near a boundary is individually inspected, and that an intelligent decision is made as to which complex (or taxonomic class) it should belong. Rules for reaching such decisions are discussed in section 4.7.1. In Figures 4.3 and 4.4, similar representations are shown for the C-complex and the X-complex, respectively.

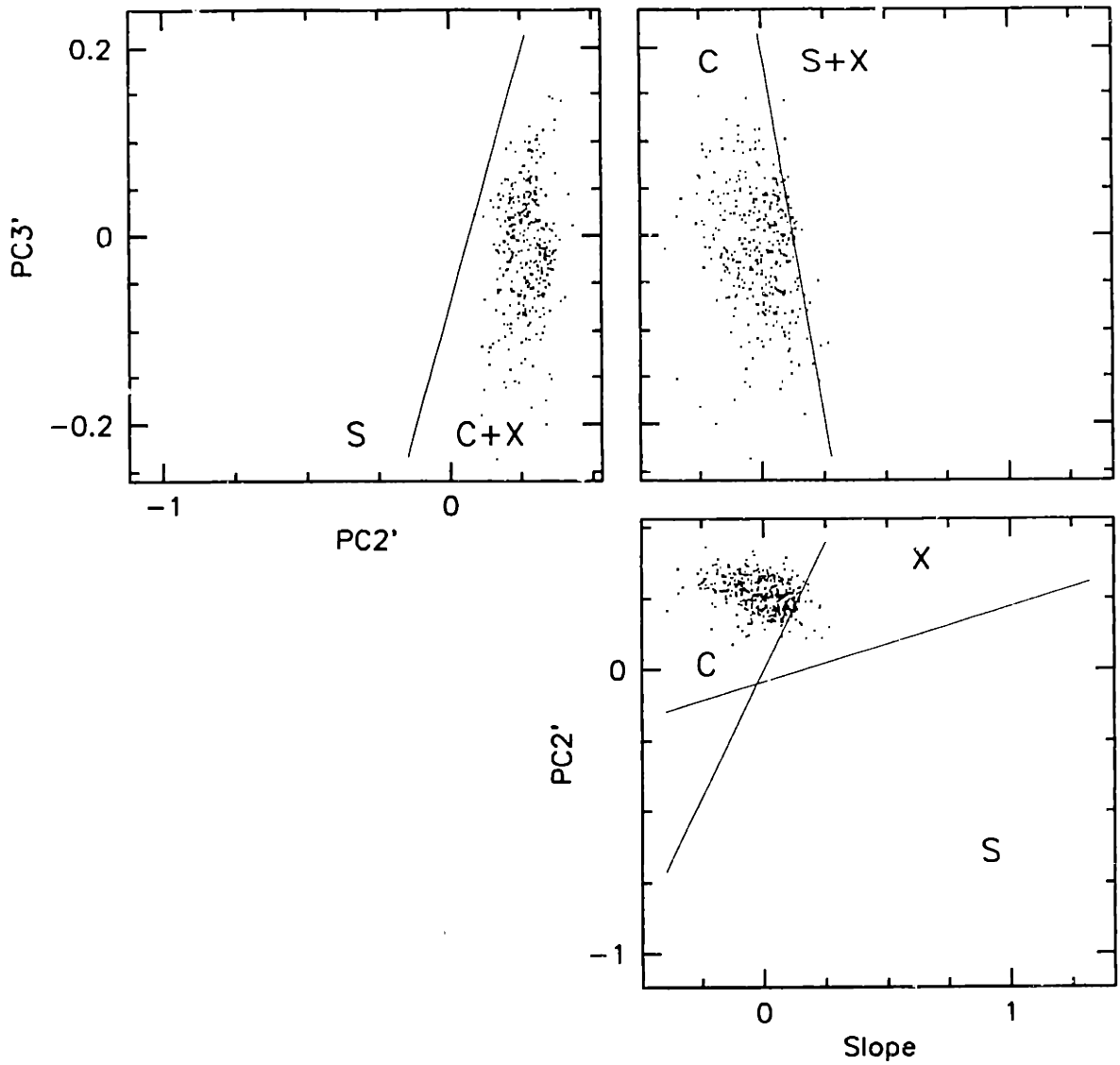

Figure 4.3: Same as Figure 4.1, but showing only the 360 SMASSII asteroids belonging to the C-complex.

4.3 Description of outlying spectral classes

There is a significant number of SMASSII asteroids whose spectra lie outside of the nominal ranges defined for the C-, X-, and S-complexes. These objects all plot on the periphery of component space, and are divided into two distinct regions. The first of these regions is well separated from the three main complexes, and occupies the lower left corner of the primary component plane defined by PC2' versus Slope. The second

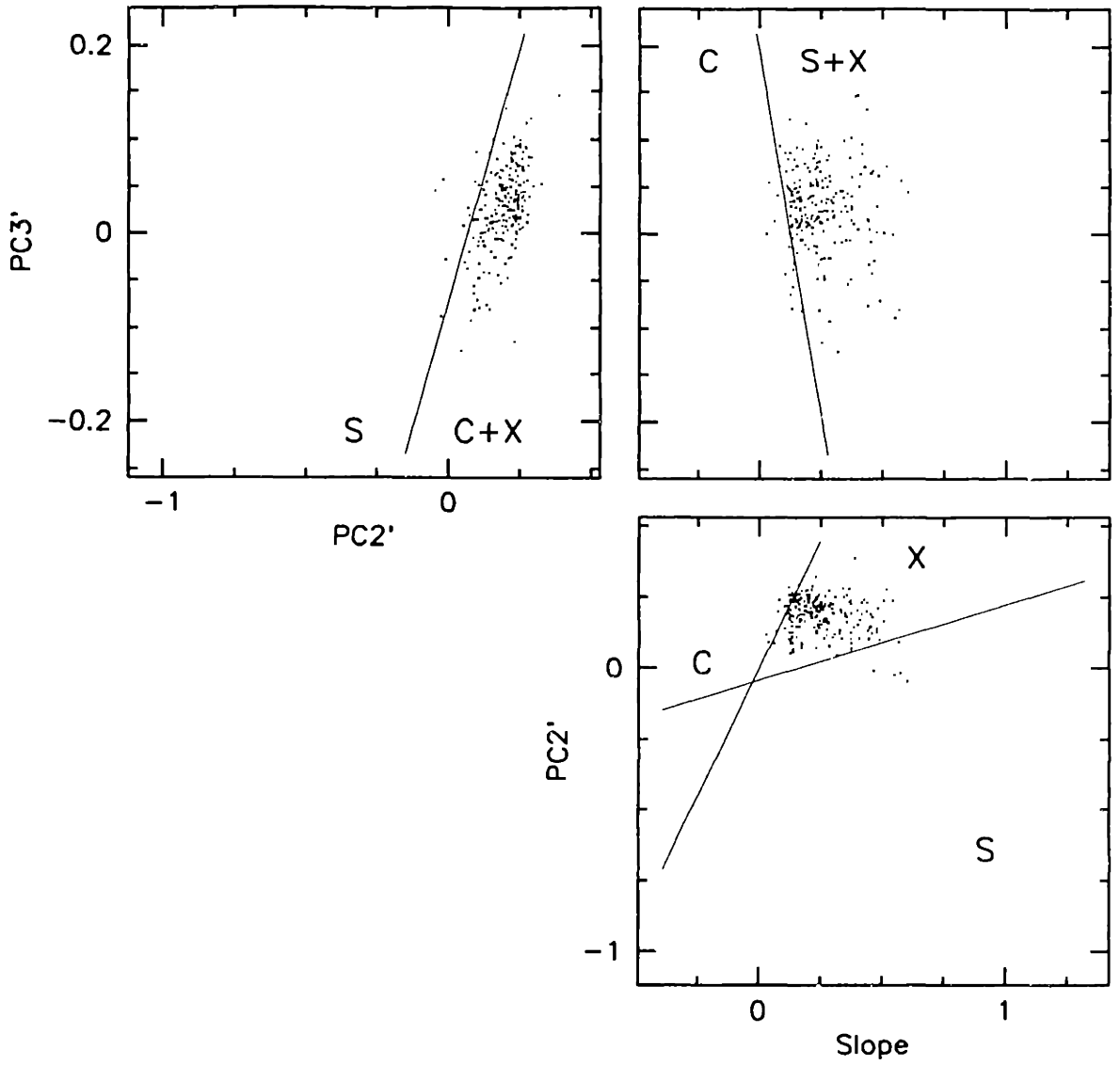

Figure 4.4: Same as Figure 4.1, but showing only the 220 SMASSII asteroids belonging to the X-complex.

region of outliers is more closely associated with both the X- and S-complexes, lying in the upper right-hand corner of the spectral component plane, but the spectra of these objects clearly do not fit within the classical definitions of either the X- or S-types. These outliers are assigned to one of five different spectral classes: the D-, T-, Ld-, O- and V-classes. The location of these spectral classes in component space is shown in Figure 4.5.

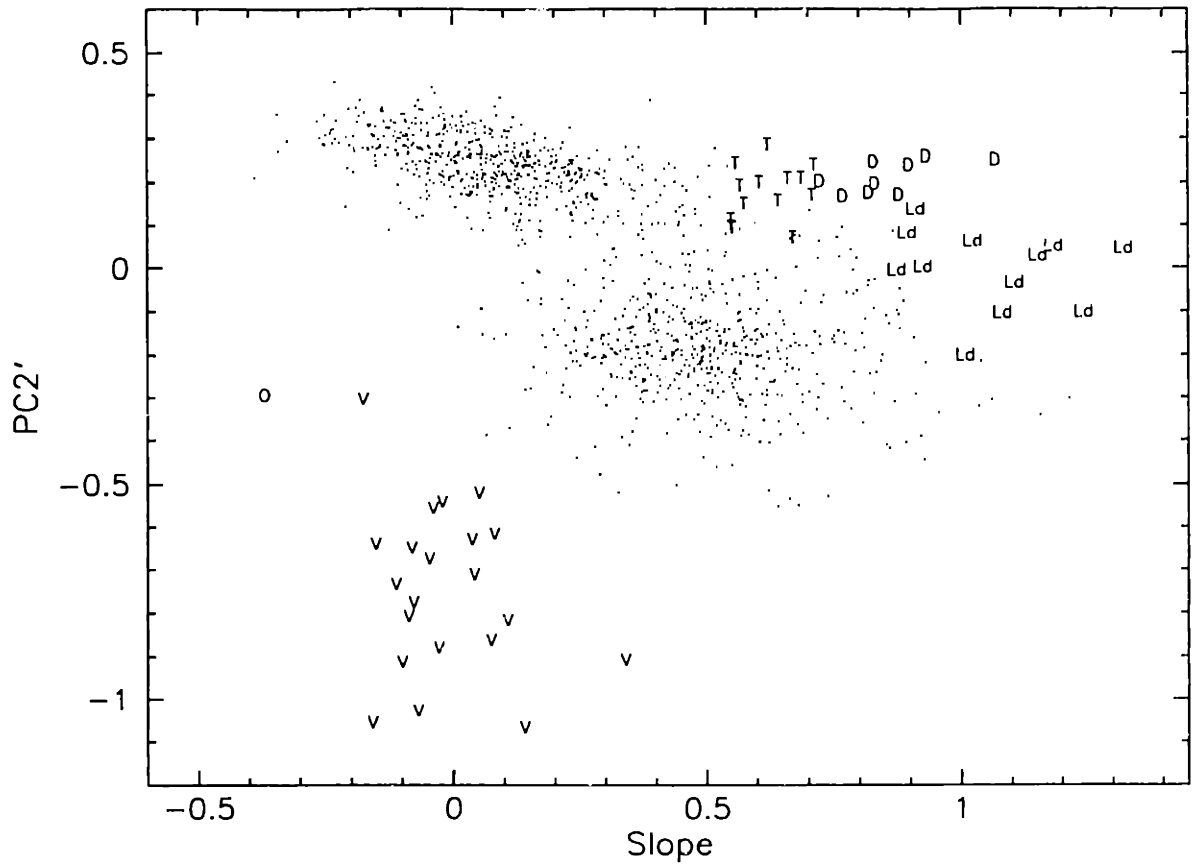

Figure 4.5: Component plot identifying those objects with spectral types that lie outside of the S-, C-, and X-complexes.

The first classes to be considered were the D- and T-types. Defining the boundaries for these two classes was based, in part, on the mean broad-band colors calculated by Tholen for the D- and T-classes, and on the scatter in spectral component space of those SMASSII asteroids previously classified as D- or T-types (Tholen 1984, Barucci *et al.* 1987, Howell *et al.* 1994). The spectra of objects in these two classes are relatively featureless, having a moderate to steep slope shortward of 0.75 μm, but often becoming less steep longward of 0.75 μm, with this change in spectral slope being gradual over a broad wavelength interval. The primary characteristic that differentiates the two classes is the average spectral slope, with D-types being steeper, or redder in color, than the T-types. In component space, the two classes plot side-by-side, with the boundary separating them being located at a Slope value of −0.72. The location of the T-types in component space is significant, in that they lie on one end of the boundary separating the X- and S-complexes, and are in close proximity to members of both the

Xk-class (of the X-complex, described in a later section) and the L-class (of the S-complex, also discussed in a later section). The fact that the T-types bridge this space, forming a continuum between the Xk-, L-, and D-types, may help to explain the variety of compositional interpretations that have been made regarding T-type asteroids (Gaffey *et al.* 1993b). Objects classified as D-types are predominantly found in the outer asteroid belt, especially among the Trojan asteroids (French *et al.* 1989, Lagerkvist *et al.* 1993), and are thought to be composed of relatively primitive, organic material. Since outer-belt asteroids were not a focus of the SMASSII survey, D-types are greatly undersampled in our spectral results. Even so, we classify nine asteroids as being D-types, eight of these having semimajor axes between 2.6 and 3.9 AU. This number is consistent with the findings of SMASSI (Xu *et al.* 1995), where three D-types were identified in the main belt from a total survey sample of 316 asteroids.

The remaining outliers on the right-hand side of this component plane were classified as Ld-types. The spectra of these asteroids have a very steep red slope shortward of 0.7 μm, and become essentially flat longward of 0.75 μm, with a maximum relative reflectance of roughly 1.3. This is a fairly unusual spectral type and was essentially unsampled in the ECAS survey, with only one of the twelve SMASSII asteroids assigned to the Ld-class being previously classified (234 Barbara, designated as an S-type, Tholen 1984, and as an S0-type, Barucci *et al.* 1987). The component space occupied by these twelve objects is large, filling the region bounded by the edge of the S-complex, and extending along the PC2' axis from the bottom edge of the D-class to the top of the A-class (in the lower right-hand corner of the S-complex). The designation "Ld" was selected to reflect the fact that, spectrally, these objects are most similar to the L-types (discussed in the next section), but have a much steeper slope, like the D-types.

Located on the left-hand edge of the spectral component plane is a single object representing the O-class. This class was defined by Binzel *et al.* (1993b) based on the unusual spectral properties of the asteroid 3628 Božněmcová. This spectrum is described by a moderately red slope from 0.44 to 0.54 μm, followed by a generally linear, but much shallower spectral slope that reaches a maximum relative reflectance of only 1.05 at 0.7 μm. The short-wavelength half of a very deep silicate absorption feature is then seen longward of 0.75 μm. Based on comparisons with meteorite data, Binzel *et al.* found the spectrum 3628 to be most consistent with that of L6 and LL6 ordinary

chondrites, and suggested this main-belt asteroid may represent a possible link to ordinary chondrite meteorites found on Earth. The unique nature of this object is greatly reinforced by the fact that in the results of the SMASSII survey, no other main-belt asteroid was observed whose spectral properties even approach those of 3628 Božněmcová.

The V-class was first proposed by Tholen (1984) to describe the unusual spectral properties of the asteroid 4 Vesta. The visual reflectance spectrum of Vesta has a moderately steep, red slope shortward of 0.7 μm, and a very deep absorption band longward of 0.75 μm, similar to the spectra of basaltic achondrite (HED) meteorites (McCord *et al.* 1970). During the SMASSI survey, Binzel and Xu (1993) identified over 20 asteroids that are not only spectrally similar to Vesta, but also have orbital parameters similar to those of Vesta. This clustering of V-type asteroids in orbital parameter space not only helps confirm the existence of a suspected dynamical family (Williams 1979, Zappalà *et al.* 1990), but because of this cluster's proximity to both secular (ν_6) and mean-motion (3:1) resonances, it provides possible pathways for delivering HED meteorites to Earth (Greenberg and Chapman 1983). In classifying the "Vesta chips", Binzel and Xu actually divided the spectral class, designating those objects with particularly deep 1 μm bands as J-types ("J" for Johnstown diogenite). Observations of asteroids in the Vesta zone were continued throughout the SMASSII survey, with nearly 20 additional V-type asteroids being added to the total known.

In all, twenty-one V-types are plotted in the lower left-hand corner of the spectral component plane shown in Figure 4.5. The dispersion of these points in component space is quite large, consistent with the wide range of spectral variation observed among these objects. Even so, I do not to adopt the division between the V- and J-classes, but rather, include all members of this group in a single V class. To be consistent with this feature-based taxonomy, any future subdivision of this spectral space should be labelled as subclasses of the V-types (for example, a Vj class).

In Figure 4.6, the average spectrum for each of these five outlying classes is plotted, along with envelopes representing the 1σ range in spectral variation. Because these classes of asteroids plot on the periphery of spectral component space, the average spectra plotted here are examples of some of the extremes in spectral characteristics observed thus far among the main-belt asteroids.

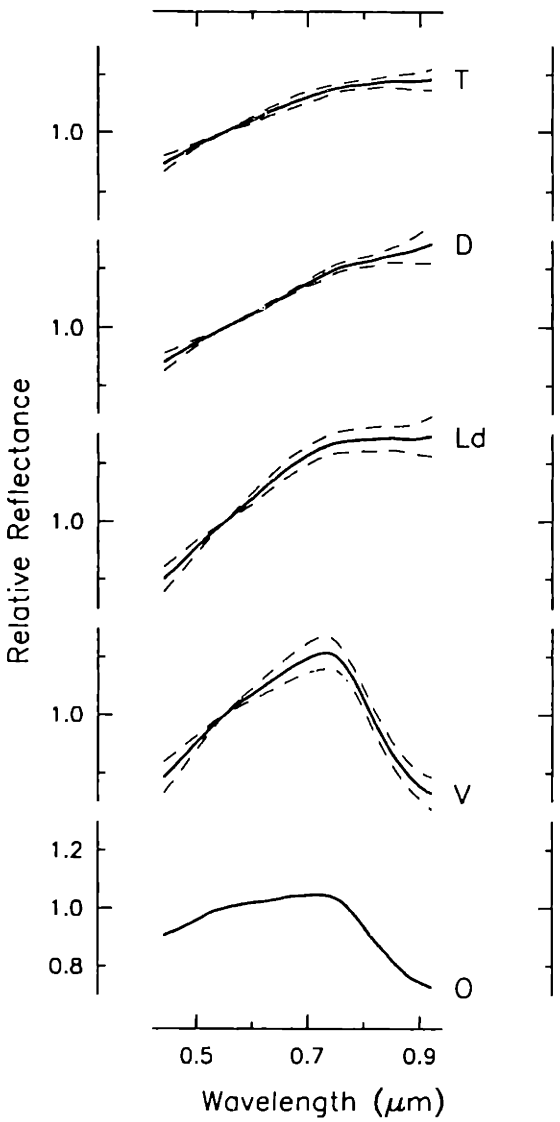

Figure 4.6: The mean reflectance spectrum (solid curve) for each of the five outlying spectral classes. The dashed lines represent the 1σ envelope determined from the variance in each wavelength channel.

4.4 The S-complex

In the component space defined by Slope, PC2' and PC3', the S-complex is represented by a triaxially-symmetric, centrally-condensed cloud of points, as plotted in Figure 4.2. All of the asteroids contained in this complex have the common spectral characteristic of a moderate to steep red slope over the wavelength interval from 0.44 to 0.70 μm, usually reaching a maximum reflectance between 0.72 and 0.76 μm.

Longward of this peak reflectance (out to the limit of our observations at 0.92 μm), these spectra can range from being approximately flat, or neutral in color, to having a very deep silicate absorption band that reaches minimum reflectance at around 1 μm. Because the UV slope (shortward of 0.70 μm) and the 1 μm band are the two most dominant features observed in the visible spectra of asteroids, these features dominate the variance described by the lower-order spectral components, particularly Slope and PC2'. The shape of the S-complex in spectral component space (both the concentration of objects at the center, and the approximate triaxial symmetry of the distribution) indicates that the variations observed in the UV slope and 1 μm band depth within the S-complex should be treated as continuous, and suggests that subdividing this complex into smaller spectral classes could be achieved, in part, using analytical methods.

4.4.1 Description of the A-, Q-, and R-classes

Three spectral classes defined in the Tholen taxonomy (the A-, Q-, and R-types) plot on the lower perimeter of the S-complex (as projected in the primary plane of PC2' vs. Slope). The spectra of these objects contain moderate to very deep 1 μm absorption bands, consistent with their lower (or more negative) values of component PC2'. What differentiates these asteroids from others in the bottom half of the S-complex is subtle peculiarities in the shape and width of the reflectance peak, and to a smaller extent, in the shape of the 1 μm silicate absorption band over the wavelength sampled. In particular, for most asteroids contained in the S-complex, the spectral reflectance maximum is located between 0.72 and 0.76 μm, and the interval over which significant curvature occurs (that interval over which the spectral slope transitions from the UV slope to the 1 μm absorption band) is typically 0.07 to 0.09 μm wide. For those asteroids classified by Tholen as A-, Q-, or R-types, the width of the spectral peak is usually outside of this nominal range, with some asteroids having reflectance maxima that are especially narrow or sharply peaked (with the curvature being confined to an interval of ~0.05 μm), while other asteroids have spectral reflectance maxima that are particularly broad (interval of curvature ≥0.1 μm). In addition to these variations in the shape of the reflectance peak, the 1 μm absorption band often appears to be more rounded, or "bowl-shaped", than is typical for S-type asteroids.

Based on the ECAS results, Tholen uniquely identified five asteroids as A-types: 246 Asporina, 289 Nenetta, 446 Aeternitas, 863 Benkoela, and 2501 Lohja (Tholen

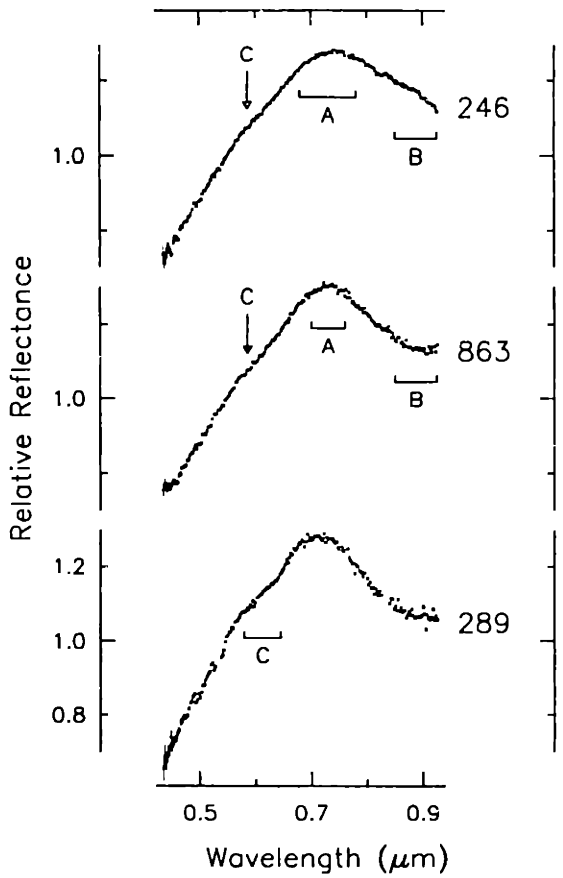

Figure 4.7: Three examples of A-type spectra, showing the range of variation observed for different spectral features. The reflectance maximum, marked A, is seen to be fairly narrow, or sharply peaked in some A-type spectra (such as 863 Benkoela), but in other A-types, such as 246 Asporina, the maximum can be quite broad. The 1μm absorption band can appear significantly rounded (see B for asteroid 863) though the presence of a rounded absorption feature is usually correlated with a sharply-peaked maximum. When the reflectance maximum is broad, the absorption feature is likely to be more linear in appearance, as is seen in 246 Asporina. Most A-types appear to have a subtle bend, or deflection, in the red slope, centered around 0.625 μm (King and Ridley, 1987). This feature is marked with an arrow and labelled C in the first two spectra, but in the spectrum of 289 Nenetta, this feature is quite pronounced, with a width of over 0.07μm as shown by the labelled bracket.

1989). Two other ECAS asteroids were assigned the letter "A" as part of a multiple designation: 1658 Innes (AS) and 1747 Wright (AU:). During the SMASSII survey, we reobserved each of the five unambiguous A-types identified by Tholen, and used these in defining the limits of the A-class in our feature-based taxonomy. The A-types have an unusually steep red slope shortward of 0.70 μm, and a moderately deep 1 μm band. Mineralogically, there is little debate over the interpretation of these spectra, which are

characteristic of an olivine composition (Gaffey 1994, Lucey and Keil 1997). However, based on our observations of the five ECAS asteroids, we find that there are actually two distinct spectral forms associated with the A-class. The first of these forms has a reflectance maximum that is narrow, or sharply peaked, and a 1 μm band that is particularly rounded. Two examples of this form (289 Nenetta and 863 Benkoela) are plotted in Figure 4.7. The other spectral form has a reflectance peak that is much broader, and a 1 μm feature that shows little or no curvature (is essentially linear) out to the end of the observed spectrum (at 0.92 μm). An example of this spectral type (246 Asporina) is also plotted in Figure 4.7. In those A-type spectra with sufficiently good signal-to-noise, a subtle bend, or deflection is commonly observed in the UV slope, centered around 0.625 μm (King and Ridley 1987, Sunshine *et al.* 1998). In some spectra, such as that of 289 (see Figure 4.7), this feature can have a substantial width, and appears to result from the combination of multiple band components.

A total of 15 A-type asteroids were identified in the SMASSII survey, including the five A-types previously known from the ECAS survey. While these objects occupy a relatively large, elongated region of spectral component space (see Figure 4.8), the apparent correlation between the components Slope and PC2' can be reasonably explained. Those A-types that exhibit a sharp reflectance peak, and correspondingly more rounded (and thus deeper) 1 μm absorption band will be fitted by a lower average spectral slope (measure of component Slope). In contrast, those spectra with broader reflectance maxima, and thus more linear or shallow 1 μm bands will be fitted by a steeper average slope. In Figure 4.8, arrows have been added to show the approximate directions in which the UV slope and 1 μm band depth increase. It is clear that the A-types cluster in an orientation along the line of variable 1 μm band depth, while the UV slope tends to be more constant (consistently very steep, or red). Though the A-types are generally isolated in the lower right-hand corner of Figure 4.8, inclusion of an asteroid in the A-class must ultimately depend on inspection of the shapes of the reflectance maximum and 1 μm band. The differences in the 1 μm band strength have been confirmed through observations in the near-IR by SMASSIR (Burbine *et al.* 1999). Arguments could be made to subdivide the A-class based on these differences in shape and strength of the 1 μm band, but until more A-types are observed and the range of spectral variability is better established through mapping the full structure of the 1 μm band, we suggest maintaining a single A class, thus preserving the definition of Tholen.

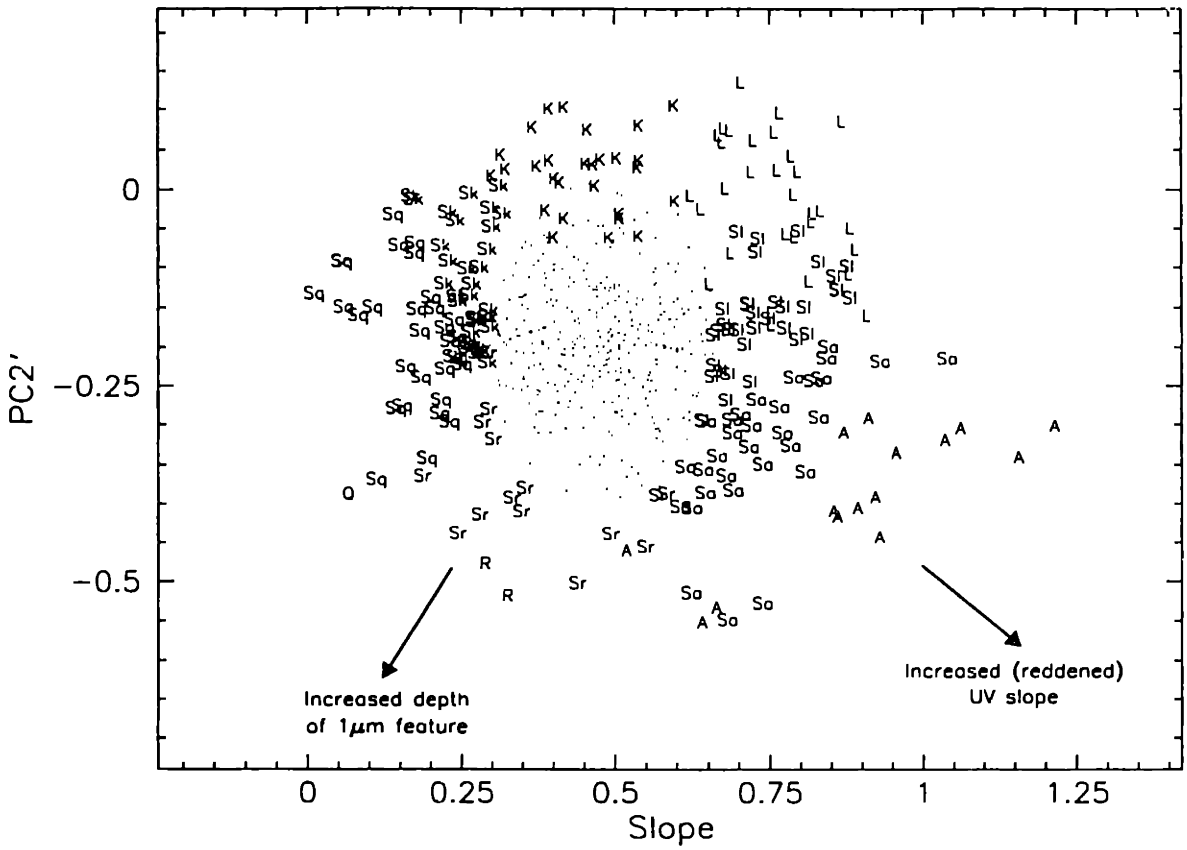

Figure 4.8: Component plot showing the subdivision of asteroids within the S-complex. For clarity, those asteroids classified as "S" (with no subscript) are shown as dots. Arrows are plotted to show the general trends of primary spectral features in component space. The depth of the 1 μm feature trends from negligible in the K- and L-types, to very deep in the R- and Q-types. Note also that the trend for increasing UV slope (the slope for that part of the spectrum shortward of roughly 0.7 μm) is skewed with respect to the Slope axis (the Slope axis being a measure of the average slope over the entire spectral interval.)

The earliest definition of the R-class (Bowell *et al.* 1978) contained several asteroids whose spectra have a steep UV slope and a strong 1 μm absorption feature. However, with the addition of near-IR spectrophotometric measurements, and the introduction of the A-class, the R-class became very exclusive. Tholen found only one definitive R-type in his classification of the ECAS asteroids, 349 Dembowska. The maximum reflectance in the Dembowska spectrum is very sharply peaked, and somewhat skewed due to the steep drop-off of the 1 μm absorption band. Unlike the A-types, whose near-IR spectra reveal a single absorption band centered near 1 μm (indicating a composition dominated by olivine), the near-IR spectrum of Dembowska exhibits strong absorption features at both 1 and 2 μm, interpreted as resulting from a

mixture of olivine and pyroxene, with little or no NiFe metal (Feierberg *et al.* 1980, Gaffey *et al.* 1989). In the SMASSII data, we have identified one other asteroid, 1904 Massevitch, whose visible wavelength spectrum is nearly identical to that of 349 Dembowska. However, a comparison of the proper orbital elements for these two asteroids (for Dembowska, a = 2.925 AU, e' = 0.055, sin i' = 0.135, while for 1904 Massevitch, a = 2.744 AU, e' = 0.039, sin i' = 0.205, from proper element file version 6.8.5, Milani and Knežević 1994) suggests that it is unlikely these two objects originated from the same disrupted parent body.

The only asteroid unambiguously identified as a Q-type by Tholen is the near-Earth asteroid (NEA) 1862 Apollo. This asteroid, as well as 74 other NEAs, were observed as part of SMASSII. As discussed earlier, results from our observations of NEAs are being reported on separately by Binzel *et al.* (1999b), with preliminary findings already given by Binzel et al. (1996). While we do not include the spectrum of 1862 Apollo in Appendix B, we do include the fitted channels for this asteroid in our calculation of spectral components, thus providing a benchmark for the Q-class within our feature-based taxonomy. The spectrum of 1862 Apollo contains a moderately steep UV slope and a deep 1 μm absorption feature. The reflectance maximum (centered at roughly 0.71 μm) is noticeably broader, and more rounded, than is typical for S-type asteroids. Similarly, the 1 μm absorption feature is very rounded, or "bowl-shaped". Using the position of the 1 μm band, McFadden *et al.* (1984, 1989) interpreted the surface composition of Apollo to be a mixture of olivine and pyroxene, similar to that found in ordinary chondrite meteorites. While several asteroids have been identified among the NEA population whose spectral properties are similar to that of 1862 Apollo (Binzel *et al.* 1996), no asteroids in the main belt have been found whose spectral characteristics are sufficiently close to those of Apollo to be included in the Q-class.

4.4.2 Description of the K- and L-classes

Asteroids plotting in the upper portion of the S-complex, as viewed in the primary plane of PC2' versus Slope, have spectra in which the 1 μm band tends to be shallow. Specifically, for those asteroids located on the upper perimeter of this complex, the 1 μm band depth is essentially zero, leaving an approximately flat, or neutral spectrum over the interval longward of 0.75 μm (where the UV slope has ended). The transition from the UV slope to this flat segment occurs smoothly, usually over a wavelength interval of

~0.05 μm. To describe this spectral form, I have reserved the term "smoothly angled". In the definitions of both the K- and L-classes, the spectral segment longward of 0.75 μm is not required to be absolutely flat (the slope over this segment can range from moderately bluish to slightly reddish), but it must be linear, with no significant concave-up curvature like that normally associated with the 1 μm absorption band. While several asteroids having this spectral form were measured during ECAS, in the Tholen taxonomy, these objects were assigned to the S-class, and have traditionally been referred to as "featureless" S-types.

Gradie and Zellner (1977) found that asteroids belonging to the Eos family have UBV colors and radiometric albedos that are intermediate between those of C- and S-type asteroids. Over the visible wavelengths, the spectra of Eos family members are generally similar to those of S-type asteroids in that they exhibit a moderate UV slope shortward of 0.7 μm. However, over the interval of 0.75 to 0.92 μm, these spectra contain no significant 1 μm feature. In spectral component space, the Eos family asteroids cluster around a PC2' value of 0.0, and plot as a continuous extension from the densely-populated core of S-types. The first proposal for a separate K-class was made by Bell (1988), based on near-IR spectrophotometry of Eos family objects in which he found the 1 μm silicate absorption feature to be particularly shallow, and the 2 μm band to be essentially absent. Bell found a close similarity between the spectral and albedo data for these K-types and that of anhydrous CV3 and CO3 chondrite meteorites. Tedesco *et al.* (1989) also defined a K-class based on their three-parameter taxonomy, but included extra objects in the class that are not associated with the Eos family. A thorough study of the Eos family was conducted by Doressoundiram *et al.* (1998) using CCD spectroscopy, in which a wide range of spectral slopes among the family members was revealed. This spread in spectral slopes was interpreted as a record of compositional variation within the Eos parent body, though Doressoundiram *et al.* also found evidence suggesting that surface weathering processes may have reddened many of the spectra. In the SMASSII data, we have identified 28 asteroids as K-types, though only about half of these objects are directly associated with the Eos family.

Based on his principal component analysis of the combined ECAS and 52-color survey data, Burbine (1991) identified two S-type asteroids, 387 Aquitania and 980 Anacostia, that have an unusual near-IR spectrum when compared with those of typical S-types (Gaffey *et al.* 1990, 1993a). These same asteroids were also noted as being

unusual by Britt and Lebofsky (1992). The spectra of both Aquitania and Anacostia contain a moderately deep, broad 2 μm absorption band, while the 1 μm feature is very weak. In mixtures of olivine and pyroxene, it is the 1 μm absorption band that is usually strongest, with the relative intensity of the 2 μm band approaching that of the 1 μm feature only in assemblages that are dominated by pyroxene (Cloutis *et al.* 1986). Burbine *et al.* (1992) interpreted these anomalous spectra as indicating the presence of spinel, which is commonly found in inclusions contained in CV3 and CO3 meteorites.

Over the visible wavelengths, 387 Aquitania and 980 Anacostia have spectra that are generally similar to those of K-types. There is a moderately steep UV slope shortward of 0.70 μm, and relatively flat, featureless interval longward of 0.75 μm, with the transition being smoothly angled. The primary characteristic separating these asteroids from the K-class is the fact that the UV slope is considerably steeper for Aquitania and Anacostia than for the average K-type asteroid. In SMASSI, Xu *et al.* (1995) identified 6 inner main-belt S-type asteroids whose visible wavelength spectra are similar to those of Aquitania and Anacostia. In SMASSII, we have identified 31 such asteroids, leading us to propose a new spectral class to describe them, and denoting this class by the letter "L". The letter L was chosen to stress the apparent spectral continuum these asteroids form with relation to the K-types, as well as the S-types. In the SMASSII spectral component space, the separation between the K- and L-classes occurs at a Slope value of about 0.60. Burbine *et al.* (1992) noted the similarities in orbital semimajor axes and inclinations (proper sin i) of Aquitania and Anacostia, suggesting a possible Aquitania-Anacostia family formed by the disruption of a spinel-bearing CV3-type parent body, and indicated that 599 Luisa and 729 Watsonia may also be members of this family. The SMASSII observations tend to support this hypothesis, with Luisa and Watsonia being classified as K- and L-types, respectively. We have also found that most members of the proposed Henan family (Zappalà *et al.* 1995) are L-types (these family memberships will be discussed at length in Chapter 5). This fact that the Eos family primarily contains K-types, while the proposed Aquitania-Anacostia and Henan families are dominated by L-types, was significant in our decision to form the separate "L" spectral class, rather than simply expanding the boundaries of the K-class.

4.4.3 Subdividing the core of the S-complex

Once the A-, K-, L-, Q-, and R-types had been identified among the SMASSII asteroids, and removed from further steps in the classification process, a total of 476 objects still remained as unclassified within the S-complex. While all of these asteroids shared the common S-type characteristics of a moderately wide reflectance maximum, usually centered between 0.72 and 0.76 μm, and a 1 μm feature that shows moderate concave curvature, there was still considerable diversity among these spectra, especially in the steepness of the UV slopes, and in the depths of the 1 μm bands.

Previous efforts to subdivide the S-class (e.g. Chapman 1987, Gaffey *et al.* 1993a, Howell *et al.* 1994) were primarily driven by mineralogical considerations. Based on observations in the near-IR, measurements of the 1 and 2 μm silicate absorption bands provide direct evidence for the olivine and/or pyroxene compositions of S-type asteroids (Burns 1970, Adams 1974, 1975, Cloutis *et al.* 1986). While the SMASSII observations are limited to the visible wavelength region and record only the shorter wavelength half of the 1 μm band, it must be argued that the first two spectral components (Slope and PC2') calculated from the SMASSII data are fully capable of separating the A-, Q-, and R-type asteroids (as well as the K- and L-types) with their wide diversity of inferred mineralogies (as shown in Figure 4.8). Because we have interpreted the S-complex to be a continuous distribution of spectral forms, with the A-, K-, L-, Q-, and R-classes representing endmembers of this distribution, it follows that a trend in silicate composition may also extend throughout the S-complex as plotted in spectral component space. There were many asteroids observed during SMASSII whose overall spectral slope, and depth of the 1 μm band closely matched those of A-type asteroids, but which were not classified as A-types because the shape of the reflectance maximum and the degree to which the 1 μm feature was either rounded or linear did not meet the criteria that we had established in defining the A-class. During SMASSI (Xu *et al.* 1995), eight asteroids were identified as having spectra similar to those of A-types, but which were ultimately not included in the A-class. Instead, these SMASSI asteroids were noted as being "olivine-rich" or "clinopyroxene-rich" S-types. In the SMASSII data, we have similarly found many asteroids whose spectra come close to matching those of the two identified R-type asteroids (349 Dembowska and 1904 Massevitch), but which were not classified as R-types because their reflectance maxima and 1 μm bands appeared too "rounded" in shape. By maintaining these seemingly strict definitions for determining

those objects to be included in the A- and R-classes (and similarly, those asteroids included in the K-, L-, and Q-classes), we attempt to preserve these classes as true endmembers of the spectral continuum.

The Slope and PC2' components account for the majority of the variance in our spectra. It therefore follows that the spectral variations found among asteroids in the S-complex (which are primarily manifested as differences in the UV slope and 1 μm band depth, where these features are isolated by the Slope and PC2' components) can be separated based solely on a measure of spectral variance. This suggests that a simple, quantitative approach can be used to classify asteroids in the S-complex, which is independent of principal component analysis. The procedure we have adopted uses the dissimilarity (defined in Eqn. 3.2) to measure the deviation between individual spectra and the mean spectra calculated for different regions of the S-complex. In Table 4.1, the reflectance values are listed for the mean spectra of all asteroids contained in each of the A-, K-, L-, Q-, and R-classes. For the Q-class, the values presented in this table are those for the single asteroid 1862 Apollo. Likewise, for the R-class, the values listed represent the mean of two spectra (asteroids 349 Dembowska and 1904 Massevitch), while the mean spectrum for the L-class is derived from 31 different asteroids. Also listed in Table 4.1 is the mean spectrum for the "core" of the S-complex, which includes all 476 members of the complex which had not already been classified as A-, K-, L-, Q-, or R-types.

The primary calculation involves determining the dissimilarity (Euclidean distance, as given by Eqn. 3.2) for each asteroid in the core of the S-complex (any asteroid not yet classified) with respect to each of the six mean spectra in Table 4.1. Examining the distribution of dissimilarities for all 476 asteroids with respect to the mean core spectrum (this dissimilarity with respect to the core of the S-complex is denoted by d_s), we find that 1σ (68%) of these asteroids have dissimilarities $d_s \leq 0.25$. Using this 1σ definition, any asteroid in the S-complex with a value of $d_s \leq 0.25$ was classified as an S-type (with no subscript) in our feature-based taxonomy. For the remaining unclassified asteroids, with values of $d_s > 0.25$, the classification of each object was determined from the set of dissimilarities [d_a, d_k, d_l, d_q, d_r] that were calculated with respect to the mean spectra of A-, K-, L-, Q-, and R-types listed in Table 4.1. By finding which of these five dissimilarities is smallest (finding the minimum value contained in the set, denoted as

Table 4.1: Mean spectra used in subdividing the S-complex

Wavelength (μm)	Mean relative reflectance					
	Core of S-complex	A-types	K-types	L-types	Q-types	R-types
0.44	0.8111	0.7106	0.8598	0.8170	0.8178	0.7934
0.45	0.8296	0.7368	0.8740	0.8348	0.8332	0.8110
0.46	0.8481	0.7632	0.8881	0.8525	0.8488	0.8289
0.47	0.8663	0.7897	0.9020	0.8702	0.8644	0.8472
0.48	0.8842	0.8162	0.9156	0.8876	0.8805	0.8656
0.49	0.9017	0.8426	0.9290	0.9050	0.8970	0.8829
0.50	0.9188	0.8691	0.9423	0.9220	0.9143	0.8989
0.51	0.9358	0.8958	0.9552	0.9386	0.9321	0.9158
0.52	0.9527	0.9226	0.9674	0.9548	0.9502	0.9366
0.53	0.9691	0.9483	0.9789	0.9702	0.9679	0.9599
0.54	0.9848	0.9746	0.9896	0.9851	0.9845	0.9808
0.55	1.0000	1.0000	1.0000	1.0000	1.0000	1.0000
0.56	1.0144	1.0243	1.0099	1.0147	1.0146	1.0184
0.57	1.0273	1.0471	1.0192	1.0285	1.0283	1.0355
0.58	1.0388	1.0680	1.0275	1.0414	1.0410	1.0502
0.59	1.0497	1.0879	1.0355	1.0538	1.0526	1.0632
0.60	1.0611	1.1075	1.0440	1.0664	1.0629	1.0770
0.61	1.0732	1.1274	1.0531	1.0797	1.0725	1.0904
0.62	1.0858	1.1474	1.0626	1.0932	1.0820	1.1028
0.63	1.0981	1.1674	1.0715	1.1060	1.0915	1.1163
0.64	1.1103	1.1884	1.0796	1.1185	1.1010	1.1334
0.65	1.1223	1.2103	1.0877	1.1305	1.1105	1.1507
0.66	1.1340	1.2317	1.0960	1.1419	1.1198	1.1664
0.67	1.1451	1.2507	1.1037	1.1526	1.1287	1.1808
0.68	1.1548	1.2671	1.1103	1.1623	1.1361	1.1948
0.69	1.1632	1.2808	1.1161	1.1709	1.1412	1.2064
0.70	1.1709	1.2917	1.1214	1.1791	1.1442	1.2154
0.71	1.1778	1.3002	1.1255	1.1869	1.1453	1.2232
0.72	1.1833	1.3059	1.1286	1.1935	1.1440	1.2267
0.73	1.1876	1.3087	1.1323	1.1992	1.1405	1.2285
0.74	1.1900	1.3086	1.1360	1.2041	1.1354	1.2313
0.75	1.1889	1.3047	1.1378	1.2067	1.1281	1.2266
0.76	1.1841	1.2961	1.1371	1.2068	1.1173	1.2117
0.77	1.1765	1.2842	1.1344	1.2056	1.1031	1.1892
0.78	1.1675	1.2713	1.1309	1.2044	1.0852	1.1644
0.79	1.1574	1.2584	1.1276	1.2031	1.0638	1.1384
0.80	1.1457	1.2446	1.1238	1.2010	1.0395	1.1086
0.81	1.1331	1.2305	1.1197	1.1988	1.0137	1.0768
0.82	1.1209	1.2174	1.1168	1.1975	0.9884	1.0498
0.83	1.1096	1.2061	1.1153	1.1969	0.9651	1.0301
0.84	1.0979	1.1951	1.1132	1.1957	0.9443	1.0108
0.85	1.0852	1.1831	1.1092	1.1929	0.9264	0.9877
0.86	1.0729	1.1717	1.1041	1.1898	0.9119	0.9660
0.87	1.0617	1.1624	1.0986	1.1873	0.9009	0.9488
0.88	1.0520	1.1554	1.0931	1.1857	0.8926	0.9358
0.89	1.0445	1.1504	1.0881	1.1851	0.8860	0.9272
0.90	1.0392	1.1468	1.0841	1.1851	0.8804	0.9225
0.91	1.0359	1.1442	1.0817	1.1861	0.8757	0.9217
0.92	1.0340	1.1425	1.0805	1.1880	0.8717	0.9243

min[d_a, d_k, d_l, d_q, d_r]), we assign each of the remaining asteroids to one of five spectral classes, the Sa-, Sk-, Sl-, Sq-, and Sr-classes. For example, those asteroids in the S-complex for which $d_s > 0.25$, and for which $d_a = \min[d_a, d_\kappa, d_l, d_q, d_r]$ (and which had not been previously classified as A-types) were assigned to the Sa-class.

Figure 4.8 shows the distribution of spectral classes making up the S-complex, plotted in the component plane of PC2' versus Slope. Members of the A-, K-, L-, Q-, and R-classes are clearly seen occupying different regions around the perimeter of this distribution. Also seen are the relative locations of members belonging to the Sa-, Sk-, Sl-, Sq-, and Sr-classes. For clarity, those asteroids classified as S-types are represented by the dots concentrated in the center of this distribution. In this plot, those asteroids classified as Sa-types occupy the region between the S-types and the A-types. This results from the fact that the dissimilarity between the S-types and A-types is significant, leaving a relatively large gap of component space between the positions of A-types and the center of the S-type distribution that can be allocated to the Sa-class. Likewise, the R-type asteroids (and the Q-type asteroid 1862 Apollo) plot relatively far from the center of the S-type distribution, so that the Sr- and Sq-type asteroids plot in intermediate locations on this component plane. The relatively large values of dissimilarity between the A- and S-types, the Q- and S-types, and the R- and S-types are what led Tholen (1984) to identify the A-, Q- and R-classes as being distinct from the S-class in his minimum tree analysis. The asteroids that we assign to the Sa-, Sq-, and Sr-classes are generally small in size, and were not well sampled by the ECAS observations that provided the basis for Tholen's taxonomy. The trends in spectral shape, marked by arrows in Figure 4.8, indicate that the primary difference between the A-types and the Sa-types is the steepness of the UV slope (this is in addition to the subtle differences in the shapes of the reflectance peaks and the 1 μm bands that were described above). Likewise, the R- and Q-types differ from the Sr- and Sq-types primarily in the depth of the 1 μm absorption band. These differences, while relatively minor, can be seen in Figure 4.9, where the mean spectra for each of the classes in the S-complex is plotted. The case for the Sk- and Sl-classes, and their relationships to the K- and L-classes in spectral component space is slightly different. The UV slopes (and correspondingly, the average spectral slopes) for asteroids in both the K- and L-classes are not significantly different from those of the S-class asteroids. Thus, the only characteristic that really distinguishes the K- and L-types from the S-class is the absence

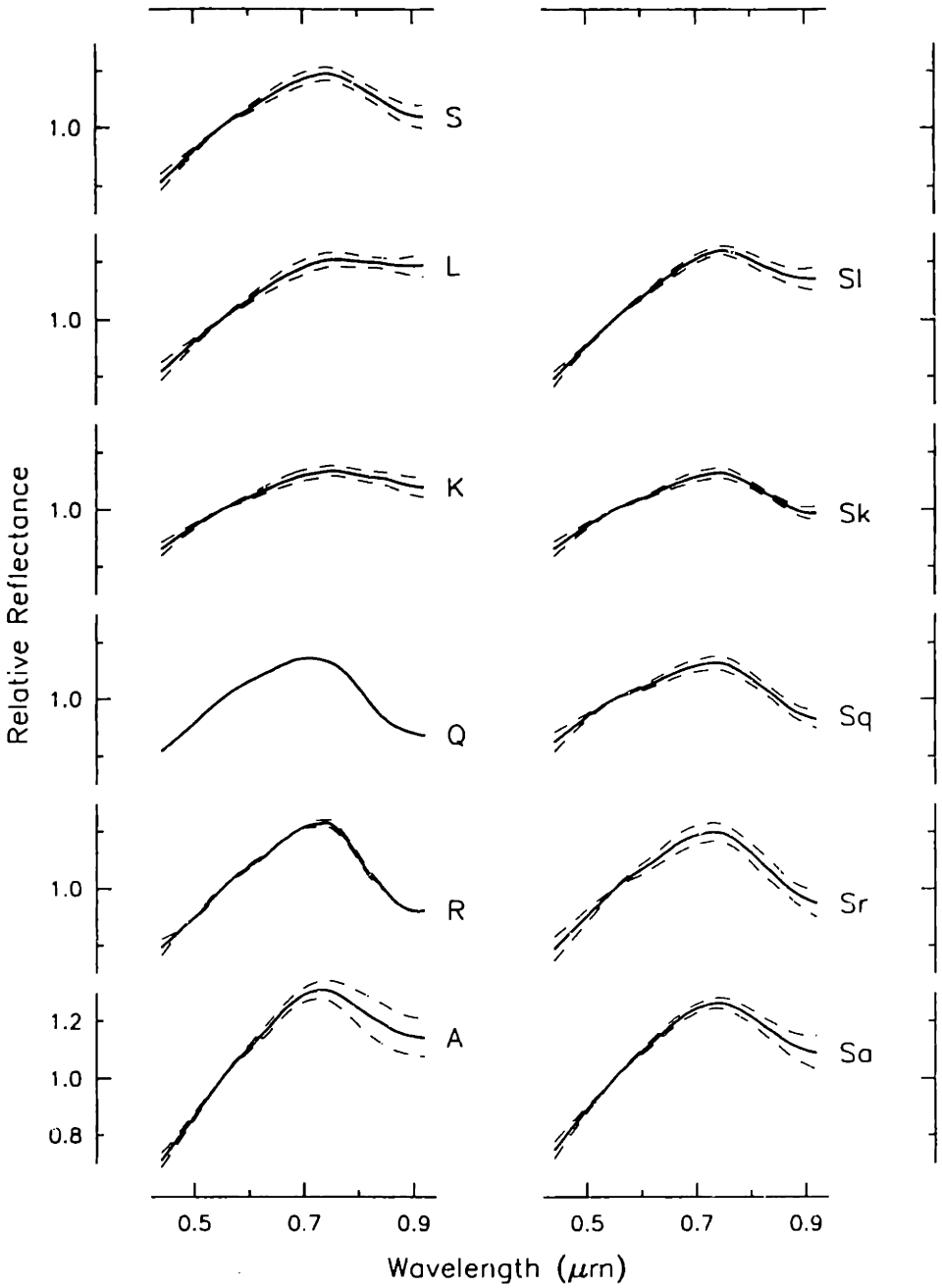

Figure 4.9: Similar to Figure 4.6, but showing the mean spectra for those classes contained in the S-complex.

of any substantial curvature in the 1 μm band, while the magnitude of the spectral variance separating the K- and L-types from the S-class is relatively small. As a result, the K- and L-classes plot immediately adjacent to the S-types in spectral component space, leaving the Sk- and Sl-types to plot on the perimeter of the distribution shown in

Figure 4.8. The Sk-types occupy a space bounded by not only the K- and S-classes, but also by the Sq-class. Similarly, the Sl-class is bounded by the L-, S-, and Sa-classes. The positions of these various classes in the PC2' versus Slope plane illustrates the fact that not only do the Sk- and Sl-types have more substantial 1 μm bands than the K- and L-types, but also that the UV slopes of the Sk- and Sl-types bracket the range of slopes found among asteroids assigned to the S-class. These relationships between the K-, L-, S-, Sk- and Sl-classes are also apparent in the mean spectra plotted in Figure 4.9.

4.4.4 Previous classifications of S-types

This description of six separate classes (the S-, Sa-, Sk-, Sl-, Sq- and Sr-classes) within the core of the S-complex is not the first subdivision of S-type asteroids to be proposed. Due to the large spectral diversity among the S-types, there have been several previous attempts to identify subclasses within this group (Chapman and Gaffey 1979, Barucci *et al.* 1987, Chapman 1987, Gaffey *et al.* 1993a, Howell *et al.* 1994), often based on mineralogical considerations that are justified by the presence of silicate absorption bands in the S-type spectrum. While only one of these silicate absorption features (the 1 μm band) is partially measured in the SMASSII spectra, and even though our approach in subdividing the core of the S-complex was strictly analytical, there may be trends resulting from our analysis of the SMASSII data that have some mineralogical significance. In particular, if our ability to clearly differentiate the A-, K-, L-, Q-, and R-types within the PC2' versus Slope component plane is extended to include the core of the S-complex, then it should be possible to separate those S-type asteroids whose compositions are more "olivine-rich" from those that are more "pyroxene-rich". To test this, we compare the SMASSII results with previous classifications of S-types provided by Chapman (1987), Gaffey *et al.* (1993a) and Howell *et al.* (1994).

The analysis by Chapman (1987) involved the combination of several different datasets, including broadband UBV colors, 24-color spectrophotometry (Chapman and Gaffey 1979), ECAS colors (Zellner *et al* 1985), and IRAS albedos (Veeder *et al.* 1989). Using the spectral parameters of BEND, DEPTH, and IR (Chapman and Gaffey 1979), together with albedo, Chapman classified the S-type asteroids as being either silicate-rich or silicate-poor (rich in metal or opaques). By estimating the position of the 1 μm band center and determining the IR parameter (infrared reflectance, defined as $r_{1.05}$ - $r_{0.73}$), many of the silicate-rich S-types were further classified as being either olivine-rich

or pyroxene-rich. In frame A of Figure 4.10, 46 asteroids observed during SMASSII that had been previously identified as olivine- or pyroxene-rich S-types by Chapman are plotted in the PC2' versus Slope component plane. This plot shows the olivine-rich (o) and pyroxene-rich (p) objects to be relatively well mixed in component space, with only a small indication of olivine-rich objects separating towards the lower-right corner in this plane (and similarly the pyroxene-rich objects show a slight tendency for plotting more towards the upper left).

Gaffey *et al.* (1993a) used the combined spectrophotometric data from ECAS, the 24-color survey, and the 52-color survey (Bell *et al.* 1988), providing spectral coverage over the wavelength interval of 0.32 to 2.5 μm. Using the spectral slope, positions of the 1 and 2 μm band centers, the depth of the 1 μm band, and the ratio of areas between the 2 μm and 1 μm bands, Gaffey *et al.* were able to estimate the olivine to pyroxene abundance ratios, as well as determine the Ca^{2+} and Fe^{2+} content of the pyroxenes (differentiating the clinopyroxenes and orthopyroxenes) for 39 S-type asteroids. Based on their findings, these S-type asteroids were grouped into seven classes, ranging from the olivine-rich S(I)-class to the most orthopyroxene-rich class, S(VII). In frame B of Figure 4.10, the Gaffey *et al.* classifications for 29 SMASSII asteroids have been plotted, though for clarity, the seven spectral classes, S(I) - S(VII) have been grouped into three broader categories: the olivine-rich classes, S(I) and S(II) are indicated by the label "o", the more clinopyroxene-rich classes S(III) - S(V) are labelled "c", and the orthopyroxene-rich classes S(VI) and S(VII) have been plotted with the letter "p". The clinopyroxene-rich objects are fairly well scattered over much of the plotted distribution, but there appears to be more of a separation between points representing the orthopyroxene-rich asteroids, which are concentrated toward the upper left, and those for the olivine-rich objects, which appear to plot mostly in the lower-right corner.

In the work of Howell *et al.* (1994), an artificial neural network was used to analyze the combined ECAS and 52-color datasets. In this analysis, Howell *et al.* found two end-member subclasses among the S-type asteroids that were interpreted as being compositionally distinct: the olivine-rich "So" class and the pyroxene-rich "Sp" class. Again, in frame C of Figure 4.10, the locations for 27 asteroids observed during SMASSII that had been at least partially classified as So- or Sp-types in the Howell taxonomy are plotted in the PC2' versus Slope plane. In this case, the tendency towards

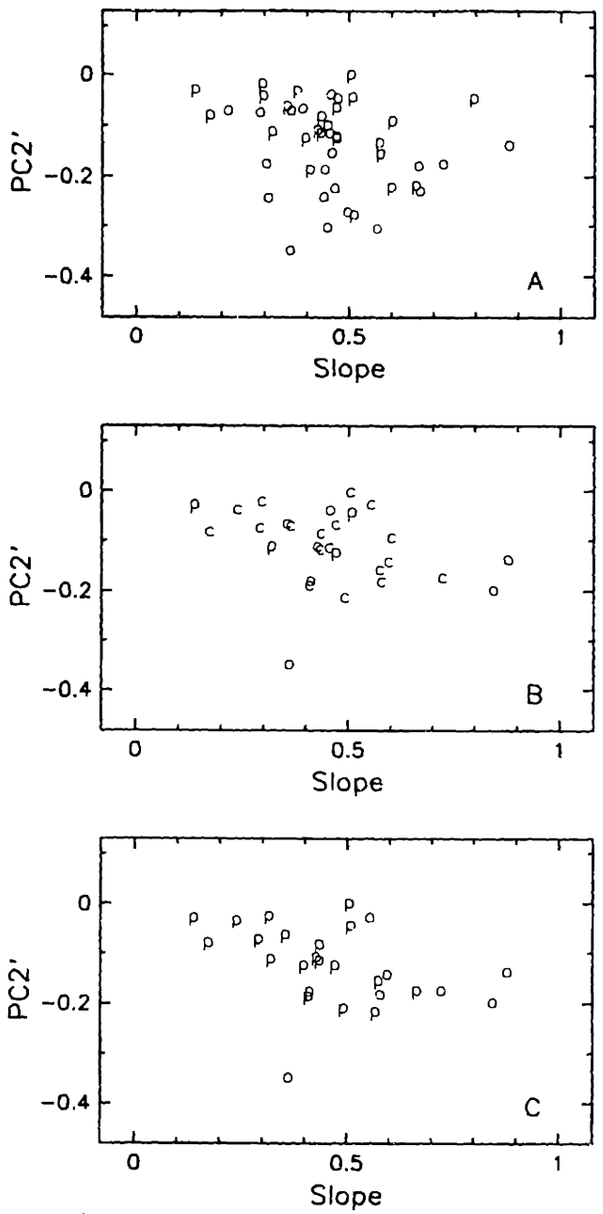

Figure 4.10: Comparing the subclassifications of S-types. In part A, asteroids that were classified by Chapman (1987), and which were observed during SMASSII, are plotted by their first two spectral components (Slope and PC2'). Only those objects for which Chapman used the "p" (pyroxene) or "o" (olivine) discriminators are shown. Similarly, in part B, asteroids classified by Gaffey *et al.* (1993) are shown. For clarity, objects classified by Gaffey *et al.* as types SI or SII (olivine-rich) are shown with the label "o", while objects in classes SVI or SVII (orthopyroxene-rich) are plotted as "p". Intermediate classes, SIII - SV (clinopyroxene-rich) are plotted as "c". In part C, those S-types classified by Howell *et al.* (1994) in the subclass Sp (pyroxene-rich) are plotted as "p", while So types (olivine-rich) are plotted with the label "o".

separation of asteroids classified as being either olivine-rich or pyroxene-rich by Howell *et al.* appears to be more substantial, with olivine-rich objects clearly tending to plot in the right half of our spectral component plane.

This increasing agreement between our spectral component analysis and previous classifications of S-type asteroids (seen in frame A-C in Figure 4.10) might be partially explained by the increased spectral coverage available to Gaffey *et al.* and Howell *et al.* with the addition of the 52-color data. However, the choice of spectral parameters and the analysis techniques used must also play a role. For example, a comparison of the Gaffey *et al.* classifications with those of Howell *et al.* shows some inconsistencies, even though roughly identical datasets, covering the same wavelength interval were used in the two analyses (Howell *et al.* 1994). The general agreement between our SMASSII results and the Howell *et al.* classifications might result from the use of analysis techniques (PCA and an artificial neural network, respectively) that account for all variations within the spectral data, rather than on discrete measurements of individual features or characteristics, as in those techniques used by Chapman (1987) and Gaffey *et al.* (1993a).

4.4.5 Secondary features in S-type spectra

In addition to the UV slope, shortward of 0.7 μm, and the 1 μm absorption feature, which are the primary spectral characteristics that distinguish the S-type asteroids, the SMASSII spectra also reveal other, much more subtle features in the spectra of S-type asteroids, primarily appearing as deviations in the UV slope. In Figure 4.11, four representative S-type spectra are plotted, showing two particular variations in the UV slope that are commonly seen in the SMASSII spectra. The first of these is a gentle to moderate deflection in the slope that can be described as an "angled" UV drop-off. This bend in the UV slope typically occurs at a wavelength of 0.53 μm, with the spectral interval shortward of 0.53 μm always appearing steeper, or redder in slope. This UV drop-off is due to charge transfer absorptions (Adams 1975), similar to the more rounded drop-offs seen in the spectra of C-type asteroids. The second of these features is even more subtle, and can usually be seen only in spectra with sufficiently high signal-to-noise ratios, or in the spline-fitted spectrum. This feature is usually noticed as a small bump, or deflection in the UV slope, located 0.58 to 0.59 μm. However, in the best examples of this feature, it is clear that this feature spans the interval from approximately 0.565 to

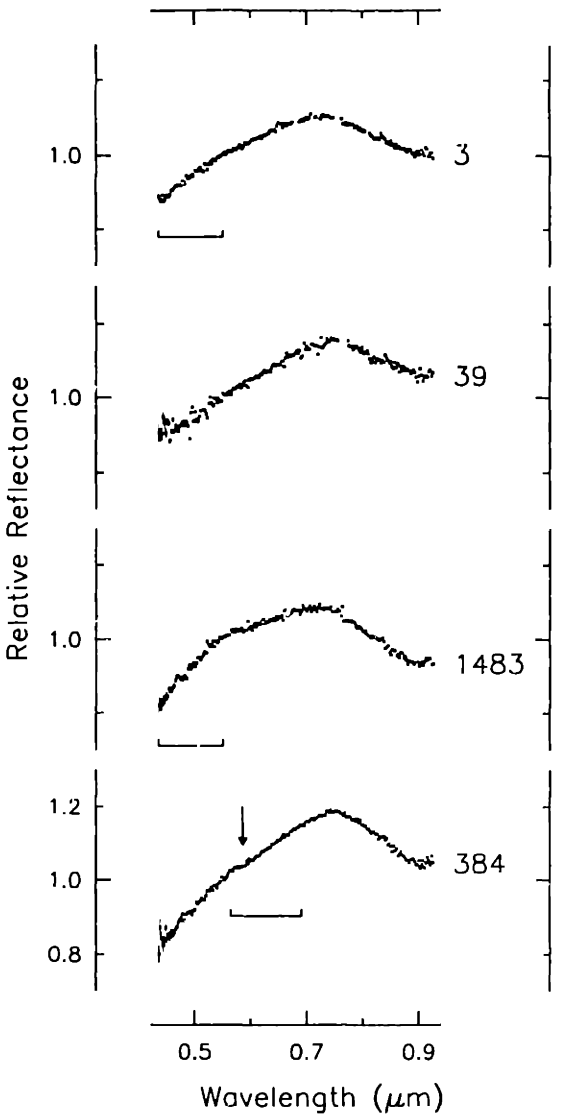

Figure 4.11: Four SMASSII spectra are shown, highlighting differences that are observed in the UV slope (shortward of 0.7 μm) among S-types. The spectrum of 3 Juno is representative of the most common S-type, where the spectrum shows a slight increase (reddening) of the UV slope shortward of 0.53 μm (as marked). A nearly linear or featureless UV slope, as seen in the spectrum of 39 Laetitia, is found to be much less common. In the case of 1483 Hakoila, the spectral slope over the interval shortward of 0.53 μm is very red. An example of a rather common, though subtle absorption feature is seen in the spectrum of 384 Burdigala. This feature (actually described as two absorption bands by Hiroi *et al.* 1996) spans the interval from approximately 0.565 to 0.69 μm (centered around 0.62 μm), though in the SMASSII spectra, this feature is usually best detected as an inflection in the UV slope at around 0.585 μm (marked with arrow).

0.69 μm. A feature similar to this is described by Cloutis *et al.* (1986) in laboratory mixtures of olivine and orthopyroxene. However, the specific nature of this band, centered at 0.65 μm was not determined. Hiroi *et al.* (1996) examined this feature in the spectra of 9 S-type asteroids, and found it to be the composite of two separate absorption bands, centered at roughly 0.60 and 0.67 μm. They interpret the presence of these minor bands as indicating the presence of either oxidized iron compounds or spinel-group minerals.

In our spectral component analysis of the SMASSII data, subtle, higher-order features such as the 0.60 and 0.67 μm bands are easily lost in the total variance that is contributed by the entire dataset. However, this does not preclude us from separately analyzing a subset of the SMASSII data, with the goal of better isolating these features using multivariate techniques. The spectra of all 476 asteroids making up the core of the S-complex (the S-, Sa-, Sk-, Sl-, Sq-, and Sr-types) were reanalyzed, using only those wavelength channels covering the UV slope, from 0.44 to 0.70 μm. As in our original analysis of the SMASSII data, an average slope, γ, was first determined for the spectral interval of 0.44 to 0.70 μm by fitting a line to the spline-fitted channels, where this line is constrained to have a value of 1.0 at 0.55 μm, as given by Eqn. 3.3. The fitted spectrum is then divided by this line, producing a residual spectrum whose mean value, averaged over all channels from 0.44 to 0.70 μm, is roughly 1.0. These residual spectra were then analyzed using PCA. The first three spectral components resulting from this new analysis are called $Slope_{(S1)}$, $PC2'_{(S1)}$, and $PC3'_{(S1)}$, where the subscript $_{(S1)}$ identifies these components as pertaining to this special treatment of the UV slope in S-type spectra, and are listed in Table 4.2. For convenience, I refer to these new components, calculated based on subsets of the SMASSII data, as secondary components.

The secondary component plane of $PC3'_{(S1)}$ versus $PC2'_{(S1)}$ is plotted in Figure 4.12, showing the locations for all 476 asteroids making up the core of the S-complex. Because these components were calculated specifically to isolate subtle features in the UV slopes of the S-type asteroids, trends in the spectral components can be empirically identified that correspond to variations in the strengths of these features. In Figure 4.12, these trends are marked with arrows, indicating the directions of increasing strength for the angled UV drop-off, which is most closely correlated with component $PC2'_{(S1)}$, and for the 0.62 μm band (identified as the combined 0.60 and 0.67 μm bands by Hiroi *et al.*

Table 4.2: Secondary spectral components for S-types

Asteroid	Type	Spectral components					Asteroid	Type	Spectral components				
		Slope (S1)	PC2' (S1)	PC3' (S1)	PC2' (S2)	PC3' (S2)			Slope (S1)	PC2' (S1)	PC3' (S1)	PC2' (S2)	PC3' (S2)
3	Sk	0.855	0.0182	-0.0019	0.0508	0.0115	198	S	1.001	0.0571	0.0248	0.0225	-0.0014
5	S	1.096	0.0154	-0.0017	-0.0004	-0.0027	208	Sk	1.078	0.0257	0.0062	0.0215	-0.0033
6	S	1.153	0.0394	0.0032	0.0369	0.0038	226	S	1.029	0.0349	0.0078	0.0258	-0.0046
7	S	1.167	0.0078	0.0022	0.0164	0.0049	230	Sl	1.431	0.0558	0.0102	0.0378	0.0037
11	Sk	0.861	0.0166	-0.0145	0.0484	0.0042	237	S	1.375	-0.0196	0.0046	0.0047	-0.0096
14	S	0.930	0.0188	0.0093	0.0409	-0.0129	243	S	1.073	0.0260	-0.0046	0.0172	-0.0020
15	S	0.971	0.0132	0.0035	0.0366	-0.0076	244	Sa	1.742	-0.0111	-0.0344	-0.0248	0.0044
17	Sl	1.323	0.0175	-0.0035	0.0348	-0.0018	245	S	1.288	0.0344	0.0063	0.0046	0.0059
18	S	1.159	0.0045	-0.0032	0.0448	0.0040	263	S	1.253	-0.0140	0.0016	0.0288	-0.0185
20	S	0.984	0.0349	0.0086	0.0088	-0.0041	264	S	1.057	0.0650	0.0111	0.0012	-0.0129
25	S	1.392	0.0229	0.0105	-0.0230	-0.0091	278	S	1.202	-0.0328	-0.0029	0.0038	-0.0106
26	S	1.222	0.0036	0.0098	-0.0037	0.0082	281	S	1.421	-0.0246	-0.0127	0.0048	0.0059
28	S	1.305	-0.0116	-0.0090	0.0249	0.0046	288	S	1.406	-0.0243	0.0015	-0.0026	-0.0311
29	S	1.047	0.0244	0.0211	0.0461	0.0010	295	S	1.249	0.0204	0.0039	0.0047	0.0129
30	Sl	1.400	0.0286	0.0034	0.0321	0.0137	306	S	1.461	-0.0159	-0.0069	-0.0311	-0.0134
32	S	1.131	0.0168	-0.0013	0.0168	-0.0036	310	S	1.322	-0.0559	-0.0005	0.0426	0.0244
33	Sq	0.769	0.0274	0.0099	0.0124	-0.0098	312	Sk	0.995	0.0267	0.0241	-0.0151	-0.0131
37	S	1.343	0.0205	-0.0036	0.0326	0.0046	321	S	1.067	0.0243	-0.0036	0.0256	0.0000
39	S	1.007	0.0906	0.0269	0.0243	-0.0004	327	Sl	1.495	-0.0167	0.0012	-0.0017	0.0137
40	S	1.179	0.0424	0.0038	0.0125	0.0028	346	S	1.065	-0.0143	-0.0153	0.0320	0.0046
43	Sk	0.929	-0.0044	0.0051	0.0291	0.0045	352	Sl	1.548	-0.0163	0.0075	0.0029	0.0006
57	S	1.077	0.0416	0.0078	0.0297	-0.0077	353	S	1.356	-0.0006	-0.0020	0.0097	0.0027
60	S	1.341	0.0038	0.0118	-0.0133	0.0050	354	Sl	1.748	0.0162	0.0134	-0.0037	0.0291
61	S	1.263	0.0077	0.0053	0.0152	-0.0249	355	S	1.502	-0.0024	0.0035	-0.0207	0.0111
63	Sa	1.781	0.0605	0.0035	-0.0013	0.0032	371	S	1.344	-0.0016	0.0042	0.0010	-0.0059
67	S	1.190	-0.0065	-0.0030	0.0021	-0.0210	374	S	1.226	-0.0060	0.0007	-0.0115	-0.0069
80	S	1.373	0.0049	0.0066	0.0093	0.0186	378	S	1.249	-0.0056	0.0204	-0.0011	-0.0158
82	Sq	0.592	0.1098	0.0220	0.0088	-0.0114	384	S	1.295	-0.0076	0.0101	-0.0016	-0.0073
100	S	1.160	0.0047	-0.0018	0.0395	-0.0150	389	S	0.967	0.0277	0.0001	0.0326	-0.0003
101	S	1.449	-0.0093	-0.0118	0.0108	0.0062	391	S	1.324	-0.0084	-0.0017	0.0074	-0.0267
103	S	1.375	-0.0043	-0.0037	-0.0047	-0.0283	394	S	1.076	0.0026	0.0075	0.0150	-0.0202
108	Sl	1.502	-0.0231	-0.0102	-0.0006	-0.0216	405	S	1.132	-0.0214	0.0030	0.0174	0.0064
113	S	1.528	-0.0664	0.0169	-0.0543	0.0148	416	Sl	1.454	0.0503	0.0163	0.0288	-0.0191
115	S	1.396	0.0392	0.0026	0.0121	0.0076	432	S	1.444	0.0334	0.0058	-0.0056	-0.0057
116	Sk	0.856	0.0309	0.0040	0.0248	0.0028	443	Sl	1.532	0.1063	0.0239	-0.0045	0.0050
118	S	1.210	0.0167	0.0208	-0.0003	-0.0042	453	S	1.544	-0.0388	-0.0123	0.0001	0.0083
119	Sl	1.585	-0.0083	-0.0031	-0.0134	0.0032	456	S	1.367	-0.0189	0.0079	-0.0172	0.0132
123	S	1.398	0.0374	0.0018	0.0055	-0.0023	462	S	1.079	-0.0129	0.0076	0.0398	0.0036
124	S	1.289	0.0124	-0.0028	0.0240	0.0106	470	S	1.333	0.0313	0.0024	0.0053	-0.0026
148	S	1.288	-0.0174	-0.0090	0.0183	-0.0050	471	S	0.972	0.0180	0.0113	0.0234	0.0058
151	Sl	1.613	-0.0262	-0.0128	0.0167	0.0040	477	S	1.423	-0.0111	0.0044	0.0045	0.0029
158	S	1.086	0.0013	0.0016	0.0017	-0.0111	484	S	1.306	-0.0367	-0.0092	0.0236	-0.0037
167	Sk	0.799	0.0317	0.0122	0.0479	-0.0025	485	S	0.967	0.0372	0.0174	0.0183	-0.0103
169	Sl	1.456	0.0245	0.0061	0.0050	-0.0004	496	S	1.609	-0.0020	-0.0008	-0.0394	-0.0187
174	S	1.326	-0.0278	-0.0121	-0.0086	-0.0293	509	S	1.199	0.0062	-0.0014	0.0161	-0.0143
179	Sk	0.836	0.0705	0.0077	0.0264	-0.0055	512	S	1.486	0.0040	-0.0085	-0.0185	0.0083
183	S	1.108	-0.0320	-0.0039	-0.0023	-0.0038	519	S	1.110	0.0241	0.0235	0.0301	0.0104
188	S	1.405	-0.0173	0.0055	0.0070	-0.0038	532	S	1.059	0.0594	0.0168	0.0259	-0.0026
192	Sl	1.587	0.0209	0.0017	0.0097	0.0058	533	S	1.164	0.0053	0.0117	0.0149	-0.0157
193	Sk	0.762	0.0240	0.0130	0.0412	0.0012	534	Sk	0.970	0.0061	0.0067	0.0230	0.0051
196	S	0.971	0.0352	0.0095	0.0236	-0.0004	553	S	1.564	-0.0303	-0.0027	-0.0311	0.0008
197	S	1.407	-0.0419	-0.0099	-0.0167	0.0028	556	S	0.888	0.0907	0.0192	0.0359	0.0031

Table 4.2: Secondary spectral components for S-types

Asteroid	Type	Spectral components					Asteroid	Type	Spectral components				
		Slope (S1)	PC2' (S1)	PC3' (S1)	PC2' (S2)	PC3' (S2)			Slope (S1)	PC2' (S1)	PC3' (S1)	PC2' (S2)	PC3' (S2)
563	Sl	1.632	-0.0037	-0.0076	0.0151	0.0083	1134	S	1.212	-0.0011	-0.0158	0.0213	-0.0126
571	S	1.220	0.0270	0.0013	-0.0137	-0.0073	1139	S	1.625	-0.0015	-0.0128	-0.0277	0.0195
584	Sl	1.557	-0.0033	0.0011	-0.0113	-0.0001	1140	S	1.361	0.0007	0.0021	-0.0025	0.0036
597	S	1.040	0.0231	0.0129	0.0001	-0.0026	1147	S	1.663	-0.0528	-0.0093	0.0036	0.0080
600	S	1.248	0.0156	0.0091	-0.0135	0.0008	1152	Sl	1.692	-0.0422	-0.0148	0.0025	-0.0064
622	S	1.247	-0.0082	0.0050	0.0091	-0.0047	1165	S	1.471	-0.0125	-0.0009	-0.0240	0.0073
625	Sa	1.900	0.0592	-0.0129	-0.0004	0.0063	1186	Sk	0.707	-0.0244	-0.0159	0.0578	0.0189
631	S	1.335	-0.0131	0.0050	-0.0110	-0.0062	1188	S	1.528	-0.0198	0.0018	-0.0075	-0.0041
633	S	1.352	0.1019	-0.0358	0.0533	0.0147	1204	S	1.239	0.0243	-0.0007	0.0241	0.0082
649	Sk	1.017	0.0082	0.0101	-0.0049	-0.0085	1228	S	1.345	-0.0168	0.0077	-0.0349	-0.0102
670	S	1.024	0.0065	0.0158	0.0073	-0.0088	1248	S	1.398	0.0209	-0.0040	-0.0095	0.0070
673	S	1.190	0.0415	-0.0169	0.0604	0.0133	1252	S	1.448	0.0335	-0.0121	-0.0114	-0.0152
675	S	1.102	0.0013	-0.0012	0.0301	0.0085	1272	Sl	1.687	-0.0115	-0.0033	0.0098	0.0278
677	Sl	1.539	-0.0167	0.0042	0.0270	-0.0209	1278	S	1.406	-0.0178	-0.0055	0.0056	-0.0269
699	Sk	0.825	0.0038	0.0097	0.0184	-0.0012	1293	Sq	1.209	-0.0128	0.0112	-0.0428	-0.0122
716	S	1.302	0.0443	-0.0189	0.0041	-0.0149	1316	Sr	1.454	-0.0677	-0.0109	-0.0278	-0.0210
720	Sq	0.806	-0.0081	-0.0014	0.0323	0.0044	1324	Sq	0.717	0.0151	0.0340	0.0093	0.0275
737	S	1.358	-0.0242	0.0043	0.0132	-0.0046	1329	S	1.503	-0.0110	-0.0058	0.0005	0.0121
749	S	1.365	-0.0297	0.0037	0.0150	0.0062	1336	S	1.426	-0.0134	-0.0305	0.0022	-0.0025
782	S	1.374	0.0569	-0.0119	0.0169	0.0112	1348	Sl	1.730	0.0415	-0.0177	0.0167	0.0022
793	S	1.231	-0.0091	0.0027	-0.0121	-0.0103	1350	Sa	1.950	-0.1643	0.0060	-0.0281	-0.0052
797	S	1.366	0.0057	-0.0093	0.0098	0.0011	1374	Sq	1.080	-0.0532	0.0123	-0.0066	0.0039
808	Sk	1.002	0.0347	0.0099	-0.0128	-0.0106	1385	S	1.457	-0.0277	-0.0093	0.0063	-0.0113
819	S	1.407	-0.0468	-0.0013	-0.0057	0.0032	1423	S	1.148	0.0367	0.0316	0.0065	0.0027
825	S	1.656	-0.0421	-0.0032	-0.0421	-0.0007	1433	S	1.199	-0.0326	-0.0159	-0.0020	0.0071
847	S	1.328	-0.0048	0.0036	-0.0137	0.0006	1458	S	1.654	-0.0478	-0.0183	-0.0109	0.0143
862	S	1.167	-0.0430	0.0030	-0.0211	-0.0309	1480	S	1.081	-0.0211	-0.0043	0.0327	0.0070
870	S	1.650	-0.0167	0.0079	-0.0198	0.0056	1483	Sq	0.893	-0.1045	0.0079	0.0172	0.0132
897	Sl	1.377	-0.0279	-0.0063	0.0467	-0.0128	1494	Sr	1.842	0.0036	0.0128	-0.0311	0.0056
898	Sl	1.529	0.0288	-0.0014	0.0203	-0.0054	1549	S	1.564	-0.0182	0.0005	-0.0283	-0.0129
913	Sa	1.734	-0.0462	-0.0126	-0.0226	0.0059	1550	S	1.273	-0.0078	-0.0020	0.0019	0.0090
929	S	1.642	0.0009	-0.0203	-0.0150	0.0042	1553	S	1.399	-0.0288	-0.0257	-0.0013	-0.0028
950	Sa	1.982	-0.0356	-0.0369	-0.0010	0.0015	1562	S	1.619	-0.0057	-0.0078	-0.0154	0.0063
951	S	1.380	-0.0351	0.0035	-0.0069	-0.0064	1563	Sa	1.785	-0.0325	-0.0110	-0.0281	0.0137
970	S	1.092	-0.0134	-0.0028	-0.0041	0.0093	1565	Sq	1.017	-0.0892	-0.0010	-0.0183	-0.0168
984	Sr	1.879	-0.0004	0.0184	-0.0770	0.0311	1587	Sa	1.904	-0.0086	-0.0084	-0.0334	0.0077
985	S	1.502	0.0404	-0.0135	-0.0029	-0.0014	1593	S	1.749	0.0194	0.0065	-0.0346	0.0300
994	S	1.084	0.0516	-0.0073	0.0414	-0.0010	1594	S	1.254	0.0200	0.0156	-0.0003	0.0019
1011	Sr	1.958	-0.0974	0.0122	-0.0205	-0.0043	1601	Sl	1.576	0.0691	0.0076	-0.0241	-0.0089
1016	S	1.320	-0.0253	-0.0085	-0.0294	-0.0067	1618	S	1.173	0.0348	-0.0060	0.0202	0.0036
1020	S	1.461	0.0360	-0.0208	0.0061	-0.0018	1629	S	1.532	-0.0377	-0.0009	-0.0155	0.0033
1052	S	1.375	-0.0340	-0.0115	0.0012	0.0078	1634	Sr	1.154	0.0489	0.0149	-0.0139	0.0239
1055	S	1.228	-0.0210	0.0078	-0.0067	-0.0058	1635	S	1.012	0.0243	-0.0132	0.0417	-0.0085
1056	S	1.425	0.0000	-0.0029	0.0058	0.0012	1640	S	1.162	0.0343	0.0131	0.0240	0.0110
1058	S	1.400	0.0114	0.0072	-0.0088	0.0084	1642	S	1.633	-0.0303	0.0214	-0.0168	-0.0325
1065	S	1.552	0.0713	0.0047	-0.0187	-0.0035	1659	S	0.965	0.0729	0.0192	0.0471	-0.0225
1069	S	1.332	0.0474	0.0132	0.0021	-0.0114	1660	S	1.200	0.0163	0.0021	0.0037	-0.0058
1088	S	1.364	-0.0262	-0.0093	-0.0011	-0.0065	1662	Sr	1.783	-0.0171	0.0275	-0.0341	-0.0032
1102	S	1.340	0.0229	0.0053	-0.0007	-0.0275	1664	S	1.446	-0.0174	-0.0012	-0.0082	-0.0108
1106	S	1.097	0.0464	-0.0092	0.0473	0.0083	1667	Sa	1.913	0.0234	-0.0060	-0.0153	-0.0013
1110	S	1.320	-0.0083	-0.0001	-0.0034	0.0133	1680	S	1.317	0.0335	0.0210	-0.0128	-0.0035
1131	S	1.624	0.0563	0.0051	-0.0144	0.0166	1738	S	1.244	-0.0111	0.0002	0.0213	0.0002

Table 4.2: Secondary spectral components for S-types

Asteroid	Type	Spectral components					Asteroid	Type	Spectral components				
		Slope (S1)	PC2' (S1)	PC3' (S1)	PC2' (S2)	PC3' (S2)			Slope (S1)	PC2' (S1)	PC3' (S1)	PC2' (S2)	PC3' (S2)
1751	S	1.434	-0.0207	0.0011	0.0190	0.0018	2467	Sl	1.672	-0.0100	-0.0077	-0.0268	0.0051
1777	Sq	1.076	-0.0128	-0.0011	0.0035	-0.0145	2478	S	1.266	-0.0187	0.0108	0.0020	0.0008
1785	Sk	1.096	0.0454	0.0202	0.0144	0.0112	2482	S	1.146	-0.0027	-0.0026	0.0073	0.0046
1798	S	1.523	-0.0483	-0.0047	-0.0108	0.0059	2493	S	1.364	0.0779	-0.0243	0.0100	0.0127
1807	S	1.152	0.0536	-0.0032	0.0145	0.0125	2504	Sk	0.908	-0.0055	-0.0041	0.0241	-0.0031
1830	S	1.379	-0.0419	0.0017	-0.0326	-0.0091	2521	S	1.176	-0.0224	-0.0356	0.0171	0.0013
1831	S	1.564	-0.0408	0.0016	-0.0101	0.0165	2575	Sr	1.753	-0.0203	-0.0291	-0.0589	0.0155
1839	S	1.335	-0.0404	0.0221	-0.0067	-0.0363	2604	Sa	2.218	-0.0465	-0.0444	-0.0749	-0.0029
1848	S	1.788	-0.0744	0.0221	0.0099	-0.0103	2625	S	1.435	-0.0182	-0.0029	-0.0037	0.0078
1856	S	1.421	-0.0253	-0.0025	0.0022	-0.0037	2631	S	1.313	0.0305	0.0212	-0.0005	-0.0116
1857	S	1.379	-0.0292	0.0021	-0.0119	0.0043	2635	S	1.552	-0.0746	-0.0089	-0.0320	-0.0135
1888	S	1.239	0.0408	0.0002	-0.0124	0.0075	2703	S	1.039	0.0235	0.0039	-0.0003	-0.0133
1948	S	1.113	0.0634	0.0036	0.0155	0.0025	2709	S	1.331	0.0276	0.0076	-0.0142	0.0054
1968	S	1.243	-0.0123	-0.0040	-0.0031	-0.0176	2737	S	1.374	-0.0221	-0.0068	-0.0066	-0.0004
1977	Sk	0.663	0.0867	-0.0253	0.0624	0.0010	2744	S	1.387	-0.0504	-0.0052	-0.0335	0.0014
2019	S	1.288	0.0271	0.0236	0.0151	0.0052	2746	Sr	1.367	-0.0382	0.0015	-0.0420	-0.0035
2022	S	1.579	-0.0528	0.0046	-0.0259	0.0094	2748	S	0.945	0.0651	0.0047	0.0303	-0.0124
2038	Sa	1.998	0.0827	-0.0301	0.0148	-0.0067	2750	S	1.196	-0.0549	0.0221	-0.0058	-0.0072
2042	Sq	1.180	-0.0144	-0.0010	0.0111	-0.0020	2754	Sa	1.859	-0.0262	-0.0068	-0.0213	0.0017
2053	S	1.245	0.0636	0.0302	-0.0242	0.0213	2789	S	1.161	-0.0139	-0.0031	0.0150	-0.0202
2056	S	1.379	-0.0200	-0.0063	-0.0173	-0.0063	2801	S	1.499	0.0089	-0.0177	0.0029	0.0077
2078	Sk	0.958	-0.0038	-0.0027	0.0060	-0.0049	2818	S	1.726	0.0044	-0.0114	-0.0265	0.0000
2088	S	1.536	0.0442	-0.0182	-0.0538	0.0054	2834	S	1.468	0.0561	0.0135	-0.0236	-0.0102
2089	Sq	0.975	0.0037	-0.0113	0.0047	-0.0072	2855	Sl	1.647	0.0476	-0.0055	0.0573	-0.0011
2107	S	1.615	0.0408	0.0017	-0.0108	0.0044	2873	S	1.276	-0.0174	-0.0029	-0.0072	-0.0032
2118	S	1.081	0.0279	0.0044	0.0014	-0.0017	2874	S	1.474	-0.0287	-0.0033	-0.0100	0.0008
2131	S	1.195	0.0097	0.0127	0.0283	-0.0031	2875	S	1.538	-0.0116	0.0068	0.0118	0.0062
2141	Sl	1.510	-0.0073	-0.0141	0.0171	-0.0110	2881	S	1.123	0.0339	-0.0156	-0.0140	0.0093
2157	S	1.495	0.0515	-0.0311	0.0156	0.0000	2902	Sq	1.269	-0.0107	0.0086	-0.0398	0.0061
2167	S	1.532	-0.0317	0.0106	-0.0059	-0.0016	2905	S	1.085	0.0505	0.0053	0.0392	0.0162
2185	S	1.436	-0.0350	-0.0107	0.0038	0.0130	2911	S	1.496	0.0604	-0.0117	0.0024	0.0066
2189	S	1.242	-0.0289	0.0122	-0.0052	-0.0079	2917	S	1.304	-0.0273	0.0107	-0.0199	0.0119
2268	S	1.259	0.0171	-0.0107	-0.0066	-0.0049	2949	S	1.164	-0.0470	-0.0018	-0.0017	-0.0001
2280	Sa	1.855	-0.0329	-0.0106	-0.0369	0.0292	2953	S	1.366	-0.0148	0.0005	0.0002	-0.0032
2282	S	1.190	-0.0290	0.0006	0.0247	0.0016	2955	S	1.572	-0.0162	-0.0095	-0.0146	0.0143
2305	S	1.389	-0.0219	0.0013	0.0016	0.0048	2956	Sr	1.516	-0.0578	-0.0134	-0.0520	-0.0058
2308	S	1.416	-0.1273	-0.0029	0.0310	0.0192	2977	S	1.356	0.0198	-0.0162	0.0157	0.0154
2317	S	1.426	-0.0317	0.0086	0.0128	0.0104	2988	S	1.653	0.0014	-0.0067	-0.0395	0.0131
2335	Sa	1.916	0.0373	-0.0002	-0.0342	0.0024	3020	Sl	1.673	-0.0275	-0.0083	0.0177	0.0096
2353	S	1.207	-0.0088	0.0077	0.0233	-0.0021	3040	S	1.730	0.0399	0.0005	-0.0197	0.0171
2369	S	1.194	0.0374	0.0197	0.0326	0.0048	3060	S	1.630	-0.0165	-0.0034	-0.0693	-0.0178
2373	S	1.103	-0.0101	0.0172	0.0012	-0.0214	3121	S	1.154	0.0367	0.0109	0.0222	0.0036
2386	S	1.334	0.0146	0.0004	0.0147	0.0111	3151	S	1.343	0.0137	-0.0207	0.0059	0.0036
2396	Sa	1.810	0.0589	-0.0033	-0.0119	-0.0020	3170	S	1.108	-0.0376	0.0238	-0.0039	0.0000
2401	S	1.234	0.0270	-0.0071	-0.0126	-0.0163	3181	S	1.379	-0.0256	0.0105	-0.0187	0.0008
2402	Sl	1.746	-0.0778	-0.0089	-0.0128	0.0137	3209	S	1.321	0.0119	0.0109	0.0087	-0.0141
2409	S	1.307	0.0415	0.0076	-0.0005	0.0048	3216	S	1.376	0.0891	-0.0137	0.0260	0.0100
2410	S	1.582	0.0014	0.0140	0.0016	0.0130	3255	S	1.148	-0.0014	0.0108	-0.0224	-0.0037
2427	Sk	0.838	0.0535	-0.0014	0.0168	-0.0068	3258	S	1.560	0.0245	-0.0022	-0.0073	-0.0029
2430	Sl	1.548	0.0781	-0.0229	0.0170	0.0098	3306	S	1.282	0.0181	0.0085	-0.0057	0.0222
2438	S	1.552	-0.0514	0.0130	-0.0211	-0.0039	3309	S	1.516	0.0062	-0.0144	0.0045	0.0015
2451	S	1.326	-0.0120	-0.0065	0.0261	0.0030	3314	S	1.430	-0.0044	0.0041	-0.0258	-0.0099

Table 4.2: Secondary spectral components for S-types

Asteroid	Type	Spectral components					Asteroid	Type	Spectral components				
		Slope (S1)	PC2' (S1)	PC3' (S1)	PC2' (S2)	PC3' (S2)			Slope (S1)	PC2' (S1)	PC3' (S1)	PC2' (S2)	PC3' (S2)
3340	S	1.223	0.0563	-0.0170	0.0115	0.0027	4116	Sl	1.528	0.0963	-0.0065	0.0209	-0.0013
3363	Sq	0.988	-0.0139	-0.0009	-0.0149	-0.0195	4182	Sr	1.259	-0.0206	0.0111	-0.0135	-0.0117
3364	S	1.402	-0.0046	-0.0116	0.0096	0.0073	4200	S	1.221	-0.0247	-0.0003	0.0173	0.0010
3371	Sr	1.066	-0.0038	0.0088	-0.0345	-0.0127	4222	S	1.346	-0.0563	-0.0067	-0.0131	0.0114
3376	Sq	1.053	0.0357	0.0013	-0.0786	-0.0306	4261	Sq	0.725	0.0260	0.0098	0.0188	-0.0115
3385	S	1.489	-0.0456	0.0047	-0.0267	-0.0001	4287	S	1.541	-0.0703	-0.0012	0.0230	-0.0060
3394	S	1.206	0.0007	0.0032	0.0016	0.0119	4299	S	1.478	-0.0404	0.0019	-0.0112	0.0098
3395	Sr	1.264	-0.0399	-0.0043	-0.0196	-0.0169	4305	S	1.202	0.0324	-0.0064	0.0186	0.0113
3401	S	1.194	0.0289	0.0056	0.0107	-0.0014	4327	Sk	0.890	0.0608	-0.0066	0.0369	-0.0106
3416	Sa	2.092	0.0237	0.0099	-0.0218	0.0327	4340	S	1.167	-0.0117	0.0019	0.0017	-0.0026
3417	S	1.290	0.0161	-0.0006	-0.0047	0.0000	4352	S	1.382	-0.0372	-0.0024	-0.0061	0.0032
3430	Sk	1.024	-0.0096	-0.0040	0.0022	-0.0090	4372	S	1.150	-0.1235	0.0235	0.0476	-0.0322
3474	Sa	1.738	-0.0045	-0.0034	-0.0049	-0.0056	4374	S	1.332	0.0043	0.0105	-0.0114	-0.0110
3491	Sq	1.032	-0.0541	0.0066	0.0010	0.0223	4382	Sa	1.914	0.0430	-0.0044	-0.0312	0.0089
3493	S	1.738	0.0058	-0.0038	-0.0386	0.0054	4407	Sa	1.859	-0.0357	0.0119	-0.0046	0.0163
3511	S	1.495	-0.0450	-0.0082	-0.0252	0.0055	4417	S	1.695	0.0606	-0.0157	-0.0169	0.0012
3534	S	1.443	-0.0406	-0.0026	-0.0029	0.0024	4422	S	1.342	-0.0211	-0.0028	0.0080	0.0010
3545	Sa	1.783	0.0422	-0.0030	-0.0136	0.0080	4435	S	1.330	-0.0165	0.0036	-0.0285	-0.0105
3546	Sa	1.747	0.0007	-0.0075	-0.0084	0.0005	4479	S	1.507	-0.0538	0.0096	-0.0233	0.0107
3592	S	1.210	0.0065	0.0049	0.0300	-0.0019	4512	Sa	1.881	-0.0537	0.0006	-0.0133	0.0189
3635	S	1.290	0.0754	-0.0029	-0.0254	-0.0001	4516	Sa	1.815	0.0242	-0.0180	0.0146	0.0133
3636	S	1.293	-0.0366	0.0112	-0.0179	0.0080	4536	S	1.344	-0.0066	-0.0107	0.0000	-0.0047
3640	S	1.336	-0.0059	0.0047	0.0060	0.0069	4558	S	1.204	0.0114	0.0067	-0.0162	-0.0122
3669	S	1.302	-0.0252	-0.0025	0.0003	0.0037	4570	Sa	1.890	-0.0453	-0.0054	0.0119	0.0108
3674	Sk	0.942	0.0097	0.0013	0.0022	-0.0228	4611	S	1.587	-0.0312	0.0021	-0.0425	0.0140
3678	S	1.306	0.0015	-0.0074	-0.0233	-0.0008	4628	S	1.487	-0.0202	-0.0045	-0.0099	0.0099
3700	Sk	1.006	0.0025	0.0146	0.0026	-0.0191	4649	S	1.490	-0.0098	0.0054	-0.0512	0.0117
3701	S	1.355	0.0121	-0.0104	0.0004	0.0053	4702	S	1.032	0.0396	0.0154	0.0277	0.0212
3712	S	1.258	0.0315	0.0028	0.0215	-0.0008	4733	Sq	0.933	0.0364	0.0079	-0.0106	0.0285
3767	Sa	1.885	-0.0176	-0.0219	-0.0012	0.0085	4748	S	1.581	-0.0714	-0.0100	-0.0501	0.0120
3788	S	1.461	0.0244	-0.0323	0.0284	0.0117	4767	S	1.401	-0.0266	-0.0047	0.0108	0.0109
3792	S	1.191	-0.0083	0.0331	-0.0299	-0.0054	4774	S	1.249	0.0483	0.0134	0.0076	0.0047
3800	S	1.755	-0.0039	0.0002	-0.0274	0.0175	4824	Sr	1.070	0.0632	0.0067	-0.0883	-0.0361
3809	S	1.268	0.0166	0.0078	-0.0065	-0.0122	4844	S	1.480	0.0073	0.0019	-0.0233	-0.0015
3813	S	1.080	0.0262	0.0213	0.0271	0.0175	4853	S	1.103	0.0117	-0.0026	0.0252	-0.0058
3819	Sr	1.578	-0.1018	0.0387	-0.0955	0.0083	4884	S	1.344	-0.0286	-0.0068	0.0047	0.0119
3831	S	1.533	-0.0031	-0.0268	0.0216	0.0022	4910	S	1.612	0.0524	-0.0243	0.0027	0.0106
3853	S	1.049	-0.0229	-0.0033	0.0162	-0.0015	4923	S	1.319	0.0045	0.0020	-0.0201	-0.0241
3858	Sa	2.179	-0.1380	-0.0010	-0.0543	-0.0092	4945	S	1.754	0.0251	0.0298	-0.0072	-0.0155
3860	S	1.475	0.0921	-0.0400	0.0076	0.0053	4950	Sk	1.057	0.0535	0.0036	-0.0137	-0.0006
3861	S	1.192	0.0027	0.0133	0.0174	0.0038	4951	S	1.573	-0.0260	0.0060	-0.0360	0.0078
3862	S	1.510	0.0327	-0.0099	0.0047	-0.0022	4968	Sq	0.956	-0.0097	-0.0074	0.0043	-0.0094
3903	Sq	0.912	0.0083	-0.0104	0.0098	-0.0087	4995	S	1.106	-0.0098	0.0152	-0.0073	-0.0018
3910	S	1.502	-0.0506	-0.0186	-0.0088	0.0066	5008	S	1.322	0.0180	-0.0201	0.0193	0.0152
3920	Sa	1.960	0.0066	-0.0102	-0.0312	0.0329	5010	S	1.089	0.0053	0.0011	-0.0158	-0.0168
3949	Sq	1.128	-0.0049	0.0001	-0.0133	0.0035	5013	Sl	1.563	-0.0202	-0.0116	-0.0011	-0.0013
3972	S	1.179	0.0389	-0.0115	-0.0105	-0.0009	5038	S	1.258	-0.0012	-0.0008	0.0196	-0.0032
4001	S	1.074	-0.0005	-0.0082	0.0165	-0.0078	5069	S	1.440	-0.0125	-0.0003	-0.0133	-0.0050
4037	Sk	1.144	-0.0211	-0.0093	-0.0021	0.0096	5134	Sl	1.631	-0.0087	-0.0042	0.0078	0.0098
4039	S	1.555	-0.0435	-0.0095	-0.0629	-0.0012	5142	Sq	1.048	0.0181	0.0255	-0.0011	-0.0034
4051	Sq	0.636	0.0589	0.0216	0.0001	-0.0074	5159	S	1.464	0.0052	-0.0126	0.0012	0.0145
4096	Sl	1.698	0.1086	-0.0142	-0.0121	0.0038	5195	Sa	1.733	-0.0235	-0.0067	-0.0188	0.0113

Table 4.2: Secondary spectral components for S-types

Asteroid	Type	Spectral components					Asteroid	Type	Spectral components				
		Slope (S1)	PC2' (S1)	PC3' (S1)	PC2' (S2)	PC3' (S2)			Slope (S1)	PC2' (S1)	PC3' (S1)	PC2' (S2)	PC3' (S2)
5196	S	1.354	-0.0190	-0.0106	0.0022	-0.0137	6086	Sl	1.647	-0.0029	0.0004	0.0058	0.0119
5208	S	0.960	-0.0212	-0.0031	0.0217	-0.0043	6146	Sq	1.121	-0.0078	-0.0089	0.0086	-0.0056
5214	S	1.190	-0.0072	-0.0065	-0.0052	0.0055	6192	S	1.467	-0.0175	-0.0198	-0.0317	0.0120
5242	Sq	0.930	0.0177	-0.0102	0.0235	-0.0087	6211	Sr	1.443	0.0610	-0.0055	-0.0520	-0.0038
5253	S	1.642	-0.0237	-0.0001	-0.0170	-0.0042	6364	S	1.283	0.0025	-0.0031	0.0002	0.0050
5261	Sr	1.648	-0.0385	0.0396	-0.0454	0.0392	6386	S	1.388	0.0820	-0.0074	-0.0138	-0.0044
5275	Sa	2.051	-0.0655	-0.0062	-0.0378	-0.0053	6585	Sk	1.049	-0.0359	0.0004	-0.0043	-0.0058
5392	Sl	1.657	-0.0561	-0.0092	-0.0049	0.0069	6592	Sq	1.020	0.0024	0.0033	-0.0005	-0.0165
5397	S	1.471	0.0469	-0.0035	0.0530	0.0167	6669	S	1.342	-0.0416	0.0001	-0.0233	-0.0021
5401	S	1.416	-0.0058	-0.0167	0.0166	0.0029	6847	Sk	0.913	-0.0152	0.0041	0.0181	-0.0203
5407	Sk	0.776	0.0057	0.0039	0.0411	-0.0222	6908	S	1.128	0.0371	0.0012	0.0065	-0.0147
5448	S	1.479	-0.0300	-0.0029	0.0011	0.0008	7056	Sq	1.080	-0.0224	-0.0037	-0.0098	-0.0126
5482	Sa	1.914	0.0016	-0.0260	-0.0298	0.0020	7170	S	1.550	-0.0178	-0.0206	0.0231	0.0060
5485	S	1.420	0.0116	0.0091	0.0052	0.0043	7211	S	1.076	0.0384	0.0082	0.0149	0.0034
5510	S	1.738	0.0296	-0.0108	-0.0378	0.0245	7224	Sq	1.070	-0.0771	0.0138	-0.0435	-0.0135
5534	S	1.123	0.0031	-0.0034	0.0363	0.0062	7225	S	1.620	-0.0525	0.0019	-0.0224	0.0156
5552	S	1.076	0.0081	0.0029	0.0238	-0.0113	7397	S	1.518	-0.0654	-0.0024	0.0185	0.0025
5563	S	1.253	-0.0709	-0.0002	-0.0042	-0.0149	7451	S	1.292	-0.0225	-0.0142	0.0138	0.0117
5565	S	1.296	0.0040	0.0038	0.0174	-0.0128	7564	S	1.260	-0.0246	0.0111	-0.0214	-0.0123
5595	S	1.205	-0.0313	0.0004	0.0022	-0.0085	8333	Sq	1.037	-0.0080	0.0037	-0.0195	-0.0019
5610	S	1.066	-0.0224	0.0030	0.0154	-0.0084	8334	S	1.090	-0.0271	0.0260	0.0289	-0.0058
5622	Sk	1.148	-0.1108	-0.0011	-0.0076	-0.0063	8516	S	1.297	-0.0396	-0.0026	-0.0329	-0.0005
5647	S	1.331	0.0076	-0.0016	-0.0232	0.0011	1977AW2	Sq	0.720	0.0093	0.0115	0.0439	-0.0111
5685	S	1.272	-0.0232	0.0154	0.0101	0.0120	1987UF5	Sl	1.568	-0.0405	-0.0040	0.0044	0.0118
5817	S	1.659	0.0571	-0.0182	-0.0274	0.0090	1991PE10	S	1.154	0.0334	-0.0007	0.0345	0.0113
5892	S	1.312	-0.0230	-0.0016	-0.0093	-0.0057	1992AE1	Sq	1.177	-0.0230	0.0005	-0.0069	0.0000
5965	Sa	1.806	0.0085	-0.0010	-0.0007	-0.0060	1995BM2	Sq	1.157	-0.0175	-0.0046	-0.0087	-0.0179
6071	S	1.150	-0.0041	-0.0099	-0.0036	-0.0028	1996UK	Sq	0.839	0.0207	0.0026	0.0225	0.0028
6077	Sq	0.836	-0.0344	-0.0007	0.0069	0.0057	1996VC	S	1.232	-0.0609	-0.0108	0.0044	0.0080
6078	S	1.269	-0.1049	0.0214	0.0016	-0.0092	1997CZ5	S	1.203	-0.0290	0.0076	-0.0235	-0.0092

1996), which is most closely correlated with $PC3'_{(S1)}$. Those asteroids classified as S-types are shown as dots in this figure, while members of the Sa-, Sk-, Sl-, Sq-, and Sr-classes are specifically labelled. Because the actual distribution of spectral classes is hard to determine from this plot, these components have been replotted in the form of histograms in Figure 4.13, where the distribution for each spectral class is separately shown for all three secondary components. We find that the UV slope, as quantified by the component $Slope_{(S1)}$, is highly correlated with spectral class. This should be expected, since the primary component Slope (the average slope over the entire spectral interval of 0.44 to 0.92 μm) is also clearly correlated with spectral class. As for the components $PC2'_{(S1)}$ and $PC3'_{(S1)}$, trends with respect to taxonomic class appear to be small. However, we note that members of the Sr-class appear more likely to have

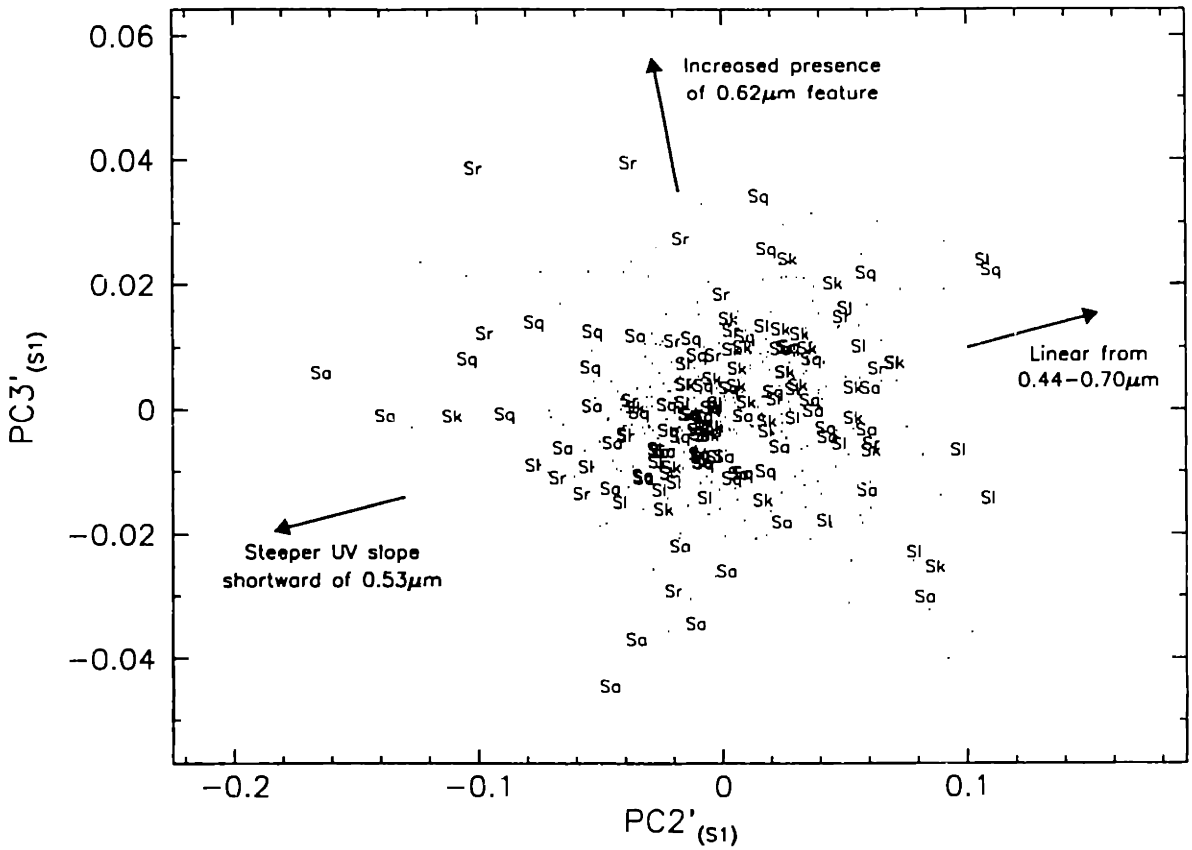

Figure 4.12: Plot of the secondary spectral components $PC2'_{(S1)}$ and $PC3'_{(S1)}$ for S-type asteroids (including all subclasses of S-types). $PC2'_{(S1)}$ is sensitive to the bend in the spectrum around 0.53 μm, where the spectrum shortward of 0.53 μm can be redder (steeper) than that over the interval from 0.53 to 0.70 μm. Arrows on this plot indicate the general direction of this trend. By comparison, the component $PC3'_{(S1)}$ is most sensitive to the presence of the broad (though very subtle) absorption feature centered near 0.62 μm. The trend in component space for objects whose spectra contain this feature is marked.

strong UV drop-offs in their spectra shortward of 0.53 μm, as compared with the other spectral classes. Likewise, the spectra of asteroids belonging to the Sk-, Sq-, and Sr-classes appear more likely to contain the 0.62 μm feature.

A major reason for examining these secondary features in the spectra of S-type asteroids is to look for possible correlations with mineralogy. If such correlations exist, the olivine-rich or pyroxene-rich composition of S-types might be inferred from the presence or absence of these features in our CCD spectra. In Figure 4.14, the secondary component planes of $PC3'_{(S1)}$ versus $PC2'_{(S1)}$ are shown for those SMASSII asteroids that had been previously classified by Chapman (1987), Gaffey *et al.* (1993a),

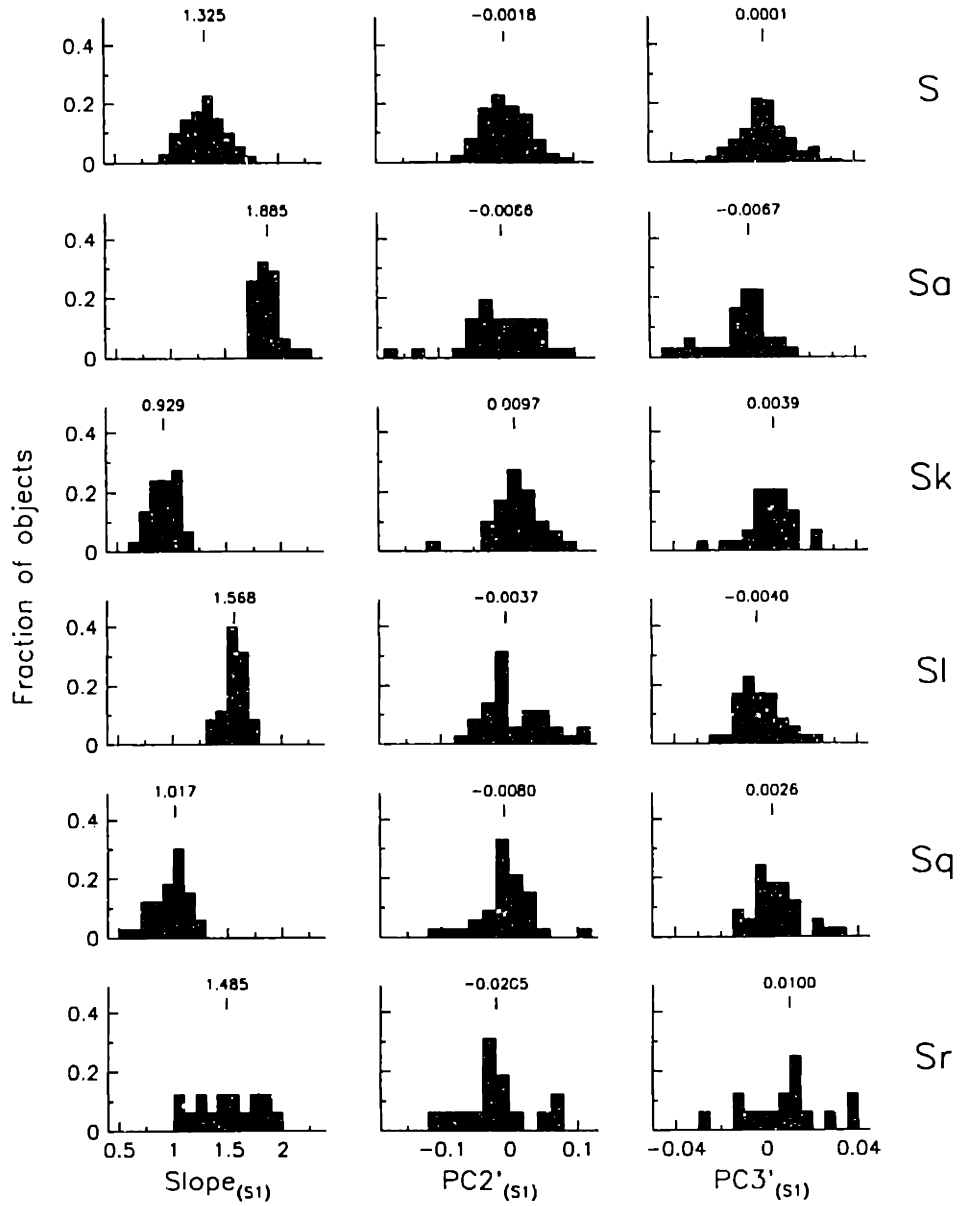

Figure 4.13: Histograms showing the frequency distribution of S-types (including all subclasses of S-types) as functions of the three secondary spectral components $Slope_{(S1)}$, $PC2'_{(S1)}$, and $PC3'_{(S1)}$. The component of $Slope_{(S1)}$ is highly correlated with spectral class, as would be expected, since the trend in UV slope is very apparent in the primary spectral component plane of Slope vs. PC2' (see Figure 4.8). At the top of each histogram, the location and value of the median for that distribution are shown. The other two secondary components do not show any significant correlations with spectral type, though there seem to be some subtle trends. In particular, the distributions with respect to $PC2'_{(S1)}$ indicates that asteroids belonging to the class Sr are more likely to exhibit a bend in the spectral reflectance (reddening of the slope) shortward of 0.53 μm, while the spectra of Sk-types are least likely to contain this bend in the UV slope. Likewise, inspection of component $PC3'_{(S1)}$ shows that Sk-, Sq- and Sr-type spectra are more likely to contain the 0.62 μm feature.

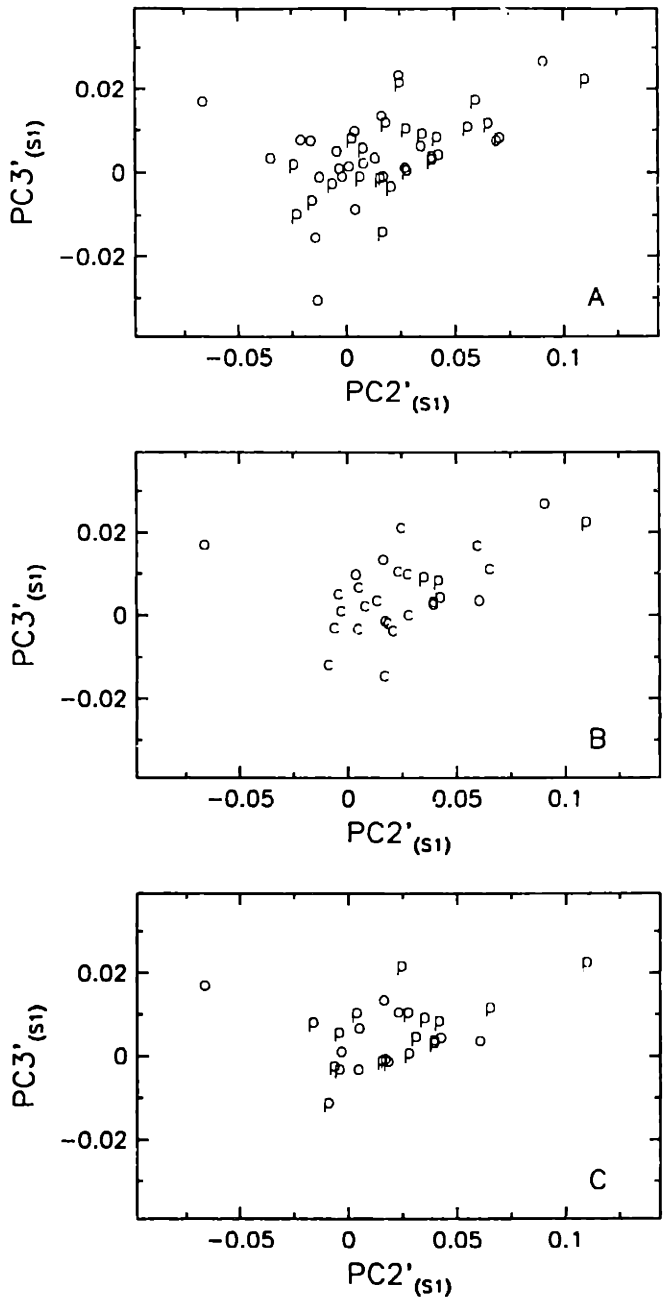

Figure 4.14: Similar to Figure 4.10, but objects are plotted by the two secondary components $PC2'_{(S1)}$ and $PC3'_{(S1)}$. This figure suggests there is no obvious correlation between spectral features over the interval of 0.44 to 0.70 μm (either the bend in the UV slope or the presence of the 0.62 μm feature) and other spectral features (in the near-IR) that reveal the presence of olivine or pyroxene.

and Howell *et al.* (1994). These three plots use the same criteria for the labelling of asteroids that was used in Figure 4.10. Figure 4.14 shows that there is no significant correlations between either the UV drop-off or the presence of the 0.62 μm feature, and the silicate composition of these asteroids. In particular, frame C of this figure shows the distribution of secondary components for asteroids classified by Howell *et al.* as either olivine-rich or pyroxene-rich. There is no apparent separation of these compositional types by either component $PC2'_{(S1)}$ or $PC3'_{(S1)}$, while in Figure 4.10, these same objects were reasonably well separated by the primary components of Slope and PC2'.

We also considered whether the shape of the reflectance maximum, or the wavelength at which that maximum is centered, might be correlated with composition. By isolating that part of the spectrum containing the reflectance peak, we can use PCA to parameterize its shape in a way that allows for simple comparisons. For this investigation, the spectra of all 476 asteroids making up the core of the S-complex were again included, but only those wavelength channels covering the interval from 0.65 to 0.84 μm were used. Since these channels represent values from the spline-fitted spectrum that was originally normalized at 0.55 μm, we first renormalized each of these shorter spectral segments to a value of 1.0 at 0.65 μm. Next, the average slope was determined for each of these shortened spectral segments, where the line being fit was forced to have a value of 1.0 at 0.65 μm. Each spectrum was then divided by its fitted line, and the resulting residual spectra (each having a mean value of roughly 1.0 over the entire interval of 0.65 to 0.84 μm) were analyzed using PCA. The secondary spectral components derived from this analysis are denoted by the subscript $_{(S2)}$, and the two most relevant components, $PC2'_{(S2)}$ and $PC3'_{(S2)}$, are listed in Table 4.2. These two secondary components are also plotted in Figure 4.15, where the trends corresponding to variations in the width of the reflectance peak, and in the wavelength (center) of that peak, have been marked. To better understand the distributions of these components as functions of spectral class, histograms for $PC2'_{(S2)}$ and $PC3'_{(S2)}$ are plotted in Figure 4.16. These histograms do reveal some interesting, and useful trends, especially with regard to the width of the spectral peak, given by component $PC2'_{(S2)}$. For example, the Sa- and Sr-classes tend to have reflectance maxima that are narrower in shape than do the Sk- and Sl-classes, as determined by $PC2'_{(S2)}$. Since the Sa- and Sr-classes also typically have the deepest 1 μm bands, this immediately suggests a

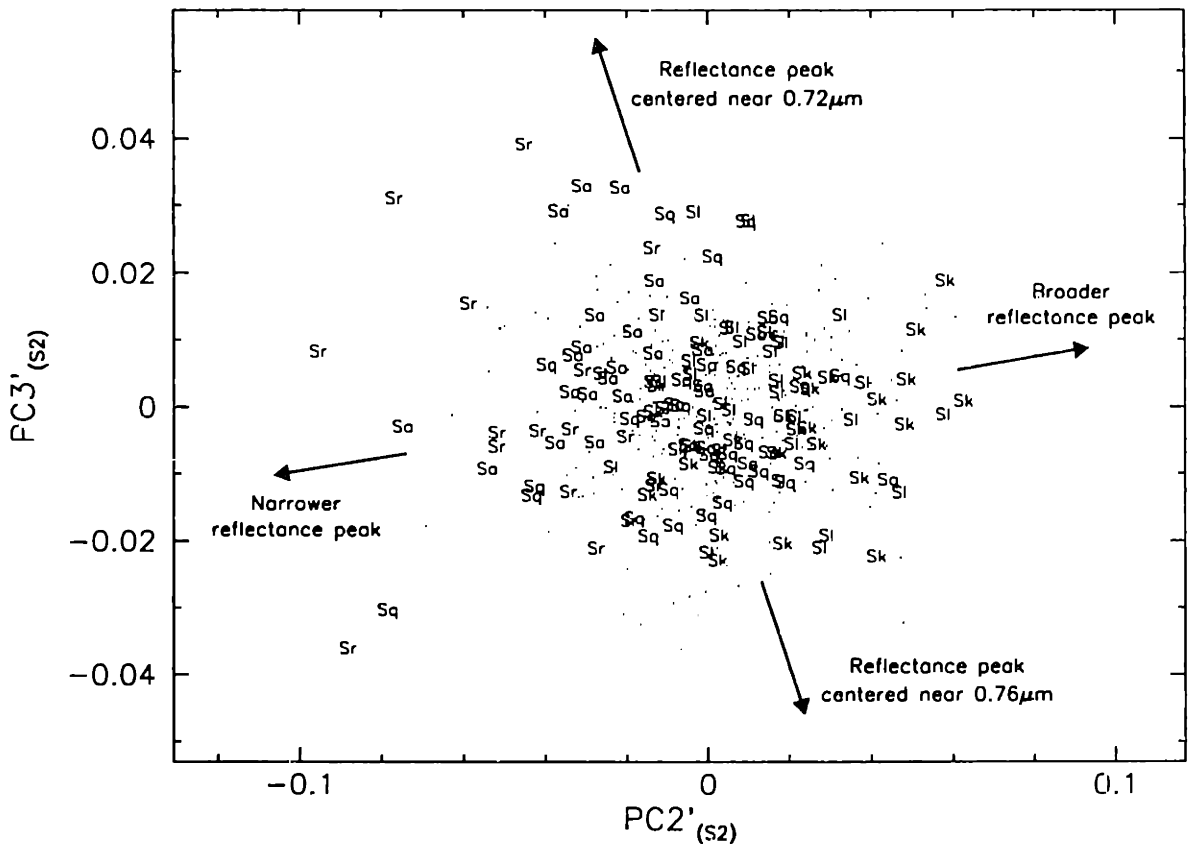

Figure 4.15: Plot of the secondary spectral components $PC2'_{(S2)}$ and $PC3'_{(S2)}$ for S-type asteroids (including all subclasses of the S-types). $PC2'_{(S2)}$ is sensitive to the width of the peak in spectral reflectance, while $PC3'_{(S2)}$ is an indicator of the wavelength at which that peak is located.

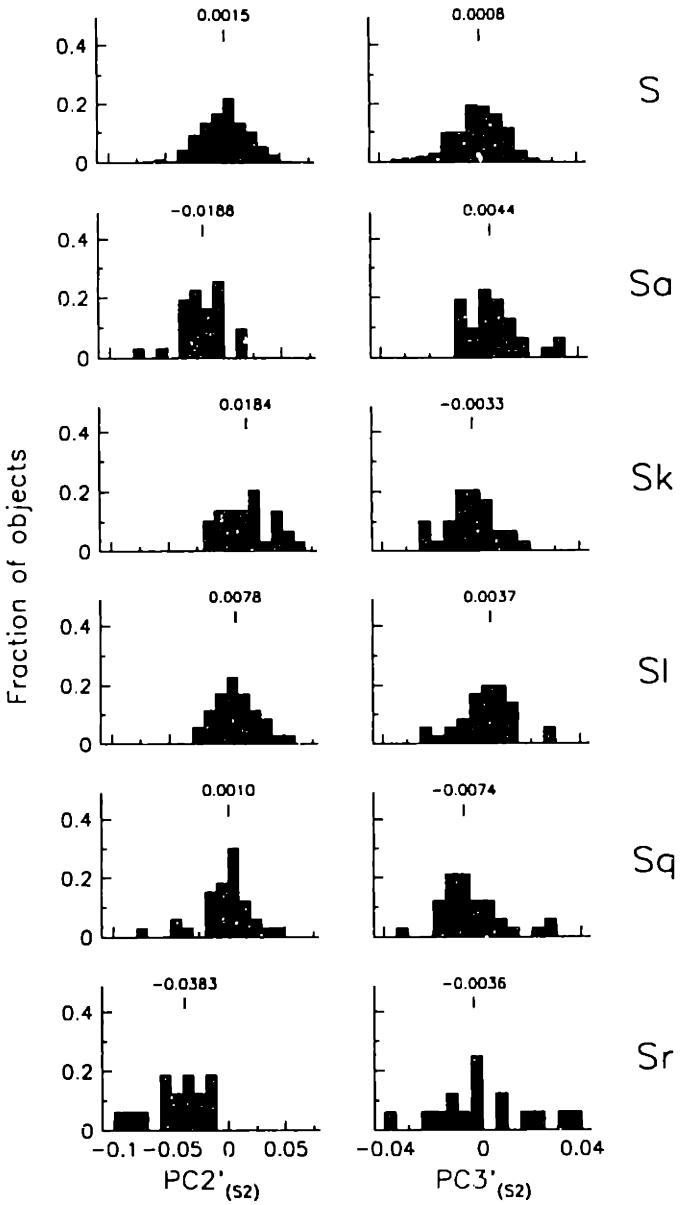

Figure 4.16: Histograms showing the frequency distribution for all classes of S-types as functions of the two secondary components $PC2'_{(S2)}$ and $PC3'_{(S2)}$. The plots of $PC2'_{(S2)}$ indicate that Sa- and Sr-types have a narrower (more sharply peaked) maximum in spectral reflectance than do the Sk- or Sl-types. This width of the reflectance peak is strongly correlated with the depth of the 1μm feature, represented by the primary spectral component PC2' (as shown in Figure 4.15). Inspection of the distributions in $PC3'_{(S2)}$ shows that the wavelength at which the maximum reflectance occurs is slightly bluer (approaching 0.72 μm) for Sa- and Sl-types, while maximum is typically at redder wavelengths (approaching 0.76 μm) for Sk-, Sq-, and Sr-types. This trend in the wavelength at which peak reflectance occurs is somewhat correlated with the primary spectral component Slope.

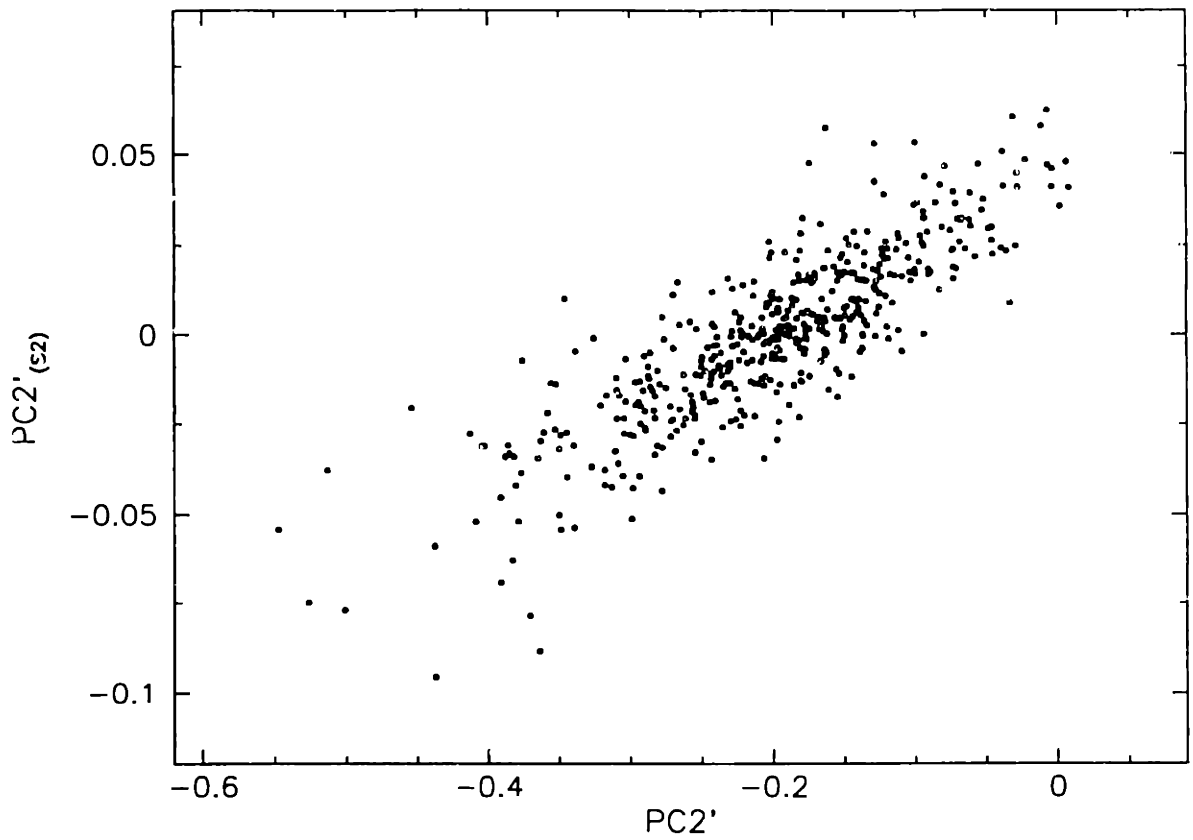

Figure 4.17: Plot of the relationship between the secondary spectral component PC2'$_{(S2)}$, which is a measure of the width of the spectral reflectance peak, and the primary component PC2', which is most strongly correlated with the depth of the 1μm band. This relationship shows that as the 1μm band becomes deeper, the maximum reflectance tends to be more sharply peaked.

possible relationship between PC2'$_{(S2)}$ and the primary component PC2'. This rather strong correlation between the 1 μm band depth (PC2') and the width of the reflectance peak (PC2'$_{(S2)}$) is demonstrated in Figure 4.17.

To determine if the secondary components describing the width and location of the reflectance peak might be indicative of mineralogy, comparisons are again made with the Chapman (1987), Gaffey *et al.* (1993a) and Howell *et al.* (1994) taxonomies, as shown in Figures 4.18, 4.19 and 4.20. This time, however, we show these data in the form of pairwise plots, and include not only the two components describing the reflectance peak (PC2'$_{(S2)}$ and PC3'$_{(S2)}$), but also include the measure of UV slope, provided by Slope$_{(S1)}$. In each of these plots, the plane that appears to be most useful in separating the olivine-rich asteroids from the pyroxene-rich objects is that defined by

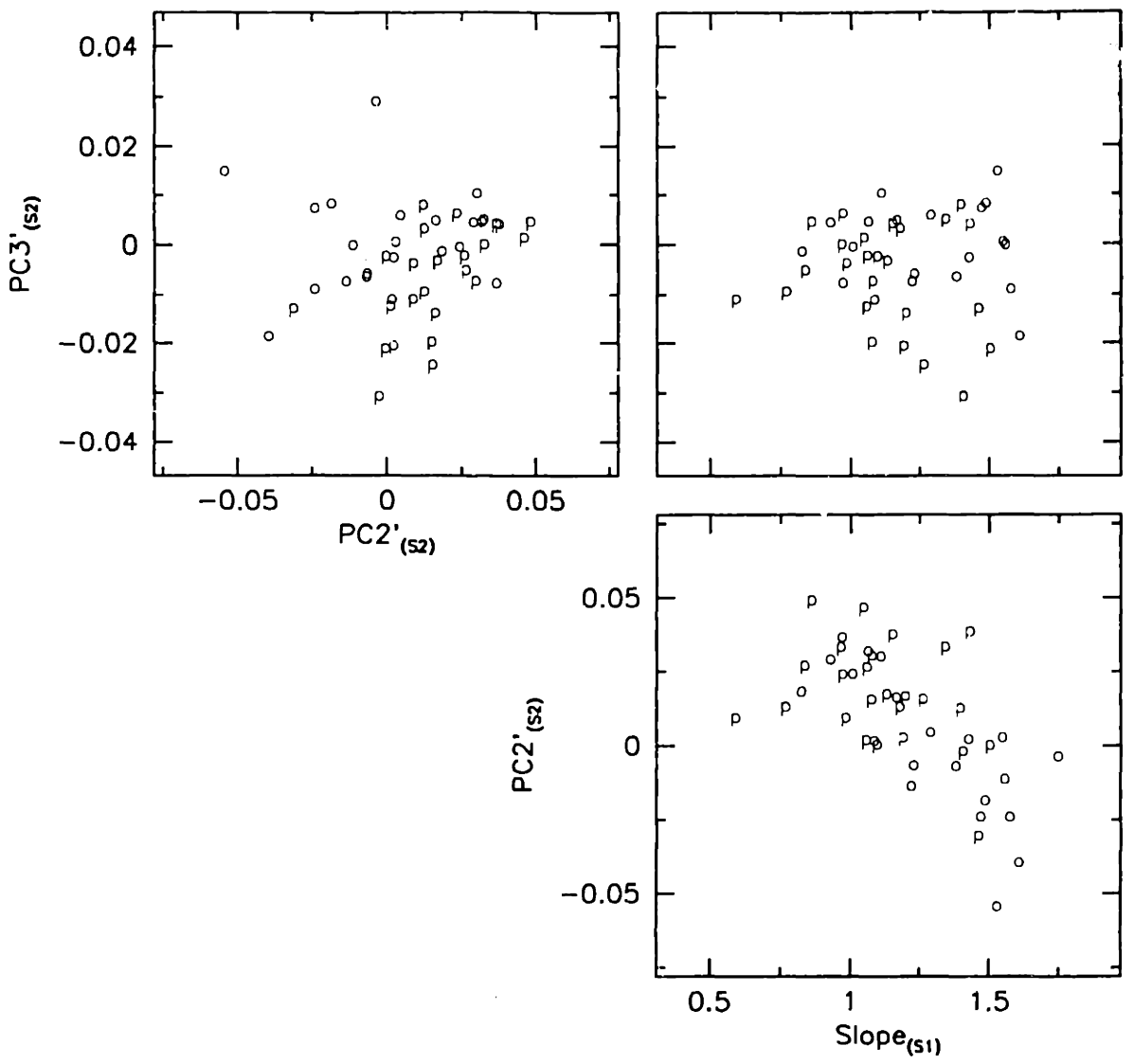

Figure 4.18: Plots showing all pairwise combinations of the secondary spectral components $Slope_{(S1)}$, $PC2'_{(S2)}$, and $PC3'_{(S2)}$ for S-types classified by Chapman (1987), and which were observed during SMASSII. Following the same criteria used for Fig. 4.10, only those objects for which Chapman used the discriminators "p" (pyroxene) or "o" (olivine) are included. While statistically insignificant, there is a subtle indication in each of the component planes that olivine-rich objects preferentially plot on one side of the distribution, while pyroxene-rich objects tend to cluster toward the other side of the distribution..

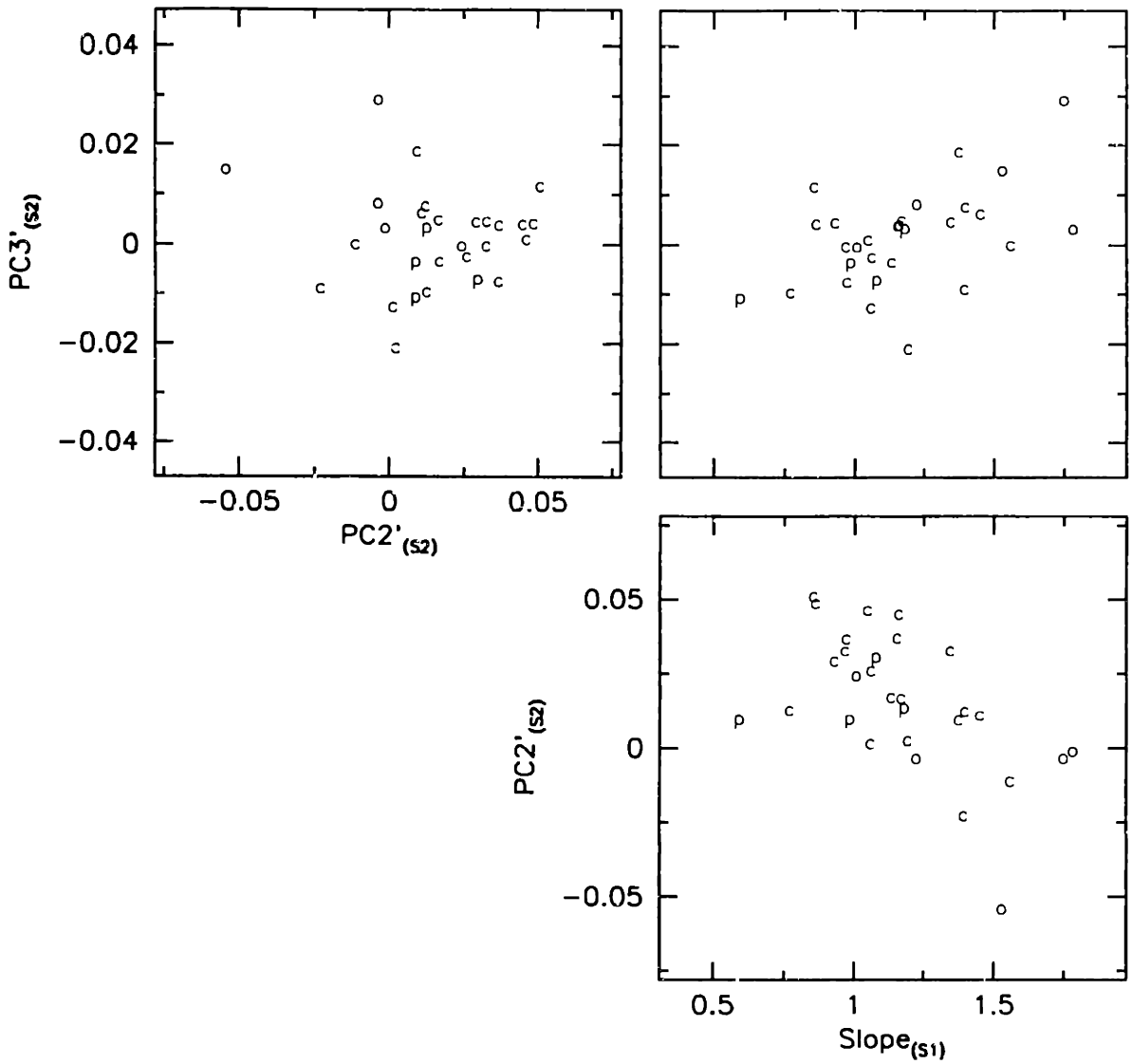

Figure 4.19: Similar to Fig. 4.18, but plotting asteroids classified by Gaffey *et al.* (1993). For clarity, those objects classified by Gaffey *et al.* as SI or SII (olivine rich) are shown with the label "o", while objects in classes SVI or SVII (orthopyroxene rich) are plotted as "p". Intermediate classes, SIII - SV (clinopyroxene rich) are plotted as "c".

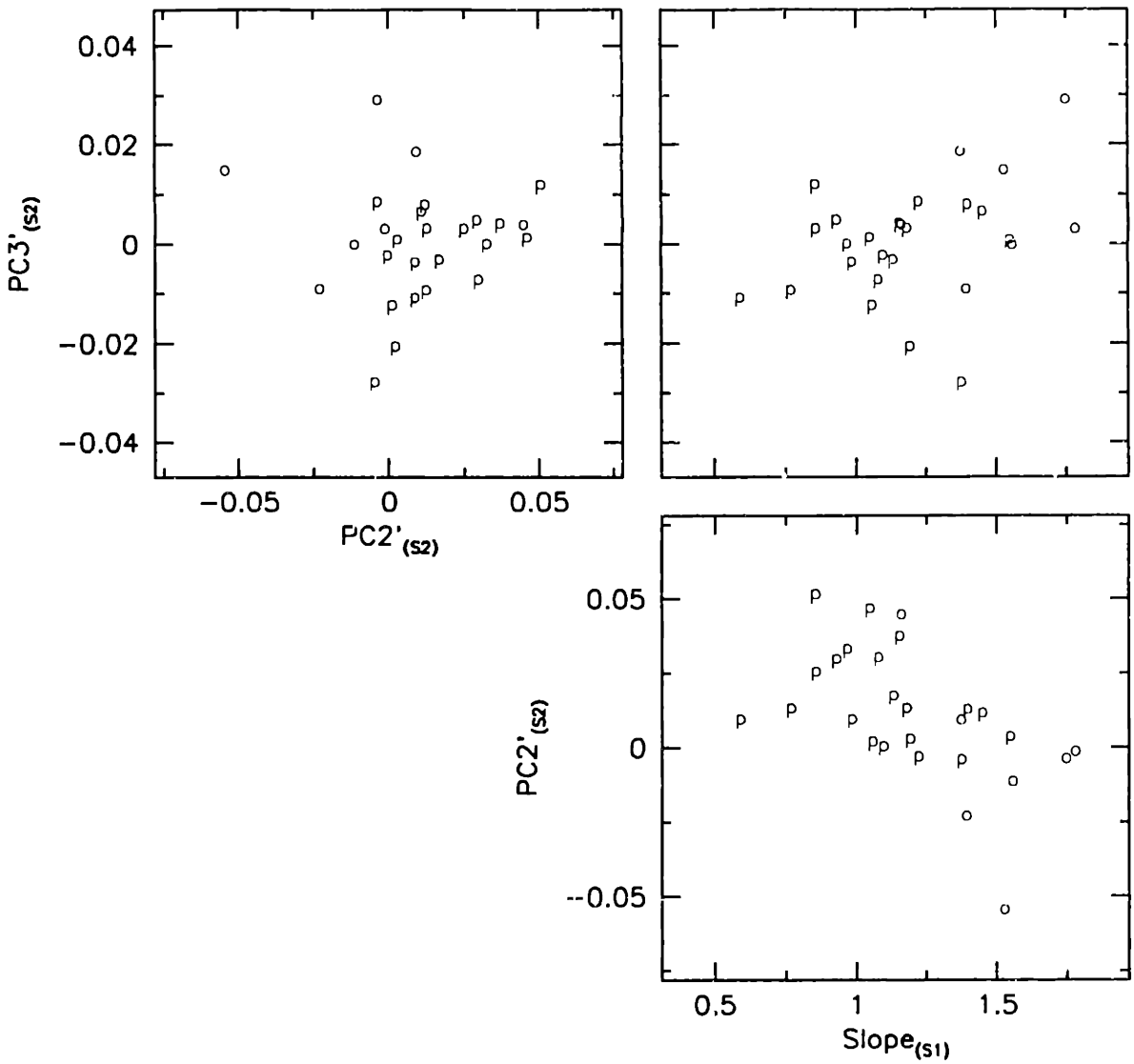

Figure 4.20: Similar to Fig. 4.18, but using the classifications of Howell *et al.* (1994). Those S-types classified by Howell *et al.* in the subclass Sp (pyroxene rich) are plotted as "p", while So types (olivine rich) are plotted with the label "o". Separation of these two mineralogical domains, based on the shape and location of the reflectance peak in S-type spectra, appears possible from these three component planes.

the secondary components $PC2'_{(S2)}$ and $Slope_{(S1)}$, while the wavelength of the reflectance peak ($PC3'_{(S2)}$) does not seem to be as important for distinguishing mineralogical differences. A careful comparison of these three figures with the corresponding plots in Figure 4.10 shows there to be no significant improvement, or decline in the ability to separate olivine-rich and pyroxene-rich asteroids based on the secondary components $Slope_{(S1)}$ and $PC2'_{(S2)}$, as compared with using the primary components Slope and PC2'. This suggests that simply knowing the UV slope, and the shape of the spectral reflectance maximum for an S-type asteroid may, to some extent, be diagnostic of its silicate mineralogy. To further test this, however, a more thorough sampling of S-type asteroids is required in the near-IR, such as that currently being provided by the SMASSIR survey (Burbine *et al.* 1999). Only through expanded, and improved observations and measurements of the 1 and 2 μm silicate absorption bands can some of the discrepancies between the classifications given by Chapman (1987), Gaffey et al. (1993a), and Howell et al. (1994) be clarified.

4.5 The C-complex

Based on the ECAS colors, Tholen (1984) defined four classes to describe those asteroids whose spectra are generally flat and featureless longward of 0.4 μm, and which can have ultraviolet drop-offs in reflectance (Fe-O charge transfer absorptions) shortward of 0.4 μm. These classes, denoted by the letters B, C, F, and G, are often referred to as sub-classes of a larger C-class or "C-group", reflecting the fact that the spectral differences separating these classes are small. By Tholen's definition, the B-type asteroids have spectra containing a moderate-strength UV absorption feature and an overall slope (longward of 0.4 μm) that ranges from slightly bluish to neutral in color. By comparison, Tholen's C-types have a UV feature of similar depth, but the overall slope is more reddish in color. The F-class was reserved for those asteroids with the smallest UV drop-offs, while G-types have the deepest UV features. Tholen considered measurements of albedo as a means for separating these classes, but as with the spectral features, variations in albedo among these asteroids are relatively small, with only the B-class having a mean albedo that is statistically distinguishable (higher) from the mean values for the other three classes.

The extent of our C-complex, as defined in Section 4.2, is essentially equal to that of the C-group (the B-, C-, F-, and G-classes) described by Tholen. In spectral

component space, the C-complex is not centrally-condensed, but rather plots as a bifurcated cloud with two broad, but relatively distinct concentrations of points that are best separated in the spectral component plane of PC3' versus PC2' (see Figure 4.3). In the PC2' versus Slope plane, this distribution is generally elliptical in shape, except for the sharp boundary with the X-complex, resulting from the continuous variation of spectral forms between the two complexes. In separating the X- and C-complexes, spectral slope is the primary distinguishing factor, though spectral shape also plays a important role. In particular, in our feature-based taxonomy, the presence of a broad, distinct concave-down curvature, located in the middle of a "C-like" spectrum is attributed to members of the X-complex. As the magnitude of this curvature increases (represented by a decrease, or more negative value of PC2'), the fitted average slope of the spectrum (component Slope) decreases. This correlation between the Slope and PC2' components accounts for the fact that the plane separating the C- and X-complexes is not normal to the Slope axis, as depicted in Figure 4.3.

The bifurcated distribution of the C-complex, in component space, results from two relatively distinct populations within the complex that are differentiated based on the presence or absence of a broad absorption feature, centered near 0.7 μm (correlated primarily with PC2'). In addition to the 0.7 μm feature, the PC3' versus PC2' plane is also sensitive to the depth of the UV absorption (mostly correlated with PC3'). The order in which the C-complex was divided into taxonomic classes was based on the dominance of these two spectral features in component space. Spectra containing a deep UV feature were classified first, followed by objects whose spectra exhibit a 0.7 μm band. Finally, those spectra with shallow to non-existent UV absorptions were subdivided, based primarily on their spectral slope.

In separating the G-class asteroids from the B- and C-types, Tholen had the advantage of colors derived from the ECAS *s*-, *u*-, and *b*-bandpasses (with bandcenters of 0.337, 0.359 and 0.437 μm, respectively) in determining the strength of the UV absorption, which is normally associated with an Fe-O intervalence charge transfer transition in the structure of silicate minerals (Gaffey 1976, Gaffey *et al.* 1989). This wavelength interval is not sampled in the SMASSII spectra, which begin at 0.44 μm, and therefore, cannot be used to characterize the UV feature to the same extent as was possible with the ECAS data. However, in the SMASSII spectra, the subtle curvature associated with this UV absorption usually begins just shortward of 0.55 μm, so that over

the interval from 0.44 to 0.55 μm, a diagnostic portion of the feature is measured. In the spectral component plane shown in Figure 4.21, the trend for increased depth of the UV feature extends to the left (as marked), corresponding primarily to a decrease in the value of component PC3'. This plot was used as a guide in defining a boundary between those C-type asteroids with moderate UV features, and those with deep features. To denote those asteroids with deep UV features, the letter "g" is appended to the class label of "C", thus maintaining some level of consistency with the Tholen G-class.

In Figure 4.21, those asteroids plotting in the region of the distribution extending from upper-center to the left have spectra containing the 0.7 μm absorption feature. This feature, first reported by Vilas and Gaffey (1989), has been identified in the spectra of many low-albedo asteroids (Sawyer 1991, Vilas *et al.* 1993, and others). A similar feature is found in the spectra of CM carbonaceous chondrite meteorites, leading to the suggestion that, in asteroid spectra, this absorption is due to the presence of oxidized iron in phyllosilicates, formed through aqueous alteration processes (Vilas and Gaffey 1989). However, a similar absorption feature has been found in the spectra of other mineral forms (King and Clark 1997), raising questions about the true identity of the 0.7 μm band measured in the asteroidal spectra. Following the suggestion of Burbine and Bell (1993), the letter "h" has been appended to the label "C" to identify those asteroids whose spectra contain the 0.7 μm feature. Fourteen of the asteroids observed during SMASSII have spectra containing both the 0.7 μm band and a deep UV drop-off, and are assigned the designation "Cgh". These two spectral types (the Ch- and Cgh-types, containing the 0.7 μm band) are observed to be the major constituents of some dynamical families. For example, the Dora family (discussed in Chapter 5) is made up almost entirely of Ch-type asteroids, while the Chloris family consists of a mixture of both Ch- and Cgh-types.

Once the Cg-, Ch-, and Cgh-types had been identified, they were removed from further steps in the classification process. The spectra of those objects remaining in the C-complex have UV absorption features that range from moderately deep to nonexistent (spectra that are essentially linear down to 0.44 μm), and have overall slopes varying from moderately bluish to slightly reddish. These characteristics fall within the ranges defined by Tholen for the B-, C-, and F-classes, though as before, the limited wavelength interval over which the UV feature is sampled in the SMASSII spectra makes it difficult to

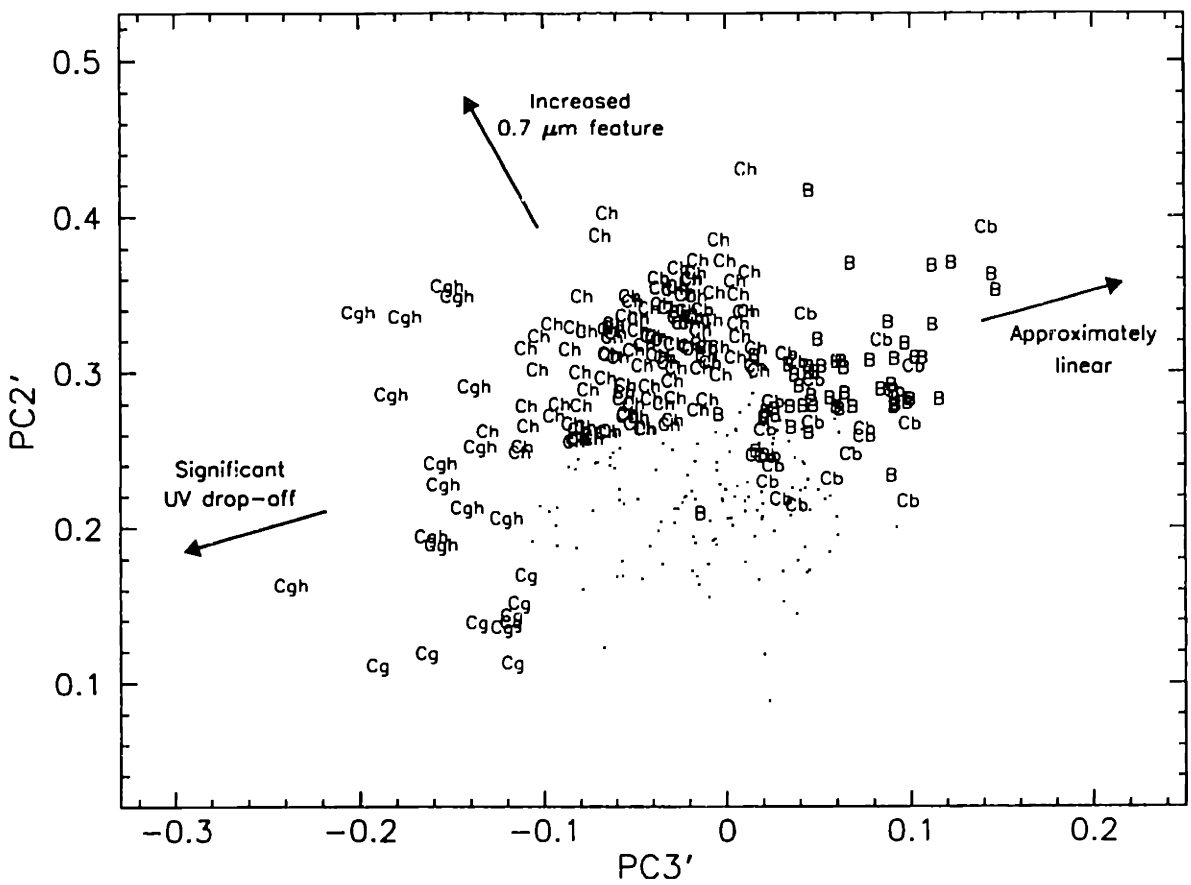

Figure 4.21: Plot of the primary spectral components PC2' versus PC3' for asteroids in the C-complex. For clarity, those asteroids classified as "C" (with no subscript) are shown as dots. Arrows indicate distinct spectral trends that are represented in this component plane. Most notably, asteroids whose spectra contain a broad 0.7μm feature (classified as Ch- and Cgh-types) cluster in the upper-left half of this plot. The C-types (dots) do not show this absorption feature, and asteroids plotting in the lower-right part of this distribution actually show a slight convex-up shape in the middle of the spectrum. On the left-hand side of the plot, spectra tend to have a deep UV drop-off (objects classified as Cg and Cgh), while spectra that are essentially linear in shape plot to the upper right. An asteroid located in the middle of this distribution will have a moderate UV drop-off, and will be approximately linear over the interval from 0.55 to 0.92μm. Because the UV drop-off and 0.7 μm absorptions dominate the variance represented in this plane, the Cg, Ch, and Cgh classes separate well. However, the spectral classes that do not include these absorption features, but rather are defined based primarily on the average spectral slope (the C-, B-, and Cb-types), do not separate out well in this plane.

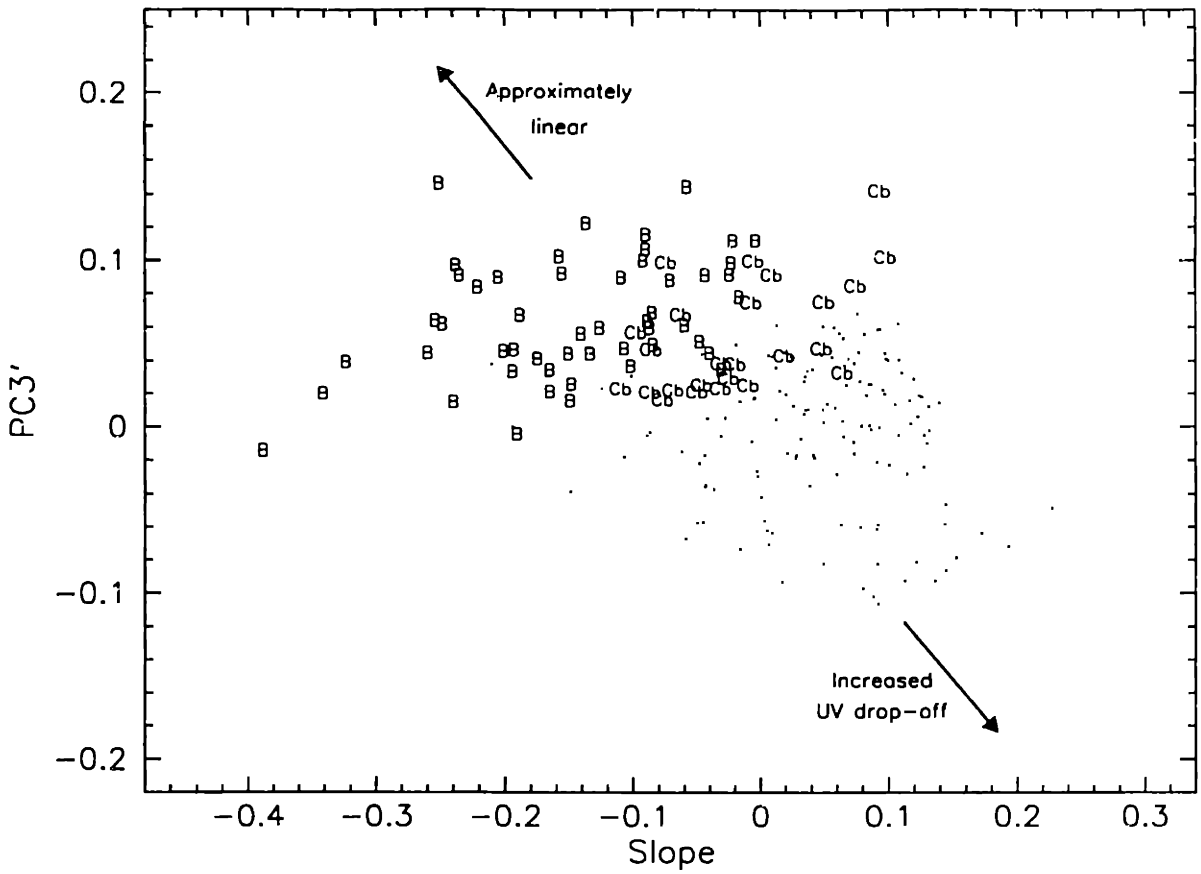

Figure 4.22: Plot of the primary components Slope and PC3', showing only the C-, B-, and Cb-classes. The B- and Cb-type asteroids are roughly linear in shape, with the classes being divided primarily on spectral slope. The B-type spectra tend to be the most linear, while the Cb-type spectra can show some subtle curvature due to the UV absorption feature. This presence of curvature among the Cb-types is the reason the boundary separating the B- and Cb-classes is not sharply defined at a Slope value of 0.0. The C-types exhibit a slight to moderate UV drop-off, as indicated by the arrow.

apply Tholen's definitions directly to these data. In particular, when comparing the SMASSII spectra of objects previously classified by Tholen as either B- or F-types, we find these two classes to be indistinguishable. Even so, the region of component space occupied by the remaining C-complex asteroids is not small, especially when replotted in the PC3' versus Slope plane (as shown in Figure 4.22), where variations in the average spectral slope and UV drop-off are best represented. When the spectral makeup of pertinent dynamical families is also taken into account, we find that further subdivision of this part of the C-complex is justified. In particular, most asteroids belonging to the Pallas family (see Chapter 5) have spectra that are essentially linear (featureless), with a

slight to moderate bluish slope, and cluster in the upper-left half of the distribution shown in Figure 4.22. By comparison, asteroids contained in both the Astrid and Hoffmeister families have spectra with slopes that are neutral to slightly reddish and a UV absorption that is shallow to moderate in depth (clustering primarily in the lower-right half of Figure 4.22). Based on these considerations, the asteroids plotted in Figure 4.22 are divided into three classes: the B-, C-, and Cb-types. The B-class is reserved for those asteroids whose spectra are linear, showing no substantial evidence of curvature related to a UV absorption feature, and for whom the measure of average spectral slope (component Slope) has a value less than zero. Those asteroids with spectra having well-defined UV features, ranging in depth from shallow to moderate, and for which the middle of the spectrum (the interval from roughly 0.6 to 0.8 μm) varies from being flat to having a very slight concave-down curvature, are assigned to the C-class. Based on these definitions, the B- and C-classes are spectrally distinct, making it difficult to classify those asteroids with intermediate spectral shapes. To fill this gap, the Cb-class was formed. Asteroids classified as Cb-types have Slope values ranging from -0.1 to 0.1, and have UV features ranging from very shallow (for those objects with Slope values approaching -0.1) to nonexistent, thus including those spectra that are linear, but which have Slope values slightly greater than zero. The mean spectra for all six classes contained in the C-complex are plotted in Figure 4.23, along with envelopes showing the 1σ variation for each class.

Over the past two decades, there has been growing interest in determining the hydration state of asteroids by looking for the presence of hydrated minerals on their surfaces (Lebofsky 1978, Feierberg *et al.* 1981, Jones *et al.* 1990). In particular, a series of absorption features, centered around 3 μm, has been observed in the reflectance spectra of many asteroids, and is interpreted as resulting from the presence of both structural OH ions and interlayer H_2O molecules in hydrated silicates. An investigation by Jones *et al.* (1990) showed that, among low-albedo asteroids, the hydration state of these objects, as determined from the 3 μm feature, is related to heliocentric distance, with asteroids in the inner belt being more likely to have undergone an episode of heating and aqueous alteration than those asteroids in the outer belt, where any water present is likely to remain in the form of subsurface ices. Due to the difficulties inherent in near-IR observations, including lower flux levels, and the increased presence of telluric absorption bands, accurate measurements of the 3 μm band are

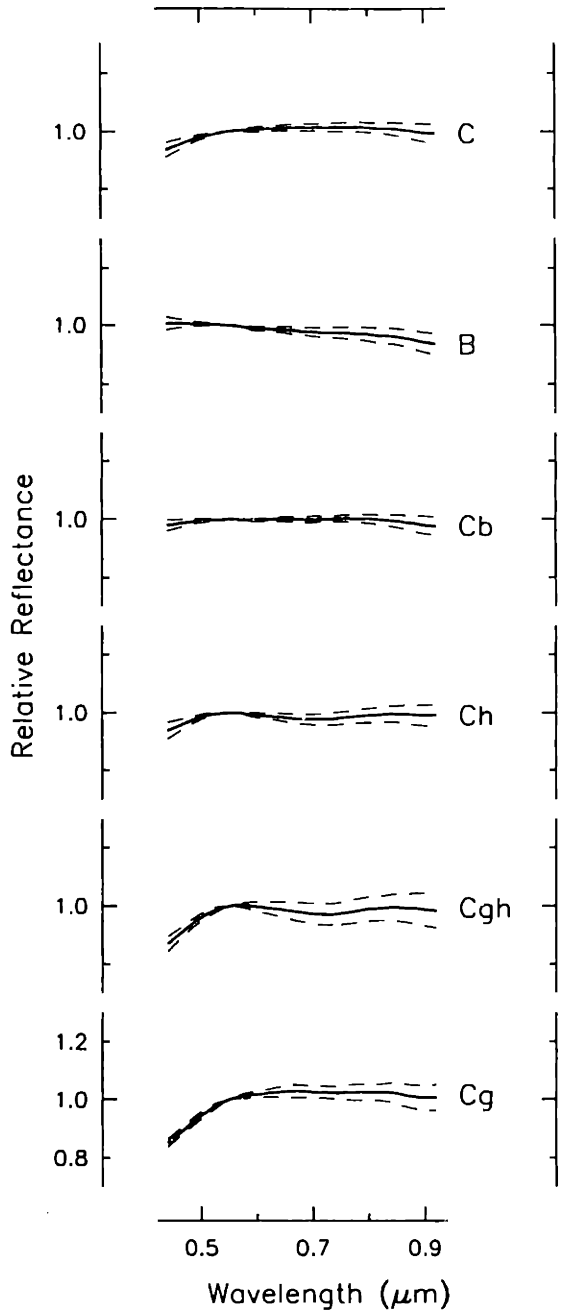

Figure 4.23: Similar to Figure 4.6, but showing the mean spectra for those classes contained in the C-complex.

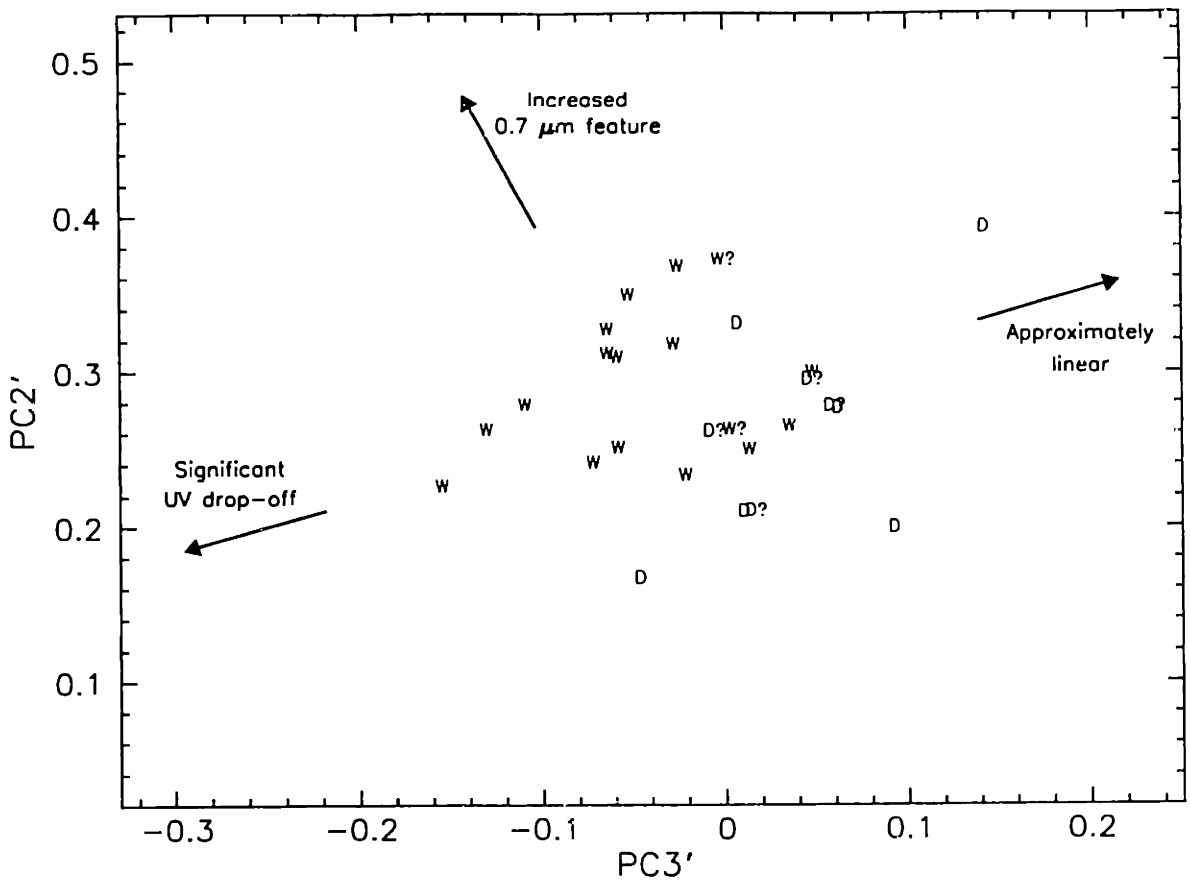

Figure 4.24: The primary spectral component plane, PC2' versus PC3', plotted with the same limits as used in Figure 4.21. Twenty-six SMASSII asteroids are plotted for which a hydration state has been determined, based on observations of the 3 μm water band. Objects are labelled as "W"et or "D"ry, as listed in Table I of Merényi *et al.* (1997). The tendency for hydrated objects (Wet) to plot towards the upper left of this plot, while dry objects tend to plot to the lower right appears to be correlated with increased strengths of both the UV drop-off and the 0.7 μm feature.

often problematic. Because of this, Merényi *et al.* (1997) investigated whether the presence of water in asteroids could be predicted based on spectral features shortward of 3 μm, using artificial neural network techniques. In the case of C-type asteroids, Vilas (1994) found a strong correlation between the presence of a 3 μm hydration band and the presence of the 0.7 μm phyllosilicate band, affirming the idea that the 0.7 μm band results from aqueous alteration processes. In Figure 4.24, the position of 26 SMASSII asteroids are plotted in the PC2' versus PC3' component plane (to the same scale as plotted in Figure 4.21), where these asteroids have been labelled as either "W"et or "D"ry, based on the compilation in Table I of Merényi *et al.* (1997). While the separation

between wet and dry asteroids is not perfect in Figure 4.24, the tendency for wet objects to plot in the upper-left portion of this plane, while dry objects cluster toward the lower-right half, is significant. This plot confirms the correlation found by Vilas (1994), with 10 out of the 11 SMASSII asteroids classified as Ch- or Cgh-types being designated as wet, based on 3-μm band observations. The mixture of wet and dry asteroids in the center of the distribution in Figure 4.24 should be expected, and reinforces the idea of continuous variations in spectral, and presumably mineralogical properties (including the hydration states) among the asteroids. In searching for hydrated asteroids, those plotting in the upper-left portion of Figure 4.21 should be especially targeted, and in particular, measurements of the 3 μm feature in the spectra of Dora and Chloris family members may help put constraints on thermal processing in the interiors of asteroids.

4.6 The X-complex

As described in Section 4.2, membership in the X-complex is limited to those asteroids whose spectral characteristics are similar to those of the X-types (including the E-, M-, and P-types) identified in earlier taxonomies. In particular, SMASSII asteroids that had been previously classified as X-, E-, M-, or P-types by Tholen (1984), Barucci *et al.* (1987) or Howell *et al.* (1994) were used to define the extent of the X-complex. In past discussions of taxonomy, the spectra of X-type asteroids have been described as generally featureless (linear) over the visible wavelength interval from 0.4 to 1.0 μm, with slopes that range from slightly- to moderately-red in color. To formally assign an asteroid to one of the E-, M-, or P-classes, its albedo must be known. Even though albedo was never directly considered in the development of our feature-based taxonomy, it was a significant parameter in both the Tholen and Barucci *et al.* taxonomies. Because we have relied on these earlier classifications of Tholen and Barucci *et al.* in forming the basis of our feature-based taxonomy, it must be assumed that albedo has indirectly influenced our definition of the X-complex, and, in particular, how its boundary with the C-complex was established.

Based on the wide range of albedos, and physical evidence provided by meteorites, asteroids classified as E-, M-, or P-types have traditionally been interpreted as having very different mineralogies and thermal histories. The low-albedo P-type asteroids are thought to be composed of primitive, undifferentiated materials, while the high-albedo E-type asteroids are interpreted as being differentiated, and having a low-

iron, enstatite composition. The M-class asteroids have intermediate albedos, closely matching those of nickel-iron meteorites, leading to the idea that these asteroids are the collisionally-produced fragments of differentiated metal cores (e.g. Bell *et al.* 1989). However, based on recent findings, these broad interpretations, particularly those for the E- and M-classes, are being challenged. For example, polarimetric measurements (Lupishko and Belskaya 1989) and radar observations (Ostro *et al.* 1985) of selected M-type asteroids have revealed surface properties that are, in some cases, inconsistent with metallic iron. Even more notable is the possible evidence for hydrated minerals on the surfaces of some E- and M-type asteroids (Jones *et al.* 1990, Rivkin *et al.* 1995), the existence of which would be in direct contradiction with the high temperatures (1400 to 1900 K) associated with the differentiation of iron-silicate mixtures (Haack *et al.* 1990).

The SMASSII observations reveal that the visible-wavelength spectra of asteroids contained in the X-complex are not uniformly featureless. Instead, we find a set of subtle, but distinct spectral features that seem to be uniquely associated with this complex. The shapes and locations of these features can be accurately described, and to some extent, can be correlated with trends that are observed in spectral component space. Most significantly, these features provide a means for subdividing the X-complex that is independent of albedo. The presence (or absence) of two particular features, an absorption band centered near 0.49 μm and a broad, concave-down curvature, extending from roughly 0.55 to 0.8 μm, provides the basis for dividing this complex into four spectral classes.

The first of these classes is defined by a combination of three spectral features, the most significant being the 0.49 μm band. This band was first recognized as a prominent feature in the spectrum of asteroid 64 Angelina. This same band has been subsequently identified, though at much weaker levels, in the spectra of 26 other SMASSII asteroids, not including the near-Earth objects. Among the NEAs (Binzel *et al.* 1999b), the spectrum of 3103 Eger contains a particularly strong 0.49 μm feature, second in strength only to that observed in the Angelina spectrum. In those spectra with sufficiently high levels of signal-to-noise, a second, much weaker absorption feature is observed, centered near 0.59 μm. In addition, a smoothly-angled, convex deflection in the spectral slope occurs near 0.72 μm. These three features are labelled in the spectrum of 64 Angelina, which is plotted in Figure 4.25. Also plotted in this figure are the spectra of

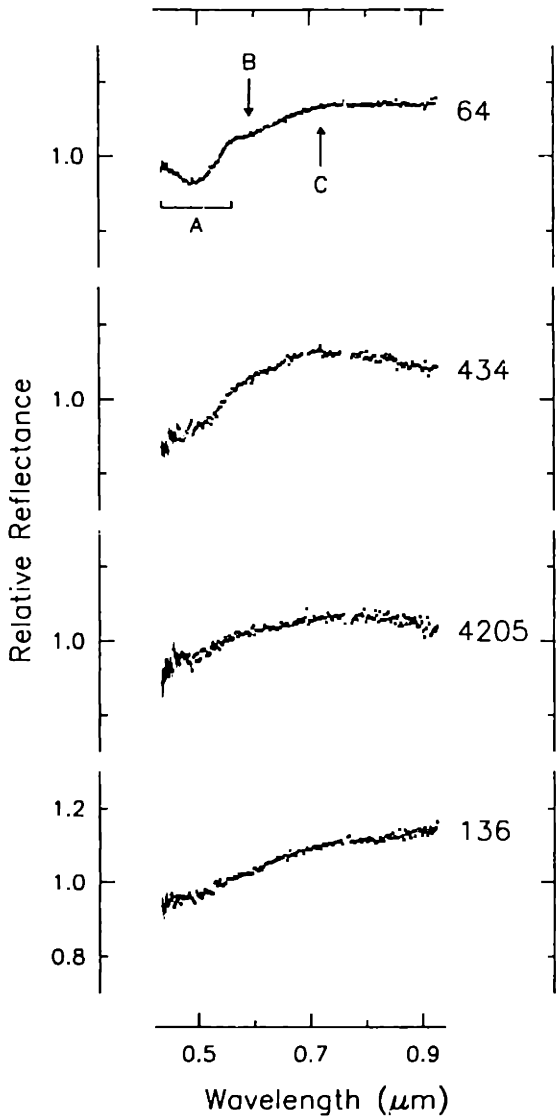

Figure 4.25: Representative spectra of asteroids belonging to the Xe-class. A combination of three features are used in defining this class, though often these features are very subtle, as is apparent in the spectra of 4205 David Hughes and 136 Austria. The prototype spectrum for this class is 64 Angelina, shown at the top of this panel. The most prominent feature in the Angelina spectrum is the "hook-shaped" absorption feature centered near 0.49 μm (labelled A). A second, much shallower absorption can be seen around 0.59 μm (labelled B), as well as the smoothly angled bend in the spectrum around 0.72 μm (labelled C). These features have been intentionally left unlabeled in the other three spectra, so as to not influence a critical inspection of these data. In the cases of 4205 and 136, the most diagnostic feature is the slight concave-up curvature of the 0.49 μm band, though recognizing its presence usually requires the fitting of a smoothing function, such as a spline, to the data.

434 Hungaria, 4205 David Hughes, and 136 Austria, demonstrating the various degrees at which these features can be present. In many cases, only by examining the fitted (smoothed) spectrum can these features be properly identified. Of the 27 asteroids whose spectra contain the 0.49 μm band, 13 had been previously classified by Tholen, with the largest fraction (6 objects) being assigned to the E-class based on their high albedos. For this reason, these 27 asteroids have been assigned to a spectral class labelled "Xe". Burbine *et al.* (1998) suggested that the 0.49 μm feature in these spectra arises from the presence of troilite (FeS). Troilite is often found in enstatite-rich aubrite meteorites, which are thought to be derived from E-type asteroids (Zellner *et al.* 1977, Gaffey *et al.* 1992).

The other principal characteristic used in dividing the X-complex is a broad, and very gradual convex curvature, covering the wavelength interval from roughly 0.55 to 0.8 μm. Once the Xe-class asteroids had been identified, and removed from further consideration, nearly half of the remaining X-complex asteroids were found to exhibit this spectral curvature. These asteroids tend to fill a gap in the spectral continuum between the C-types, where those members of C-class lying on the lower right-hand edge of the distribution in Figure 4.22 tend to have a very slight concave-down curvature in the middle of their spectra, and the K- and T-type asteroids, whose spectra have a more substantial, and more sharply defined curvature. Because of the wide range in average spectral slopes among these asteroids, two classes were formed, the Xc- and the Xk-types, with the division between these classes occurring at a Slope value of 0.26.

The fourth taxonomic class contains all remaining members of the X-complex. The spectra of these asteroids are generally linear in form, except for minor absorption features that can be present at either end of the SMASSII spectral range. Because the reflectance spectra of these asteroids most closely match the traditional definition of the "X-class" (including the E-, M-, and P-types defined in previous taxonomies), the label "X" is used to designate this class in our feature-based taxonomy. The spectra of four representative X-class asteroids are plotted in Figure 4.26, showing that, in general, the absorption features present are relatively weak. In the spectrum of 139 Juewa, a UV absorption feature is marked, very similar in shape to the rounded UV features (Fe-O charge-transfer bands) present in the spectra of C-class asteroids. Among the X-types, however, the depth of this UV feature rarely exceeds that exhibited by 139 Juewa. At the red end of these spectra, a weak to moderate absorption band is often detected near

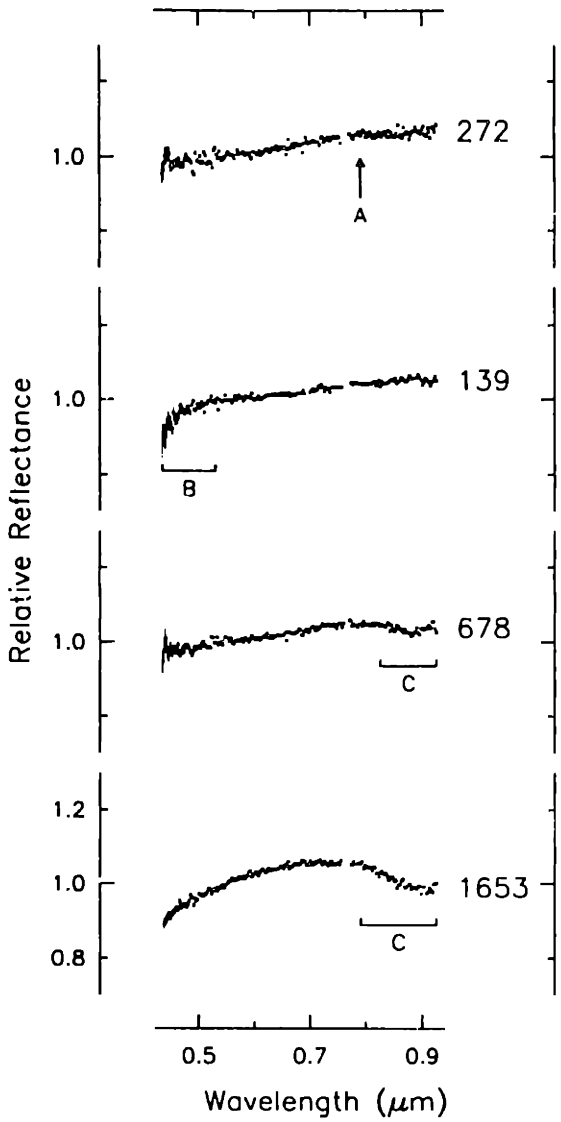

Figure 4.26: Representative spectra of asteroids belonging to the X-class. These spectra are generally linear in shape, and have a slight to moderate reddish slope. Many X-type spectra that appear linear actually contain a VERY subtle bend, usually centered between 0.78 and 0.80μm. An example of this is seen in the spectrum of 272 Antonia (labelled A). A shallow UV drop-off is also commonly observed, though a deeper drop-offs, such as that seen in the spectrum of 139 Juewa (labelled B), are relatively uncommon. Finally, many X-type spectra are found to have a shallow feature centered near 0.9 μm. Most often, this feature is relatively narrow (less than 0.1 μm wide) like that in the spectrum of 678 Fredegundis, though occasionally it can be broader (1653 Yakhontovia). The spectrum of 1653 is particularly anomalous, appearing to be an intermediate spectral phase between the X- and the S-complexes.

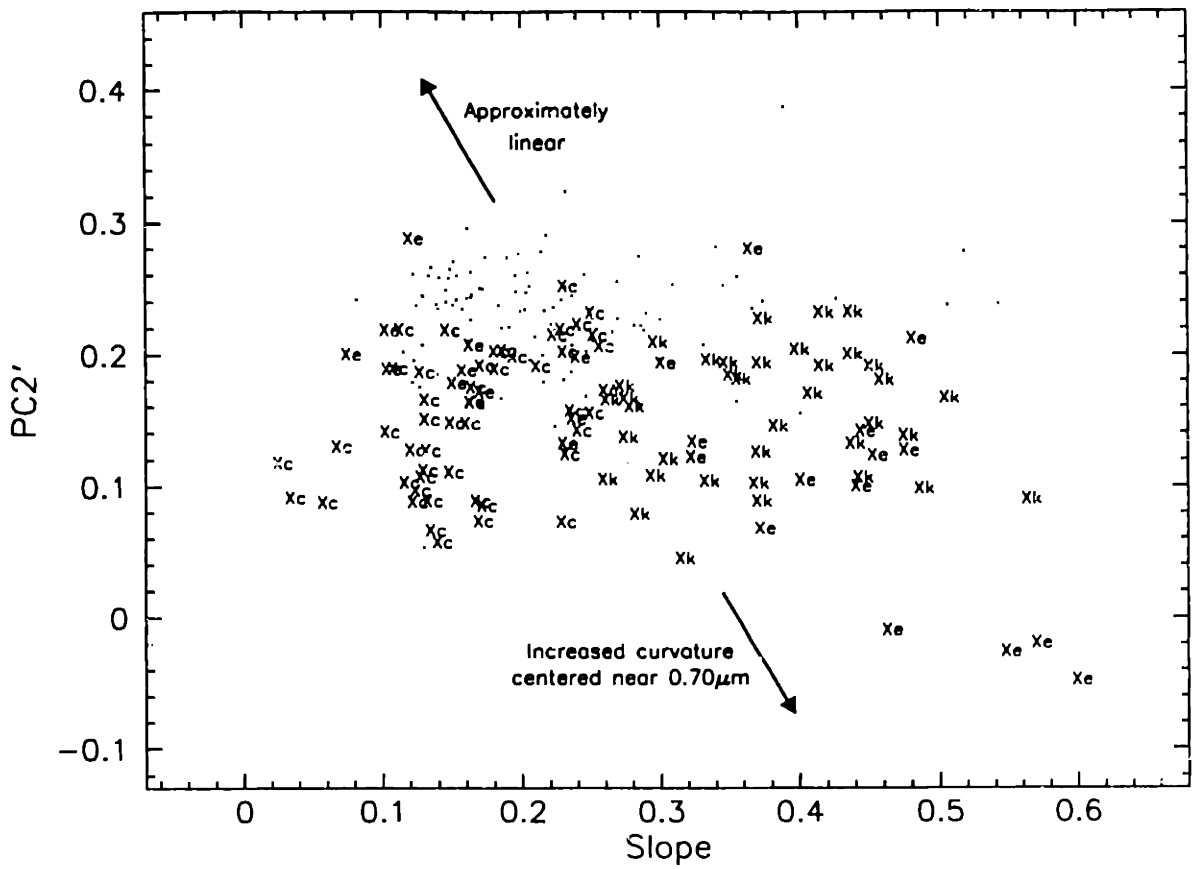

Figure 4.27: Plot of the primary spectral components Slope and PC2' for the X-complex. Due to the subtle nature of the features observed in these spectra, the boundaries separating the spectral classes are not well defined in spectral component space. A fairly clear division is seen between the Xc- and Xk-classes based on the average slope (Slope ≈ 0.26), but no clear boundaries exist for the X-types or Xe-types. Arrows show the general trend for increasing (or decreasing) spectral curvature that defines the difference between the X-types and the Xc- and Xk-types.

0.9 μm, an example of which is marked in the spectrum of 678 Fredegundis. This feature probably results from the presence of silicates (pyroxene or olivine), similar to the 1 μm band contained in S-type spectra. The spectrum of 1653 Yakhontovia, shown in Figure 4.26, is somewhat anomalous, and has been included in the X-class through a process of elimination. An equally unusual spectrum of 1653 Yakhontovia was obtained during SMASSI (Xu *et al.* 1995) that was interpreted as showing similar characteristics to that of 44 Nysa. The intermediate nature of the Yakhontovia spectrum, with characteristics belonging to both the S- and X-complexes, reinforces the concept of a continuum in spectral reflectance properties that links these two complexes. At the top

of Figure 4.26, the spectrum of 272 Antonia is plotted, showing that even in the most featureless spectra, small deflections in slope are often present. The spectra contained in the X-class have average slopes ranging from slightly- to moderately-red, with Slope values in the range of 0.08 to 0.55, though, as seen in Figure 4.27, the majority of the asteroids in this class have spectral slopes clustering in the lower half of this range, with a median value for the Slope component of 0.21. An additional argument for forming the X-class, and recognizing these asteroids as distinct from the Xc- and Xk-types, is provided by members of the Lydia and Phaeo families (see Chapter 5). These asteroids are predominantly classified as X-types, with most members having linear spectra that show no broad curvature like that present in the Xc- and Xk-type spectra.

Figure 4.27 shows the distribution of all X-complex asteroids in the spectral component plane of PC2' versus Slope. A general trend is apparent, with those asteroids in the X-class (objects with spectra that are relatively featureless) plotting in the upper-left portion of this distribution, while those asteroids whose spectra exhibit more curvature (the Xc- and Xk-types) plot lower in the distribution. However, the separation of these two spectral forms is not distinct in this lower-order component plane. Asteroids belonging to the Xe-class, which exhibit unique, but usually weak spectral characteristics, seem to plot almost anywhere within this distribution. The only classes that are fully separated in this component plane are the Xc- and Xk-classes, which are distinguished based on spectral slope.

In an attempt to more quantitatively isolate those spectral features that distinguish the four X-complex classes, a new set of secondary spectral components, based solely on the X-complex, were calculated. Because the primary spectral features described above (the 0.49 μm and 0.59 μm bands observed in the Xe-type spectra, and the spectral curvatures that are centered near 0.7 μm) are contained within the wavelength interval from 0.44 to 0.80 μm, only that portion of each spectrum was included in this new analysis. Following the standard procedures described in Chapter 3, the average slope, γ, was first recalculated for each spectrum, using the least-squares solution to Eqn. 3.3 for those spectral channels between 0.44 and 0.80 μm. As before, this fitted line is constrained to have a value of 1.0 at 0.55 μm. The spectrum of each asteroid (over the interval of 0.44 to 0.80 μm) was then divided by its slope function, producing a residual spectrum with mean reflectance, over all channels, of approximately 1.0. The residual spectra for all X-complex asteroids were then analyzed using principal

Table 4.3: Secondary spectral components for X-types

Asteroid	Type	Spectral components				Asteroid	Type	Spectral components			
		Slope (X1)	PC2' (X1)	PC3' (X1)	PC4' (X1)			Slope (X1)	PC2' (X1)	PC3' (X1)	PC4' (X1)
16	X	0.6036	-0.0107	-0.0016	-0.0070	336	Xk	0.5416	0.0641	-0.0237	-0.0100
21	Xk	0.4641	-0.0309	-0.0163	0.0136	337	X	0.2394	0.0013	0.0098	-0.0093
22	X	0.4312	-0.0143	0.0271	0.0020	338	Xk	0.5236	-0.0588	-0.0223	-0.0070
44	Xe	0.1884	0.0471	-0.0132	0.0339	348	X	0.2241	0.0173	0.0199	0.0066
46	Xc	0.2986	0.0781	-0.0150	-0.0063	359	X	0.1987	0.0854	0.0028	0.0045
55	X	0.3224	0.0327	0.0203	0.0057	363	X	0.3669	0.0402	0.0251	-0.0020
56	Xk	0.5799	-0.0428	-0.0437	-0.0105	375	Xc	0.3744	-0.0728	-0.0162	-0.0198
64	Xe	0.6507	-0.0142	-0.0776	0.1041	393	Xc	0.2976	-0.1159	0.0427	0.0066
65	Xc	0.2814	0.0037	-0.0295	-0.0117	396	Xe	0.2738	-0.0131	0.0249	0.0179
69	X	0.4097	0.0168	0.0173	-0.0041	399	X	0.2195	0.0860	0.0119	0.0108
71	Xe	0.6197	-0.0809	-0.0183	0.0193	409	Xc	0.3325	0.0573	-0.0065	0.0002
75	Xk	0.5598	-0.0309	-0.0335	-0.0098	413	X	0.2252	0.0242	0.0171	0.0033
76	X	0.2083	0.0063	0.0223	0.0007	417	Xk	0.5569	-0.0914	0.0324	-0.0104
83	X	0.4137	0.0861	-0.0212	-0.0041	434	Xe	0.7602	-0.1111	-0.0795	0.0293
87	X	0.3739	0.0390	0.0238	-0.0007	441	Xk	0.6426	-0.0275	-0.0110	0.0077
92	Xc	0.3234	0.0546	-0.0054	0.0026	504	X	0.1889	0.0303	0.0101	0.0077
99	Xk	0.3860	-0.0566	0.0139	-0.0034	507	X	0.3228	0.0544	0.0070	-0.0061
107	X	0.2624	0.0393	-0.0343	-0.0053	516	X	0.4084	-0.0222	0.0256	0.0014
110	X	0.2896	0.0113	0.0209	-0.0009	523	X	0.2493	0.0634	0.0138	0.0125
114	Xk	0.6179	0.0247	-0.0194	-0.0093	543	Xe	0.3000	-0.0344	0.0251	0.0106
117	X	0.3276	0.0105	0.0217	-0.0137	547	Xk	0.5222	0.1137	-0.0632	-0.0130
125	X	0.2904	0.0039	0.0326	0.0010	559	Xk	0.5903	-0.1093	0.0020	-0.0022
129	X	0.2416	0.1084	-0.0215	-0.0017	564	Xc	0.3484	-0.0162	0.0141	0.0058
131	Xc	0.3533	-0.0964	0.0205	-0.0006	578	Xc	0.3817	-0.1117	0.0208	0.0053
132	Xe	0.2623	-0.0202	-0.0116	0.0417	581	Xk	0.4730	-0.0561	-0.0259	0.0010
135	Xk	0.6776	-0.1128	0.0100	-0.0034	598	X	0.4030	0.0200	0.0137	-0.0052
136	Xe	0.5837	0.0406	-0.0373	0.0108	604	Xc	0.3112	-0.1155	0.0292	-0.0088
139	X	0.2259	0.0141	0.0398	-0.0048	627	X	0.4462	0.0478	-0.0105	-0.0096
140	Xc	0.3408	0.0439	-0.0374	-0.0046	629	X	0.4273	0.0047	0.0262	-0.0028
143	Xc	0.2049	0.0557	-0.0300	-0.0017	634	X	0.1477	0.0718	-0.0105	-0.0064
153	X	0.2397	0.0203	0.0270	-0.0066	671	Xk	0.4580	0.0065	0.0232	-0.0029
161	Xc	0.2951	0.0021	0.0038	-0.0025	678	X	0.2253	0.0598	0.0106	0.0091
166	Xe	0.3336	-0.0499	0.0239	0.0147	687	X	0.3734	0.0638	-0.0046	0.0050
173	Xk	0.4106	-0.0581	-0.0157	-0.0074	712	X	0.3142	-0.0642	0.0136	0.0011
184	X	0.2998	0.0606	0.0022	0.0077	715	X	0.3645	-0.0366	0.0480	-0.0074
190	X	0.1929	0.0404	0.0165	0.0068	718	X	0.2886	0.0190	0.0083	-0.0164
199	X	0.5598	0.0719	0.0048	0.0032	731	Xe	0.4916	-0.0319	-0.0314	0.0169
201	X	0.3268	0.0198	0.0216	-0.0045	739	X	0.3743	0.0043	0.0167	-0.0046
209	Xc	0.3280	-0.0528	-0.0415	-0.0197	741	X	0.2108	0.0607	0.0070	0.0024
214	Xc	0.3675	-0.0953	-0.0253	-0.0054	757	Xk	0.4857	0.0062	-0.0207	-0.0047
216	Xe	0.4042	0.0788	0.0010	0.0208	759	X	0.2045	0.0218	-0.0014	0.0066
242	Xc	0.3480	0.0303	0.0175	-0.0027	771	X	0.1796	0.0788	0.0096	0.0078
247	Xc	0.2746	-0.0315	-0.0449	-0.0096	779	X	0.2523	0.0479	0.0171	-0.0042
250	Xk	0.5518	-0.0056	-0.0384	-0.0059	781	Xc	0.2830	-0.0091	-0.0032	-0.0046
259	X	0.2606	-0.0252	0.0247	-0.0021	789	X	0.3115	-0.0139	0.0025	0.0155
261	X	0.3027	0.0413	0.0051	0.0106	792	X	0.3972	0.0266	-0.0024	-0.0056
272	X	0.2456	0.0816	0.0014	0.0112	796	X	0.2293	0.0309	0.0004	-0.0005
279	X	0.3375	0.1682	-0.0241	-0.0036	815	Xe	0.6046	-0.0368	-0.0477	0.0317
304	Xc	0.2936	0.0041	0.0003	-0.0140	844	X	0.3641	0.0354	0.0116	-0.0105
317	Xe	0.2264	0.0378	-0.0025	0.0201	860	X	0.1978	0.0708	0.0136	0.0084
322	X	0.4136	0.0424	-0.0048	-0.0130	866	X	0.3460	0.0045	0.0017	-0.0310
332	Xk	0.3930	0.0133	-0.0006	-0.0043	872	X	0.3250	0.0073	0.0156	-0.0144

Table 4.3: Secondary spectral components for X-types

Asteroid	Type	Spectral components				Asteroid	Type	Spectral components			
		Slope (X1)	PC2' (X1)	PC3' (X1)	PC4' (X1)			Slope (X1)	PC2' (X1)	PC3' (X1)	PC4' (X1)
907	Xk	0.4345	-0.0983	-0.0283	-0.0234	1891	X	0.2131	0.0401	0.0128	0.0006
924	X	0.2084	0.0351	0.0121	0.0134	1998	Xc	0.3014	-0.0087	0.0065	-0.0128
941	X	0.2944	-0.0016	0.0280	-0.0017	2001	Xe	0.2955	-0.0333	0.0116	0.0439
961	X	0.2216	-0.0029	0.0285	-0.0108	2035	Xe	0.6448	-0.0352	-0.0199	0.0339
965	Xc	0.2435	0.0142	-0.0264	-0.0056	2065	Xc	0.3483	-0.1334	0.0157	0.0104
973	Xk	0.4741	-0.1440	0.0427	-0.0050	2073	X	0.2569	0.0188	0.0120	0.0073
1014	Xe	0.9641	-0.0478	-0.1063	0.0021	2194	Xc	0.2681	0.0047	-0.0213	-0.0103
1015	Xc	0.2933	-0.0573	-0.0106	-0.0217	2306	X	0.2463	-0.0043	0.0241	0.0036
1022	X	0.4297	0.0251	-0.0035	-0.0001	2349	Xc	0.3014	-0.0651	-0.0092	0.0031
1025	Xe	0.8523	-0.1694	-0.0362	0.0165	2390	X	0.2607	-0.0113	0.0001	0.0083
1032	X	0.3543	0.0266	-0.0076	0.0024	2507	Xe	0.5075	-0.0004	-0.0185	0.0190
1039	X	0.4522	-0.0252	-0.0096	0.0022	2559	Xk	0.4504	0.0232	0.0148	0.0021
1046	Xe	0.2627	0.0106	0.0296	0.0246	2560	Xc	0.2941	-0.0575	0.0227	-0.0090
1071	Xk	0.5535	0.0305	-0.0388	-0.0107	2567	Xc	0.4418	-0.0791	0.0212	-0.0008
1094	Xk	0.5931	0.0369	-0.0137	-0.0182	2582	Xc	0.3767	-0.0619	0.0187	-0.0149
1098	Xe	0.1582	0.1180	-0.0063	0.0212	2606	Xk	0.6288	-0.0772	-0.0017	-0.0059
1103	Xk	0.4140	0.0032	-0.0235	0.0013	2681	Xk	0.7556	-0.1275	-0.0161	-0.0169
1104	Xk	0.5656	0.1016	-0.0439	0.0000	2861	Xc	0.2458	-0.0785	0.0621	0.0142
1107	Xc	0.3170	-0.0230	0.0263	-0.0020	2879	X	0.2227	0.0191	0.0118	0.0022
1114	Xc	0.2305	0.0261	-0.0188	-0.0060	2906	Xc	0.3005	0.0128	0.0122	-0.0275
1135	Xk	0.4008	0.0171	-0.0062	-0.0099	2996	Xc	0.3080	-0.0307	-0.0554	-0.0040
1155	Xe	0.4043	0.0076	-0.0550	0.0008	3214	Xc	0.2379	-0.0074	-0.0126	-0.0068
1181	X	0.2789	0.0512	0.0107	0.0151	3224	X	0.1784	0.0553	0.0168	0.0049
1187	X	0.5678	-0.0073	0.0100	-0.0109	3256	X	0.3517	0.0219	0.0167	-0.0069
1196	X	0.2862	0.0256	0.0035	-0.0120	3262	X	0.3118	0.0135	-0.0104	-0.0150
1201	Xc	0.3946	0.0563	-0.0349	-0.0167	3367	X	0.1883	0.0185	0.0097	-0.0023
1212	X	0.3306	0.0734	0.0010	-0.0112	3406	X	0.3441	-0.0093	0.0171	-0.0025
1214	Xk	0.4849	-0.0282	-0.0437	-0.0114	3440	X	0.3345	-0.0405	0.0148	0.0131
1222	X	0.2194	0.0258	0.0129	0.0025	3451	X	0.1921	0.0219	0.0225	-0.0014
1251	X	0.2569	0.0591	0.0183	0.0057	3533	Xk	0.4711	0.0858	0.0072	0.0161
1304	X	0.3620	0.0223	0.0184	0.0041	3567	Xc	0.2306	0.0257	0.0083	-0.0063
1323	Xc	0.2760	-0.0136	-0.0052	-0.0091	3575	X	0.2283	0.0710	0.0455	0.0048
1327	X	0.3395	0.0356	0.0087	-0.0085	3670	X	0.2350	-0.0039	0.0409	0.0116
1351	Xk	0.5364	-0.0300	-0.0443	-0.0383	3686	X	0.2265	0.0193	-0.0063	0.0056
1352	X	0.3403	-0.0080	0.0266	0.0084	3704	Xk	0.4308	-0.0301	-0.0434	-0.0140
1407	X	0.2620	-0.0237	0.0306	0.0041	3730	Xk	0.5051	0.0021	0.0009	-0.0165
1420	X	0.2254	0.0288	0.0437	-0.0007	3759	X	0.2137	0.0022	0.0268	-0.0025
1424	X	0.2522	0.0092	0.0305	-0.0302	3958	Xc	0.2584	-0.0481	-0.0522	-0.0135
1428	Xc	0.3920	-0.0240	0.0107	-0.0145	3976	X	0.4938	0.0076	0.0085	-0.0029
1493	Xc	0.3099	-0.0544	-0.0278	-0.0177	3985	X	0.5424	-0.0297	0.0070	-0.0064
1502	Xc	0.3207	0.0462	-0.0159	-0.0093	4205	Xe	0.3812	-0.0212	-0.0153	0.0221
1517	X	0.2374	0.0186	0.0073	-0.0062	4332	Xe	0.2014	0.0649	-0.0088	0.0164
1541	Xc	0.2003	-0.0475	0.0109	-0.0056	4342	Xc	0.2945	-0.1239	0.0313	0.0263
1548	Xk	0.6392	-0.0364	-0.0050	-0.0164	4353	Xe	0.9067	-0.0296	-0.0840	-0.0159
1592	X	0.2220	0.0090	0.0260	0.0092	4369	Xk	0.5051	0.0696	0.0179	-0.0031
1604	Xc	0.3316	0.0240	-0.0363	-0.0124	4424	Xk	0.5313	-0.1859	-0.0022	0.0154
1638	X	0.2601	0.0048	0.0351	0.0064	4461	X	0.3760	-0.0189	0.0166	-0.0025
1653	X	0.3686	-0.0580	-0.0136	-0.0075	4547	X	0.1877	0.0071	0.0124	-0.0024
1715	X	0.3255	0.0063	0.0160	-0.0028	4701	Xe	0.4070	-0.0048	0.0118	0.0155
1730	Xe	0.6021	-0.0349	-0.0461	0.0061	4750	X	0.3121	-0.0149	0.0037	-0.0079
1847	Xc	0.3991	-0.0562	0.0225	-0.0067	4786	Xc	0.3929	-0.0434	-0.0558	-0.0023
1860	X	0.1841	0.0583	-0.0012	-0.0062	4845	X	0.3391	0.0189	-0.0087	-0.0087

Table 4.3: Secondary spectral components for X-types

Asteroid	Type	Spectral components				Asteroid	Type	Spectral components			
		Slope (X1)	PC2' (X1)	PC3' (X1)	PC4' (X1)			Slope (X1)	PC2' (X1)	PC3' (X1)	PC4' (X1)
4942	X	0.3918	0.0429	0.0011	0.0123	5588	X	0.2977	0.0814	0.0060	0.0104
5087	X	0.2955	-0.0238	0.0489	-0.0047	5632	Xc	0.3265	-0.1055	0.0236	0.0074
5103	X	0.1768	0.0327	0.0287	0.0081	6249	Xe	0.6005	-0.0040	-0.0427	0.0056
5294	X	0.2618	0.0371	-0.0005	0.0099	1973AW3	Xc	0.2379	-0.0065	-0.0064	-0.0154
5467	X	0.5012	0.0587	0.0013	-0.0187	1990WA5	X	0.1994	0.0062	0.0337	0.0027
5578	Xk	0.4626	-0.0748	0.0175	-0.0071	1996TE11	Xc	0.2811	-0.0463	-0.0031	0.0120

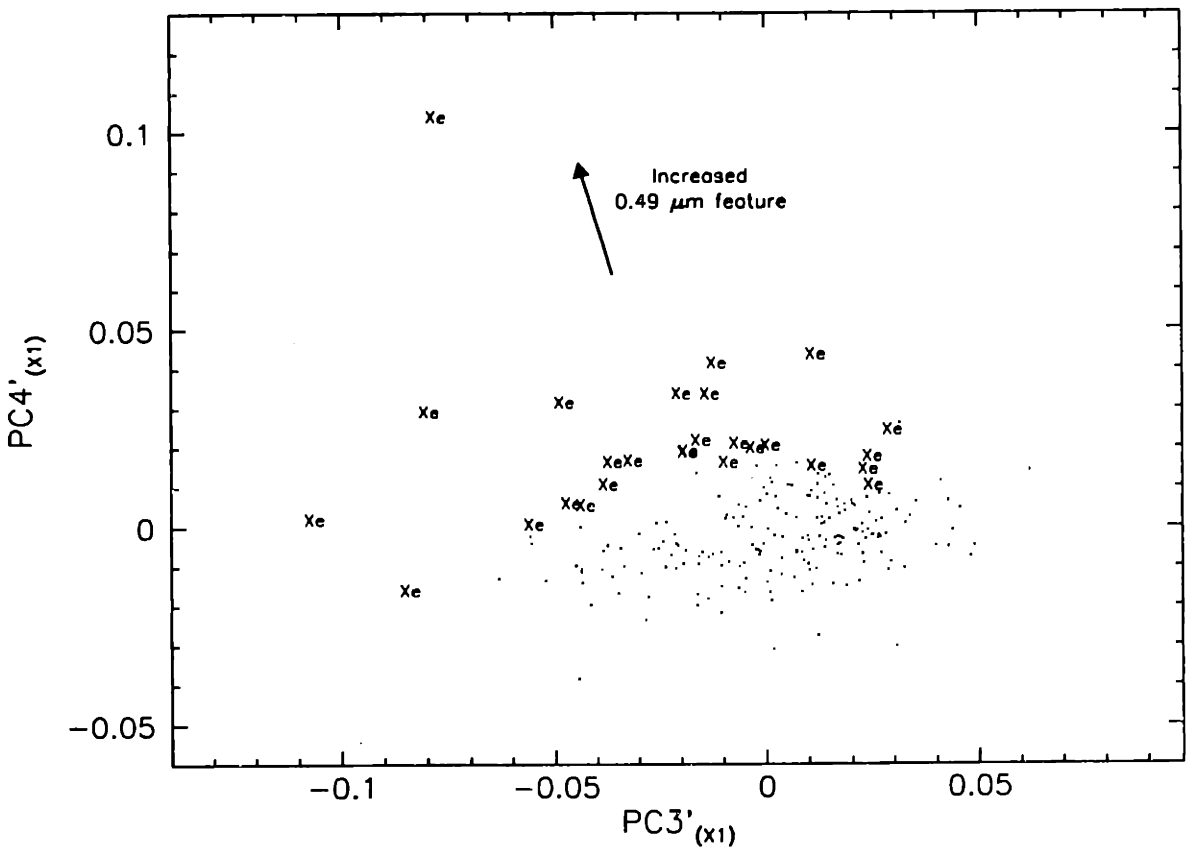

Figure 4.28: Plot of the secondary spectral components $PC4'_{(X1)}$ versus $PC3'_{(X1)}$ for all asteroids in the X-complex. The high-order component ($PC4'_{(X1)}$) is relatively efficient at separating the Xe-class asteroids from the rest of the X-complex objects.

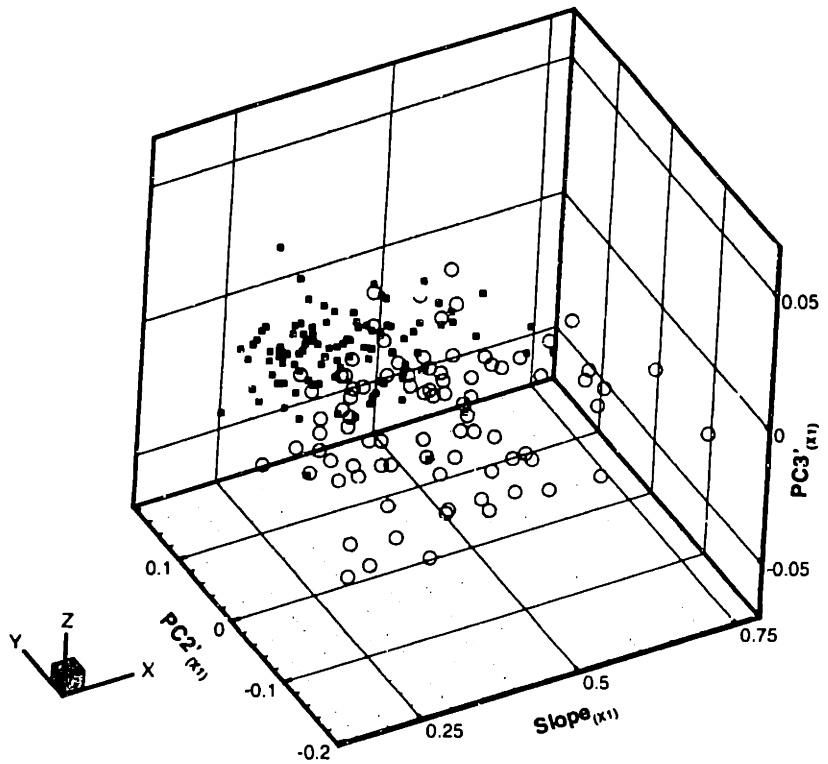

Figure 4.29: A 3-D plot showing the secondary spectral components $Slope_{(X1)}$, $PC2'_{(X1)}$, and $PC3'_{(X1)}$ for the X-types (shown as small, filled squares), and the Xc- and Xk-types (shown combined as open circles). The Xe-types are not plotted. While this set of secondary spectral components is efficient at separating the Xe-types from the rest of the X-complex (as shown in Figure 4.28), the separation between the X-types and the combined Xc- and Xk-types appears only slightly improved compared with Figure 4.27, where the two primary components of Slope and PC2' were used.

component analysis. To differentiate these new, or secondary spectral components from other components previously calculated, the subscript of $_{(X1)}$ is appended to the component labels (for example, $Slope_{(X1)}$, $PC2'_{(X1)}$, etc.). In Table 4.3, the first four components from this analysis are listed. The secondary component plane of $PC4'_{(X1)}$ versus $PC3'_{(X1)}$ is shown in Figure 4.28. All members of the X-complex have been included, though for clarity, those asteroids classified as X-, Xc-, or Xk-types are plotted as points. In this plane, it is clear that the spectral characteristics defining the Xe-class, particularly the 0.49 μm band, can be isolated. In Figure 4.29, members of the Xe-class have been removed, and the remaining X-, Xc-, and Xk-types are plotted in the 3-dimensional space of $Slope_{(X1)}$, $PC2'_{(X1)}$, and $PC3'_{(X1)}$, to determine if these classes can

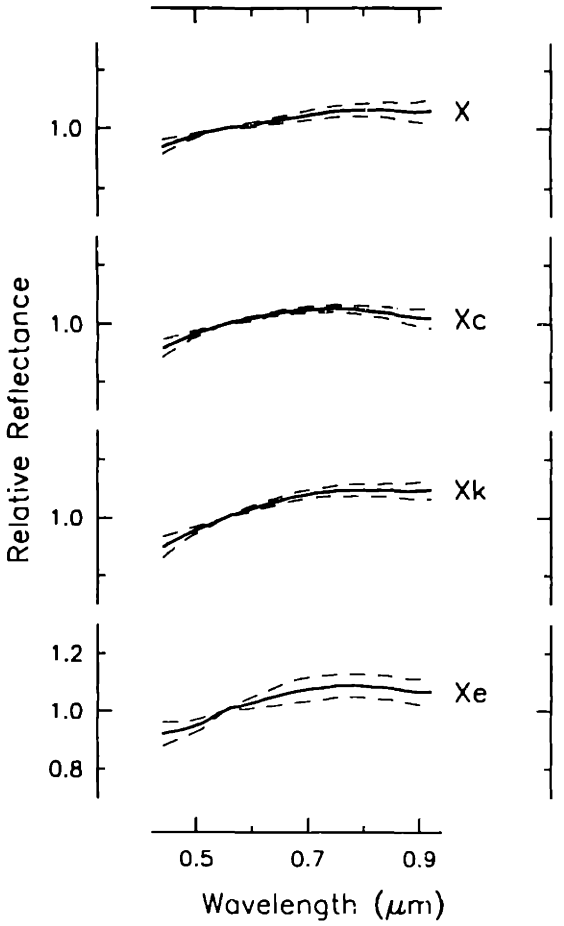

Figure 4.30: Similar to Figure 4.6, but showing the mean spectra for the four classes contained in the X-complex.

be better separated based on these new secondary components. However, this plot shows that the boundary between the X-types and the combined Xc- and Xk-types is still vague, with little to nc improvement over the separation that was achieved by the primary components Slope and PC2' in Figure 4.27. This difficulty in quantitatively separating the X-class from the Xc- and Xk-types results, in part, from the subtle nature of the spectral curvature used to differentiate the classes, and how that curvature was evaluated in each individual spectrum. Another factor contributing to the scatter along this boundary in component space is the higher-frequency, random variations in each fitted spectrum that contribute to the overall variance described by these lower-order spectral components. Finally, in Figure 4.30, the mean spectrum is plotted for each of the four classes contained in the X-complex, along with envelopes representing the 1σ

variation, as a function of wavelength, for all of the spectra contained in each of those classes.

4.7 Discussion

In the general scheme of asteroid taxonomy, the question can be asked: "What sets this new feature-based taxonomy apart from previous efforts to classify asteroids?" After all, every other taxonomy has been based on measurements of how incident sunlight interacts with, and is reflected from mineral grains on the surfaces of asteroids, and thus, in principle have relied on variations in spectral features. We assert that the taxonomy presented here differs from earlier classification systems in two important ways: 1) this is the first time results from high-resolution CCD spectroscopy have been use as the basis for development of a complete asteroid taxonomy, and 2) we have relied on the detection of distinct, though sometimes subtle differences in spectral features for developing our taxonomic classes, rather than basing these classes directly on the results of multivariate analysis techniques. In the preceding discussions, we routinely used results from principal component analysis, and referred to projections of asteroid spectra in component space as a means of visualizing the differences between those spectra. However, we made every effort to relate the variance described by those spectral components to trends in specific features contained in the spectra. In the end, it is the presence or absence of these spectral features, along with the recognition of variations in those features, that form the foundation of this taxonomy. The procedures followed in developing the taxonomy can best be described as a "human neural network", in which, as information was gained and assimilated throughout the learning process, decisions were made as to how to best proceed with the structuring of the taxonomy, and with assigning objects to individual spectral classes. An objective test of this taxonomy will be to train an artificial neural network, based on the rules used here in defining each spectral class, and to reanalyze the SMASSII dataset, comparing the resulting classifications from that analysis with the taxonomic designations we present in Appendix A.

4.7.1 Application to new asteroids

An important aspect of any taxonomy, and a measure of its usefulness to subsequent scientific efforts, is how easily the taxonomy can be applied to newly

observed, but as yet unclassified members of a population. When a taxonomy is derived using multivariate techniques, it can be difficult to incorporate new members into that taxonomy, and often requires that the multivariate solution be recalculated based on an expanded dataset, consisting of the original sample plus the newly observed members of the population. If instead, the rules and procedures around which the taxonomy is developed are based on specific identifiable (and quantifiable) characteristics of the population, then it should be possible to apply those rules to any new member in a straightforward manner, without requiring any reanalysis of the original sample.

A concise summary of our new feature-based asteroid taxonomy is shown in Figure 4.31. All 26 spectral classes are plotted with constant horizontal and vertical scalings, and are arranged in a way that approximates the relative position of each class in the primary spectral component plane of PC2' versus Slope. This key provides a particularly instructive comparison of these 26 classes by emphasizing the continuous relationship between adjacent classes, and demonstrating how the major spectral features (in particular, the average spectral slope and the 1 μm band) vary across this continuum. However, this figure does not, in itself, provide any specific rules by which a new asteroid might be classified, and therefore should only be considered a "quick reference" to this taxonomy. A more thorough summary of the individual classes is needed, though how this information is best presented depends, in large part, on how it is intended to be used. For example, if a large number of asteroid spectra are to be classified, then it might be more efficient to consider each spectral class separately, and to identify all of those asteroids whose spectral properties belong to that class. One the other hand, if only a single asteroid is being considered, then it might more appropriate to ask what spectral features or characteristics are present, and based on those characteristics, quickly focus in on a proper classification. In either case, accurate descriptions of the pertinent spectral features are fundamental to successfully applying this taxonomy to other asteroids. Figure 4.32 summarizes all of the primary spectral features and characteristics that are used in defining our spectral classes. Throughout the text, I have tried to maintain a consistent terminology when describing the different forms of these features.

Descriptions for all 26 classes are listed in Table 4.4. These descriptions are qualitative in nature, highlighting those features or characteristics in the spectrum that are considered diagnostic. Also listed in this table are the permanent numbers of up to

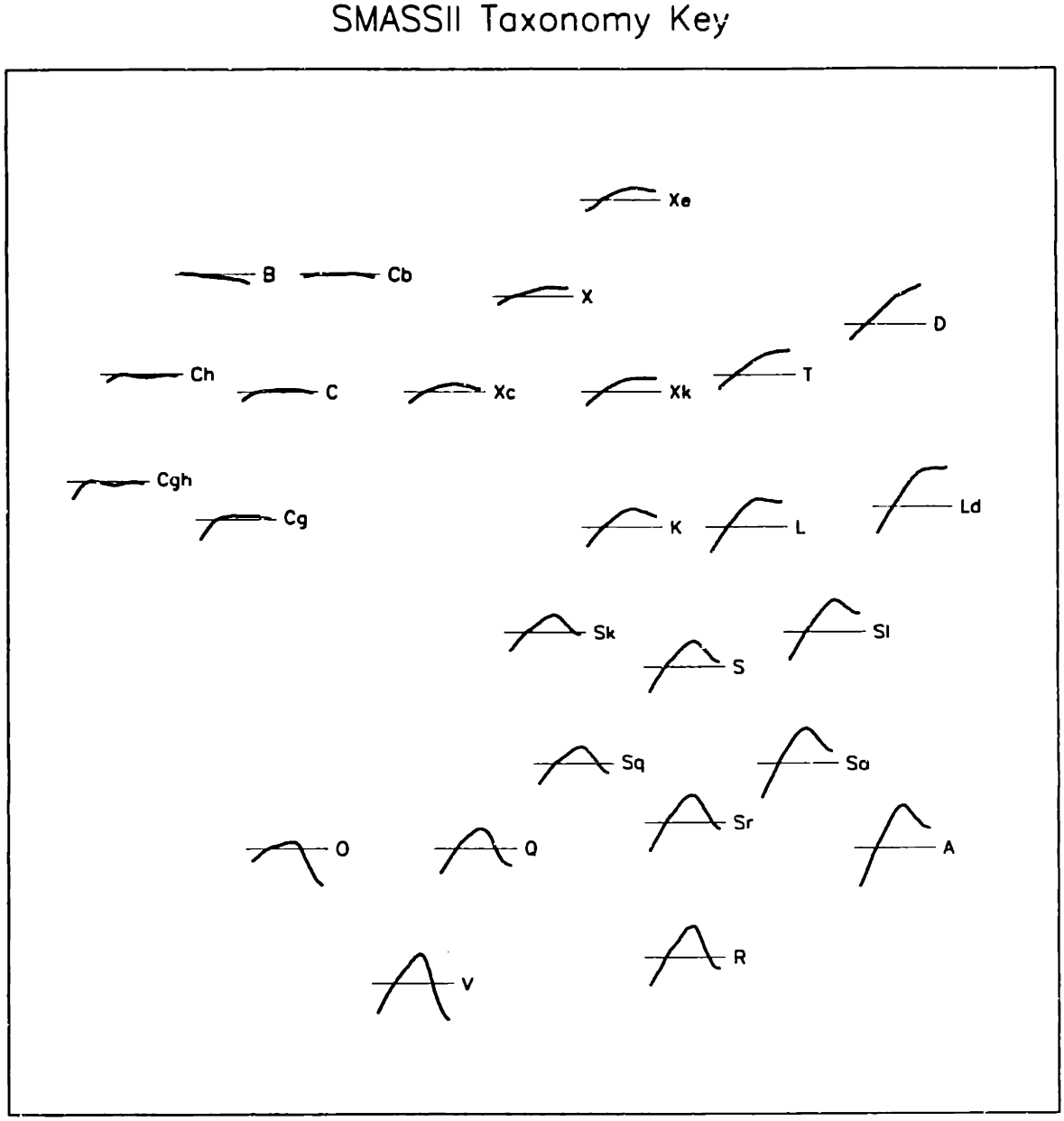

Figure 4.31: Key showing all 26 SMASSII taxonomic classes. The spectra are arranged in a pattern that approximates the class location in spectral component (PCA) space. Thus, depth of the 1 μm band generally increases from top to bottom, and average spectral slope increases from left to right. Due to the spectral complexity of the C- and X-complexes, the locations of some of these classes do not strictly follow the pattern. The horizontal lines to which each spectrum is referenced shows the normalized reflectance of 1.00.

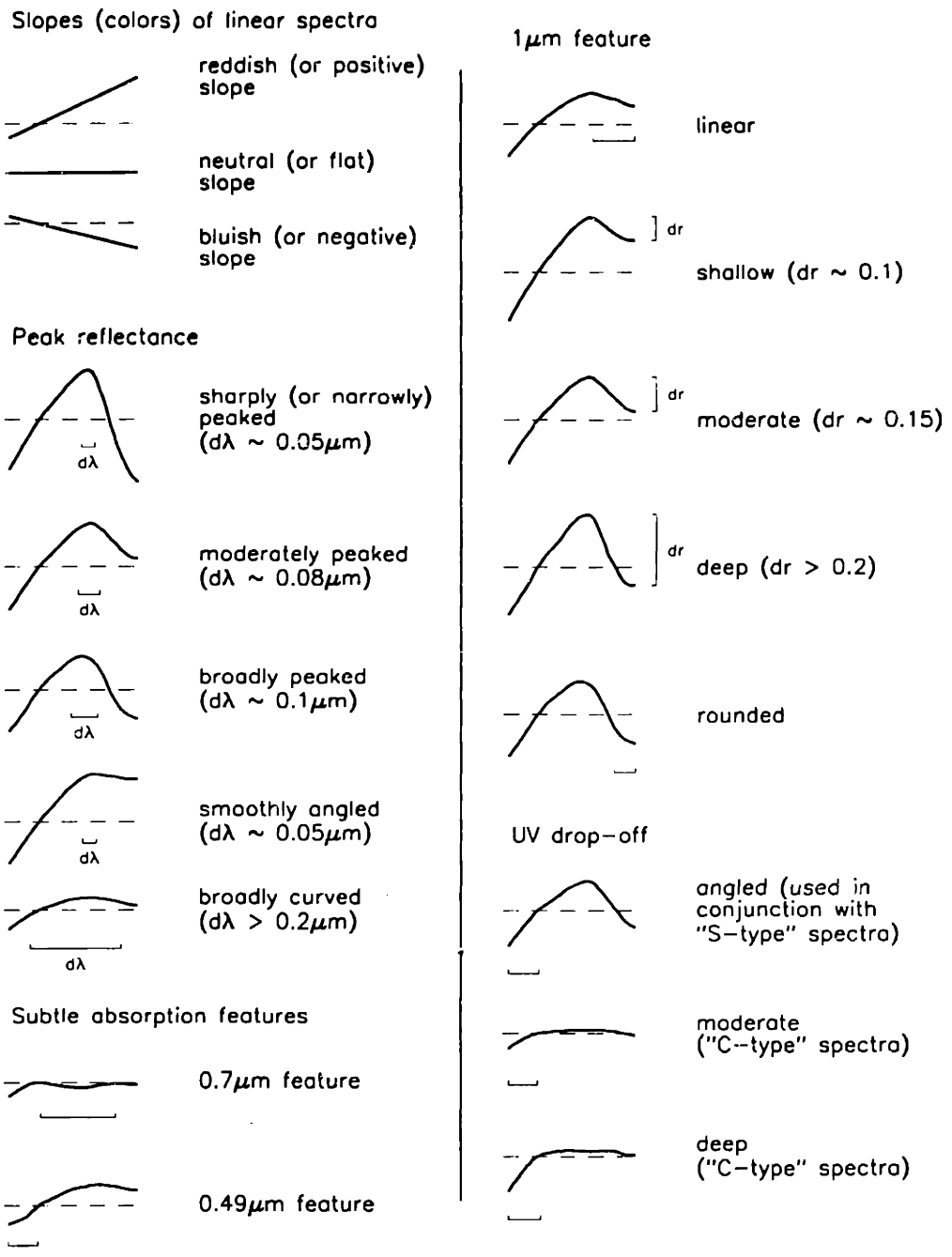

Figure 4.32: Definitions of the primary spectral features used in defining this taxonomy. The terms used to describe these features are used in subsequent tables and figures, as well as throughout the text. Brackets define the important region of each spectrum (showing the limits of the pertinent feature). Measures of dλ (interval of wavelength) or dr (interval in relative reflectance) are given as guides. The dashed lines refer to a normalized reflectance of 1.00.

Table 4.4: Description of classes within this feature-based taxonomy

Type	Description	Examples of spectral type
A	Very steep to extremely steep red slope shortward of 0.75 μm, and a moderately deep absorption feature, longward of 0.75 μm. The shape of the spectrum around 0.75 μm, where the reflectance is maximum, can either be sharply peaked, or can be quite broad, with the shape of the peak being possibly tied to the shape and roundness of the 1μm feature. A subtle absorption feature is often present around 0.63 μm.	246, 289, 863
B	Linear, featureless spectrum over interval of 0.44 to 0.92 μm, with negative (bluish) to flat slope.	2, 24, 85
C	Weak to medium UV absorption feature shortward of 0.55 μm, generally flat to slightly reddish and featureless longward of 0.55 μm.	1, 10, 52
Cb	Generally linear, featureless spectrum over interval of 0.44 to 0.92 μm (though very subtle curvature is possible), with a flat to slightly reddish slope.	150, 210, 2060
Cg	Strong UV absorption feature shortward of 0.55 μm and generally flat to slightly reddish slope longward of 0.55 μm, occasionally with a shallow absorption feature longward of 0.85 μm.	175, 1300, 1695
Cgh	Similar to Cg spectrum, except for addition of broad, moderately shallow absorption band centered near 0.7 μm.	38, 106, 706
Ch	Similar to C spectrum, except for addition of broad, relatively shallow absorption band centered near 0.7 μm.	19, 48, 49
D	Relatively featureless spectrum with very steep red slope. A decrease in spectral slope (less red) is sometimes observed longward of 0.75 μm.	1542, 2246, 4744
K	Moderately steep red slope shortward of 0.75 μm, a smoothly angled maximum and a basically flat to slightly negative (bluish) slope longward of 0.75 μm, showing little or no curvature of the absorption band.	221, 579, 679
L	Very steep red slope shortward of 0.75 μm, becoming approximately flat, with a relative reflectance of about 1.2 longward of 0.75 μm.	42, 236, 908
Ld	Very steep red slope shortward of 0.7 μm, becoming essentially flat, with a relative reflectance of roughly 1.3 longward of 0.75 μm. Spectrum is generally steeper over the interval of 0.44 to 0.7 μm, and is flatter from 0.75 to 0.92 μm, than is typical for D-types.	269, 1406, 2850

Table 4.4: Description of classes within this feature-based taxonomy

Type	Description	Examples of spectral type
O	Moderately red slope from 0.44 to 0.54 μm, then less steep over interval of 0.54 to 0.7 μm, reaching peak relative reflectance of 1.05. Deep absorption feature longward of 0.75 μm. Single type object (3628 Božněmcová) in class.	3628
Q	Moderately steep red slope shortward of 0.7 μm, and a deep, very rounded absorption feature longward of 0.75 μm that reaches a minimum reflectance level of about 0.9. Single type object (1862 Apollo) in class.	1862
R	Very steep red slope shortward of 0.7 μm, and a deep absorption feature longward of 0.75 μm. The shape of the spectrum, near maximum reflectance, is more sharply peaked than it is in S-type spectra, and is somewhat skewed due to the absorption band that reaches a minimum at roughly 0.9 μm with a relative reflectance level of 0.9. Additional small absorption feature is centered near 0.52 μm.	349, 1904
S	Moderately steep, reddish slope shortward of 0.7 μm, and a moderate to deep absorption band longward of 0.75 μm. Average S-type spectrum has a peak reflectance of about 1.2 at 0.73 μm. The spectral slope is almost always slightly steeper over the wavelength interval of 0.44 to 0.55 μm than it is from 0.55 to 0.7 μm, and often, there is a broad, but shallow absorption feature centered around 0.63 μm.	5, 7, 20
Sa	Spectrum intermediate between S- and A-types. Very steep red slope shortward of 0.7 μm. Shape of the spectrum around maximum reflectance is more gently rounded than it is in A-types.	63, 244, 913
Sk	Intermediate between S- and K-type spectra. Absorption feature longward of 0.75 μm shows moderate curvature, unlike the K-type spectra, which are approximately linear over that interval. Compared with other S-types, the 0.63 μm feature can be strong.	3, 11, 43
Sl	Intermediate between S- and L-type spectra. Absorption feature longward of 0.75 μm is shallow to moderately deep, unlike L-types, where this spectral interval is essentially flat.	30, 192, 354
Sq	Spectrum intermediate between S- and Q-types. Compared with other S-types, can contain a relatively strong 0.63 μm feature.	33, 720, 1483
Sr	Intermediate between S- and R-type spectra. Very steep red slope shortward of 0.7 μm and a deep absorption feature longward of 0.75 μm. Reflectance peak is broader and more symmetrical in shape than it is for R-types.	984, 1494, 2956

Table 4.4: Description of classes within this feature-based taxonomy

Type	Description	Examples of spectral type
T	Moderately steep red slope shortward of 0.75 μm, becoming flat with a relative reflectance between 1.15 and 1.2 longward of 0.85 μm. The change in spectral slope occurs very gently.	96, 596, 3317
V	Moderate to very steep red slope shortward of 0.7 μm, with an extremely deep absorption band longward of 0.75 μm that usually reaches a minimum relative reflectance level of 0.7 tc 0.8. The spectral slope between 0.44 and 0.55 μm is usually slightly steeper than that over the interval of 0.55 to 0.7 μm. An additional small absorption feature, centered near 0.52 μm, is occasionally seen. The largest member, 4 Vesta, is anomalous in that its slope and band depth are less extreme than for other members of this spectral class.	4, 1929, 2912
X	A generally featureless spectrum, with slight to moderate reddish slope. A subtle UV absorption feature, shortward of 0.55 μm, can be present, as well as an occasional shallow feature longward of 0.85 μm.	22, 55, 69
Xc	A slightly reddish spectrum, generally featureless except for a gentle curvature, concave-side down, over the middle and red portions of the spectrum.	46, 65, 92
Xe	Overall slope that is slightly to moderately red, with a series of subtle absorption features. Most dominate feature is an absorption band, shortward of 0.55 μm, that exhibits a concave-side up curvature (especially visible in the spectrum of 64 Angelina, where the center of this band is clearly seen at 0.49 μm). Often present is a very shallow absorption feature centered around 0.6 μm. Also, a decrease in spectral slope (becoming less red or even bluish) is usually seen longward of 0.75 μm.	64, 71, 434
Xk	Moderately red slope, shortward of about 0.75 μm, and generally flat longward of 0.75 μm with a peak relative reflectance of roughly 1.1, the change in slope occurring very gradually. Similar in spectral shape to Xc, but redder in overall slope.	21, 56, 114

Table 4.5: Statistics for selected wavelength channels in each spectral class

Type (No. of objects)		Wavelength (μm)								
		0.44	0.50	0.60	0.65	0.70	0.75	0.80	0.85	0.92
A (15)	High	0.747	0.886	1.139	1.248	1.330	1.359	1.337	1.297	1.243
	Low	0.659	0.841	1.095	1.179	1.243	1.215	1.112	1.052	1.033
	Mean	0.711	0.869	1.108	1.210	1.292	1.305	1.245	1.183	1.143
	StDev	0.025	0.013	0.011	0.019	0.025	0.037	0.060	0.069	0.067
B (51)	High	1.075	1.025	1.006	1.006	1.002	1.005	1.002	1.009	1.009
	Low	0.967	0.985	0.977	0.961	0.945	0.932	0.900	0.880	0.838
	Mean	1.007	1.004	0.988	0.984	0.977	0.974	0.968	0.960	0.935
	StDev	0.022	0.007	0.007	0.011	0.014	0.018	0.024	0.027	0.039
C (137)	High	0.977	1.002	1.032	1.038	1.042	1.059	1.061	1.064	1.064
	Low	0.872	0.952	0.971	0.984	0.973	0.967	0.959	0.931	0.856
	Mean	0.935	0.978	1.007	1.013	1.015	1.016	1.014	1.008	0.993
	StDev	0.025	0.009	0.009	0.011	0.013	0.016	0.017	0.023	0.034
Cb (25)	High	1.039	1.010	1.009	1.028	1.030	1.023	1.032	1.039	1.041
	Low	0.957	0.981	0.986	0.990	0.983	0.977	0.978	0.964	0.929
	Mean	0.980	0.995	0.997	1.000	1.000	1.003	1.002	0.994	0.978
	StDev	0.019	0.007	0.005	0.008	0.010	0.011	0.015	0.020	0.032
Cg (9)	High	0.868	0.962	1.028	1.050	1.052	1.057	1.067	1.082	1.057
	Low	0.825	0.924	0.999	0.993	0.989	0.988	0.992	0.969	0.927
	Mean	0.852	0.945	1.018	1.028	1.027	1.025	1.026	1.022	1.007
	StDev	0.013	0.013	0.012	0.020	0.020	0.023	0.027	0.036	0.044
Cgh (14)	High	0.912	0.992	1.024	1.027	1.026	1.030	1.047	1.063	1.076
	Low	0.811	0.937	0.966	0.934	0.904	0.903	0.912	0.913	0.870
	Mean	0.868	0.961	0.998	0.986	0.974	0.975	0.990	0.995	0.983
	StDev	0.025	0.013	0.016	0.027	0.035	0.038	0.042	0.047	0.060
Ch (124)	High	1.021	1.004	1.013	1.014	1.015	1.026	1.046	1.056	1.073
	Low	0.878	0.962	0.970	0.945	0.928	0.931	0.937	0.925	0.911
	Mean	0.939	0.985	0.992	0.983	0.977	0.983	0.991	0.996	0.992
	StDev	0.028	0.009	0.008	0.014	0.018	0.021	0.025	0.029	0.038
D (9)	High	0.936	0.971	1.055	1.108	1.171	1.234	1.252	1.300	1.408
	Low	0.843	0.933	1.041	1.089	1.139	1.184	1.201	1.218	1.199
	Mean	0.882	0.951	1.046	1.098	1.150	1.199	1.222	1.247	1.287
	StDev	0.029	0.012	0.005	0.006	0.010	0.015	0.018	0.026	0.067
K (28)	High	0.897	0.959	1.073	1.128	1.166	1.168	1.153	1.153	1.175
	Low	0.809	0.922	1.031	1.066	1.092	1.106	1.084	1.063	1.029
	Mean	0.860	0.942	1.044	1.083	1.121	1.138	1.124	1.109	1.081
	StDev	0.023	0.009	0.010	0.016	0.019	0.018	0.019	0.023	0.036

Table 4.5: Statistics for selected wavelength channels in each spectral class

Type (No. of objects)		Wavelength (μm)								
		0.44	0.50	0.60	0.65	0.70	0.75	0.80	0.85	0.92
L (31)	High	0.875	0.947	1.094	1.172	1.232	1.263	1.242	1.232	1.268
	Low	0.743	0.892	1.048	1.098	1.139	1.168	1.166	1.157	1.097
	Mean	0.817	0.922	1.066	1.130	1.179	1.207	1.201	1.193	1.188
	StDev	0.032	0.014	0.013	0.021	0.026	0.025	0.021	0.019	0.041
Ld (12)	High	0.875	0.951	1.111	1.210	1.267	1.327	1.359	1.373	1.403
	Low	0.717	0.875	1.049	1.117	1.178	1.216	1.230	1.224	1.204
	Mean	0.800	0.913	1.080	1.164	1.228	1.270	1.281	1.286	1.292
	StDev	0.044	0.022	0.018	0.028	0.031	0.035	0.039	0.041	0.069
O (1)	High	-	-	-	-	-	-	-	-	-
	Low	-	-	-	-	-	-	-	-	-
	Mean	0.907	0.960	1.019	1.034	1.045	1.035	0.936	0.822	0.727
	StDev	-	-	-	-	-	-	-	-	-
Q (1)	High	-	-	-	-	-	-	-	-	-
	Low	-	-	-	-	-	-	-	-	-
	Mean	0.818	0.914	1.063	1.110	1.144	1.128	1.040	0.926	0.872
	StDev	-	-	-	-	-	-	-	-	-
R (2)	High	0.814	0.899	1.082	1.152	1.216	1.236	1.117	0.990	0.926
	Low	0.773	0.899	1.072	1.149	1.215	1.217	1.101	0.985	0.922
	Mean	0.793	0.899	1.077	1.151	1.215	1.227	1.109	0.988	0.924
	StDev	0.029	0.000	0.008	0.003	0.001	0.014	0.011	0.004	0.003
S (332)	High	0.907	0.947	1.100	1.172	1.236	1.244	1.204	1.158	1.153
	Low	0.742	0.872	1.038	1.076	1.116	1.132	1.094	1.026	0.935
	Mean	0.813	0.919	1.060	1.121	1.169	1.188	1.146	1.086	1.036
	StDev	0.029	0.012	0.012	0.019	0.024	0.024	0.023	0.027	0.040
Sa (31)	High	0.789	0.912	1.116	1.209	1.285	1.316	1.290	1.247	1.230
	Low	0.668	0.857	1.076	1.152	1.221	1.233	1.167	1.099	0.972
	Mean	0.746	0.891	1.094	1.180	1.244	1.261	1.215	1.149	1.089
	StDev	0.029	0.012	0.010	0.014	0.015	0.020	0.024	0.035	0.059
Sk (29)	High	0.915	0.972	1.055	1.105	1.144	1.158	1.113	1.057	1.040
	Low	0.781	0.917	1.026	1.052	1.082	1.085	1.055	1.019	0.943
	Mean	0.860	0.941	1.038	1.083	1.117	1.130	1.090	1.033	0.987
	StDev	0.026	0.011	0.007	0.012	0.017	0.018	0.013	0.011	0.025
Sl (35)	High	0.847	0.924	1.097	1.179	1.239	1.272	1.254	1.216	1.225
	Low	0.730	0.891	1.062	1.121	1.173	1.208	1.180	1.123	1.055
	Mean	0.789	0.909	1.075	1.148	1.208	1.238	1.208	1.165	1.140
	StDev	0.027	0.008	0.009	0.013	0.015	0.016	0.020	0.026	0.041

Table 4.5: Statistics for selected wavelength channels in each spectral class

Type (No. of objects)		Wavelength (μm)								
		0.44	0.50	0.60	0.65	0.70	0.75	0.80	0.85	0.92
Sq (33)	High	0.948	0.964	1.057	1.113	1.157	1.166	1.104	1.028	0.986
	Low	0.803	0.918	1.022	1.056	1.077	1.072	1.021	0.950	0.849
	Mean	0.848	0.936	1.039	1.084	1.118	1.125	1.073	1.000	0.929
	StDev	0.034	0.011	0.009	0.017	0.021	0.024	0.021	0.020	0.032
Sr (16)	High	0.868	0.941	1.096	1.178	1.244	1.242	1.181	1.098	1.049
	Low	0.713	0.865	1.042	1.092	1.140	1.149	1.068	0.982	0.859
	Mean	0.788	0.904	1.068	1.137	1.189	1.194	1.125	1.035	0.948
	StDev	0.043	0.023	0.018	0.029	0.034	0.032	0.034	0.034	0.047
T (14)	High	0.938	0.968	1.061	1.119	1.164	1.180	1.187	1.209	1.243
	Low	0.854	0.942	1.024	1.055	1.091	1.128	1.137	1.143	1.131
	Mean	0.894	0.956	1.041	1.083	1.119	1.150	1.164	1.175	1.183
	StDev	0.027	0.008	0.011	0.016	0.019	0.015	0.015	0.021	0.038
V (21)	High	0.893	0.959	1.111	1.208	1.298	1.317	1.152	0.954	0.806
	Low	0.665	0.858	1.022	1.048	1.074	1.092	0.998	0.771	0.609
	Mean	0.784	0.905	1.071	1.139	1.198	1.206	1.054	0.870	0.730
	StDev	0.054	0.024	0.020	0.038	0.052	0.050	0.036	0.041	0.056
X (107)	High	1.011	0.996	1.037	1.067	1.092	1.116	1.135	1.154	1.189
	Low	0.889	0.957	1.000	1.008	1.019	1.028	1.034	1.009	0.989
	Mean	0.940	0.977	1.013	1.030	1.045	1.058	1.063	1.061	1.060
	StDev	0.024	0.008	0.007	0.012	0.016	0.019	0.021	0.026	0.038
Xc (49)	High	0.979	0.987	1.038	1.061	1.072	1.084	1.076	1.073	1.104
	Low	0.863	0.943	1.006	1.020	1.026	1.036	1.010	0.994	0.934
	Mean	0.918	0.969	1.020	1.039	1.050	1.054	1.047	1.037	1.020
	StDev	0.031	0.011	0.008	0.008	0.010	0.012	0.015	0.020	0.034
Xe (27)	High	1.014	0.989	1.076	1.137	1.167	1.174	1.173	1.141	1.155
	Low	0.815	0.905	0.999	1.009	1.021	1.036	1.037	1.015	0.992
	Mean	0.923	0.950	1.030	1.057	1.077	1.089	1.088	1.081	1.068
	StDev	0.041	0.021	0.020	0.035	0.042	0.040	0.040	0.041	0.049
Xk (37)	High	0.979	0.980	1.062	1.094	1.120	1.126	1.140	1.139	1.172
	Low	0.822	0.922	1.018	1.032	1.057	1.063	1.065	1.055	1.043
	Mean	0.899	0.959	1.033	1.061	1.084	1.096	1.098	1.098	1.100
	StDev	0.037	0.013	0.010	0.013	0.014	0.018	0.020	0.023	0.034

three asteroids, observed during the SMASSII survey, which are representative examples of that spectral class. Listed in Table 4.5 are the high and low values, the mean, and the standard deviation for nine spectral channels, based on all of the SMASSII asteroids contained in each spectral class. When combined, the information contained in Tables 4.4 and 4.5, along with the graphical representations of the mean spectra (such as those shown in Fig. 4.31, and with greater detail in Figs. 4.6, 4.9, 4.23 and 4.30) provides a sufficient foundation for applying this taxonomy in the classification of other asteroids. If an asteroid is to be classified using these general class descriptions, the CCD spectrum needs to meet some limited requirements: 1) the spectrum should ideally cover the wavelength interval of 0.44 to 0.92 μm, though, as long as the spectrum extends far enough in both directions that features such as the UV drop-off or 0.49 μm band (at the blue end), and the degree of curvature, or linearity, in the 1 μm band (at the red end) can be recognized, a shorter wavelength coverage is acceptable, 2) the spectrum must be properly calibrated to a solar analog star, and normalized to unity at 0.55 μm, 3) any discrepant values, or systematic (instrumental) features in the spectrum should be removed, or at least the intervals over which those features occur must be determined and their effects on the spectrum accounted for, and 4) the spectrum should be fitted by a smoothing function to reduce the random noise level of individual channels.

Another method for applying this taxonomy is provided by Figure 4.33. This flowchart, or decision tree, presents a logical series of questions, each requiring a binary response of "yes" or "no". The structure of this decision tree follows a natural thought process, which begins by asking if the most prominent spectral feature, the 1 μm silicate absorption band, is present. Subsequent steps in the flowchart determine if less prominent features or characteristics are present, until a unique classification can be established. Many of the questions included in this flowchart are quantitative in nature, and require finding the relative reflectance, r, at a specific wavelength channel, calculating the average spectral slope, γ (analogous to the primary spectral component Slope, as defined by Eqn. 3.3), or determining a series of dissimilarities with respect to mean spectra (using Eqn. 3.2 and the mean spectra associated with the S-complex, listed in Table 4.1). Other questions in the flowchart that ask if specific spectral features are present can require decisions to be made that are necessarily more subjective. In most cases, spectral features are quite obvious, especially in the fitted (smoothed)

Procedure for Classifying New Asteroids

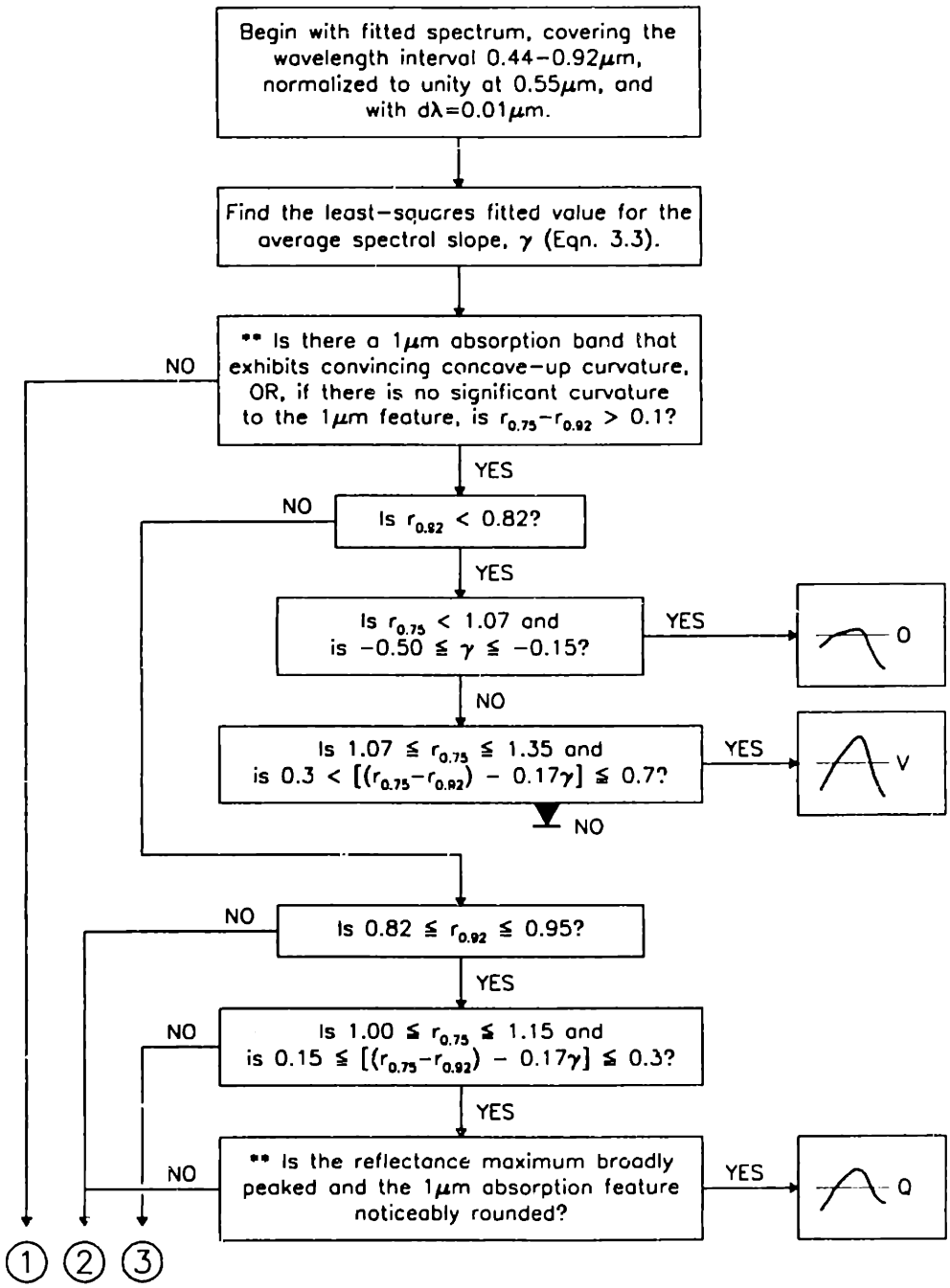

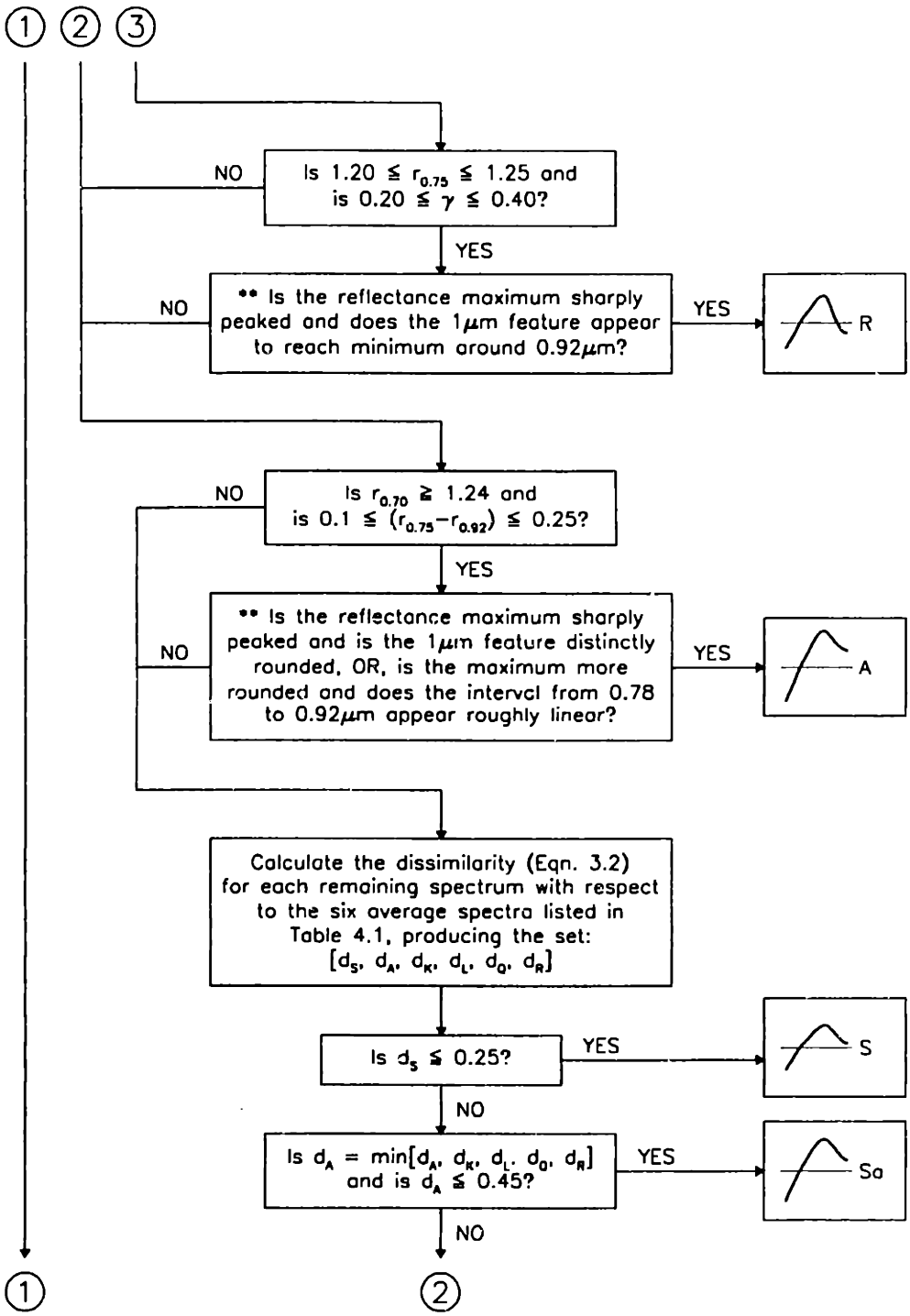
1
2
3
NO
Is 1.20 ≤ $r_{0.75}$ ≤ 1.25 and is 0.20 ≤ γ ≤ 0.40?
YES
NO
** Is the reflectance maximum sharply peaked and does the 1μm feature appear to reach minimum around 0.92μm?
YES
R
NO
Is $r_{0.70}$ ≥ 1.24 and is 0.1 ≤ ($r_{0.75}$−$r_{0.92}$) ≤ 0.25?
YES
NO
** Is the reflectance maximum sharply peaked and is the 1μm feature distinctly rounded, OR, is the maximum more rounded and does the interval from 0.78 to 0.92μm appear roughly linear?
YES
A
Calculate the dissimilarity (Eqn. 3.2) for each remaining spectrum with respect to the six average spectra listed in Table 4.1, producing the set: [d_S, d_A, d_K, d_L, d_O, d_R]
Is d_S ≤ 0.25?
YES
S
NO
Is d_A = min[d_A, d_K, d_L, d_O, d_R] and is d_A ≤ 0.45?
YES
Sa
NO
1
2

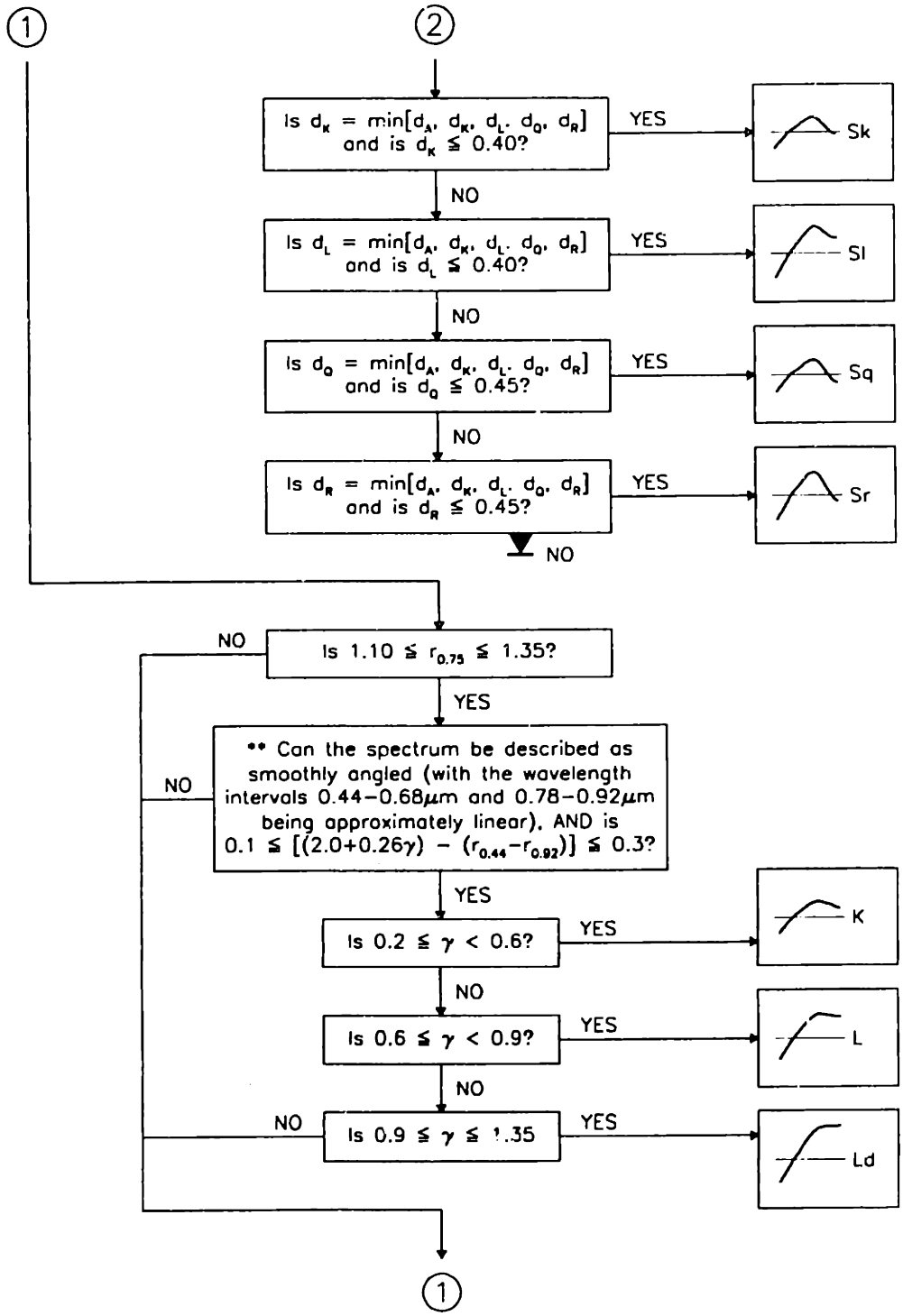
1
2
Is d_K = min[d_A, d_K, d_L, d_Q, d_R] and is $d_K \leqq 0.40$?
YES
Sk
NO
Is d_L = min[d_A, d_K, d_L, d_Q, d_R] and is $d_L \leqq 0.40$?
YES
Sl
NO
Is d_Q = min[d_A, d_K, d_L, d_Q, d_R] and is $d_Q \leqq 0.45$?
YES
Sq
NO
Is d_R = min[d_A, d_K, d_L, d_Q, d_R] and is $d_R \leqq 0.45$?
YES
Sr
NO
NO
Is $1.10 \leqq r_{0.75} \leqq 1.35$?
YES
** Can the spectrum be described as smoothly angled (with the wavelength intervals 0.44–0.68μm and 0.78–0.92μm being approximately linear), AND is $0.1 \leqq [(2.0+0.26\gamma) - (r_{0.44}-r_{0.92})] \leqq 0.3$?
NO
YES
Is $0.2 \leqq \gamma < 0.6$?
YES
K
NO
Is $0.6 \leqq \gamma < 0.9$?
YES
L
NO
NO
Is $0.9 \leqq \gamma \leqq 1.35$
YES
Ld
1

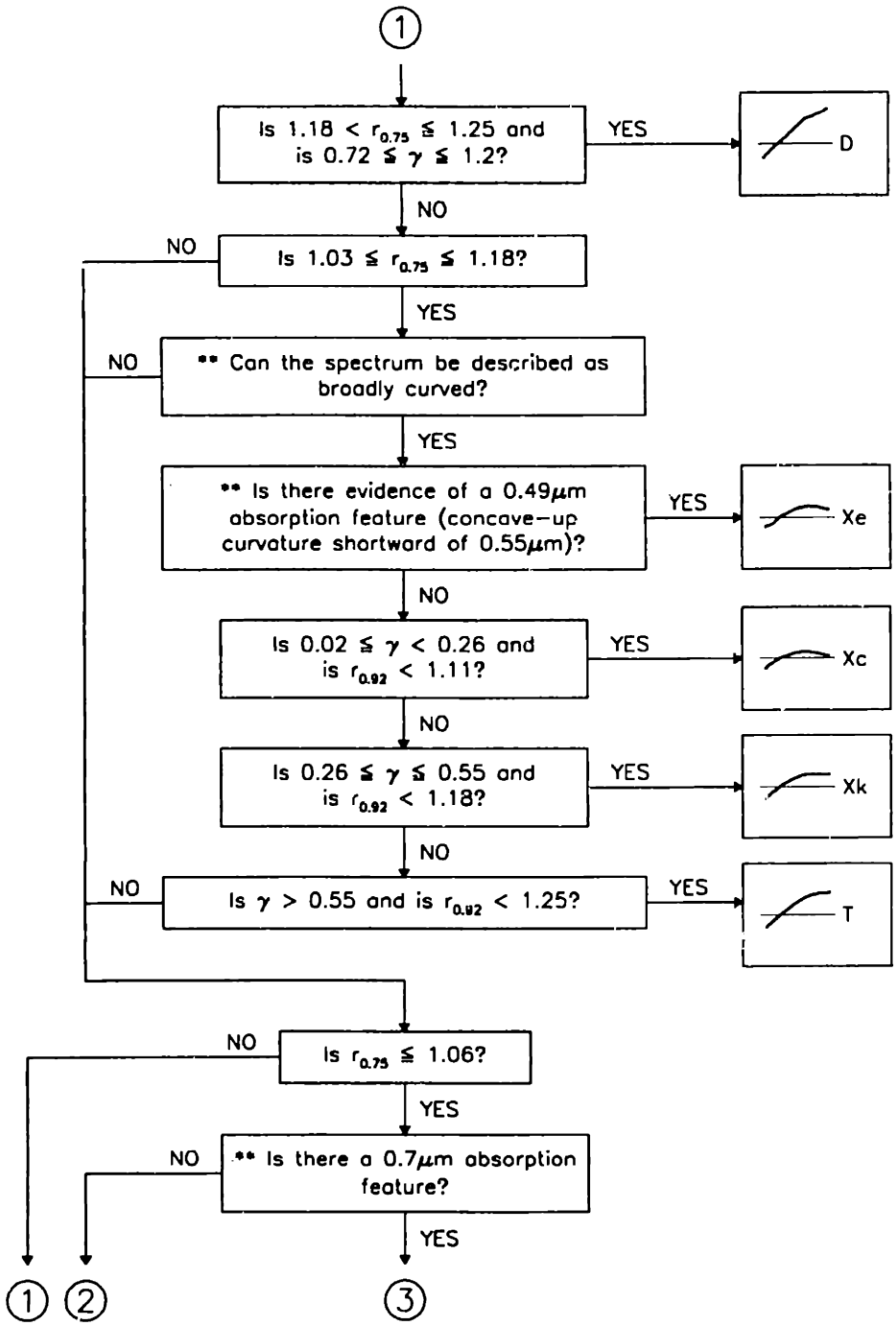
1
Is 1.18 < $r_{0.75}$ ≦ 1.25 and is 0.72 ≦ γ ≦ 1.2?
YES
D
NO
NO
Is 1.03 ≦ $r_{0.75}$ ≦ 1.18?
YES
NO
** Can the spectrum be described as broadly curved?
YES
** Is there evidence of a 0.49μm absorption feature (concave-up curvature shortward of 0.55μm)?
YES
Xe
NO
Is 0.02 ≦ γ < 0.26 and is $r_{0.92}$ < 1.11?
YES
Xc
NO
Is 0.26 ≦ γ ≦ 0.55 and is $r_{0.92}$ < 1.18?
YES
Xk
NO
NO
Is γ > 0.55 and is $r_{0.92}$ < 1.25?
YES
T
NO
Is $r_{0.75}$ ≦ 1.06?
YES
NO
** Is there a 0.7μm absorption feature?
YES
1
2
3

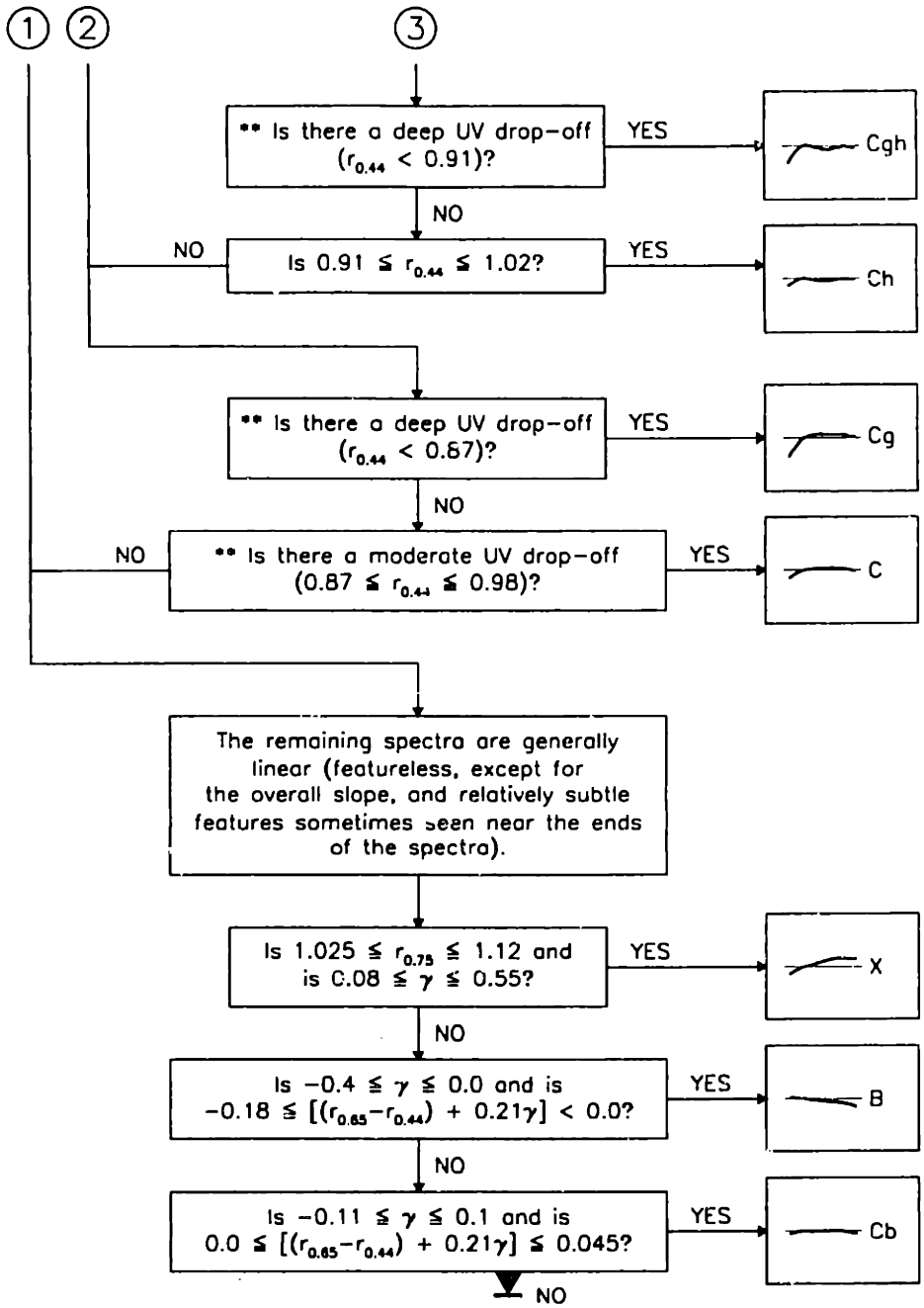

Figure 4.33: Flowchart mapping out a procedure by which this taxonomy can be applied to a newly observed asteroid. Many steps in this procedure are quantitative, requiring very basic measurements from the spectrum (a normalized reflectance at a certain wavelength, or the measure of the average spectral slope, γ). Some of the steps, however, are subjective (does a particular feature occur in the spectrum, etc.). Subjective steps are flagged by a double asterisk (**). At three points, the symbol ▼ indicates an exit from the process. At these exit points, if the answer to that question is "NO", then there is no need to go on. The asteroid is undefined in this taxonomy.

spectrum. However, because of the continuous distribution in spectral forms, deciding if a particular feature is present or absent will occasionally be difficult. Those questions in the decision tree that are considered to be potentially subjective in nature are identified by a double asterisk (**). This decision tree is complete, as defined by the SMASSII dataset. Thus, any asteroid whose spectrum lies within the range of spectral forms sampled by SMASSII can be classified using this procedure. However, if a new spectral form is encountered, it will not be possible to classify that asteroid within the 26 classes that have defined, thus far, in this feature-based taxonomy. Three points exist in the flowchart, marked by the symbol ▼, which are exits from the procedure. If the spectrum being considered reaches an exit point in the flowchart without meeting the criteria for that class, then the effort to classify that asteroid should be stopped: The object is not classifiable within this taxonomy.

To properly follow the procedure outlined in Figure 4.33, the spectrum being classified must meet more rigorous requirements than were listed above (in connection with the first classification strategy). In particular, the spectrum must cover the wavelength interval of 0.44 to 0.92 μm, since the relative reflectances at these spectral extremes are regularly required in answering questions posed in the decision tree. Also, the spectrum must be fitted, preferably with a resampling step, dλ, of 0.01 μm, so that values of the relative reflectance, r, are less influenced by random noise contained in the original spectrum.

4.7.2 Comparison with other taxonomies

Many of the asteroids observed in the SMASSII survey had been previously classified in other recent taxonomies (e.g. Tholen 1984, Barucci *et al.* 1987, Tedesco *et al.* 1989, Howell *et al.* 1994). These earlier classifications helped form the foundation of our feature-based taxonomy, particularly in the definition of major boundaries between the C-, S-, and X-complexes. By taking into consideration these previous works, we have ensured a reasonable level of consistency between our taxonomy and that of others. A comparison between the SMASSII spectral classes and the taxonomic designations assigned by Tholen (1984) is given for 406 asteroids in Table 4.6. For each spectral class, the full distribution of Tholen designations is listed, with the number of objects assigned to each designation given in parentheses. A cursory examination of this table reveals trends that, for the most part, should be expected given the strategies

Table 4.6: Comparison with Tholen (ECAS) designations

SMASSII type	Fraction classified by Tholen	Distribution of objects by Tholen classes
A	5 / 15	A (5)
B	20 / 51	C (3) F (3) B (2) BC (1) BFC (1) BFU (1) BFX (1) CF (1) CP (1) FBCU (1) FC (1) FCB (1) FP (1) FX (1) XFU (1)
C	42 / 137	C (21) X (4) CX (2) F (2) PC (2) B (1) BCF (1) CF (1) CU (1) FC (1) FXU (1) G (1) P (1) PU (1) XC (1) XDC (1)
Cb	11 / 25	C (4) CD (2) B (1) CF (1) CX (1) M (1) XFCU (1)
Cg	3 / 9	C (3)
Cgh	3 / 14	C (2) G (1)
Ch	64 / 124	C (40) G (5) CX (3) XC (3) CG (2) BU (1) CP (1) CPF (1) CU (1) DCX (1) FC (1) PD (1) SCTU (1) STU (1) X (1) XD (1)
D	2 / 9	D (1) DU (1)
K	13 / 28	S (12) TSD (1)
L	14 / 31	S (9) D (1) ST (1) STGD (1) SU (1) T (1)
Ld	1 / 12	S (1)
O	0 / 1	
Q	1 / 1	Q (1)
R	1 / 2	R (1)
S	96 / 332	S (90) C (1) DU (1) GU (1) QSV (1) SR (1) SU (1)
Sa	2 / 31	S (2)
Sk	11 / 29	S (11)
Sl	17 / 35	S (17)
Sq	4 / 33	S (4)
Sr	1 / 16	S (1)
T	5 / 14	T (2) D (1) PCD (1) ST (1)
V	1 / 21	V (1)
X	40 / 107	M (12) X (8) P (5) C (3) CX (3) CP (2) XC (2) B (1) D (1) E (1) XB (1) XD (1)
Xc	19 / 49	C (6) P (3) CDX (1) CP (1) CPU (1) CX (1) E (1) F (1) M (1) SU (1) X (1) XSCU (1)
Xe	13 / 27	E (6) M (3) CD (1) GC (1) S (1) X (1)
Xk	17 / 37	M (6) C (4) D (1) E (1) P (1) T (1) X (1) XD (1) XF (1)

Table 4.7: Comparisons with other recent taxonomies

SMASSII type	Distribution among Barucci *et al.* classes	Distribution among Tedesco *et al.* classes	Distribution among Howell *et al.* classes
A	A0 (4)	A (2) r (1)	A (4)
B	C0 (6) B0 (2) B1 (2) B3 (2)	C (4) F (3) C? (1) FC (1) m (1)	Cx (2) BCv (1)
C	C0 (25) B1 (1) B3 (1) D2 (1) G0 (1)	C (26) C? (1) G? (1) I (1)	B+F (2) CvB (1) Cx (1)
Cb	C0 (4) B2 (1)	C (2) CF (1) CP (1) m (1)	Cx (1)
Cg	C0 (1)	C (1)	
Cgh	C0 (1) G0 (1)	C (1) G (1)	Cv (1)
Ch	C0 (30) B3 (1) G0 (1) S1 (1)	C (31) G (3) C? (1)	Cv (2) CvP (2) Cx (2)
D	D0 (1)		D (1)
K	S0 (7) D3 (1) S1 (1)	K (3) S (2) SK (2) TK (1)	K (3)
L	S0 (4) D3 (1) S3 (1)	S (5)	So (1) Sp (1) T (1)
Ld	S0 (1)	S (1)	
R	V0 (1)	r (1)	R (1)
S	S0 (48) S2 (3) S1 (2)	S (41) r (2) K (1) SK (1)	Sp (13) S (6) So (3) S,SoT (1) SSp (1)
Sa	S0 (1)	S (1)	So (1)
Sk	S0 (5)	S (7)	Sp (2) S (1) Sp,S (1)
Sl	S0 (10) S2 (2) S3 (1) V0 (1)	S (9)	So (2) SSp (1)
Sq	S0 (1)	S (1)	Sp (2)
T	D0 (1) D3 (1) S0 (1)	I (2) D (1)	D (1) T (1) TSo (1)
V	V0 (1)	r (1)	V (1)
X	M0 (13) C0 (7) B3 (1) D0 (1) E0 (1)	M (11) C (4) CP (2) I (2) D (1) E (1) E? (1) P (1) PC (1)	M (3) P (2)
Xc	C0 (5) M0 (2) D3 (1) E0 (1) S1 (1)	C (3) M (2) C? (1) E (1) KCT (1)	P (2) M (1)
Xe	E0 (2) M0 (2) S0 (1)	E (3) M (1) M? (1) S (1)	E (3)
Xk	M0 (6) C0 (4) D0 (1) D3 (1)	M (6) C (3) D (1) E (1) KS (1) T (1) I (1)	D (1) M (1) M,T (1) T (1)

used in defining the two taxonomies. In the Tholen system, asteroids are more likely to be assigned multiple designations when the classes involved are small, and the boundaries dividing them are less distinct (based on the magnitude of the dissimilarities separating individual spectra). This is clear in the distribution of Tholen classes for asteroids contained in the C-complex, particularly the B-, C-, and Ch-classes where the number of objects classified in both taxonomies is greatest. In the X-complex, there is likewise a large dispersion of Tholen classes that is compounded by the inclusion of the E-, M-, and P-classes, defined by Tholen based on albedo. In contrast, asteroids belonging to the S-complex (the A-, K-, L-, Q-, R-, S-, Sa-, Sk-, Sl-, Sq-, and Sr-classes) compare very consistently with the Tholen classifications with relatively few multiple, or discrepant designations due to the large size (and corresponding spectral diversity) of Tholen's S-class. Similar comparisons are made with the Barucci *et al.* (1987), Tedesco *et al.* (1989) and Howell *et al.* (1994) taxonomies in Table 4.7.

4.7.3 Albedo

Even though albedo was not a parameter in the development of this feature-based taxonomy, it is appropriate to investigate the general relationship between albedo and the SMASSII spectral classes. IRAS albedos (from IMPS Final Product files #102 and #103, Veeder *et al.* 1989) for 625 SMASSII asteroids are listed in the summary of observations given in Appendix A. These values were used in Figure 3.12, where the relationship between albedo and spectral component space was first examined. From this figure, it can be seen that albedo is most strongly correlated with the component PC2', indicating a relationship between albedo and the strength of spectral absorption features. To explore this correlation further, Figure 4.34 shows a log-linear plot of IRAS albedo versus PC2', where each object has been labelled by its spectral class. The general distribution of points in this plot reflects the bimodal nature of albedos that was discussed at length in Chapter 3, with a pronounced separation between the C- and S-complexes. In addition, the wide range of albedos associated with members of the X-complex is clearly represented in this figure. The most intriguing aspect of this plot is the detailed distribution of asteroids belonging to the S-complex, and the apparent relationship between albedo and depth of the 1 μm silicate absorption band. The K- and L-type asteroids have 1 μm bands that are essentially nonexistent, and as a result, have the highest values of PC2'. On average, these asteroids also have the lowest IRAS albedos. By comparison, asteroids belonging to the A- and R-classes have the deepest

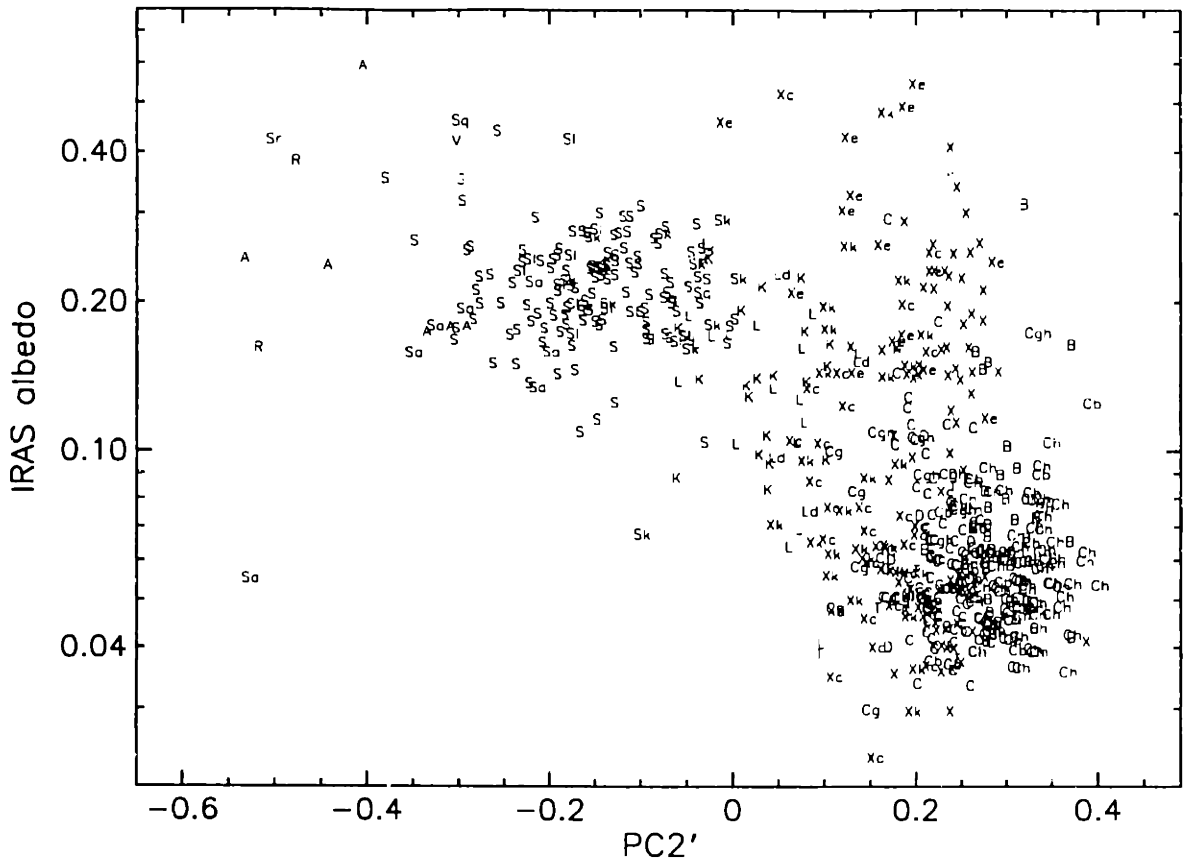

Figure 4.34: Relationship between albedo and the magnitude of spectral features (primarily the depth of the 1 μm band) as described by PC2'. The bimodal distribution of albedos is clearly seen in the separation of asteroids belonging to the C- and S-complexes. Also very evident is the range of albedos for asteroids belonging to the X-complex.

1 μm bands while, on average, having the highest albedos. This apparent relationship is also seen in Table 4.8, which lists statistics based on the IRAS albedos, including the mean and standard deviation for each of the SMASSII taxonomic classes. The general explanation for differences in albedo between the C- and S-class asteroids is based on the presence of opaque materials in the mineral matrix of C-type objects. The addition of opaques, such as carbon/organics or iron oxides (magnetite), to silicate mixtures has the effect of both reducing the reflectivity (albedo) of the material, and masking the silicate spectral absorption bands (Johnson and Fanale 1973). However, extending this explanation to the various classes (and presumably diverse mineral assemblages) making up the entire S-complex may be difficult. While we note that this apparent relationship between albedo and spectral band-depth among the S-complex asteroids

may exist, any detailed discussion of its significance is beyond the scope of this present work.

Table 4.8: Statistics for IRAS albedo measurements of SMASSII asteroids

Spectral type	No. in sample	High	Low	Median	Mean	StDev	~ H mag. for D = 20km
A	6	0.60	0.17	0.21	0.27	0.16	10.6
B	32	0.32	0.04	0.07	0.08	0.06	11.9
C	87	0.29	0.01	0.06	0.07	0.04	12.0
Cb	16	0.12	0.04	0.06	0.06	0.02	12.2
Cg	6	0.10	0.03	0.05	0.06	0.03	12.2
Cgh	10	0.17	0.05	0.08	0.09	0.03	11.8
Ch	96	0.10	0.04	0.05	0.06	0.01	12.2
D	6	0.09	0.04	0.06	0.06	0.02	12.2
K	21	0.24	0.08	0.14	0.15	0.05	11.2
L	17	0.26	0.04	0.16	0.15	0.05	11.2
Ld	4	0.23	0.08	0.12	0.14	0.07	11.3
O	0	-	-	-	-	-	-
Q	0	-	-	-	-	-	-
R	2	0.38	0.16	0.27	0.27	0.16	10.6
S	112	0.44	0.02	0.21	0.22	0.06	10.8
Sa	7	0.22	0.06	0.16	0.16	0.05	11.1
Sk	12	0.29	0.07	0.22	0.22	0.06	10.8
Sl	18	0.43	0.17	0.22	0.23	0.06	10.7
Sq	3	0.46	0.20	0.21	0.29	0.15	10.5
Sr	1	-	-	0.42	0.42	-	10.1
T	10	0.09	0.04	0.05	0.05	0.01	12.4
V	2	0.42	0.04	0.23	0.23	0.27	10.7
X	75	0.41	0.03	0.10	0.12	0.09	11.5
Xc	35	0.52	0.02	0.07	0.09	0.09	11.8
Xe	15	0.55	0.12	0.24	0.28	0.14	10.5
Xk	32	0.48	0.03	0.06	0.11	0.09	11.5

4.7.4 Bias corrections

The upper half of Figure 4.35 shows a plot of absolute magnitude, H, versus semimajor axis for asteroids observed during the SMASSII survey, excluding the near-Earth objects. There are two notable concentrations of objects in this plot, centered near 2.2 and 2.75 AU, that result from our intentional targeting of small asteroids in these regions to investigate certain dynamical families. For comparison, the lower half of this figure shows a similar plot, containing all numbered asteroids (excluding the NEAs) through asteroid 8980. In this larger sample of objects, the effect of heliocentric distance on the completeness of discovery (and on the eventual numbering) of asteroids is clearly visible. Among the numbered asteroids shown, the mean absolute magnitude for objects with semimajor axes around 2.2 AU is $H \approx 13.5$, while for asteroids with semimajor axes around 3.2 AU, this mean value drops to $H \approx 11.5$, consistent with an r^{-2} dependence of apparent brightness on the combined heliocentric and geocentric distances of asteroids (which predicts a $\Delta H \approx -2.1$ mag). Also seen in Figure 4.35 are the effects of mean motion resonances with Jupiter that result in gaps in the number density of asteroids as a function of orbital semimajor axis. Only the three lowest-order resonances have been marked in this figure.

In Figures 4.36 and 4.37, the upper plot of Figure 4.35 has been replicated to show the distributions of absolute magnitude and semimajor axis for each of the SMASSII taxonomic classes. Considerable structure is present in some of these plots, especially those devoted to the more populated spectral classes. The large scale concentrations of points at fainter magnitudes primarily result from the selective sampling of asteroids in specific regions of the belt, as mentioned above. However, smaller groupings can also be seen in the distributions of certain taxonomic classes that can be attributed to the spectral similarities of objects within asteroid families. A careful examination of these figures reveals several large-scale trends, and differences between the various classes, many of which, like the dominance of S-type asteroids in the inner belt, and conversely, the dominance of C-types in the outer belt, have long been recognized (e.g. Chapman *et al.* 1975, Gradie *et al.* 1989). The identification of significant trends in composition, as inferred from the distribution of spectral types within the asteroid belt, can help put constraints on models of the early inner solar system. Similarly, determining the distributions of asteroid sizes can lead to a better understanding of their collisional histories.

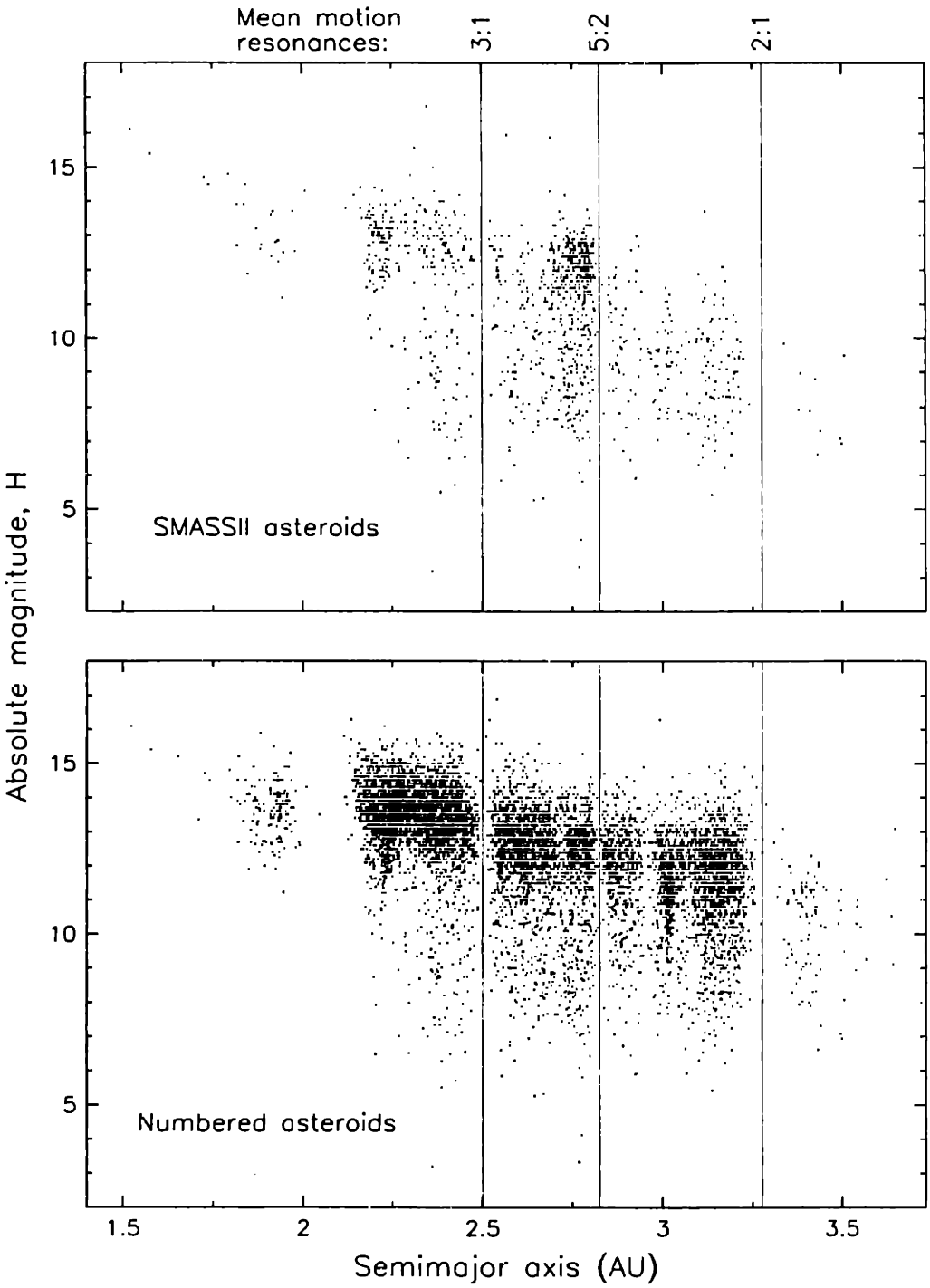

Figure 4.35: The distribution of asteroids (by semimajor axis and absolute magnitude) observed during SMASSII. For comparison, 8815 numbered asteroids are shown plotted to the same scale in the bottom panel. Three major mean motion resonances are marked, in part to help compare the two plots by eye, and to mark boundaries used in calculating a first-order bias correction for the SMASSII sample.

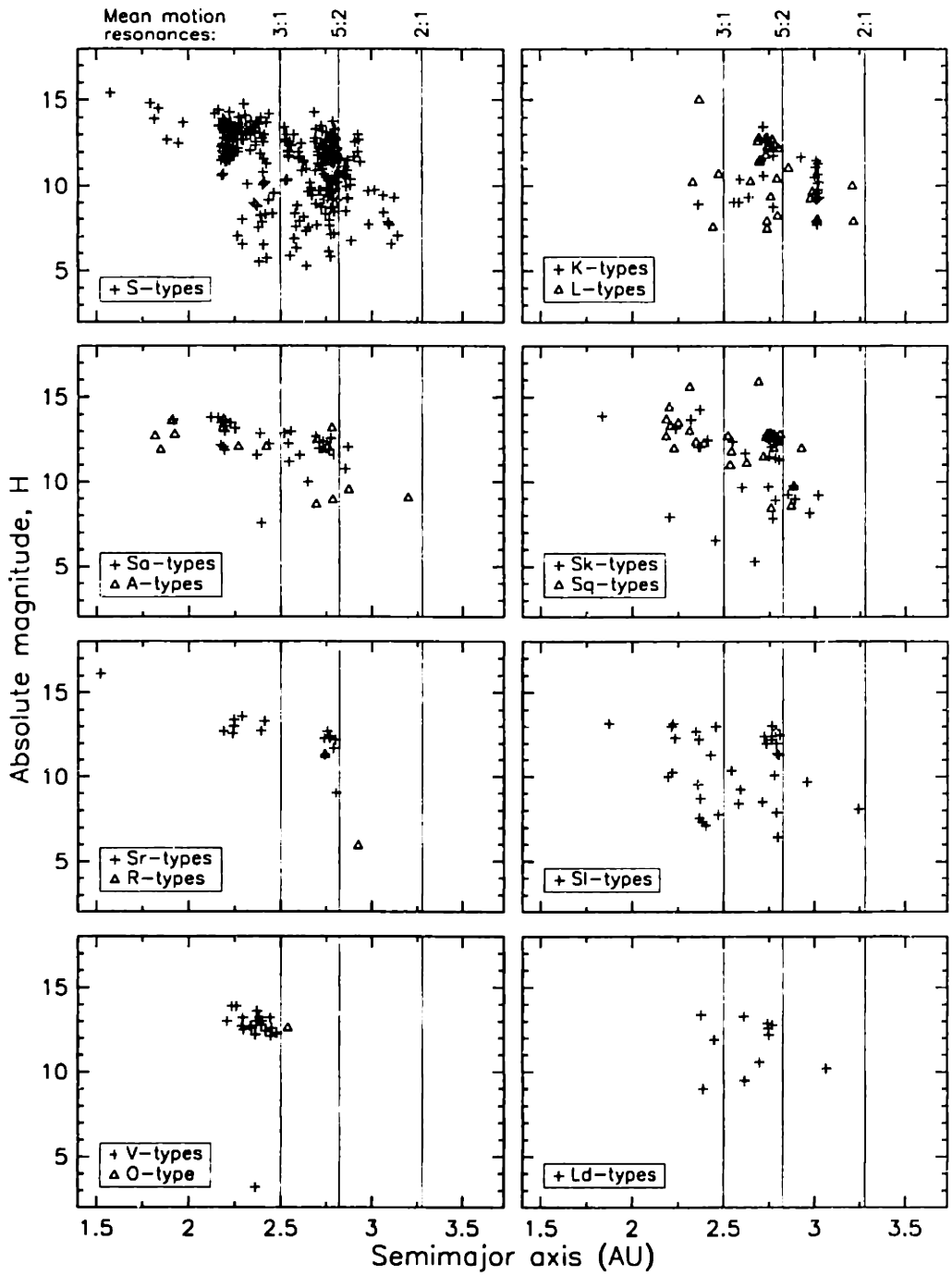

Figure 4.36: Plots of semimajor axis versus absolute magnitude, H, showing the raw (non-bias-corrected) distributions of SMASSII asteroids by taxonomic class. The three lines representing the mean motion resonances are duplicated in each frame to aid in comparing the different plots. In many cases, two closely related spectral types are plotted together in the same frame. The spectral types shown here belong to the S-complex, or to outlying spectral classes that surround the S-complex (Ld-, O-, and V-types).

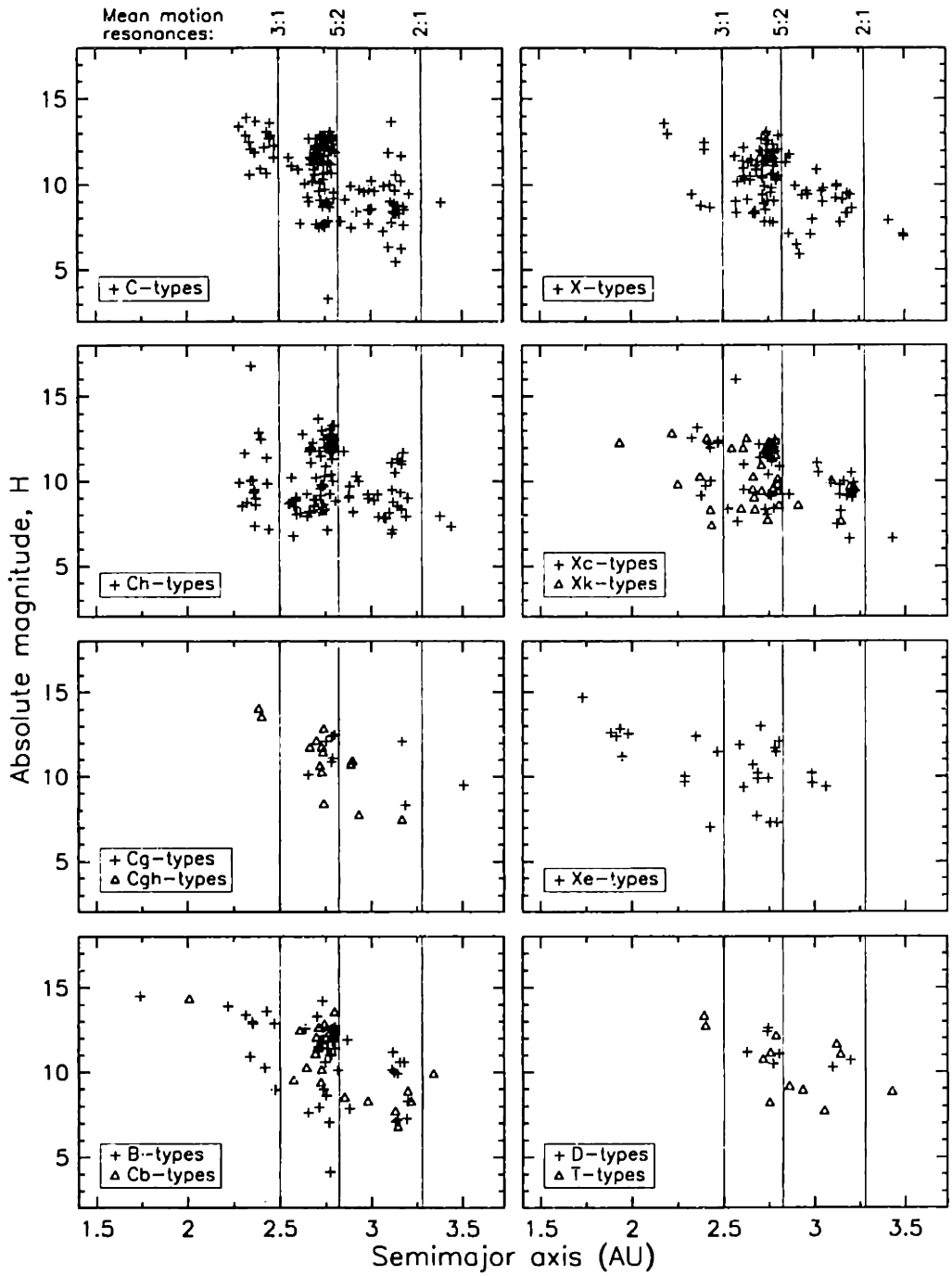

Figure 4.37: Same as for Figure 4.36, except for asteroids belonging to the C- and X-complexes, and the outlying D- and T-classes.

The plots contained in Figures 4.36 and 4.37 show the raw distributions of asteroids that were observed and characterized as part of the SMASSII survey. To properly interpret the underlying factors and physical processes that led to these distributions, however, it is important that corrections are first applied for the observational biases that influence these apparent distributions. In the SMASSII survey, a substantial fraction of the observational effects arises from the fact that bright asteroids are easier to observe than faint ones, leading to a natural selection of inner-belt S-type asteroids over outer-belt C-type asteroids. For example, a 10 km diameter S-type asteroid with a heliocentric distance of 2.2 AU (observed at opposition) poses the same observational challenge as a 45 km diameter C-type object with a heliocentric distance of 3.2 AU. Beyond this basic consideration of brightness, there were several other, more subtle factors that influenced the SMASSII observations that stemmed from both the observing strategy followed and our scientific goals. A high priority was placed on obtaining spectral observations of planet-crossing asteroids, including both NEAs and Mars-crossing objects. In addition, our studies of dynamical families focused on the region of the belt surrounding the asteroid 4 Vesta, extending from the ν_6 secular resonance to the 3:1 mean motion resonance, and on the region between 2.69 and 2.82 AU, where 15 different families were investigated (the results of which are presented in Chapter 5). At the telescope, the decision of which asteroid to observe was driven by these scientific objectives, but ultimately depended on the immediate sky conditions, and the object's position in the sky with respect to the meridian. Asteroids were sometimes selected for observation because of unusual orbital parameters, such as a high eccentricity or inclination. At other times, an asteroid might be targeted simply because it was named in honor of a friend or colleague.

A general approach for correcting observational biases was described by Chapman *et al.* (1975), and was later adopted by Zellner (1979) and Chapman (1987). This method uses the entire set of numbered asteroids as the foundation for estimating the true population and distribution of objects in the main belt. The belt is first divided into several zones based on orbital parameters, and the distribution of numbered asteroids contained in each of these zones is then determined as a function of magnitude. Because the discovery and numbering of asteroids is not complete for apparent magnitudes fainter than V ~ 15.5, Zellner extended the magnitude-frequency relationship for each zone beyond V = 15.75 by assuming a constant slope, using the

relationship *log*(N) ≈ 0.39V that was determined during the Palomar-Leiden Survey (van Houten *et al.* 1970), where N is the number of asteroids per 0.5 magnitude bin. The bias correction factor, *f*, for a particular zone and magnitude bin is simply the ratio of the total number of asteroids in that bin to the number of classified asteroids in the bin. In applying this correction factor, the assumption is made that for each classified asteroid in a particular zone and magnitude bin, there are *f*-1 asteroids in the same magnitude bin, and of the same spectral class, that have not yet been classified.

This same approach was used in correcting for the observational biases and selection effects inherent in the SMASSII dataset, though a few minor, but notable changes were made to the procedures outlined by Zellner (1979) and Chapman (1987). These changes primarily involved restricting the region of the belt over which the correction factors were calculated, and the number of zones into which this region was divided. First, because of the increased number of spectral classes contained in our taxonomy, our analysis of the population is confined to that region of the asteroid belt between 2.10 and 3.278 AU, where a sufficiently large number of asteroids were observed that we could reasonably avoid small-number statistics in calculating the bias corrections. Likewise, we divided the belt into only three zones, with limits of $2.100 \leq a < 2.501$, $2.501 \leq a < 2.825$, and $2.825 \leq a < 3.278$, where these boundaries are defined by the locations of major mean motion resonances. These zones have very similar boundaries to zones I, II, and III defined by Zellner (1979), though we do not include any limits on eccentricity or inclination. The other zones identified by both Zellner and Chapman, which isolate some of the larger asteroid families and dynamical regions in the belt, were not included in our analysis. Using these additional zones did not seem practical, given that the focus of the SMASSII survey was on numerous small asteroid families. Separately correcting the biases in these additional zones, many of which were not significantly sampled during SMASSII, would again have led to some calculations being based on small numbers. One final difference in our application of this procedure was the use of absolute magnitudes, rather than apparent magnitudes, in determining the magnitude-frequency distribution for each of the zones. This choice was based on the apparent step-wise drops in the limiting absolute magnitude, as a function of semimajor axis, seen in the upper plot of Figure 4.35. These drops are more pronounced than the gradual fall-off in H observed among the numbered asteroids plotted in the lower half of this figure, and are presumably artifacts resulting from our

efforts to concentrate on particular regions of the belt during the SMASSII survey. Our use of absolute magnitude in determining the magnitude-frequency relationships means that the correction factors, listed in Table 4.9, are also presented as a function of absolute magnitude, H.

In applying the correction factors given in Table 4.9, we assumed that, for every SMASSII asteroid with an orbital semimajor axis between 2.10 and 3.278 AU, there were f-1 other asteroids (as defined above) with the same absolute magnitude and spectral class, and with semimajor axes that are normally distributed about that of the known object, with a 1σ deviation of ±0.1 AU. By assuming this distribution in semimajor axis, we avoid the creation of artificial "families" of asteroids at locations where the bias correction factors are large. Similarly, the boundaries of real families are blurred by this correction. Since our interest in this analysis is determining the broad trends in spectral types as a function of heliocentric distance, the smoothing of finer detailed structures, such as families, does not alter the overall results. Figure 4.38 illustrates the bias-corrected distributions of various spectral classes for asteroids with diameters of 20 km or greater. Using the mean IRAS albedo for each spectral class, listed in Table 4.8, the absolute magnitude of an asteroid 20 km in diameter was calculated, and is listed in the last column of this table. Only those asteroids with absolute magnitudes equal to or brighter than this cutoff magnitude were used in deriving the distributions shown in Figure 4.38. Revising this plot to include asteroids that are even smaller, based on the SMASSII dataset, becomes increasingly problematic, as the bias correction factors become larger, and less well determined, particularly in the outer part of the main belt.

4.7.5 Distributions by size and heliocentric distance

Gross trends in the distribution of asteroids contained in the three complexes, as a function of orbital semimajor axis, are clearly visible in Figure 4.38. Considering only those asteroids that are 20 km in diameter or larger, the percentage that belong to the C-complex increases from roughly 25%, for asteroids with semimajor axes $a \approx 2.1$ AU, to almost 65%, for objects with $a \approx 3.28$ AU. In contrast, for those asteroids in the S-complex, this percentage decreases from 55% to just 5% over the same interval of semimajor axis, while the distribution of asteroids belonging to the X-complex appears to be relatively flat, at a level of ~ 20%. Plotted in the lower-right hand corner of Figure 4.38 is the average shifted histogram for each of the three complexes, as well as that for

Table 4.9: Bias-correction values

Interval of absolute magnitude, *H*	Interval of semimajor axis (AU)								
	2.100 ≤ a < 2.501			2.501 ≤ a < 2.825			2.825 ≤ a < 3.278		
	Numbered objs.	Observed objs.	Correction factor	Numbered objs.	Observed objs.	Correction factor	Numbered objs.	Observed objs.	Correction factor
3.0 ≤ *H* < 3.5	1	1	1.0	1	1	1.0	0	0	
3.5 ≤ *H* < 4.0	0	0		0	0		0	0	
4.0 ≤ *H* < 4.5	0	0		1	1	1.0	0	0	
4.5 ≤ *H* < 5.0	0	0		0	0		0	0	
5.0 ≤ *H* < 5.5	0	0		2	2	1.0	1	1	1.0
5.5 ≤ *H* < 6.0	2	2	1.0	2	2	1.0	3	2	1.5
6.0 ≤ *H* < 6.5	3	1	3.0	3	3	1.0	3	3	1.0
6.5 ≤ *H* < 7.0	4	3	1.3	6	2	3.0	6	5	1.2
7.0 ≤ *H* < 7.5	7	6	1.2	11	11	1.0	14	11	1.3
7.5 ≤ *H* < 8.0	9	8	1.1	23	22	1.0	29	22	1.3
8.0 ≤ *H* < 8.5	5	4	1.3	42	31	1.4	45	25	1.8
8.5 ≤ *H* < 9.0	18	12	1.5	50	28	1.8	45	15	3.0
9.0 ≤ *H* < 9.5	13	6	2.2	56	38	1.5	91	33	2.8
9.5 ≤ *H* < 10.0	12	7	1.7	46	27	1.7	130	38	3.4
10.0 ≤ *H* < 10.5	20	13	1.5	66	46	1.4	139	15	9.3
10.5 ≤ *H* < 11.0	31	8	3.9	69	31	2.2	257	14	18.4
11.0 ≤ *H* < 11.5	42	8	5.3	134	66	2.0	384	13	29.5
11.5 ≤ *H* < 12.0	92	24	3.8	290	95	3.1	517	13	39.8
12.0 ≤ *H* < 12.5	220	44	5.0	432	114	3.8	810[a]	2	50[b]
12.5 ≤ *H* < 13.0	491	60	8.2	676[a]	79	8.6	1269[a]	3	60[b]
13.0 ≤ *H* < 13.5	787	55	14.3	1060[a]	18	15[b]	1988[a]	0	70[b]
13.5 ≤ *H* < 14.0	1233[a]	32	38.5	1661[a]	2	20[b]	3115[a]	1	80[b]

[a] Extrapolation, based on a logarithmic slope of 0.39 determined during the PLS (van Houten *et al.* 1970)
[b] Bias-correction factors are estimated, due to the small number of asteroids in the SMASSII sample

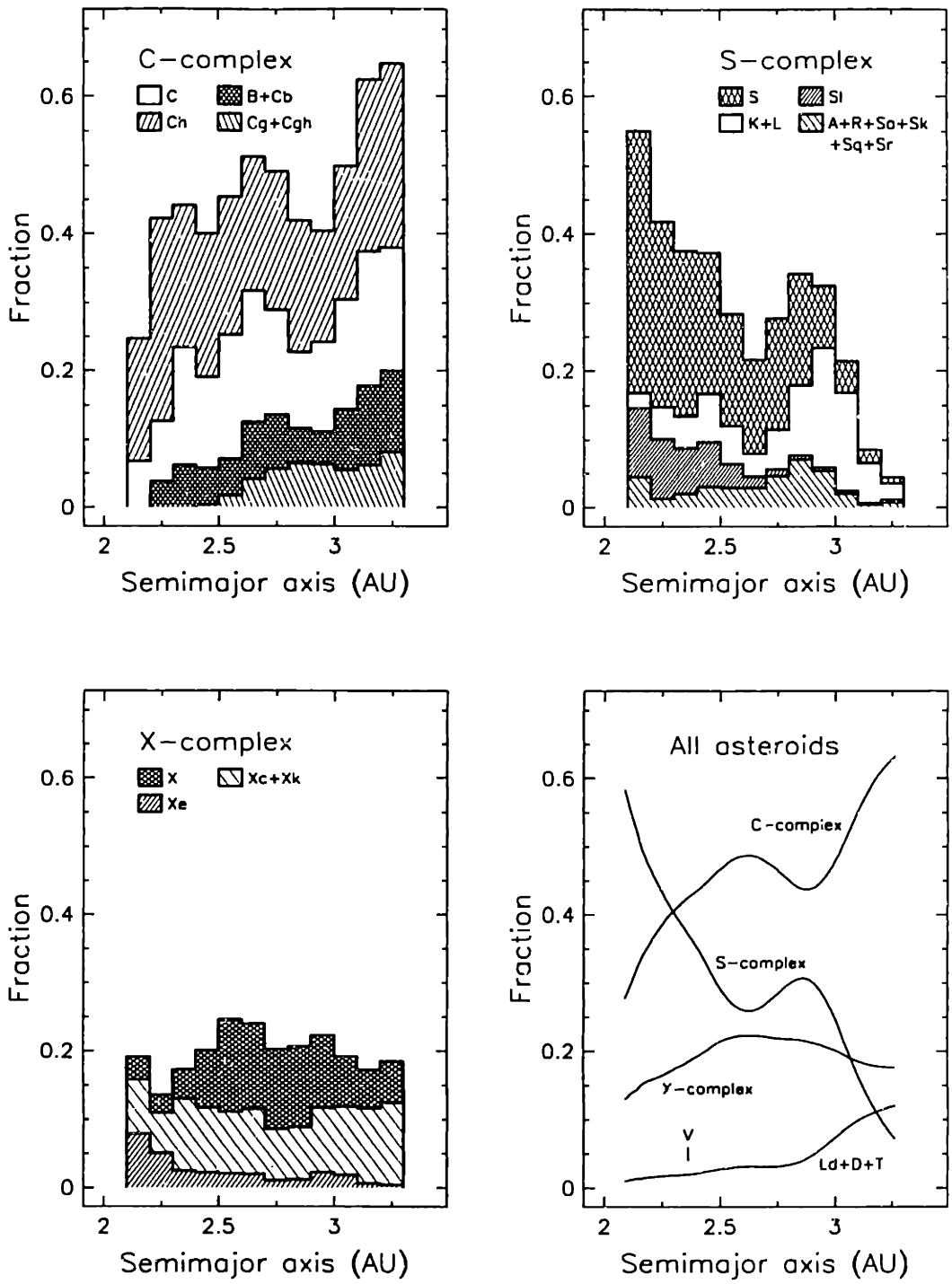

Figure 4.38: Histograms showing the bias-corrected distributions for spectral classes as a function of semimajor axis. Individual histograms give the cumulative fractional distributions for classes within each complex, where the fractions are calculated based on the entire population (the total distribution for all classes combined). In the lower right, the average shifted histograms for each of the complexes are overlaid, along with the combined contribution from outlying classes.

the combined outlying spectral classes. These smoothed curves reveal higher-order structure (secondary peaks) in the distributions of objects belonging to the C- and S-complexes. The curve representing the C-complex contains a secondary peak at a ≈ 2.6 AU, closely corresponding to a plateau in the individually plotted points (not the fitted curve) for C-types shown in Fig 1.4 (reproduced from Gradie *et al.* 1989). Similarly, a secondary peak in the curve for the S-complex, located at a ≈ 2.85 AU, corresponds to a feature in the bias-corrected distribution of S-type asteroids calculated by Chapman (1987), shown in Figure 1.5 (also reproduced from Gradie *et al.* 1989).

In addition to the large-scale differences between the distributions of asteroids in the three complexes, Figure 4.38 also reveals differences between the classes within each complex. In the C-complex, the B-, C-, Cb-, Cg-, and Cgh-classes all have distributions that increase as a function of semimajor axis, paralleling the trend for the C-complex as a whole. However, the distribution of Ch-types appears to be much flatter over the entire interval of 2.1 ≤ a ≤ 3.28 AU. This difference between the Ch-class and other classes in the C-complex is also apparent in the raw distributions shown in Figure 4.37, where a number of bright Ch-type asteroids plot in the region shortward of a = 2.5 AU, while a similar concentration of bright objects is not found among the other classes of the C-complex. Within the S-complex, the distribution of K- and L-type asteroids stands out as being most distinct, with a strong peak occurring at a ≈ 3.0 AU. This concentration of K- and L-types is partly due to a number of large members in the Eos family (predominantly K-types, with semimajor axes a ≈ 3.0 AU), but also includes some objects from the Henan and Watsonia families (predominantly L-types, described in Chapter 5). Along with these asteroids, there are a number of objects classified as K- or L-types that are not apparently associated with dynamical families, but which are found scattered throughout the middle of the asteroid belt. Several of the spectral classes making up the S-complex, specifically the A-, R-, Sa-, Sk-, Sq- and Sr-classes, have very few large members (with diameters of 20 km or greater), leading to their relatively small contribution in Figure 4.38. It is somewhat surprising, however, that the contribution from the Sk- and Sq-classes is not greater, since the number of bright objects plotted in Figure 4.36 seems more significant in the interval of 2.7 < a < 3.0 AU. In the bias correction, this apparent discrepancy can be accounted for by differences in albedo (with the Sq-class having a particularly high mean albedo), and by the fact that this region of the belt was the most thoroughly surveyed during SMASSII, leaving the

Sk- and Sq-types to represent only a small fraction of the total. The distribution of classes contained in the X-complex also shows some structure as a function of heliocentric distance. In particular, the fraction of those asteroids classified as X-types peaks at a ≈ 2.6 AU, while the distribution of Xc- and Xk-type objects appears to be more bimodal.

The same bias correction factors listed in Table 4.9, along with the mean IRAS albedos given in Table 4.8, were used to produce the cumulative size-frequency plots shown in Figure 4.39. The population represented by these curves is limited to that region of the asteroid belt between 2.1 and 3.28 AU, so that the population of spectral classes that dominate the outer belt, such as the T- and D-types, are drastically underestimated. These curves generally follow a power-law distribution, with slopes ranging from -1.5 to -2.5 (marked in each plot for reference), though for those spectral classes containing only smaller asteroids, such as the Sa-, Sq-, and Sr-classes, the slopes of the distributions are steeper. There is an apparent turnover, or decrease in the slopes of the size-frequency distributions for the X-, Xc-, and Xk-classes (at smaller sizes) that is much more pronounced than that seen in the other spectral classes. While incomplete bias corrections at faint magnitudes cannot be ruled out as the source for this turnover in slope, the fact that this effect is primarily limited to classes in the X-complex is intriguing.

Numerous comparisons can be made between distributions of asteroid sizes and spectral classes, but one particular comparison stands out. Figure 4.40 plots the spectral components corresponding to two different features contained in S-type spectra as functions of absolute magnitude, H. These plots include all members of the S-complex belonging to the S-, Sa-, Sk-, Sl-, Sq- and Sr-classes, for which the secondary component sets $_{(S1)}$ and $_{(S2)}$ were previously calculated (see Section 4.4.4). The upper plot in the figure, marked frame A, shows the relationship between the 1 μm band depth (described by component PC2') and absolute magnitude. As smaller S-type asteroids are observed, the dispersion in PC2' becomes larger, indicating a greater variety of depths of the 1 μm feature. A comparison of this figure (frame A) and Figure 4.8 shows that those asteroids with the deepest bands, belonging primarily to the Sa-, Sq-, and Sr-classes (as well as many belonging to the S-class), are also inherently the faintest, and thus, the smallest. This is consistent with the cumulative size-frequency distributions for

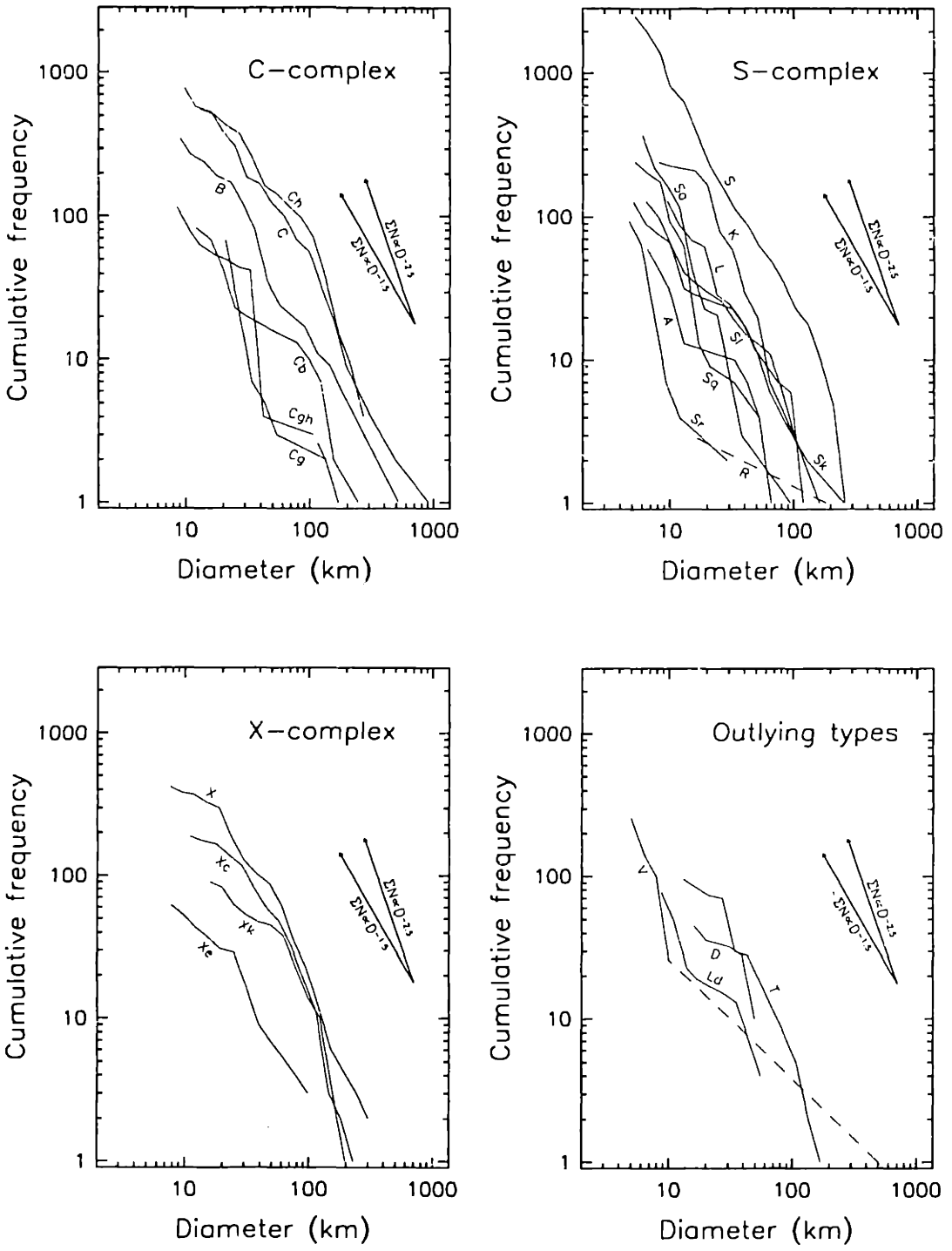

Figure 4.39: Bias-corrected cumulative size-frequency plots (*log-log*) for 24 of the 26 SMASSII taxonomic classes (O- and Q-types are not included, since these classes contain only one member each). These plots represent the population in the main belt from 2.1 to 3.27 AU, the interval over which a first-order bias correction to the population was feasible.

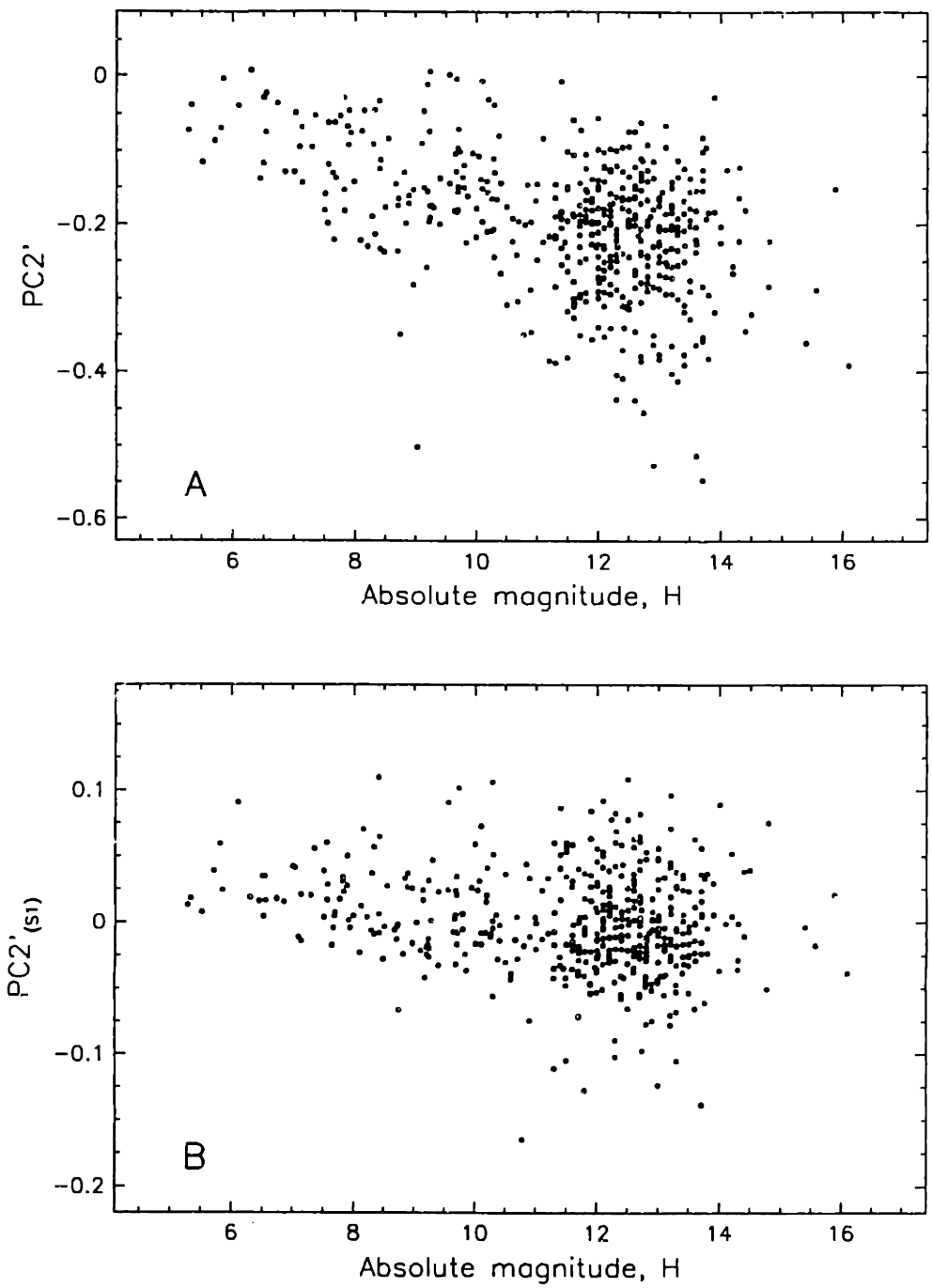

Figure 4.40: Magnitude dependence on S-type asteroid spectral properties. In Frame A, the primary spectral component PC2' (measure of 1μm band depth) is plotted against absolute magnitude, H. For fainter asteroids, the dispersion in spectral properties is greater, with more asteroids having deeper 1μm bands. This dispersion leads to the continuum in spectral types observed throughout the S-complex. Frame B plots the secondary component $PC2'_{(S1)}$, a measure of the strength of the UV drop-off, as a function of H.

the Sa-, Sr-, and Sq- classes shown in Figure 4.39, and with the fact that these spectral types were essentially unsampled during the ECAS observations, providing Tholen with clear gaps separating his A-, R-, and Q-classes from the rest of the S-types. The distribution shown in frame A is very similar to that derived by Binzel *et al.* (1998), where the spectral dependency on magnitude (size) is even more apparent among the smaller near-Earth asteroids. This size dependent effect is likely the result of variations in surface properties such as exposure age and the extent of regolith development (commonly called "space weathering"), with the smallest asteroids having the youngest and presumably least altered surfaces (e.g. Chapman 1996). Frame B, in Figure 4.40, shows the relationship between absolute magnitude, and strength of the angled UV drop-off, where smaller (more negative) values of $PC2'_{(S1)}$ are correlated with a stronger UV feature (see Figure 4.12). While the relationship in this plot is not as strong as that shown in frame A, there is an apparent trend for the variability of this UV feature, and thus potential for stronger bands, to be the greatest among the smaller S-type asteroids.

4.7.6 Comparison with meteorites

When the principal component solution was generated for the 1189 SMASSII spectra discussed in this work, we included the near-Earth asteroid 1862 Apollo to provide a spectral benchmark for the Q-class. In addition, we included the laboratory spectra of 78 meteorite samples, measured by Gaffey (1976). These meteorite spectra were first fitted with a smoothing spline over the wavelength interval of 0.44 to 0.92 μm, and binned to 0.01 μm channels, in order to match the characteristics of the spline-fitted asteroid data. A residual spectrum was created for each of these meteorites by first fitting for, and then dividing by the average spectral slope. These residual spectra were then combined with the residual spectra of the asteroids in the principal component analysis. The first three spectral components for these meteorite samples, Slope, PC2', and PC3', are listed in Table 4.10.

A broad view of spectral component space, showing the plotted positions of all 78 meteorite samples with respect to the SMASSII spectral classes, is presented in Figure 4.41. Of particular interest in this plot is the extent of the basaltic achondrites in component space, and our ability to separate these classes (the Eucrites, Howardites and Diogenites) from the ordinary chondrites in the PC2' versus PC3' plane. The large "V" in this plot shows the mean location of all V-type asteroids classified during

Table 4.10: Spectral component scores for 80 meteorite samples

Type	Meteorite name	Component scores		
		Slope	PC2'	PC3'
EH4	Abee	0.4979	0.2847	0.1018
EL6	Hvittis	0.5683	0.0426	-0.0650
EL6	Pillistfer	0.5094	0.0845	-0.0473
EL6	Khairpur	0.7767	0.0162	-0.0485
H3	Tieschitz	0.2099	-0.1058	-0.0653
H4	Ochansk	-0.0058	-0.1232	0.0339
H5	Castalia	0.2372	-0.2854	-0.0676
H5	Collescipoli	-0.0229	-0.1948	0.0347
H5	Pantar	0.1794	-0.1566	-0.0553
H6	Lancon	-0.0695	-0.3121	-0.0063
L4	Bald Mountain	0.1480	-0.2143	-0.0558
L4	Cynthiana	0.2651	-0.3381	0.0019
L4	Saratov	0.3415	-0.1371	-0.0379
L5	Homestead	0.4003	-0.4011	-0.0424
L5	Shelburne	0.1497	-0.5565	-0.0102
L6	Aumale	-0.1913	-0.4029	-0.0252
L6	Bruderheim	-0.2070	-0.2698	0.0016
L6	Buschof	-0.3270	-0.6160	-0.0192
L6	Cabeza de May	-0.4819	-0.4999	0.0100
L6	Colby	-0.0874	-0.3606	-0.0358
L6	Drake Creek	-0.1531	-0.8789	-0.0071
L6	Girgenti	-0.1037	-0.6075	-0.0573
L6	Leedey	0.0194	-0.3670	-0.0437
L6	Nerft	-0.1365	-0.4950	0.0033
L6	St. Michel	-0.1034	-0.7436	-0.0121
L6	Tourinnes La Grosse	-0.2523	-0.5205	-0.0035
L6	Zavid	-0.1491	-0.3550	-0.0027
LL4	Soko Bonja	0.2398	-0.3996	-0.0731
LL5	Olivenza	0.0373	-0.3303	0.0024
LL6	Jelica	0.0465	-0.2638	-0.0686
LL6	Manbhoom	-0.3047	-0.5113	-0.0766
LL6	Vavilovka	-0.2265	-0.3987	-0.0387
LL5b	Paragould	0.4204	0.1701	0.0433
L5b	Farmington	-0.0194	0.0213	0.0553
L5b	Sevrukovo	0.1888	0.1551	0.0686
Iron	Casey County	0.7778	0.2358	0.0124
Iron	Butler	0.9220	0.1841	-0.0531
Iron	Chulafinee	0.6884	0.2110	0.0073
Iron	Babb's Mill	0.4893	0.1800	-0.0062
St.Iron	Veramin	1.3191	0.1070	0.1273

Table 4.10: Spectral component scores for 80 meteorite samples

Type	Meteorite name	Component scores		
		Slope	PC2'	PC3'
Euc	Bereba	-0.2645	-0.4703	0.1563
Euc	Padvarninkai	-0.4878	-0.8121	0.1785
Euc	Sioux County	-0.1545	-0.2795	0.1708
Euc	Jonzac	-0.2984	-0.8802	0.2616
Euc	Haraiya	0.0568	-0.5752	0.2396
Euc	Pasamonte	0.1764	-0.5876	0.1893
Euc	Juvinas	-0.1655	-0.8264	0.2409
Euc	Stannern	-0.0421	-0.3291	0.2399
Euc	Nobleboro	0.0121	-0.6806	0.2370
How	Pavlovka	-0.5642	-0.8404	0.1574
How	Frankfort	-0.8059	-1.2657	0.1334
How	Le Teilleul	-0.3921	-0.8506	0.1933
How	Petersburg	-0.1160	-0.6634	0.2126
Dio	Johnstown	-0.8018	-1.7138	0.0048
Dio	Roda	-0.6978	-1.0915	0.0995
Dio	Tatahouine	-1.2643	-1.5702	-0.0367
Dio	Shalka	-0.7775	-1.0059	0.2525
CI	Orgueil	0.9049	-0.0660	-0.2234
CM	Cold Bokkeveld ps<.075mm	0.3416	0.0716	-0.1709
CM	Cold Bokkeveld .075-.15mm	-0.1047	0.1993	-0.1848
CM	Cold Bokkeveld .15-.50mm	-0.1922	0.2042	-0.2179
CM	Mighei ps <.075mm	0.0874	0.2463	-0.2458
CM	Murchison	0.0859	0.2173	-0.2202
CM	Murray	0.2952	0.1292	-0.1886
CM	Nogoya	-0.0556	0.2352	-0.3273
CO	Kainsaz	0.3535	0.0259	-0.0280
CO	Ornans	0.3988	0.0351	-0.0664
CO	Warrenton ps<.075mm	0.3249	0.0043	-0.0803
CO	Warrenton .075-.15mm	0.1985	-0.0130	-0.0293
CV	Allende	0.3731	0.1056	0.0165
CV	Grosnaja .075mm	0.4668	-0.0293	-0.1909
CV	Grosnaja .075-.15mm	-0.1509	0.1875	-0.1613
CV	Grosnaja .15-.50mm	-0.0449	0.1443	-0.1369
CV	Leoville	0.6738	-0.1501	-0.2108
CV	Mokoia	0.4979	0.1228	0.0449
CV	Vigarano	0.3627	0.0296	-0.0719
Ure	Novo Urei	0.1229	-0.1112	-0.0960
Kak	Kakangari	0.6917	-0.2279	-0.2430

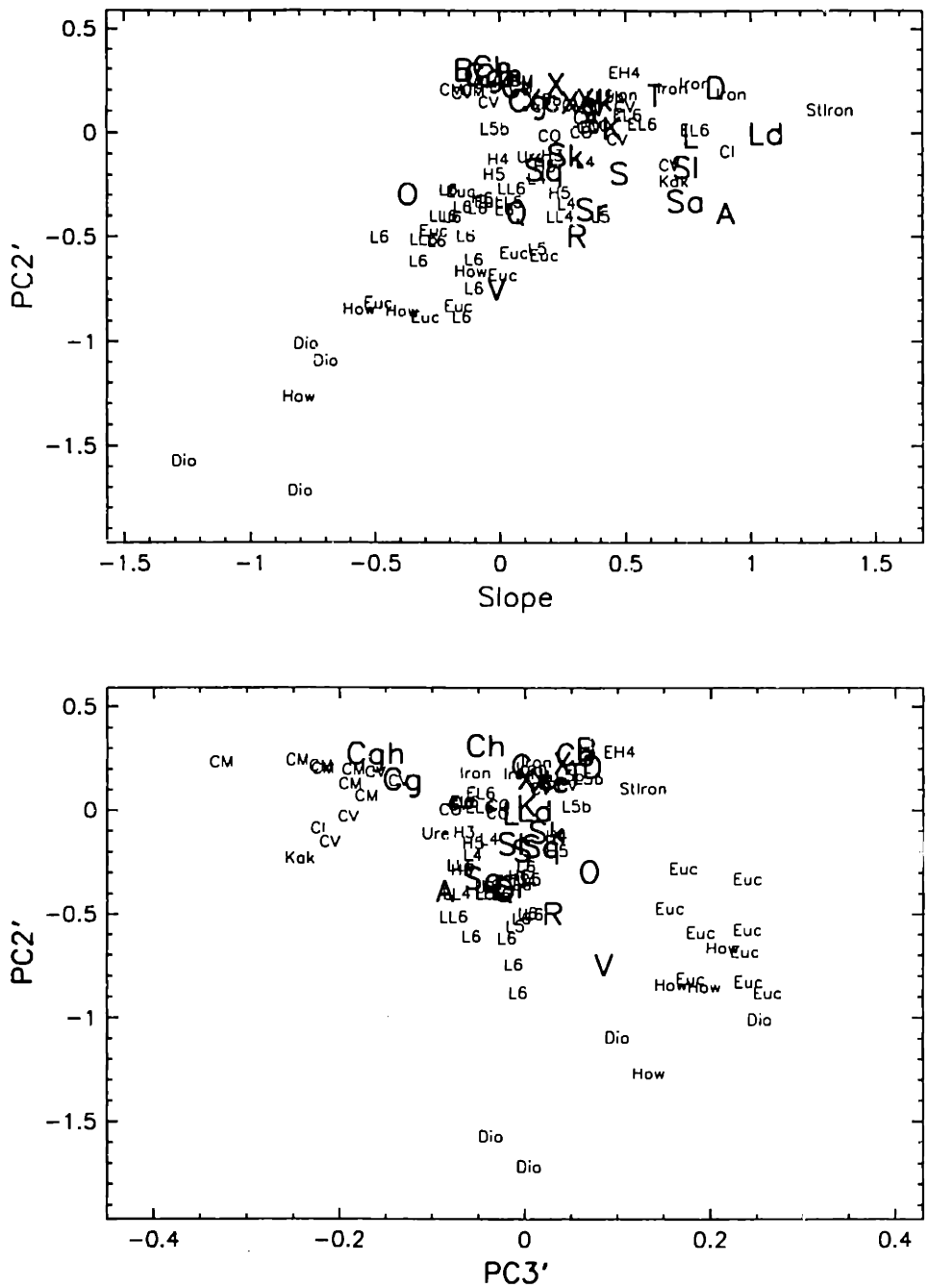

Figure 4.41: Spectral component plots showing the relationship of 78 meteorite spectra (Gaffey 1976) to the mean locations of the SMASSII taxonomic classes (large font). This broad view shows the range of the HED meteorites with respect to the variance in the asteroid data.

SMASSII. The HEDs, which are thought to be derived from Vesta (Binzel and Xu 1993) have spectra very similar to V-type asteroids, though, as seen in Figure 4.41, there are offsets between the HED meteorites and the V-class. An offset in the component Slope is seen in the upper plot in this figure, but a more substantial offset is present between the HED meteorites and the V-class in component PC3'. This offset occurs because the meteorite spectra have reflectance maxima that are more sharply peaked than that normally seen among the V-type asteroids, and the center of these peaks tend to be shifted redward (to longer wavelengths, typically by 0.02 μm) of the peaks seen in the asteroid spectra.

Figure 4.42 provides a magnified view of spectral component space, showing the positions of all SMASSII spectral classes except for the V-class. Likewise, most of the meteorite spectra are represented except for most of the HEDs and a few ordinary chondrites. By comparing both of the primary component planes plotted in this figure, several trends can be seen among the meteorite types, as well as relationships between the meteorite classifications and the asteroid classes. Focusing on the PC2' versus PC3' plane, we note the concentration of ordinary chondrites in the lower center of this plot, extending from the bottom edge of the plot, where L- and LL-type chondrites dominate, to the middle of the plot where the H-type chondrites are found. In the center of this distribution is the letter "Q", denoting the position of the asteroid 1862 Apollo. The Sk- and Sq-classes also plot in this region, toward the upper portion of the ordinary chondrite distribution (where the H-types dominate), in general agreement with the findings of Binzel *et al.* (1996) who show the continuum of spectral characteristics among S-type asteroids, especially within the NEA population, approach the observed spectral characteristics of ordinary chondrites. The CM carbonaceous chondrites plot in the upper left corner of the PC2' versus PC3' plane, corresponding most closely to the Cg- and Cgh-asteroid classes. The spectra of these meteorites have deep UV drop-offs, and may or may not contain 0.7 μm absorption bands, consistent with the two different asteroid classifications. Vilas and Gaffey (1989) suggested the CM chondrites as possible analogs to those C-type asteroids containing the 0.7 μm feature, though as seen in this figure, no meteorites plot close to the more heavily populated Ch-class, primarily because of the reduced strength of the UV feature in the Ch-type asteroid spectra. Just above the center in this plot (and just above the center of the PC2' versus Slope plane) is a small concentration of CO carbonaceous chondrites. These meteorites

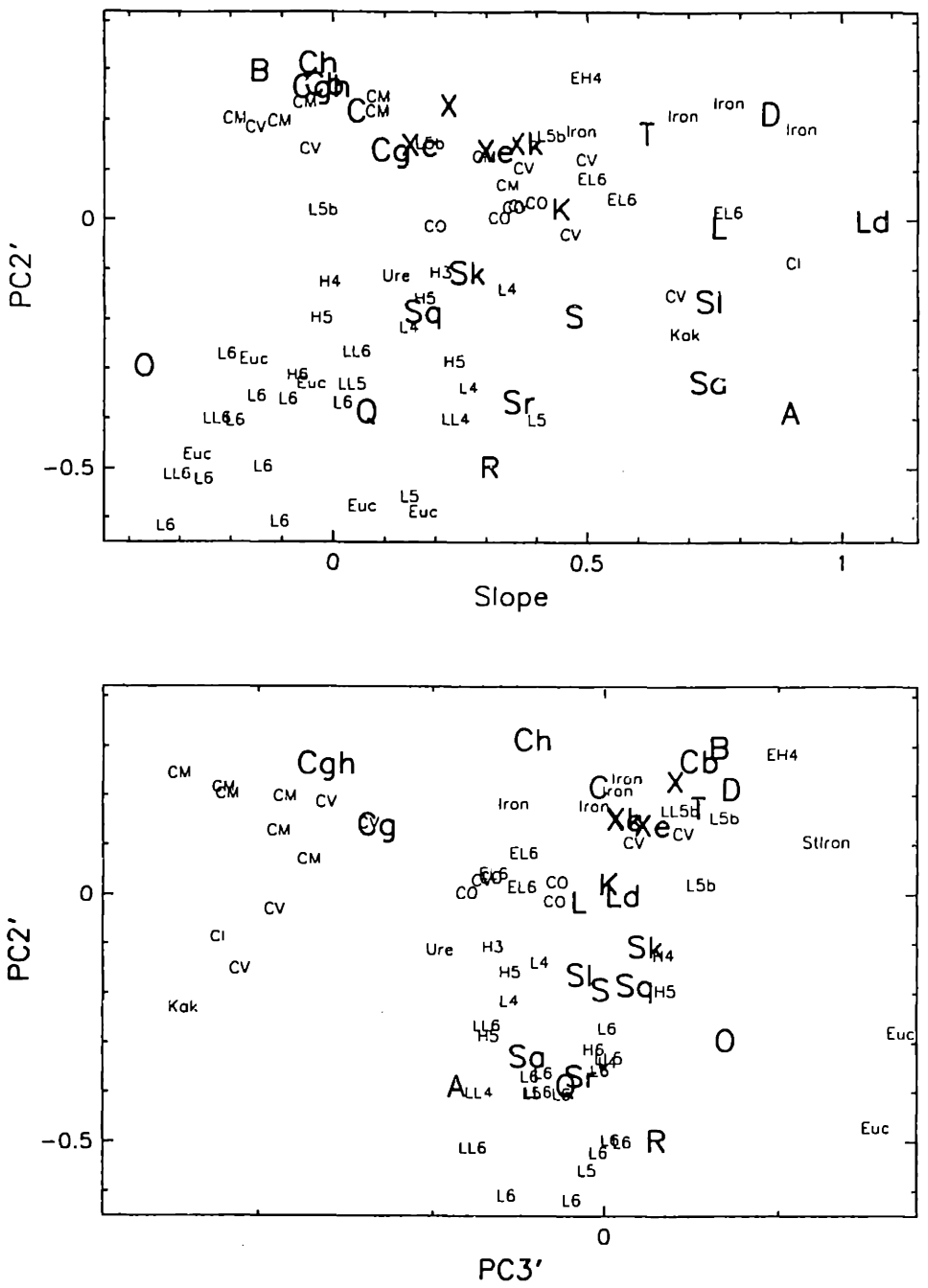

Figure 4.42: Similar to Figure 4.41, but a magnified view centered on the region occupied by the SMASSII asteroid classes (except for the V-class). Agreement between some asteroid classes and the proposed meteorite analogs is quite good - in particular, the Q-class (1862 Apollo) plots nicely in the ordinary L- and LL-ordinary chondrite field (McFadden *et al.* 1984). Likewise, the asteroid classes Cg and Cgh plot close to the CM meteorites which have been suggested as an analog (Vilas and Gaffey 1989).

plot most closely to the K-class, consistent with the identification by Bell (1988) of CV3 and CO3 chondrites as possible analogs of K-type asteroids. There are some unexplainable offsets between certain asteroid classes, and their assumed meteorite analogs, as was previously noted by Britt *et al.* (1992) and Xu *et al.* (1995). Most notable is the offset between iron meteorites and the X-type asteroids (including all class of the X-complex, except the Xe-types which are assumed to have an enstatite composition). This offset between the iron meteorites and the X-types is primarily confined to differences in spectral slope, and thus may suggest these color variations are tied to aging or processing of the asteroid surfaces at scales comparable to the observed wavelengths of reflected light.

Chapter 5

The reality of dynamical asteroid families located between 2.7 and 2.8 AU

5.1 Identification of dynamical families

The heliocentric orbit of an asteroid is described at any particular epoch by a set of six elements. Two of these elements, the semimajor axis (a) and the eccentricity (e), give the size and the shape of the elliptical orbit as constrained by Kepler's First Law. Three angles, the inclination (i), the longitude of the ascending node (Ω), and the argument of perihelion (ω), provide the orientation of this orbit within a heliocentric reference frame that is defined by the ecliptic plane and the vernal equinox. The sixth element, the time of perihelion (T), is necessary for locating the asteroid at any time along its orbital path. However, due to gravitational perturbations by the major planets, this simple two-body representation of the asteroid's motion around the Sun, called the osculating orbit, is not constant over time (Danby 1992).

The effects of gravitational perturbations can be grouped into two categories. The first of these depends on the actual orbital longitude of an asteroid, and that of the perturbing planet, as functions of time. When the orbital period of the asteroid is commensurate with that of a major planet (most notably, Jupiter), the asteroid and planet will regularly have closest approaches that occur at the same orbital longitude. These repeated encounters, and the resulting gravitational perturbations are the basis for mean-motion resonances. Some of these resonances are responsible for gaps in the number density of asteroids at specific values of semimajor axis within the main belt, called the Kirkwood Gaps (Kirkwood 1867), while other mean-motion resonances, such

as the 1:1 resonance, provide regions of long-term orbital stability (e.g. Yoder 1979). For certain resonances with Jupiter, the orbit of an asteroid whose mean motion too closely matches the resonance value can become chaotic, resulting in potentially large fluctuations in orbital eccentricity (Wisdom 1982, 1983). If fragments of asteroids are injected into these "chaotic zones" as a result of mutual collisions within the belt, these resonances can provide dynamical pathways for delivering this asteroidal material into the inner solar system, and are thus ways of resupplying the observed near-Earth asteroid and meteoroid populations (Greenberg and Nolan 1989, Wetherill 1989).

The second category of perturbations does not depend on the exact location of a planet in its orbit over time, but rather on the long-term effects that the planet has when the gravitational contribution of its mass is averaged over its entire orbit. The combined gravitational effects of all of the major planets leads to a series of fundamental precessional frequencies in the solar system (Brouwer and van Woerkom 1950, Nobili *et al.* 1989). The orbit of each asteroid is subject to the effects of these secular perturbations, resulting in the precessions of both the longitude of the ascending node and the argument of perihelion, with corresponding oscillations in orbital inclination and eccentricity of the asteroid, where these oscillations have periods that are typically of order 10^4 to 10^5 years. The semimajor axis of the orbit, which represents the total energy in the two-body problem, is not subject to secular perturbations, and is stable.

To understand the dynamical history of the asteroid belt, it is therefore necessary to first determine a set of orbital elements, called proper elements (semimajor axis, a', proper eccentricity, e', and proper sine of inclination, sin i'), from which the more significant effects of these secular perturbations have been removed. This is a complex problem, especially when one of these precessional frequencies (either the nodal or apsidal frequency of the asteroid) closely matches one of the fundamental frequencies for the major planets. An asteroid whose orbit is near one of these secular resonances can experience large perturbations. This is especially true for the ν_5 and ν_6 resonances (in apsidal frequencies), and the ν_{16} resonance (in nodal frequency), which are closely tied to the orbital precession rates of Jupiter and Saturn.

In his initial work, Hirayama (1918) identified three apparent groupings of asteroids based on similarities in their orbital mean motion and on the systematic orientations of the poles of their osculating orbital planes. Based on his understanding of the effects of

secular perturbations, Hirayama suggested that each of these three groupings might have originated from a common source, such as the break-up of a parent asteroid. The first three Hirayama families, the Eos, Koronis, and Themis families, are still the most widely recognized of all dynamical groupings, and are labelled in the proper element plot of a' versus sin i' shown in Figure 5.1. In his subsequent investigations, Hirayama used the computations of proper elements to further study the clustering of asteroids, ultimately adding Maria and Flora to his list of "classical" families (Hirayama 1923). As with many aspects of asteroid research, however, little progress was made in the studies of these dynamical families during the three decades immediately following Hirayama's work. Brouwer (1951) resurrected the interest in asteroid families by applying his theory of secular perturbations (Brouwer and van Woerkom 1950) in the calculation of proper elements for over 1500 asteroids. Brouwer identified a total of 28 potential groupings that included the original five families noted by Hirayama. Since that time, significant advances have been made on several different fronts related to the dynamical studies of asteroids.

Certainly the most measurable advance in the study of asteroids has been in the number of objects that have been discovered. During the mid-1920's when Hirayama found the first clusters of asteroids in proper element space, there were roughly 1000 asteroids known. Today, over 10,000 asteroids have orbits that are sufficiently well determined that they have received permanent numbers in the IAU system for the cataloguing of asteroids. In addition, several thousand other asteroids have well determined orbits, but which have not yet achieved the criteria necessary for numbering. This exponential growth in the discovery rate of asteroids as a function of time was discussed by Bowell *et al.* (1989a), and shows no sign of slowing, especially with the recent introduction of CCD cameras, along with automated scanning and astrometric techniques for the large-scale surveying of asteroids (Monet *et al.* 1997, Stokes *et al.* 1998). By increasing the number of asteroids known, a more complete picture of the distribution of orbits is developed, including a better statistical understanding of asteroid groupings in orbital element space. The effect of increasing the known population is clearly seen in lower half of Figure 5.1. Coinciding with this rapid growth in asteroid discoveries has been the monumental advances in computer technology. This increase in computing power has helped prompt the development of different secular perturbation theories, as well as the use of various techniques for identifying clusters of asteroids

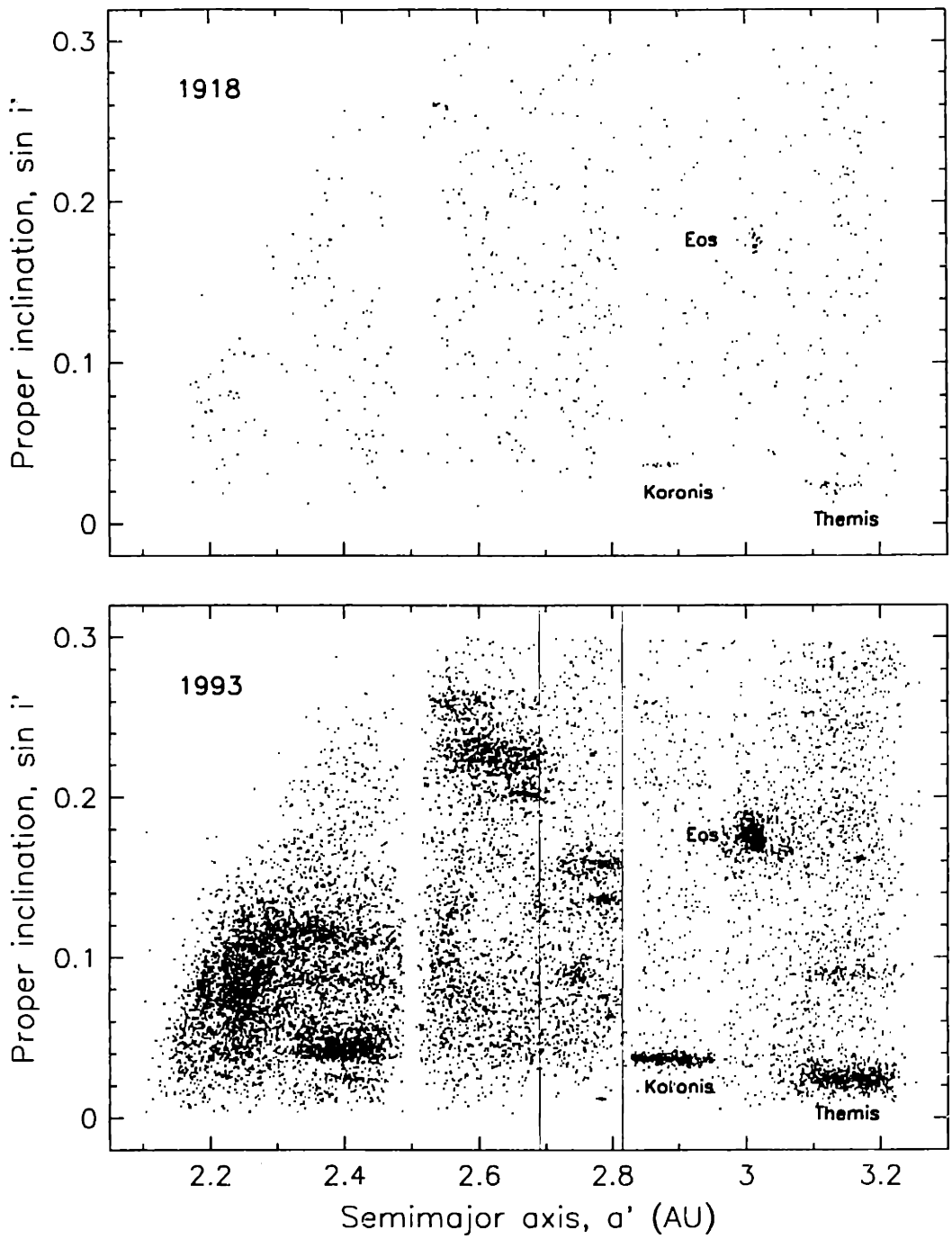

Figure 5.1: Plots showing the distribution of proper elements (a' versus sin i') for those asteroids known in 1918 (upper panel) and in 1993 (lower panel). The Eos, Koronis, and Themis families, first recognized by Hirayama (1918) are labelled. By increasing the number of known asteroids, the structure and number of individual groupings found in proper element space increases dramatically. In the bottom panel, two vertical lines have been added at 2.690 and 2.815 AU to denote the region studied in this project. Figure adapted from Binzel (1994).

among the resulting proper elements. Even with these advances, however, there are still limitations in the different perturbation theories, in the long-term reliability of the calculated proper elements, and in the methods used to identify potential dynamical families.

Lemaitre (1993) compared three different methods for calculating proper elements: (1) the semi-analytical theory of Williams (1969), (2) an analytical theory developed through the combined efforts of Yuasa (1973), Milani and Knežević (1990), and (3) the semi-analytical theory of Henrard (1990) that was adapted in the method of Lemaitre and Morbidelli (1994). The analytical method of Yuasa, Milani and Knežević has the advantage of being fast and simple to apply, making it a preferred method when large numbers of orbits (real or simulated) are being considered. However, due to the truncated series expansions used in this method (in lieu of numerical integrations), it is only applicable for asteroids having relatively small orbital eccentricities and inclinations. By comparison, the semi-analytical methods of Williams (1969) and Lemaitre and Morbidelli (1994) are more suitable for computations involving highly inclined or eccentric orbits. For the family analysis presented in this chapter, we have adopted the proper element triplets (a', e', sin i') that were computed by Milani and Knežević (1994, from their file version 6.8.5, which contains the proper elements for a total of 12,487 asteroids). Because 32 of the asteroids observed during SMASSII in the region between 2.7 and 2.8 AU have high values of orbital inclination or eccentricity, we supplemented the data of Milani and Knežević with proper elements provided by A. Lemaitre (private communication).

In the search for dynamical families, the goal is to identify those clusters of asteroids in proper element space that are statistically more significant than any chance accumulations of non-family, background asteroids. When a large number of asteroids are clustered very closely in proper element space, there is usually little question about the reality of the family. However, for those potential families that have fewer members, and for which the locations of those members in element space are more dispersed, the possibility that the cluster is a statistical fluke becomes greater. Even if the family is real, defining the boundaries or the exact membership of a dispersed grouping of objects becomes problematic. For this reason, various methods have been described to identify possible families, each with its own set of strengths and weaknesses, and its own degree of subjectivity. A very basic approach for finding families is that described by

Williams (1992) who used a visual, stereoscopic examination of proper elements in the three-dimensional space of a', e', sin i' to locate potential clusterings. Poisson statistics were applied *a posteriori* to test the significance for each of the detected clusters, and the family was accepted as real only if the chance that it was a random accumulation was considered to be sufficiently small. Based on a sample of 2823 asteroids (of which 1753 were numbered, and 1070 were objects from the Palomar-Leiden Survey, van Houten *et al.* 1970), Williams found 104 clusterings within the main belt that he considered to be statistically significant.

Zappalà *et al.* (1990, 1994, 1995) used the multivariate technique of hierarchical clustering to search for families of asteroids. The hierarchical clustering method (HCM) is a distance technique, similar to the minimum-spanning tree (MST) algorithm discussed in Chapter 3. Unlike MST, however, the clustering in HCM occurs by agglomeration, where the objects are clustered together in order of increasing values of dissimilarity (the pair of objects with the smallest value of dissimilarity is linked first). In the single-linkage method used by Zappalà *et al.*, the distance between two clusters is measured by the dissimilarity of the closest pair of objects between them, such that the agglomeration occurs based on the shortest possible linkage. The advantage of HCM is the ability to display the clustering solution as a dendrogram, as was demonstrated for the case of spectral dissimilarities in Figure 3.7. To apply this technique, Zappalà *et al.* first transformed the proper elements a', e', and sin i' into dissimilarities (distances) using the two metrics:

$$D_1 = na' \sqrt{\frac{5}{4}\left(\frac{\delta a'}{a'}\right)^2 + 2(\delta e')^2 + 2(\delta \sin i')^2} \tag{5.1}$$

and

$$D_2 = na' \sqrt{\frac{1}{2}\left(\frac{\delta a'}{a'}\right)^2 + \frac{3}{4}(\delta e')^2 + 4(\delta \sin i')^2} \tag{5.2}$$

where $\delta a'$, $\delta e'$, and $\delta \sin i'$ are the differences in proper elements between each pair of asteroids, and n and a' are the average mean motion and proper semimajor axis for that pair. Eqn. 5.1 was considered the "standard metric", while Eqn. 5.2 was used to test the robustness of the clustering solutions. These dissimilarities are expressed in units c.

m/s, and are related to the relative velocities of fragments being ejected from the gravitational potential of a parent body (Zappalà *et al.* 1995). In determining what clusters were statistically significant, Zappalà *et al.* adopted a quasi-random level, a value of D_1 (or D_2) above which clusters with a minimum number of members might be considered to be a random grouping of background (non-family) objects. By setting this quasi-random level sufficiently low, any clusters with values of D_1 (or D_2) smaller than this cut-off criteria have a high probability of being real. Based on the Milani and Knežević sample of 12,487 asteroids, Zappalà *et al.* (1995) identified 32 nominal families, as well as 31 "clumps" that are less certain.

Another technique, called the wavelet analysis method (WAM), was adapted by Bendjoya (Bendjoya *et al.* 1991, Bendjoya 1993, Zappalà *et al.* 1995) in his search for asteroid families. In this method, a wavelet transform is applied to the distribution of proper elements in three-dimensional space, revealing the locations of overdensities (concentrations of points) within that space. These overdensities are mapped at different resolutions by varying the scale-length of the transform, using the metrics given in Eqns. 5.1 and 5.2. By varying the resolution, the wavelet method becomes sensitive to various scales of structure within the data, and is considered to be more efficient at detecting clusters with respect to their local background than HCM. Based on the same sample of 12,487 objects from Milani and Knežević, this method identified 30 dynamical families within the mainbelt, along with 24 "tribes" and 9 "marginal groupings", where these latter categories indicate groupings that are less certain. Zappalà *et al.* (1995) compared the results from both the HCM and WAM techniques, providing an important foundation on which the reality of each of the proposed dynamical families can be judged.

While Hirayama (1918, 1923) hypothesized that asteroid families result from the internal break-up of larger parent bodies, much like that observed in the splitting of cometary nuclei (Sekanina 1979), the long-held notion has been that clusters of asteroids in proper element space result from collisional processes (Kuiper 1950). Because the instantaneous ejection velocities of collisional fragments are understood to be much smaller (<1 km/s, Zappalà *et al.* 1984) than the orbital velocity of the parent (~20 km/s), the fragments will assume osculating orbits that are similar to that of the parent. These orbits will evolve over time, due in part to subsequent collisional or

dynamical processes, but primarily due to the effects of secular perturbations. However, finding clusters of asteroids in orbital space does not, in itself, prove that there is a genetic relationship between the objects (that is, that there is a compositional tie between the individual members that can be traced to the original formation, subsequent thermal evolution, and ultimate breakup of a single parent body). Because the dynamical families are statistical by nature, only by including physical observations of the individual members is it possible to uniquely define the boundaries of a family, and to identify the exact membership, as well as potential interlopers that are not genetically related to the family (Chapman *et al.* 1989). Proving that these families are real genetic relationships is an important step in understanding both the early, formational circumstances of the asteroid belt, and the collisional evolution of the asteroids over time. If these dynamical families are the result of collisions, then they provide natural experiments from which to study the physics of collisions at sizes and energies many orders of magnitude greater than is possible in the laboratory. True, genetic families will also allow us the unique chance to examine the exposed interiors of once much larger, and possibly differentiated bodies.

5.2 Previous spectral studies of families

By measuring the spectral reflectance properties of asteroids in a proposed family, it is possible to address the question of whether the family makes "cosmochemical sense". If the spectral signatures of the family members are similar to each other, but distinct from the distribution of spectral types making up the background, this provides strong evidence that the family results from the collisional breakup of a relatively homogenous parent. If, on the other hand, a variety of spectral types are observed among the members of a purported family, the interpretation becomes more difficult. The disruption of a differentiated parent could result in a family with a variety of spectral types, related to the different mineralogical layers within that parent. Such a family might consist of various fragments from the iron core, the olivine-rich mantle region, and the silicate-rich crust. Identifying an asteroid family as the breakup of a differentiated body, however, requires that the mineralogical interpretations of the various spectral types observed are secure. Even in such a heterogeneous family, it should be expected that, as more members are observed, groups of fragments from each mineralogical layer will be found that will exhibit similar spectral properties. If the members of a proposed family are interpreted as coming from both differentiated (high-temperature) and

undifferentiated (low-temperature, primitive) sources, then it is unlikely that the family resulted from the breakup of a single body. In any of these scenarios, however, it is important that the spectral makeup of the background population is determined as well, providing a basis against which the potential family members can be compared. Whether the members of a family indicate a parent body was homogeneous or heterogeneous, if that family has the same distribution of spectral types as the background population, then little is gained from this spectral information that can confirm a genetic origin for the family, or constrain the actual size or membership of the family.

The first notable investigation of the spectral properties of asteroid families was carried out by Gradie and Zellner (1977). Based on broadband UBV photometry and radiometric measurements of asteroids belonging to the Eos and Koronis families, they found that each of these families appears to be the result of the collisional disruption of a homogeneous parent. Using the classifications available in the TRIAD file (Bowell *et al.* 1979), Gradie *et al.* (1979) extended this work by examining 48 dynamical families that had been proposed by Williams (1979). Again, the Eos and Koronis families were described as being spectrally similar, with Eos primarily containing U-type (nearly S-type) asteroids, while the Koronis family contains objects that were more clearly identified as S-types. In addition, the Themis family was found to be comprised of neutral colored C-types. Among the smaller families, over half were described as containing similar taxonomic types, but the remaining families had members that were spectrally dissimilar, usually mixtures of S- and C-types, a combination that cannot be readily explained based on the implied mineralogies. Because these small families tended to reflect the same taxonomic makeups as the local background population, Gradie *et al.* concluded that the small asteroid families have undergone the same formational and collisional evolution as the non-family objects, and that large homogeneous families, such as the Themis, Eos and Koronis families, are the anomalies.

Chapman (1987) utilized a variety of datasets, including the ECAS colors (Zellner *et al.* 1985) and the IRAS albedos (Veeder *et al.* 1989) to place taxonomic constraints on 1721 asteroids, of which 939 where uniquely assigned to specific taxonomic classes. From this large sample, Chapman was able to test the reality of many proposed asteroid families, including 84 families identified by Williams (1979), 72 families from Kozai (1979), and 19 families proposed by Carusi and Massaro (1978). By comparing the

distribution of taxonomic types for each of these families with the distribution of types among the local background, Chapman identified those families that appeared taxonomically (and presumably compositionally) distinct from the background. Chapman postulated that the more distinct a family is from its immediate background, the more likely that family might be real. From this analysis, he found that about half of the well-sampled Williams families were distinct from the local background, and should be considered real; some others were found to be spectrally homogeneous and sufficiently similar to the background that a genetic relationship could not be ruled out.

Bell (1989) used the expanded taxonomy of Tholen to examine the reality of proposed families by assuming a mineralogical interpretation for each of the Tholen classes. Bell found only five families that he considered to be real genetic relationships: the Themis, Eos, Koronis, and Flora families, and part of the combined Nysa/Hertha family. Each of these five groupings are spectrally homogeneous, and no families were identified in which spectrally diverse members could be interpreted as originating in various regions of a single differentiated parent. In contrast to the findings of Chapman, Bell concluded that most of the small dynamical families are not true genetic relationships, because the taxonomic classifications of their members suggest geochemical or mineralogical associations that are not compatible with a common origin.

The introduction of CCD spectroscopy enhances the prospects of solving some of the major questions surrounding dynamical families. Several spectroscopic campaigns have focused on measuring the reflectance properties of specific families, and have obtained observations of sufficiently large samples of objects, including relatively small members, that the true nature of the these families is now being revealed. As part of the SMASSI survey (Xu *et al.* 1995), Binzel and Xu (1993) reported on the distribution of asteroids with spectra resembling those of basaltic achondrite (HED) meteorites in the vicinity of the asteroid 4 Vesta, thus confirming the existence of a dynamical family associated with Vesta, and placing constraints on its boundary in proper element space. Observations of the Vesta region continued during the SMASSII survey, the results of which will be reported in an upcoming paper. In addition to these observations of the Vesta family, spectral studies of the Koronis (Binzel *et al.* 1993a), Veritas (Di Martino *et al.* 1997), Eos (Doressoundiram *et al.* 1998), and Themis (Florczak *et al.* 1999) families have also been reported. For each of these families, the spectral observations reveal strong similarities in the details of absorption features among the different members,

suggesting these families are relatively homogenous in terms of their spectral types. However, variations in the spectral slope are routinely noted (e.g.. Di Martino *et al.* 1997, Doressoundiram *et al.* 1998) that have been attributed to both compositional variations within the parent body, and variations in resurfacing processes tied to space weathering. Until the physical processes that alter the optical characteristics of asteroid surfaces are better understood, determining the source of the variations in spectral slope among asteroid family members will be difficult.

Except for our study of the Vesta region, each of the CCD surveys cited above has focused on observing asteroids that have been listed as probable members of their respective dynamical families. By assuming that the family memberships determined from dynamical studies (the computation of proper elements, and the search for groupings in orbital element space) is correct, these spectral observations primarily address the question of the genetic reality of the family. Except for the identification of interlopers within the listed membership, the true extent of the family in orbital space is not determined. Finding the true boundaries of a family requires that the distribution of spectral types making up the local background is also known. The importance of thoroughly sampling the region containing, and surrounding a possible family should not be underestimated.

5.3 Analysis of the SMASSII observations

In the sections that follow, I will describe the initial results obtained from a spectroscopic survey of asteroid families located between 2.7 and 2.8 AU. This region of the main belt was chosen for study for two primary reasons. The first is the variety of spectral types that might be expected in this part of the belt. Prior to this work, it was known that the fraction of C- and S-type asteroids in this region should be about equal, and that a significant number of X-types should also be present (Gradie *et al.* 1989). As can be seen in Figure 4.38, the mix of classes within the C-complex, with roughly equal numbers of objects exhibiting either the presence or absence of the 0.7 μm absorption feature, and the mixture within the S-complex, with a significant fraction of K- and L-type asteroids being present, makes this a very diverse region of the belt. This mixture of spectral types is important in helping to define the extent of families that might be spectrally homogenous with respect to the background population. The second reason for choosing this region for study was the number of small families that had already been

identified through dynamical studies by Williams (1992), Zappalà *et al.* (1990, 1994, 1995), and others. By comparing the lists of proposed families from each of these works, we estimated there may be as many as 12 to 15 families between 2.7 and 2.8 AU that could be adequately studied, and placed in the context of the broader background population, by obtaining CCD spectra for a total of 400 to 500 asteroids. The goal of this project was to measure the spectral properties of a large, representative sample of asteroids throughout this region of the main belt, equally sampling members of many proposed families and the background population, so that the reality of those small dynamical families could be tested. For those families that are real, we hoped to more accurately determine their memberships and boundaries in orbital element space, and to identify possible interlopers.

In this analysis, we use the spectra of 465 asteroids observed during the SMASSII survey, all with semimajor axes between 2.690 to 2.815 AU. The latter boundary in semimajor axis corresponds to the inner edge of the 5:2 mean-motion resonance with Jupiter, centered at 2.825 AU, while the boundary at 2.69 AU was chosen as the best compromise for separating the small families that we had targeted for study from the much larger Eunomia family that extends from roughly 2.55 to 2.70 AU. During the observations, somewhat greater weight was giving to obtaining spectra of objects in particularly small families, such as the Astrid, Hoffmeister and Chloris families defined by Zappalà *et al.* (1995, using the HCM technique), to ensure that these families were sufficiently sampled. In general, however, an equal effort was made to obtain observations of non-family (background) asteroids as was made for objects suspected of being family members. The distribution of these 465 asteroids in proper element space is shown in Figures 5.2 and 5.3.

A goal throughout the entire SMASSII survey was to observe as many small asteroids as possible, though there was always a natural tendency to observe the brighter objects, especially when the sky conditions were less than ideal. The limiting magnitude of our observations was V ~ 17.5, which corresponds to an absolute magnitude of H ~ 13.5 for asteroids in the middle of the main belt. Thus, the smallest asteroids in the sample of 465 discussed here have diameters ranging from ~6 km (for S-type asteroids), to ~12 km (for C-types). In Figure 5.4, the cumulative number of asteroids we observed is plotted as a function of absolute magnitude. For comparison,

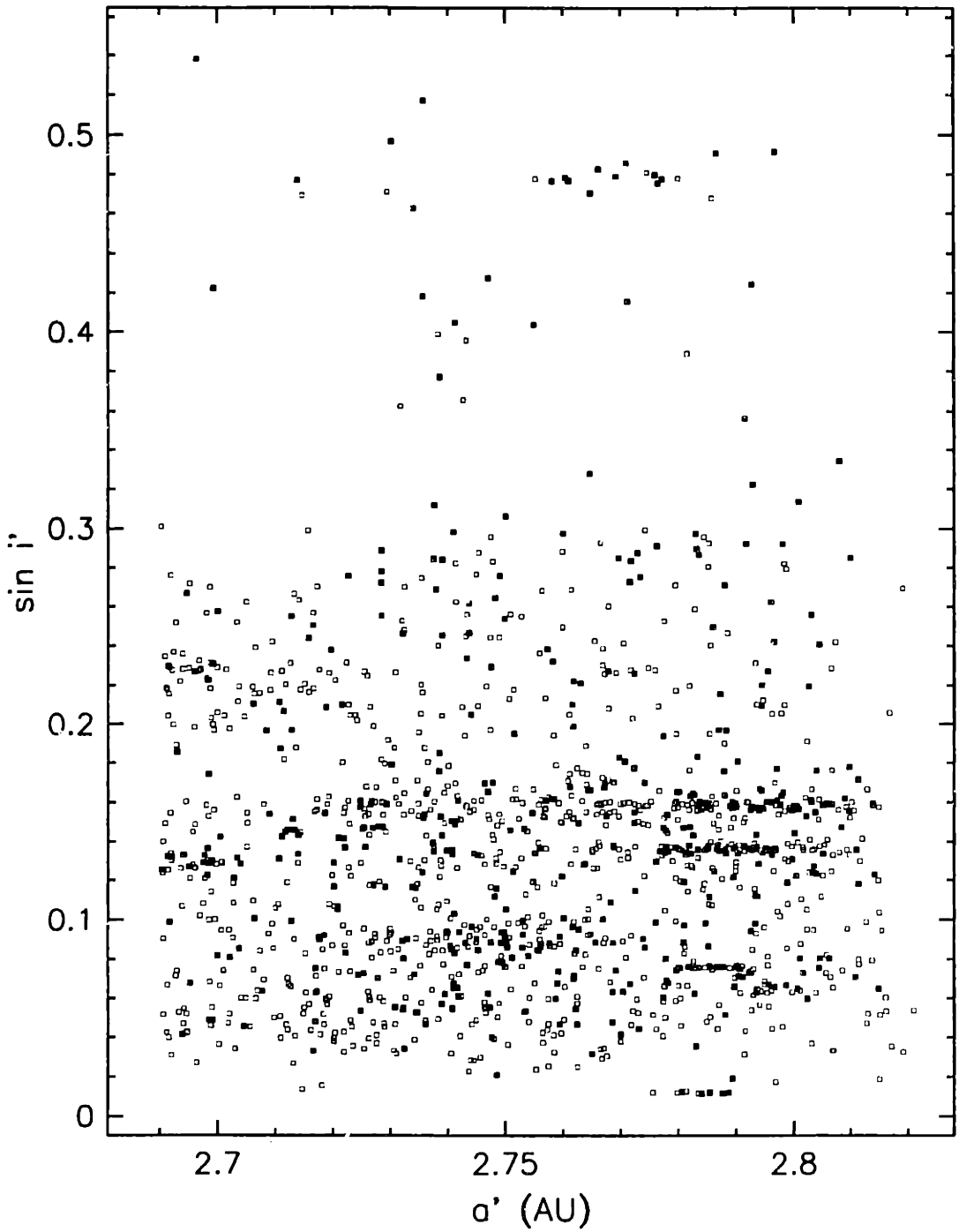

Figure 5.2: Detailed distribution of asteroids in proper element space (a' versus sin i') between 2.690 and 2.815 AU. Those objects plotting with sin $i' < 0.30$ are from the proper element file (version 6.8.5) of Milani and Knežević (1994), while the elements for objects with higher inclinations were provided by A. Lemaitre (private communication). The 465 objects observed as part of the SMASSII survey are plotted as solid symbols, while those objects that were not observed during SMASSII are shown as open symbols.

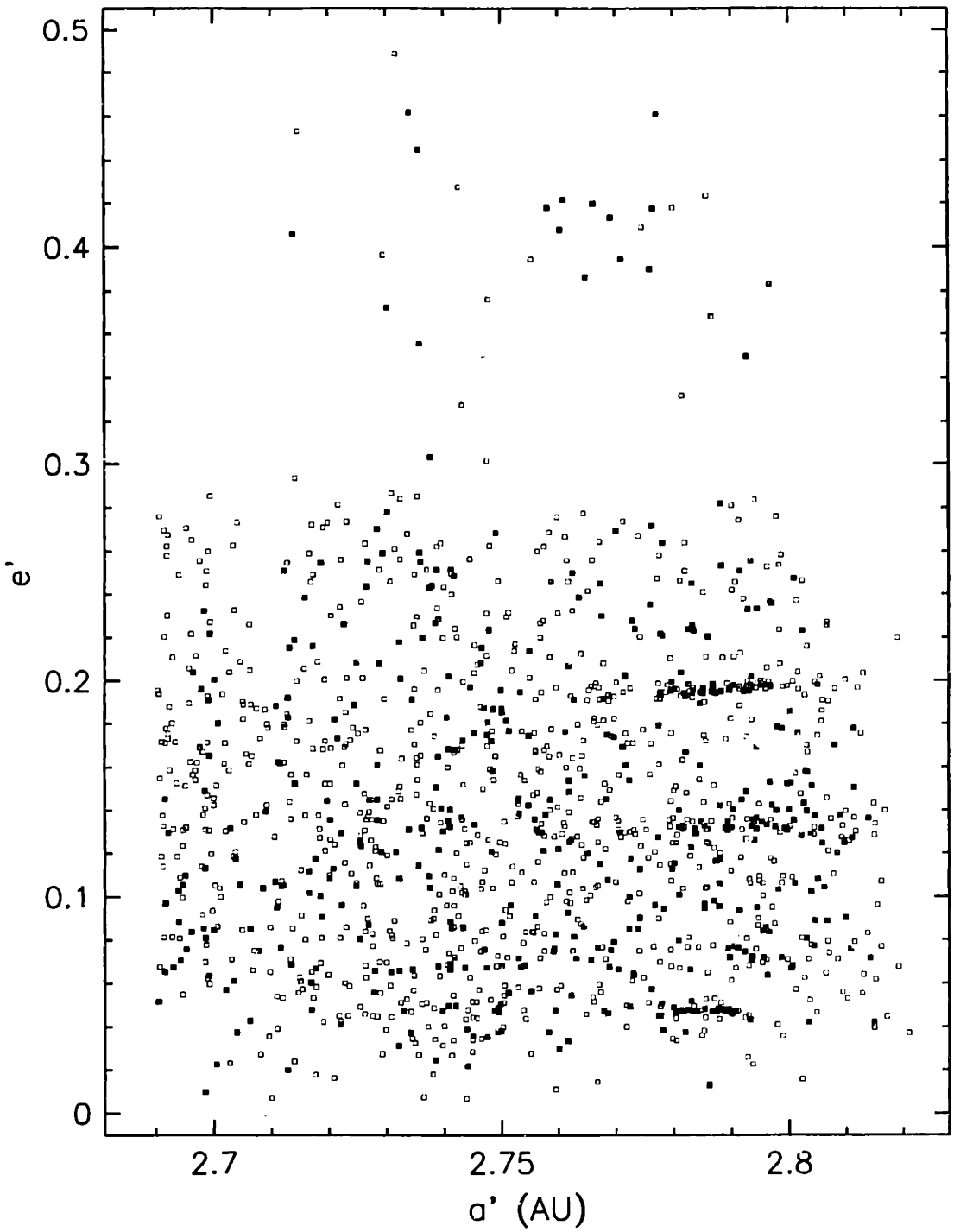

Figure 5.3: Similar to Figure 5.2, but showing the distribution of a' versus e'. Again, the proper elements for those objects with $e' > 0.3$ were provided by Lemaitre.

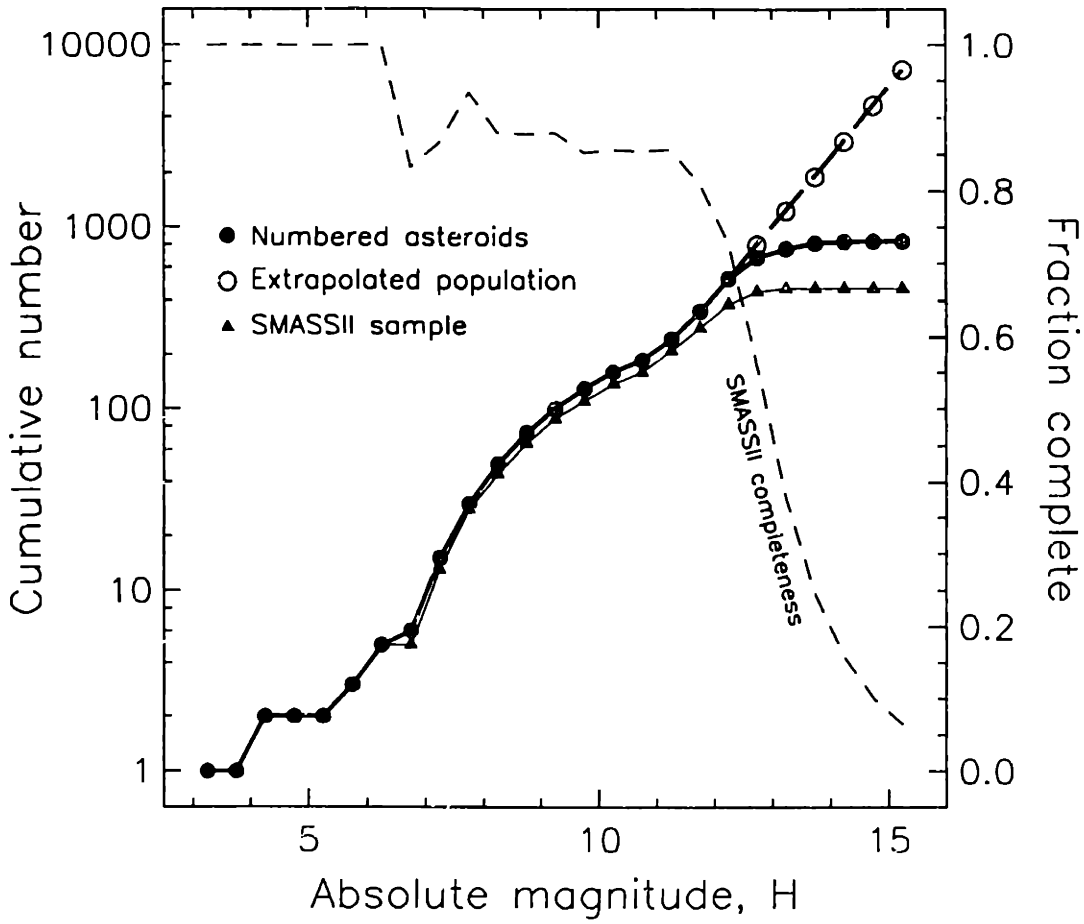

Figure 5.4: Completeness of the SMASSII survey (between 2.690 and 2.815 AU) as a function of absolute magnitude, H. The numbered asteroid population (solid circles) is plotted as the cumulative number, and is assumed to be complete down to H = 12.25. For smaller asteroids, this cumulative population is extrapolated (open circles), assuming a log slope of 0.39 per magnitude for the non-cumulative distribution, determined from the Palomar-Leiden Survey (van Houten *et al.* 1970). The cumulative distribution for asteroids observed during SMASSII is also plotted. The dashed line (short dashes) is the linear fraction of the SMASSII objects relative to the total population (referred to the scale on the right). From this plot, we see that the SMASSII survey (for this narrow region of the main belt) is complete at the 85% level down to an absolute magnitude of 11.5. This completeness falls off rapidly for smaller asteroids.

the cumulative distribution for the numbered asteroids is also plotted. From this, we see that our sampling of the region between 2.7 and 2.8 AU is about 85% complete for absolute magnitudes brighter than H = 11.5, corresponding to asteroids with diameters of 15 km (for S-types) to 30 km (for C-types). This completeness falls off rapidly, however, with only ~60% of all asteroids in the region brighter than H = 12.5 having been observed.

In the early phases of this project, visual examinations of the spectra revealed that many of the families proposed by both Williams (1992) and Zappalà *et al.* (1994, 1995) appeared to be spectrally homogeneous (Bus *et al.* 1996). That is, for each of these families, most members have spectra showing very similar reflectance characteristics, with most of the variation between members being in the overall slopes of the spectra. These variations in slope are similar in magnitude to those described for the Veritas and Eos families (Di Martino *et al.* 1997, Doressoundiram *et al.* 1998), and might be attributed to minor compositional variations, to processes of resurfacing and space weathering, or possibly to differences in observational geometry (phase-reddening). Because these variations in slope are typically larger than we expect from uncertainties in the individual observations, we have adopted the term "quasi-homogeneous" to describe those families whose members exhibit relatively strong spectral similarities, but which may have small differences in composition or in surface properties between them. A cursory examination of the spectral variance within each of the families reveals a very loose correlation with the depth of the 1 μm band, so that families composed of S-type asteroids tend to have a greater degree of variation between their spectra than families composed of C-types. This relationship is consistent with the overall increase in spectral variance with a decrease in the component PC2' for the various taxonomic classes discussed in Chapter 4.

Because most dynamical families appear to have members that are spectrally similar, this raises the possibility of combining a measure of the spectral variance with the orbital dissimilarity, allowing for an independent search of asteroid families that directly incorporates both the orbital and spectral information. In the ideal case, it is mathematically straightforward to add the spectral and orbital metrics, producing a single measure of dissimilarity that could be analyzed using various distance techniques such as hierarchical clustering (HCM). Unfortunately, while the orbital dissimilarity, as defined by Eqns. 5.1 and 5.2, relates directly to ejection velocity, and thus, to kinetic energy as a smoothly varying function, defining a meaningful spectral metric is much more difficult. Distinctions between taxonomic classes are not smoothly related to the spectral variance on which a metric would most naturally be based. As was discussed in Chapter 3, attempts to define a single metric for the development of our feature-based taxonomy were not successful, leading us to rely on the ordination technique of principal component analysis as a way to visualize the taxonomic results.

Rather than trying to directly incorporate the spectral variance in our search for asteroid families, we have adopted a more simplistic approach. By treating the variance between a pair of spectra as a conditional test of similarity, we can define a metric that is a simple step function, which will filter asteroid pairs that are spectrally similar from those pairs that are not similar. By combining this simplified spectral metric with the orbital metric, we can interactively search for asteroid groupings that are both dynamically and spectrally similar. A major advantage of this approach is the ease and simplicity with which the results can be interpreted. On the other hand, because this method is based only on a measure of the spectral variance, it is insensitive to taxonomic boundaries, so that care must be used in interpreting the results. To apply this technique, a standard measure of the spectral dissimilarity, s, must first be defined (we actually define two different spectral metrics, denoted as s_1 and s_2, in the discussion below). A variable ε is also defined as a cutoff value of spectral dissimilarity below which a pair of spectra are considered similar. Finally, a height z is established for the step function where z is expressed in m/s, comparable to the relative ejection velocities given by Eqns. 5.1 and 5.2. By selecting a sufficiently high value of z, the effect will be to artificially raise the relative ejection velocity for any asteroid pair that is spectrally dissimilar, postponing the linkage of that pair in the cluster analysis. This simplified spectral metric $\nu(s)$ can be defined as:

$$\nu(s) = 0 \quad \text{for } s < \varepsilon, \text{ and}$$

$$\nu(s) = z \quad \text{for } s \geq \varepsilon,$$

where the value of z that we have adopted is 2000 m/s, significantly larger than any ejection velocities we might expect in true, genetic families. The metric $\nu(s)$ is then combined with the orbital metric D_1, given in Eqn. 5.1, by:

$$D' = \sqrt{D_1^{\,2} + \nu(s)^2} \tag{5.3}$$

Two measures of the spectral dissimilarity, s, were defined. The first is given by:

$$s_1 = 4\sqrt{\left(\frac{\delta\gamma}{1 - 0.6\overline{PC2'}}\right)^2 + \left(\frac{3d'}{2(1 - 0.3\overline{PC2'})}\right)^2} \tag{5.4}$$

where $\delta\gamma$ is the differences in average spectral slope between the pair of asteroids (γ is defined in Eqn. 3.3), d' is the Euclidean distance between the two residual spectra, and $\overline{PC2'}$ is average value of PC2' for the pair. The coefficients were determined empirically, as a means of equalizing the differences in spectral variance between families of S-type asteroids and those composed of C-type asteroids. The factor of 4, at the beginning of Eqn. 5.4, is introduced to scale the dissimilarities, increasing the mean value of s_1 to ~ 1.0 for families that are spectrally quasi-homogeneous, and is included only to make the interpretation of the dissimilarities easier. While the derivation of Eqn. 5.4 may seem somewhat arbitrary, I feel that it accurately relates the fractions of spectral variance that can be attributed to both the slope, and to the higher-order spectral features. However, as a test, I have defined a second measure of dissimilarity by:

$$s_2 = \frac{9}{2}d \tag{5.5}$$

where d is the Euclidean distance between two original spectra (where the average slopes of the spectra have not been removed), and the scaling factor of 9/2 again raises the mean value of the dissimilarity within the various families to ~1.0. As will be seen from the following results, the choice of dissimilarity (s_1 or s_2) has little effect on the determination of family memberships.

5.4 Results for the primary families

The procedure I used to identify possible asteroid families was based on the computation of a series of clustering solutions, where the value of ε (the cutoff in spectral dissimilarity) was increased incrementally. This procedure was repeated using both definitions of dissimilarity, s_1 and s_2, given in Eqns. 5.4 and 5.5, and the results were intercompared. An important tool for the visualization of clustering results is the clustering tree, or dendrogram. Dendrograms will be repeatedly used in the following discussions of asteroid families. As a primer, a simple example of a dendrogram is shown in Figure 5.5, and the different components of this graphical tool are explained.

As a starting point for our analysis, Figure 5.6 shows the single-linkage hierarchical clustering solution for all 465 asteroids, based only on orbital dissimilarities (no spectral information has been included). In this plot, the groupings that correspond to several

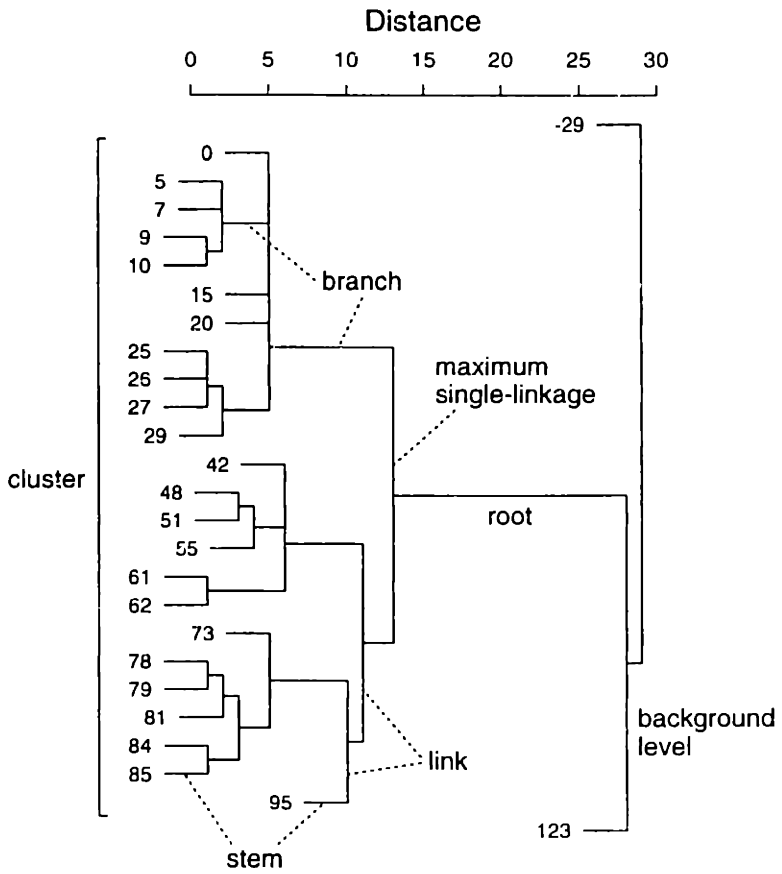

Figure 5.5: Key to reading a dendrogram (clustering tree). This example is borrowed (and slightly modified) from Anderberg (1973) and shows a very simplified version of a single-linkage clustering dendrogram. The clustered objects (in this case, integers) are labelled to the left of the tree. For this example, the distance (dissimilarity) between any pair of objects is given by the magnitude of the difference between the two numbers. This tree is made up of branches that are linked together at successively higher distances, until all of the groups have joined together at the root (the long branch, farthest to the right). This root then joins the cluster with the background level, shown here at the right-hand edge of the plot. The length of the initial stems (the lowest-order branches, farthest to the left) is arbitrary. The length of these stems has been set to be 10% of the length of the distance axis plotted at the top. The position of the vertical segment that links any pair of stems (or higher-level branches) gives the value of the dissimilarity at which that linkage occurs. For the single-linkage algorithm, this distance is defined by the nearest pair of objects from the two groups that are being linked. For example, we see that the two groups [48, 51, 55] and [61, 62] are linked with a dissimilarity of 6, since this is the shortest distance between these two sets (the distance between 55 and 61). From this plot, it is also readily seen that the set of numbers [25, 26, 27, 29] form a more tightly-bound cluster (it clusters farther to the left) than the set containing [48, 51, 55]. The final linkage that occurs before the root (in this case, at a distance of 13) is called the maximum single-linkage for that cluster. For our asteroid spectra, those groupings of objects that are most similar (based on the combination of spectral and orbital properties, as given by D', Eqn. 5.3) will cluster farthest to the left. The longer the root (the connecting branch between a particular cluster and the background level), the more isolated the cluster is from the background.

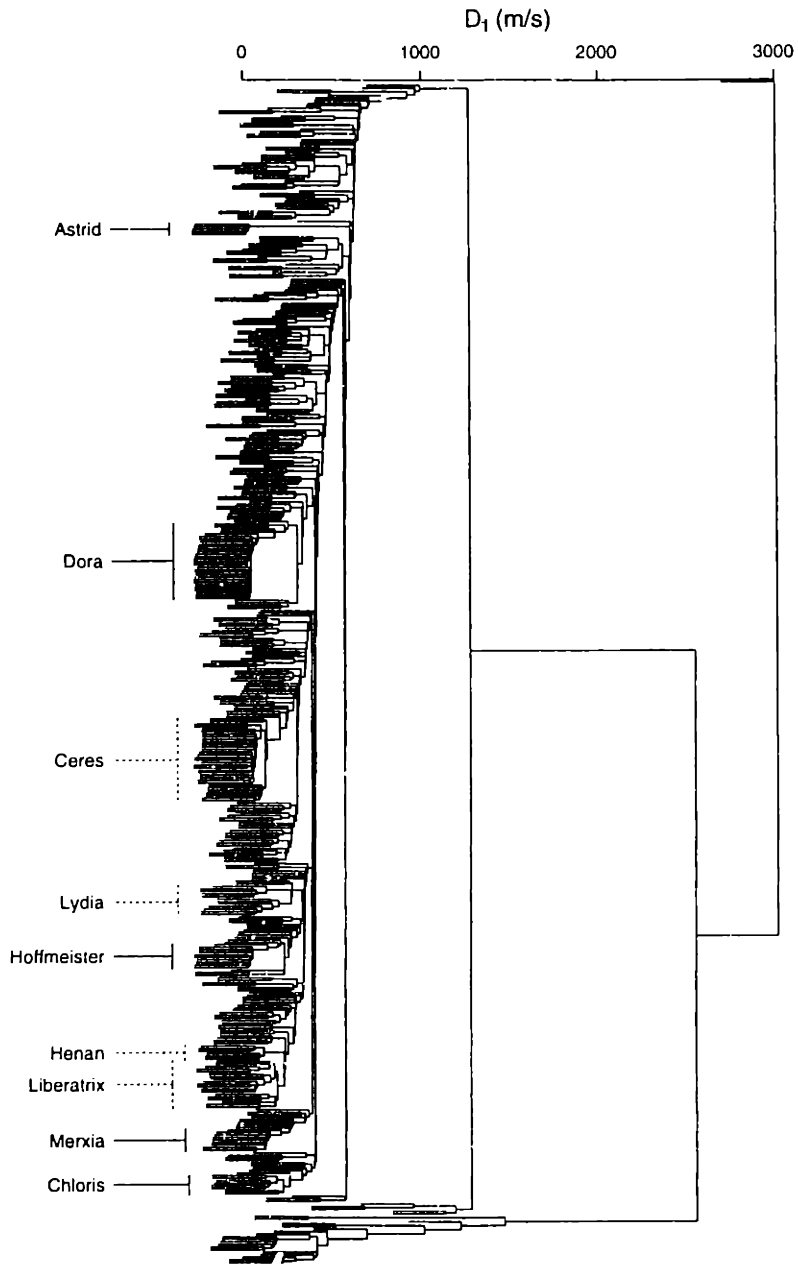

Figure 5.6: Dendrogram for the single-linkage hierarchical clustering solution for 465 SMASSII asteroids located between 2.690 and 2.815 AU. In this solution, only the orbital information has been included, where the dissimilarities are based on the metric D_1, given by Eqn. 5.1 (from Zappalà *et al.* 1995). For clarity, the labels for individual objects have been omitted, but significant clusters are marked with the family names (as given by Zappalà *et al.* 1995). Some groupings like the Astrid and Dora families stand out very well (in the case of the Astrid family, note the particularly long root that connects this cluster with the background). Because this solution is derived from a small subset of the objects analyzed by Zappalà *et al.*, this solution is different from the one they obtained. In particular, those families marked by dotted lines are groupings that are substantially different from those found by Zappalà *et al.*

dynamical families identified by Zappalà *et al.* (1995) have been marked, though for clarity, the labels of the individual asteroids have been omitted. The names assigned to these families are those given by Zappalà *et al.* based on their results using the HCM technique. Some families, particularly the Astrid family, stand out as very distinctive from the background based only on this orbital information. Other families, like Henan and Liberatrix, are less well defined in this plot. Since the number of objects included here is only a subset of the total used by Zappalà *et al.* in their investigation, differences in the solutions should be expected, and many of the potential families that they noted will not be as clearly differentiated in this clustering solution.

The effect of introducing the spectral information is seen in Figure 5.7, where the spectral dissimilarity s_1 has been included with a cutoff of $\varepsilon = 0.3$. The addition of 2000 m/s to any pair of asteroids not meeting this cutoff criteria forms an artificial threshold, below which groupings of objects will drop only if they are spectrally very similar. Even for this very low value of ε, the nuclei of some families, especially the Dora family, are beginning to develop. In Figure 5.8, ε has been increased to 0.6, thus relaxing the constraint on how similar a pair of spectra must be for them to cluster below the 2000 m/s threshold. In this plot, many more groupings are visible, and different clustering patterns for the members of the various families are becoming apparent. For example, the Hoffmeister family is very compact, with all members linking together at very small values of D'. The relatively long root connecting this small group of seven objects to the background level indicates that the Hoffmeister family is relatively isolated from the background, at least with respect to those surrounding objects that are spectrally similar, as constrained by ε. Other families, such as Agnia and Henan, show a bifurcation in the clustering. The largest families, Gefion and Dora, each consist of a relatively compact concentration of objects, but there are tails in these clustering distributions that indicate each family is surrounded by a halo of spectrally similar objects with increasingly higher values of D'. In Figure 5.9, the cutoff in spectral dissimilarity is relaxed even further, with $\varepsilon = 1.0$. Most of the families marked appear to be mature, well-defined groupings, separated from their surroundings by relatively long roots. The algorithm used in generating these dendrograms optimizes the ordering of clusters, based on the dissimilarity at which each linkage occurs, and on the lengths of the joining branches. To ensure that no branches cross, the ordering of the individual objects and clusters

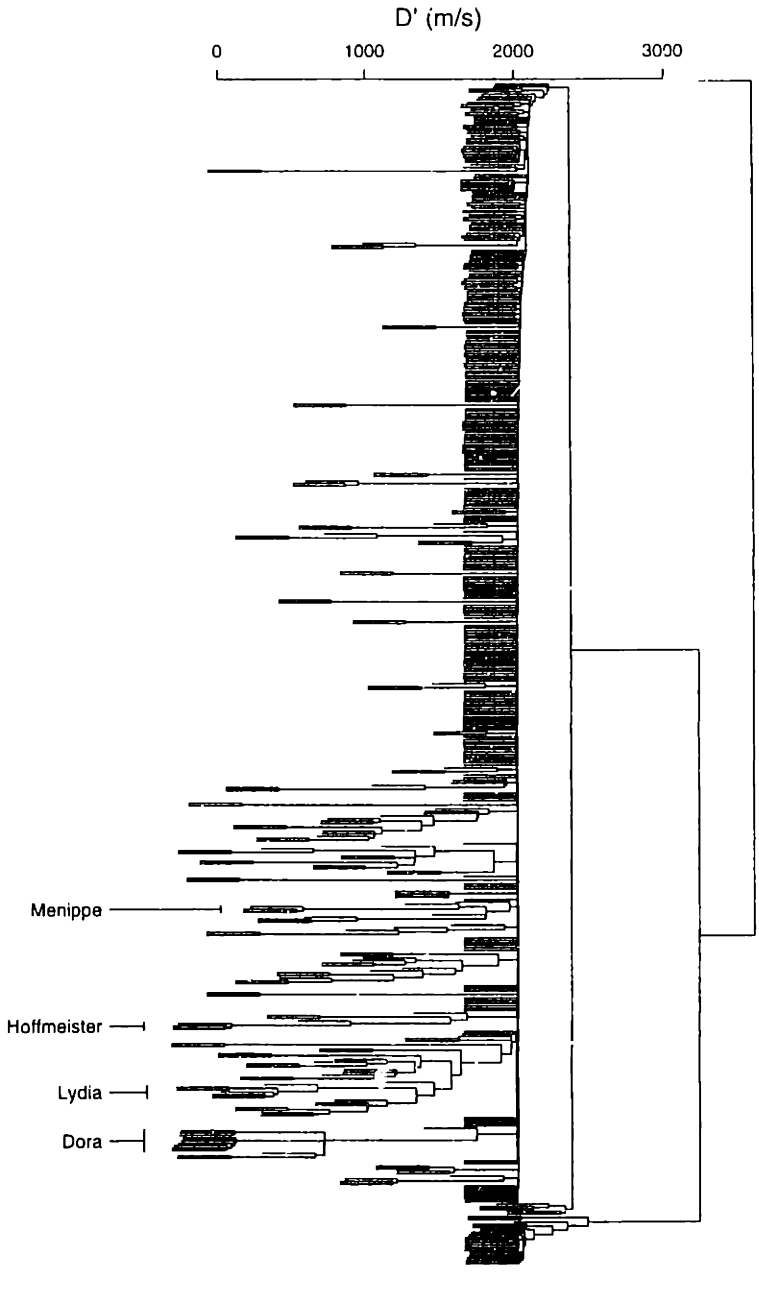

Figure 5.7: Similar to Figure 5.6, but spectral information has been included by way of the metric D', given by Eqn 5.3. The dissimilarity s_1 has been used, with a spectral cutoff at $\varepsilon = 0.3$. An offset of $z = 2000$ m/s is applied to any pair of objects whose spectral dissimilarity is greater than 0.3. An artificial boundary is formed at 2000 m/s, and only those groups of objects that are spectrally very similar will cluster at values of D' lower than 2000 m/s. Even at this minimal value of ε, many groups of objects are beginning to cluster. In particular, a substantial nucleus of the Dora family is already forming.

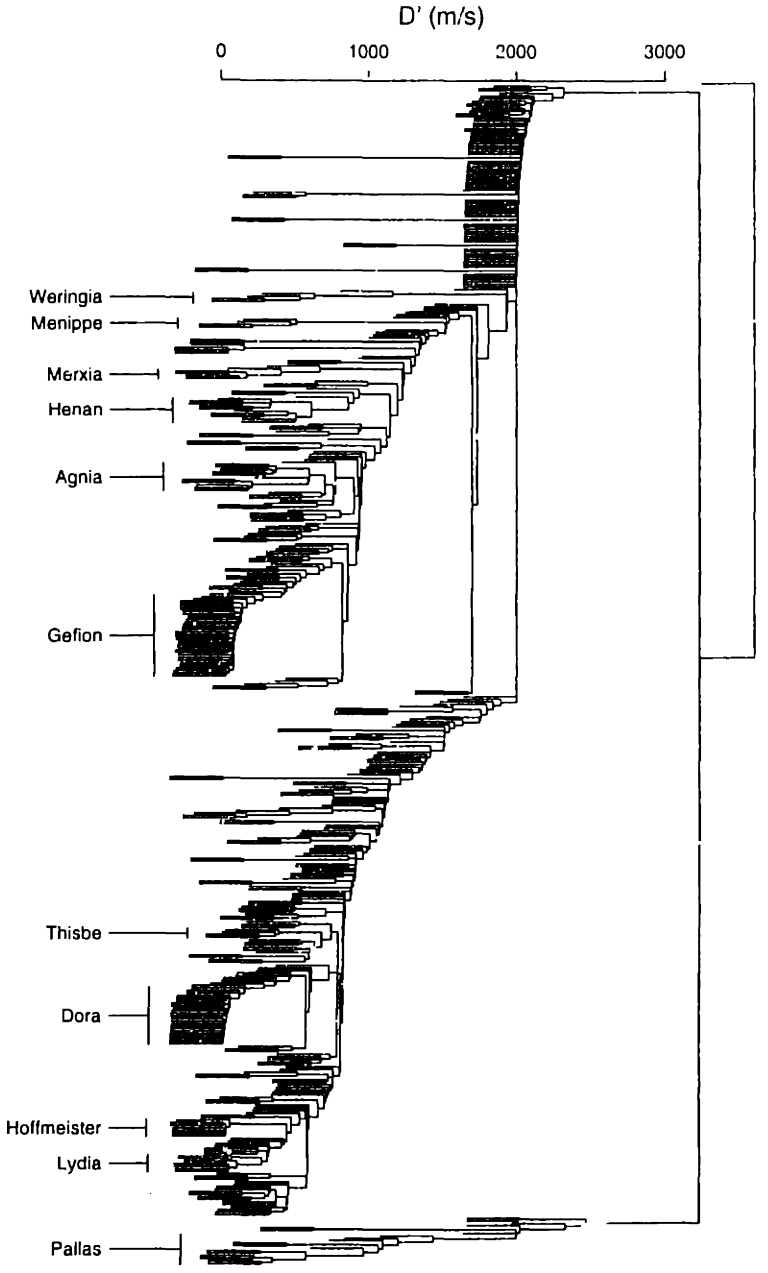

Figure 5.8: Similar to Figure 5.7, but for $\varepsilon = 0.6$. The clustering structure is becoming much more apparent, with the Dora and Gefion families becoming well formed. The Henan and Agnia families both appear to be bifurcated, with two separate subclusters being apparent at this value of ε. This subgrouping is transient, and disappears as ε is further increased.

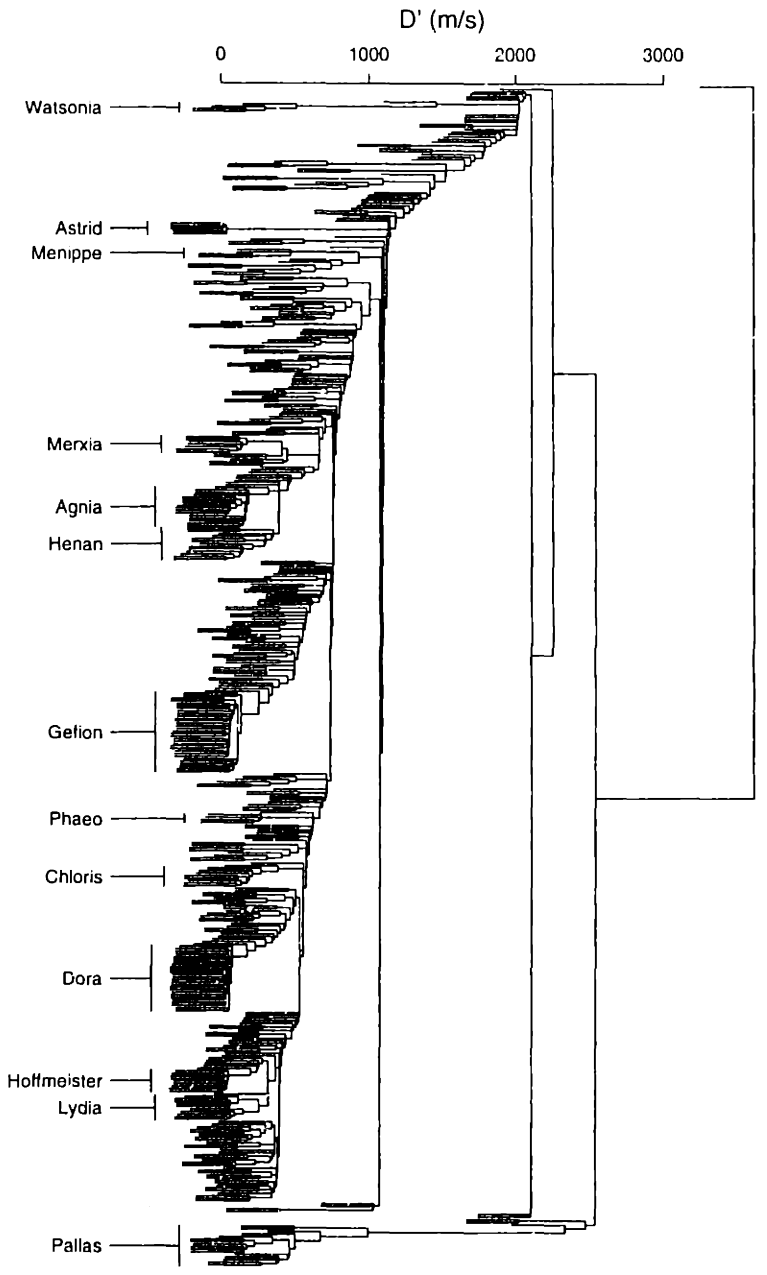

Figure 5.9: Similar to Figure 5.6, but for $\varepsilon = 1.0$. Most of the families that are marked are very mature, well-defined clusters, often with significant roots linking these clusters to the background.

changes in successive plots as the value of ε, and correspondingly, the number of possible linkage combinations, is increased.

The criteria that I have adopted for defining a family is somewhat subjective. Unlike the procedure used by Zappalà *et al.*, I have not tried to determine a quasi-random level in D' that would place limits on the possible ejection velocities within groupings. By setting such a cutoff, it is likely that spectrally real families would be truncated, or missed entirely. Instead, I use the "stability" of the clustering with varying values of ε to judge the robustness of any particular grouping. First, the clustering solutions were found for the entire set of 465 asteroids by varying the value of ε from 0.2 to 1.9, at increments of 0.1. Independent solutions were derived using both dissimilarities s_1 and s_2. Plots (dendrograms) for each of these solutions were then inspected visually for distinct groups consisting of at least four members. The evolution of each of these groupings was then examined as ε was increased, and the set of objects that was found to be most robust over the largest range in ε was considered to be the "locus" of the family. In almost all cases, the loci determined using the dissimilarity s_1 are identical to those found using s_2. A locus can be described as ranging from very compact and isolated to dispersed, depending on the spread in spectral and orbital characteristics of its members, and on the relationship of that locus to the background population. The boundaries in a', e' and sin i' were determined for the locus, and that volume of proper element space was inspected for possible interlopers that had not shown up in the clustering solutions. Also, as each locus evolved with increasing ε, there were often extraneous, but spectrally similar objects that would show up in the clustering solutions, but which were not included as members of the final locus. These objects were noted, and were individually evaluated as potential members of the family. The process of adding an additional member to the family included determining a new boundary for the family in proper element space, and inspecting that volume for interlopers. Additional objects were considered as real members of the family only if the fraction of additional interlopers included within the boundary of the family was small.

In this phase of the analysis, the loci for 15 spectrally similar groupings were identified among the 465 SMASSII asteroids. To describe each of these spectral families, I have divided the proper element space between 2.69 and 2.815 AU into eight zones of varying dimensions, depending on the density of background objects, and the

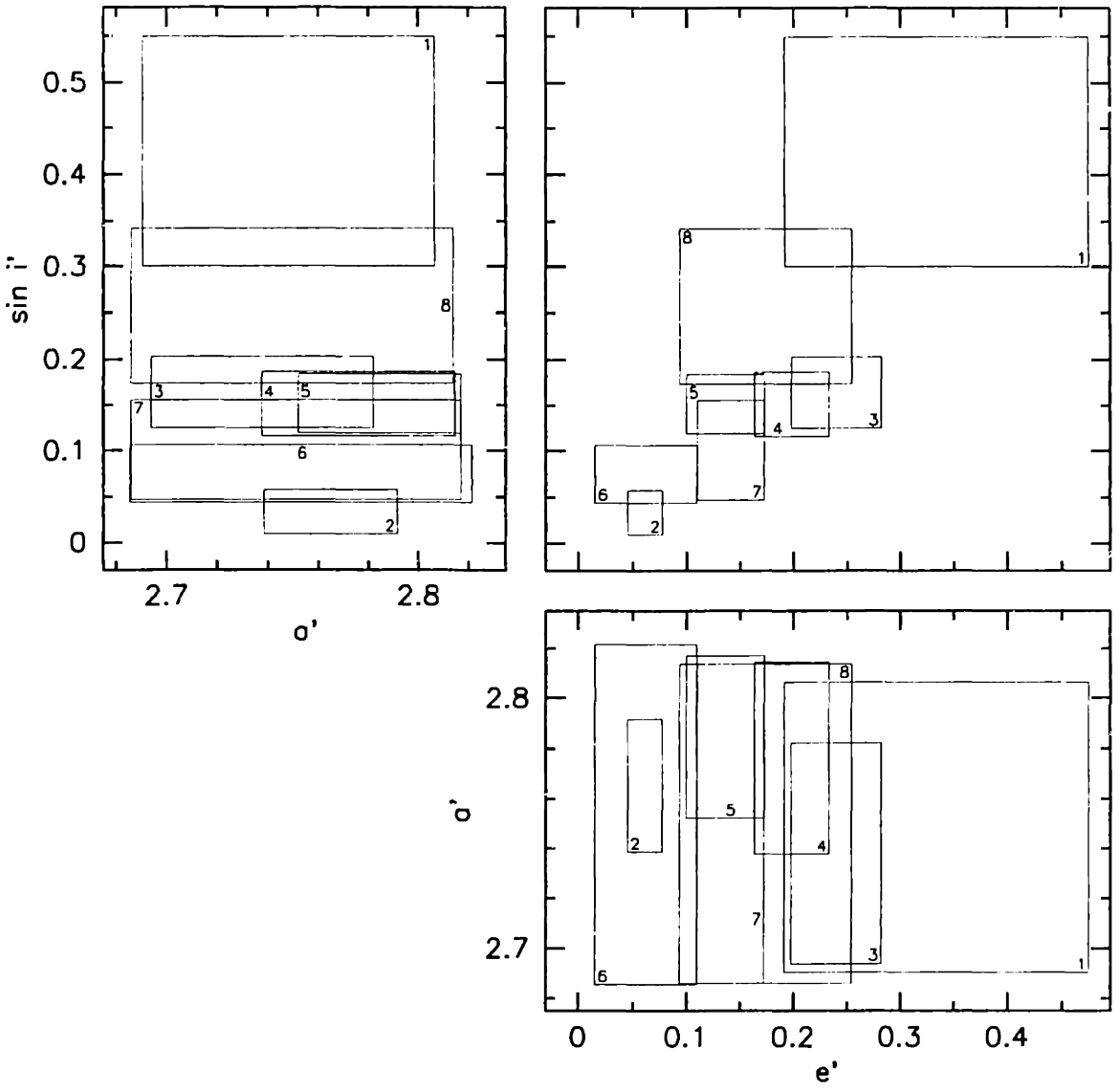

Figure 5.10: Pairwise plots of proper element space, showing the locations of all eight zones discussed in this section.

number and sizes of the families included. The boundary for each of these zones is represented in Figure 5.10. Each zone, and the included families are discussed in the following subsections, and a compilation of the memberships and boundaries determined for all of these families is given as part of the discussion in section 5.6.

5.4.1 Zone 1 - Pallas family

Zone 1 contains 27 asteroids with particularly high orbital eccentricities ($0.20 < e' < 0.47$) and inclinations ($0.31 < \sin i' < 0.54$). Even though this region of proper element space is outside of the domain investigated by Milani and Knežević (1994), we targeted these asteroids as a means of testing the reality of the Pallas family, proposed by Kozai (1979), Williams (1989) and Lemaitre and Morbidelli (1994). The proper elements we used in the analysis of this zone were provided by A. Lemaitre (private communication).

Pallas family - *The Pallas family appears to be a true genetic association that has resulted from one or more cratering events involving the asteroid 2 Pallas. This family is defined by 16 SMASSII asteroids, all with very high orbital eccentricities and inclinations, and all being classified as B- and C-types. This family was identified by Williams (1979, 1989, 1992), Kozai (1979), and Lemaitre and Morbidelli (1994).*

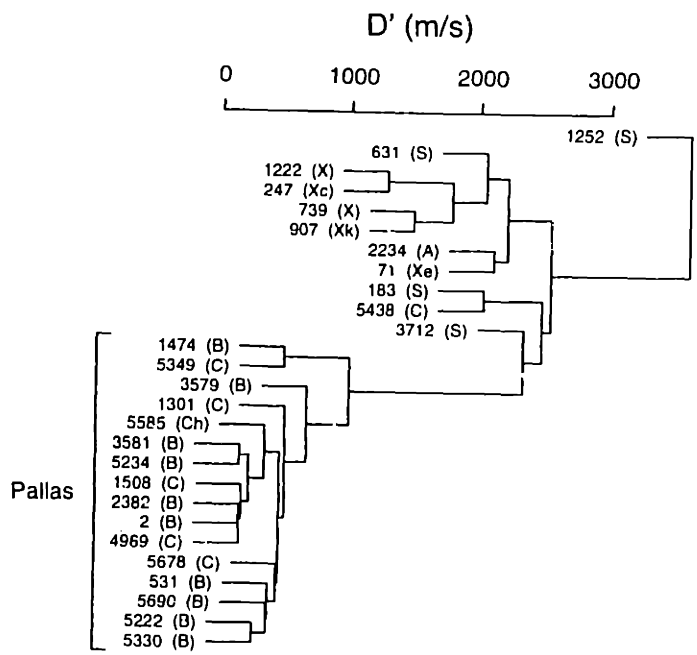

Figure 5.11: Dendrogram showing the single-linkage hierarchical clustering solution for 27 asteroids contained in zone 1. The dissimilarity s_1 has been used, with a cutoff of $\varepsilon = 1.0$. Each stem is labelled with the permanent number of the asteroid, along with the taxonomic class (in parentheses). The Pallas family is clearly visible as an isolated cluster, with a root that is ~1300 m/s in length connecting this cluster to the background distribution.

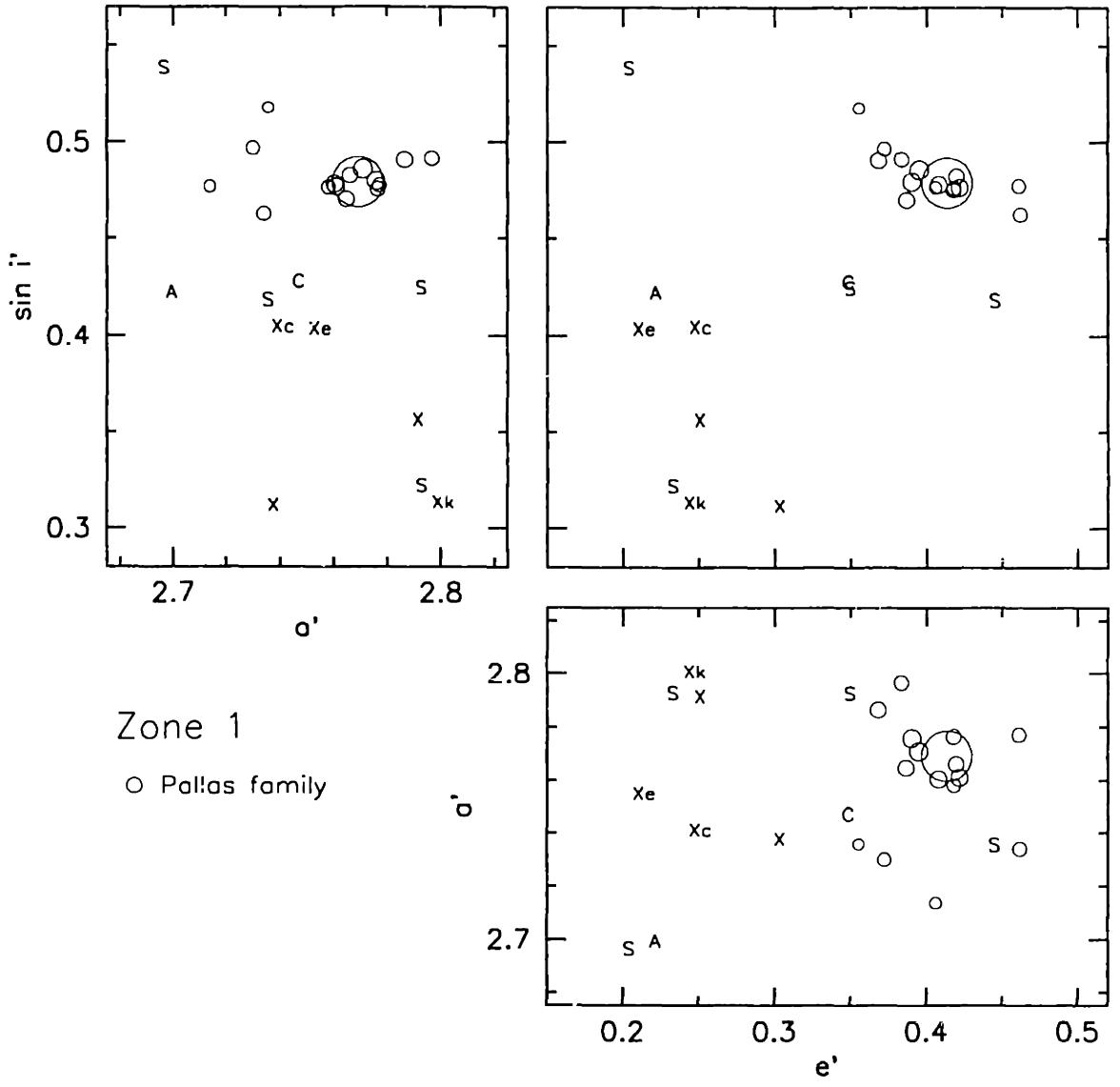

Figure 5.12: Pairwise plots for zone 1, showing the locations of Pallas family members (open circles) and background objects (labelled by taxonomic class) in the three planes of sin i' versus a', sin i' versus e', and a' versus e'. The sizes of the circles representing the family members have been scaled by the cube-root of the asteroid diameters, so that the largest circle is the location of 2 Pallas in proper element space.

A hierarchical clustering (HCM) solution that is based on these 27 asteroids is plotted in Figure 5.11. The Pallas family plots as an isolated, though fairly dispersed group of 16 objects, comprised entirely of B- and C-type asteroids (with one object being classified as a Ch-type). By comparison, Figure 5.12 shows that the background asteroids near the Pallas family in proper element space are primarily classified as S-

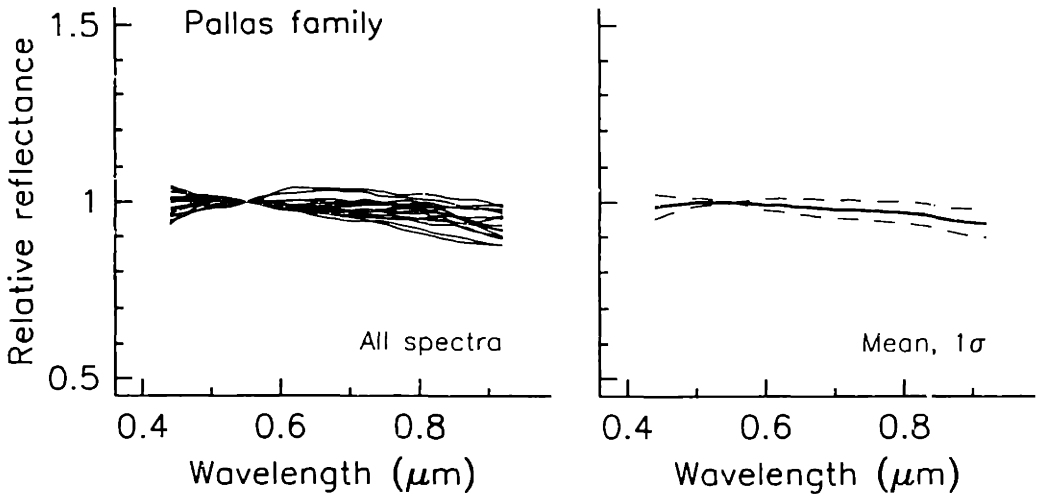

Figure 5.13: Spectra of the Pallas family members. The panel on the left shows the SMASSII spectra for all 16 Pallas family asteroids. The right-hand panel shows the mean for these 16 objects, as well as a 1σ envelope, representing the scatter among the spectra as measured in each of the 49 spectral channels (from 0.44 to 0.92 μm, at 0.01 μm increments).

and X-types. The clustering is very robust, with all 16 asteroids being included in the locus. The locus is stable over the intervals of $0.8 \leq \varepsilon \leq 1.9$, as measured using the dissimilarity s_1, and $0.7 \leq \varepsilon \leq 1.9$, based on s_2. In Figure 5.11, we see that the uppermost linkage for members in the Pallas grouping occurs at a value of D' ~ 1 km/s, though, as pointed out by Zappalà *et al.* (1995), any dynamical interpretations based on the metrics D_1 and D_2 (Eqns. 5.1 and 5.2) must be made cautiously. In particular, D_1, which corresponds to our metric D' when the spectra of the asteroids are sufficiently similar (as defined by Eqn. 5.3), can overestimate the true separation velocities by as much as a factor of 1.9 when the disruption is characterized by an isotropic explosion. The relative sizes of members in the Pallas family classifies this disruption as a cratering event, with the 15 small fragments in our sample making up much less than 0.1% of the mass of Pallas. Based on a diameter of 523 ± 20 km (Tedesco 1989) and a density of 2.6 ± 0.5 g/cm^3 (Millis and Dunham 1989), the surface escape velocity for Pallas is roughly 300 m/s. The distributions of masses and velocities found within the Pallas family compare very closely with those observed for the Vesta family, where fragments that are spectrally similar to Vesta have been identified with relative velocities also approaching 1 km/s (Binzel *et al.* 1999a). Another similarity to the Vesta family is the fact that Pallas lies very near the center of its family in proper element space, as seen in Figure 5.12. In Figure 5.13, the spectra of all 16 Pallas family objects are plotted,

revealing moderate variations between objects, especially in spectral slope. The B-types all have spectra that are relatively linear in shape, and range from slightly bluish in slope (as is the case for the spectrum of Pallas itself) to very blue. The spectrum of 5585 Parks is somewhat noisy, but a mild concave curvature in the middle of its spectrum supports the classification of "Ch" for this asteroid.

The locus we defined for the Pallas family is generally consistent with the family members identified by Kozai, Williams, and Lemaitre and Morbidelli. Both Williams (private communication) and Lemaitre and Morbidelli (1994) have tended to underestimate the size of the Pallas family by omitting two asteroids (5349 Paulharris and 5678 DuBridge), and one asteroid (1474 Beira), from their respective lists of family members. On the other hand, the earlier work by Kozai (1979) included the asteroid 1252 Celestia, an S-type that is clearly not a member of this family.

5.4.2 Zone 2 - Astrid family

Astrid family *- Based on the observations of five SMASSII asteroids, the Astrid family is found to be a very compact, isolated grouping of C-type asteroids that are assumed to be genetically related. This family was proposed by Zappalà et al. (1995) using both the HCM and WAM techniques.*

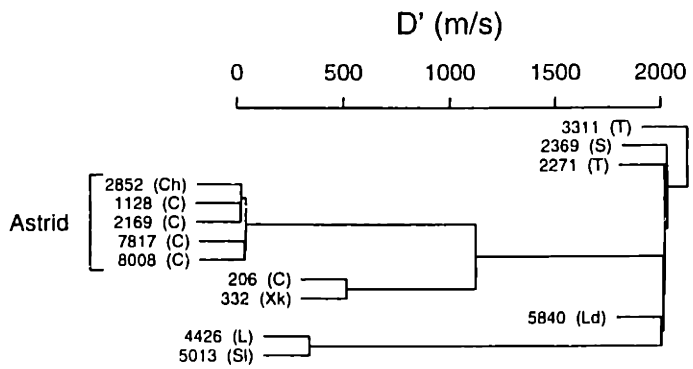

Figure 5.14: Similar to Figure 5.11, but for 13 SMASSII asteroids contained in zone 2. Dissimilarity s_1 was used, with a spectral cutoff of $\varepsilon = 1.0$. The locus of the Astrid family is marked.

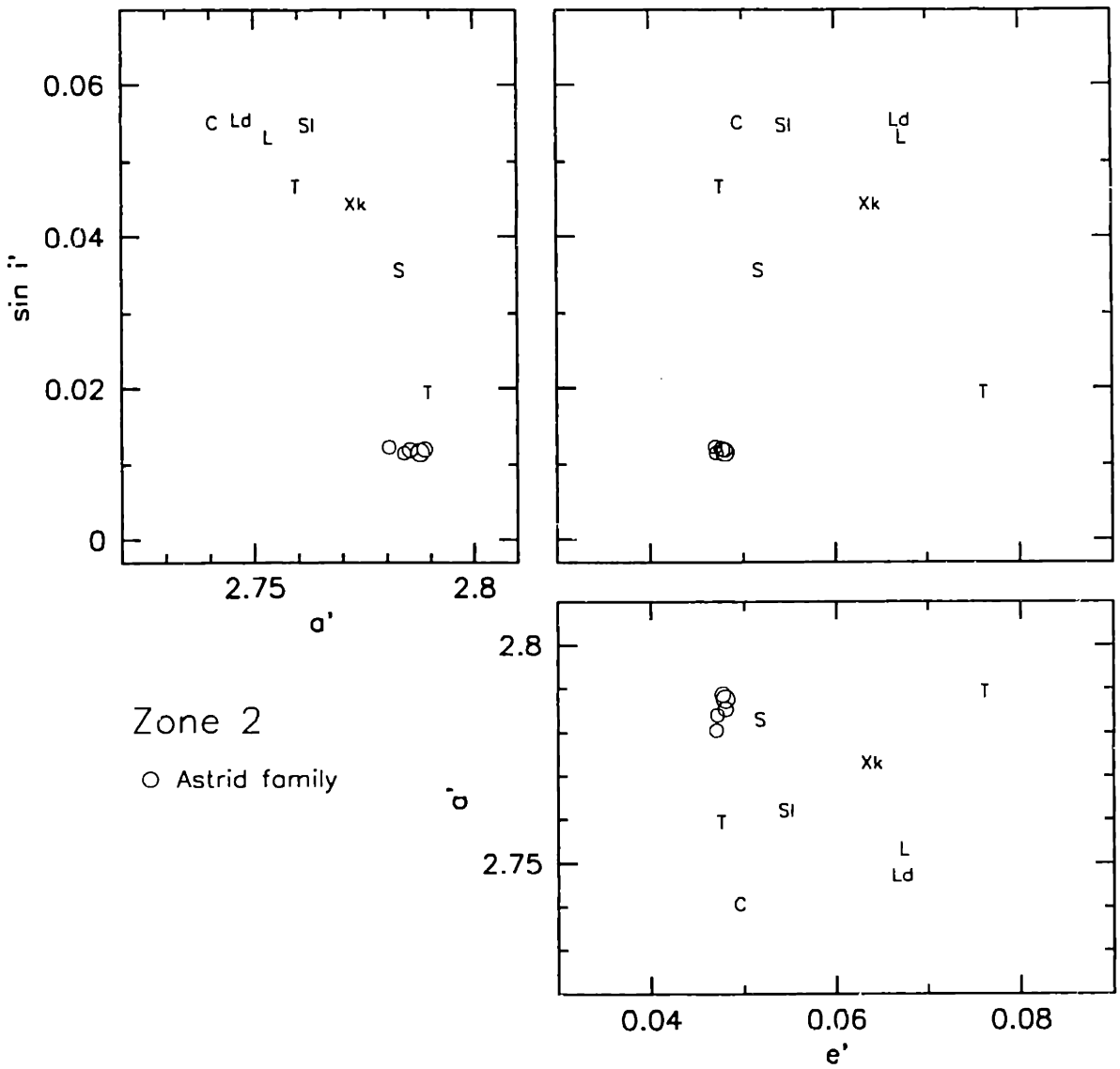

Figure 5.15: Similar to Figure 5.12. Pairwise plots for zone 2, showing the locations of Astrid family members.

The Astrid family lies on the inner edge of proper element space, with orbital eccentricities and inclinations that are very low. This family is extremely compact, and isolated from the background population, as can be seen in both Figures 5.14 and 5.15. The clustering solution is very robust, remaining constant over the intervals in ε of 0.9 - 1.9, based on the dissimilarity s_1, and 0.7 - 1.9, based on s_2. The longest single linkage within this grouping occurs at a value of D' ~ 30 m/s. The Astrid family was identified by Zappalà *et al.* (1995) based on their analyses using both the HCM and WAM techniques,

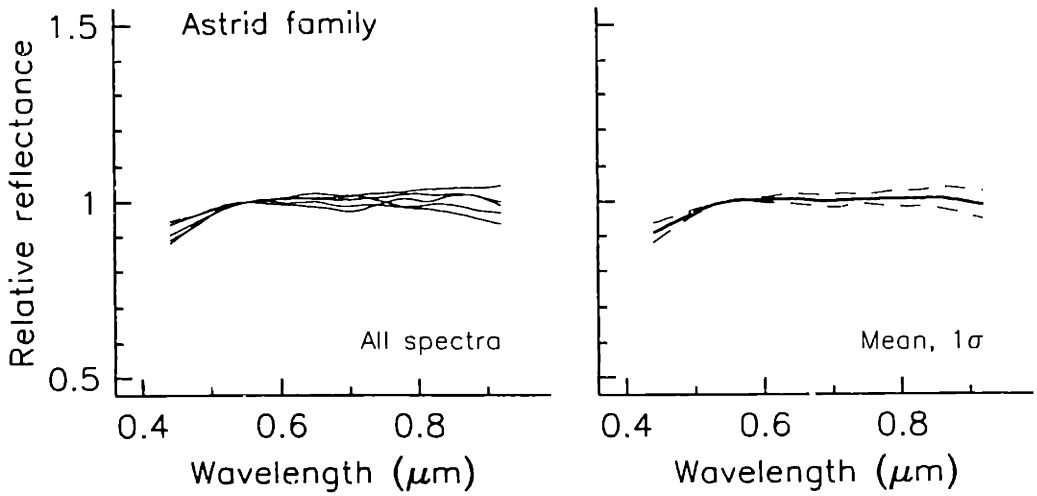

Figure 5.16: Similar to Figure 5.13, showing the spectra of five Astrid family members.

from which they identified a total of 10 and 11 family members, respectively. Of these purported members, we were able to observe five during the course of the SMASSII survey. Spectrally, these five asteroids appear quite similar, with four of the observed members being classified as C-types, and the remaining object being classified as a Ch-type. The variation in spectral slopes among the members is moderate, as seen in Figure 5.16, accounting for the fact that this family did not fully develop in the clustering solutions at lower values of ε. All five members do show a moderate UV drop-off in their spectra. In addition, there are very subtle indications for a 0.7 μm band in four of the five spectra, though this band is strong enough only in the spectrum of 2852 Declercq to satisfy a classification of "Ch". All five members are contained in the locus of the family, with no additional asteroids being observed surrounding the locus that could be considered possible members of the family. Within the boundary of zone 2, there are eight asteroids, in addition to the Astrid family members, that constitute a local background sample. The taxonomic mix among these background asteroids is very random, with only one of these eight asteroids being classified as a C-type.

5.4.3 Zone 3 - Chloris family

Chloris family *- Nine asteroids observed during SMASSII make up the relatively compact Chloris family, a cluster of C-type asteroids that appear to be genetically related. Steep UV drop-offs in many of these spectra differentiate the Chloris family members from other C-types in the surrounding background. This family was proposed*

by Kozai (1979), Bendjoya (1993), and Zappalà et al. (1994) as the family Idelsonia, and by Zappalà et al. (1995) as the Chloris family using both the HCM and WAM techniques.

The locus of the Chloris family is a moderately isolated grouping of eight asteroids, centered in proper element space at $e' \sim 0.25$ and $\sin i' \sim 0.16$, and extending from 2.71 to 2.74 AU in semimajor axis. The members of this family all belong to the C-complex, with the majority being classified as Ch- or Cgh-types, and having spectra that are noteworthy for the strengths of their UV drop-offs. The presence of both the strong UV feature and the 0.7 μm absorption band help distinguish these asteroids from a local background population that is mostly a mix of C- and S-types. The existence of this family was suggested by Kozai (1979, as family no. 33), by Zappalà *et al.* (1994) as the Idelsonia family, and by Zappalà *et al.* (1995) as the Chloris family, based on results from both the HCM and WAM techniques. Williams (1992) does not identify a family association with Chloris, though in his listing of proper elements, Williams (1989) does note three of the asteroids included in this locus (521 Brixia, 1534 Nasi, and 1613 Smiley) as being near the ν_{10} resonance. The uncertainties in proper elements

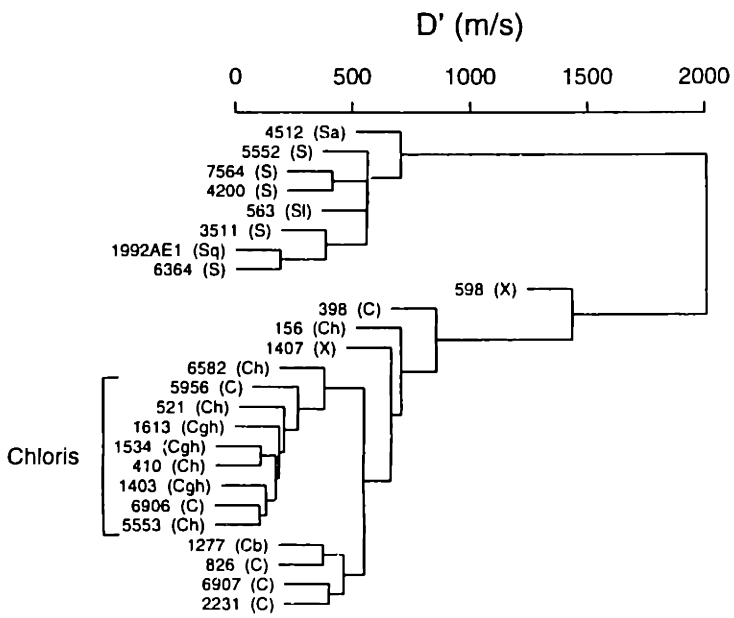

Figure 5.17: Similar to Figure 5.11, but for 25 SMASSII asteroids contained in zone 3. Dissimilarity s_1 was used, with a spectral cutoff of $\varepsilon = 1.0$. The locus of the Chloris family (8 objects) is marked.

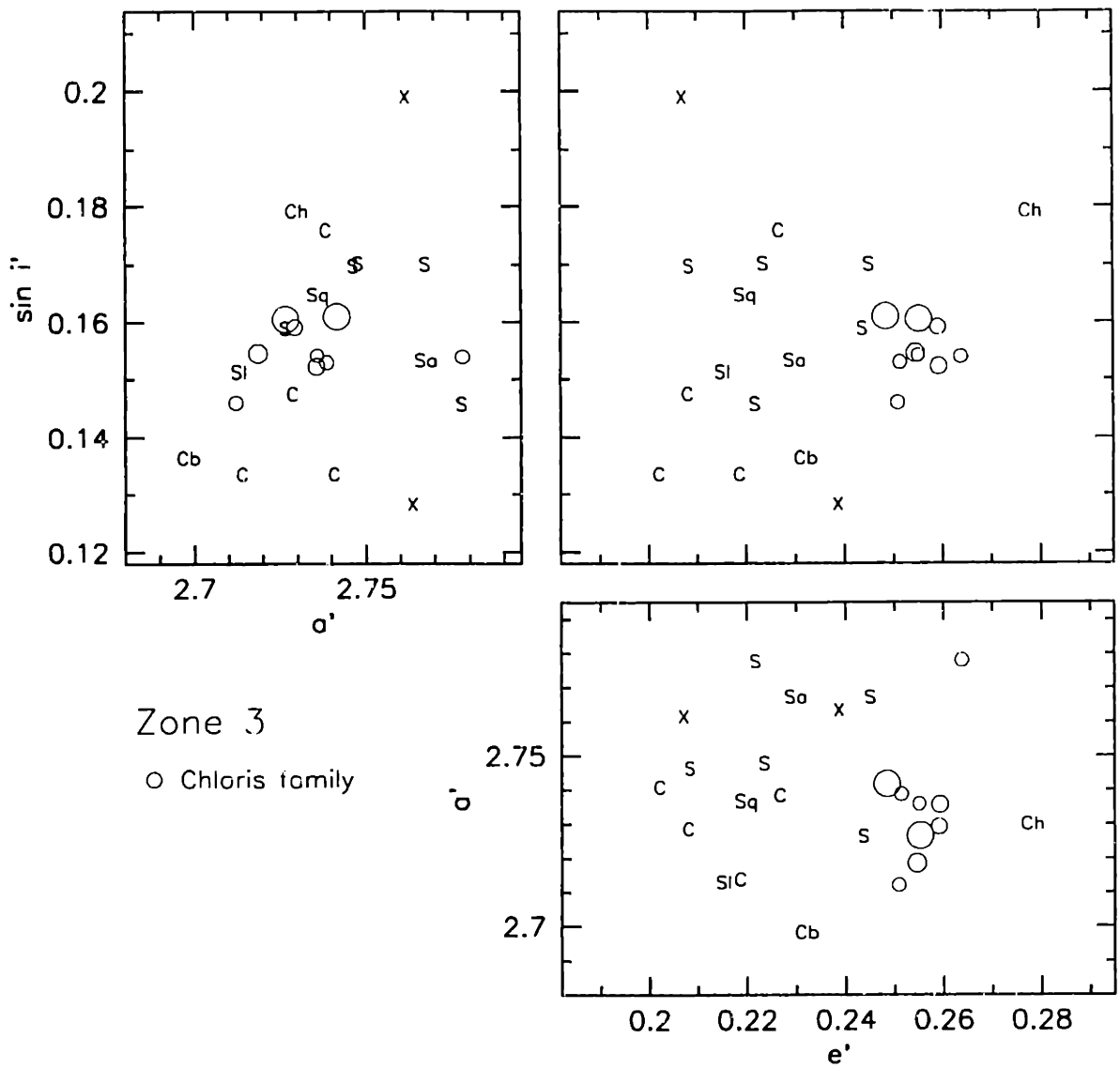

Figure 5.18: Similar to Figure 5.12. Pairwise plots for zone 3, showing the locations of Chloris family members.

resulting from this proximity to the ν_{10} resonance is a possible reason that Williams did not recognize this dynamical clustering. The locus of the Chloris family is very robust, remaining stable over ranges in ε from 0.8 to 1.9 using the dissimilarity s_1, and from 0.9 to 1.9 using s_2. As seen in Figure 5.17, the maximum value of D' linking the objects in the locus is ~240 m/s. The locations of these family members, with respect to the local background objects, are plotted in Figure 5.18. There is an additional asteroid, 6582 1981 VS, however, that is on the periphery of the cluster, and which can be added as

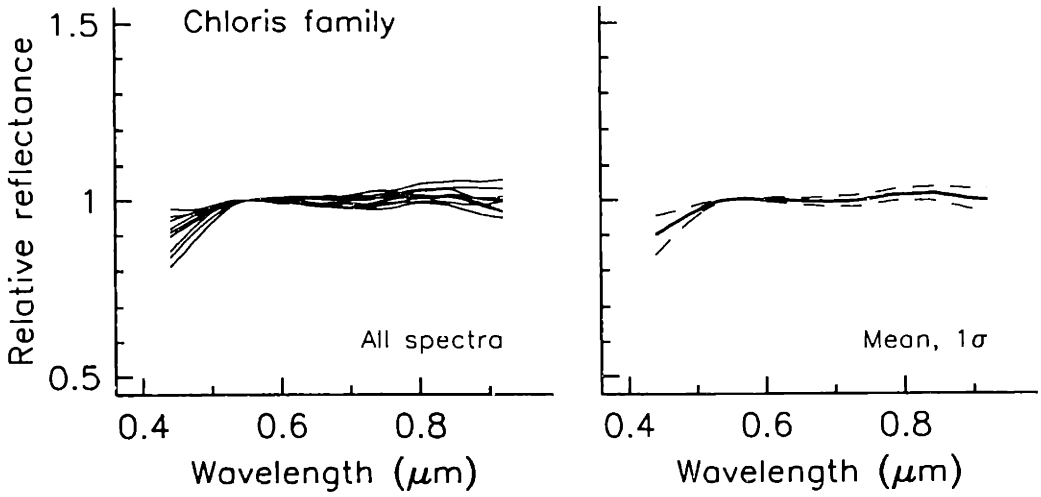

Figure 5.19: Similar to Figure 5.13, showing the spectra of nine Chloris family members.

member of this family. This object is classified as a Ch-type, and is located very near the locus of the family. Adding this object does require increasing the more distant boundary of the family in semimajor axis to 2.78 AU, and increases the maximum single linkage in the clustering solution to D' ~ 330 m/s. Among our sample, there are no other asteroids in the vicinity of the locus that appear to be related to this family. Even by increasing the volume of proper element space to include 6582 as a member of the family, no spectral interlopers are found within the boundary of the Chloris family. The spectra of all nine members, including 6582, are plotted together in Figure 5.19.

5.4.4 Zone 4 - Dora and Phaeo families

The boundary of zone 4 was chosen to encompass two distinct and very different dynamical families. The Dora family is a very densely populated and well defined family, while the Phaeo family is much smaller, with only four observed members, and is much more dispersed in orbital space. A clustering solution, based on the 55 SMASSII asteroids contained in this zone, is shown in Figure 5.20. In Figure 5.21, the locations of these two families are shown in proper element space. Note that the centers of the Dora and Phaeo families are almost identical in a' (~ 2.785 AU) and e' (~ 0.195), but are significantly offset in sin i'.

***Dora family** - The Dora family is a very well-defined, compact genetic association. A total of 29 members of the Dora family were observed during SMASSII. A majority of*

these objects are classified as Ch-types, with distinct 0.7 μm absorption bands being present in the spectra. The Dora family was identified by Williams (1979, 1989, 1992), Kozai (1979), Bendjoya (1993), Lindblad (1994), and Zappalà et al. (1990, 1994, 1995).

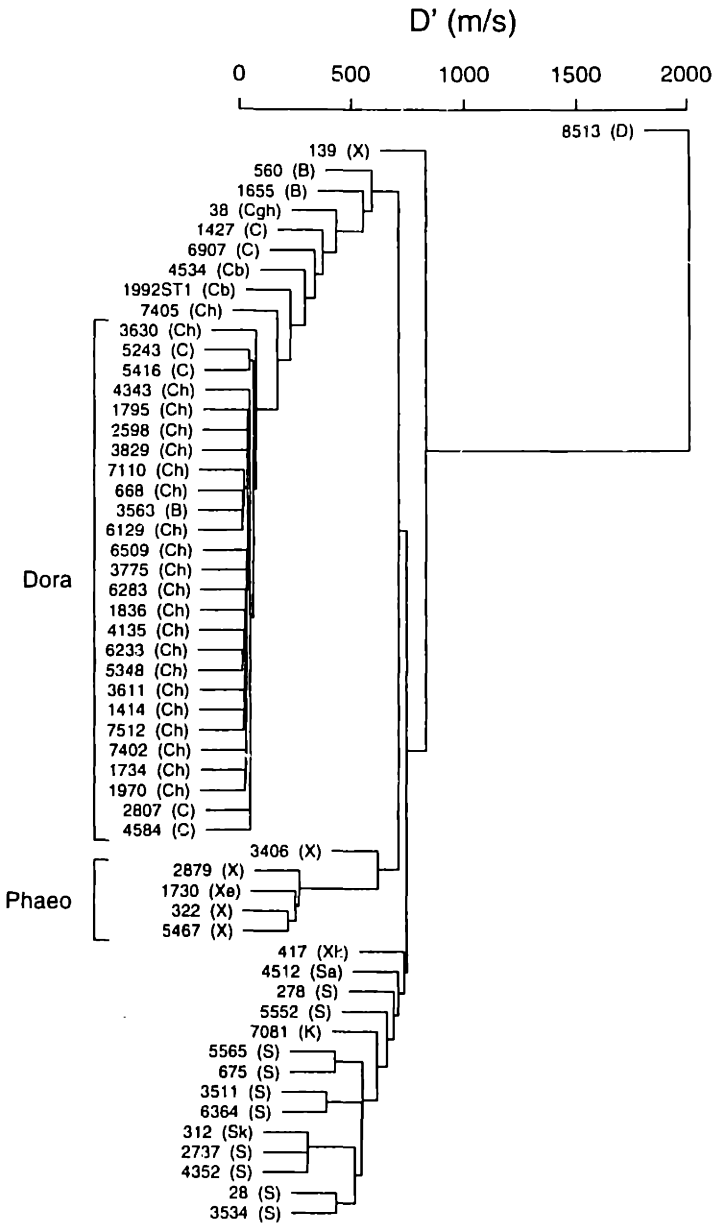

Figure 5.20: Similar to Figure 5.11, but for 55 SMASSII asteroids contained in zone 4. Dissimilarity s_1 was used, with a spectral cutoff of $\varepsilon = 1.0$. The loci of the Dora family (26 objects) and Phaeo family (4 objects) are marked.

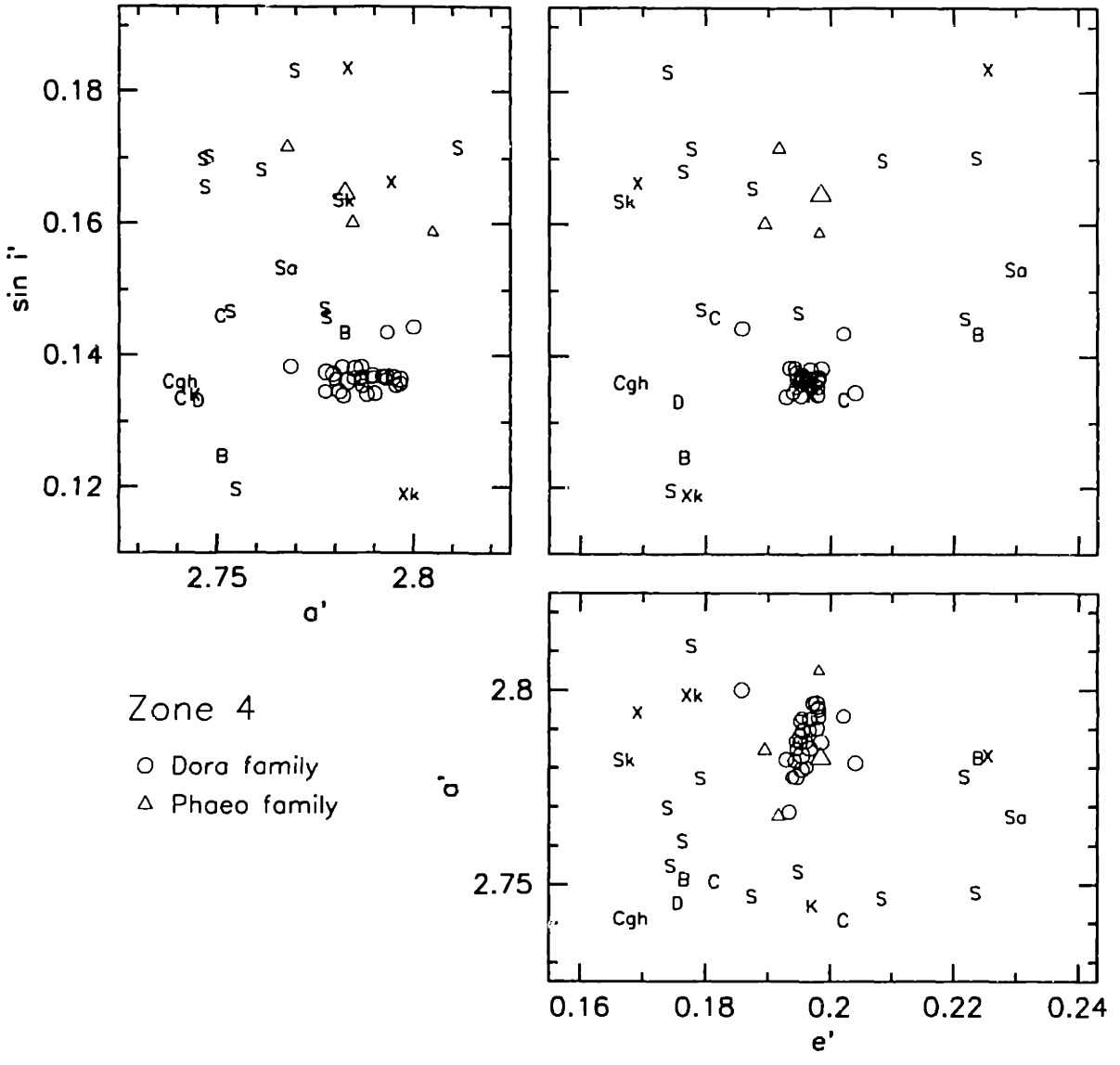

Figure 5.21: Similar to Figure 5.12. Pairwise plots for zone 4, showing the locations of Dora family members (open circles) and Phaeo family members (open triangles). Note that the Phaeo family overlies the Dora family in the a' versus e' plane, but that they are offset in sin i'.

Existence of the Dora family was proposed by Williams (1992, family 128), Lindblad (1994), and Zappalà *et al.* (1990, 1994). Most recently, Zappalà *et al.* (1995), recognized 78 members in the Dora family based on the HCM results, and 79 members using the WAM technique. Members of this family were also listed as part of a more liberal family grouping by Kozai (1979, family no. 39). From the SMASSII results, we define a locus for the Dora family that contains 26 asteroids. This locus is very stable,

being defined over the intervals in ε of 0.8 - 1.9 and 0.6 - 1.9 for the dissimilarities s_1 and s_2, respectively. This family is composed entirely of asteroids belonging to the C-complex, with a majority of the objects having spectra containing a 0.7 μm absorption feature (Ch-types). The local background, defined over the volume of zone 4, is a mixture of spectral types, roughly divided between members of the C- and S-complexes as seen in Figure 5.21. However, there are three asteroids immediately surrounding the locus of the Dora family that, based on spectral similarities with the locus members, I have included as outlying members of the family. These three asteroids, 7405 1988FF (a Ch-type), 1992ST1, and 4534 Rimskij-Korsakov (both Cb-types), are the first objects to cluster along the tail that extends above the locus of the Dora family in Figure 5.20. By including these outlying asteroids in the family, the longest single linkage within the clustering solution increases from D' ~ 75 m/s to D' ~ 290 m/s. The boundary of the family in proper element space is also expanded, primarily in the dimensions of eccentricity and inclination. Expanding this boundary, however, does not introduce any additional asteroids from our sample that could be interpreted as spectral interlopers. The reflectance spectra for all 29 members of the Dora family (26 members comprising the locus, and the three outlying objects) are plotted in Figure 5.22. In addition to variations in the spectral slope, moderate variations in the strengths of both the UV drop-off and the 0.7 μm band are observed among the Dora family members.

In comparing our results for the Dora family with previous dynamical studies, we find very good agreement. All of the SMASSII asteroids that had been identified as Dora family members by Lindblad (1994), and by Williams (private communication), are within the boundary of our defined locus. In the HCM analysis of Zappalà *et al.* (1995), the boundary of the Dora family is expanded to include two objects, 6907 1990 WE and 7081 1987 QF7. While 6907 is classified as a C-type, and could be considered a member of the family, 7081 is a K-type asteroid, and is clearly not a member. Similarly, the WAM results of Zappalà *et al.* included the S-type asteroid 3534 Sax, as well as 7081, neither of which should be considered members.

Phaeo family - *The Phaeo family is a small, dispersed family, with only four members being observed during SMASSII. Of these four asteroids, three are classified as X-types, while the fourth object is an Xe-type. The genetic reality of the Phaeo family*

is less certain. This family has been previously identified by Zappalà et al. (1995) using the WAM clustering technique.

The reality of the Phaeo family is much less certain than that described for the Dora family. The Phaeo family was proposed by Zappalà *et al.* (1995) based only on the WAM results, from which a total of 14 family members were identified. In their HCM analysis, Zappalà *et al.* labelled this same set of 14 asteroids as background, or non-family objects. The two largest members of this purported family, 322 Phaeo and 1730 Marceline, were also included in family no. 39 by Kozai (1979). Of the four possible

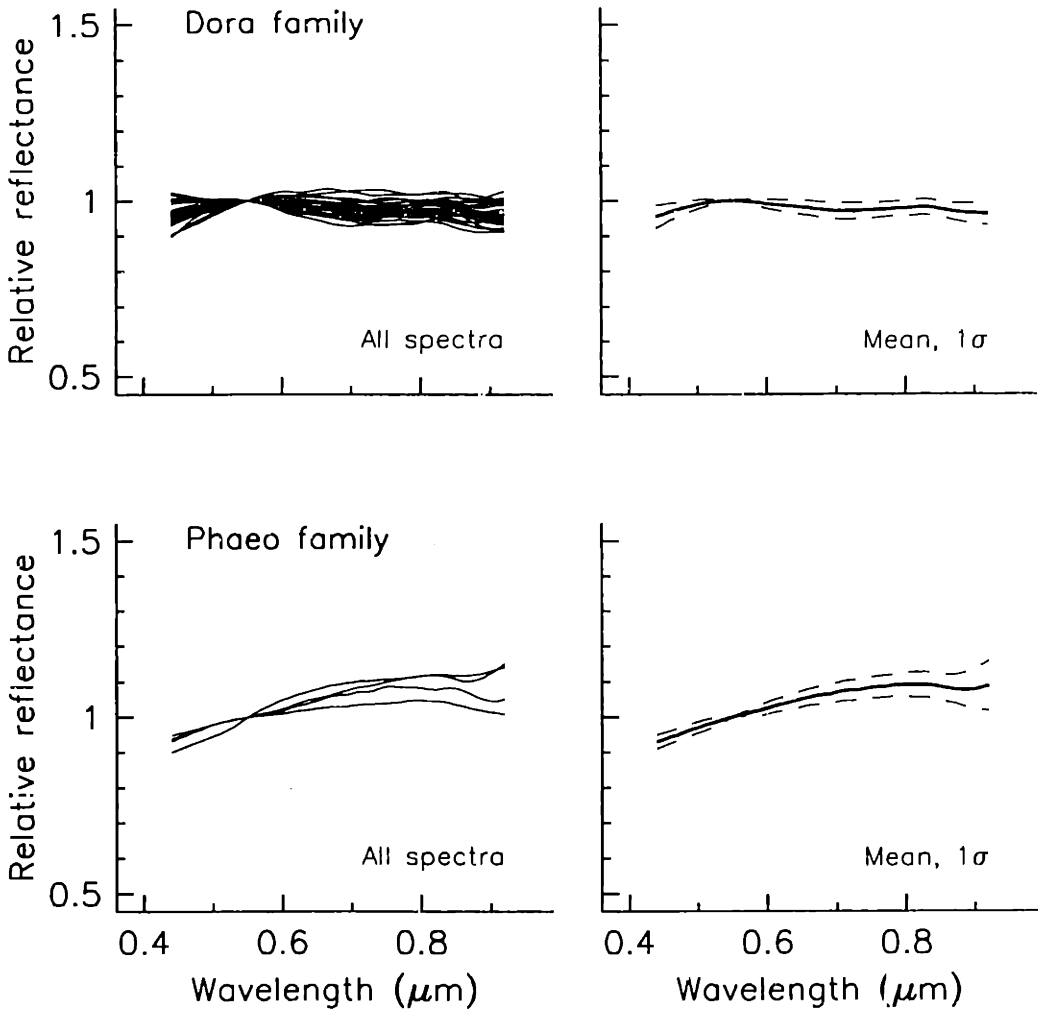

Figure 5.22: Similar to Figure 5.13, showing the spectra for 29 Dora family members, and 4 Phaeo family asteroids.

members observed during SMASSII (322, 1730, 2879 Shimizu, and 5467 1988 AG), three are classified as X-types, while the fourth is assigned the classification "Xe". The variations in spectral reflectance between these four objects is seen in Figure 5.22, where most of the variation is accounted for by differences in spectral slope. The object classified as an Xe-type, 1730 Marceline, does have a moderately strong concave curvature at the blue end of the spectrum associated with the 0.49 μm band, reinforcing this taxonomic classification. In the spectra of the other three members, however, no evidence of the 0.49 μm band is observed. Even with this difference, these four potential members of the Phaeo family are spectrally distinct from the background population. These objects are dispersed in proper element space, as shown in Figures 5.20 and 5.21, though in our clustering solutions, the locus is found to be moderately robust. The clustering of these four asteroids is stable over the interval of $0.9 \leq \varepsilon \leq 1.9$ based on the dissimilarity s_1, but is somewhat less stable when defined by dissimilarity s_2, with $1.1 \leq \varepsilon \leq 1.7$. The maximum single linkage occurs at D' ~ 270 m/s, and within the boundary of the family, as defined by the locus, there are no spectral interlopers. Similarly, no additional asteroids are identified along the periphery of the locus that might be considered members of the family. In the WAM results of Zappalà *et al.* (1995), the asteroid 3511 Tsvetaeva was included as a member of the Phaeo family, but based on the SMASSII observations, this object is classified as an S-type, and is not included here as a genetically related member of the Phaeo family..

5.4.5 Zone 5 - Gefion family

Gefion family *- The Gefion family is a very densely populated, moderately compact family containing S-type asteroids. In total, 36 members of the Gefion family were observed during SMASSII, providing very strong evidence for this family being a true genetic association. This family was proposed by Williams (1979, 1989, 1992), Bendjoya (1993), Lindblad (1994), and Zappalà et al. (1990, 1994, 1995).*

The Gefion family is a large, well-defined spectral grouping, consisting almost entirely of S-type asteroids. Based on the SMASSII dataset, 32 objects are identified in the locus of this family, as illustrated in both the HCM clustering solution shown in Figure 5.23 and the pairwise plots of proper element space shown in Figure 5.24. In semimajor axis, this locus extends from approximately 2.78 to 2.815 AU, with the more distant boundary corresponding to the inner edge of the 5:2 resonance. A total of 57 SMASSII

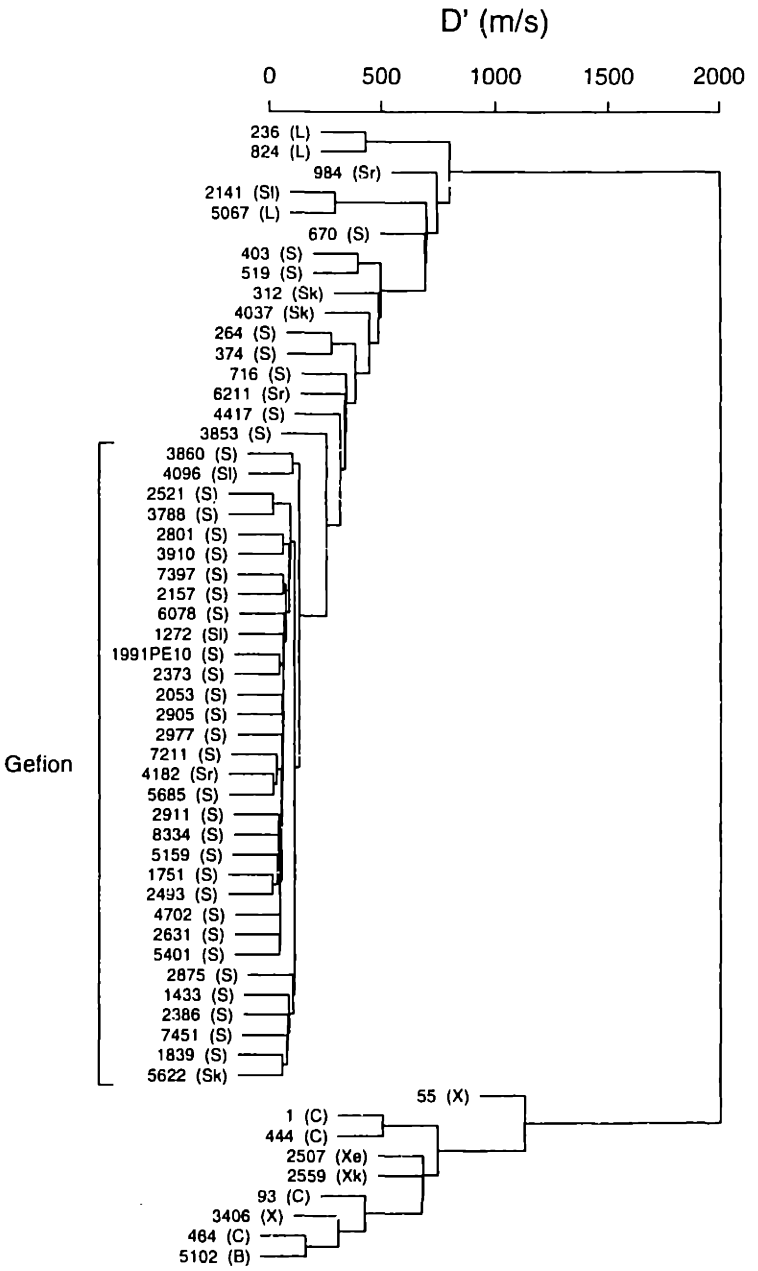

Figure 5.23: Similar to Figure 5.11, but for 57 SMASSII asteroids contained in zone 5. Dissimilarity s_1 was used, with a spectral cutoff of $\varepsilon = 1.0$. The locus of the Gefion family (32 objects) is marked.

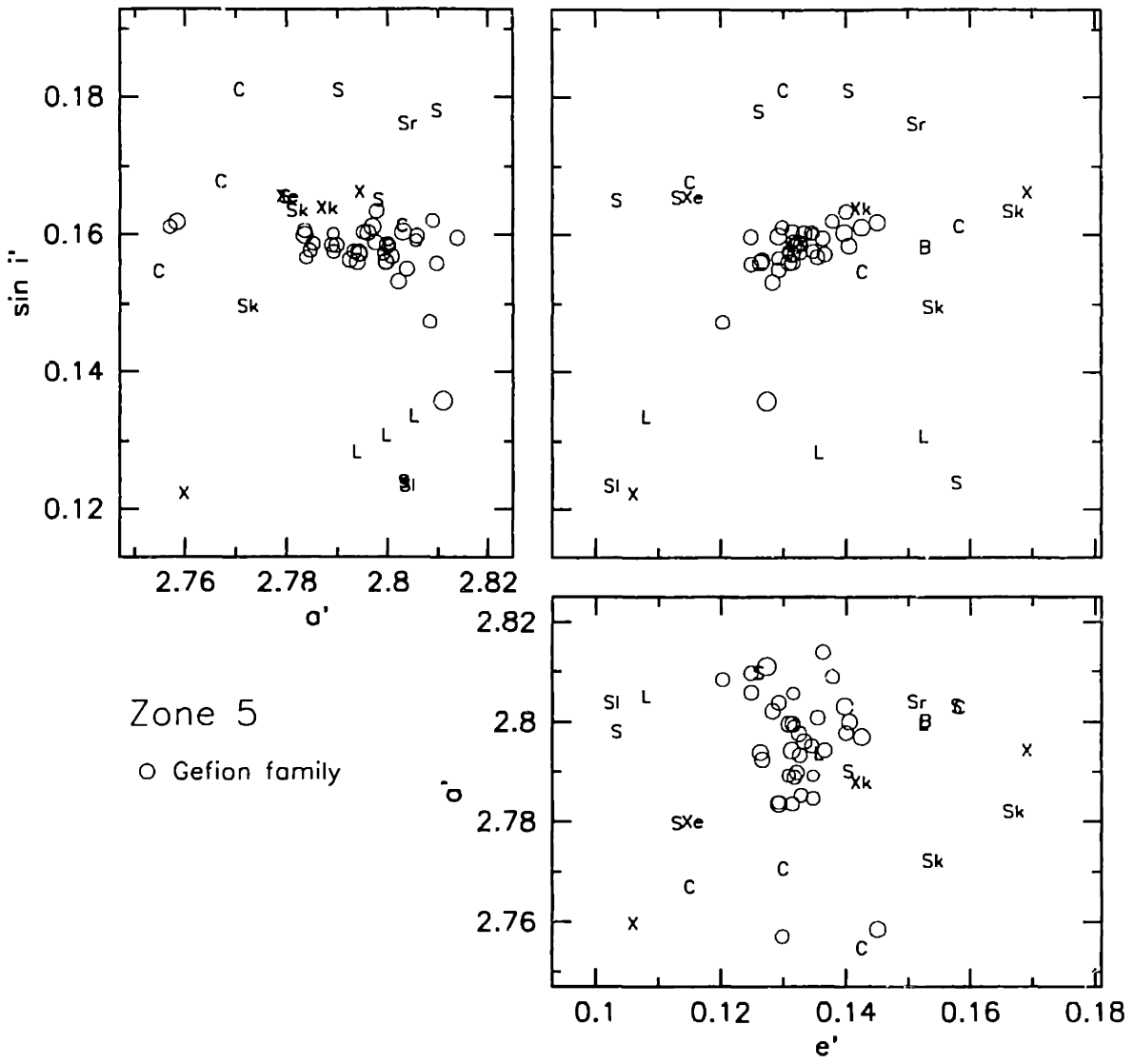

Figure 5.24: Similar to Figure 5.12. Pairwise plots for zone 5, showing the locations of Gefion family members.

asteroids are contained within the volume of zone 5, providing 25 background objects against which the locus of the Gefion family can be compared. The locus is very stable, remaining constant over values of $0.6 \leq \varepsilon \leq 1.9$ and $0.7 \leq \varepsilon \leq 1.9$ for the dissimilarities s_1 and s_2, respectively, with the maximum single linkage occurring at a value of D' ~ 120 m/s. The Gefion family appears similar to the Dora family in many aspects, though comparing Figures 5.21 and 5.24 shows that the Gefion family is somewhat more dispersed in proper element space. In particular, the distribution of Gefion members in

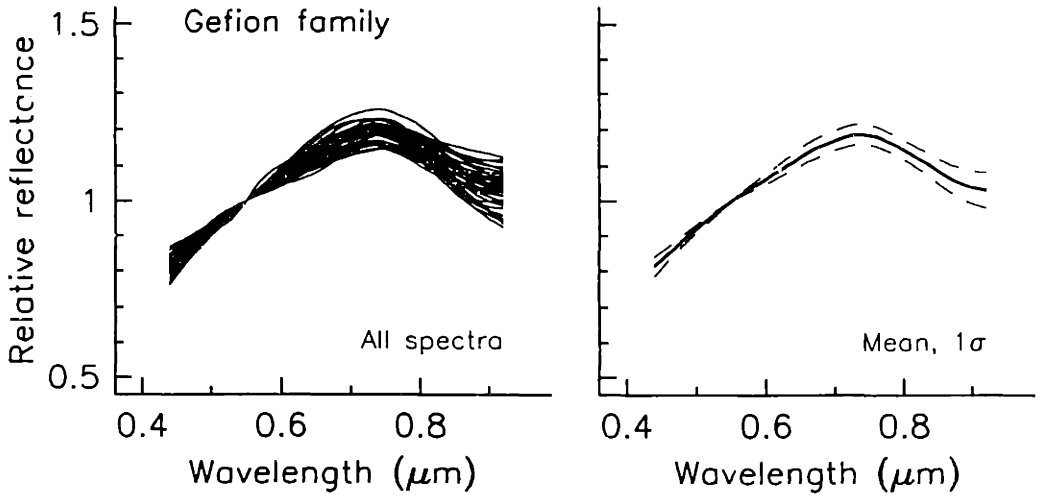

Figure 5.25: Similar to Figure 5.13, showing the spectra for 36 Gefion family members.

the sin *i'* versus *e'* plane is noticeably elongated, in contrast to the more compact clustering of the Dora family asteroids. This greater dispersion in proper elements, combined with a background population that contains a significant number of S-type objects, makes defining a true boundary for the Gefion family more challenging. In Figure 5.23, a relatively shallow tail of S-type asteroids is seen to extend above, and to the right (higher values of D') of the Gefion locus. The four objects closest to the locus, 716 Berkeley, 3853 Haas, 4417 Lecar, and 6211 1991DO, all have spectral signatures that are within the range of variations observed among the locus members. These objects can easily be added to the membership of the Gefion family by extending the family boundaries in orbital space, primarily in semimajor axis and inclination, without introducing any spectral interlopers into the family. By including these four asteroids in the family membership, the maximum single linkage increases to D' ~ 340 m/s. The spectra for all 36 members of the family are plotted in Figure 5.25.

Several studies have led to the identification of the Gefion family as a dynamical grouping. Williams (1992) described a family (family 127) consisting of ten members, of which the largest member was the C-type asteroid, 93 Minerva. However, by increasing the number of asteroids in his analysis, Williams (private communication) redefined this family to include 22 potential members, but excluded Minerva as a possible member due to its apparently weak connection with the more densely populated core of the family. During the SMASSII survey, we observed all 22 of these objects, and include all but one

in the locus of the Gefion family. The asteroid that we have excluded from the locus is 2559 Svoboda, classified as an Xk-type, and probably not genetically related to the Gefion family. Lindblad (1994) identified two separate families within the Gefion grouping, the Oppavia-Gefion family and the Nuki family. The combined membership of the Oppavia-Gefion and Nuki families is, again, almost identical to our locus, except that Lindblad included the same non-family asteroid, 2559 Svoboda, in his list of Oppavia-Gefion family members. Bendjoya (1993) and Zappalà *et al.* (1994) both analyzed a set of 6,479 asteroids, using the wavelet analysis (WAM) and hierarchical clustering (HCM) techniques, respectively. The Gefion family was identified in both of these analyses, again with lists of probable members that very closely matches our definition of the locus. Bendjoya slightly overestimated the size of the family by including the background asteroid 2559, while Zappalà *et al.* slightly underestimated the size of the family by omitting the asteroids 1433 Geramtina and 1839 Ragazza. In Zappalà *et al.* (1995), however, the analysis of 12,487 asteroids resulted in significant overestimations of the size of the Gefion family by both the HCM and WAM techniques. In the WAM analysis, 93 Minerva was included in the family, while in the HCM results, 1 Ceres (a C-type asteroid) was identified as the primary member of the family. I have listed these various details because, contrary to what might be expected, the increase in the total number of asteroids that were considered in the different analyses appears to have had an adverse affect on how accurately the boundary of this family has been determined.

Though the C-type asteroids 1 Ceres and 93 Minerva are clearly not members of the Gefion family (based on their spectral properties), Williams (1979, 1989, 1992) does identify a separate Ceres family (family 67) that is distinct from the Gefion grouping (family 127). Kelley and Gaffey (1996) obtained spectral observations of the seven known members comprising the Williams family 67, and based on mineralogical interpretations of their spectra, found a possible genetic relationship between those asteroids. Similarly, during the SMASSII survey, all seven of the asteroids in Williams family 67 were observed, and a mixture of taxonomic classes were found, with one C-type (Ceres), one A-type, one Xk-type, and four S-types making up this proposed association. While that subset of objects consisting of the A- and S-types might be considered as a possible genetic relationship, we point out that the spectra of the four S-types, 39 Laetitia, 264 Libussa, 374 Burgundia, and 403 Cyane, are nearly identical over the visible wavelength interval, and are also very similar to the mean spectral reflectance

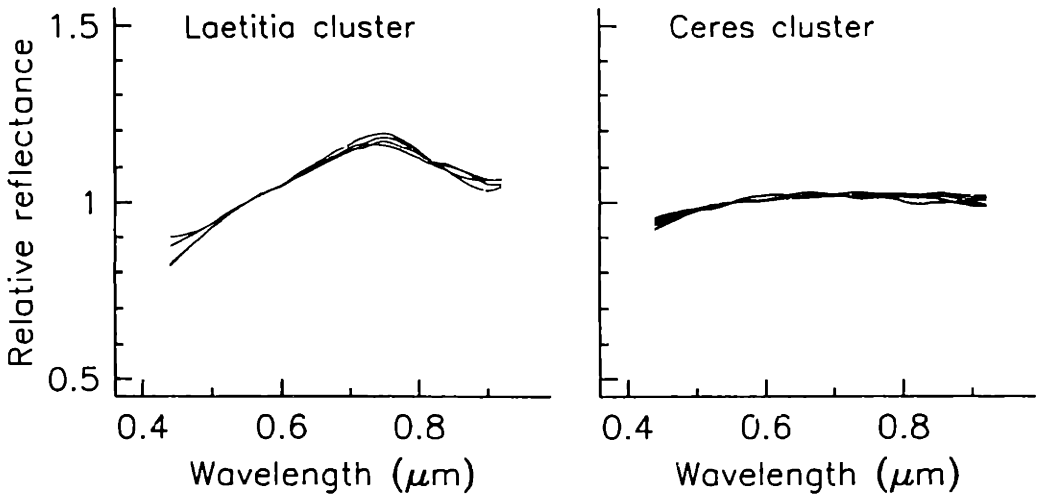

Figure 5.26: Spectra of asteroids near the Gefion family. In the left panel, spectra for the four S-type asteroids 39 Laetitia, 264 Libussa, 374 Burgundia, and 403 Cyane are plotted. These four asteroids are spectrally very similar to many Gefion family members, and may be genetically related to the Gefion family. In the right-hand panel, spectra for five large C-type asteroids are plotted, including the spectra of 1 Ceres, 93 Minerva, 444 Gyptis, 464 Megaira, and 688 Melanie. These spectra are essentially identical over the visible wavelengths, and suggests these may be the oid, dispersed remnants of a true Ceres family.

of the Gefion family asteroids, as shown in Figure 5.26. This suggests the possibility that 39, 264, 374, 403 and the parent body of the Gefion family are the large remaining remnants from an earlier collisional event, and that the present Gefion family is the result of a more recent, second-generation disruption. Because these larger S-type asteroids are dispersed in proper element space (with $2.769 \leq a' \leq 2.810$, $0.068 \leq e' \leq 0.133$, and $0.158 \leq \sin i' 0.178$, where the center of mass of the currently observed Gefion family is included in these limits), we can neither verify, nor dismiss this possible larger relationship based on our SMASSII results. Proving such a relationship may be difficult without more extensive physical observations, such as extended measurements in the near infrared. Similarly, ! point out the very strong spectral similarities between the C-type asteroids 1 Ceres, 93 Minerva, 444 Gyptis, 464 Megaira, and 688 Melanie, as shown in Figure 5.26. Again, these large asteroids are dispersed over a relatively large volume of proper element space, with $2.699 \leq a' \leq 2.803$, $0.113 \leq e' \leq 0.158$, and $0.155 \leq \sin i' \leq 0.181$. The maximum single linkage within this cluster is D' ~ 750 m/s, so that demonstrating any significant relationship between these asteroids is not possible, based solely on the SMASSII results. To prove the existence of a real Ceres family will, again, require more extensive physical studies of these individual asteroids.

5.4.6 Zone 6 - Agnia, Henan, Hoffmeister, and Lydia families

Zone 6 is bounded in proper element space by the intervals $2.692 \leq a' \leq 2.815$ AU, $0.020 \leq e' \leq 0.105$, and $0.047 \leq \sin i' \leq 0.103$, and contains a total of 90 asteroids that were observed during the SMASSII survey. The dendrogram of a hierarchical clustering solution for these asteroids is shown in Figure 5.27, where the cutoff in spectral dissimilarity is defined by a value of $\varepsilon = 0.8$. Figure 5.28 shows these same asteroids in a set of pairwise plots of proper element space. The distribution of taxonomic types in this zone is very mixed, with a large number of K-, L-, and X-type asteroids being observed, in addition to the normal mixture of C- and S-types. Even among the S-type asteroids in this region, there is a significant number that are classified as Sq-types. Past searches for asteroid families have identified several potential groupings within the boundary of this zone, though only one of these dynamical families (the Hoffmeister family) is a well-defined, compact grouping in proper element space. The other proposed families are significantly more dispersed, resulting in family boundaries that are less certain, and making this zone the most complex of the eight regions studied in this project. Even when the spectral classifications for these objects are taken into account, precisely determining the boundaries and memberships for these different families is not always possible given the limited number of asteroids for which we currently have spectral data.

Based on an analysis of the numbered asteroids, up to and including asteroid 2125, Kozai (1979) identified a single, all-encompassing family, no. 30, that includes nearly all of the bright (large) objects contained in zone 6. By comparison, Williams (1979, 1989) has identified six much smaller, but statistically significant clusters within this same region (Williams families 36, 37, 38, 130, 132, 134). The most recent work of Williams (1992) still recognizes these six families as being real associations. The latest work of Zappalà *et al.* (1995) identifies five families (Henan, Hoffmeister, Liberatrix, Lydia, and Nemesis) within this zone by the HCM technique, and five families (Agnia, Antonia, Concordia, Lydia, and Tirza) using the WAM technique, but there are significant differences in the boundaries and memberships determined for these families based on these two clustering methods. The difficulty in precisely defining the asteroid families in this region stems from their close proximity to one another, and the fact that only the Hoffmeister family appears to have a well-defined, densely populated locus. In this analysis, we have identified four primary families that are spectrally distinct, with the

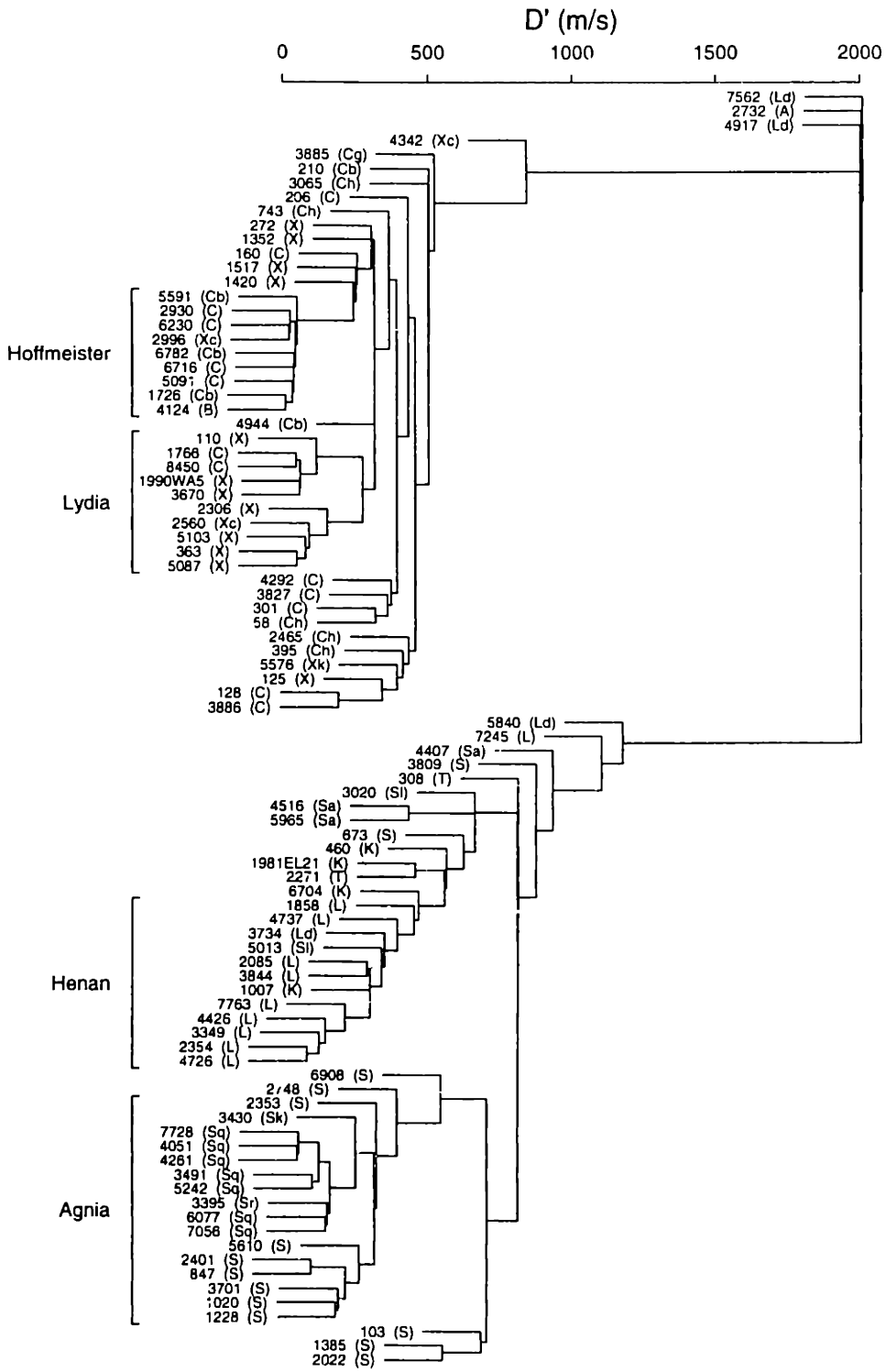

Figure 5.27: Similar to Figure 5.11, but for 90 SMASSII asteroids contained in zone 6. Dissimilarity s_1 was used, with a spectral cutoff of $\varepsilon = 0.8$. The loci of the Agnia, Henan, Hoffmeister, and Lydia families are marked.

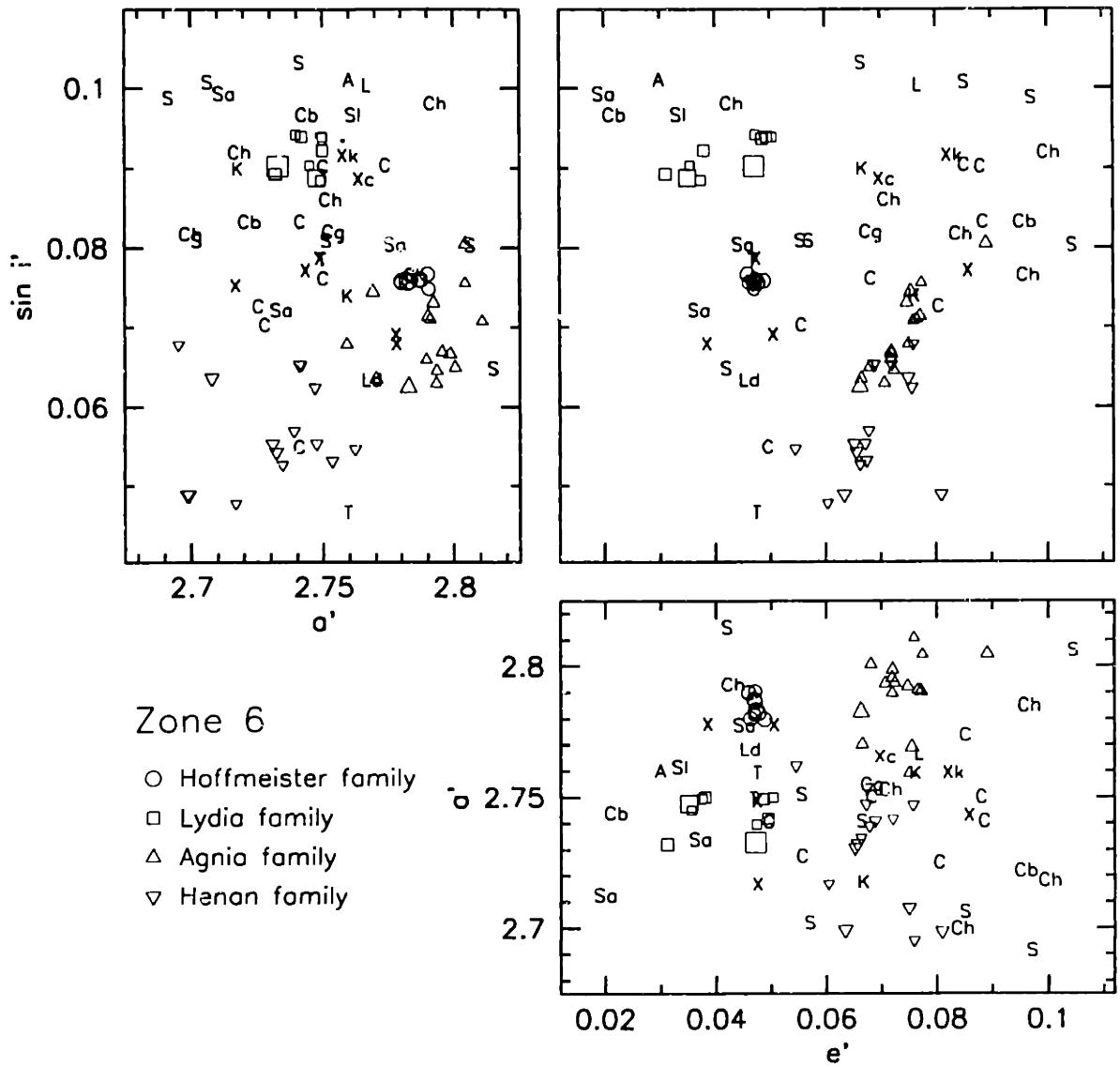

Figure 5.28: Similar to Figure 5.12. Pairwise plots for zone 6, showing the locations of Agnia, Henan, Hoffmeister, and Lydia family members. While the Hoffmeister and Lydia families appear to be relatively isolated, the Agnia and Henan families are more widely dispersed. The bifurcated nature of the Lydia family is clearly seen in the e' dimension.

Hoffmeister family being composed of C-type asteroids, the Lydia family containing primarily X-types, the Agnia family being made up of S-types, and the Henan family consisting primarily of L-type asteroids. While there is little question about the genetic reality of any of these families, the Henan family is the most dispersed in proper element space, and its boundary is the most difficult of the four families to define. In a secondary analysis of the background asteroids described in section 5.5 of this chapter, a fifth

family, Liberatrix, is also identified in this zone, though the reality of the Liberatrix family is not as certain as that of these four primary families.

Hoffmeister family *- The Hoffmeister family is a very compact and well-defined grouping. Based on the SMASSII observations of nine members, we find the Hoffmeister asteroids to be spectrally similar, with the majority of the members being classified as C-types. While there is some spectral variation, there is strong evidence that this is a real genetic relationship. Members of the Hoffmeister family were originally included as part of a larger Antonia family by Williams (1979, 1989, 1992). The more compact Hoffmeister grouping was later recognized by Zappalà et al. (1994, 1995).*

The locus of the Hoffmeister family contains nine asteroids that cluster together with a maximum single linkage value of D' ~ 35 m/s, as seen in Figure 5.27. The clustering solution is very robust, remaining constant over the intervals of $0.7 \leq \varepsilon \leq 1.9$ and $0.8 \leq \varepsilon \leq 1.9$ for the dissimilarities s_1 and s_2, respectively. The spectra of these nine family members are plotted in Figure 5.29, with all but one of the objects being classified within the C-complex (4 C-types, 3 Cb-types, 1 B-type, and 1 Xc-type). This is consistent with the results of Migliorini *et al.* (1996) who found the spectrum of 1726 Hoffmeister (a Cb-type) to be similar to that of C- and F-type asteroids in the Tholen taxonomy. A moderate degree of spectral variation is seen among the Hoffmeister family members, some of which can be accounted for by differences in their average spectral slopes. In addition to these differences in slope, however, several of the objects have spectra containing a small concave absorption feature at the red end of the spectrum, centered around 0.9 μm, and an associated convex inflection located at about 0.82 μm. The 0.9 μm feature is relatively subtle, but is often observed in the spectra of asteroids classified as C-, Ch-, and X-types. Immediately surrounding the Hoffmeister locus in proper element space are several X-type asteroids that are substantially redder in color than the Hoffmeister spectra, and are probably not related to this family. Instead, these X-type asteroids may be more closely related to the nearby Lydia family. No spectral interlopers are identified within the boundary of the Hoffmeister locus based on our SMASSII sample. In the analysis of Zappalà *et al.* (1994, 1995), the HCM results identified an additional asteroid, 4516 Pugovkin, as a potential member of the Hoffmeister family. Pugovkin was observed during the SMASSII survey, and is classified as an Sa-type, suggesting that this object is not genetically related to

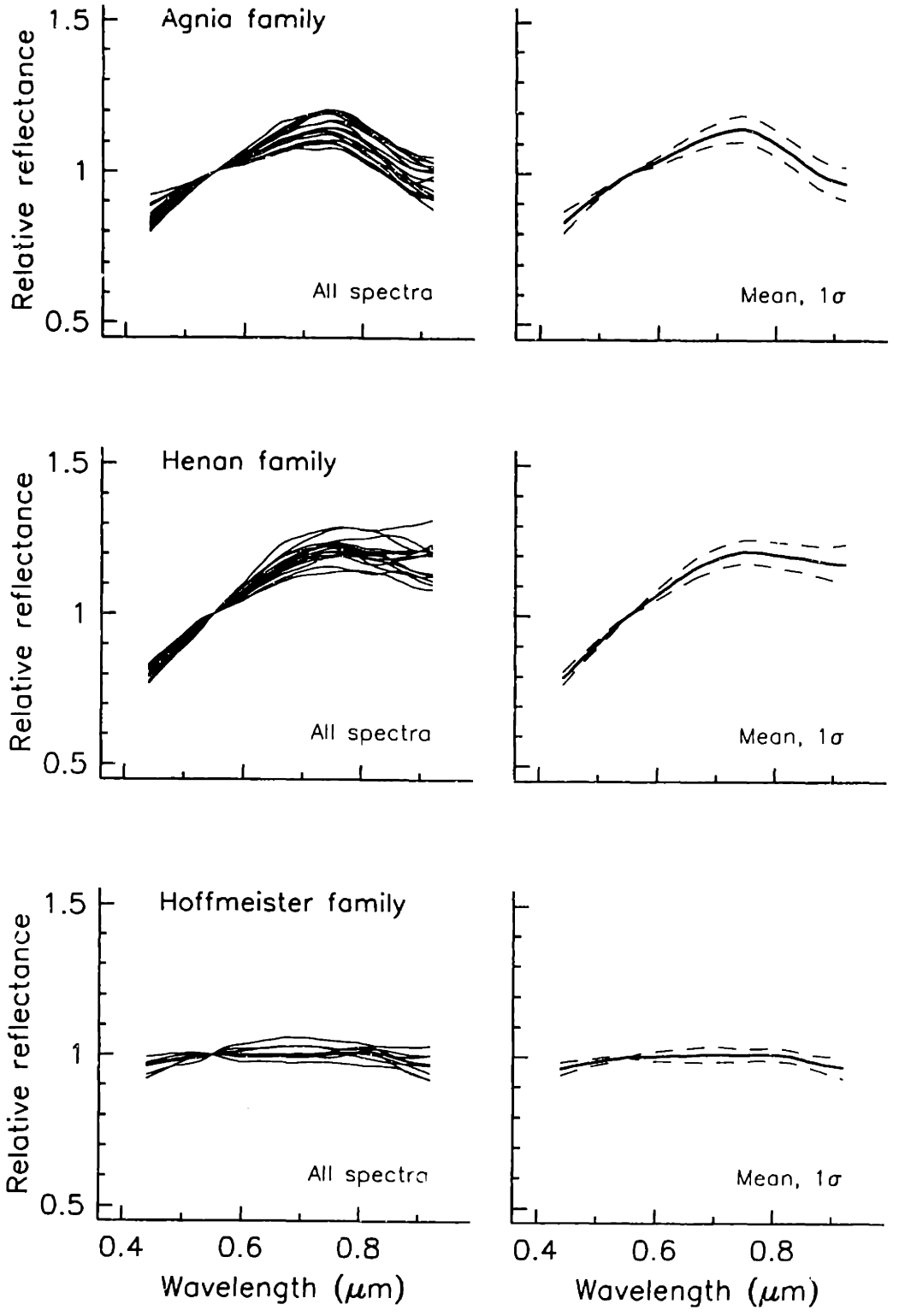

Figure 5.29: Similar to Figure 5.13, showing the spectra for 16 Agnia family members, 15 Henan family members, 9 Hoffmeister family members, and 10 Lydia family members.

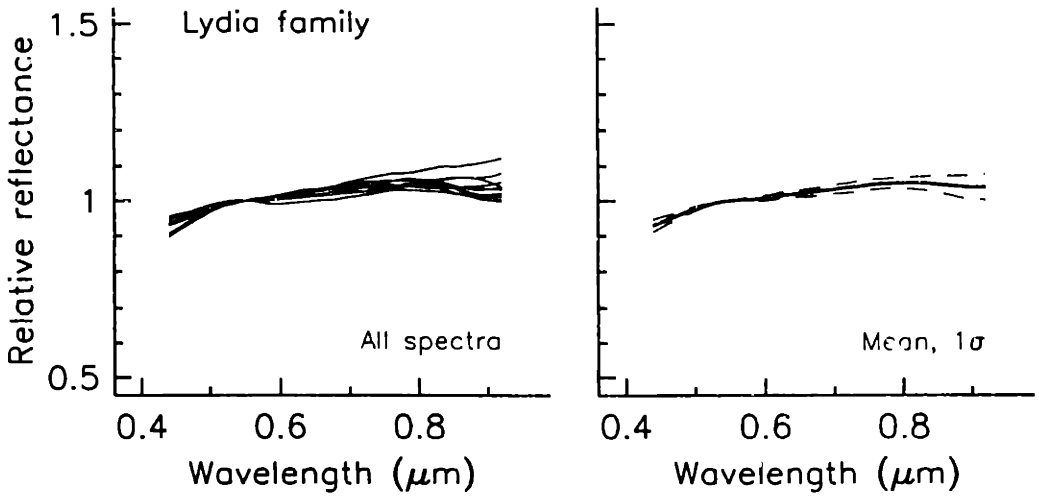

Figure 5.29: continued.

Hoffmeister. The Hoffmeister group was identified as part of a larger Antonia family by Williams (1992), though he later noted that 272 Antonia and 1352 Wawel may not actually be members (private communication), resulting in much more compact Hoffmeister family. In their WAM analysis, Zappalà *et al.* found members of the Hoffmeister family to be divided between the Antonia and Lydia families, where interestingly, the lower numbered, and presumably larger members of the Hoffmeister family all clustered with the Antonia grouping, while the unnumbered, and presumably smaller members were all identified with the Lydia group.

Lydia family *- Ten asteroids observed during the SMASSII survey are included in the Lydia family. This family is moderately compact, and contains asteroids that are spectrally similar, but straddle the boundary between the C- and X-complexes, with the majority of observed members being classified as X-types. This grouping is probably a real genetic relationship, even though the taxonomic mixture of C- and X-types might suggest otherwise. There are additional, more widely-dispersed asteroids that are spectrally similar, and which may belong to this family, but are not included in our membership. This family was most accurately identified by Williams (1989, 1992) and by Zappalà et al. (1990, 1995).*

Among the four primary families in zone 6, the next best-defined grouping belongs to the Lydia family. We have identified ten asteroids making up the locus of this family,

though as seen in both Figures 5.27 and 5.28, the locus appears to be bifurcated, with two distinct clusters, separated in eccentricity by $\Delta e' \sim 0.01$. The clustering solutions are stable over the intervals in ε of 0.8 - 1.9 and 0.9 - 1.9 for dissimilarities s_1 and s_2, respectively, with the maximum single linkage between the two clusters occurring at $D' \sim$ 250 m/s. Each of the two groupings contains one large member, 110 Lydia and 363 Padua. Spectrally, all of the objects contained in the Lydia family locus are very similar, as seen in Figure 5.29, with the majority being classified as X-types, and the remaining objects being assigned to the C-class, straddling the boundary that separates the C- and X-complexes in spectral component space. The largest members are spectrally featureless, except for a moderately reddish slope, while spectra of the smaller objects (with absolute magnitudes H > 11.0) typically contain shallow absorption features centered near 0.9 μm. There are five additional objects in the vicinity of the Lydia family that are spectrally very similar (160 Una, 272 Antonia, 1352 Wawel, 1420 Radcliffe, and 1517 Beograd), and which could be considered as widely dispersed members of the Lydia family. These asteroids plot just to the left of the Hoffmeister family in the HCM clustering solution shown in Figure 5.27, and generally surround the Hoffmeister family in the *e'* versus sin *i'* plane in Figure 5.28. Including these asteroids in the Lydia family requires significantly expanding the boundary defined by the locus, and does introduce several spectral interlopers (primarily S-types) into the family that are probably not genetically related to Lydia. Therefore, these five additional objects are not included in the Lydia membership defined here, though we note their spectral similarities to the Lydia family members, and cannot rule out a possible genetic relationship.

Agnia family - *The Agnia family is moderately dispersed, making it difficult to accurately define a boundary. However, this family appears to be a real genetic association. Sixteen asteroids were observed during SMASSII, all classified as S-types, though variations in the average slopes of these spectra appear to depend on the sizes of the asteroids, with the smallest objects having the lowest average slopes. This family was proposed by Williams (1979, 1989, 1992), Bendjoya (1993), Lindblad (1994), and Zappalà et al. (1990, 1994, 1995).*

The Agnia family is a grouping of spectrally similar S-type asteroids that are moderately dispersed in proper element space. A locus containing 16 Agnia family members is reasonably robust based on the dissimilarity s_1, with clustering solutions

remaining stable for ε over the interval of 0.7 to 1.1. Based on the dissimilarity s_2, however, the membership of the locus is not as clearly defined. All 16 asteroids are again recognized for values of ε = 0.7 and 0.8, but two additional S-types, 2748 Patrick Gene and 6908 1990 WB3, are also included. I have adopted the 16 SMASSII asteroids identified by dissimilarity s_1 to be the locus of the Agnia family. At higher values of ε, this locus begins to blend with spectrally similar asteroids in the background, and in particular, with the L-type asteroids contained in the adjoining Henan family. Within the boundary of the locus in proper element space, one interloper is recognized, 6704 1988 CJ, a K-type that may be related to the Henan family. The maximum single linkage for members of the Agnia locus is D' ~ 340 m/s, as seen in Figure 5.27. While the asteroids 2748 Patrick Gene and 6908 1990 WB3 may be real members of the Agnia family, their addition to the family increases the maximum single linkage to 540 m/s. Adding these two asteroids would also introduce another spectral interloper within the boundary of the family, the Ch-type asteroid 395 Delia. Based on these considerations, these two S-type objects are not included in the Agnia membership defined here, though a genetic tie with Agnia should not be ruled out. The spectral variations observed among the Agnia family members is primarily accounted for by differences in the average spectral slope, as seen in Figure 5.29. The smaller members of the Agnia family tend to have average spectral slopes that are shallower than those observed for the larger members, leading to the classification of "Sq" for many of these smaller objects. This apparent decrease in spectral slope for smaller objects is identical to that observed among the near-Earth asteroids (Binzel *et al.* 1996), and may be related to size-dependent resurfacing or space weathering processes.

Henan family *- Fifteen SMASSII asteroids are included in the Henan family. These asteroids are very dispersed in proper element space, but are spectrally very distinct from the background population, with the majority of the members being classified as L-types. There is little doubt about the genetic reality of this family, though defining an actual boundary for the family is difficult due to the orbital dispersion. This family was best identified by Williams (1989, 1992) and by Zappalà et al. (1994, 1995), first as the Lavrov family, and later as the Henan family.*

The Henan family is the most distinctive of the four primary groupings in zone 6, with a majority of its members being classified as L-types. However, due to the

dispersion of the Henan family asteroids in proper element space, the boundary of this family is also the most difficult of the four groupings to define. In Figure 5.27, the Henan family cluster plots as a stepwise chain of objects, ordered by increasing values of D'. This stepwise configuration in a dendrogram results when there is no strong concentration of asteroids forming a well-defined locus in proper element space. As the value of ε is increased, different linkages between the members of the family occur as objects whose spectra are increasingly dissimilar are allowed to link together. This results in a continual reordering of objects in the clustering solutions as ε is incremented. For the Henan family, the locus I have adopted consists of ten asteroids whose clustering remains consistent over the intervals of $0.6 \leq \varepsilon \leq 0.7$ and $0.8 \leq \varepsilon \leq 1.0$ for the dissimilarities s_1 and s_2, respectively. The maximum single linkage for this group of asteroids is D' ~ 450 m/s. Within the volume of proper element space containing these ten objects, there are five other asteroids for which we have spectral classifications. Four of these asteroids, 1007 Pawlowia, 3734 Waland, 4917 Yurilovia, and 5840 1978 ON, are spectrally similar to the locus members (with classifications of K, Ld, Ld, and Ld) and are considered part of the Henan family. The fifth object within the boundary of the locus, 3430 Bradfield, is classified as an Sk-type, and is identified as a member of the Agnia family. By slightly expanding the lower boundary of the locus in inclination, the K-type asteroid 1981 EL21 can also be added to the family membership without introducing any additional interlopers. The spectra for all 15 of these Henan family members are plotted in Figure 5.29. These spectra exhibit a moderate degree of variation, especially in the peak level of relative reflectance. These differences can be generally attributed to variations in the average spectral slope, the primary characteristic that distinguishes K-, L-, and Ld-type asteroids. Two additional K-type asteroids, 460 Scania and 6704 1988 CJ, may also be related to the Henan family, though expanding the family boundary to include these objects would introduce a greater number of spectral interlopers. Therefore, while we recognize 460 Scania and 6704 1988 CJ as having possible genetic ties to Henan, these two objects are not included in our list of Henan family members. Zappalà *et al.* (1994) assigned the name Lavrov to this grouping. In an earlier discussion of our results (Bus 1998), this family was referred to as the Pawlowia family, in recognition of 1007 Pawlowia being the lowest numbered asteroid in the family. However, Pawlowia is not included in our current definition of the locus. Instead, the lowest numbered member of the locus is 1858 Lobachevskij. However, adding in the additional complication that 460 Scania might be genetically

linked to this grouping makes the naming of this family even more confusing. I have thus reverted back to the name Henan (in recognition of 2085 Henan) that was proposed by Zappalà *et al.* (1995) based on their most recent HCM clustering results, and suggest maintaining this name until a more rigorous determination of the family membership can be made.

5.4.7 Zone 7 - Merxia and Thisbe families

Zone 7 contains 53 asteroids that were observed during the SMASSII survey. Within this region, two primary families are identified: the Merxia family, which is a moderately-compact grouping of asteroids belonging to the S-complex, and the Thisbe family, a dispersed collection of four B-type asteroids. The local background is well sampled, and is found to be a mixture of C-, S-, and X-type objects. In Figure 5.30, a dendrogram shows the HCM clustering solution for this zone, where the range in spectral dissimilarity has been constrained by $\varepsilon = 0.8$. Pairwise plots giving the locations of all 53 asteroids in proper element space are shown in Figure 5.31.

Merxia family *- The Merxia family is identified based on nine SMASSII asteroids. This group is relatively compact in proper element space, but shows a moderate degree of spectral variation among the members, which are classified as S-, Sk-, and Sq-types. Even with this spectral variation, this is considered a genetic association, where the variation may indicate either compositional variations within the parent, or variations in surfacing processes. Members of the Merxia family were recognized by Williams (1979, 1989, 1992) and Bendjoya (1993) as part of the Lilaea family, while Zappalà et al. (1994, 1995) identified this grouping as the Merxia family.*

The locus of the Merxia family contains seven asteroids that are clustered together with a maximum single linkage value of D' ~ 120 m/s. This locus is stable over the interval of ε from 0.8 to 1.4, based on the dissimilarity s_1, and from 1.1 to 1.9 using the dissimilarity s_2. While the Merxia locus is relatively compact in proper element space, there is a moderate degree of spectral variation among these asteroids, as seen in Figure 5.32. Because of this variation in spectral reflectances, the locus of the Merxia family is not well isolated from the background population, where several similar S-type asteroids are observed that may have potential genetic ties to Merxia. These background objects surround the locus in both a' and e', but have values of sin *i'* that are

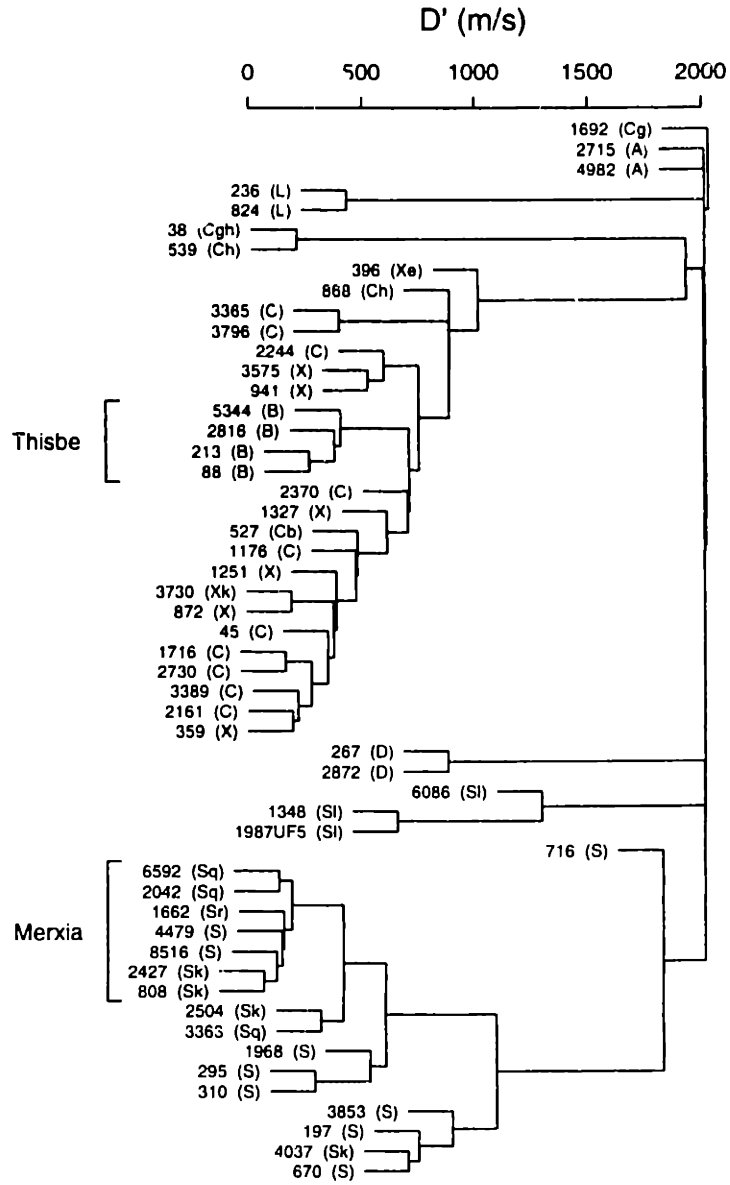

Figure 5.30: Similar to Figure 5.11, but for 53 SMASSII asteroids contained in zone 7. Dissimilarity s_1 was used, with a spectral cutoff of $\varepsilon = 0.8$. The loci of the Merxia and Thisbe families are marked. Between the Merxia and Thisbe groupings in this dendrogram, another group of objects appears to be significant, but is not marked. This group belongs to a secondary family called Eugenia that will be discussed in Section 5.5.

equal to or lower than those of the locus members. From the clustering solution shown in Figure 5.30, we note two asteroids in particular, 2504 Gaviola (an Sk-type) and 3363 Bowen (an Sq-type), which are spectrally very similar to members of the Merxia locus, and which are added to the membership of the family. By extending the family boundary

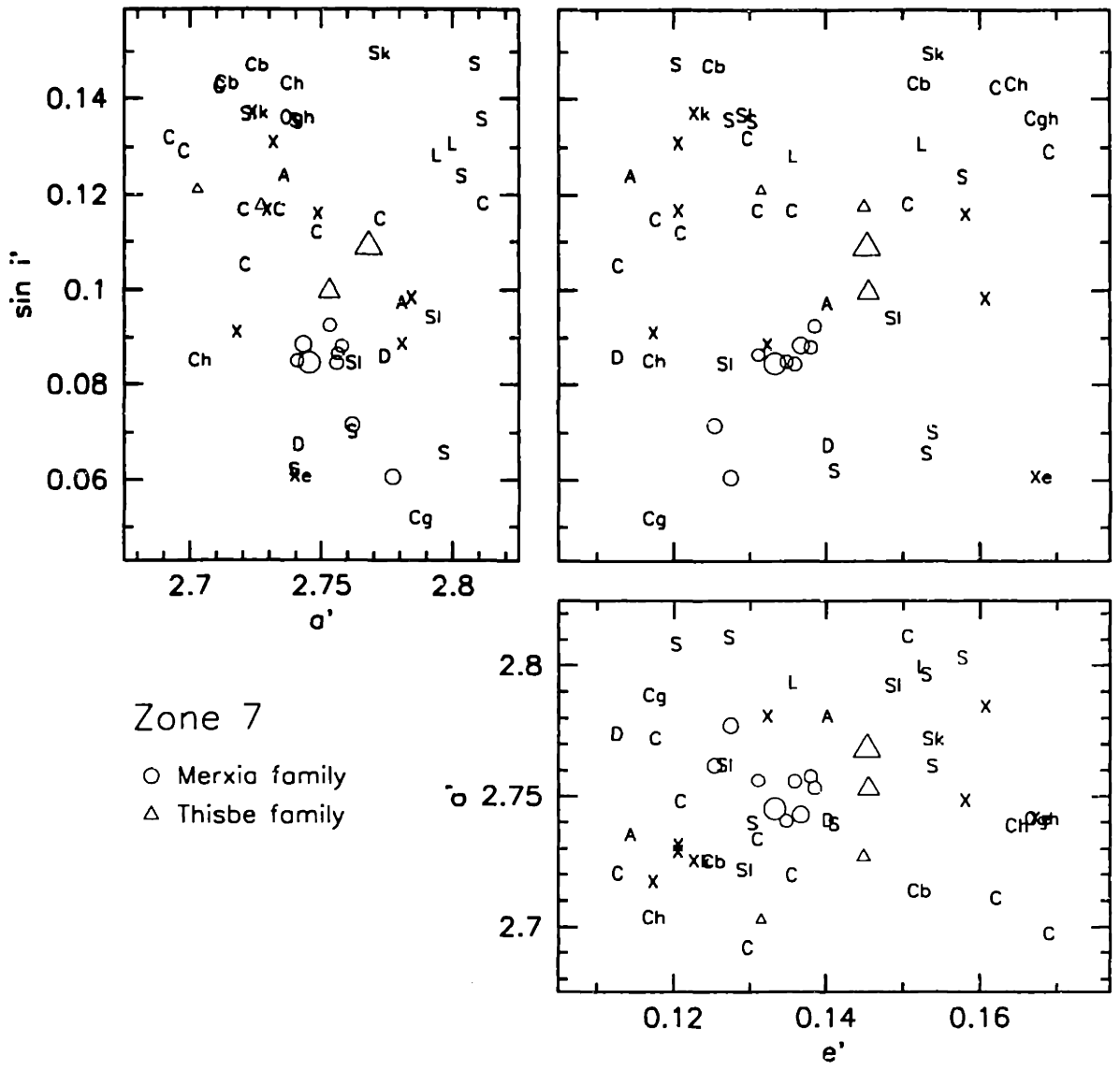

Figure 5.31: Similar to Figure 5.12. Pairwise plots for zone 7, showing the locations of Merxia and Thisbe family members.

in proper element space to include these two objects, however, we also introduce the asteroid 1987 UF5, which is classified as an Sl-type, and is sufficiently dissimilar from the other Merxia family members that it is considered a spectral interloper. The addition of 2504 Gaviola and 3363 Bowen increases the maximum single linkage for the Merxia family to D' ~ 400 m/s. The Merxia family was identified by Williams (1989) as family 40, and contained four asteroids among the numbered objects up to and including asteroid 2065. Our definition of the Merxia family includes three of these asteroids (808 Merxia,

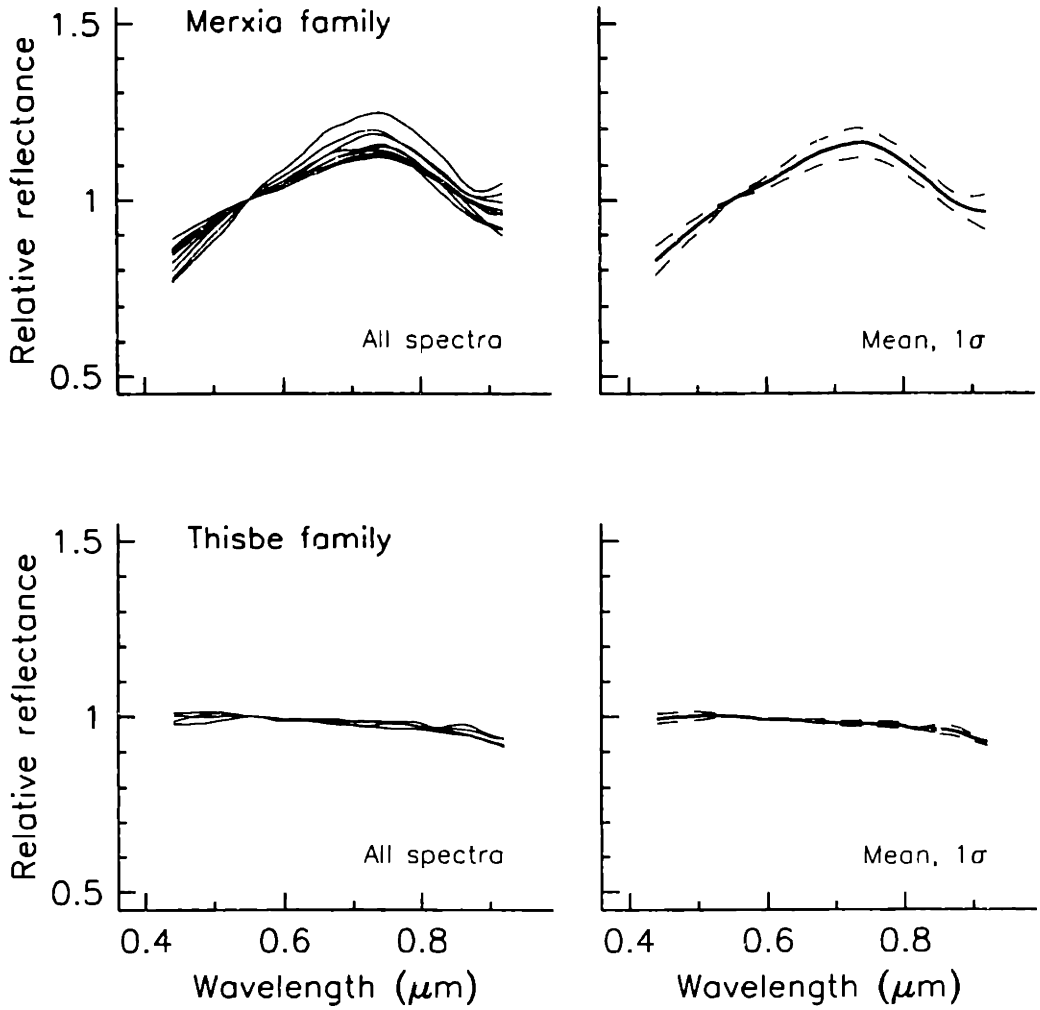

Figure 5.32: Similar to Figure 5.13, showing the spectra of 9 Merxia family members and 4 Thisbe family members.

1662 Hoffmann, and 2042 Sitarski) as members, but we find the fourth object listed by Williams, 1327 Namaqua (an X-type), to be a spectral interloper. Zappalà *et al.* (1995) also identified the Merxia family, using both the HCM and WAM techniques. The resulting memberships from these two analyses of Zappalà *et al.* are internally consistent, and closely match our description of the locus, though Zappalà *et al.* also includes the two interlopers 1327 Namaqua and 1987 UF5 as potential members of the Merxia family.

Thisbe family - *The Thisbe family is defined based on four SMASSII asteroids. This grouping is uncertain, with the four members being spectrally identical B-types, but*

being very dispersed in proper element space. No previcus identifications of a Thisbe family are known to exist.

The Thisbe family is a more questionable grouping, with the four members being spectrally almost identical, but being significantly dispersed in all three elements of orbital space. Because of the strong spectral similarities between the members, as seen in Figure 5.32, the clustering becomes stable at very low values of ε, with this grouping being defined over the intervals of $0.4 \leq \varepsilon \leq 0.9$ and $0.4 \leq \varepsilon \leq 1.0$ for the dissimilarities s_1 and s_2, respectively. For higher values of ε, these B-type asteroids begin to merge with the spectrally similar C-type asteroids in the background population, and the clustering solution for the Thisbe family begins to dissolve. The two largest members of this locus, 88 Thisbe and 213 Lilaea, are closest in proper element space, being separated primarily in sin i'. The linkage between these two larger members is D' ~ 260 m/s, while the maximum single linkage for all four members of the Thisbe locus is D' ~ 400 m/s. One spectral interloper is found within the volume of proper element space containing the Thisbe locus. This asteroid, the C-type 2730 Barks, has a spectral slope significantly redder than the Thisbe family members, and is very similar to the other C-types in the vicinity that are found to make up a secondary grouping called Eugenia, which will be described in section 5.5. The significance of the Thisbe family is corroborated by a search of the background population extending outside of zone 7, which shows this group of asteroids to be moderately isolated. The next closest asteroid in proper element space that is spectrally similar to the Thisbe family members is 2251 Tikhov, a Cb-type that is separated from the Thisbe cluster by D' ~ 680 m/s. No prior identification of the Thisbe family is known to exist.

5.4.8 Zone 8 - Menippe, Watsonia and Weringia families

Zone 8 contains a total of 56 asteroids with moderately high orbital eccentricities ($0.1 \leq e' \leq 0.25$) and inclinations ($0.18 \leq \sin i' \leq 0.34$). Three potential families are identified within this zone, based on the spectral similarities between the members of each grouping. However, the locus for each of these families contains only four asteroids, the minimum number needed for a grouping to be considered real in this analysis. In addition, the members of these families are moderately to widely dispersed in proper element space, raising questions about the validity of these groupings as true genetic associations. I believe that the spectral evidence for each of these families is

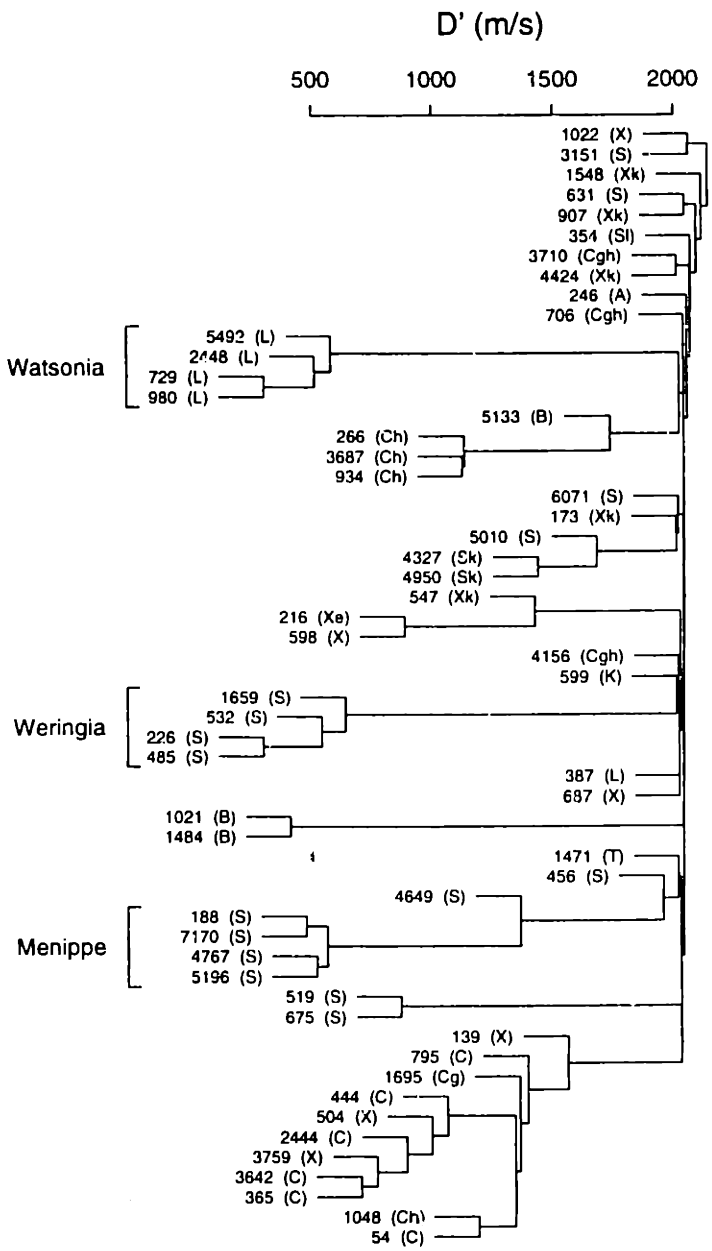

Figure 5.33: Similar to Figure 5.11, but for 56 SMASSII asteroids contained in zone 8. Dissimilarity s_2 was used, with a spectral cutoff of $\varepsilon = 0.6$. The loci of the Menippe, Watsonia, and Weringia families are marked. While the loci for all three groups appear to be very isolated, this changes quickly as the value of ε is increased. In particular, other surrounding K- and L-type asteroids begin to merge with the Watsonia family at higher levels of D'.

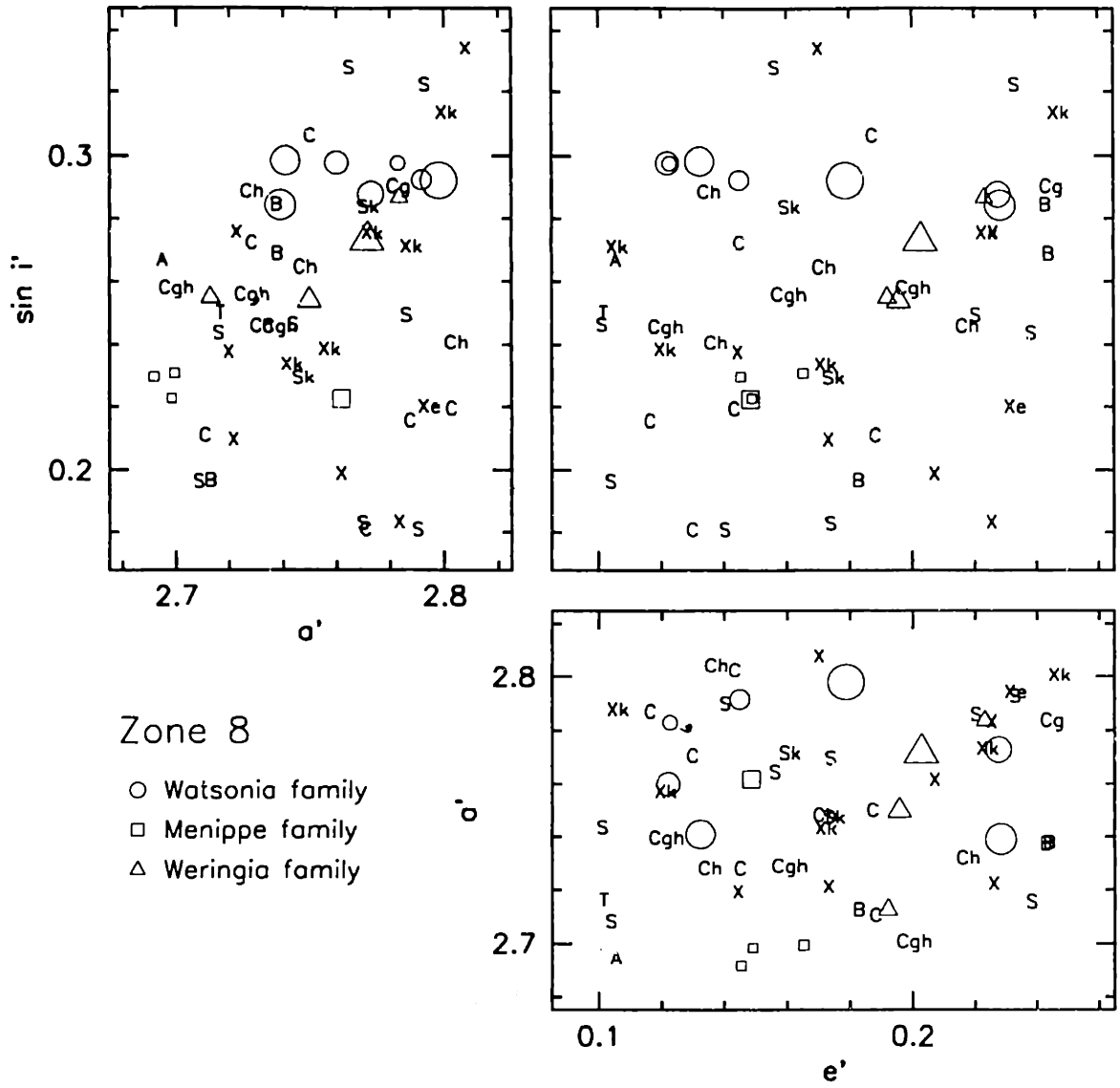

Figure 5.34: Similar to Figure 5.12. Pairwise plots for zone 8, showing the locations of Menippe, Watsonia, and Weringia family members.

strong, and in the case of the Watsonia and Menippe families, additional asteroids outside of the locus help provide a much clearer picture of the true nature of these families. The asteroids forming the loci of all three families are marked in the dendrogram shown in Figure 5.33, and in the pairwise plots of proper element space shown in Figure 5.34.

Watsonia family - *The Watsonia family contains seven SMASSII asteroids that are spectrally similar, and distinct from the background, being primarily classified as L-types. The observed members are all relatively large, lower-numbered asteroids, and are very dispersed in proper elements, suggesting this may be the remaining remnants of an older collisional event. This family was proposed by Burbine et al. (1992) based on the unusual spectral properties of asteroids 387 Aquitania and 980 Anacostia.*

The locus of the Watsonia family is a very isolated grouping, due in part to the high orbital inclinations of its members, with sin $i' \sim 0.30$. The four asteroids making up this locus are classified as L-types. They are spectrally very similar, but stand out as relatively unique against the background population that consists of a mixture of C-, S-, and X-types. The clustering solution for this locus is stable over the intervals in ε of 0.8 - 1.9 and 0.6 - 1.9 for the dissimilarities s_1 and s_2, respectively, and has a maximum single linkage of $D' \sim 510$ m/s. In addition to these four locus members, there are three other asteroids observed during the SMASSII survey that are spectrally similar to Watsonia, but which are more widely dispersed in orbital eccentricity: 354 Eleonora (an Sl-type), 387 Aquitania (L-type), and 599 Luisa (K-type). To include these three asteroids as members of the Watsonia family, the boundary of the family must be expanded to cover the interval in eccentricity of $0.122 \leq e' \leq 0.228$, while the range in inclination remains much more tightly constrained by $0.284 \leq \sin i' \leq 0.299$. Adding these three asteroids to the family also increases the maximum single linkage value to $D' \sim 1250$ m/s. This large dispersion of family members, with $\Delta\varepsilon \sim 0.1$ and relative velocities in excess of 1 km/s, is comparable to that found for members of the Pallas family. The Vesta family also contains fragments whose relative ejection velocities are in excess of 1 km/s (Binzel *et al.* 1999a). By expanding the family boundary to include 354 Eleonora, 387 Aquitania and 599 Luisa, the S-type asteroid 1659 Punkaharju is also introduced, a spectral interloper that is included as a member of the adjacent Weringia family which is described below. The spectra of all seven members of the Watsonia family are plotted in Figure 5.35. This family was proposed by Burbine *et al.* (1992) who noted the spectral similarities and orbital proximity of 387 Aquitania and 980 Anacostia. Burbine *et al.* also suggested that 599 Luisa and 729 Watsonia may be members of this potential family, based solely on orbital similarities.

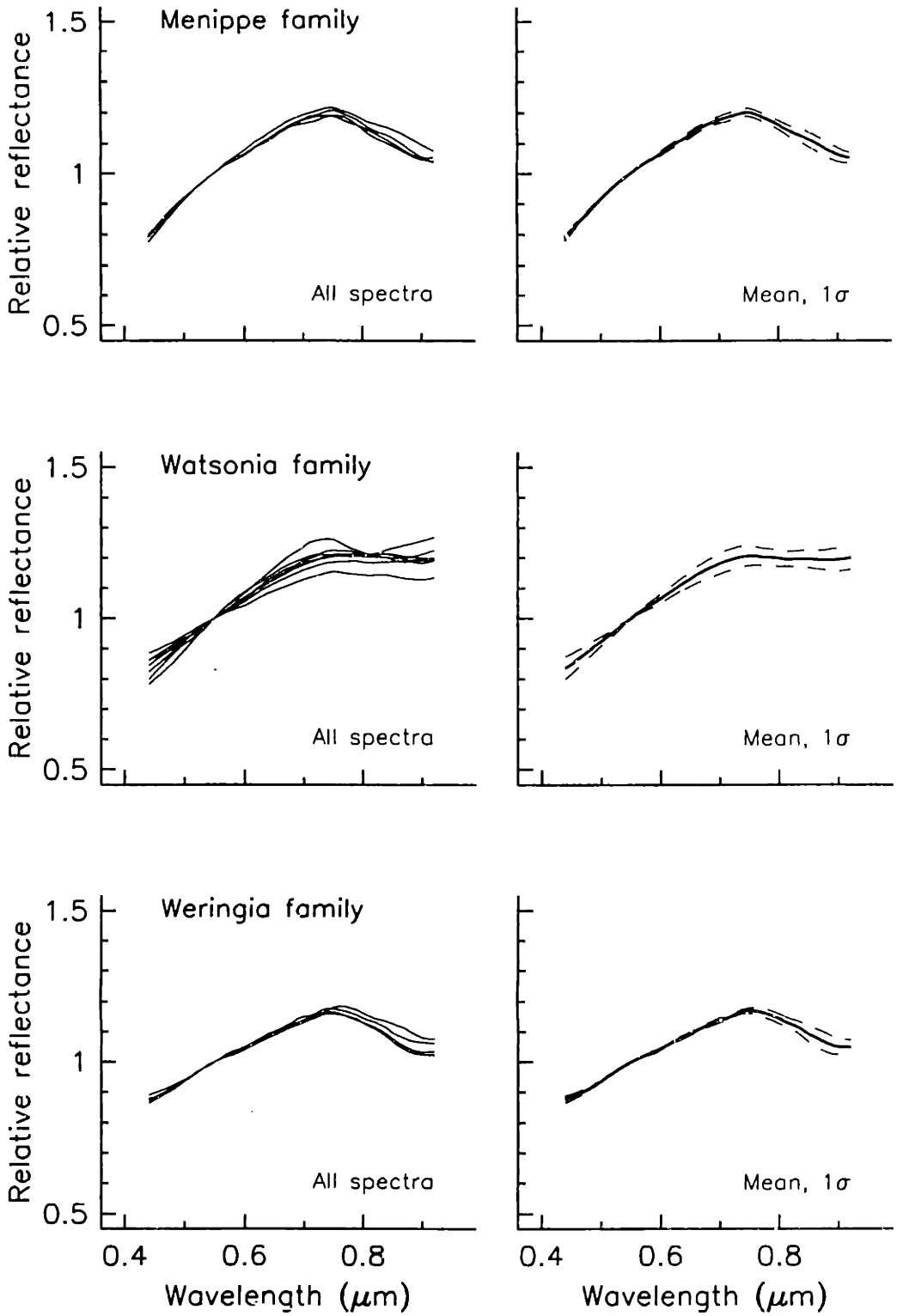

Figure 5.35: Similar to Figure 5.13, showing the spectra of 4 Menippe family members, 7 Watsonia family members, and 4 Weringia family members.

Menippe family - *The Menippe grouping is a cluster of four spectrally identical S-type asteroids observed during SMASSII. The three smaller members of this group (excluding 188 Menippe) are recognized as members of the Eunomia family (Zappalà et al. 1995), which is located just outside of our sample region. This "Menippe family" is probably an artifact of the boundaries defined for our survey, and I suggest that 188 Menippe might actually be a widely separated member of the Eunomia family.*

We identify a grouping of four S-type asteroids that are spectrally very similar, and associated with the large asteroid 188 Menippe. This grouping remains constant over the ranges of spectral dissimilarity given by $0.5 \leq \varepsilon \leq 1.0$ and $0.6 \leq \varepsilon \leq 1.4$, using s_1 and s_2, respectively. While this small Menippe cluster is very robust, it is probably an artifact related to the much larger Eunomia family that lies just outside of the inner edge of our survey region. The three smaller asteroids in this cluster, 4767 1987 GC, 5196 Bustelli, and 7170 1987 MK, are all identified as Eunomia members in the HCM results of Zappalà *et al.* (1995), while 188 Menippe is listed as a background (non-family) asteroid. In Figure 5.34, the locations of these four asteroids are plotted in proper element space. A dynamical family associated with Menippe was initially suggested by Bowell (private communication) based on a clustering in the distribution of a' versus sin i' in the proper elements of Milani and Knežević (file version 6.8.5), but this grouping was not formally recognized by Zappalà *et al.* (1995)

The Eunomia family is bounded in eccentricity by the interval $0.127 \leq e' \leq 0.170$ and in inclination by $0.223 \leq \sin i' \leq 0.241$ (Williams 1992, family 140), consistent with the Menippe cluster we have defined. While sampling the Eunomia family was not a high priority during the SMASSII survey, we did obtain spectra of 17 objects identified as family members by Zappalà *et al.* (1995) based on their HCM analysis. The SMASSII spectra reveal a mixture of taxonomic types among the purported Eunomia members, but there is a narrow core of asteroids, bounded by $0.145 \leq e' \leq 0.165$ and $0.222 \leq \sin i' \leq 0.238$ that are spectrally very similar to our Menippe family members. This suggests that 188 Menippe might be genetically related to this core of objects within the Eunomia family. Recent work by Lazzaro *et al.* (1999) shows the Eunomia family to be primarily composed of S-type asteroids, and that only a small number of spectral interlopers exist within the family boundary. While the range of spectral variation among the Eunomia S-types observed by Lazzaro *et al.* is somewhat larger than we observed in our more

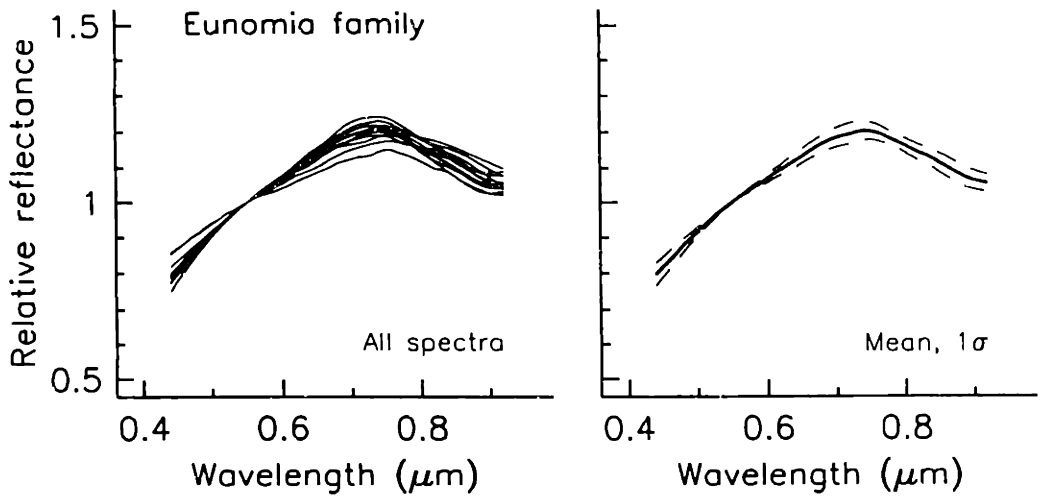

Figure 5.36: Similar to Figure 5.13, but showing a total of 13 SMASSII spectra for S-type asteroids belonging to the Eunomia family. This plot includes the spectra of 4767 1987 GC, 5196 Bustelli, and 7170 1987 MK, three members of the Menippe grouping that we have recognized in our analysis, but which are identified as members of the Eunomia family (Zappalà *et al.* 1995). The spectrum of 188 Menippe is also included.

limited sample, the results from these two spectral surveys are very consistent. In Figure 5.35, the spectra are plotted for the four asteroids we identify within the Menippe cluster. For comparison, I have replotted these four objects, along with the remaining Eunomia S-types observed during SMASSII, in Figure 5.36.

Weringia family *- The Weringia family consists of four SMASSII asteroids that are spectrally nearly identical S-types. These asteroids are very dispersed in proper element space, making this a relatively uncertain grouping. All four members are lower-numbered asteroids, suggesting that these may the be larger remaining remnants of an older disruption event. There are no previous identifications of a Weringia family.*

The Weringia family is the most uncertain of the three groupings identified in zone 8. The four S-type asteroids included in the locus of this family are spectrally very similar, as shown in Figure 5.35, and form a very isolated cluster for small values of ε, as seen in Figure 5.33. The clustering solutions for the Weringia locus are stable for both s_1 and s_2 over the interval of $0.5 \leq \varepsilon \leq 0.7$, with a maximum single linkage of D' ~ 630 m/s. As ε is increased, however, additional asteroids merge into the clustering solution, including the K-type asteroid 599 Luisa, which is a member of the adjoining Watsonia family. No other SMASSII asteroids were observed within the boundary of the Weringia

locus. The significance of the Weringia locus as a spectrally isolated grouping is tested by searching the background population, extending outside of zone 8, for any asteroids that are spectrally similar to the locus members. This was the same approach used to estimate the robustness of the Thisbe family in zone 7. We find that the nearest asteroid with a spectral signature similar to the Weringia family members is separated from this locus by a value of D' ~ 1.9 km/s. This isolation from spectrally similar background objects suggests that the Weringia grouping is significant. The fact that all the observed members are larger, lower numbered asteroids may be indicative of the age of the Weringia family, where over time, the smaller members of the family have been collisionally ground down, while the larger surviving members have been dispersed in proper element space through mutual collisions or other dynamical processes.

5.5 Secondary analysis of the background

Fifteen primary families, accounting for a total of 177 asteroids (38% of the 465 asteroids making up our total sample), were identified during the first phase of our analysis, described in section 5.4. These fifteen groupings were sufficiently well represented in the different clustering solutions that a consistent locus of objects was identified as the core membership for each of these families. A well-defined locus appears when a group of asteroids is relatively isolated, both spectrally and physically (in orbital space), from the surrounding background. From the previous discussions of the individual families, it is clear that there are different degrees of isolation, and correspondingly, different levels of certainty with which these families can be described. Families like Astrid and Hoffmeister have very well determined memberships and boundaries based on the SMASSII sample. By comparison, families such as Lydia or Watsonia have more poorly determined boundaries, even though the reality of these families as being genetic associations is strongly supported by our spectral observations. In our search for asteroid families, even more tenuous groupings of objects were identified. These groupings may represent true genetic associations, but were difficult to define because a unique locus of objects could not be readily identified.

To test the reality of these secondary clusters of asteroids, and potentially add them to our list of families between 2.7 and 2.8 AU, I repeated the hierarchical cluster analysis, including only those 272 background asteroids that remained after the original fifteen families had been identified. This set of 272 asteroids does not include any

objects with $e' > 0.3$ or $\sin i' > 0.3$. Again, a series of clustering solutions were generated for both dissimilarities s_1 and s_2 by incrementing the value of ε. Since all members of the major families have been removed, these new clustering solutions reveal structures that are more subtle, and less convincing than those found during the initial analysis. The dendrogram representing one of these clustering solutions is shown in Figure 5.37. In this figure, four groupings are marked that appear significant, and consistent enough over a range of ε to be considered as potentially real associations. Because the objects included in each of these four groupings are dispersed over a large volume of proper element space, their clustering solutions are generally unstable with changes in ε. For each of these groupings, the same set of asteroids will tend to cluster together, but the order of linkage and the exact membership of the grouping may vary for consecutive values of ε. This makes it difficult to determine a unique locus of objects based on the criteria used in defining the first fifteen families. The approach used in describing these four additional groupings is, therefore, more qualitative and subjective. A magnified view of the lower half of Figure 5.37 is presented in Figure 5.38.

The clustering solutions for each of the four groupings were inspected over the range of $0.5 \leq \varepsilon \leq 1.5$, and those asteroids that were most commonly included as members of the group were considered part of the locus. The volume of proper element space containing this locus was then inspected for interlopers. If the number of spectral interlopers was ≤ 1, the family boundary was expanded to include the next closest asteroid that had been identified in the cluster analysis. This process was continued until the number of interlopers became greater than 1. To be considered a spectral interloper in this part of the analysis, the asteroid has to be a member of this background population of 272 objects. If an asteroid had already been identified as belonging to one of the fifteen primary families, it could be located inside the boundary of the newer grouping, but would not be considered an interloper, since its relationship to the primary family had already been established. This allowed for the identification of families whose boundaries overlap. In Figures 5.39, 5.40 and 5.41, the locations of these families are plotted in the e' versus a', $\sin i'$ versus a', and $\sin i'$ versus e' planes of proper element space.

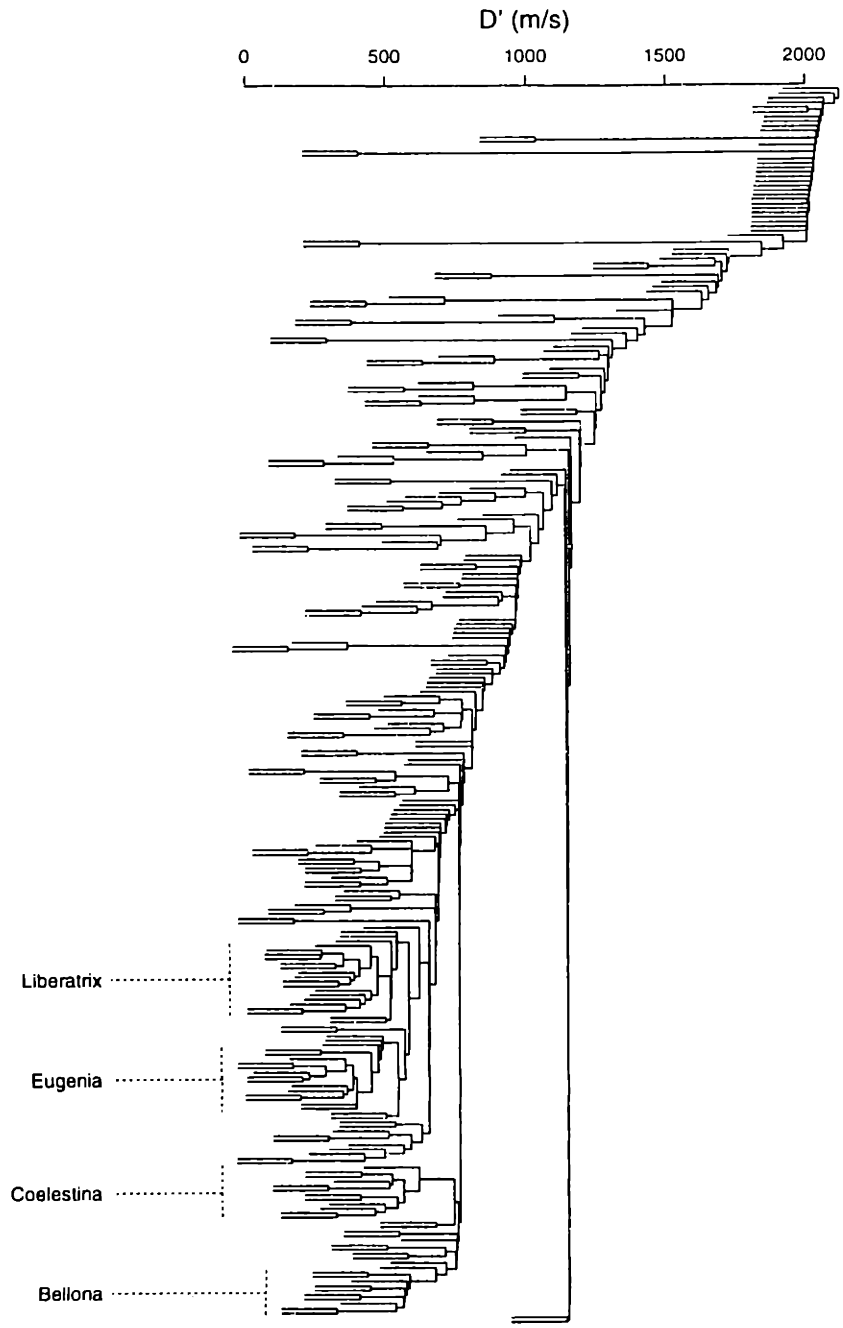

Figure 5.37: Dendrogram showing a hierarchical clustering solution for 272 background objects (after the primary family members have been identified, and removed). Only those background asteroids with $e' < 0.3$ and $\sin i' < 0.3$ have been included. This solution is based on the dissimilarity s_1, and uses a spectral cutoff of $\varepsilon = 0.8$. For clarity, the individual object labels have been omitted. Instead, the four most prominent groupings are marked with the family names of Bellona, Coelestina, Eugenia, and Liberatrix. Dotted lines are used to denote the interval for each family, signifying an uncertainty in the exact boundaries for these groups. These clusters are relatively unstable, with no unique subset of objects defining a consistent locus as ε is varied.

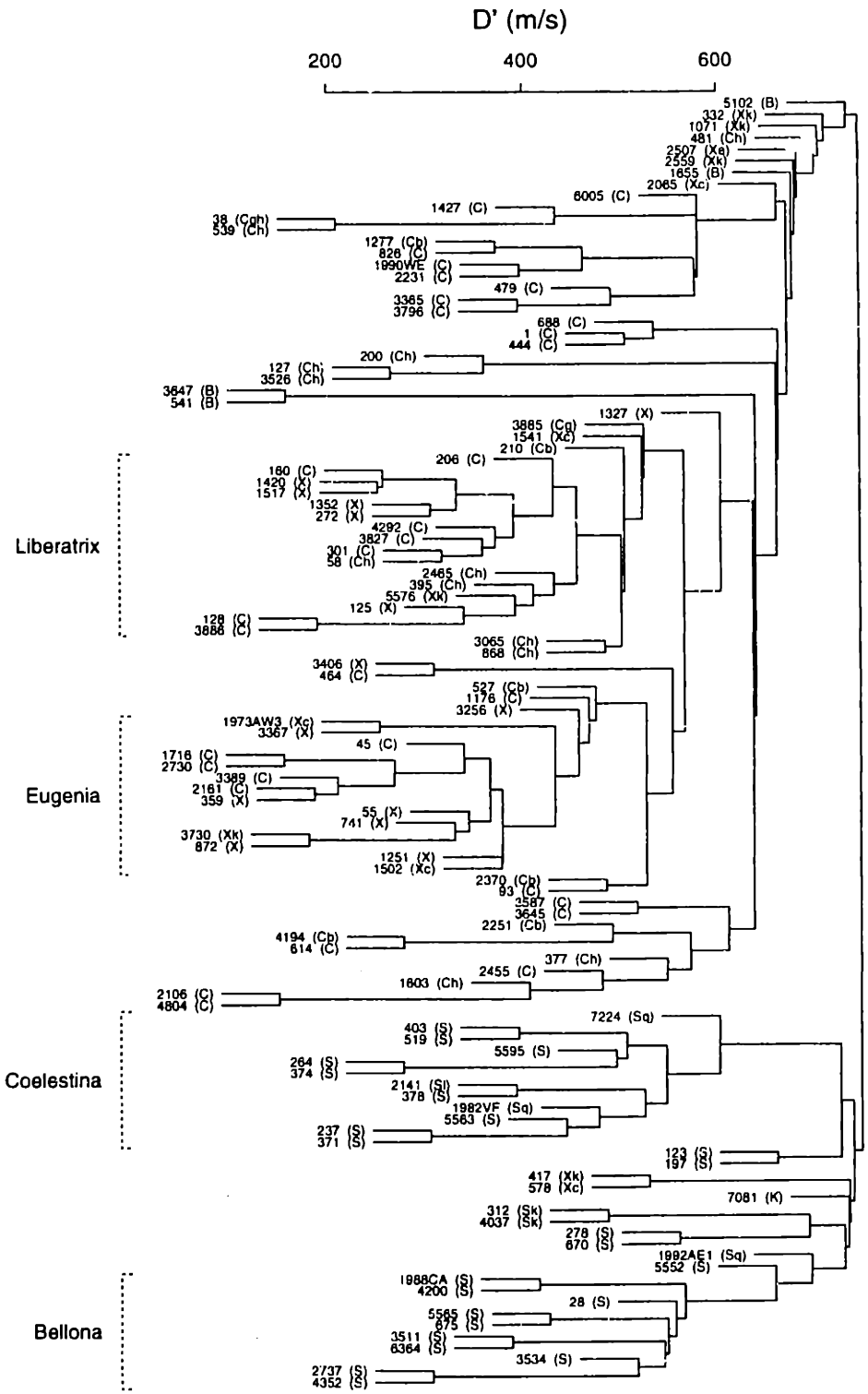

Figure 5.38: A magnified view of the lower half of Figure 5.37, where individual asteroids have been labelled.

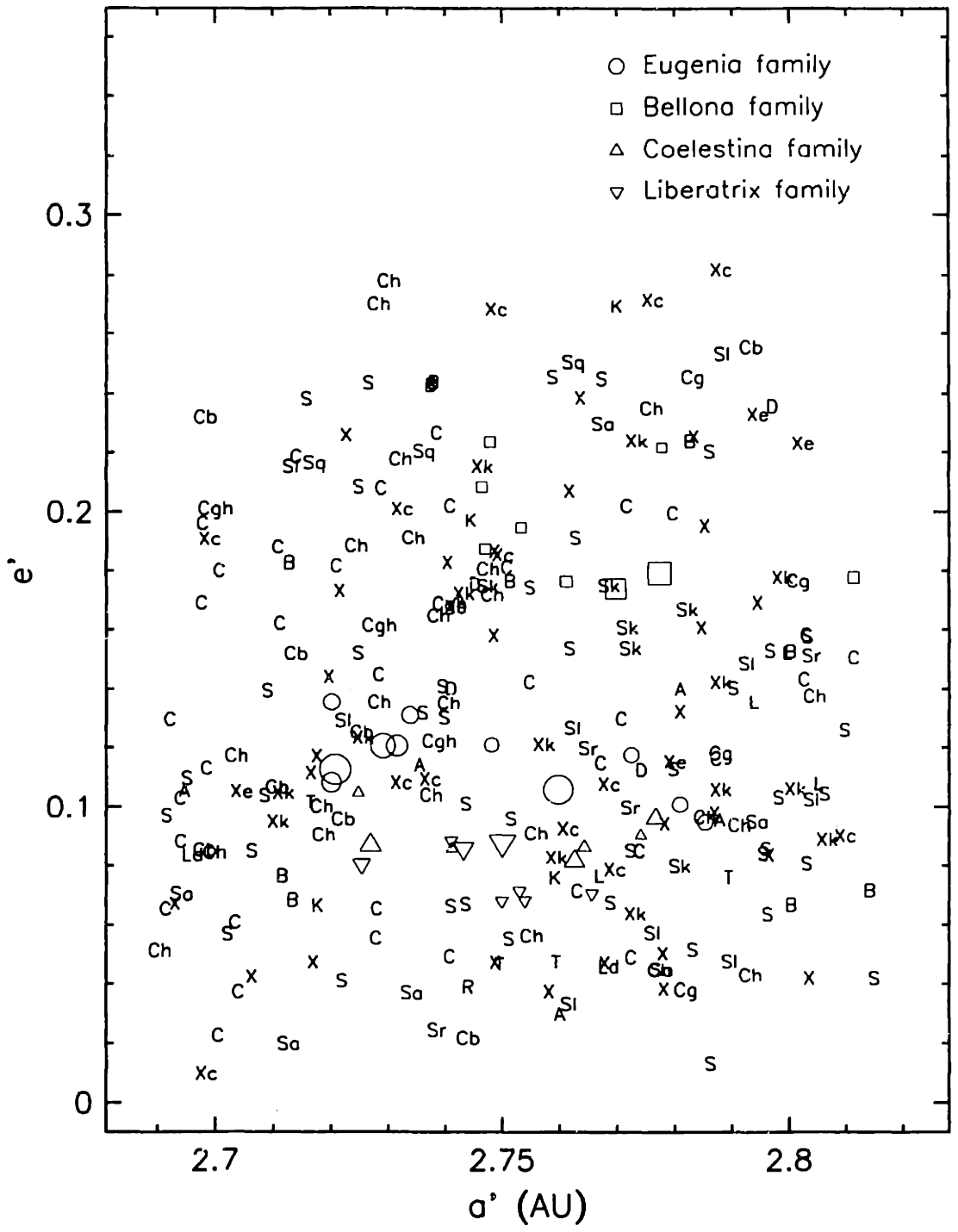

Figure 5.39: Plot of the proper element plane e' versus a', where a total of 272 objects are plotted. Only those asteroids with $e' < 0.3$ and $\sin i' < 0.3$ have been included. Of this subset of SMASSII asteroids, 35 have been identified as belonging to secondary families. Objects belonging to the Bellona, Eugenia, Coelestina and Liberatrix families are plotted as open symbols, where the size of those symbols has been scaled by the cube-root of the asteroid diameters.

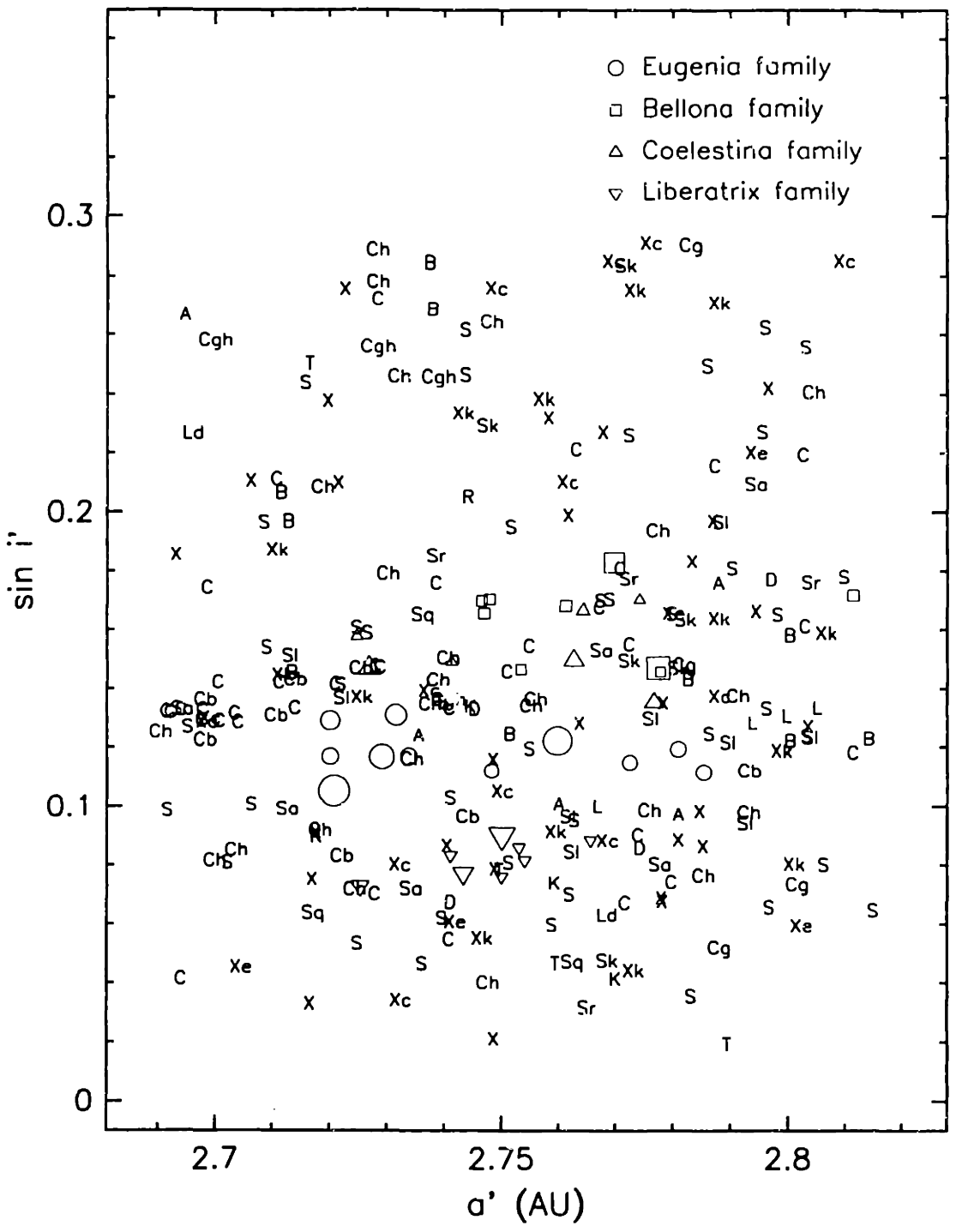

Figure 5.40: Similar to Figure 5.39, but showing the proper element plane of sin *i'* versus *a'*.

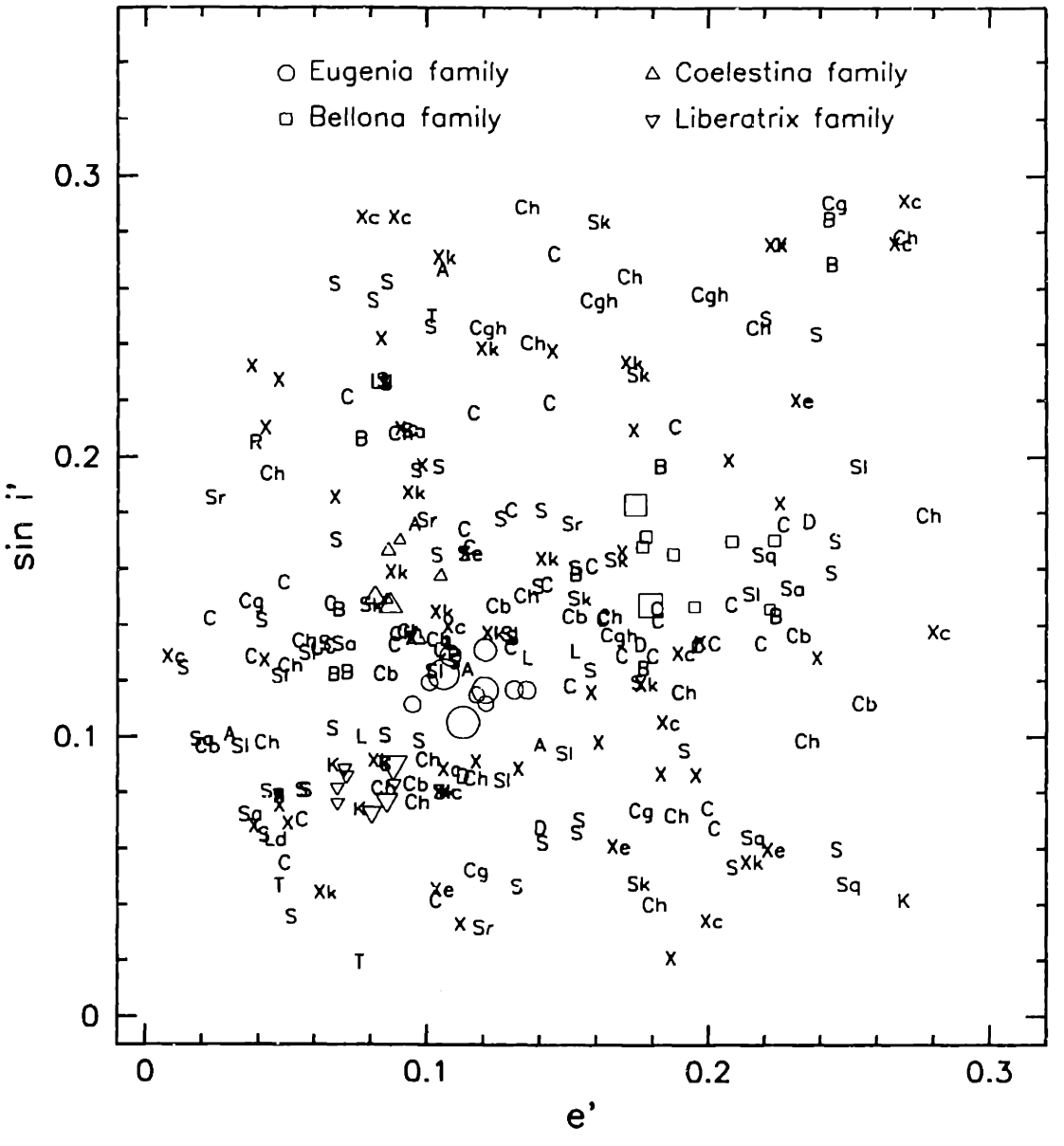

Figure 5.41: Similar to Figure 5.39, but showing the proper element plane of sin *i'* versus *e'*.

Eugenia family *- Eleven SMASSII asteroids are included in the Eugenia family. These asteroids are spectrally similar, even though they straddle the taxonomic boundary between the C- and X-complexes. These objects are moderately dispersed in proper element space, and blend into a background population that also contains a significant fraction of C- and X-type asteroids. While I believe this grouping to be a real genetic association, its boundary is very difficult to define. The Eugenia family had been previously proposed by Williams (1979, 1989, 1992).*

Of the four secondary groupings, the Eugenia family is the most robust, with seven asteroids making up a locus that is quasi-stable over the intervals of ε of 0.6 - 0.9 and 0.5 - 1.5 for the dissimilarities s_1 and s_2, respectively. The maximum single linkage connecting members within this locus is D' ~ 450 m/s. The spectra of these asteroids are very similar, as shown in Figure 5.42, while the taxonomic classes assigned to these objects straddle the division between the C- and X-complexes. One interloper is identified within the boundary of this locus based on the SMASSII sample, the A-type asteroid 2715 Mielikki. By slightly expanding the boundary of this family in all three dimensions, four additional asteroids can be included as members of the Eugenia family, reducing the maximum single linkage to D' ~ 360 m/s. These four asteroids are spectrally very similar to the locus members except for minor increases in the average spectral slope, with the X-type 55 Pandora being the reddest of the family members. These variations in spectral slope are relatively small, however, compared with the range of slopes encountered in many of the primary families. The inclusion of 2715 Mielikki (A-type) within the boundary of this family is intriguing, and raises the question of whether the Eugenia family might be fragments of a differentiated parent. Tholen (1984) classified both 55 Pandora and 872 Holda as M-type asteroids based on their moderately-high albedo, though Jones *et al.* (1990) showed 55 Pandora to be hydrated, inconsistent with this being a fragment of a metallic core. Williams (1989, 1992) identified this grouping as a dynamical family (Williams family 133), providing a membership that very closely matches our definition of the Eugenia family except that Williams does include the S-type asteroid 197 Arete as a potential member.

Coelestina family - *The Coelestina family contains seven SMASSII asteroids. These objects are spectrally similar S-types, though there is some variation among the members in their average spectral slopes that appears to be size dependent. These asteroids are moderately dispersed in proper element space, and blend with other S-types in the background, making it difficult to accurately define the family boundary. This family was identified by Zappalà et al. (1995) based on results from the WAM analysis.*

The Coelestina family is a grouping of seven asteroids belonging to the S-complex that is reasonably stable over the intervals of $0.7 \leq \varepsilon \leq 1.1$ and $0.9 \leq \varepsilon \leq 1.3$ for the dissimilarities s_1 and s_2, respectively, and has a maximum single linkage of D' ~ 530 m/s. Within the boundary of this locus in proper element space, there is one interloper,

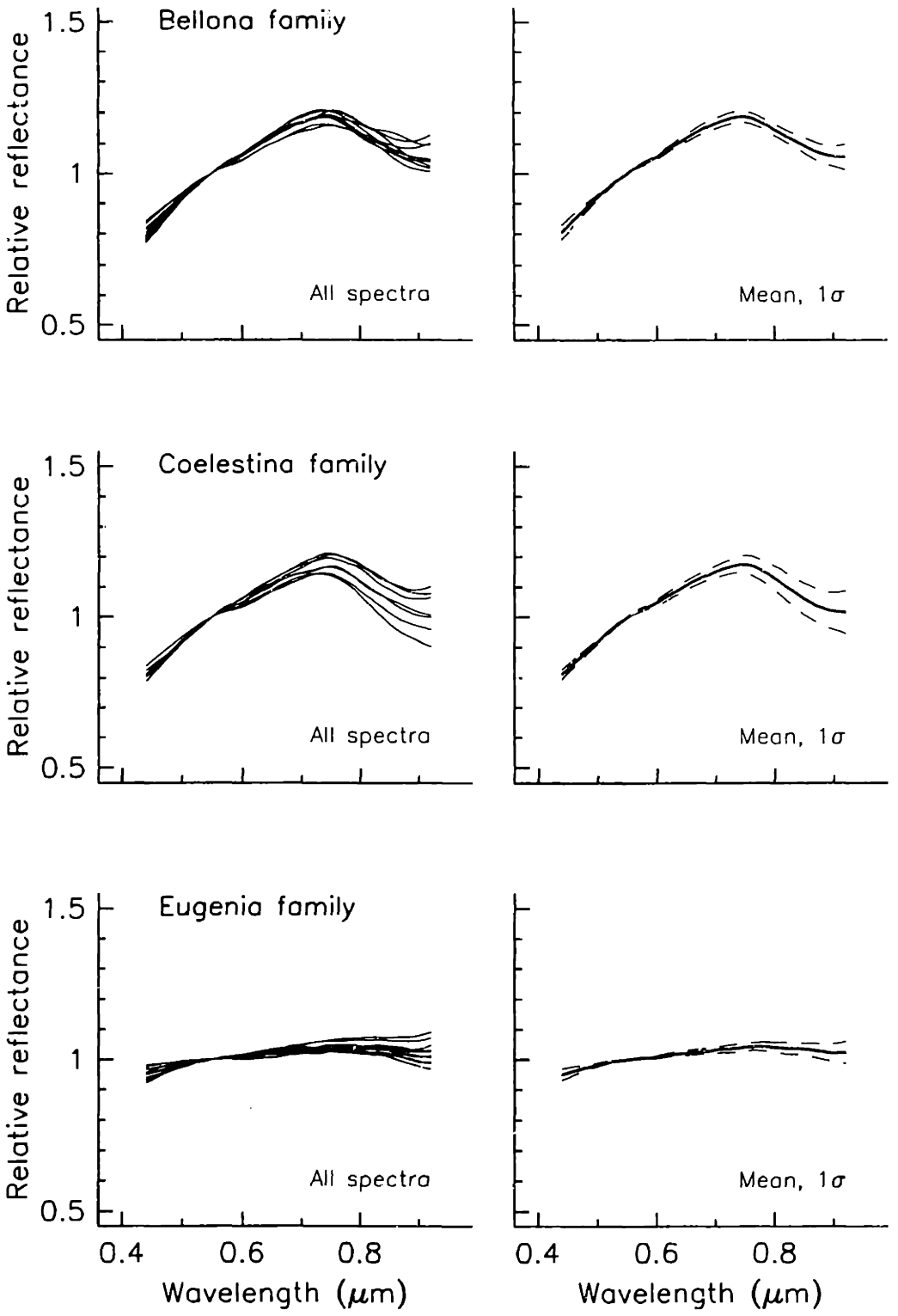

Figure 5.42: *Similar to Figure 5.13, showing the spectra of 9 Bellona family members, 7 Coelestina family members, 11 Eugenia family members, and 8 Liberatrix family members.*

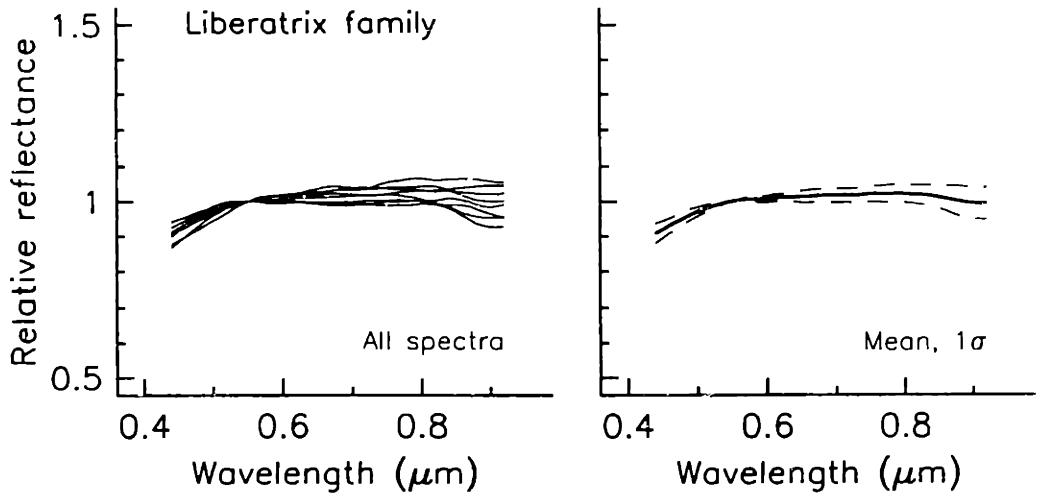

Figure 5.42: Continued

the Ch-type asteroid 127 Johanna. The spectra of the Coelestina members are very similar in shape, as seen in Figure 5.42, though there is a systematic offset in the height of the reflectance maxima (and correspondingly in the level of 1 μm minima) that appears to be size dependent. The three largest members of this family have the highest reflectance maxima while the smaller members (two of which are classified as Sq-types) have lower maxima. This size-dependent trend is consistent with that observed among the small S-type asteroids making up the near-Earth asteroid population (Binzel *et al.* 1996). The Coelestina family was identified in the WAM analysis of Zappalà *et al.* (1995), though the family suggested by Zappalà *et al.* is smaller, and only partially overlaps the Coelestina family grouping that we have identified based on the SMASSII spectra.

Bellona family *- The Bellona family consists of nine SMASSII asteroids that are spectrally very similar S-types. This family probably is a real genetic association, though these asteroids are moderately dispersed in orbital space, and blend with other S-types in the background. The boundary of the Bellona family encloses the four members of the Phaeo family, raising the question of whether the Phaeo and Bellona groupings might represent different layers of a differentiated parent. There are no previous identifications of a Bellona family.*

The Bellona family is characterized by a locus of five spectrally very similar S-type asteroids that are identified as a part of a larger grouping in the clustering solutions bounded by $0.8 \leq \varepsilon \leq 0.9$ (using dissimilarity s_1) and $0.9 \leq \varepsilon \leq 1.2$ (based on s_2). These five particular asteroids are chosen as the locus because they occupy the smallest volume of proper element space, without including any other spectral interlopers. The boundary of this locus is defined by $0.174 \leq e' \leq 0.187$ and $0.147 \leq \sin i' \leq 0.183$. However, the Bellona family is undoubtedly much larger, with several additional asteroids, all spectrally very similar S-types, appearing in both sets of clustering solutions. By extending the upper boundary in eccentricity to $e' \leq 0.224$, four other SMASSII asteroids can be included in the Bellona family, though one spectral interloper, the C-type asteroid 1427 Ruvuma, is also introduced. The maximum single linkage for these nine family asteroids is D' ~ 660 m/s. In addition to the interloper 1427 Ruvuma, this expanded boundary for the Bellona family also encloses the entire Phaeo family of X-type asteroids. This is the only case found between 2.7 and 2.8 AU for one family, the Bellona grouping, completely encircling a smaller family, the Phaeo grouping. It can be argued that there may be a genetic link between these two groupings, with the Phaeo family representing the metallic core and the Bellona family being fragments of the silicate crust of a differentiated parent. To support such an argument, however, more extensive physical studies of both families are needed, as well as a more secure understanding of the mineralogy associated with these different spectral types. For now, I treat these two families as two independent collisional events. The spectra of all nine Bellona family members are plotted in Figure 5.42.

Liberatrix family *- Eight SMASSII asteroid are contained in the Liberatrix family. These objects are primarily classified as C-types, though there is a moderate degree of spectral variation between them. This grouping is adjacent to both the Lydia and Hoffmeister families in proper element space, but appears to be spectrally distinct from both of these families. The genetic reality of this Liberatrix family is difficult to judge based on the limited number of objects in our sample. Members of this group are divided among various families identified by Zappalà et al. (1995), though Williams (1989, 1992) does recognize most of this grouping as part of his Concordia family (Williams family 132).*

The Liberatrix family is probably the least robust of the four families described here. This cluster of objects is located in zone 6, but is clearly separate from the four primary families in this zone. The locus consists of seven asteroids, mainly classified as C-types, whose spectral signatures show a moderate degree of variation, as seen in Figure 5.42. The Liberatrix locus can be traced through the clustering solutions derived from both dissimilarities s_1 and s_2 over the range in ε from 0.7 to 1.5, but this group is not well isolated from the background population of C-types, leading to many potentially spurious linkages with background objects as ε is varied. The Liberatrix family asteroids have slopes that are generally shallower than those found among the Lydia family members, and have UV drop-offs that are steeper than those observed among the Hoffmeister family asteroids, making the Liberatrix family asteroids spectrally distinct from the two nearby families that are comprised of C- and X-type objects. Similar to both the Hoffmeister and Lydia families, however, the smaller Liberatrix family asteroids do tend to have shallow 0.9 μm absorption features. By slightly extending the outer edge of the family boundary in semimajor axis, an additional asteroid, 4342 Freud, can be added to the Liberatrix family, though expanding this boundary does introduce one interloper, the K-type asteroid 6704 1988 CJ. The maximum single linkage for all eight members of the Liberatrix family is D' ~ 370 m/s. Williams (1989, 1992) identified family 132 in which the Ch-type asteroid 58 Concordia is the largest member, and which partially overlaps our Liberatrix grouping. Adding 58 Concordia to our Liberatrix family would require significantly expanding the family boundary in semimajor axis, though no new spectral interlopers from the SMASSII sample would be introduced. The reason for not including 58 Concordia in our family is that it is spectrally distinct from the other Liberatrix members, particularly in the depth of its 0.7 μm absorption feature, though we cannot rule out a possible genetic tie between 58 Concordia and our Liberatrix family. Zappalà *et al.* (1995) recognized a Concordia family within the WAM results that, likewise, partially overlaps our Liberatrix grouping. Among the HCM results of Zappalà *et al.* (1995), members of our Liberatrix family are equally divided between the HCM families of Liberatrix, Lydia, and Nemesis.

5.6 Discussion

From the results presented in the previous two sections, we find that each of the small dynamical families sampled have members who share very common spectral characteristics, and conclude that these are all real genetic associations. Essentially

every dynamical family that had been previously identified between 2.7 and 2.8 AU appears to be a real spectral family, though the boundaries that were determined based purely on the statistical searches of proper elements were often inaccurate. Difficulties in determining the membership and boundary of a family, using only the cluster analysis of proper elements, occur when the members of the family are very dispersed (and therefore blend with the background population), or when two or more families are in close proximity in orbital space. Both of these scenarios reflect the limitations of the statistical approaches used.

Combining spectral information with the orbital parameters produces a noticeable enhancement of the groupings found in our hierarchical clustering solutions. This enhancement leads to more robust determinations of the family boundaries and memberships, even for families whose members are more widely dispersed. Still, there are limitations. Even by including the spectral information, we still find instances of families whose members have spectral signatures that are in common with those of the background asteroids. In this case, the spectral information adds little to improving the accuracy of the boundary determination.

The memberships and boundaries for all 19 families identified during this project are listed in Tables 5.1 and 5.2. In Table 5.1, the permanent numbers (or provisional asteroid designations) are given for all of the SMASSII asteroids identified as members of each family. Those asteroids defining the locus are listed first. If any additional members of the family were identified after the locus had been defined (by expanding the family boundary in proper elements), these objects are also listed, denoted by parentheses ( ). This table also identifies asteroids that are considered to be spectral interlopers. Those interlopers listed without parentheses reside within the boundary of the locus in proper element space, while those interlopers that were added by expanding the family boundary are shown in parentheses. Some of the interlopers are marked with an asterisk. These objects are identified as being members of other, adjacent families, and, as such, are listed elsewhere in the membership column. In the case of the Bellona family, all four Phaeo family members reside within the boundary of the Bellona family, and are therefore listed as spectral interlopers of the Bellona family.

Table 5.2 lists the boundaries for all 19 families as determined from our SMASSII sample. These boundaries are defined as intervals (ranges) of semimajor axis a', proper

Table 5.1: List of asteroid family members

Family	Members	Interlopers
Agnia	847, 1020, 1228, 2353, 2401, 3395, 3430, 3491, 3701, 4051, 4261, 5242, 5610, 6077, 7056, 7728	6704
Astrid	1128, 2169, 2852, 7817, 8008	
Bellona	28, 675, 2737, 4352, 5565, (3511), (3534), (5552), (6364)	(322)*, (1427), (1730)*, (2879)*, (5467)*
Chloris	410, 521, 1403, 1534, 1613, 5553, 5956, 6906, (6582)	
Coelestina	237, 371, 378, 5563, 5595, 7224, 1982 VF	127
Dora	668, 1414, 1734, 1795, 1836, 1970, 2598, 2807, 3563, 3611, 3630, 3775, 3829, 4135, 4343, 4584, 5243, 5348, 5416, 6129, 6233, 6283, 6509, 7110, 7402, 7512, (4534), (7405), (1992ST1)	
Eugenia	45, 359, 741, 1716, 2161, 2730, 3389, (55), (872), (3367), (1973 AW3)	2715
Gefion	1272, 1433, 1751, 1839, 2053, 2157, 2373, 2386, 2493, 2521, 2631, 2801, 2875, 2905, 2911, 2977, 3788, 3860, 3910, 4096, 4182, 4702, 5159, 5401, 5622, 5685, 6078, 7211, 7397, 7451, 1984 CF, 1991 PE10, (716), (3853), (4417), (6211)	
Henan	1858, 2085, 2354, 3349, 3844, 4426, 4726, 4737, 5013, 7763, (1007), (3734), (4917), (5840), (1981 EL21)	3430*
Hoffmeister	1726, 2930, 2996, 4124, 5091, 5591, 6230, 6716, 6782	
Liberatrix	125, 128, 301, 2465, 3827, 3885, 4292, (4342)	(6704)
Lydia	110, 363, 1766, 2306, 2560, 3670, 5087, 5103, 1977 QL1, 1990 WA5	
Menippe	188, 4767, 5196, 7170	
Merxia	808, 1662, 2042, 2427, 4479, 6592, 1991 TW1, (2504), (3363)	(1987 UF5)
Pallas	2, 531, 1301, 1474, 1508, 2382, 3579, 3581, 4969, 5222, 5234, 5330, 5349, 5585, 5678, 5690	
Phaeo	322, 1730, 2879. 5467	
Thisbe	88, 213, 2816, 5344	2730*
Watsonia	729, 980, 2448, 5492, (354), (387), (599)	(1659)
Weringia	226, 485, 532, 1659	

Members of the locus are listed first, followed by additional members (in parentheses) that were identified once the locus had been defined. Those interlopers marked with an asterisk (*) are listed as members of another, adjacent family.

Table 5.2: Family boundaries

Family	Range in proper elements			Center of mass		
	a'	e'	sin i'	a'	e'	sin i'
Agnia	2.7590-2.8108	0.0663-0.0891	0.0625-0.0805	2.7906	0.0738	0.0689
Astrid	2.7805-2.7887	0.0470-0.0480	0.0115-0.0123	2.7851	0.0475	0.0119
Bellona	2.7470-2.8113 (2.7465-2.8113)	0.1739-0.1874 (0.1739-0.2235)	0.1472-0.1830 (0.1458-0.1830)	2.7732 (2.7649)	0.1793 (0.1956)	0.1677 (0.1629)
Chloris	2.7121-2.7417 (2.7121-2.7780)	0.2484-0.2593 (0.2484-0.2638)	0.1460-0.1610 (0.1460-0.1610)	2.7296 (2.7356)	0.2543 (0.2555)	0.1545 (0.1544)
Coelestina	2.7247-2.7767	0.0816-0.1048	0.1354-0.1702	2.7529	0.0906	0.1546
Dora	2.7687-2.7968 (2.7687-2.8001)	0.1929-0.1985 (0.1858-0.2040)	0.1339-0.1382 (0.1339-0.1443)	2.7870 (2.7874)	0.1959 (0.1960)	0.1363 (0.1368)
Eugenia	2.7201-2.7725 (2.7201-2.7853)	0.1083-0.1355 (0.0948-0.1355)	0.1052-0.1290 (0.1052-0.1310)	2.7366 (2.7474)	0.1216 (0.1155)	0.1162 (0.1177)
Gefion	2.7836-2.8139 (2.7570-2.8139)	0.1248-0.1425 (0.1203-0.1450)	0.1532-0.1634 (0.1358-0.1634)	2.7963 (2.7949)	0.1326 (0.1324)	0.1583 (0.1576)
Henan	2.6953-2.7621 (2.6953-2.7621)	0.0545-0.0809 (0.0545-0.0809)	0.0489-0.0678 (0.0478-0.0678)	2.7306 (2.7300)	0.0683 (0.0683)	0.0566 (0.0569)
Hoffmeister	2.7800-2.7906	0.0459-0.0488	0.0749-0.0767	2.7847	0.0471	0.0759
Liberatrix	2.7253-2.7540 (2.7253-2.7656)	0.0682-0.0885 (0.0682-0.0885)	0.0727-0.0902 (0.0727-0.0902)	2.7455 (2.7483)	0.0778 (0.0768)	0.0808 (0.0819)
Lydia	2.7320-2.7499	0.0311-0.0503	0.0884-0.0942	2.7441	0.0421	0.0916
Menippe	2.6916-2.7618	0.1454-0.1652	0.2224-0.2307	2.7090	0.1522	0.2266
Merxia	2.7406-2.7577 (2.7406-2.7773)	0.1311-0.1385 (0.1254-0.1385)	0.0845-0.0926 (0.0606-0.0926)	2.7506 (2.7547)	0.1355 (0.1335)	0.0872 (0.0825)
Pallas	2.7138-2.7966	0.3555-0.4619	0.4627-0.5173	2.7597	0.4044	0.4831
Phaeo	2.7678-2.8050	0.1895-0.1984	0.1587-0.1716	2.7856	0.1943	0.1635
Thisbe	2.7028-2.7682	0.1315-0.1455	0.0997-0.1211	2.7317	0.1407	0.1135
Watsonia	2.7409-2.7917 (2.7390-2.7980)	0.1221-0.1449 (0.1221-0.2283)	0.2924-0.2984 (0.2843-0.2984)	2.7716 (2.7706)	0.1303 (0.1604	0.2965 (0.2934)
Weringia	2.7128-2.7834	0.1920-0.2232	0.2539-0.2868	2.7530	0.2040	0.2673

eccentricity e', and proper inclination sin i'. For those families defined entirely by the locus, and for which no other members were added, there is only one boundary listed. For those families in which other members were included, in addition to the locus, two boundaries are given. The boundary defined by the locus is listed first, while the expanded boundary (containing all members of the family) is listed below, denoted by parentheses. An approximate center of mass has also been calculated for each family. The center of mass was determined separately for each element, using the absolute magnitudes, H, and assuming a constant albedo for all of the members. Again, only one center of mass is given for those families defined entirely by the locus, while two centers are listed for those families for which other members (in addition to the locus) have been included.

In Table 5.3, the distribution of taxonomic types is listed for each of the families. Statistics for IRAS albedo measurements are also given. An IRAS albedo is available for at least one member of every family, except for the Henan family. A cursory examination of this table reveals the similarities of spectral classes within each family, consistent with the similarities in spectral properties discussed in the earlier sections. These distributions have been displayed in Figure 5.43, where bar plots have been constructed for each family. A consistent scaling has been used throughout this plot, so that the numbers of objects can be easily intercompared between the families. The ordering of the families, and of the spectral classes, has been carefully chosen to best depict the continuum between spectral types.

Two general observations can be made from Figure 5.43. First, all three of the spectral complexes (the C-, S-, and X-complexes) appear capable of family formation. Asteroids belonging to the S-complex appear to be most associated with family formation (55% of S-complex members are identified as belonging to families), while 49% of the C-complex asteroids are found to be family members, and just 24% to the X-complex asteroids are identified with families. Those asteroid types that are least represented among the background population (the T-, D-, R-, A-, and Sa-types) do not contribute any members to the families we have defined. Somewhat surprisingly, no Xk-types are found among these families, even though the Xk-types are spectrally intermediate between the Xc- and K-type asteroids, and are well represented in our SMASSII sample. Secondly, there appear to be some strong divisions between spectral groups. In particular, the division separating the combined C- and X-complexes, and the

Table 5.3: Spectral classes and IRAS albedos of family members

Family	No. of obj.	Distribution of taxonomic classes	IRAS albedos			
			No.	Mean	High	Low
Agnia	16	S(7) Sq(7) Sk(1) Sr(1)	1	0.17	-	-
Astrid	5	C(4) Ch(1)	2	0.09	0.10	0.08
Bellona	9	S(9)	1	0.18	-	-
Chloris	9	Ch(4) Cgh(3) C(2)	5	0.07	0.11	0.05
Coelestina	7	S(5) Sq(2)	3	0.23	0.30	0.19
Dora	29	Ch(22) C(4) Cb(2) B(1)	10	0.06	0.09	0.04
Eugenia	11	C(5) X(5) Xc(1)	7	0.15	0.30	0.04
Gefion	36	S(31) Sl(2) Sr(2) Sk(1)	2	0.16	0.15	0.18
Henan	15	L(9) Ld(3) K(2) Sl(1)	0	-	-	-
Hoffmeister	9	C(4) Cb(3) B(1) Xc(1)	3	0.05	0.07	0.04
Liberatrix	8	C(4) Cg(1) Ch(1) X(1) Xc(1)	6	0.09	0.23	0.05
Lydia	10	X(7) C(2) Xc(1)	2	0.14	0.18	0.11
Menippe	4	S(4)	2	0.19	0.24	0.14
Merxia	9	Sk(3) Sq(3) S(2) Sr(1)	1	0.22	-	-
Pallas	16	B(10) C(5) Ch(1)	6	0.16	0.32	0.01
Phaeo	4	X(3) Xe(1)	2	0.07	0.09	0.05
Thisbe	4	B(4)	3	0.08	0.09	0.07
Watsonia	7	L(5) K(1) Sl(1)	6	0.16	0.19	0.13
Weringia	4	S(4)	4	0.18	0.21	0.17

S-complex is very strong, with no families being found to cross this boundary, even though in spectral component space, there is a non-negligible continuum of objects spanning this region. An important division is found between the "S-types" (including the S-, Sk-, Sq- and Sr-classes), and the K- and L-types. While there are a few Sl-types shown to span these two groups, the separation between the S-types and the K- and L-types among these families appears relatively strong, and suggests a real compositional

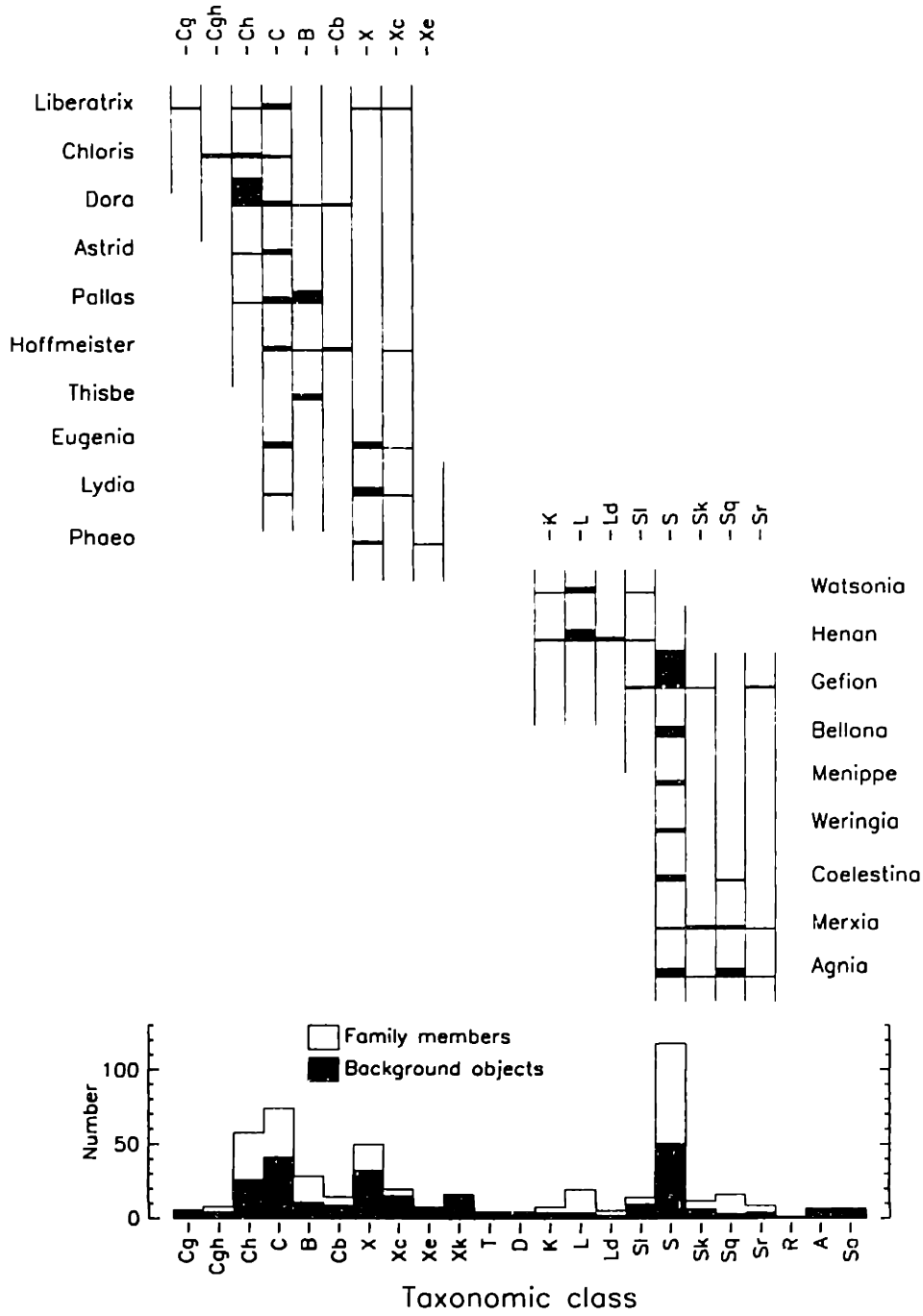

Figure 5.43: The upper portion of this plot shows the distribution of spectral types for all 19 families identified in the region between 2.690 and 2.815 AU, using those values listed in Table 5.3. The ordering of the families (and of the taxonomic classes) has been arranged so that the smoothest visual progression through the different spectral classes could be achieved. In the lower portion of this plot, a histogram shows the number of asteroids that are identified as family members from each of the taxonomic classes. No asteroids classified as Xk-, T-, D-, R-, A-, or Sa-types were included in any of the 19 families.

distinction between these two spectral types. By comparison, the division between the C- and X-complexes appears to be somewhat vague. Four families, the Liberatrix, Hoffmeister, Eugenia and Lydia families all consist of mixtures of C- and X-types, with the Eugenia family being evenly split between Cs and Xs. If five suspected outliers of the Lydia family were included as actual members, then the Lydia family would also consist of roughly equal numbers of C- and X-types. The association between C- and X-type asteroids in these families is supported by the range of IRAS albedo measurements for the family members. In particular, the Eugenia and Liberatrix families (where IRAS measurements exist for 7 and 6 of the members, respectively), show wide ranges in albedos. More detailed studies of the Eugenia and Liberatrix families (as well as the Lydia family) may help shed some light on the relationship between the C- and X-type asteroids.

The spectral similarities within each of these families suggest that they are "quasi-homogeneous" in nature. The variations that are observed can be traced primarily to differences in the average slopes of the spectra. This may indicate real mineralogical variations within the parent body, or might be explained by various surface alteration processes (regolith development or space weathering) or differences in observing geometry (phase reddening). While our cluster analysis is strongly biased towards finding groups of objects with similar spectra, a significant effort was made to search each of the groupings for spectral interlopers that might be genetically related to the family, and thus indicating the disruption of a differentiated body. The one association that stands out is the relationship between the Phaeo family (X-types), and the Bellona family (S-types). Both of these are widely dispersed families, but their approximate centers of mass are very similar. Another association that has been noted is the A-type asteroid, 2715 Mielikki, which is an interloper within the Eugenia family (made up of C- and X-types). The Eugenia family is a relatively dispersed family in proper elements, and so a single A-type within the family may be coincidental.

To search further for possible associations that might be remnants of differentiated parents, I preformed a separate cluster analysis, in which each family was represented by its calculated center of mass, and included all background asteroids classified as A-, R-, Sa- and Sr-types (a total of 17 asteroids). This cluster analysis was based on the Zappalà et al. metric D_1, and so contained no restriction on spectral variations. The

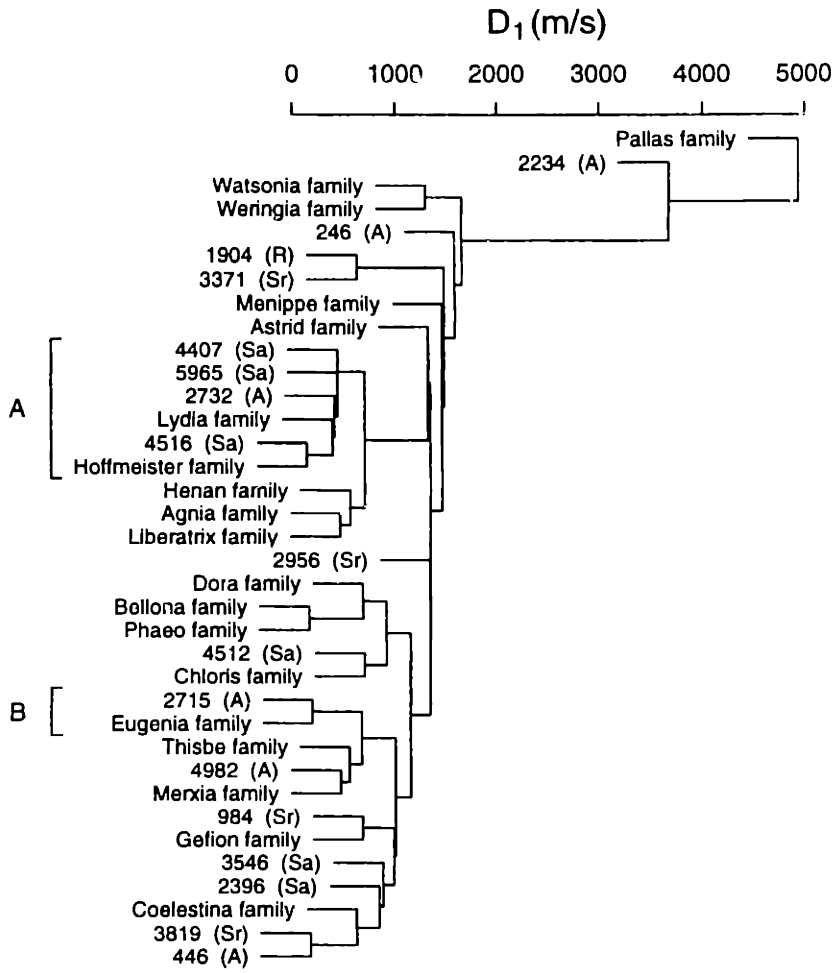

Figure 5.44: Clustering solution based on the center of mass for each of the 19 spectral families. Also included are 17 background asteroids that are classified as A-, R-, Sa-, and Sr-types. The Zappalà *et al.* metric D_1 (Eqn. 5.1) was used, so that no spectral information was included. This plot should reveal any close associations between our spectral families, and olivine-rich objects, which are assumed to be the remnants of differentiated parents. Two groupings stand out in particular. The group marked "B" shows the close proximity of the A-type asteroid 2715 Mielikki to the Eugenia family, as was discussed in section 5.5. The grouping marked "A" is more intriguing. Here, the Lydia family (composed primarily of X-type asteroids) is surrounded by four asteroids classified as A- or Sa-types, with a maximum single-linkage of $D_1 \sim 430$ m/s. This is the best example found within this region of the main belt for a possible family consisting of cosmochemically related fragments.

dendrogram for this clustering analysis is plotted in Figure 5.44. This plot clearly demonstrates the close relationships between families, such as the Phaeo and Bellona families, and the close proximity of the Henan, Agnia, and Liberatrix families. The association between 2715 Mielikki and the Eugenia family is also seen (marked "B").

However, this plot reveals a rather interesting association (marked "A") between the Lydia and Hoffmeister families, and four potentially olivine-rich asteroids (1 A-type, and 3 Sa-types). The Hoffmeister family is a very densely packed family, composed primarily of C-types, and is probably not a genetically-related part of this association. On the other hand, the Lydia family is more dispersed, and is composed primarily of X-types. Because there are so few A- and Sa-type asteroids that have been observed in this region, this closely-packed cluster of four olivine-rich objects is, in itself, significant. It's close association with the Lydia family makes this grouping the best candidate we have found for the disruption of a differentiated parent, in which the Lydia family might represent core material, and the surrounding olivine-rich objects would be fragments of the mantle.

In Table 5.4, a comparison is made between the families we have identified in this analysis, and the dynamical families that have been found by various researchers based on groupings in orbital element space. I have limited this comparison to nine previous works, including the family lists of Kozai (1979), Williams (1989, and private communications), Bendjoya (1993), Lindblad (1994), Lemaitre and Morbidelli (1994), and Zappalà et al. (1990, 1994, 1995). Before making the comparisons with these different works, I first tried to quantify a level of confidence for each of the 19 spectral families found by our clustering method.

In our analysis, there are two factors that contribute to the degree of confidence for any particular family: how isolated the family is, spectrally, from the background population, and how isolated it is, dynamically, in orbital space, from the surrounding background. In the procedure we followed, a series of clustering solutions was generated by varying the amount of spectral dissimilarity allowed, as defined by ε. The range of ε, over which the locus of a family is defined, indicates the degree to which that grouping is spectrally isolated from its surroundings. Similarly, the length of the root associated with the locus (that branch in the clustering solution that connects the cluster, in this case, the locus, to the background level) is an indication of how isolated the locus is in orbital space. Based on these two considerations, I have adopted a measure of confidence, Q, defined as:

$$Q^2 = \sum_{i=\varepsilon_{min}}^{\varepsilon_{max}} \varepsilon_i \left(\frac{D'_{bi} - D'_{li}}{D'_{li}} \right) \qquad (5.6)$$

were ε_{min} and ε_{max} define the range of ε over which the locus was stable, D'_{li} is the maximum single-linkage value for the *i*-th clustering solution, and D'_{bi} is the background level (the value of D' at which the root connects to the background) for the *i*-th solution. Those families that are very isolated from the background will have a high confidence level, such as the Astrid (Q=20.4) or Hoffmeister (7.9) families, while families that blend in with the background will have a much lower confidence level, such as Agnia (Q=0.9) and Henan (0.7). Q provides an estimate of how well the boundary of a family can be determined, and is not a measure of whether or not these are true genetic relationships. I believe that all of the families listed here are real, especially those that are spectrally distinct, like Henan. However, because Henan is so diffuse, it is difficult to identify a unique boundary. Because Q depends on uniquely defining a locus, the four secondary families, Bellona, Coelestina, Eugenia, and Liberatrix do not have values for Q associated with them.

Another measure of robustness is defined by Bendjoya (1993) to relate the number of objects in common when comparing the results from different analyses. This value, R, is defined as:

$$R = 1 - \frac{1}{2}\left(\frac{N_1 - N_c}{N_1} + \frac{N_2 - N_c}{N_2} \right) \qquad (5.7)$$

where N_1 is the total number of members in a family from analysis 1, N_2 is the total number of family members identified by analysis 2, and N_c is the number of objects in common. A value of R = 1.00 indicates a perfect match between the results from the two analyses.

In Table 5.4, a value of Q is given for the 15 primary families. For each family, all known prior identifications are also listed, along with the number of objects in common with the SMASSII family, and the value of R, which compares how well the results of these previous family searches match the SMASSII findings. Only asteroids that could

Table 5.4: Comparison with previous family searches

Family	Q	Reference	No. in common	R
Agnia	0.9	Zappalà *et al.* (1990) Agnia	7	0.818
		Williams (Priv. comm.) Family 37	9	0.909
		Bendjoya (1993) Agnia	8	0.586
		Lindblad (1994) Agnia	9	0.909
		Zappalà *et al.* (1994) Agnia	6	0.773
		Zappalà *et al.* (1995) HCM-Liberatrix	15	0.826
		Zappalà *et al.* (1995) WAM-Agnia	15	0.769
Astrid	20.4	Zappalà *et al.* (1995) HCM-Astrid	5	1.000
		Zappalà *et al.* (1995) WAM-Astrid	5	1.000
Bellona		None		
Chloris	3.0	Kozai (1979) Family No. 33	4	0.800
		Zappalà *et al.* (1994) Idelsonia	4	0.833
		Zappalà *et al.* (1995) HCM-Chloris	7	0.826
		Zappalà *et al.* (1995) WAM-Chloris	8	0.689
Coelestina		Zappalà *et al.* (1995) WAM-Coelestina	3	0.589
Dora	4.4	Kozai (1979) Family No. 39	3	0.438
		Zappalà *et al.* (1990) Dora	14	1.000
		Williams (Priv. comm.) Family 128	15	1.000
		Bendjoya (1993) Dora	25	0.960
		Lindblad (1994) Dora	14	1.000
		Zappalà *et al.* (1994) Dora	25	0.980
		Zappalà *et al.* (1995) HCM-Dora	29	0.968
		Zappalà *et al.* (1995) WAM-Dora	29	0.968
Eugenia		Williams (1989) Family 133	5	0.833
Gefion	3.3	Zappalà *et al.* (1990) Gefion	19	0.913
		Williams (Priv. comm.) Family 127	21	0.934
		Bendjoya (1993) Gefion	26	0.930
		Lindblad (1994) Oppavia-Gefion	12	0.722
		Lindblad (1994) Nuki	9	0.696
		Zappalà *et al.* (1994) HCM-Gefion	24	0.914
		Zappalà *et al.* (1995) HCM-Ceres	33	0.881
		Zappalà *et al.* (1995) WAM-Minerva	33	0.930
Henan	0.7	Williams (1989) Family 36	2	1.000
		Bendjoya (1993) Agnia	9	0.700
		Zappalà *et al.* (1994) Lavrov	6	0.875

Table 5.4: Comparison with previous family searches

Family	Q	Reference	No. in common	R
		Zappalà *et al.* (1995) HCM-Henan	8	0.711
		Zappalà *et al.* (1995) HCM-Liberatrix	3	0.171
		Zappalà *et al.* (1995) WAM-Agnia	9	0.480
Hoffmeister	7.9	Williams (Priv. comm.) Family 38	4	0.750
		Zappalà *et al.* (1994) Hoffmeister	7	0.938
		Zappalà *et al.* (1995) HCM-Hoffmeister	9	0.950
		Zappalà *et al.* (1995) WAM-Antonia	5	0.505
		Zappalà *et al.* (1995) WAM-Lydia	4	0.340
Liberatrix		Williams (1989) Family 132	8	0.688
		Zappalà *et al.* (1995) HCM-Nemesis	2	0.325
		Zappalà *et al.* (1995) HCM-Liberatrix	2	0.173
		Zappalà *et al.* (1995) HCM-Lydia	4	0.355
		Zappalà *et al.* (1995) WAM-Concordia	3	0.375
Lydia	2.0	Williams (1989) Family 130	3	0.800
		Zappalà *et al.* (1990) Lydia	4	0.833
		Zappalà *et al.* (1994) Padua	5	0.813
		Zappalà *et al.* (1995) HCM-Lydia	10	0.763
		Zappalà *et al.* (1995) WAM-Lydia	10	0.794
Menippe	2.4	None (Probably subset of Eunomia family)		
Merxia	3.3	Williams (1989) Family 40	3	0.875
		Bendjoya (1993) Lilaea	6	0.708
		Zappalà *et al.* (1994) Merxia	6	0.804
		Zappalà *et al.* (1995) HCM-Merxia	7	0.778
		Zappalà *et al.* (1995) WAM-Merxia	7	0.778
Pallas	3.9	Kozai (1979) Family No. 31	5	0.917
		Williams (Priv. comm.) Family 129	14	0.938
		Lemaitre and Morbidelli (1994)	8	0.944
Phaeo	3.6	Kozai (1979) Family No. 39	2	0.625
		Zappalà *et al.* (1995) WAM-Phaeo	4	0.900
Thisbe	1.8	None		
Watsonia	3.9	Burbine *et al.* (1992) Spectral prediction.		
Weringia	1.5	None		

truly be in common with both analyses were considered in the calculation of R. Therefore, only those asteroids observed during SMASSII were considered in the comparison. Likewise, for the older works of Kozai or Williams, only those SMASSII objects numbered up to the cutoff in their analysis were used. Many subtle conclusions could be drawn from this table. However, in broad terms, there is generally good agreement between the spectral families identified by the method presented here, and those dynamical families that have been previously found. Those dynamical families that are very compact and isolated, like Dora and Astrid, agree almost exactly between the various results. By comparison, those families that are more diffuse pose a greater problem. In particular, the close proximity of the Agnia, Henan, Hoffmeister, Liberatrix and Lydia families appears to have been the greatest challenge for previous family searches. Even the very compact and relatively isolated Hoffmeister family (Q=7.9) was poorly resolved in the wavelet analysis (WAM) results of Zappalà *et al.* (1995). With the SMASSII observations, we have been able to define relatively accurate boundaries for each of these families.

Chapter 6

Conclusions and future work

6.1 Summary of conclusions

• *New spectral diversity is found in the main belt*

Visible wavelength spectroscopic measurements provide a tool for investigating the diversity within the population of asteroids. Through the high spectral resolution provided by the Small Main-belt Asteroid Spectroscopic Survey (SMASSII), the measurement of 1189 asteroids has revealed new evidence for asteroid diversity. Several new distinct spectral classes are defined, such as the L- and Ld-type asteroids, which display a steep, red slope over the short wavelength half of their spectrum. Their mineralogical nature remains uncertain. Diversity in the C-class is revealed by the presence or absence of a 0.7 μm feature attributed to the presence of phyllosilicates. Asteroids belonging to the previously spectrally degenerate X-class are found to display a range of measurable features, allowing this class to be subdivided. In particular, the Xe-class shows a distinct 0.49 μm feature that may be associated with troilite (FeS).

• *Asteroids display a continuous transition between spectral groups*

The SMASSII sample reveals that previously apparent separations in the spectral distribution between major taxonomic classes become filled as asteroids in smaller diameter ranges are sampled. Most significant is the transitions between S-type asteroids and the previously separated classes of A-types, R-types, and Q-types. Another example of a smooth transition is that seen between the S- and X-complexes.

As asteroids are sampled at smaller sizes, individual objects may be more likely to consist of a single geologic unit. Through the sampling of numerous small asteroids, the full diversity of all geologic units may become apparent in the form of a continuous spectral distribution. Variations in regolith particle sizes and possible surface alteration effects could also contribute toward creating a continuous spectral distribution.

- ***New evidence is found for substantial collisional evolution in the asteroid belt***

Validation or refutation of proposed dynamical families can be accomplished through spectroscopic measurements of family members. By utilizing the SMASSII subset of 465 spectra of asteroids in the 2.690 to 2.815 AU region of the asteroid belt, we have shown that members of 14 proposed dynamical families have spectral characteristics consistent with the disruption of quasi-homogeneous parent bodies. Five additional clusters of asteroids are found (not identified by previous family searches) that are comprised of spectrally similar members, though these asteroids are more dispersed in orbital elements, and may represent the remnants of older collisional events. This spectral validation provides strong new evidence that the asteroid belt has indeed been subject to substantial collisional evolution.

- ***All observed families appear to be relatively homogeneous***

Asteroid families represent the outcomes of natural collision experiments allowing us to see into the interiors of larger asteroids. In nearly all cases where such examination has been possible, the results show relatively homogeneous spectral properties between family members, implying little variation in internal mineralogy of the parent body. Of the 19 families studied between 2.690 and 2.815 AU, only the Lydia family and the Bellona/Phaeo cluster provide any evidence for the possible disruptions of differentiated parent bodies, though even this evidence is not strong. The presence of iron meteorites and metal-rich asteroids implies that a substantial number of differentiated bodies must have been disrupted. It remains a mystery as to why there are no clearer examples of disrupted differentiated parent bodies among the families studied to date.

6.2 Future work

Apparent temporal variations in the CCD spectra of asteroids must be better understood. Individual asteroids that have been reobserved during different observing runs often show spectral variations that, if real (and not instrumental in origin), may indicate measurable compositional heterogeneities on their surfaces, or may result from differences in observing geometry. A more detailed analysis of the SMASSII results, and comparisons with the results of other spectroscopic surveys, such as SMASSI, may provide further insight into these variations.

Several of the families studied have members that bridge the boundaries between the C- and X-complexes and also appear to show wide ranges in albedos. Further studies of these families, most especially additional albedo information, may help in understanding the mineralogical relationships between objects that have been traditionally labeled as C-types and X-types.

Further spectral studies of proposed members within the Lydia family may provide stronger evidence for this family being the remnants of a differentiated parent body.

Small and very compact families, such as the Astrid and Hoffmeister families, are likely formed from collisions having energies just above the disruption threshold. Lightcurve measurements revealing the rotation states and shapes of their members may provide the best basis for comparison with similar measurements derived from laboratory collision experiments.

The Dora and Gefion families have similar dimensions in orbital space and similarly large populations. However, Dora is comprised of presumably weaker objects (Ch-types) than Gefion (S-types). Comparative studies between these two families may reveal distinguishing characteristics for the collisional outcomes of bodies having different strengths.

References

Abbott, L. A., F. A. Bisby, and D. J. Rogers 1985. *Taxonomic Analysis in Biology.* Columbia University Press, New York.

Adams, J. B. 1974. Visible and near-infrared diffuse reflectance spectra of pyroxenes as applied to remote sensing of solid objects in the solar system. *J. Geophys. Res.* **79**, 4829-4836.

Adams, J. B. 1975. Interpretation of visible and near-infrared diffuse reflectance spectra of pyroxenes and other rock-forming minerals. In *Infrared and Raman Spectroscopy of Lunar and Terrestrial Minerals* (C. Karr, Ed.), pp. 91-116. Academic Press, New York.

Anderberg, M. R. 1973. *Cluster Analysis for Applications.* Academic Press, New York.

Barucci, M. A., M. T. Capria, A. Coradini, and M. Fulchignoni 1987. Classification of asteroids using G-mode analysis. *Icarus* **72**, 304-324.

Bell, J. F. 1988. A probable asteroidal parent body for the CV or CO chondrites. *Meteoritics* **23**, 256-257.

Bell, J. F. 1989. Mineralogical clues to the origins of asteroid dynamical families. *Icarus* **78**, 426-440.

Bell, J. F., P. D. Owensby, B. R. Hawke, and M. J. Gaffey 1988. The 52-color Asteroid Survey: Final results and interpretation. *Lunar and Planet. Sci. Conf. Abstr.* **XIX**, 57-58.

Bell, J. F., D. R. Davis, W. K. Hartmann, and M. J. Gaffey 1989. Asteroids: The big picture. In *Asteroids II* (R. P. Binzel, T. Gehrels, and M. S. Matthews, Eds.), pp. 921-945. Univ. of Arizona Press, Tucson.

Belton, M. J. S., J. Veverka, P. Thomas, P. Helfenstein, D. Simonelli, C. Chapman, M. E. Davies, R. Greeley, R. Greenberg, and J. Head 1992. Galileo encounter with 951 Gaspra - First pictures of an asteroid. *Science* **257**, 1647-1652.

Bendjoya, P., E. Slezak, and C. Froeschlé 1991. The wavelet transform: A new tool for asteroid family determination. *Astron. Astrophys.* **251**, 312-330.

Bendjoya, P. 1993. A classification of 6479 asteroids into families by means of the wavelet clustering method. *Astron. Astrophys. Sup.* **102**, 25-55.

Binzel, R. P. 1989. An overview of the asteroids. In *Asteroids II* (R. P. Binzel, T. Gehrels, and M. S. Matthews, Eds.), pp. 3-18. Univ. of Arizona Press, Tucson.

Binzel, R. P. 1992. The optical spectrum of 5145 Pholus. *Icarus* **99**, 238-240.

Binzel, R. P. 1994. Physical Studies of Hirayama families: Recent results and future prospects. In *Seventy-five Years of Hirayama Asteroid Families: The Role of Collisions in the Solar System History* (Y. Kozai, R. P. Binzel, and T. Hirayama, Eds.), pp. 251-258. Astron. Soc. of the Pacific, San Francisco.

Binzel, R. P., and S. Xu 1993. Chips off of asteroid 4 Vesta: Evidence for the parent body of basaltic achondrite meteorites. *Science* **260**, 186-191.

Binzel, R. P., S. Xu, and S. J. Bus 1993a. Spectral variations within the Koronis family - Possible implications for the surface colors of Asteroid 243 Ida. *Icarus* **106**, 608-611.

Binzel, R. P., S. Xu, S. J. Bus, M. F. Skrutskie, M. R. Meyer, P. Knezek, and E. S. Barker 1993b. Discovery of a main-belt asteroid resembling ordinary chondrite meteorites. *Science* **262**, 1541-1543.

Binzel, R. P., S. J. Bus, T. H. Burbine, and J. M. Sunshine 1996. Spectral properties of near-Earth asteroids: Evidence for sources of ordinary chondrite meteorites. *Science* **273**, 946-948.

Binzel, R. P., S. J. Bus, and T. H. Burbine 1998. Size dependence of asteroid spectral properties: SMASS results for near-Earth and main-belt asteroids. In *Lunar and Planetary Science* **XXIX**, Abstract #1222, Lunar and Planetary Institute, Houston (CD-ROM).

Binzel, R. P., S. J. Bus, and T. H. Burbine 1999a. The orbital distribution of Vesta-like asteroids. In *Lunar and Planetary Science* **XXX**, Abstract #1216, Lunar and Planetary Institute, Houston (CD-ROM).

Binzel, R. P., *et al.* 1999b. In preparation

Bobrovnikoff, N. T. 1929. The spectra of minor planets. *Lick Obs. Bull.* **14**, 18-27.

Bowell, E., C. R. Chapman, J. C. Gradie, D. Morrison, and B. Zellner 1978. Taxonomy of asteroids. *Icarus* **35**, 313-335.

Bowell, E., Gehrels, T., and Zellner, B. 1979. Magnitudes, colors, types and adopted diameters of the asteroids. In *Asteroids* (T. Gehrels, Ed.), pp. 1108-1129. Univ. of Arizona Press, Tucson.

Bowell, E., N. S. Chernykh, and B. G. Marsden 1989a. Discovery and follow up of asteroids. In *Asteroids II* (R. P. Binzel, T. Gehrels, and M. S. Matthews, Eds.), pp. 21-38. Univ. of Arizona Press, Tucson.

Bowell, E., B. Hapke, D. Domingue, K. Lumme, J. Peltoniemi, and A. W. Harris 1989b. Application of photometric models to asteroids. In *Asteroids II* (R. P. Binzel, T. Gehrels, and M. S. Matthews, Eds.), pp. 524-556. Univ. of Arizona Press, Tucson.

Britt, D. T., and L. A. Lebofsky 1992. Spectral variation within asteroid classes. *Lunar and Planet. Sci. Conf. Abstr.* **XXIII**, 161-162.

Britt, D. T., D. J. Tholen, J. F. Bell, and C. M. Pieters 1992. Comparison of asteroid and meteorite spectra: Classification by principal component analysis. *Icarus* **99**, 153-166.

Brouwer, D. 1951. Secular variations of the orbital elements of minor planets. *Astron. J.* **56**, 9-32.

Brouwer, D., and A. J. J. van Woerkom 1950. The secular variations of the orbital elements of the principal planets. *Astron. Papers U. S. Naval Obs. Naut. Almanac Off.* **13**, 81-107.

Burbine, T. H. 1991. *Principal component analysis of asteroid and meteorite spectra from 0.3 to 2.5* μm. Master's thesis, University of Pittsburgh.

Burbine, T. H., M. J. Gaffey, and J. F. Bell 1992. S-asteroids 387 Aquitania and 980 Anacostia: Possible fragments of the breakup of a spinel-bearing parent body with CO3/CV3 affinities. *Meteoritics* **27**, 424-434.

Burbine, T. H., and J. F. Bell 1993. How diverse is the asteroid belt? *Lunar and Planet. Sci. Conf. Abstr.* **XXIV**, 223-224.

Burbine, T. H., R. P. Binzel, and S. J. Bus 1997. SMASS and SMASSIR - Visible and near-infrared spectral studies of main-belt and near-Earth asteroids. *Lunar and Planet. Sci. Conf. Abstr.* **XXVIII**, 179.

Burbine, T. H., E. A. Cloutis, S. J. Bus, A. Meibom, and R. P. Binzel 1998. The detection of troilite (FeS) on the surfaces of E-class asteroids. *Bull. Am. Astron. Soc.* **30**, 1025-1026.

Burbine, T. H., R. P. Binzel, and S. J. Bus 1999. Near-infrared spectra of pyroxene- and olivine-rich asteroids. In *Lunar and Planetary Science* **XXX**, Abstract #1777, Lunar and Planetary Institute, Houston (CD-ROM).

Burns, R. G. 1970. *Mineralogical Applications of Crystal Field Theory*. Cambridge Univ. Press, New York.

Bus, S. J., R. P. Binzel, T. H. Burbine 1996. Asteroid families: Myth or reality? *Bull. Am. Astron. Soc.* **28**, 1097.

Bus, S. J. 1998. Testing the validity of asteroid families between 2.69 and 2.82 AU: Results from SMASS II (Abstract). Presented at *5th Workshop on Catastrophic Disruption in the Solar System* (July 1-3, 1998. Timberline Lodge, Oregon).

Carusi, A, and E. Massaro 1978. Statistics and mapping of asteroid concentrations in the proper element space. *Astron. Astrophys. Sup.* **34**, 81-90.

Chapman, C. R. 1987. Compositional structure of the asteroid belt and its families. Unpublished manuscript.

Chapman, C. R. 1996. S-type asteroids, ordinary chondrites, and space weathering: The evidence from Galileo's fly-bys of Gaspra and Ida. *Meteorit. Planet. Sci.* **31**, 699-725.

Chapman, C. R., T. V. Johnson, and T. B. McCord 1971. A review of spectrophotometric studies of asteroids. In *Physical Studies of Minor Planets* (T. Gehrels, Ed.), pp. 51-65. NASA SP-267.

Chapman, C. R., D. Morrison, and B. Zellner 1975. Surface properties of asteroids: A synthesis of polarimetry, radiometry, and spectrophotometry. *Icarus* **25**, 104-130.

Chapman, C. R., and M. J. Gaffey 1979. Reflectance spectra for 277 asteroids. In *Asteroids* (T. Gehrels, Ed.), pp. 655-687. Univ. of Arizona Press, Tucson.

Chapman, C., P. Paolicchi, V. Zappalà, R. P. Binzel, and J. F. Bell 1989. Asteroid families; Physical properties and evolution. In *Asteroids II* (R. P. Binzel, T. Gehrels, and M. S. Matthews, Eds.), pp. 386-415. Univ. of Arizona Press, Tucson.

Cloutis, E. A., M. J. Gaffey, T. L. Jackowski, and K. L. Reed 1986. Calibrations of phase abundance, composition, and particle size distribution for olivine-orthopyroxene mixtures from reflectance spectra. *J. Geophys. Res.* **91**, 11641-11653.

Cochran, A. L., and T. G. Barnes, III 1981. Spectrophotometry with a self-scanned silicon photodiode array. I - Instrumentation and reductions. *Astrophys. J. Suppl. S.* **45**, 73-81.

Danby, J. M. A. 1992. *Fundamentals of celestial mechanics*, 2nd ed. Willmann-Bell, Inc. U.S.A.

Dillon, W. R., and M. Goldstein 1984. *Multivariate analysis: methods and applications*. Wiley, New York.

Di Martino, M., F. Migliorini, V. Zappalà, A. Manara, and C. Barbieri 1997. Veritas asteroid family: Remarkable Spectral Differences inside a primitive parent body. *Icarus* **127**, 112-120.

Doressoundiram, A., M. A. Barucci, M. Fulchignoni, and M. Florczak 1998. Eos family: A spectroscopic study. *Icarus* **131**, 15-31.

Feierberg, M. A., H. P. Larson, U. Fink, and H. A. Smith 1980. Spectroscopic evidence for two achondrite parent bodies: Asteroids 349 Dembowska and 4 Vesta. *Geochim. Cosmochim. Ac.* **44**, 513-524.

Feierberg. M. A., L. A. Lebofsky, and H. P. Larson 1981. Spectroscopic evidence for aqueous alteration products on the surfaces of low-albedo asteroids. *Geochim. Cosmochim. Ac.* **45**, 971-981.

Filippenko, A. V. 1982. The importance of atmospheric differential refraction in spectroscopy. *Publ. Astron. Soc. Pac.* **94**, 715-721.

Florczak, M., D. Lazzaro, T. Mothé-Diniz, C. A. Angeli, and A. S. Betzler 1999. A spectroscopic study of the Themis family. *Astron. Astrophys. Sup.* **134**, 463-471.

French, L. M., and R. P. Binzel 1989. CCD photometry of asteroids. In *Asteroids II* (R. P. Binzel, T. Gehrels, and M. S. Matthews, Eds.), pp. 54-65. Univ. of Arizona Press, Tucson.

French, L. M., F. Vilas, W. K. Hartmann, and D. J. Tholen 1989. Distant asteroids and Chiron. In *Asteroids II* (R. P. Binzel, T. Gehrels, and M. S. Matthews, Eds.), pp. 468-486. Univ. of Arizona Press, Tucson.

Gaffey, M. J. 1976. Spectral reflectance characteristics of the meteorite classes. *J. Geophys. Res.* **81**, 905-920.

Gaffey, M. J. 1994. Nature and origins of the olivine-dominated A- and S(I)-type asteroids. *Lunar and Planet. Sci. Conf. Abstr.* **XXV**, 399-400.

Gaffey, M. J. 1997. Surface lithologic heterogeneity of asteroid 4 Vesta. *Icarus* **127**, 130-157.

Gaffey, M. J., J. F. Bell, and D. P. Cruikshank 1989. Reflectance spectroscopy and asteroid surface mineralogy. In *Asteroids II* (R. P. Binzel, T. Gehrels, and M. S. Matthews, Eds.), pp. 98-127. Univ. of Arizona Press, Tucson.

Gaffey, M. J., J. F. Bell, R. H. Brown, and T. H. Burbine 1990. Mineralogical variations within the S-asteroid population. *Lunar and Planet. Sci. Conf. Abstr.* **XXI**, 399-400.

Gaffey, M. J., K. L. Reed, and M. S. Kelley 1992. Relationship of E-type Apollo asteroid 3103 (1982 BB) to the enstatite achondrite meteorites and the Hungaria asteroids. *Icarus* **100**, 95-109.

Gaffey, M. J., J. F. Bell, R. H. Brown, T. H. Burbine, J. L. Piatek, K. L. Reed, and D. A. Chaky 1993a. Mineralogical variations within the S-type asteroid class. *Icarus* **106**, 573-602.

Gaffey, M. J., T. H. Burbine, and R. P. Binzel 1993b. Asteroid spectroscopy: Progress and perspectives. *Meteoritics* **28**, 161-187.

Gehrels, T. 1991. Scanning with charge-coupled devices. *Space Sci. Rev.* **58**, 347-375.

Gradie, J. C., and B. Zellner 1977. Asteroid families: Observational evidence for common origins. *Science* **197**, 254-255.

Gradie, J. C., C. R. Chapman, and J. G. Williams 1979. Families of minor planets. In *Asteroids* (T. Gehrels, Ed.), pp. 359-390. Univ. of Arizona Press, Tucson.

Gradie, J., and E. F. Tedesco 1982. Compositional structure of the asteroid belt. *Science* **216**, 1405-1407.

Gradie, J. C., C. R. Chapman, and E. F. Tedesco 1989. Distribution of taxonomic classes and the compositional structure of the asteroid belt. In *Asteroids II* (R. P. Binzel, T. Gehrels, and M. S. Matthews, Eds.), pp. 316-335. Univ. of Arizona Press, Tucson.

Greenberg, R., and C. R. Chapman 1983. Asteroids and meteorites: Parent bodies and delivered samples. *Icarus* **55**, 455-481.

Greenberg, R., and M. C. Nolan 1989. Delivery of asteroids and meteorites to the inner solar system. In *Asteroids II* (R. P. Binzel, T. Gehrels, and M. S. Matthews, Eds.), pp. 778-804. Univ. of Arizona Press, Tucson.

Haack, H., K. L. Rasmussen, and P. H. Warren 1990. Effects of regolith/megaregolith insulation on the cooling histories of differentiated asteroids. *J. Geophys. Res.* **95**, 5111-5124.

Hardorp, J. 1978. The sun among the stars. I - A search for solar spectral analogs. *Astron. Astrophys.* **63**, 383-390.

Hayes, D. S., and D. W. Latham 1975. A rediscussion of the atmospheric extinction and the absolute spectral-energy distribution of Vega. *Astrophys. J.* **197**, 593-601.

Henrard, J. 1990. A semi-numerical perturbation method for separable Hamiltonian systems. *Celest. Mech. Dyn. Astr.* **49**, 43-67.

Hiroi, T., F. Vilas, and J. M. Sunshine 1996. Discovery and analysis of minor absorption bands in S-asteroid visible reflectance spectra. *Icarus* **119**, 202-208.

Hirayama, K. 1918. Groups of asteroids probably of common origin. *Astron. J.* **31**, 185-188.

Hirayama, K. 1923. Families of asteroids. *Japan J. Astron. Geophys.* **1**, 55-93.

Hirayama, K. 1928. Families of asteroids. Second paper. *Japan J. Astron. Geophys.* **5**, 137-162.

Hirayama, K. 1933. Present state of the families of asteroids. *Proc. Japan Academy* **9**, 482-485.

Hoffleit, D. 1982. *The bright star catalogue*, 4th rev. ed. Yale University Observatory, New Haven, Conn.

Howell, E. S. 1995. *Probing asteroid composition using visible and near-infrared spectroscopy.* Doctoral thesis, University of Arizona.

Howell, E. S., E. Merényi, and L. A. Lebofsky 1994. Classification of asteroid spectra using a neural network. *J. Geophys. Res.* **99**, 10847-10865.

Janesick, J., and T. Elliott 1992. History and advancement of large array scientific CCD imagers. In *Astronomical CCD Observing and Reduction Techniques* (S. B. Howell, Ed.), pp. 1-67. Astron. Soc. of the Pacific, San Francisco.

Johnson, T. V., and F. P. Fanale 1973. Optical properties of carbonaceous chondrites and their relationship to asteroids. *J. Geophys. Res.* **78**, 8507-8518.

Jones, T. D., L. A. Lebofsky, J. S. Lewis, and M. S. Marley 1990. The composition and origin of the C, P, and D asteroids: Water as a tracer of thermal evolution in the outer belt. *Icarus* **88**, 172-192.

Kaler, J. B. 1989. *Stars and their spectra: An introduction to the spectral sequence.* Cambridge University Press, Cambridge.

Kelley, M. S., and M. J. Gaffey 1996. A genetic study of the Ceres (Williams #67) asteroid family. *Bull. Am. Astron. Soc.* **28**, 1097.

Kepler, J. 1596. *Mysterium Cosmographicum.*

King, T. V. V., and W. I. Ridley 1987. Relation of the spectroscopic reflectance of olivine to mineral chemistry and some remote sensing implications. *J. Geophys. Res.* **92**, 11457-11469.

King, T. V. V., and R. N. Clark 1997. The presence of a single absorption feature: What it does and doesn't imply. *Lunar and Planet. Sci. Conf. Abstr.* **XXVIII**, 727-728.

Kirkwood, D. 1867. *Meteoritic astronomy: A treatise on shooting-stars, fireballs, and Aerolites*, Ch. 13 (Philadelphia: J. B. Lippincott).

Kozai, Y. 1979. The dynamical evolution of the Hirayama families. In *Asteroids* (T. Gehrels, Ed.), pp. 334-358. Univ. of Arizona Press, Tucson.

Kuiper, G. P. 1950. On the origin of asteroids. *Astron. J.* **55**, 164.

Lagerkvist, C.-I., A. Fitzsimmons, P. Magnusson, and I. P. Williams 1993. Investigations of D-type asteroids. *Mon. Not. R. Astron. Soc.* **260**, 679-680.

Lazzaro, D., T. Mothé-Diniz, J. M. Carvano, C. A. Angeli, A. S. Betzler, M. Florczak, A. Cellino, M. Di Martino, A. Doressoundiram, M. A. Barucci, E. Dotto, and P. Bendjoya 1999. The Eunomia family: A visible spectroscopic survey. Submitted to *Icarus.*

Lebofsky, L. A. 1978. Asteroid 1 Ceres: Evidence for water of hydration. *Mon. Not. R. Astron. Soc.* **182**, 17-21.

Lemaitre, A. 1993. Proper elements: What are they? *Celest. Mech. Dyn. Astr.* **56**, 103-119.

Lemaitre, A., and A. Morbidelli 1994. Proper elements for highly inclined asteroidal orbits. *Celest. Mech. Dyn. Astr.* **60**, 29-56.

Lindblad, B. A. 1994. A study of asteroid dynamical families. In *Seventy-five Years of Hirayama Asteroid Families: The Role of Collisions in the Solar System History* (Y. Kozai, R. P. Binzel, and T. Hirayama, Eds.), pp.62-75. Astron. Soc. of the Pacific, San Francisco.

Lipschutz, M. E., M. J. Gaffey, and P. Pellas 1989. Meteoritic parent bodies: Nature, number, size and relation to present-day asteroids. In *Asteroids II* (R. P. Binzel, T. Gehrels, and M. S. Matthews, Eds.), pp. 740-777. Univ. of Arizona Press, Tucson.

Lockwood, G. W., and D. T. Thompson 1986. Atmospheric extinction - The ordinary and volcanically induced variations, 1972-1985. *Astron. J.* **92**, 976-985.

Lucey, P. G., and K. Keil 1997. The silicate chemistry of the A-type asteroids. *Meteorit. Planet. Sci.* **32**, A82.

Lucey, P. G., and K. Keil 1998. The influence of temperature on the spectra of the A-asteroids and implications for their silicate chemistry. *J. Geophys. Res.* **103**, 5865-5871.

Lucey, P. G., J. L. Hinrichs, and M. S. Robinson 1998. Dependence of spectral properties of olivine and pyroxene on temperature: Implications for NEAR observations of Eros. In *Lunar and Planetary Science* **XXIX**, Abstract #1357, Lunar and Planetary Institute, Houston (CD-ROM).

Lupishko, D. F., and I. N. Belskaya 1989. On the surface composition of the M-type asteroids. *Icarus* **78**, 395-401.

Luu, J. X., and D. C. Jewitt 1990. Charge-coupled device spectra of asteroids. I - Near-earth and 3:1 resonance asteroids. *Astron. J.* **99**, 1985-2011.

McCord, T. B., and C. R. Chapman 1975. Asteroids - Spectral reflectance and color characteristics. *Astrophys. J.* **195**, 553-562.

McCord, T. B., J. B. Adams, and T. V. Johnson 1970. Asteroid Vesta: Spectral reflectivity and compositional implications. *Science* **168**, 1445-1447.

McFadden, L.-A., M. J. Gaffey, and T. B. McCord 1984. Mineralogical-petrological characterization of near-Earth asteroids. *Icarus* **59**, 25-40.

McFadden, L.-A., D. J. Tholen, and G. J. Veeder 1989. Physical properties of Aten, Apollo and Amor asteroids. In *Asteroids II* (R. P. Binzel, T. Gehrels, and M. S. Matthews, Eds.), pp. 442-467. Univ. of Arizona Press, Tucson.

Merényi, E., E. S. Howell, A. S. Rivkin, and L. A. Lebofsky 1997. Prediction of water in asteroids from spectral data shortward of 3 μm. *Icarus* **129**, 421-439.

Migliorini, F., A. Manara, M. Di Martino, and P. Farinella 1996. The Hoffmeister asteroid family: inferences from physical data. *Astron. Astrophys.* **310**, 681-685.

Milani, A., and Z. Knežević 1990. Secular perturbation theory and computation of asteroidal proper elements. *Celest. Mech. Dyn. Astr.* **49**, 347-411.

Milani, A., and Z. Knežević 1994. Asteroid proper elements and the dynamical structure of the asteroid main belt. *Icarus* **107**, 219-254.

Millis, R. L., and D. W. Dunham 1989. Precise measurement of asteroid sizes and shapes from occultations. In *Asteroids II* (R. P. Binzel, T. Gehrels, and M. S. Matthews, Eds.), pp. 148-170. Univ. of Arizona Press, Tucson.

Miner, E., and J. Young 1976. Five-color photoelectric photometry of asteroid 433 Eros. *Icarus* **28**, 43-51.

Monet, A. K. B., E. Bowell, and D. G. Monet 1997. "Hands-free" asteroid astrometry. *Bull. Am. Astron. Soc.* **29**, 1273.

Moroz, L. V., A. V. Fisenko, L. F. Semjonova, C. M. Pieters, and N. N. Korotaeva 1996. Optical effects of regolith processes on S-asteroids as simulated by laser shots on ordinary chondrite and other mafic materials. *Icarus* **122**, 366-382.

Morrison, D. 1974. Radiometric diameters and albedos of 40 asteroids. *Astrophys. J.* **194**, 203-212.

Mueller, B. E. A., D. J. Tholen, W. K. Hartmann, and D. P. Cruikshank 1992. Extraordinary colors of asteroidal object (5145) 1992 AD. *Icarus* **97**, 150-154.

Nobili, A. M., A. Milani, and M. Carpino 1989. Fundamental frequencies and small divisors in the orbits of the outer planets. *Astron. Astrophys.* **210**, 313-336.

Olbers, W. 1803. *Ann. Physik* **14**, 38.

Ostro, S. J., D. B. Campbell, and I. I. Shapiro 1985. Main-belt asteroids: Dual-polarization radar observations. *Science* **229**, 442-446.

Pieters, C. M., and L. A. McFadden 1994. Meteorite and asteroid reflectance spectroscopy: Clues to early solar system processes. *Annu. Rev. Earth Pl. Sc.* **22**, 457-497.

Poutanen, M., E. Bowell, L. J. Martin, and D. T. Thompson 1985. Photoelectric photometry of asteroid 69 Hesperia. *Astron. Astrophys. Sup.* **61**, 291-297.

Rabinowitz, D. L. 1991. Detection of earth-approaching asteroids in near real time. *Astron. J.* **101**, 1518-1529.

Reinsch, C. H. 1967. Smoothing by spline functions. *Numer. Math.* **10**, 177-183.

Ridley, M. 1986. *Evolution and Classification: The Reformation of Cladism.* Longman Group Limited, Essex, England.

Rivkin, A. S., E. S. Howell, D. T. Britt, L. A. Lebofsky, M. C. Nolan, and D. D. Branston 1995. 3-μm spectrophotometric survey of M- and E-class asteroids. *Icarus* **117**, 90-100.

Sawyer, S. R. 1991. *A high resolution CCD spectroscopic survey of low albedo main belt asteroids.* Doctoral thesis, University of Texas.

Sekanina, Z. 1979. Relative motions of fragments of the split comets. III - A test of splitting and comets with suspected multiple nuclei. *Icarus* **38**, 300-316.

Stokes, G. H., H. E. M. Viggh, F. L. Shelly, M. S. Blythe, and J. S. Stuart 1998. Results from the Lincoln Near Earth Asteroid Research (LINEAR) Project. *Bull. Am. Astron. Soc.* **30**, 1042.

Sunshine, J. M., and C. M. Pieters 1993. Estimating modal abundances from the spectra of natural and laboratory pyroxene mixtures using the modified Gaussian model. *J. Geophys. Res.* **98**, 9075-9087.

Sunshine, J. M., R. P. Binzel, T. H. Burbine, and S. J. Bus 1998. Is asteroid 239 Nenetta compositionally analogous to the Brachinite meteorites? In *Lunar and Planetary Science* **XXIX**, Abstract #1430, Lunar and Planetary Institute, Houston (CD-ROM).

Tedesco, E. F. 1989. Asteroid magnitudes, UBV colors, and IRAS albedos and diameters. In *Asteroids II* (R. P. Binzel, T. Gehrels, and M. S. Matthews, Eds.), pp. 1090-1138. Univ. of Arizona Press, Tucson.

Tedesco, E. F., J. G. Williams, D. L. Matson, G. J. Veeder, J. C. Gradie, and L. A. Lebofsky 1989. Three-parameter asteroid taxonomy classifications. In *Asteroids II* (R. P. Binzel, T. Gehrels, and M. S. Matthews, Eds.), pp. 1151-1161. Univ. of Arizona Press, Tucson.

Tholen, D. J. 1984. *Asteroid taxonomy from cluster analysis of photometry.* Doctoral thesis, University of Arizona.

Tholen, D. J. 1989. Asteroid taxonomic classifications. In *Asteroids II* (R. P. Binzel, T. Gehrels, and M. S. Matthews, Eds.), pp. 1139-1150. Univ. of Arizona Press, Tucson.

Tholen, D. J., and M. A. Barucci 1989. Asteroid taxonomy. In *Asteroids II* (R. P. Binzel, T. Gehrels, and M. S. Matthews, Eds.), pp. 298-315. Univ. of Arizona Press, Tucson.

Tody, D. 1993. IRAF in the Nineties. In *Astronomical Data Analysis Software and Systems II* (R. J. Hanisch, R. J. V. Brissenden, and J. Barnes, Eds.), p. 173. Astron. Soc. of the Pacific, San Francisco.

van Houten, C. J., I. van Houten-Groeneveld, P. Herget, and T. Gehrels 1970. The Palomar-Leiden Survey of faint minor planets. *Astron. Astrophys. Sup.* **2**, 339-448.

Veeder, G. J., E. F. Tedesco, and D. L. Matson 1989. Asteroid results from the IRAS survey. In *Asteroids II* (R. P. Binzel, T. Gehrels, and M. S. Matthews, Eds.), pp. 282-289. Univ. of Arizona Press, Tucson.

Venables, W. N., and B. D. Ripley 1994. *Modern Applied Statistics with S-Plus.* Springer-Verlag, New York.

Vilas, F. 1994. A cheaper, faster, better way to detect water of hydration on solar system bodies. *Icarus* **111**, 456-467.

Vilas, F., and B. A. Smith 1985. Reflectance spectrophotometry (~0.5-1.0 μm) of outer-belt asteroids: Implications for primitive, organic Solar System material. *Icarus* **64**, 503-516.

Vilas, F., and M. J. Gaffey 1989. Phyllosilicate absorption features in main-belt and outer-belt asteroid reflectance spectra. *Science* **246**, 790-792.

Vilas, F., S. M. Larson, E. C. Hatch, and K. S. Jarvis 1993. CCD reflectance spectra of selected asteroids. II. Low-albedo asteroid spectra and data extraction techniques. *Icarus* **105**, 67-78.

Wetherill, G. W. 1989. Cratering of the terrestrial planets by Apollo objects. *Meteoritics* **24**, 15-22.

Williams, J. G. 1969. *Secular perturbations in the solar system.* Doctoral thesis, University of California, Los Angeles.

Williams, J. G. 1971. Proper elements, families, and belt boundaries. In *Physical Studies of Minor Planets* (T. Gehrels, Ed.), pp. 177-181. NASA SP-267.

Williams, J. G. 1979. Proper elements and family memberships of the asteroids. In *Asteroids* (T. Gehrels, Ed.), pp. 1040-1063. Univ. of Arizona Press, Tucson.

Williams, J. G. 1989. Asteroid family identifications and proper elements. In *Asteroids II* (R. P. Binzel, T. Gehrels, and M. S. Matthews, Eds.), pp. 1034-1072. Univ. of Arizona Press, Tucson.

Williams, J. G. 1992. Asteroid families - An initial search. *Icarus* **96**, 251-280.

Wisdom, J. 1982. The origin of the Kirkwood gaps: A mapping for asteroidal motion near the 3/1 commensurability. *Astron. J.* **87**, 577-593.

Wisdom, J. 1983. Chaotic behavior and the origin of the 3/1 Kirkwood gap. *Icarus* **56**, 51-74.

Wisniewski, W. Z., and R. S. McMillan 1987. Differential CCD photometry of faint asteroids in crowded star fields and nonphotometric sky conditions. *Astron. J.* **93**, 1264-1267.

Wood, J. H., and G. P. Kuiper 1963. Photometric studies of asteroids. *Astrophys. J.* **137**, 1279-1285.

Xu, S., R. P. Binzel, T. H. Burbine, and S. J. Bus 1995. Small Main-belt Asteroid Spectroscopic Survey: Initial results. *Icarus* **115**, 1-35.

Yoder, C. F. 1979. Notes on the origin of the Trojan asteroids. *Icarus* **40**, 341-344.

Yuasa, M. 1973. Theory of secular perturbations of asteroids including terms of higher orders and higher degrees. *Publ. Astron. Soc. Jpn.* **25**, 399-445.

Zappalà, V., P. Farinella, Z. Knežević, and P. Paolicchi 1984. Collisional origin of the asteroid families: Mass and velocity distributions. *Icarus* **59**, 261-285.

Zappalà, V., A. Cellino, P. Farinella, and Z. Knežević 1990. Asteroid families: I. Identification by hierarchical clustering and reliability assessment. *Astron. J.* **100**, 2030-2046.

Zappalà, V., A. Cellino, P. Farinella, and A. Milani 1994. Asteroid families: Extension to unnumbered multi-opposition asteroids. *Astrophys. J.* **107**, 772-801.

Zappalà, V., P. Bendjoya, A. Cellino, P. Farinella, and C. Froeschlé 1995. Asteroid families: Search of a 12,487-asteroid sample using two different clustering techniques. *Icarus* **106**, 291-314.

Zellner, B. 1973. Polarimetric albedos of asteroids. *Bull. Am. Astron. Soc.* **5**, 388.

Zellner, B. 1979. Asteroid taxonomy and the distribution of the compositional types. In *Asteroids* (T. Gehrels, Ed.), pp. 783-806. Univ. of Arizona Press, Tucson.

Zellner, B., M. Leaka, J. G. Williams, and D. Morrison 1977. The E asteroids and the origin of the enstatite achondrites. *Geochim. Cosmochim. Ac.* **41**, 1759-1767.

Zellner, B., D. J. Tholen, and E. F. Tedesco 1985. The eight-color asteroid survey: Results for 589 minor planets. *Icarus* **61**, 355-416.

Appendix A

Summary of the SMASSII observations and taxonomic classifications

This table contains a summary of the observational circumstances and classification results for 1189 asteroids observed during SMASSII.

The first three columns provide general information for each asteroid. The permanent number and name (or provisional designation) is listed in the first column. This is followed by *H*, the visual absolute magnitude calculated in the *H,G* system (Bowell *et al.* 1989b). These values of *H* were extracted from the Lowell Observatory asteroid database (update version January 1998). For those asteroids observed by IRAS, the third column contains the value for p_H, the IRAS (*V*-band, geometric) albedo, which is also calculated based on the *H,G* system. These albedos were obtained from the IMPS Final Product files #102 and #103. Six entries (marked with a pair of asterisks, **) were not included in these two final product files because the IRAS observations did not meet certain final quality criteria. Instead, these six values were obtained from an earlier listing of IRAS albedos (p_V) by Tedesco *et al.* (1989).

Columns 4 through 9 describe the observational circumstances for the SMASSII data. Any observation that was rejected during the reduction process, and not included in the final reduced spectrum of the asteroid (as plotted in Appendix B), is not included in this tabulation. Multiple lines provide the nightly details for those asteroids that were observed on more than one date. Column 4 gives the UT Date of the observations. The information contained in columns 5 through 9 has been condensed, and correspondingly, the table headings for these columns have been abbreviated to the

letters *a* - *e*. Column *a* gives the telescope and detector combination, where 1 = the 1.3-m (f/7.5) McGraw-Hill telescope, 2 = the 2.4-m (f/7.6) Hiltner telescope, C = "Charlotte" (a SITE 1024x1024 thinned, backside illuminated CCD), and W = "Wilbur" (a Loral 2048x2048 thick, front-side illuminated CCD). Column *b* gives the total exposure time, in seconds, followed by the number of CCD exposures (in parentheses). Column *c* gives the mean airmass of the observations, calculated from the airmass values recorded at the beginning of each exposure. The sky conditions at the time of the observations are summarized in column *d*, where the letter c = cloudy, roughly defined as the presence of clouds (usually noted in the observing log) that led to erratic variations (greater than 5%) in the observed flux of either the solar-analog stars or asteroids, h = a relative humidity greater than 70%, and m = moonlight, where the lunar illumination is greater than 50%, and the moon's altitude above the horizon is greater than 20°. Column *e* gives the solar-analog star used in the calibration of the asteroid spectra, where s1 = 16 Cyg B (HD186427), s2 = Hyades 64 (HD28099), s3 = HR4486 (HD101177), and s4 = HR5384 (HD126053).

Columns 10 through 12 give the primary spectral components Slope, PC2', and PC3' that were calculated based on the entire SMASSII dataset as described in Chapter 3. The Slope component has units of μm^{-1}, where the line fitted to each spectrum is forced to have a value of 1.00 at 0.55 μm, as given by Eqn. 3.3. The estimated uncertainties in these components are: ±0.05 in Slope, ±0.025 in PC2', and ±0.02 in PC3' for any asteroid that was measured on just one observing run. An explanation of these uncertainties is given in Section 3.5. For asteroids classified by Tholen based on his analysis of the ECAS colors (Tholen 1984), those spectral classes are given in column 13 under the heading of "Old". The new spectral classes, based on the feature-based taxonomy described in Chapter 4, are listed in the final column under the heading of "New".

Asteroid	H	p_H	Observational circumstances						Spectral components			Classification	
			UT Date	a	b	c	d	e	Slope	PC2'	PC3'	Old	New
1 Ceres	3.3	0.11	22 Aug 1993	1C	10(2)	1.16	c	s1	0.0910	0.2339	-0.0211	G	C
			7 Jan 1994	2C	6(2)	1.16		s2					
2 Pallas	4.1	0.16	22 Aug 1993	1C	30(2)	1.11		s1	-0.0312	0.2652	0.0351	B	B
3 Juno	5.3	0.24	23 Feb 1994	2C	20(2)	1.26		s3	0.2393	-0.0385	-0.0018	S	Sk
			12 Oct 1996	2C	5(5)	1.28		s1					
4 Vesta	3.2	0.42	18 Apr 1996	1W	4(5)	1.33		s1	-0.1756	-0.3024	0.1180	V	V
5 Astraea	6.8	0.23	8 Feb 1995	2C	20(4)	1.05	m	s2	0.3972	-0.1283	0.0277	S	S
6 Hebe	5.7	0.27	31 Mar 1994	2C	30(2)	1.20	m	s3	0.4348	-0.0859	0.0025	S	S
7 Iris	5.5	0.28	4 Sep 1995	1W	30(3)	1.03		s2	0.4551	-0.1146	0.0044	S	S
			28 Jan 1996	2C	25(5)	1.03	cm	s2					
10 Hygiea	5.4	0.07	6 Jan 1994	2C	60(2)	1.35		s2	-0.0275	0.2629	0.0054	C	C
			22 Feb 1994	2C	20(2)	1.43		s3					
			23 Feb 1994	2C	20(2)	1.43	m	s3					
			12 Oct 1996	2C	50(5)	1.08		s1					
11 Parthenope	6.6	0.18	8 Feb 1995	2C	25(5)	1.03		s2	0.2965	-0.0224	0.0061	S	Sk
13 Egeria	6.7	0.08	4 Sep 1995	1W	360(3)	1.05		s2	0.0218	0.3277	-0.0642	G	Ch
14 Irene	6.3		28 Oct 1995	1C	300(5)	1.03		s2	0.4588	0.0079	0.0243	S	S
15 Eunomia	5.3	0.21	22 Apr 1996	1W	300(5)	1.54		s1	0.3643	-0.0716	0.0256	S	S
			23 Apr 1996	1C	225(5)	1.53		s1					
16 Psyche	5.9	0.12	27 Feb 1997	2C	60(4)	1.11	m	s3	0.5425	0.2383	-0.0005	M	X
17 Thetis	7.8	0.17	21 Aug 1993	1C	200(2)	1.17	c	s1	0.6955	-0.0530	-0.0021	S	Sl
18 Melpomene	6.5	0.22	19 Jan 1997	2C	100(5)	1.15		s2	0.5529	-0.0283	-0.0190	S	S
			8 Apr 1997	2C	75(5)	1.06		s1					
19 Fortuna	7.1		13 Nov 1994	2C	60(2)	1.04	h	s2	0.0184	0.3495	-0.0525	G	Ch
20 Massalia	6.5	0.21	9 Dec 1995	2C	45(3)	1.14	m	s2	0.3198	-0.1161	0.0485	S	S
21 Lutetia	7.4	0.22	29 Nov 1996	2C	300(5)	1.51		s2	0.3522	0.1847	-0.0063	M	Xk
22 Kalliope	6.4	0.14	12 Oct 1996	2C	100(5)	1.02		s1	0.3667	0.2349	-0.0059	M	X
24 Themis	7.1		15 Nov 1994	2C	450(3)	1.41	cm	s1	-0.1071	0.3004	0.0477	C	B
			16 Nov 1994	2C	480(2)	1.41	m	s1					
25 Phocaea	7.8	0.23	20 Jan 1997	2C	300(5)	1.37	m	s2	0.5781	-0.1820	0.0190	S	S
26 Proserpina	7.5	0.20	1 May 1996	2C	75(5)	1.66	m	s1	0.4110	-0.1808	0.0086	S	S
28 Bellona	7.1	0.18	30 Nov 1996	2C	75(5)	1.11	m	s2	0.5863	-0.0942	-0.0309	S	S
29 Amphitrite	5.8	0.18	24 Feb 1997	2C	30(2)	1.49	m	s2	0.5043	-0.0036	0.0086	S	S
30 Urania	7.6	0.17	6 Jan 1994	2C	400(2)	1.01	c	s2	0.7301	-0.0619	-0.0042	S	Sl
31 Euphrosyne	6.7	0.05	5 Nov 1994	1W	240(2)	1.26		s1	0.0480	0.2957	0.0476	C	Cb
32 Pomona	7.6	0.26	17 Jan 1997	2C	150(5)	1.06	m	s2	0.4338	-0.1181	0.0205	S	S
33 Polyhymnia	8.6		15 Dec 1995	2C	180(3)	1.02	h	s2	0.1729	-0.0831	0.0484	S	Sq
34 Circe	8.5	0.05	14 Nov 1994	2C	120(2)	1.04	h	s1	0.0011	0.3502	-0.0217	C	Ch
			12 Feb 1995	2C	200(2)	1.07	m	s2					
35 Leukothea	8.5	0.07	14 May 1995	2C	240(2)	1.15	m	s3	0.0886	0.2140	-0.1021	C	C
37 Fides	7.3	0.18	6 Jan 1994	2C	240(2)	1.01	c	s2	0.6023	-0.0942	-0.0148	S	S
			1 Apr 1994	2C	120(2)	1.05		s3					
38 Leda	8.3	0.06	27 Feb 1997	2C	120(4)	1.25	m	s3	0.1478	0.2902	-0.1377	C	Cgh
39 Laetitia	6.1	0.29	8 Sep 1996	2C	15(5)	1.41		s1	0.4570	-0.0394	0.0819	S	S
40 Harmonia	7.0	0.24	8 Feb 1996	2C	150(5)	1.26	m	s2	0.4711	-0.1282	0.0431	S	S
41 Daphne	7.1	0.08	28 Mar 1994	2C	40(2)	1.12	m	s3	0.0554	0.2837	-0.0561	C	Ch
42 Isis	7.5	0.17	5 Nov 1994	1W	60(2)	1.14		s1	0.6373	-0.0233	0.0190	S	L
43 Ariadne	7.9	0.27	18 Jan 1997	2C	150(5)	1.05		s2	0.2914	-0.0755	-0.0003	S	Sk
44 Nysa	7.0	0.55	5 Nov 1994	1W	120(2)	1.33		s1	0.0780	0.2008	0.0731	E	Xe
45 Eugenia	7.5	0.04	19 Apr 1996	1W	600(5)	1.33		s1	0.0621	0.2203	0.0563	FC	C
			20 Apr 1996	1W	600(5)	1.34		s1					
46 Hestia	8.4	0.05	5 Nov 1994	1W	120(2)	1.05		s1	0.2333	0.2517	0.0924	P	Xc
			9 Feb 1995	2C	200(2)	1.06	m	s2					
47 Aglaja	7.8	0.08	5 Nov 1994	1W	400(2)	1.15		s1	-0.1021	0.2986	0.0371	C	B
48 Doris	6.9	0.06	10 Dec 1995	2C	135(3)	1.11	m	s2	-0.1811	0.3884	-0.0688	CG	Ch
49 Pales	7.8	0.06	18 Apr 1996	1W	900(2)	1.37		s1	-0.1239	0.3232	-0.1024	CG	Ch

Asteroid	H	p_H	Observational circumstances						Spectral components			Classification	
			UT Date	*a*	*b*	*c*	*d*	*e*	Slope	PC2'	PC3'	Old	New
50 Virginia	9.2	0.04	24 Feb 1997	2C	480(2)	1.11	m	s2	-0.2028	0.3680	-0.0256	X	Ch
51 Nemausa	7.4	0.09	15 Dec 1995	2C	360(3)	1.14		s2	0.1821	0.2789	-0.1094	CU	Ch
52 Europa	6.3	0.06	20 Feb 1994	2C	20(2)	1.02	m	s3	0.1440	0.1673	-0.0462	CF	C
54 Alexandra	7.7	0.06	20 Feb 1994	2C	120(1)	1.01	m	s3	0.0923	0.1913	-0.1063	C	C
55 Pandora	7.8	0.30	11 Sep 1996	2C	300(5)	1.02	h	s2	0.2690	0.2550	0.0387	M	X
56 Melete	8.3	0.07	20 Feb 1994	2C	120(2)	1.17		s3	0.3731	0.0891	0.0151	P	Xk
57 Mnemosyne	7.0	0.21	22 Feb 1997	2C	720(3)	1.43		s2	0.5083	-0.0484	0.0441	S	S
58 Concordia	8.9	0.06	29 Jan 1996	2C	1080(2)	1.22	cm	s2	-0.0898	0.3367	-0.0543	C	Ch
			17 Jan 1997	2C	360(3)	1.05	h	s2					
59 Elpis	7.9	0.04	8 Dec 1995	2C	360(3)	1.12	m	s2	-0.0041	0.3304	0.1119	CP	B
60 Echo	8.2	0.25	30 Apr 1996	2C	600(5)	1.60		s1	0.4758	-0.2302	0.0227	S	S
61 Danaë	7.7	0.22	5 Nov 1994	1W	400(2)	1.32		s1	0.5722	-0.1366	0.0315	S	S
62 Erato	8.8	0.06	6 Jan 1994	2C	600(2)	1.02	c	s2	-0.2304	0.2987	-0.0026	BU	Ch
63 Ausonia	7.6	0.16	31 Mar 1994	2C	120(2)	1.02		s3	0.8445	-0.1986	0.0015	S	Sa
64 Angelina	7.7	0.43**	17 Jan 1997	2C	150(5)	1.11	h	s2	0.4783	0.1273	0.0302	E	Xe
			14 Apr 1997	2C	150(5)	1.08		s1					
65 Cybele	6.6	0.07	19 Feb 1994	2C	100(2)	1.12	h	s3	0.1835	0.2030	0.0293	P	Xc
67 Asia	8.3	0.26	18 Apr 1996	1W	1200(2)	1.14		s1	0.4081	-0.1897	0.0214	S	S
			25 Apr 1996	1C	1350(3)	1.13	c	s1					
69 Hesperia	7.0	0.14	1 May 1996	2C	360(4)	1.42		s1	0.2999	0.1968	0.0408	M	X
70 Panopaea	8.1	0.07	23 Aug 1993	1C	300(3)	1.18		s1	0.0738	0.3101	-0.0589	C	Ch
			14 Nov 1994	2C	240(2)	1.00	h	s1					
71 Niobe	7.3	0.31	5 Nov 1994	1W	600(3)	1.02		s1	0.4558	0.1239	-0.0414	S	Xe
			28 Oct 1995	1C	540(3)	1.06		s2					
74 Galatea	8.7	0.04	23 Feb 1994	2C	240(2)	1.16	m	s3	-0.0050	0.2113	0.0168	C	C
75 Eurydike	9.0	0.15	10 Feb 1995	2C	240(2)	1.02	cm	s3	0.4530	0.1919	-0.0078	M	Xk
76 Freia	7.9	0.04	20 Apr 1996	1W	1800(3)	1.08		s1	0.1462	0.2397	0.0164	P	X
80 Sappho	8.0	0.18	29 Apr 1996	2C	150(5)	1.46	cm	s1	0.5952	-0.1421	-0.0069	S	S
81 Terpsichore	8.5	0.05	11 Dec 1995	2C	240(2)	1.01	m	s2	0.0499	0.2643	0.0750	C	Cb
82 Alkmene	8.4	0.21	8 Sep 1996	2C	900(3)	1.52		s1	0.1384	-0.0332	0.1358	S	Sq
83 Beatrix	8.7	0.09	23 Feb 1997	2C	480(2)	1.01	cm	s2	0.3455	0.2521	0.0996	X	X
84 Klio	9.3	0.05	6 Jan 1994	2C	360(2)	1.02	c	s2	0.0003	0.3232	-0.0382	G	Ch
85 Io	7.6	0.07	8 Dec 1995	2C	135(3)	1.12	m	s2	-0.0845	0.3212	0.0498	FC	B
87 Sylvia	6.9	0.04	21 Apr 1996	1W	720(4)	1.43		s1	0.2863	0.2222	0.0572	P	X
88 Thisbe	7.0	0.07	9 Sep 1996	2C	300(5)	1.03		s1	-0.1265	0.2785	0.0597	CF	B
90 Antiope	8.3	0.06	14 Nov 1994	2C	480(2)	1.55	hm	s1	0.0094	0.2253	0.0427	C	C
91 Aegina	8.8	0.04	22 Jan 1997	2C	180(3)	1.06	cm	s2	0.1230	0.2794	-0.0793	CP	Ch
			27 Feb 1997	2C	240(2)	1.08	m	s3					
92 Undina	6.6	0.25	17 Nov 1994	2C	60(2)	1.05	hm	s2	0.2312	0.2194	0.0769	X	Xc
93 Minerva	7.7	0.09	27 Oct 1995	1C	270(3)	1.27		s1	0.0847	0.2578	0.0258	CU	C
95 Arethusa	7.8	0.07	8 Sep 1996	2C	300(5)	1.01		s2	0.0319	0.3313	-0.0614	C	Ch
96 Aegle	7.7	0.05	22 Apr 1996	1W	1200(2)	1.11		s1	0.5669	0.1933	0.0765	T	T
			23 Apr 1996	1C	900(3)	1.10		s1					
99 Dike	9.4	0.06	20 Feb 1994	2C	240(2)	1.16	c	s3	0.2637	0.1656	-0.0254	C	Xk
			24 Feb 1994	2C	300(2)	1.14	cm	s2					
			30 Mar 1994	2C	180(1)	1.27	cm	s3					
100 Hekate	7.7	0.19	5 Nov 1994	1W	360(2)	1.14		s1	0.5660	-0.0614	0.0162	S	S
101 Helena	8.3	0.19	11 Feb 1995	2C	120(2)	1.06	hm	s3	0.4913	-0.2137	-0.0433	S	S
102 Miriam	9.3	0.05	7 Feb 1996	2C	1200(2)	1.21	m	s2	0.0920	0.2247	-0.0585	P	C
103 Hera	7.7	0.18	21 Apr 1996	1W	720(4)	1.50		s1	0.5671	-0.2209	0.0362	S	S
105 Artemis	8.6	0.05	29 Nov 1996	2C	540(3)	1.26		s2	0.0785	0.3169	-0.0196	C	Ch
106 Dione	7.4	0.09	20 Feb 1994	2C	120(2)	1.01	m	s3	-0.0699	0.2404	-0.1563	G	Cgh
107 Camilla	7.1	0.05	31 Mar 1994	2C	120(2)	1.06		s3	0.2058	0.2513	0.0521	C	X
108 Hecuba	8.1	0.24	19 Apr 1996	1W	900(3)	1.29		s1	0.6582	-0.2220	0.0048	S	Sl
110 Lydia	7.8	0.18	7 Apr 1997	2C	150(5)	1.50		s1	0.2383	0.2517	0.0178	M	X
111 Ate	8.0	0.06	6 Sep 1996	2C	300(5)	1.03	h	s2	-0.0167	0.3558	-0.0264	C	Ch

Asteroid	H	p_H	Observational circumstances						Spectral components			Classification	
			UT Date	*a*	*b*	*c*	*d*	*e*	Slope	PC2'	PC3'	Old	New
112 Iphigenia	9.8	0.04	7 Apr 1997	2C	1200(2)	1.11		s1	0.0580	0.2670	-0.0309	DCX	Ch
113 Amalthea	8.7	0.26	24 Apr 1996	1C	540(3)	1.54		s1	0.3614	-0.3485	-0.0765	S	S
114 Kassandra	8.3	0.09	11 Dec 1995	2C	90(3)	1.04	m	s2	0.4530	0.1474	0.0654	T	Xk
115 Thyra	7.5	0.27	30 Mar 1994	2C	120(2)	1.05	c	s3	0.5743	-0.1585	0.0104	S	S
116 Sirona	7.8	0.26	15 Oct 1996	2C	300(5)	1.03	c	s2	0.3157	-0.0293	0.0342	S	Sk
117 Lomia	8.0	0.05	22 Jan 1997	2C	360(3)	1.03	m	s2	0.2547	0.2298	0 0249	XC	X
118 Peitho	9.1	0.22	17 Jan 1997	2C	180(3)	1.00	m	s2	0.4804	-0.1500	0.0295	S	S
119 Althaea	8.4	0.23	29 Jan 1996	2C	360(3)	1.20		s2	0.6816	-0.2333	-0.0034	S	Sl
			21 Apr 1996	1W	1200(2)	1.12		s1					
120 Lachesis	7.8	0.05	22 Jan 1997	2C	540(3)	1.01	cm	s2	0.0929	0.2248	-0.0004	C	C
121 Hermione	7.3	0.05	19 Jan 1997	2C	360(3)	1.03	m	s2	0.0459	0.3311	-0.0951	C	Ch
122 Gerda	7.9	0.19	22 Feb 1997	2C	240(2)	1.22	m	s2	0.8795	-0.0481	-0.0021	ST	L
123 Brunhild	8.9	0.21	28 Mar 1994	2C	480(2)	1.13	m	s3	0.5543	-0.1718	0.0101	S	S
124 Alkeste	8.1	0.17	29 Nov 1996	2C	540(3)	1.18		s2	0.6190	-0.0733	-0.0073	S	S
125 Liberatrix	9.0	0.23	2 Sep 1995	1W	1800(3)	1.10		s2	0.2231	0.2359	0.0140	M	X
			8 Apr 1997	2C	900(3)	1.08		s1					
127 Johanna	8.3		15 Oct 1996	2C	360(3)	1.00	c	s2	0.0751	0.3100	-0.0331	CX	Ch
128 Nemesis	7.5	0.05	29 Jan 1996	2C	180(3)	1.13	cm	s2	0.1237	0.2056	0.0191	C	C
129 Antigone	7.1		1 Dec 1996	2C	450(5)	1.57		s1	0.1898	0.2729	0.1170	M	X
130 Elektra	7.1	0.08	19 Feb 1994	2C	40(1)	1.05	ch	s3	-0.0386	0.2627	-0.1305	G	Ch
131 Vala	10.0	0.11	22 Jan 1997	2C	900(2)	1.04	m	s2	0.1383	0.0665	-0.0375	SU	Xc
132 Aethra	9.4	0.17	6 Sep 1996	2C	1200(2)	1.13	h	s2	0.1605	0.1883	0.0081	M	Xe
			9 Sep 1996	2C	1200(2)	1.16		s2					
134 Sophrosyne	8.8	0.04	7 Jan 1994	2C	480(2)	1.03		s2	0.1107	0.3161	-0.0037	C	Ch
			19 Feb 1994	2C	40(1)	1.02	ch	s3					
135 Hertha	8.2	0.14	10 May 1995	2C	480(2)	1.10	m	s3	0.4889	0.0988	-0.0702	M	Xk
136 Austria	9.7	0.15	5 Jan 1994	2C	360(2)	1.11		s2	0.4837	0.2127	0.0627	M	Xe
139 Juewa	7.8	0.06	2 Sep 1995	1W	1800(3)	1.03		s2	0.1979	0.2759	0.0120	CP	X
140 Siwa	8.3	0.07	11 May 1995	2C	60(2)	1.44	cm	s4	0.2327	0.2027	0.0722	P	Xc
141 Lumen	8.2	0.05	8 Dec 1995	2C	180(3)	1.00	m	s2	0.0876	0.3519	-0.0062	CPF	Ch
142 Polana	10.3	0.05	25 Apr 1996	1C	1350(3)	1.70	c	s1	-0.2213	0.2898	0.0837	F	B
143 Adria	9.1	0.05	15 Oct 1996	2C	1200(2)	1.31	c	s1	0.1161	0.2193	0.0806	C	Xc
			16 Oct 1996	2C	600(2)	1.32		s1					
144 Vibilia	7.9	0.06	6 Jan 1994	2C	800(2)	1.02	c	s2	-0.0371	0.3462	-0.0509	C	Ch
			7 Jan 1994	2C	40(2)	1.00		s2					
			24 Feb 1994	2C	120(2)	1.08	cm	s2					
145 Adeona	8.1	0.04	15 Nov 1994	2C	600(3)	1.77	cm	s1	-0.0787	0.2830	-0.0100	C	Ch
146 Lucina	8.2	0.05	7 Feb 1995	2C	120(2)	1.01		s2	-0.0569	0.2726	-0.0944	C	Ch
			24 Apr 1996	1C	900(3)	1.53		s1					
147 Protogeneia	8.3	0.05	22 Apr 1996	1W	900(1)	1.37	c	s1	0.0368	0.2559	0.0339	C	C
			23 Apr 1996	1C	1800(3)	1.37		s1					
148 Gallia	7.6	0.16	7 Apr 1997	2C	300(5)	1.11		s1	0.5217	-0.1297	-0.0290	GU	S
150 Nuwa	8.2	0.04	5 Nov 1994	1W	900(3)	1.02		s1	0.0641	0.3123	0.0350	CX	Cb
151 Abundantia	9.2	0.17	18 Jan 1997	2C	900(3)	1.05	m	s2	0.7725	-0.1749	-0.0336	S	Sl
153 Hilda	7.5	0.06	7 Apr 1997	2C	540(3)	1.18		s1	0.2141	0.2776	0.0202	P	X
154 Bertha	7.6	0.05	24 Feb 1997	2C	60(1)	1.05	m	s2	0.0528	0.2969	0.0139		C
			7 Apr 1997	2C	150(5)	1.04		s1					
156 Xanthippe	8.6	0.04	12 Sep 1996	2C	540(3)	1.07	h	s2	0.0302	0.3144	-0.0503	C	Ch
158 Koronis	9.3	0.28	22 Jan 1997	2C	900(2)	1.03	cm	s2	0.3058	-0.1745	0.0167	S	S
159 Aemilia	8.1	0.06	15 Dec 1995	2C	480(2)	1.21	h	s2	-0.1125	0.3150	-0.0854	C	Ch
160 Una	9.1	0.06	15 Oct 1996	2C	540(3)	1.01	c	s2	0.1165	0.2509	0.0158	CX	C
161 Athor	9.2	0.20	11 Dec 1995	2C	270(3)	1.03	m	s2	0.1838	0.1893	0.0295	M	Xc
162 Laurentia	8.8	0.05	18 Apr 1996	1W	1800(2)	1.11		s1	0.0398	0.2924	-0.0549	STU	Ch
163 Erigone	9.5	0.05	21 Apr 1996	1W	1350(3)	1.16		s1	0.1021	0.3184	-0.0278	C	Ch
165 Loreley	7.6	0.08	25 Apr 1996	1C	1350(3)	1.17	c	s1	-0.0315	0.2469	0.0235	CD	Ch
166 Rhodope	9.9		24 Feb 1997	2C	600(2)	1.02	cm	s2	0.2422	0.1985	-0.0320	GC:	Xe

Asteroid	H	p_H	Observational circumstances						Spectral components			Classification	
			UT Date	*a*	*b*	*c*	*d*	*e*	Slope	PC2'	PC3'	Old	New
167 Urda	9.2	0.22	5 Jan 1994	2C	360(2)	1.04		s2	0.3105	0.0063	0.0311	S	Sk
168 Sibylla	7.9	0.05	24 Feb 1997	2C	360(2)	1.16	m	s2	-0.1288	0.3233	-0.0403	C	Ch
169 Zelia	9.6	0.23	18 Jan 1997	2C	600(2)	1.00	m	s2	0.7124	-0.1442	0.0258	S	Sl
171 Ophelia	8.3	0.06	19 Feb 1994	2C	100(2)	1.05	h	s3	0.0213	0.2542	-0.0157	C	C
			22 Feb 1994	2C	120(2)	1.09	m	s3					
			24 Feb 1994	2C	120(2)	1.06	cm	s2					
173 Ino	7.7	0.06	27 Mar 1994	2C	360(2)	1.18	m	s3	0.2810	0.1604	-0.0257	C	Xk
			1 Apr 1994	2C	240(2)	1.17	m	s3					
174 Phaedra	8.5	0.15	20 Apr 1996	1W	1800(2)	1.07		s1	0.4758	-0.2374	0.0099	S	S
175 Andromache	8.3	0.08	26 Feb 1997	2C	960(2)	1.47	m	s3	0.1050	0.1348	-0.1230	C	Cg
176 Iduna	7.9	0.08	10 May 1995	2C	600(2)	1.16		s1	-0.1444	0.2969	-0.0659	G	Ch
179 Klytaemnestra	8.2	0.16	10 Dec 1995	2C	135(3)	1.04	m	s2	0.2984	-0.0461	0.0786	S	Sk
183 Istria	9.7	0.19	24 Apr 1996	1C	2700(3)	1.05		s1	0.3102	-0.1834	-0.0125	S	S
184 Dejopeja	8.3	0.19	24 Feb 1997	2C	360(2)	1.05	cm	s2	0.2455	0.2605	0.0677	X	X
185 Eunike	7.6	0.06	20 Apr 1996	1W	900(3)	1.03		s1	-0.0310	0.2619	-0.0057	C	C
186 Celuta	8.9	0.19	7 Apr 1997	2C	540(3)	1.05		s1	0.4101	0.0096	-0.0888	S	K
188 Menippe	9.2	0.24	22 Aug 1993	1C	601(2)	1.37	c	s1	0.5496	-0.1967	-0.0145	S	S
			7 Feb 1996	2C	1200(2)	1.29	m	s2					
190 Ismene	7.6		18 Jan 1997	2C	900(3)	1.13	m	s2	0.1489	0.2644	0.0456	P	X
192 Nausikaa	7.1	0.23	5 Jan 1994	2C	20(2)	1.00		s2	0.7587	-0.1429	-0.0179	S	Sl
			6 Jan 1994	2C	60(2)	1.01	c	s2					
			1 Apr 1994	2C	120(2)	1.02		s3					
193 Ambrosia	9.7		9 Dec 1995	2C	180(3)	1.05	m	s2	0.2619	-0.0039	0.0264		Sk
194 Prokne	7.7	0.05	27 Mar 1994	2C	180(2)	1.21		s3	0.1722	0.2402	-0.0638	C	C
			31 Mar 1994	2C	180(2)	1.21	m	s3					
195 Eurykleia	9.0	0.06	17 Nov 1994	2C	360(2)	1.00	hm	s2	-0.0144	0.3290	-0.0827	C	Ch
196 Philomela	6.5	0.23	13 May 1995	2C	45(3)	1.47	m	s1	0.3492	-0.0740	0.0352	S	S
197 Arete	9.2	0.44	9 Feb 1996	2C	1200(2)	1.15	m	s2	0.4360	-0.2578	-0.0367	S	S
198 Ampella	8.3	0.25	23 Feb 1997	2C	400(2)	1.08	cm	s2	0.4330	-0.0454	0.0557	S	S
199 Byblis	8.3		22 Feb 1997	2C	600(2)	1.07	m	s2	0.5180	0.2778	0.0728		X
200 Dynamene	8.3	0.05	7 Jan 1994	2C	120(2)	1.00		s2	0.0279	0.3600	-0.0191	C	Ch
201 Penelope	8.4	0.16	9 Feb 1995	2C	200(2)	1.03	m	s2	0.2513	0.2277	0.0359	M	X
205 Martha	9.2	0.05	27 Oct 1995	1C	1200(2)	1.05		s2	-0.0087	0.3151	-0.0177	C	Ch
206 Hersilia	8.7		9 Feb 1995	2C	240(2)	1.21	h	s2	0.1006	0.2195	-0.0227	C	C
207 Hedda	9.9	0.06	13 May 1995	2C	600(2)	1.19	m	s3	0.0881	0.2629	-0.0634	C	Ch
208 Lacrimosa	9.0	0.27	10 May 1995	2C	600(2)	1.33	m	s4	0.2937	-0.1527	0.0153	S	Sk
209 Dido	8.2	0.03	20 Feb 1994	2C	240(2)	1.34	c	s3	0.1513	0.1111	0.0002	C	Xc
210 Isabella	9.3	0.04	12 Sep 1996	2C	900(3)	1.03		s2	0.0089	0.2890	0.0911	CF	Cb
211 Isolda	7.9	0.06	12 Oct 1996	2C	180(3)	1.01		s1	0.1073	0.3021	-0.1033	C	Ch
213 Lilaea	8.6	0.09	16 Oct 1996	2C	300(5)	1.21		s2	-0.1095	0.2924	0.0895	F	B
214 Aschera	9.5	0.52	22 Feb 1994	2C	240(2)	1.24		s3	0.1428	0.0574	-0.0309	E	Xc
216 Kleopatra	7.3	0.12	5 Nov 1994	1W	90(3)	1.14		s1	0.3673	0.2803	0.0823	M	Xe
221 Eos	7.7	0.14	15 Nov 1994	2C	300(2)	1.54	cm	s1	0.3221	0.0264	0.0481	S	K
226 Weringia	9.7	0.19	15 Dec 1995	2C	1008(2)	1.12		s2	0.4015	-0.0957	0.0491		S
230 Athamantis	7.4	0.17	28 Nov 1996	2C	150(5)	1.19	h	s1	0.7958	-0.0520	0.0247	S	Sl
234 Barbara	9.0	0.23	6 Apr 1997	2C	540(3)	1.22	c	s1	1.1832	0.0537	-0.0687	S	Ld
			7 Apr 1997	2C	360(3)	1.22		s1					
236 Honoria	8.2	0.13	18 Apr 1996	1W	1800(2)	1.14		s1	0.7564	0.0727	0.0033	S	L
			19 Apr 1996	1W	1800(2)	1.13		s1					
			8 Apr 1997	2C	540(3)	1.44		s1					
237 Coelestina	9.2	0.21	29 Nov 1996	2C	540(3)	1.10	cm	s2	0.5144	-0.1911	-0.0259	S	S
238 Hypatia	8.2	0.04	8 Apr 1997	2C	540(3)	1.34		s1	0.0336	0.2896	-0.0755	C	Ch
240 Vanadis	9.0	0.04	9 May 1995	2C	600(2)	1.10	m	s3	0.1932	0.2417	-0.0718	C	C
242 Krlemhild	9.2	0.16	22 Jan 1997	2C	540(3)	1.14	m	s2	0.2545	0.2151	0.0503		Xc
243 Ida	9.9	0.24	17 Jan 1997	2C	900(3)	1.01	hm	s2	0.4016	-0.1027	0.0268	S	S
244 Sita	12.2	0.19	7 Feb 1995	2C	1800(2)	1.32		s2	0.6884	-0.2929	-0.0251		Sa

Asteroid	H	p_H	Observational circumstances						Spectral components			Classification	
			UT Date	a	b	c	d	e	Slope	PC2'	PC3'	Old	New
245 Vera	7.8	0.21	31 Mar 1994	2C	300(2)	1.01		s3	0.4595	-0.1533	-0.0005	S	S
246 Asporina	8.6	0.17	7 Jan 1994	2C	360(2)	1.33		s2	0.9554	-0.3349	-0.0880	A	A
			18 Apr 1996	1W	540(3)	1.14		s1					
			19 Apr 1996	1W	540(3)	1.12		s1					
247 Eukrate	8.0	0.06	20 Feb 1994	2C	200(2)	1.20	c	s3	0.1341	0.1505	0.0106	CP	Xc
250 Bettina	7.6	0.26	19 Feb 1994	2C	120(2)	1.08	h	s3	0.3724	0.1261	0.0412	M	Xk
253 Mathilde	10.2	0.04	7 Feb 1995	2C	900(1)	1.14		s2	-0.0772	0.2469	0.0166		Cb
			8 Feb 1995	2C	1800(2)	1.13		s2					
			24 Apr 1996	1C	2700(3)	1.35		s1					
257 Silesia	9.5	0.05	18 Apr 1996	1W	1800(2)	1.42		s1	0.0067	0.2602	-0.0733	SCTU	Ch
			19 Apr 1996	1W	1800(2)	1.43		s1					
259 Aletheia	7.8	0.04	13 Apr 1997	2C	300(5)	1.34		s1	0.1992	0.2330	-0.0156	CP	X
261 Prymno	9.4	0.11	6 Jan 1994	2C	600(2)	1.05	c	s2	0.2364	0.2444	0.0524	B	X
263 Dresda	10.4	0.23	22 Aug 1993	1C	1200(2)	1.64		s1	0.5198	-0.1434	0.0034		S
264 Libussa	8.4	0.30	8 Dec 1995	2C	900(3)	1.10	m	s2	0.4271	-0.1121	0.0833	S	S
266 Aline	8.8	0.04	13 May 1995	2C	600(2)	1.61	m	s1	-0.0943	0.2836	-0.0406	C	Ch
267 Tirza	10.5	0.04	9 Dec 1995	2C	1200(2)	1.05	m	s2	0.7670	0.1691	0.1133	DU	D
269 Justitia	9.5	0.10	17 Nov 1994	2C	1200(2)	1.12	h	s2	1.3224	0.0479	0.0576		Ld
272 Antonia	10.7	0.14	5 Jan 1994	2C	600(2)	1.01		s2	0.2178	0.2904	0.0813		X
275 Sapientia	8.8	0.04**	15 Oct 1996	2C	540(3)	1.26	c	s2	0.0563	0.2409	0.0423	X	C
278 Paulina	9.4	0.25	28 Oct 1995	1C	1800(2)	1.05		s2	0.4712	-0.1361	-0.0192		S
279 Thule	8.6	0.04	22 Feb 1997	2C	1800(2)	1.02	m	s2	0.3895	0.3871	0.1458	D	X
281 Lucretia	12.0	0.20	26 May 1997	2C	1200(2)	1.66		s1	0.4245	-0.2773	-0.0205	SU	S
282 Clorinde	10.9	0.05	14 Apr 1997	2C	1350(3)	1.26		s1	-0.1931	0.2790	0.0469	BFU:	B
284 Amalia	10.0	0.06	14 Dec 1995	2C	600(2)	1.04		s2	-0.0663	0.3860	-0.0037	CX	Ch
286 Idea	9.0	0.05	21 Apr 1996	1W	2700(3)	1.09		s1	0.0447	0.3228	-0.0623	CX	Ch
288 Glauke	9.8	0.20	21 Apr 1996	1W	1800(3)	1.53		s1	0.5999	-0.2251	0.0247	S	S
289 Nenetta	9.5	0.24	13 Apr 1997	2C	1350(3)	1.06		s1	0.6633	-0.5324	-0.2096	A	A
295 Theresia	10.2	0.19	30 Apr 1996	2C	1800(3)	1.56	m	s1	0.4703	-0.1567	0.0187	S	S
301 Bavaria	10.1	0.05	29 Jan 1996	2C	1800(2)	1.22		s2	0.0052	0.2482	-0.0620		C
304 Olga	9.7	0.05	18 Apr 1996	1W	1800(2)	1.11		s1	0.1673	0.1750	0.0370	C	Xc
			19 Apr 1996	1W	1800(2)	1.10		s1					
306 Unitas	9.0	0.21	8 Feb 1995	2C	480(2)	1.08	cm	s2	0.5111	-0.2811	0.0045	S	S
308 Polyxo	8.2	0.05	9 Feb 1995	2C	120(2)	1.03	m	s2	0.6413	0.1580	0.0612	T	T
			8 Feb 1996	2C	360(3)	1.34	m	s2					
310 Margarita	10.3	0.12	12 Feb 1995	2C	1800(2)	1.09	m	s2	0.4906	-0.1287	-0.0869		S
312 Pierretta	8.9	0.20	8 Dec 1995	2C	1200(2)	1.05	m	s2	0.2917	-0.1611	0.0575	S	Sk
317 Roxane	10.0	0.49	9 Dec 1995	2C	600(2)	1.15		s2	0.1067	0.1893	0.0670	E	Xe
321 Florentina	10.0	0.23	15 Nov 1994	2C	480(2)	1.06	cm	s1	0.3862	-0.1066	0.0224	S	S
322 Phaeo	9.0	0.09	29 Jan 1996	2C	1800(2)	1.59		s2	0.2725	0.1698	0.0799	X	X
327 Columbia	10.1	0.24	17 Oct 1996	2C	1200(2)	1.01		s2	0.6726	-0.1513	-0.0362		Sl
331 Etheridgea	9.6	0.04	26 May 1997	2C	1200(2)	1.31		s1	-0.0020	0.2504	-0.0293	CX	C
332 Siri	9.5	0.17	16 Oct 1996	2C	900(3)	1.06	c	s2	0.2983	0.2099	0.0339		Xk
335 Roberta	9.0	0.06	8 Feb 1995	2C	400(2)	1.06	m	s2	-0.0601	0.2769	0.0613	FP	B
336 Lacadiera	9.8	0.05	30 Apr 1996	2C	300(5)	1.61	m	s1	0.4176	0.1919	0.0960	D	Xk
337 Devosa	8.7	0.16	26 May 1997	2C	360(3)	1.28		s1	0.1219	0.1787	0.0351	X	X
338 Budrosa	8.5	0.18	20 Feb 1994	2C	120(2)	1.16	m	s3	0.3353	0.1046	-0.0085	M	Xk
339 Dorothea	9.2	0.24	23 Feb 1994	2C	800(2)	1.10	m	s3	0.5066	-0.0302	0.0148	S	K
			1 Apr 1994	2C	900(2)	1.10		s3					
342 Endymion	10.2	0.04	8 Dec 1995	2C	600(2)	1.04	m	s2	-0.1128	0.3356	-0.0258	C	Ch
345 Tercidina	8.7	0.07	14 Dec 1995	2C	90(3)	1.08		s2	-0.0989	0.3540	-0.0291	C	Ch
346 Hermentaria	7.1	0.22	22 Feb 1997	2C	120(2)	1.07	m	s2	0.3909	-0.0675	-0.0324	S	S
			8 Apr 1997	2C	150(5)	1.03		s1					
348 May	9.4	0.04	5 Nov 1994	1W	1800(2)	1.28		s1	0.1643	0.2450	0.0266		X
349 Dembowska	5.9	0.38	1 Dec 1996	2C	100(5)	1.63		s1	0.2888	-0.4767	0.0397	R	R
352 Gisela	10.0	0.43	22 Feb 1997	2C	300(1)	1.14	m	s2	0.6649	-0.1784	-0.0459	S	Sl

Asteroid	H	p_H	Observational circumstances						Spectral components			Classification	
			UT Date	*a*	*b*	*c*	*d*	*e*	Slope	PC2'	PC3'	Old	New
			7 Apr 1997	2C	900(3)	1.13		s1					
353 Ruperto-Carola	11.0		22 Feb 1997	2C	600(1)	1.08	m	s2	0.5733	-0.1446	-0.0124		S
			9 Apr 1997	2C	1800(3)	1.03		s1					
354 Eleonora	6.4	0.19	27 Oct 1995	1C	240(4)	1.16		s2	0.8792	-0.1375	-0.0486	S	SI
			22 Feb 1997	2C	180(3)	1.28		s2					
355 Gabriella	10.4	0.23	25 Feb 1994	2C	1200(2)	1.01	cm	s2	0.5215	-0.2656	-0.0094		S
358 Apollonia	9.1	0.05	5 Nov 1994	1W	1800(2)	1.04		s1	0.1098	0.3157	-0.1095		Ch
359 Georgia	8.9	0.26	8 Dec 1995	2C	1200(2)	1.02	m	s2	0.1514	0.2700	0.0929	CX	X
360 Carlova	8.5	0.05	9 Dec 1995	2C	270(3)	1.19	m	s2	0.0065	0.2848	0.0435	C	C
363 Padua	9.0		21 Oct 1996	2C	1350(3)	1.03		s2	0.3407	0.2814	0.0395	XC	X
365 Corduba	9.2	0.03	24 Apr 1996	1C	2700(3)	1.13		s1	0.0792	0.2598	0.0004	X	C
366 Vincentina	8.5	0.08	18 Jan 1997	2C	900(2)	1.03	m	s2	0.0039	0.2570	-0.0816		Ch
371 Bohemia	8.7	0.19	22 Aug 1993	1C	900(3)	1.01	c	s1	0.5704	-0.1652	0.0071	QSV	S
			23 Aug 1993	1C	600(2)	1.02		s1					
			5 Jan 1994	2C	360(2)	1.05		s2					
372 Palma	7.2	0.07	10 Dec 1995	2C	135(3)	1.01	m	s2	-0.0220	0.3694	0.1118	BFC	B
374 Burgundia	8.7	0.30	27 Oct 1995	1C	1800(3)	1.11		s2	0.4886	-0.1452	0.0065	S	S
375 Ursula	7.5		10 Feb 1995	2C	120(2)	1.00	cm	s3	0.2626	0.1731	-0.0440	C	Xc
377 Campania	8.9	0.06	10 Apr 1997	2C	600(5)	1.25	c	s1	-0.0926	0.3547	-0.0357	PD	Ch
378 Holmia	9.8	0.30	28 Oct 1995	1C	2700(3)	1.03		s2	0.5671	-0.1191	0.0079	S	S
379 Huenna	8.9	0.06	6 Jan 1994	2C	960(2)	1.03	c	s2	-0.0438	0.2427	-0.0170	B	C
			7 Feb 1995	2C	600(2)	1.17		s2					
			15 May 1995	2C	1200(2)	1.13		s3					
381 Myrrha	8.2	0.06	9 Dec 1995	2C	900(2)	1.16	m	s2	-0.0466	0.2820	0.0256	C	Cb
383 Janina	9.9	0.09	6 Jan 1994	2C	1200(2)	1.05	c	s2	-0.2399	0.3110	0.0153	B	B
384 Burdigala	9.6	0.18	18 Jan 1997	2C	540(3)	1.06	m	s2	0.5062	-0.1817	0.0095	S	S
386 Siegena	7.4	0.07	28 Mar 1994	2C	600(2)	1.20		s3	0.1434	0.2513	-0.0581	C	C
			31 Mar 1994	2C	360(2)	1.20	m	s3					
387 Aquitania	7.4	0.19	21 Oct 1996	2C	360(3)	1.17		s2	0.8660	0.0866	-0.0261	S	L
388 Charybdis	8.6	0.05	22 Jan 1997	2C	900(3)	1.02	cm	s2	0.0686	0.2638	0.0412	C	C
389 Industria	7.9	0.20	8 Feb 1995	2C	30(3)	1.08		s2	0.3546	-0.0668	0.0267	S	S
391 Ingeborg	10.1		18 Apr 1996	1W	2700(3)	1.30		s1	0.5312	-0.1965	0.0179	S	S
392 Wilhelmina	9.7	0.06	13 May 1995	2C	900(3)	1.34	cm	s3	-0.0527	0.2488	-0.1131		Ch
393 Lampetia	8.4	0.08	9 May 1995	2C	60(3)	1.35		s3	0.2531	0.2318	-0.1145	C	Xc
394 Arduina	9.7	0.25	2 Sep 1995	1W	1800(3)	1.07		s2	0.4500	-0.1033	0.0290	S	S
			28 Oct 1995	1C	1200(2)	1.06		s2					
395 Delia	10.4	0.05	16 Oct 1996	2C	1800(3)	1.02	c	s2	0.1033	0.3159	-0.0102	C	Ch
396 Aeolia	9.9	0.17	9 Dec 1995	2C	1800(2)	1.21	m	s2	0.1534	0.1784	0.0138		Xe
397 Vienna	9.3	0.18	23 Feb 1994	2C	400(2)	1.23	m	s3	0.5376	-0.0592	0.0225	S	K
398 Admete	10.3	0.06	11 Feb 1995	2C	600(2)	1.23	hm	s3	0.1524	0.1606	-0.0786		C
399 Persephone	9.0	0.18	8 Dec 1995	2C	1200(2)	1.02	m	s2	0.1741	0.2733	0.0911		X
402 Chloë	9.0	0.15	22 Jan 1997	2C	180(3)	1.08	m	s2	0.4175	0.1032	0.0469	S	K
403 Cyane	9.1	0.17	21 Oct 1996	2C	360(3)	1.01		s2	0.4416	-0.0895	-0.0280	S	S
404 Arsinoë	9.0	0.05	7 Feb 1995	2C	300(2)	1.22		s2	0.1473	0.2725	-0.0542	C	Ch
405 Thia	8.5	0.05	2 Sep 1995	1W	900(3)	1.09		s2	0.0163	0.3494	-0.0789	C	Ch
409 Aspasia	7.6	0.06	10 Dec 1995	2C	270(3)	1.20	m	s2	0.2435	0.2233	0.0783	CX	Xc
410 Chloris	8.3	0.06	9 Dec 1995	2C	900(2)	1.17	m	s2	0.0173	0.3121	-0.0641	C	Ch
412 Elisabetha	9.0	0.05	9 Dec 1995	2C	1200(2)	1.45		s2	0.0121	0.2255	0.0359		C
413 Edburga	10.2	0.15	7 Apr 1997	2C	1800(2)	1.04		s1	0.1637	0.2430	0.0356	M	X
414 Liriope	9.5	0.06	15 May 1995	2C	1200(2)	1.14	m	s3	0.2049	0.1379	-0.1366	C	Cg
416 Vaticana	7.9	0.17	3 Sep 1995	1W	600(2)	1.21		s1	0.8281	-0.0918	0.0562	S	SI
417 Suevia	9.3	0.20	9 Sep 1996	2C	1800(3)	1.16	c	s2	0.3710	0.1029	-0.0479	X	Xk
423 Diotima	7.2	0.05	10 Feb 1995	2C	120(2)	1.01	c	s3	0.1079	0.1893	-0.0053	C	C
425 Cornelia	9.9	0.05	17 Nov 1994	2C	1200(2)	1.06	h	s2	0.1216	0.2442	-0.0811		C
432 Pythia	8.8	0.23	27 Mar 1994	2C	120(2)	1.18	m	s3	0.5810	-0.1989	0.0201	S	S
			1 Apr 1994	2C	120(2)	1.17	m	s3					

Asteroid	H	p_H	Observational circumstances						Spectral components			Classification	
			UT Date	a	b	c	d	e	Slope	PC2'	PC3'	Old	New
			9 Dec 1995	2C	540(3)	1.22	m	s2					
434 Hungaria	11.2	0.46**	11 Feb 1995	2C	1200(2)	1.29	h	s3	0.4660	-0.0090	-0.0282	E	Xe
441 Bathilde	8.5	0.14	12 Sep 1996	2C	450(5)	1.11	h	s2	0.5072	0.1671	0.0008	M	Xk
442 Eichsfeldia	10.0	0.04	18 Apr 1996	1W	1800(2)	1.05		s1	0.0076	0.3287	-0.0615	C	Ch
443 Photographica	10.3	0.19	26 Nov 1996	2C	900(2)	1.22		s1	0.8526	-0.1098	0.0883	S	Sl
444 Gyptis	7.8	0.05	11 Feb 1995	2C	120(2)	1.14	hm	s3	0.0379	0.2107	0.0103	C	C
446 Aeternitas	8.9	0.24	6 Jan 1994	2C	600(2)	1.01	c	s2	0.9282	-0.4425	-0.0807	A	A
			7 Jan 1994	2C	360(2)	1.00		s2					
			23 Feb 1994	2C	1200(2)	1.00	m	s3					
453 Tea	10.6	0.25	7 Apr 1997	2C	360(3)	1.19		s1	0.6200	-0.1918	-0.0684	S	S
456 Abnoba	9.2	0.23	27 Oct 1995	1C	1300(2)	1.04		s2	0.5801	-0.1551	-0.0210		S
458 Hercynia	9.6	0.17	13 Nov 1994	2C	600(2)	1.07	h	s2	0.8164	-0.0402	-0.0013	S	L
			15 Nov 1994	2C	600(2)	1.07		s1					
460 Scania	10.6	0.21	9 Dec 1995	2C	1800(2)	1.09	m	s2	0.4652	0.0321	0.0212		K
462 Eriphyla	9.2	0.28	6 Jan 1994	2C	1200(2)	1.03	c	s2	0.4224	-0.0731	-0.0203	S	S
464 Megaira	9.5	0.05	29 Jan 1996	2C	1800(2)	1.16		s2	0.0498	0.2065	0.0026	FXU:	C
470 Kilia	10.1	0.24	17 Jan 1997	2C	900(3)	1.07	m	s2	0.6005	-0.1385	0.0309	S	S
471 Papagena	6.7	0.20	23 Feb 1997	2C	40(2)	1.02	cm	s2	0.3783	-0.0359	0.0041	S	S
477 Italia	10.2	0.28	13 Apr 1997	2C	1350(3)	1.03		s1	0.5871	-0.1643	-0.0300	S	S
478 Tergeste	8.0	0.18	2 Sep 1995	1W	900(3)	1.07		s2	0.7612	0.0256	-0.0080	S	L
479 Caprera	9.6	0.05	9 Dec 1995	2C	600(2)	1.38		s2	0.0770	0.2113	0.0453		C
481 Emita	8.6		30 Nov 1996	2C	180(3)	1.08	m	s2	0.0641	0.3264	-0.0762	C	Ch
484 Pittsburghia	9.9	0.20	9 Dec 1995	2C	1200(2)	1.26	m	s2	0.5007	-0.1615	-0.0306		S
485 Genua	8.3	0.21	2 Sep 1995	1W	900(3)	1.17		s1	0.3757	-0.0909	0.0632		S
490 Veritas	8.3	0.06	13 Nov 1994	2C	900(3)	1.09	h	s2	0.1040	0.2700	-0.0291	C	Ch
491 Carina	8.5	0.07	19 Apr 1996	1W	2700(3)	1.12		s1	0.0869	0.2172	-0.0018		C
494 Virtus	9.0	0.06	12 Dec 1995	2C	600(2)	1.06	c	s2	-0.0710	0.3444	-0.0350	C	Ch
			14 Dec 1995	2C	600(2)	1.09		s2					
496 Gryphia	11.6	0.17	28 Nov 1996	2C	1800(2)	1.41	h	s1	0.5656	-0.3051	-0.0067	S	S
503 Evelyn	9.1	0.06	18 Oct 1996	2C	360(3)	1.08		s2	-0.0152	0.3421	-0.0310	XC	Ch
504 Cora	9.4	0.34	25 Feb 1994	2C	1170(2)	1.02	m	s2	0.1292	0.2448	0.0418		X
507 Laodica	9.1	0.21	29 Nov 1996	2C	600(2)	1.02		s2	0.2851	0.2740	0.0575		X
509 Iolanda	8.4	0.27	19 Jan 1997	2C	600(2)	1.15	m	s2	0.4700	-0.1246	0.0030	S	S
511 Davida	6.2	0.05	2 Dec 1996	2C	25(5)	1.18		s2	0.1051	0.2502	0.0134	C	C
512 Taurinensis	10.7	0.18	22 May 1997	2C	540(3)	1.53	cm	s1	0.4488	-0.3033	0.0028	S	S
			27 May 1997	2C	900(3)	1.55	m	s1					
513 Centesima	9.8	0.09	23 Feb 1994	2C	1200(2)	1.07	m	s3	0.4907	-0.0613	0.0289	S	K
516 Amherstia	8.3	0.16	4 Sep 1995	1W	900(3)	1.06		s2	0.2313	0.1282	0.0165	M	X
519 Sylvania	9.1	0.17	8 Sep 1996	2C	300(5)	1.33		s1	0.4732	-0.0465	-0.0041	S	S
521 Brixia	8.3	0.06	13 Nov 1994	2C	120(2)	1.03	h	s2	0.1622	0.3098	0.0054	C	Ch
523 Ada	9.6	0.25	9 Dec 1995	2C	900(2)	1.07	m	s2	0.1957	0.2597	0.0715		X
527 Euryanthe	10.1	0.06	1 Dec 1996	2C	1200(2)	1.04	m	s2	-0.0073	0.2594	0.0748		Cb
531 Zerlina	11.8	0.15	8 Apr 1997	2C	900(3)	1.29		s1	-0.1906	0.2733	-0.0044		B
532 Herculina	5.8	0.17	8 Dec 1995	2C	45(3)	1.05	m	s2	0.4699	-0.0689	0.0638	S	S
			21 Apr 1996	1W	150(5)	1.00		s1					
533 Sara	9.7	0.25	5 Nov 1994	1W	3600(4)	1.05		s1	0.4653	-0.1279	0.0202	S	S
534 Nassovia	9.8	0.20	15 Nov 1994	2C	1200(2)	1.27	cm	s1	0.2411	-0.1358	0.0107	S	Sk
539 Pamina	9.7	0.08	2 Sep 1995	1W	1800(3)	1.03		s2	0.1161	0.3255	-0.0603		Ch
541 Deborah	10.1	0.05	19 Jan 1997	2C	1800(2)	1.25		s2	-0.0893	0.3032	0.0638		B
543 Charlotte	9.4	0.26	28 Oct 1995	1C	1800(2)	1.09		s2	0.1663	0.1632	-0.0057		Xe
545 Messalina	8.8	0.04	15 Dec 1995	2C	600(2)	1.01	h	s2	-0.0310	0.3069	0.0387	CD	Cb
547 Praxedis	9.5	0.06	15 Oct 1996	2C	900(3)	1.22	c	s1	0.4002	0.2047	0.1474	XD:	Xk
			16 Oct 1996	2C	600(2)	1.23		s1					
551 Ortrud	9.6	0.04	17 Jan 1997	2C	900(3)	1.01	m	s2	0.1077	0.2847	0.0621	XC	C
553 Kundry	12.2		30 Apr 1996	2C	2700(3)	1.56		s1	0.4591	-0.3397	-0.0270		S
554 Peraga	9.0	0.05	22 Feb 1997	2C	460(2)	1.38	m	s2	0.1365	0.3314	0.0068	FC	Ch

Asteroid	H	p_H	Observational circumstances						Spectral components			Classification	
			UT Date	*a*	*b*	*c*	*d*	*e*	Slope	PC2'	PC3'	Old	New
555 Norma	10.6	0.06	1 May 1996	2C	1800(2)	1.43	m	s1	-0.3882	0.2095	-0.0141		B
556 Phyllis	9.6	0.19	8 Sep 1996	2C	360(3)	1.19		s1	0.4293	0.0018	0.0913	S	S
559 Nanon	9.4	0.05	9 May 1995	2C	600(2)	1.51		s3	0.4399	0.1326	-0.0750	C	Xk
560 Delila	10.6	0.07	8 Dec 1995	2C	1200(2)	1.04	m	s2	-0.0714	0.3322	0.0878		B
563 Suleika	8.5	0.25	30 Mar 1994	2C	600(2)	1.21	cm	s3	0.6960	-0.1770	-0.0591	S	Sl
564 Dudu	10.4	0.05	21 Apr 1996	1W	2700(3)	1.05		s1	0.2595	0.2069	0.0036	CDX:	Xc
569 Misa	10.1	0.03	14 May 1995	2C	900(1)	1.90	m	s3	0.2666	0.1507	-0.1136	C	Cg
570 Kythera	8.8	0.05	8 Apr 1997	2C	1350(3)	1.08		s1	0.6862	0.2110	-0.0188	ST	T
571 Dulcinea	11.6	0.02**	10 Dec 1995	2C	600(2)	1.03	m	s2	0.4431	-0.1855	0.0442	S	S
572 Rebekka	10.9	0.08	27 May 1997	2C	1200(2)	1.28		s1	-0.0215	0.2003	0.0924	XDC	C
578 Happelia	9.2	0.08	28 Mar 1994	2C	1200(2)	1.03	m	s3	0.2434	0.1422	-0.0801		Xc
579 Sidonia	7.8	0.17	8 Dec 1995	2C	720(3)	1.04	m	s2	0.3654	0.0786	0.0366	S	K
581 Tauntonia	9.4	0.06	27 Mar 1994	2C	1200(2)	1.04	m	s3	0.3055	0.1209	-0.0087		Xk
			15 May 1995	2C	1200(2)	1.56	m	s3					
584 Semiramis	8.7	0.20	23 Feb 1997	2C	240(2)	1.07	c	s2	0.7236	-0.17[illegible]	-0.0139	S	Sl
586 Thekla	9.2	0.05	5 Nov 1994	1W	1800(2)	1.08		s1	-0.0717	0.3728	-0.0152	C:	Ch
592 Bathseba	9.3		20 Apr 1996	1W	2700(3)	1.24		s1	0.4530	0.0329	-0.0004		K
596 Scheila	8.9	0.04	21 Apr 1996	1W	2700(3)	1.01		s1	0.5577	0.2449	0.0827	PCD	T
597 Bandusia	9.4	0.24	9 Dec 1995	2C	360(3)	1.04	m	s2	0.3485	-0.1373	0.0426		S
598 Octavia	9.5	0.05	19 Jan 1997	2C	540(3)	1.03	m	s2	0.3558	0.2587	0.0245	C:	X
599 Luisa	8.7	0.14	10 Dec 1995	2C	180(3)	1.04	m	s2	0.5384	0.0805	0.0370	S	K
600 Musa	10.2	0.24	10 Dec 1995	2C	1800(2)	1.08	m	s2	0.4328	-0.2100	0.0365		S
601 Nerthus	9.6	0.05	28 Mar 1994	2C	1200(2)	1.20	m	s3	0.1081	0.2124	0.0407	X	C
604 Tekmessa	9.2	0.09	1 May 1996	2C	1800(2)	1.12	m	s1	0.1254	0.0884	-0.0636		Xc
606 Brangäne	10.4	0.10	23 Apr 1996	1C	2700(3)	1.42		s1	0.5363	0.0283	0.0193	TSD	K
611 Valeria	9.2	0.11	9 Apr 1997	2C	1350(3)	1.34		s1	0.6740	0.0778	-0.0138	S	L
614 Pia	11.0	0.11	7 Feb 1996	2C	1800(2)	1.07	m	s2	-0.0368	0.1982	-0.0371		C
622 Esther	10.2		6 Sep 1996	2C	450(5)	1.13	h	s2	0.5008	-0.1412	-0.0030	S	S
625 Xenia	10.0	0.22	28 Mar 1994	2C	1200(2)	1.18	m	s3	0.9293	-0.2172	0.0047		Sa
627 Charis	10.0	0.08	15 Apr 1997	2C	900(3)	1.39		s1	0.3742	0.2402	0.0620	XB:	X
629 Bernardina	9.9	0.21	20 Apr 1996	1W	2700(3)	1.11		s1	0.3315	0.2077	0.0248		X
631 Philippina	8.7	0.18	23 Apr 1996	1C	1800(2)	1.45		s1	0.4493	-0.2364	0.0055	S	S
633 Zelima	9.7	0.19	23 Feb 1994	2C	1200(2)	1.07	m	s3	0.5659	-0.1003	0.0349	S	S
634 Ute	9.6	0.05	27 May 1997	2C	1200(2)	1.11	c	s1	0.0820	0.2416	0.0939		X
638 Moira	9.8	0.05	9 Dec 1995	2C	900(2)	1.11	m	s2	-0.0778	0.3348	-0.0479		Ch
642 Clara	10.0	0.16	5 Jan 1994	2C	600(2)	1.00		s2	0.6838	0.0753	-0.0028	S	L
649 Josefa	12.4		5 Jan 1994	2C	1800(3)	1.04		s2	0.2717	-0.1629	0.0270		Sk
653 Berenike	9.2	0.24	22 Jan 1997	2C	1200(2)	1.13	m	s2	0.3867	-0.0256	-0.0375	S	K
654 Zelinda	8.5	0.04	5 Nov 1994	1W	360(2)	1.01		s1	0.0841	0.3726	-0.0004	C	Ch
661 Cloelia	9.6	0.11	8 Dec 1995	2C	1200(2)	1.01	m	s2	0.3936	0.0372	0.0367	S	K
668 Dora	11.8	0.05	7 Feb 1995	2C	1800(2)	1.12		s2	-0.0602	0.3349	-0.0148		Ch
670 Ottegebe	9.8	0.18	23 Apr 1996	1C	2700(3)	1.30		s1	0.3065	-0.1500	0.0274		S
671 Carnegia	10.0	0.05	22 Jan 1997	2C	1200(2)	1.02	m	s2	0.3490	0.1946	0.0305		Xk
673 Edda	10.2	0.10	8 Feb 1996	2C	1800(2)	1.[illegible]	m	s2	0.6021	-0.0311	0.0253	S	S
675 Ludmilla	7.9		15 Oct 1996	2C	150(5)	1.00	c	s2	0.4816	-0.0460	-0.0127	S	S
677 Aaltje	9.7	0.28	20 Apr 1996	1W	2700(3)	1.27		s1	0.8050	-0.1488	0.0019		Sl
678 Fredegundis	9.0	0.25	10 Dec 1995	2C	600(2)	1.15	m	s2	0.1533	0.2412	0.0733		X
679 Pax	9.0	0.16	24 Feb 1997	2C	1200(2)	1.03	m	s2	0.5951	0.1062	-0.0187		K
687 Tinette	11.7		9 Dec 1995	2C	1800(2)	1.04	m	s2	0.2814	0.2223	0.0847	X	X
688 Melanie	10.6	0.06	12 Apr 1997	2C	1200(2)	1.34		s1	0.0831	0.2229	0.0191		C
699 Hela	11.7		9 Dec 1995	2C	1200(2)	1.05	m	s2	0.2152	-0.0712	0.0154	S	Sk
702 Alauda	7.2	0.06	12 Oct 1996	2C	360(2)	1.08		s1	-0.0482	0.3039	0.0516	C	B
705 Erminia	8.4	0.04	14 Apr 1997	2C	540(3)	1.00		s1	0.1258	0.2546	0.0180	X	C
706 Hirundo	10.2	0.17	17 Oct 1996	2C	1200(2)	1.02		s2	-0.1113	0.3346	-0.1752		Cgh
712 Boliviana	8.3	0.05	30 Mar 1994	2C	360(2)	1.16	c	s3	0.2363	0.2075	-0.0472	C	X
713 Luscinia	9.0	0.04	12 Dec 1995	2C	600(2)	1.12		s2	0.0914	0.2824	0.0585	C	C

Asteroid	H	p_H	Observational circumstances						Spectral components			Classification	
			UT Date	*a*	*b*	*c*	*d*	*e*	Slope	PC2'	PC3'	Old	New
			14 Dec 1995	2C	600(2)	1.12		s2					
715 Transvaalia	9.8	0.26	30 Nov 1996	2C	900(2)	1.06	m	s2	0.2883	0.2189	-0.0256		X
716 Berkeley	10.8	0.18	29 Nov 1996	2C	1800(2)	1.49		s2	0.5351	-0.1460	0.0296	S	S
718 Erida	9.8	0.04	25 Feb 1994	2C	1200(2)	1.02	m	s2	0.2286	0.2414	0.0323		X
720 Bohlinia	9.7	0.20	9 Feb 1996	2C	1800(2)	1.02	c	s2	0.1741	-0.0702	-0.0041	S	Sq
723 Hammonia	9.7	0.18	23 May 1997	2C	900(2)	1.40	cm	s1	-0.0188	0.2243	0.0498		C
			24 May 1997	2C	1800(3)	1.40	m	s1					
729 Watsonia	9.3	0.14	11 Feb 1995	2C	600(2)	1.11	h	s3	0.7886	-0.0594	-0.0390	STGD	L
731 Sorga	9.6	0.14	15 May 1995	2C	600(2)	1.38	m	s3	0.3265	0.1340	0.0089	CD	Xe
735 Marghanna	9.6	0.05	8 Feb 1996	2C	1800(2)	1.15	m	s2	-0.1378	0.3611	-0.0183	C	Ch
737 Arequipa	8.8	0.27	22 Feb 1997	2C	1200(2)	1.16	m	s2	0.6234	-0.1292	-0.0214	S	S
739 Mandeville	8.5	0.05	9 Feb 1995	2C	240(2)	1.12	h	s2	0.3000	0.2269	0.0183	X	X
741 Botolphia	10.4	0.14	21 Oct 1996	2C	1200(2)	1.26		s2	0.1458	0.2485	0.0729	X	X
742 Edisona	9.6	0.13	8 Feb 1996	2C	1200(2)	1.04		s2	0.2981	0.0178	-0.0056	S	K
743 Eugenisis	10.0	0.06	4 Sep 1995	1W	2700(3)	1.04		s2	0.1824	0.3004	-0.0798		Ch
747 Winchester	7.7	0.05	12 Apr 1997	2C	540(3)	1.11		s1	0.1171	0.2489	0.0019	PC	C
749 Malzovia	11.8		24 Feb 1997	2C	600(1)	1.19	m	s2	0.5251	-0.1552	-0.0519	S	S
			7 Apr 1997	2C	360(3)	1.13		s1					
751 Faïna	8.7	0.05	19 Feb 1994	2C	240(2)	1.03	h	s3	0.0376	0.2643	-0.0437	C	Ch
753 Tiflis	10.2	0.26	28 Nov 1996	2C	900(3)	1.13	chm	s2	0.8192	-0.0289	-0.0210	S	L
754 Malabar	9.2	0.05	25 May 1997	2C	1350(3)	1.15	c	s1	-0.0469	0.3114	-0.0376	XC	Ch
757 Portlandia	10.2	0.14	19 Jan 1997	2C	900(3)	1.01	m	s2	0.3732	0.1941	0.0303	XF	Xk
759 Vinifera	10.5	0.05	5 Nov 1994	1W	1800(2)	1.05		s1	0.1391	0.2379	0.0359		X
767 Bondia	10.0	0.10	30 Nov 1996	2C	900(2)	1.04		s2	-0.2597	0.3001	0.0450		B
771 Libera	10.5	0.13	8 Dec 1995	2C	360(3)	1.14	m	s2	0.1226	0.2606	0.0877	X	X
773 Irmintraud	9.1	0.04	7 Apr 1997	2C	1200(2)	1.10		s1	0.6601	0.2100	0.0095	D	T
776 Berbericia	7.7	0.07	1 Apr 1994	2C	300(2)	1.04		s3	0.2291	0.2267	-0.1547	C	Cgh
779 Nina	8.3	0.14	9 Dec 1995	2C	120(4)	1.09	m	s2	0.2046	0.2616	0.0553		X
781 Kartvelia	9.4	0.07	15 Apr 1997	2C	900(3)	1.17		s1	0.1892	0.2037	0.0134	CPU:	Xc
782 Montefiore	11.5	0.31	28 Nov 1996	2C	900(3)	1.05	chm	s2	0.6446	-0.1002	0.0212	S	S
783 Nora	10.6	0.06	25 May 1997	2C	540(3)	1.34	chm	s1	0.1279	0.2370	-0.0052		C
784 Pickeringia	9.0	0.06	25 Apr 1996	1C	2700(3)	1.08	c	s1	0.0971	0.2155	0.0198		C
785 Zwetana	9.4	0.12	15 Dec 1995	2C	480(2)	1.04		s2	0.0930	0.3935	0.1419	M	Cb
789 Lena	10.9		15 Nov 1994	2C	1800(2)	1.11	cm	s1	0.1852	0.1665	0.0212		X
792 Metcalfia	10.3	0.04	22 Apr 1996	1W	2700(3)	1.23		s1	0.2663	0.1762	'..0607		X
			24 Apr 1996	1C	2700(3)	1.24		s1					
793 Arizona	10.3	0.17	24 Apr 1996	1C	2700(3)	1.55		s1	0.4138	-0.2084	0.0164	DU:	S
795 Fini	9.7	0.04	5 Jan 1994	2C	600(2)	1.03		s2	0.0492	0.2172	0.0103		C
796 Sarita	9.1	0.20	14 Apr 1997	2C	900(2)	1.01		s1	0.1578	0.2343	0.0463	XD	X
797 Montana	10.3		14 Apr 1997	2C	900(3)	1.17		s1	0.5280	-0.1657	-0.0144	S	S
804 Hispania	7.8	0.05	9 Dec 1995	2C	600(2)	1.08	m	s2	0.0958	0.2636	0.0223	PC	C
808 Merxia	9.7	0.22	13 May 1995	2C	1200(2)	1.46	m	s1	0.2649	-0.1801	0.0641		Sk
			6 Sep 1996	2C	1200(2)	1.44	h	s2					
			8 Sep 1996	2C	1200(2)	1.44	c	s1					
814 Tauris	8.7	0.05	12 Apr 1997	2C	1200(2)	1.18		s1	0.0427	0.2236	-0.0186	C	C
815 Coppelia	10.7	0.21	13 May 1995	2C	1200(2)	1.62	m	s1	0.3756	0.0682	0.0273		Xe
819 Barnardiana	11.9		23 Feb 1997	2C	1800(2)	1.03	cm	s2	0.5996	-0.1642	-0.0457		S
821 Fanny	11.8		18 Oct 1996	2C	1800(2)	1.12		s2	0.0588	0.2721	-0.0480	C	Ch
824 Anastasia	10.4	0.10	18 Apr 1996	1W	1800(2)	1.34		s1	0.6769	0.0029	0.0040	S	L
			19 Apr 1996	1W	1800(2)	1.35		s1					
			21 Apr 1996	1W	1800(2)	1.34		s1					
825 Tanina	11.5	0.35	23 Apr 1996	1C	2700(3)	1.57		s1	0.4865	-0.3805	-0.0325	SR	S
826 Henrika	11.3	0.14	8 Feb 1996	2C	1800(2)	1.20	m	s2	-0.0498	0.1790	-0.0571		C
844 Leontina	9.4		29 Nov 1996	2C	900(2)	1.02	m	s2	0.3093	0.2526	0.0446		X
845 Naëma	9.7	0.08	28 Mar 1994	2C	1200(2)	1.05	m	s3	0.0915	0.2378	-0.0826		C
847 Agnia	10.3	0.17	15 Nov 1994	2C	1200(2)	1.28	cm	s1	0.4242	-0.2440	0.0082	S	S

Asteroid	H	p_H	Observational circumstances						Spectral components			Classification	
			UT Date	*a*	*b*	*c*	*d*	*e*	Slope	PC2'	PC3'	Old	New
			29 Jan 1996	2C	1200(2)	1.02	m	s2					
853 Nansenia	11.7	0.05	12 Apr 1997	2C	1350(3)	1.34		s1	-0.0860	0.2951	-0.0291	XD	Ch
			23 May 1997	2C	900(2)	1.34	cm	s1					
			24 May 1997	2C	1800(3)	1.32	cm	s1					
856 Backlunda	10.7		18 Apr 1996	1W	1800(2)	1.10		s1	0.0973	0.1730	0.0448		C
860 Ursina	10.3	0.16	10 Dec 1995	2C	900(2)	1.04	m	s2	0.1410	0.2579	0.0804	M	X
862 Franzia	10.6	0.14	4 Sep 1995	1W	2700(3)	1.01		s2	0.3682	-0.2229	0.0103		S
863 Benkoela	9.0	0.60	17 Jan 1997	2C	900(3)	1.03	h	s2	0.8921	-0.4048	-0.0650	A	A
866 Fatme	9.2	0.05	25 Feb 1994	2C	1200(2)	1.04	m	s2	0.2654	0.2176	0.0260		X
868 Lova	10.2	0.05	8 Dec 1995	2C	1350(3)	1.07	m	s2	-0.0150	0.3230	0.0079	C:	Ch
870 Manto	13.1		15 May 1995	2C	900(2)	1.42	m	s3	0.5856	-0.2930	-0.0353		S
872 Holda	9.9	0.21	30 Nov 1996	2C	900(2)	1.08	m	s2	0.2414	0.2191	0.0247	M	X
886 Washingtonia	8.7	0.07	22 Jan 1997	2C	900(2)	1.05	m	s2	0.0586	0.2291	0.0115		C
895 Helio	8.3	0.04	8 Dec 1995	2C	720(3)	1.19	m	s2	-0.1371	0.3709	0.1224	FCB	B
897 Lysistrata	10.4	0.26	3 Sep 1995	1W	900(1)	1.19		s1	0.7261	-0.0790	-0.0236	S	Sl
898 Hildegard	12.0		3 Sep 1995	1W	2700(3)	1.01		s1	0.8747	-0.0975	0.0292		Sl
907 Rhoda	9.8	0.06	11 Feb 1995	2C	1200(2)	1.14	h	s3	0.2616	0.1060	-0.0475	C	Xk
908 Buda	10.7	0.16	23 Feb 1997	2C	600(1)	1.01	cm	s2	0.7026	0.1362	-0.0115		L
			7 Apr 1997	2C	1200(2)	1.08		s1					
910 Anneliese	10.3	0.06	25 Feb 1994	2C	1200(2)	1.02	cm	s2	0.0548	0.2640	-0.0446		Ch
			13 May 1995	2C	600(2)	1.53	cm	s3					
912 Maritima	8.4	0.11	20 Apr 1996	1W	1800(2)	1.06		s1	0.0345	0.2630	0.0277		C
913 Otila	11.9		22 Feb 1997	2C	1800(2)	1.20	m	s2	0.8418	-0.2132	-0.0448		Sa
919 Ilsebill	11.3	0.07	11 May 1995	2C	1200(2)	1.00	c	s4	-0.0158	0.2110	-0.0732		C
924 Toni	9.4	0.04	14 Dec 1995	2C	480(2)	1.11		s2	0.1640	0.2620	0.0406	CX	X
929 Algunde	12.1		11 Apr 1997	2C	1800(3)	1.08		s1	0.6253	-0.2615	-0.0256		S
930 Westphalia	11.4	0.04	13 Nov 1994	2C	1800(2)	1.01	h	s2	0.0466	0.3106	-0.0104		Ch
934 Thüringia	10.3	0.05	8 Feb 1995	2C	600(2)	1.01	cm	s2	-0.0951	0.3046	-0.0457		Ch
941 Murray	11.6		8 Feb 1996	2C	1800(2)	1.01	m	s2	0.2095	0.2136	0.0170	CX	X
950 Ahrensa	11.6	0.18	30 Mar 1994	2C	1200(2)	1.38	cm	s3	0.7834	-0.3254	-0.0853		Sa
951 Gaspra	11.5		19 Jan 1997	2C	1800(2)	1.32		s2	0.4660	-0.2241	-0.0359	S	S
961 Gunnie	11.3	0.04	18 Oct 1996	2C	1200(2)	1.13		s2	0.1724	0.2493	0.0048		X
965 Angelica	9.8	0.07	1 May 1996	2C	1800(2)	1.00	m	s1	0.1304	0.1867	0.0466		Xc
970 Primula	12.4		15 Dec 1995	2C	1800(2)	1.01		s2	0.3245	-0.1641	0.0016		S
971 Alsatia	10.0	0.04	5 Nov 1994	1W	1200(2)	1.10		s1	0.1101	0.2693	0.0328		C
973 Aralia	9.6	0.10	29 Jan 1996	2C	1800(2)	1.17	cm	s2	0.2849	0.0792	-0.0919		Xk
980 Anacostia	7.8	0.17	8 Dec 1995	2C	600(2)	1.17	m	s2	0.7876	-0.0045	0.0695	SU	L
984 Gretia	9.0	0.42	25 May 1997	2C	900(3)	1.80	chm	s1	0.4394	-0.5013	-0.0307		Sr
			27 May 1997	2C	900(3)	1.77	cm	s1					
985 Rosina	12.7		31 Mar 1994	2C	1800(2)	1.22		s3	0.5062	-0.2411	-0.0004		S
994 Otthild	10.3	0.22	23 Aug 1993	1C	1200(2)	1.07		s1	0.5319	-0.0379	0.0520		S
997 Priska	12.0	0.08	7 Feb 1995	2C	1800(2)	1.04		s2	0.0571	0.3392	0.0099		Ch
1007 Pawlowia	11.5		7 Feb 1996	2C	1800(2)	1.06	m	s2	0.5072	-0.0365	-0.0098		K
1011 Laodamia	12.7		14 May 1995	2C	1800(2)	1.45	m	s3	0.5489	-0.4548	-0.1257	S	Sr
1014 Semphyra	12.1		15 May 1995	2C	1800(2)	1.31	m	s3	0.6028	-0.0470	0.0461		Xe
1015 Christa	9.0	0.05	28 Mar 1994	2C	1200(2)	1.26	m	s3	0.1521	0.1476	-0.0196	C	Xc
1016 Anitra	12.0		22 Feb 1997	2C	1800(2)	1.22	m	s2	0.5069	-0.1974	-0.0034		S
1017 Jacqueline	10.9	0.05	20 Apr 1996	1W	2700(3)	1.25		s1	0.0676	0.2541	0.0252		C
1020 Arcadia	11.9		30 Mar 1994	2C	1800(2)	1.18	cm	s3	0.5097	-0.2265	0.0049		S
1021 Flammario	9.0	0.05	28 Oct 1995	1C	1200(2)	1.11		s2	-0.0907	0.3094	0.1065	F	B
1022 Olympiada	10.5	0.16	24 Feb 1994	2C	1100(2)	1.08	cm	s2	0.2847	0.1625	0.0629		X
1025 Riema	12.6		14 May 1995	2C	1800(2)	1.03	cm	s3	0.5514	-0.0251	-0.0880	E	Xe
1032 Pafuri	10.0	0.05	23 Apr 1996	1C	2700(3)	1.39		s1	0.2301	0.1810	0.0596		X
1039 Sonneberga	11.1	0.05	7 Feb 1996	2C	1800(2)	1.20	m	s2	0.2757	0.1170	0.0254		X
1041 Asta	9.9	0.06	25 Feb 1994	2C	1200(2)	1.04	cm	s2	0.0342	0.2747	0.0076		C
1046 Edwin	10.2		22 Jan 1997	2C	1800(2)	1.01	cm	s2	0.1657	0.2077	0.0289		Xe

Asteroid	H	p_H	Observational circumstances						Spectral components			Classification	
			UT Date	*a*	*b*	*c*	*d*	*e*	Slope	PC2'	PC3'	Old	New
1048 Feodosia	9.8	0.05	18 Oct 1996	2C	1200(2)	1.12		s2	0.0588	0.2803	-0.0913	XC	Ch
1052 Belgica	12.0		8 Apr 1997	2C	1800(2)	1.13		s1	0.4710	-0.1979	-0.0507	S	S
1055 Tynka	12.0		23 Apr 1996	1C	2700(3)	1.38		s1	0.3100	-0.2431	-0.0118	S	S
1056 Azalea	11.7		17 Jan 1997	2C	1800(2)	1.04	h	s2	0.5960	-0.1738	-0.0090		S
1058 Grubba	12.0		17 Nov 1994	2C	1200(2)	1.03	hm	s2	0.5012	-0.2304	0.0111	S	S
1065 Amundsenia	13.2		31 Mar 1994	2C	1800(2)	1.19		s3	0.5563	-0.2567	0.0316		S
1069 Planckia	9.3	0.22	13 May 1995	2C	600(2)	1.24	m	s1	0.5373	-0.1773	0.0450		S
1071 Brita	10.1	0.06	13 May 1995	2C	1200(2)	1.57	m	s3	0.4096	0.1707	0.0648		Xk
1076 Viola	12.3	0.04	22 Feb 1994	2C	1200(2)	1.10	m	s3	0.0657	0.1931	-0.0060	F	C
1086 Nata	9.3	0.08	22 Feb 1997	2C	1200(2)	1.03	m	s2	-0.0921	0.3417	-0.0418		Ch
1088 Mitaka	11.4		19 Jan 1997	2C	600(2)	1.03		s2	0.4961	-0.1840	-0.0397	S	S
1094 Siberia	11.9	0.09	23 Aug 1993	1C	1200(2)	1.36		s1	0.4605	0.1812	0.0682		Xk
1098 Hakone	10.2	0.24	8 Dec 1995	2C	1200(2)	1.04	m	s2	0.1226	0.2880	0.1219		Xe
1102 Pepita	9.4	0.20	19 Apr 1996	1W	2700(3)	1.45		s1	0.5794	-0.2001	0.0615	C	S
			20 Apr 1996	1W	1800(2)	1.46		s1					
1103 Sequoia	12.2	0.48**	27 Oct 1995	1C	2700(3)	1.01		s1	0.2770	0.1664	0.0379	E	Xk
1104 Syringa	12.5	0.04	26 Nov 1996	2C	1800(2)	1.36	m	s1	0.4380	0.2010	0.1321		Xk
			28 Nov 1996	2C	1800(2)	1.35	ch	s1					
1106 Cydonia	12.0		23 Aug 1993	1C	1200(2)	1.45		s1	0.5146	-0.0554	0.0505		S
1107 Victoria	9.1	0.06	28 Jan 1996	2C	1800(3)	1.04	cm	s2	0.2135	0.1914	0.0008		Xc
1110 Jaroslawa	11.8		25 May 1997	2C	900(3)	1.50	cm	s1	0.3905	-0.2457	-0.0046		S
1114 Lorraine	9.9	0.05	29 Apr 1996	2C	1800(2)	1.27	cm	s1	0.1487	0.2188	0.0499		Xc
1126 Otero	12.1	0.18	2 Dec 1996	2C	1800(2)	1.11		s2	0.8695	-0.3093	-0.1085		A
1128 Astrid	10.7	0.08	6 Jan 1994	2C	1200(2)	1.11		s2	0.1445	0.2394	-0.0864		C
			9 Sep 1996	2C	1200(2)	1.14	c	s2					
1131 Porzia	13.0		19 Feb 1994	2C	1200(2)	1.04	h	s3	0.5324	-0.2859	-0.0032		S
1134 Kepler	14.3		3 Sep 1995	1W	2700(3)	1.10		s1	0.5075	-0.1218	0.0069		S
1135 Colchis	10.2	0.06	29 Jan 1996	2C	1440(3)	1.01	cm	s2	0.2742	0.1763	0.0515		Xk
1139 Atami	12.5		29 Apr 1996	2C	1800(2)	1.42	c	s1	0.5697	-0.3041	-0.0116	S	S
1140 Crimea	10.3	0.18	30 Apr 1996	2C	1200(2)	1.22	m	s1	0.4885	-0.2065	0.0008	S	S
1147 Stavropolis	12.0		12 Apr 1997	2C	1800(3)	1.28		s1	0.6342	-0.2581	-0.0737		S
1148 Rarahu	10.2	0.14	24 Apr 1996	1C	2700(3)	1.10		s1	0.4171	-0.0364	-0.0222	S	K
1152 Pawona	11.3	0.22	12 Sep 1996	2C	1200(2)	1.23	h	s2	0.7919	-0.1895	-0.0616		Sl
1155 Aenna	11.5	0.33	23 Feb 1994	2C	1200(2)	1.24		s3	0.2330	0.1324	0.0559		Xe
1176 Lucidor	10.9	0.08	18 Oct 1996	2C	1200(2)	1.04		s2	0.0600	0.2124	-0.0282		C
1181 Lilith	11.5		9 Dec 1995	2C	1200(2)	1.05	m	s2	0.2024	0.2341	0.0673		X
1185 Nikko	12.1		27 Apr 1996	2C	1800(2)	1.42	c	s1	0.4962	-0.2714	-0.0078	S	S
1186 Turnera	9.2	0.29	7 Feb 1996	2C	1800(2)	1.27	m	s2	0.1716	-0.0113	-0.0160	S	Sk
1187 Afra	11.3	0.05	22 Aug 1993	1C	1800(3)	1.10	c	s1	0.5062	0.2377	0.0026		X
1188 Gothlandia	11.7	0.24	8 Dec 1995	2C	900(3)	1.07	m	s2	0.6130	-0.2303	-0.0195		S
1189 Terentia	10.0	0.06	22 Jan 1997	2C	1200(2)	1.05	m	s2	0.0566	0.2556	-0.0834		Ch
1196 Sheba	10.3	0.16	25 Feb 1994	2C	1200(2)	1.01	cm	s2	0.2163	0.2333	0.0422		X
1201 Strenua	11.4	0.04	30 Apr 1996	2C	2700(3)	1.31	m	s1	0.2381	0.1570	0.1003		Xc
1204 Renzia	12.2		7 Jan 1994	2C	1200(2)	1.01		s2	0.4704	-0.1239	-0.0013		S
			19 Feb 1994	2C	1200(2)	1.01	chm	s3					
1212 Francette	9.5	0.04	27 May 1997	2C	1200(2)	1.30		s1	0.2487	0.2338	0.0935	P	X
1214 Richilde	10.9	0.06	11 Feb 1995	2C	1200(2)	1.12	hm	s3	0.2964	0.1085	0.0254		Xk
1222 Tina	10.3	0.14	13 Nov 1994	2C	1800(2)	1.05	h	s2	0.1155	0.2024	0.0501		X
1228 Scabiosa	11.5		12 Sep 1996	2C	1800(2)	1.02	h	s2	0.4640	-0.2433	0.0079		S
1234 Elyna	11.5	0.14	11 Dec 1995	2C	1800(2)	1.12	m	s2	0.4017	0.0148	0.0004		K
1248 Jugurtha	9.7		29 Nov 1996	2C	900(2)	1.02	cm	s2	0.6122	-0.1559	0.0103		S
1251 Hedera	10.5	0.41**	10 Dec 1995	2C	1800(2)	1.09	m	s2	0.1837	0.2373	0.0758	E	X
1252 Celestia	10.9	0.26	10 Feb 1995	2C	400(2)	1.04	c	s3	0.4032	-0.2875	0.0065	S	S
1262 Sniadeckia	10.2	0.05	1 May 1996	2C	1800(2)	1.16	m	s1	0.1142	0.2034	-0.0280		C
1264 Letaba	9.1	0.07	6 Jan 1994	2C	1800(3)	1.06	c	s2	0.0934	0.2703	0.0589		C
1271 Isergina	10.6	0.05	25 Feb 1994	2C	1200(2)	1.05	cm	s2	0.1361	0.2132	-0.0926		C

Asteroid	H	p_H	Observational circumstances						Spectral components			Classification	
			UT Date	*a*	*b*	*c*	*d*	*e*	Slope	PC2'	PC3'	Old	New
1272 Gefion	12.8		1 Apr 1994	2C	1800(2)	1.11		s3	0.7080	-0.1953	-0.0702		Sl
1277 Dolores	11.0	0.09	15 Oct 1996	2C	900(2)	1.05	c	s2	-0.0869	0.2637	0.0212	C	Cb
1278 Kenya	10.8		20 Apr 1996	1W	2700(3)	1.12		s1	0.6003	-0.2006	0.0095		S
1284 Latvia	10.2	0.10	17 Nov 1994	2C	600(2)	1.03	h	s2	0.6654	0.0693	0.0290	T	L
1293 Sonja	12.0	0.46	8 Sep 1996	2C	1800(3)	1.43	c	s1	0.2298	-0.2982	0.0097		Sq
1294 Antwerpia	10.2	0.12	7 Feb 1996	2C	1200(2)	1.04	m	s2	0.0418	0.1905	-0.0168		C
1300 Marcelle	10.9	0.10	15 May 1995	2C	1200(2)	1.20	m	s3	0.1718	0.1102	-0.1904		Cg
1301 Yvonne	10.8	0.16	27 Mar 1994	2C	1200(2)	1.02	m	s3	0.0736	0.1794	0.0386		C
1304 Arosa	8.6	0.23	21 Apr 1996	1W	2700(3)	1.00		s1	0.2901	0.2316	0.0371		X
			22 Apr 1996	1W	1800(2)	1.00		s1					
			23 Apr 1996	1C	2700(3)	1.00		s1					
1316 Kasan	13.3		20 Feb 1994	2C	1200(2)	1.18	m	s3	0.2799	-0.4130	-0.0272		Sr
1323 Tugela	9.9	0.06	1 May 1996	2C	1800(2)	1.00	m	s1	0.1733	0.1920	0.0138		Xc
1324 Knysna	12.7		13 Oct 1996	2C	2700(3)	1.03	c	s1	0.0105	-0.1348	0.0285		Sq
1327 Namaqua	12.1	0.04	10 Dec 1995	2C	1800(2)	1.06	m	s2	0.2542	0.2194	0.0582		X
1329 Eliane	10.9		15 Apr 1997	2C	900(3)	1.18		s1	0.5782	-0.1967	-0.0470	S	S
1331 Solvejg	10.1	0.15	22 Aug 1993	1C	1200(2)	1.64		s1	-0.1652	0.2787	0.0346	BC:	B
			23 Aug 1993	1C	1200(2)	1.66		s1					
1332 Marconia	10.2	0.08	15 May 1995	2C	1200(2)	1.91	m	s3	0.8938	0.0839	0.0030		Ld
1336 Zeelandia	10.7	0.22	15 May 1995	2C	1800(2)	1.15		s3	0.4402	-0.2411	-0.0369	S	S
1343 Nicole	11.1	0.11	24 May 1997	2C	1800(3)	1.38	m	s1	0.0409	0.2080	0.0350		C
1348 Michel	11.4		31 Mar 1994	2C	1800(2)	1.23	m	s3	0.8093	-0.1823	-0.0136		Sl
1350 Rosselia	10.8	0.16	14 May 1995	2C	1000(2)	1.36	m	s3	0.7381	-0.3489	-0.1701	S	Sa
1351 Uzbekistania	9.6	0.06	28 Mar 1994	2C	1200(2)	1.16	m	s3	0.3849	0.1457	0.0114		Xk
1352 Wawel	11.1	0.15	22 Aug 1993	1C	1800(3)	1.12	c	s1	0.2466	0.2028	0.0146		X
			23 Aug 1993	1C	1800(3)	1.15		s1					
			8 Feb 1996	2C	1800(2)	1.42	m	s2					
1372 Haremari	12.2	0.04	24 Feb 1997	2C	1800(2)	1.14	m	s2	0.7658	0.0965	-0.0214		L
1374 Isora	13.5		18 Jan 1997	2C	2700(3)	1.01	m	s2	0.2313	-0.1942	-0.0418		Sq
1385 Gelria	10.7	0.19	14 Dec 1995	2C	1800(2)	1.30		s2	0.5664	-0.1962	-0.0372		S
1403 Idelsonia	10.6	0.05	11 Dec 1995	2C	1800(2)	1.16	m	s2	0.0816	0.1882	-0.1559		Cgh
1406 Komppa	10.6	0.15	24 Apr 1996	1C	2700(3)	1.36		s1	0.9101	0.1401	0.1033		Ld
			27 Apr 1996	2C	1800(2)	1.36	cm	s1					
1407 Lindelöf	10.6	0.23	9 Apr 1997	2C	900(1)	1.13		s1	0.1858	0.2204	-0.0111		X
			10 Apr 1997	2C	1800(2)	1.14		s1					
1414 Jérôme	12.4	0.07	30 Nov 1996	2C	2700(3)	1.12	m	s2	-0.1507	0.3273	-0.0137		Ch
1420 Radcliffe	11.5		10 Dec 1995	2C	1800(2)	1.06		s2	0.1608	0.2426	0.0384		X
1423 Jose	10.5	0.16	15 Nov 1994	2C	1800(2)	1.26	cm	s1	0.3838	-0.1757	0.0477		S
1424 Sundmania	9.5	0.06	25 Feb 1994	2C	1060(2)	1.05	cm	s2	0.1962	0.2472	0.0172		X
1427 Ruvuma	10.7	0.07	11 Feb 1995	2C	1800(2)	1.05	hm	s3	0.0066	0.2423	-0.0705		C
1428 Mombasa	10.9	0.02	7 Feb 1996	2C	1800(2)	1.09	m	s2	0.2522	0.1556	0.0125		Xc
1433 Geramtina	11.4		7 Feb 1995	2C	1800(2)	1.16		s2	0.3394	-0.2049	-0.0221		S
1458 Mineura	11.5	0.15	30 Apr 1996	2C	1800(2)	1.25		s1	0.6311	-0.2628	-0.0622		S
1471 Tornio	10.7	0.08	12 Sep 1996	2C	1200(2)	1.18	h	s2	0.7116	0.2401	0.0425		T
1474 Beira	12.7		13 Nov 1994	2C	600(2)	1.68	h	s2	-0.1577	0.3096	0.1023	FX	B
1480 Aunus	13.1		8 Apr 1997	2C	1200(2)	1.17		s1	0.3387	-0.0938	-0.0484		S
1483 Hakoila	11.5		10 Dec 1995	2C	1800(2)	1.06	m	s2	0.0581	-0.1516	-0.1051		Sq
			29 Jan 1996	2C	1200(2)	1.09		s2					
1484 Postrema	12.1	0.04	10 Dec 1995	2C	1800(2)	1.05	m	s2	-0.0168	0.3077	0.0779		B
1493 Sigrid	12.0	0.05	22 Feb 1994	2C	1600(2)	1.47		s3	0.1329	0.1123	-0.0042	F	Xc
1494 Savo	12.7		11 Feb 1995	2C	1800(2)	1.16	h	s3	0.5831	-0.3860	-0.0377		Sr
1502 Arenda	11.6	0.04	21 Oct 1996	2C	2700(3)	1.25	m	s2	0.2256	0.2154	0.0700		Xc
1508 Kemi	12.0		11 Feb 1995	2C	1800(2)	1.23	h	s3	0.0356	0.1782	0.0101	BCF	C
1510 Charlois	11.2	0.10	17 Nov 1994	2C	1200(2)	1.01	hm	s2	0.1298	0.1769	-0.0099		C
1517 Beograd	11.1	0.05	9 Feb 1996	2C	1800(2)	1.14	m	s2	0.1512	0.2170	0.0388		X
1520 Imatra	10.0	0.06	25 Feb 1994	2C	1600(2)	1.05	cm	s2	0.1274	0.2164	-0.0239		C

Asteroid	H	p_H	Observational circumstances						Spectral components			Classification	
			UT Date	*a*	*b*	*c*	*d*	*e*	Slope	PC2'	PC3'	Old	New
1534 Näsi	11.7	0.08	12 Sep 1996	2C	1800(2)	1.16	h	s2	0.1176	0.2511	-0.1346		Cgh
1539 Borrelly	10.6		30 Nov 1996	2C	1200(2)	1.05	h	s2	-0.2011	0.2856	0.0461		B
1541 Estonia	11.2	0.14	11 May 1995	2C	1200(2)	2.04	cm	s4	0.0285	0.1179	0.0005		Xc
1542 Schalén	10.3	0.07	29 Nov 1996	2C	1200(2)	1.05	cm	s2	0.9312	0.2602	0.0633		D
1545 Thernöe	11.8	0.10	21 Oct 1996	2C	2700(3)	1.18	m	s2	0.3929	0.1019	0.0112		K
1548 Palomaa	11.5	0.06	10 Feb 1995	2C	1296(2)	1.03	cm	s3	0.4777	0.1384	0.0025		Xk
			12 Feb 1995	2C	1800(2)	1.01	hm	s2					
1549 Mikko	11.7	0.35	18 Jan 1997	2C	1800(2)	1.16		s2	0.5628	-0.2978	-0.0031		S
1550 Tito	11.8		17 Nov 1994	2C	1200(2)	1.03	hm	s2	0.4499	-0.1885	-0.0019		S
1553 Bauersfelda	11.7		9 Feb 1995	2C	1800(2)	1.20	h	s2	0.5070	-0.2144	-0.0278		S
1560 Strattonia	11.5		29 Jan 1996	2C	1800(2)	1.06	cm	s2	0.0277	0.1725	-0.0186		C
1562 Gondolatsch	11.8	0.25	23 Apr 1996	1C	2700(3)	1.05		s1	0.6104	-0.2909	-0.0045		S
1563 Noël	13.3		9 Feb 1995	2C	1800(2)	1.18	h	s2	0.7200	-0.3000	-0.0451		Sa
1565 Lemaître	12.3		18 Jan 1997	2C	1800(3)	1.04	m	s2	0.1831	-0.2407	-0.0237		Sq
1567 Allkoski	9.5	0.06	1 Dec 1996	2C	900(2)	1.03	m	s2	0.0150	0.2700	0.0218	PU	C
1587 Kahrstedt	11.2		22 Feb 1994	2C	1200(2)	1.31		s3	0.6451	-0.3851	-0.0465		Sa
1592 Mathieu	11.6	0.22	7 Apr 1997	2C	1800(3)	1.26		s1	0.1701	0.2499	0.0158		X
1593 Fagnes	13.2		23 Feb 1994	2C	1800(2)	1.20		s3	0.5191	-0.3648	-0.0291		S
1594 Danjon	12.2	0.17	1 May 1996	2C	900(3)	1.33	m	s1	0.4392	-0.1887	0.0249		S
1600 Vyssotsky	11.9		24 Feb 1994	2C	1200(2)	1.11	c	s2	1.0358	-0.3190	-0.0147		A
			28 Mar 1994	2C	1200(2)	1.09	m	s3					
1601 Patry	12.3		26 Nov 1996	2C	1800(2)	1.32		s1	0.6686	-0.2298	0.0486	S	SI
			28 Nov 1996	2C	1800(2)	1.30	h	s1					
1603 Neva	10.9	0.06	10 Dec 1995	2C	900(2)	1.14	m	s2	-0.0603	0.3169	-0.0202		Ch
1604 Tombaugh	10.5	0.10	13 Oct 1996	2C	1200(2)	1.12	c	s1	0.1274	0.0972	0.0872	XSCU	Xc
1613 Smiley	11.4	0.11	10 Dec 1995	2C	1800(2)	1.35		s2	-0.0504	0.1619	-0.2370		Cgh
1618 Dawn	11.5	0.12	30 Apr 1996	2C	2700(3)	1.45	m	s1	0.3997	-0.1479	0.0259		S
1629 Pecker	12.6	0.18	25 Apr 1996	1C	2700(3)	1.21	c	s1	0.5028	-0.2843	-0.0421		S
1634 Ndola	13.0		13 Oct 1996	2C	1800(2)	1.16	c	s1	0.2936	-0.2065	0.0403		Sr
1635 Bohrmann	11.1		23 Aug 1993	1C	1200(2)	1.44		s1	0.3835	-0.0824	0.0343		S
1638 Ruanda	11.5		28 Oct 1995	1C	2700(3)	1.20		s2	0.2036	0.2467	0.0101		X
1640 Nemo	13.1		7 Jan 1994	2C	1200(2)	1.00		s2	0.4981	-0.0648	0.0050		S
1642 Hill	10.5		13 May 1995	2C	1200(2)	1.54	cm	s3	0.5719	-0.3076	-0.0337		S
1653 Yakhontovia	11.4		23 Feb 1994	2C	1600(2)	1.28	m	s3	0.1299	0.0533	0.0086		X
			1 Apr 1994	2C	1800(2)	1.23		s3					
			27 Nov 1996	2C	1200(2)	1.23	c	s1					
			29 Nov 1996	2C	1200(2)	1.24		s2					
1655 Comas Solá	11.0	0.07	30 May 1997	2C	1800(2)	1.52		s1	-0.0244	0.3088	0.0912	XFU	B
1659 Punkaharju	10.1	0.17	3 Sep 1995	1W	600(3)	1.31		s1	0.5112	-0.0066	0.0908		S
1660 Wood	11.9		17 Jan 1997	2C	900(2)	1.30	m	s2	0.4426	-0.1691	0.0338		S
1662 Hoffmann	11.3		9 May 1995	2C	1800(2)	1.99		s3	0.5686	-0.3879	-0.0344		Sr
1664 Felix	12.1		19 Jan 1997	2C	1200(2)	1.06		s2	0.5097	-0.2321	-0.0268		S
1667 Pels	12.1		28 Mar 1994	2C	1800(2)	1.04	m	s3	0.7703	-0.3094	-0.0297		Sa
1680 Per Brahe	11.2	0.30	11 Dec 1995	2C	1800(2)	1.08	m	s2	0.4866	-0.2159	0.0493		S
1692 Subbotina	11.1	0.05	14 May 1995	2C	1800(2)	1.16	m	s3	0.2361	0.1118	-0.1171		Cg
1695 Walbeck	12.4	0.05	27 Apr 1996	2C	2700(3)	1.38	c	s1	0.0327	0.1688	-0.1099		Cg
1702 Kalahari	11.0	0.06	1 May 1996	2C	1800(2)	1.46		s1	0.6719	0.0609	0.0764	D	L
1715 Salli	12.1	0.05	18 Jan 1997	2C	1800(2)	1.02		s2	0.2122	0.1880	0.0344		X
1716 Peter	11.4	0.07	12 Dec 1995	2C	900(1)	1.05	c	s2	0.1313	0.2199	0.0123		C
			14 Dec 1995	2C	1800(2)	1.07	c	s2					
1724 Vladimir	11.3	0.04	15 Oct 1996	2C	2700(3)	1.45	c	s1	-0.2053	0.2338	0.0894	FBCU	B
			16 Oct 1996	2C	1800(2)	1.44		s1					
1726 Hoffmeister	12.1	0.04	16 Nov 1994	2C	1800(2)	1.13	cm	s1	-0.0095	0.2402	0.0234		Cb
			29 Jan 1996	2C	1800(2)	1.04	m	s2					
1730 Marcelline	11.5		9 May 1995	2C	1800(2)	1.33		s3	0.4472	0.1419	0.0053		Xe
1734 Zhongolovich	11.7	0.05	6 Jan 1994	2C	1200(2)	1.09	c	s2	-0.0764	0.3064	-0.0084		Ch

Asteroid	H	p_H	Observational circumstances						Spectral components			Classification	
			UT Date	a	b	c	d	e	Slope	PC2'	PC3'	Old	New
1738 Oosterhoff	12.3		7 Apr 1997	2C	1800(2)	1.17		s1	0.4780	-0.1195	-0.0322		S
1751 Herget	12 2		7 Jan 1994	2C	1200(2)	1.06		s2	0.6112	-0.1575	-0.0360		S
1766 Slipher	11.7		15 Dec 1995	2C	1800(2)	1.08		s2	0.1227	0.2267	0.0061		C
			9 Feb 1996	2C	1800(2)	1.06		s2					
1768 Appenzella	12.7	0.03	20 Feb 1994	2C	600(1)	1.18	c	s3	0.0648	0.2016	0.0034	F	C
1777 Gehrels	11.1		27 May 1997	2C	2700(3)	1.62	c	s1	0.2505	-0.2238	0.0260		Sq
1783 Albitskij	11.8	0.07	17 Nov 1994	2C	1800(2)	1.11	hm	s2	-0.1191	0.3400	-0.0212		Ch
1785 Wurm	13.2		13 Oct 1996	2C	1800(2)	1.18	c	s1	0.2957	-0.1732	0.0411		Sk
1795 Woltjer	11.8	0.05	27 Apr 1996	2C	1800(2)	1.21	cm	s1	-0.1115	0.2740	-0.0536		Ch
1796 Riga	9.8	0.04	25 May 1997	2C	1200(2)	1.15	chm	s1	-0.0253	0.2188	0.0298	XFCU	Cb
1798 Watts	12.8		6 Sep 1996	2C	1800(2)	1.06	h	s2	0.5587	-0.2431	-0.0520		S
			8 Sep 1996	2C	1800(2)	1.05		s2					
1807 Slovakia	12.1		25 May 1997	2C	1800(2)	1.64	chm	s1	0.3454	-0.1857	0.0516		S
1830 Pogson	12.4		18 Jan 1997	2C	1800(2)	1.15		s2	0.3753	-0.3104	-0.0118	S	S
1831 Nicholson	12.8		12 Oct 1996	2C	1800(2)	1.06		s1	0.5526	-0.2417	-0.0704		S
1836 Komarov	11.3		9 Dec 1995	2C	1800(2)	1.03	m	s2	-0.1357	0.3613	-0.0367		Ch
1839 Ragazza	11.8		16 Nov 1994	2C	1800(2)	1.68	m	s1	0.3690	-0.3033	-0.0016		S
1847 Stobbe	11.0	0.12	7 Feb 1996	2C	1800(2)	1.10	m	s2	0.2343	0.1243	-0.0132		Xc
1848 Delvaux	10.9		14 May 1995	2C	1800(2)	1.40	m	s3	0.5770	-0.3456	-0.1050		S
1856 Růžena	12.6		1 Dec 1996	2C	1800(2)	1.06		s2	0.6079	-0.1511	-0.0403		S
1857 Parchomenko	12.3		25 May 1997	2C	1800(2)	1.54	ch	s1	0.3714	-0.2870	-0.0220		S
			26 May 1997	2C	1800(2)	1.55	c	s1					
1858 Lobachevskij	11.5		26 Feb 1997	2C	1200(2)	1.11	m	s3	0.7747	-0.0559	-0.1026		L
1860 Barbarossa	11.7		28 May 1997	2C	1350(3)	1.35	m	s1	0.1338	0.2596	0.0692		X
1882 Rajma	11.1		12 Apr 1997	2C	1800(2)	1.46		s1	0.5966	-0.0137	-0.0632		K
1888 Zu Chong-Zhi	11.7		24 Feb 1994	2C	1200(2)	1.21	cm	s2	0.4185	-0.2022	0.0505		S
1891 Gondola	12.0		21 Oct 1996	2C	1800(2)	1.00		s2	0.1404	0.2347	0.0558		X
1903 Adzhimushkaj	10.5	0.08	11 Apr 1997	2C	1800(3)	1.02		s1	0.4767	0.0383	-0.0175		K
1904 Massevitch	11.3	0.16	9 May 1995	2C	1800(2)	1.40		s3	0.3254	-0.5179	0.0200		R
			10 May 1995	2C	1800(2)	1.41		s1					
1923 Osiris	13.1	0.06	8 Feb 1996	2C	1800(2)	1.03	m	s2	0.0909	0.2385	-0.0613		C
1929 Kollaa	12.2		22 Feb 1997	2C	1800(2)	1.06	m	s2	0.3398	-0.9074	-0.0202		V
1930 Lucifer	10.9	0.11	9 Feb 1995	2C	1800(2)	1.05	m	s2	0.1113	0.2052	-0.1205		Cgh
1936 Lugano	11.1	0.10	14 Nov 1994	2C	1800(2)	1.11	hm	s1	-0.0255	0.3496	-0.0162		Ch
1948 Kampala	12.6		7 Jan 1994	2C	1200(2)	1.08		s2	0.4925	-0.0733	0.0569		S
1968 Mehltretter	12.1		24 Apr 1996	1C	2700(3)	1.26		s1	0.3835	-0.2285	0.0127		S
1970 Sumeria	12.0	0.06	17 Nov 1994	2C	1800(2)	1.01	hm	s2	-0.0753	0.2880	-0.0558		Ch
1977 Shura	11.4		30 Apr 1996	2C	3600(4)	1.14	m	s1	0.1671	-0.0072	0.0804		Sk
1989 Tatry	12.1		6 Sep 1996	2C	1200(2)	1.60	h	s2	0.0243	0.1878	0.0425		C
1998 Titius	12.2		8 Sep 1996	2C	1800(2)	1.07		s2	0.1660	0.1640	0.0253		Xc
2001 Einstein	12.8		19 Jan 1997	2C	1800(2)	1.14	cm	s2	0.1730	0.1717	-0.0058	X	Xe
2019 van Albada	11.9		6 Jan 1994	2C	1200(2)	1.06	c	s2	0.5357	-0.1379	0.0162		S
2022 West	12.0		29 Jan 1996	2C	1800(2)	1.17		s2	0.5598	-0.2898	-0.0424		S
2035 Stearns	12.6		20 Apr 1996	1W	2700(3)	1.17		s1	0.4441	0.1005	0.0148	E	Xe
			22 Apr 1996	1W	2700(3)	1.18		s1					
2038 Bistro	12.3	0.13	27 Mar 1994	2C	1000(2)	1.07	m	s3	1.0390	-0.2135	0.0233		Sa
2040 Chalonge	11.1		12 Feb 1995	2C	1800(2)	1.05	m	s2	0.0586	0.2639	-0.0807		Ch
2042 Sitarski	12.8		10 May 1995	2C	1800(2)	1.76		s4	0.2163	-0.2697	0.0041		Sq
2053 Nuki	11.9		14 Nov 1994	2C	1800(2)	1.15	hm	s1	0.4351	-0.1963	0.0578		S
2056 Nancy	12.3		15 Apr 1997	2C	1800(2)	1.30		s1	0.4026	-0.2487	-0.0321		S
2060 Chiron	6.5		29 May 1997	2C	2700(3)	1.34		s1	0.0746	0.3209	0.0844	B	Cb
2065 Spicer	12.2		7 Feb 1996	2C	1800(2)	1.04		s2	0.1702	0.0891	-0.0807		Xc
2073 Janáček	12.7		29 Jan 1996	2C	1800(2)	1.01	m	s2	0.1397	0.1850	0.0493		X
2078 Nanking	12.1		2 Dec 1996	2C	1800(2)	1.02	m	s2	0.2431	-0.1413	0.0143		Sk
			17 Jan 1997	2C	1800(3)	1.07	h	s2					
2085 Henan	11.4		28 Oct 1995	1C	3600(4)	1.52		s2	0.7184	0.0235	-0.0698		L

Asteroid	H	p_H	Observational circumstances						Spectral components			Classification	
			UT Date	*a*	*b*	*c*	*d*	*e*	Slope	PC2'	PC3'	Old	New
2088 Sahlia	12.4		30 Apr 1996	2C	2700(3)	1.46	m	s1	0.4828	-0.3391	0.0539		S
2089 Cetacea	11.0		24 Apr 1996	1C	3600(4)	1.27		s1	0.2383	-0.1673	0.0321	S	Sq
2106 Hugo	11.7		29 May 1997	2C	1800(2)	1.39		s1	-0.0866	0.2278	-0.0033		C
2107 Ilmari	11.4	0.20	23 Feb 1994	2C	1200(2)	1.20	m	s3	0.5977	-0.2542	-0.0004		S
			30 Mar 1994	2C	1800(2)	1.16	c	s3					
2118 Flagstaff	12.0		14 Dec 1995	2C	600(2)	1.00		s2	0.3581	-0.1516	0.0427		S
2131 Mayall	12.7	0.24	18 Oct 1996	2C	1800(2)	1.28		s2	0.4875	-0.1124	0.0082	S	S
2141 Simferopol	11.3		29 May 1997	2C	2700(3)	1.72		s1	0.7135	-0.1453	-0.0204		Sl
2147 Kharadze	11.7	0.04	5 Jan 1994	2C	1200(2)	1.08		s2	0.0396	0.3353	-0.0178		Ch
2152 Hannibal	10.5	0.05	8 Dec 1995	2C	1800(3)	1.06	m	s2	-0.1391	0.3646	-0.0164		Ch
2157 Ashbrook	11.4		31 Mar 1994	2C	1800(2)	1.62	m	s3	0.5237	-0.2317	0.0146		S
2161 Grissom	12.4		14 Dec 1995	2C	1800(2)	1.09		s2	0.0816	0.1847	0.0561		C
2167 Erin	12.1		13 May 1995	2C	1800(2)	1.34	cm	s3	0.4657	-0.2904	-0.0503		S
2169 Taiwan	12.0	0.10	30 Mar 1994	2C	1800(2)	1.19	cm	s3	0.0805	0.2104	-0.0971		C
			12 Sep 1996	2C	1800(2)	1.18	h	s2					
2185 Guangdong	11.3	0.18	17 Oct 1996	2C	1800(2)	1.05		s2	0.5898	-0.1637	-0.0513		S
2189 Zaragoza	12.8		14 Apr 1997	2C	2700(3)	1.22		s1	0.3920	-0.2007	-0.0194		S
2194 Arpola	12.6		13 Apr 1997	2C	1800(3)	1.44		s1	0.1340	0.1654	0.0424		Xc
2231 Durrell	12.4		9 Dec 1995	2C	1800(2)	1.12		s2	0.0732	0.1555	-0.0094		C
2234 Schmadel	12.5		30 Mar 1994	2C	1800(2)	1.04	c	s3	0.6400	-0.5509	-0.1360		A
2244 Tesla	11.9		8 Feb 1996	2C	1800(2)	1.05	m	s2	0.0286	0.2183	-0.0168		C
2246 Bowell	10.6	0.05	7 Apr 1997	2C	1800(2)	1.27		s1	0.8272	0.2475	0.0555	D	D
2251 Tikhov	11.4	0.07	27 Oct 1995	1C	2700(3)	1.07		s2	-0.0860	0.2685	0.0472		Cb
2258 Viipuri	11.4	0.09	18 Oct 1996	2C	2700(3)	1.39		s2	0.1317	0.2187	-0.0024		C
2268 Szmytowna	11.4		7 Feb 1995	2C	1800(2)	1.35		s2	0.4317	-0.1925	0.0197		S
2271 Kiso	11.1	0.04	11 Dec 1995	2C	1800(2)	1.04	m	s2	0.5513	0.0941	0.0402		T
2280 Kunikov	13.5		9 Feb 1995	2C	1800(2)	1.04	m	s2	0.7163	-0.3270	-0.0582		Sa
2282 Andrés Bello	13.2		12 Apr 1997	2C	1200(2)	1.34		s1	0.4051	-0.1414	-0.0353		S
2305 King	11.8		7 Feb 1996	2C	1800(2)	1.00	m	s2	0.5579	-0.1939	-0.0111		S
2306 Bauschinger	11.4	0.11	29 Jan 1996	2C	1800(2)	1.22		s2	0.1274	0.1751	0.0300		X
2308 Schilt	11.8	0.11	24 Feb 1994	2C	2000(2)	1.03	cm	s2	0.5065	-0.1668	-0.1421		S
2316 Jo-Ann	12.7		20 Feb 1994	2C	1200(2)	1.04	m	s3	-0.0480	0.2204	-0.0218		C
2317 Galya	13.4		20 Feb 1994	2C	1200(2)	1.10	m	s3	0.4199	-0.2284	-0.0715		S
2328 Robeson	12.5	0.13	14 Apr 1997	2C	1350(3)	1.28		s1	0.0318	0.1916	-0.0073		C
2331 Parvulesco	12.2		25 May 1997	2C	2700(3)	1.63	chm	s1	-0.2103	0.1448	0.0380		C
			26 May 1997	2C	1800(2)	1.60	c	s1					
2335 James	13.8		20 Feb 1994	2C	1800(3)	1.38	c	s3	0.6903	-0.3818	0.0009		Sa
2346 Lilio	11.9		14 Apr 1997	2C	1200(2)	1.49		s1	0.0483	0.1715	0.0435		C
2349 Kurchenko	11.9	0.07	9 Apr 1997	2C	1800(2)	1.17		s1	0.1196	0.1031	-0.0134		Xc
2353 Alva	11.8		13 Apr 1997	2C	1800(3)	1.42		s1	0.4584	-0.1232	-0.0151		S
2354 Lavrov	11.8		9 May 1995	2C	1800(2)	1.38	m	s3	0.8774	-0.1071	-0.0662		L
2369 Chekhov	11.8		11 May 1995	2C	1200(2)	1.70	cm	s4	0.3640	-0.1794	0.0244		S
2370 van Altena	12.6	0.09	9 Feb 1995	2C	1800(2)	1.06		s2	0.0186	0.3379	0.0433		Cb
2373 Immo	12.5		11 Dec 1995	2C	1800(2)	1.20		s2	0.3192	-0.1938	0.0197		S
2378 Pannekoek	10.7	0.09	14 May 1995	2C	1800(2)	1.29	m	s3	-0.0638	0.2117	-0.1417		Cgh
2382 Nonie	11.4		11 Sep 1996	2C	1800(2)	1.04	h	s2	-0.2486	0.3073	0.0622		B
2386 Nikonov	12.2	0.15	14 Nov 1994	2C	1800(2)	1.01	h	s1	0.5275	-0.1725	0.0095		S
2390 Nežárka	12.2	0.04	9 Feb 1995	2C	1800(2)	1.01	m	s2	0.1911	0.2210	0.0082		X
2396 Kochi	11.6		10 Feb 1995	2C	1800(2)	1.13	c	s3	0.6891	-0.3097	0.0061		Sa
2401 Aehlita	12.2		8 Feb 1995	2C	1800(2)	1.02	cm	s2	0.4895	-0.1808	0.0543		S
2402 Satpaev	13.2		12 Oct 1996	2C	1800(2)	1.01		s1	0.6388	-0.2933	-0.1005		Sl
2409 Chapman	13.2		11 Sep 1996	2C	1200(2)	1.23	ch	s1	0.4930	-0.1772	0.0314		S
2410 Morrison	13.0		6 Jan 1994	2C	1200(2)	1.04	c	s2	0.6575	-0.2075	-0.0277		S
2423 Ibarruri	13.2		20 Feb 1994	2C	1200(2)	1.46	c	s3	0.8595	-0.4161	-0.0331		A
			22 Feb 1994	2C	1800(2)	1.47		s3					
2427 Kobzar	12.8		30 May 1997	2C	2700(3)	1.62		s1	0.2281	-0.0908	0.0681		Sk

Asteroid	H	p_H	Observational circumstances						Spectral components			Classification	
			UT Date	*a*	*b*	*c*	*d*	*e*	Slope	PC2'	PC3'	Old	New
2428 Kamenyar	11.0	0.09	16 Nov 1994	2C	1800(2)	1.13	m	s1	-0.1303	0.2621	-0.0657		Ch
2430 Bruce Helin	12.2		31 Mar 1994	2C	1800(2)	1.19	m	s3	0.6752	-0.1710	0.0268	S	Sl
2438 Oleshko	12.9		8 Apr 1997	2C	1800(2)	1.05		s1	0.5004	-0.2838	-0.0678		S
2444 Lederle	11.8		20 Jan 1997	2C	1800(2)	1.11	m	s2	0.1195	0.2694	0.0292		C
2446 Lunacharsky	12.9		8 Feb 1995	2C	1800(2)	1.04	c	s2	-0.0904	0.2833	0.1154		B
2448 Sholokhov	10.4	0.13	23 Feb 1994	2C	1200(2)	1.04	m	s3	0.7838	0.0435	0.0576		L
2451 Dollfus	12.1		10 Apr 1997	2C	1800(2)	1.48	c	s1	0.5632	-0.1211	-0.0292		S
			13 Apr 1997	2C	1800(2)	1.48		s1					
2455 Somville	11.7		19 Jan 1997	2C	1200(2)	1.02	cm	s2	0.1392	0.2869	0.0144		C
2465 Wilson	12.0	0.07	1 Dec 1996	2C	2700(3)	1.10	m	s2	0.1362	0.2677	-0.0499		Ch
2467 Kollontai	13.0		6 Sep 1996	2C	1800(2)	1.02	h	s2	0.6780	-0.2675	-0.0214		Sl
2478 Tokai	12.8		24 Feb 1997	2C	1200(2)	1.09	cm	s2	0.4356	-0.1666	-0.0284		S
2482 Perkin	12.7		9 Feb 1995	2C	1800(2)	1.06		s2	0.3962	-0.1399	-0.0021		S
2493 Elmer	12.5		31 Mar 1994	2C	1800(2)	1.23		s3	0.4503	-0.1996	0.0341		S
2501 Lohja	12.1		30 Nov 1996	2C	1800(2)	1.08	ch	s2	0.9213	-0.3907	-0.0973	A	A
2504 Gaviola	12.1		15 Oct 1996	2C	1800(2)	1.11	c	s2	0.2207	-0.1197	0.0140		Sk
2507 Bobone	11.7		10 Dec 1995	2C	1800(2)	1.16	m	s2	0.3257	0.1223	0.0473		Xe
2511 Patterson	12.5		15 Apr 1997	2C	1800(2)	1.07	m	s1	0.0421	-0.7093	0.0961		V
2521 Heidi	11.7		30 Nov 1996	2C	1800(2)	1.05	m	s2	0.3896	-0.1433	-0.0292		S
2559 Svoboda	12.4	0.03	12 Dec 1995	2C	1800(2)	1.04	c	s2	0.3365	0.1966	0.0471		Xk
			14 Dec 1995	2C	1800(2)	1.04		s2					
2560 Siegma	11.7		27 Apr 1996	2C	2700(3)	1.09	cm	s1	0.1348	0.1271	-0.0140		Xc
2566 Kirghizia	12.6		26 Nov 1996	2C	1800(2)	1.08	m	s1	-0.0465	-0.6740	0.1602		V
			30 Nov 1996	2C	1800(2)	1.08	h	s2					
2567 Elba	11.8		9 Feb 1995	2C	1800(2)	1.04	m	s2	0.2317	0.0732	-0.0200		Xc
2569 Madeline	11.2	0.07	12 Feb 1995	2C	1200(2)	1.02	hm	s2	0.7218	0.2035	0.1708		D
2575 Bulgaria	12.6		27 Apr 1996	2C	2700(3)	1.14	cm	s1	0.4934	-0.4381	-0.0144		Sr
2579 Spartacus	13.0		30 Apr 1996	2C	2700(3)	1.57	m	s1	-0.0685	-1.0276	0.2303		V
2582 Harimaya-Bashi	10.5	0.13	25 Apr 1996	1C	2700(3)	1.50	c	s1	0.1750	0.0856	-0.0051		Xc
			1 May 1996	2C	1800(2)	1.50	m	s1					
2598 Merlin	12.6		29 Jan 1996	2C	1351(2)	1.22		s2	-0.2082	0.3031	-0.0133		Ch
2604 Marshak	12.9	0.06	27 Mar 1994	2C	1800(3)	1.11	m	s3	0.7380	-0.5267	-0.0648		Sa
2606 Odessa	11.3		15 May 1995	2C	1800(2)	1.29	m	s3	0.4456	0.1074	-0.0321		Xk
2625 Jack London	13.1		12 Oct 1996	2C	1800(2)	1.48		s1	0.4273	-0.2698	-0.0294		S
2629 Rudra	14.5		12 Sep 1996	2C	1800(2)	1.53	h	s1	-0.2512	0.3530	0.1466		B
2631 Zhejiang	12.0		16 Nov 1994	2C	1800(2)	1.16	cm	s1	0.4599	-0.2106	0.0308		S
2635 Huggins	12.9		9 Sep 1996	2C	1800(2)	1.59		s2	0.4427	-0.3499	-0.0534		S
2640 Hällström	13.0		29 May 1997	2C	1800(2)	1.71		s1	0.0518	-0.5184	0.1117		V
2653 Principia	12.1		13 Apr 1997	2C	2700(3)	1.56		s1	-0.0277	-0.8791	0.1294		V
2659 Millis	11.2	0.08	8 Apr 1997	2C	1800(3)	1.30		s1	-0.1650	0.2753	0.0214		B
2681 Ostrovskij	12.3		10 Feb 1995	2C	1800(2)	1.04	cm	s3	0.5662	0.0909	-0.0799		Xk
2703 Rodari	13.5		6 Sep 1996	2C	1800(2)	1.53	h	s2	0.3440	-0.1370	0.0427		S
			8 Sep 1996	2C	1800(2)	1.54		s1					
2704 Julian Loewe	13.2		28 May 1997	2C	1800(2)	1.55		s1	-0.1517	-0.6382	0.0945		V
2709 Sagan	13.3		13 Oct 1996	2C	2700(3)	1.26	c	s1	0.4292	-0.2347	0.0274		S
2715 Mielikki	11.9	0.18	10 May 1995	2C	1800(2)	1.23	m	s3	0.9099	-0.2912	-0.0567		A
2720 Pyotr Pervyj	13.9		7 Feb 1995	2C	1800(2)	1.03		s2	0.0662	0.2450	0.0371		C
2724 Orlov	11.7	0.09	9 Feb 1995	2C	1800(2)	1.04	m	s2	0.5032	0.0400	0.0062		K
2730 Barks	11.6		14 Dec 1995	2C	1800(2)	1.01	c	s2	0.0980	0.2426	0.0412		C
2732 Witt	12.1		14 May 1995	2C	1800(2)	1.14	m	s3	1.1561	-0.3404	-0.1206		A
2737 Kotka	11.9		22 Jan 1997	2C	900(1)	1.06	cm	s2	0.4815	-0.1985	-0.0362		S
			8 Apr 1997	2C	1800(2)	1.06		s1					
2744 Birgitta	14.8		11 Sep 1996	2C	1800(2)	1.05	ch	s2	0.3820	-0.2829	-0.0405	S	S
2746 Hissao	13.4		2 Dec 1996	2C	1800(2)	1.14		s2	0.3019	-0.3177	-0.0334		Sr
2748 Patrick Gene	12.7		12 Sep 1996	2C	1800(2)	1.52	h	s1	0.3898	-0.0610	0.0812		S
2750 Lovlisa	13.1		22 Jan 1997	2C	1800(2)	1.04	m	s2	0.3512	-0.2069	-0.0333		S

Asteroid	H	p_H	Observational circumstances						Spectral components			Classification	
			UT Date	*a*	*b*	*c*	*d*	*e*	Slope	PC2'	PC3'	Old	New
2754 Efimov	13.5		1 Dec 1996	2C	2700(3)	1.13		s2	0.8286	-0.2898	-0.0323		Sa
2772 Dugan	13.4		5 Jan 1994	2C	1200(2)	1.06	c	s2	-0.0854	0.2784	0.0686		B
2789 Foshan	13.6		19 Jan 1997	2C	1800(2)	1.06	cm	s2	0.3636	-0.1813	0.0005		S
2795 Lepage	13.2		9 Sep 1996	2C	1800(2)	1.06		s1	0.0745	-0.8621	0.0023		V
2801 Huygens	12.2		31 Mar 1994	2C	1800(2)	1.08		s3	0.5016	-0.2425	-0.0259		S
2807 Karl Marx	12.6		28 Mar 1994	2C	1800(2)	1.01		s3	0.0856	0.2062	0.0008		C
2809 Vernadskij	13.6		23 Aug 1993	1C	1200(2)	1.58		s1	-0.2354	0.2880	0.0908	BFX	B
2813 Zappalà	11.0	0.07	23 Feb 1994	2C	1200(2)	1.30	m	s3	0.6695	0.0720	0.1131		T
2816 Pien	11.7	0.08	30 Nov 1996	2C	1800(2)	1.04	m	s2	-0.1749	0.2788	0.0414		B
2818 Juvenalis	13.7		11 Feb 1995	2C	1800(2)	1.11	h	s3	0.5272	-0.3528	-0.0379		S
2834 Christy Carol	12.0		23 Feb 1994	2C	1200(2)	1.10	m	s3	0.4824	-0.2703	0.0352		S
2850 Mozhaiskij	11.9		22 Aug 1993	1C	1600(3)	1.40	c	s1	1.0821	-0.1013	-0.0185		Ld
2851 Harbin	12.3		29 Apr 1996	2C	1800(2)	1.57	cm	s1	0.1412	-1.0653	0.0269		V
2852 Declercq	12.3		3 Sep 1995	1W	2700(3)	1.26		s1	0.0174	0.3177	-0.0445		Ch
2855 Bastian	13.0		20 Feb 1994	2C	1200(2)	1.00	cm	s3	0.7469	-0.1631	-0.0180		Sl
2857 NOT	12 7		12 Sep 1996	2C	1800(2)	1.14	h	s2	0.5741	0.1506	0.0002		T
2861 Lambrecht	12.4		12 Oct 1996	2C	1800(2)	1.48		s1	0.1057	0.1411	-0.0422		Xc
2864 Soderblom	12.5	0.06	11 Apr 1997	2C	1800(2)	1.08		s1	-0.0645	0.2765	-0.0151		Ch
2872 Gentelec	12.4	0.09	9 Apr 1997	2C	1800(2)	1.24		s1	0.8967	0.2406	0.0830		D
2873 Binzel	13.0		23 Aug 1993	1C	1200(2)	1.23		s1	0.3580	-0.2504	-0.0014		S
2874 Jim Young	13.2		17 Jan 1997	2C	1800(2)	1.02	h	s2	0.5565	-0.2319	-0.0257		S
2875 Lagerkvist	12.2		27 Feb 1997	2C	1800(2)	1.02		s3	0.5902	-0.2004	-0.0554		S
2879 Shimizu	11.7	0.05	15 Dec 1995	2C	1800(2)	1.20		s2	0.1292	0.2076	0.0438		X
2881 Melden	13.4		30 May 1997	2C	1800(2)	1.35		s1	0.3136	-0.1853	0.0334		S
2892 Filipenko	10.2	0.05	25 Feb 1994	2C	1200(2)	1.02	m	s2	0.0261	0.2794	0.0126		C
2902 Westerlund	14.4		28 May 1997	2C	1800(2)	1.47		s1	0.1934	-0.3441	0.0044		Sq
			30 May 1997	2C	900(1)	1.47		s1					
2905 Plaskett	12.1		14 Nov 1994	2C	1800(2)	1.02	hm	s1	0.3861	-0.1223	0.0476		S
2906 Caltech	10.0	0.05	24 Feb 1994	2C	1200(2)	1.02	cm	s2	0.1969	0.1989	0.0384		Xc
2911 Mlahelena	11.3		6 Jan 1994	2C	1200(2)	1.20		s2	0.5667	-0.2149	0.0223		S
			23 Feb 1994	2C	1200(2)	1.18	m	s3					
			31 Mar 1994	2C	1200(2)	1.13	m	s3					
2912 Lapalma	12.7		17 Jan 1997	2C	1800(2)	1.04	m	s2	-0.0993	-0.9121	0.0715		V
2917 Sawyer Hogg	12.0		29 Jan 1996	2C	1800(2)	1.02	cm	s2	0.3608	-0.2721	-0.0039		S
2925 Beatty	14.0		31 Mar 1994	2C	1800(2)	1.04		s3	-0.0506	0.1935	-0.1613		Cgh
2929 Harris	11.6		28 Mar 1994	2C	1800(2)	1.21	m	s3	0.5480	0.1154	0.0316		T
2930 Euripides	12.4		5 Jan 1994	2C	1200(2)	1.02		s2	0.0652	0.2184	0.0537		C
			7 Jan 1994	2C	1200(2)	1.06		s2					
2934 Aristophanes	11.2	0.08	16 Nov 1994	2C	1800(2)	1.16	cm	s1	-0.1723	0.3593	0.0050		Ch
2949 Kaverznev	13.3		6 Sep 1996	2C	1200(2)	1.35	h	s2	0.3004	-0.2032	-0.0354		S
2953 Vysheslavia	11.6		7 Feb 1995	2C	1800(2)	1.03		s2	0.5381	-0 1884	-0.0076		S
2955 Newburn	13.5		9 Feb 1995	2C	1800(2)	1.10		s2	0.5529	-0.2750	-0.0309		S
2956 Yeomans	12.4		1 May 1996	2C	2700(3)	1.56	m	s1	0.3474	-0.4089	-0.0203		Sr
2957 Tatsuo	10.2	0.22	20 Jan 1997	2C	1800(2)	1.06	m	s2	0.4554	0.0751	-0.0104		K
2973 Paola	12.9		24 Feb 1994	2C	1200(2)	1.09	cm	s2	-0.0583	0.3633	0.1444		B
2977 Chivilikhin	12.7		7 Feb 1995	2C	1800(2)	1.13		s2	0.5406	-0.1711	0.0080		S
2988 Korhonen	11.7		24 Feb 1994	2C	1200(2)	1.15	c	s2	0.6194	-0.2937	-0.0049		S
2996 Bowman	11.8	0.07	22 Feb 1994	2C	1800(2)	1.22		s3	0.1632	0.1475	0.0118		Xc
3000 Leonardo	13.0		7 Feb 1995	2C	1800(2)	1.06		s2	-0.0873	0.3070	0.0598		B
3020 Naudts	12.2		2 Dec 1996	2C	1800(2)	1.12	m	s2	0.8576	-0.1268	-0.0638		Sl
3028 Zhangguoxi	10.7	0.14	11 Dec 1995	2C	1800(2)	1.17	m	s2	0.3143	0.0443	0.0109		K
3037 Alku	11.6	0.11	10 Dec 1995	2C	1800(2)	1.43	m	s2	-0.0158	0.1946	0.0154		C
3040 Kozai	14.5		19 Feb 1994	2C	1200(2)	1.01	h	s3	0.5770	-0.3207	-0.0126		S
3060 Delcano	13.4		9 Sep 1996	2C	1800(2)	1.04		s1	0.5079	-0.3909	0.0139		S
3065 Sarahlll	11.8		20 Jan 1997	2C	1800(2)	1.07	m	s2	-0.0238	0.2843	-0.0275		Ch
3090 Tjossem	12.1		20 Feb 1994	2C	1200(2)	1.13		s3	0.0734	0.1181	-0.1639		Cg

Asteroid	H	p_H	Observational circumstances						Spectral components			Classification	
			UT Date	*a*	*b*	*c*	*d*	*e*	Slope	PC2'	PC3'	Old	New
3096 Bezruč	12.7		14 Nov 1994	2C	1800(2)	1.43	hm	s1	0.0497	0.1873	-0.0823		C
3121 Tamines	13.4		28 Nov 1996	2C	1800(2)	1.08	chm	s2	0.4253	-0.1233	0.0251		S
3151 Talbot	12.1		14 Nov 1994	2C	1800(2)	1.10	hm	s1	0.5537	-0.1787	0.0197		S
3155 Lee	12.6		12 Apr 1997	2C	1800(2)	1.40		s1	0.1080	-0.8152	0.0567		V
3170 Dzhanibekov	12.0		14 Nov 1994	2C	2700(3)	1.08	hm	s1	0.3397	-0.1777	-0.0084		S
3179 Beruti	11.9		24 Feb 1994	2C	1200(2)	1.03	cm	s2	0.0128	0.2616	0.0612		C
3181 Ahnert	12.8		17 Jan 1997	2C	1800(2)	1.07	m	s2	0.4457	-0.2444	-0.0200		S
3192 A'Hearn	13.7		7 Apr 1997	2C	1800(2)	1.44		s1	0.0998	0.2241	0.0403		C
			8 Apr 1997	2C	1800(2)	1.44		s1					
3197 Weissman	11.7	0.08	6 Jan 1994	2C	1200(2)	1.03	c	s2	-0.1863	0.3375	-0.2004		Cgh
3209 Buchwald	13.6		6 Sep 1996	2C	1800(2)	1.62	h	s2	0.4935	-0.2040	0.0289		S
			12 Sep 1996	2C	1800(2)	1.63	h	s1					
3214 Makarenko	11.1		24 May 1997	2C	2700(3)	1.20	m	s1	0.0375	0.0919	0.0558		Xc
3216 Harrington	14.0		31 Mar 1994	2C	1800(2)	1.13		s3	0.4936	-0.2030	0.0597		S
3224 Irkutsk	11.3	0.05	30 Nov 1996	2C	2700(3)	1.05	h	s2	0.1614	0.2955	0.0513		X
3248 Farinella	10.7	0.06	20 Jan 1997	2C	2700(3)	1.00	cm	s2	0.8770	0.1723	0.0089		D
3254 Bus	11.0		31 Mar 1994	2C	1800(2)	1.11		s3	0.7076	0.1716	0.1309		T
3255 Tholen	13.6		10 Dec 1995	2C	2700(3)	1.01	m	s2	0.3313	-0.2205	0.0329		S
3256 Daguerre	12.4	0.04	28 Oct 1995	1C	2700(3)	1.15		s2	0.2694	0.2276	0.0339		X
3258 Somnium	13.4		2 Dec 1996	2C	2700(3)	1.44		s1	0.6447	-0.2087	-0.0002		S
3262 Miune	10.9		29 Apr 1996	2C	1800(2)	1.25	cm	s1	0.2061	0.1963	0.0411		X
3287 Olmstead	15.0		28 Apr 1996	2C	2700(3)	1.43		s1	0.6200	-0.0061	-0.0055		L
3306 Byron	12.7		13 Oct 1996	2C	900(1)	1.04	c	s1	0.3513	-0.2410	0.0134		S
3307 Athabasca	13.9	0.04	8 Sep 1996	2C	1800(2)	1.03		s2	-0.1581	-1.0545	0.0561		V
3309 Brorfelde	13.9		9 Apr 1997	2C	900(2)	1.25		s1	0.6387	-0.1833	-0.0192		S
3311 Podobed	12.1	0.04	20 Jan 1997	2C	1800(2)	1.03	m	s2	0.6205	0.2860	0.0608		T
3314 Beals	13.1		28 Nov 1996	2C	2700(3)	1.04	chm	s2	0.5542	-0.2354	0.0134		S
3317 Paris	8.3	0.06	25 May 1997	2C	600(1)	1.14	chm	s1	0.6042	0.2002	0.1319		T
			27 May 1997	2C	1200(2)	1.19	m	s1					
3340 Yinhai	13.7		30 Nov 1996	2C	1800(2)	1.02	m	s2	0.4844	-0.1253	0.0352		S
3345 Tarkovskij	11.6	0.06	11 Feb 1995	2C	960(2)	1.25	hm	s3	0.0186	0.1730	0.0450		C
3349 Manas	12.7		11 Dec 1995	2C	1800(2)	1.04	m	s2	0.6509	-0.1195	-0.0842		L
3363 Bowen	12.0		14 Dec 1995	2C	1800(2)	1.10	c	s2	0.1588	-0.2269	0.0238		Sq
3364 Zdenka	13.8		9 Apr 1997	2C	1800(2)	1.13		s1	0.5162	-0.1836	-0.0322		S
3365 Recogne	12.1		17 Oct 1996	2C	2700(3)	1.05		s2	-0.0067	0.2047	-0.0089		C
3367 Alex	12.0		10 Apr 1997	2C	2700(3)	1.24	c	s1	0.1296	0.2437	0.0303		X
3371 Giacconi	12.3		29 Nov 1996	2C	2700(3)	1.02		s2	0.2743	-0.2066	0.0290		Sr
3376 Armandhammer	12.4		6 Sep 1996	2C	1200(2)	1.15	h	s2	0.1111	-0.3704	0.1157		Sq
			8 Sep 1996	2C	1200(2)	1.15		s2					
3385 Bronnina	12.8		18 Jan 1997	2C	1800(2)	1.07	m	s2	0.5109	-0.2893	-0.0195		S
3389 Sinzot	12.3	0.05	29 Nov 1996	2C	1800(2)	1.20		s2	0.0761	0.2513	0.0680		C
3394 Banno	13.4		29 May 1997	2C	1800(2)	1.36		s1	0.4021	-0.1675	-0.0034		S
3395 Jitka	11.7		14 Dec 1995	2C	1800(2)	1.08	cm	s2	0.2839	-0.2961	-0.0085		Sr
3401 Vanphilos	12.6		17 Jan 1997	2C	900(3)	1.01	h	s2	0.4994	-0.1209	0.0322		S
3406 Omsk	11.3	0.29	8 Feb 1996	2C	1800(2)	1.07		s2	0.2353	0.1870	0.0192		X
3416 Dorrit	13.7		20 Feb 1994	2C	1200(2)	1.05	c	s3	0.8073	-0.3582	-0.0594		Sa
3417 Tamblyn	13.7		25 Feb 1997	2C	1800(2)	1.00	m	s2	0.5452	-0.1393	0.0098		S
3430 Bradfield	12.4		9 Feb 1996	2C	1800(2)	1.01	m	s2	0.2733	-0.1662	0.0177		Sk
3435 Boury	12.9		15 Apr 1997	2C	2700(3)	1.22		s1	0.0353	0.1723	0.0305		C
3440 Stampfer	12.1		10 Apr 1997	2C	2700(3)	1.10	c	s1	0.2514	0.2111	-0.0265		X
3443 Leetsungdao	13.3		14 Apr 1997	2C	1800(3)	1.24		s1	0.5491	0.0976	-0.0089		T
3451 Mentor	8.1		25 Apr 1996	1C	2700(3)	1.13	c	s1	0.1479	0.2577	0.0291		X
3474 Linsley	13.0		13 May 1995	2C	1800(2)	1.42		s1	0.7023	-0.2861	-0.0201		Sa
3491 Fridolin	12.4		15 Nov 1994	2C	1800(2)	1.12		s1	0.2222	-0.1771	-0.0397		Sq
3493 Stepanov	13.4		15 Nov 1994	2C	1800(2)	1.07		s1	0.5719	-0.3767	-0.0036		S
3507 Vilas	11.3		7 Feb 1995	2C	1800(2)	1.04		s2	-0.0181	0.3187	-0.0133		Ch

Asteroid	H	p_H	Observational circumstances						Spectral components			Classification	
			UT Date	*a*	*b*	*c*	*d*	*e*	Slope	PC2'	PC3'	Old	New
3511 Tsvetaeva	12.3		1 Dec 1996	2C	1800(2)	1.05	m	s2	0.5069	-0.2628	-0.0459		S
3526 Jeffbell	12.1	0.04	15 Oct 1996	2C	2700(3)	1.01	c	s2	0.0796	0.3014	0.0179		Ch
3533 Toyota	12.8		7 Jan 1994	2C	1200(2)	1.08		s2	0.3740	0.2276	0.1028		Xk
3534 Sax	12.4		10 Dec 1995	2C	1800(2)	1.12		s2	0.5301	-0.2390	-0.0226		S
3542 1964 TN_2	11.7		8 Feb 1995	2C	1800(2)	1.24	c	s2	-0.1489	0.2374	-0.0385		C
3545 Gaffey	12.1		23 Feb 1994	2C	2000(2)	1.42		s3	0.6131	-0.3520	0.0121		Sa
3546 Atanasoff	12.7		17 Oct 1996	2C	2700(3)	1.43		s2	0.7885	-0.2381	-0.0170		Sa
3563 Canterbury	11.9		5 Jan 1994	2C	1163(2)	1.12	c	s2	-0.0405	0.4167	0.0449		B
			7 Jan 1994	2C	1800(3)	1.12		s2					
3567 Alvema	12.5		28 Oct 1995	1C	2700(3)	1.05		s2	0.1115	0.1898	0.0521		Xc
3575 Anyuta	11.9		19 Jan 1997	2C	2700(3)	1.01	cm	s2	0.2318	0.3240	0.0536		X
3579 1977 YA	14.2		15 Dec 1995	2C	1800(2)	1.23	h	s2	-0.1555	0.2799	0.0918		B
3581 Alvarez	12.1		28 Oct 1995	1C	2700(3)	1.11		s2	-0.3237	0.2919	0.0394		B
3587 Descartes	12.2	0.06	8 Feb 1996	2C	1800(2)	1.03		s2	0.0031	0.2154	-0.0560		C
3592 Nedbal	13.7		5 Jan 1994	2C	1200(2)	1.03		s2	0.5401	-0.0812	-0.0024		S
3611 1981 YY_1	12.7		14 Dec 1995	2C	1800(2)	1.08	cm	s2	-0.1628	0.3272	-0.0477		Ch
			9 Feb 1996	2C	1800(2)	1.03		s2					
3628 Božněmcová	12.6		11 Dec 1995	2C	1800(2)	1.15		s2	-0.3699	-0.2939	0.0693		O
3630 Lubomir	12.5	0.05	14 Nov 1994	2C	1800(2)	1.00	hm	s1	-0.0344	0.4025	-0.0647		Ch
3635 1981 WO_1	14.8		29 May 1997	2C	2700(3)	1.39		s1	0.4567	-0.2230	0.0813		S
3636 Pajdušáková	14.0		18 Jan 1997	2C	1800(2)	1.02	m	s2	0.4116	-0.2251	-0.0217		S
3640 Gostin	12.9		12 Apr 1997	2C	1800(3)	1.55		s1	0.4725	-0.1795	-0.0236		S
3642 Frieden	11.2	0.05	7 Feb 1996	2C	1800(2)	1.08	m	s2	0.1125	0.1889	-0.0927		C
3645 Fabini	12.1		27 Oct 1995	1C	2700(3)	1.01		s2	0.0005	0.1885	-0.0418		C
3647 Dermott	11.4	0.05	12 Feb 1995	2C	1800(2)	1.06	hm	s2	-0.0230	0.2809	0.0983		B
3669 Vertinskij	13.2		15 Apr 1997	2C	1800(2)	1.30		s1	0.3672	-0.2067	-0.0490		S
3670 Northcott	12.0		11 Dec 1995	2C	1800(2)	1.03	m	s2	0.1637	0.2262	0.0100		X
3674 Erbisbühl	12.1		19 Jan 1997	2C	1200(2)	1.18		s2	0.2658	-0.1202	0.0261		Sk
3678 Mongmanwai	12.6		9 Feb 1995	2C	1800(2)	1.22	h	s2	0.3751	-0.2614	0.0138		S
3684 Berry	13.4	0.05	27 Feb 1997	2C	1200(2)	1.04	m	s3	0.0388	0.1768	-0.0351		C
3686 Antoku	12.4	0.10	8 Feb 1996	2C	1800(2)	1.06	m	s2	0.1228	0.1956	0.0486		X
3687 Dzus	11.5	0.05	9 Apr 1997	2C	2700(3)	1.60		s1	-0.0687	0.2805	-0.0506		Ch
3700 Geowilliams	12.5		14 Apr 1997	2C	1800(2)	1.59		s1	0.2622	-0.1342	0.0042		Sk
3701 Purkyně	12.3		9 Feb 1995	2C	1800(2)	1.29	h	s2	0.4869	-0.2213	0.0222		S
3704 1981 YX_1	12.5		30 Mar 1994	2C	1800(2)	1.16	c	s3	0.2767	0.1372	0.0160		Xk
3710 Bogoslovskij	12.8		15 Oct 1996	2C	1800(2)	1.13	c	s2	-0.3437	0.3546	-0.1522		Cgh
3712 Kraft	11.6		5 Jan 1994	2C	360(2)	1.04	c	s2	0.5625	-0.1049	0.0232		S
3713 Pieters	11.3		1 May 1996	2C	2700(3)	1.20	m	s1	0.4005	-0.0607	0.0310		K
3730 Hurban	11.8	0.04	29 Nov 1996	2C	1800(2)	1.03		s2	0.4384	0.2325	0.0165		Xk
3734 Waland	12.6		11 Sep 1996	2C	2700(3)	1.46	h	s1	0.9252	0.0041	0.0292		Ld
3744 Horn-d'Arturo	12.8	0.06	1 Dec 1996	2C	1800(2)	1.10	m	s2	0.0292	0.2582	-0.0804		Ch
3759 Pilronen	11.9	0.03	21 Oct 1996	2C	1800(2)	1.01		s2	0.1509	0.2375	0.0129		X
3767 1986 LC	11.6		28 Mar 1994	2C	1200(2)	1.08	m	s3	0.7652	-0.2762	-0.0763		Sa
3775 Ellenbeth	12.8		10 May 1995	2C	1800(2)	1.39	m	s4	-0.1525	0.3062	-0.0314		Ch
3788 1986 QM_3	11.9		30 Mar 1994	2C	1800(2)	1.13	cm	s3	0.5597	-0.1808	0.0282		S
3792 Preston	13.4		17 Nov 1994	2C	1800(2)	1.01	hm	s2	0.3227	-0.2503	0.0230		S
3796 Lena	11.9		9 Apr 1997	2C	1800(2)	1.17		s1	0.0864	0.1981	0.0258		C
3800 Karayusuf	15.4		23 Feb 1994	2C	2700(3)	1.03	m	s3	0.5372	-0.3607	-0.0411		S
3809 Amici	12.6		13 Apr 1997	2C	2700(3)	1.06		s1	0.4320	-0.2010	0.0202		S
3813 Fortov	13.3		13 Oct 1996	2C	1800(2)	1.11	c	s1	0.3611	-0.1119	0.0137		S
3819 Robinson	12.3		20 Jan 1997	2C	1800(2)	1.00	m	s2	0.2439	-0.4373	-0.1103		Sr
3827 Zdenekhorský	12.3		10 Dec 1995	2C	1800(2)	1.06		s2	-0.0451	0.1692	-0.0570		C
3829 Gunma	12.2	0.04	2 Dec 1996	2C	1800(2)	1.13	m	s2	0.0124	0.2675	-0.0841		Ch
3831 Pettengill	13.5		11 May 1995	2C	1200(2)	1.32	cm	s4	0.5998	-0.2024	-0.0336		S
3844 1966 BZ	11.8		16 Oct 1996	2C	2700(3)	1.03	c	s2	0.7945	0.0240	-0.0301		L
3850 Peltier	13.9		6 Sep 1996	2C	1800(2)	1.16	h	s2	-0.0862	-0.8064	0.0537		V

Asteroid	H	p_H	Observational circumstances						Spectral components			Classification	
			UT Date	*a*	*b*	*c*	*d*	*e*	Slope	PC2'	PC3'	Old	New
3853 Haas	12.7		27 Oct 1995	1C	2700(3)	1.18		s2	0.3347	-0.1095	-0.0226		S
3858 Dorchester	13.7		14 May 1995	2C	1800(2)	1.28	m	s3	0.6807	-0.5475	-0.1211		Sa
3860 Plovdiv	12.1		30 Mar 1994	2C	1800(2)	1.35	cm	s3	0.6003	-0.2045	0.0660		S
3861 Lorenz	12.4		15 Nov 1994	2C	1800(2)	1.06	m	s1	0.4234	-0.1498	-0.0004		S
3862 Agekian	13.0		7 Jan 1994	2C	1200(2)	1.14		s2	0.6225	-0.2078	0.0131		S
3885 Bogorodskij	12.1		29 Jan 1996	2C	1800(2)	1.06	m	s2	-0.0848	0.1380	-0.1180		Cg
3886 Shcherbakovia	12.5		15 Dec 1995	2C	1800(2)	1.12	h	s2	0.0494	0.1954	0.0605		C
3900 Knežević	13.6		8 Sep 1996	2C	1800(2)	1.10		s2	-0.0774	-0.7748	0.1122		V
3903 Kliment Ohridski	12.0		8 Feb 1995	2C	1800(2)	1.15	c	s2	0.1995	-0.1397	0.0236		Sq
3910 Liszt	12.1		7 Feb 1995	2C	1800(2)	1.05		s2	0.5451	-0.2505	-0.0451		S
3920 Aubignan	13.2		20 Feb 1994	2C	1200(2)	1.10	c	s3	0.6048	-0.4026	-0.0629		Sa
3949 Mach	13.3		15 Apr 1997	2C	1800(2)	1.56		s1	0.2356	-0.2132	-0.0099		Sq
3958 1953 TC	12.3		20 Feb 1994	2C	1200(2)	1.29	c	s3	0.0606	0.0881	0.0139		Xc
3971 Voronikhin	11.8	0.04	8 Feb 1995	2C	1800(2)	1.21		s2	-0.1645	0.3318	-0.0234		Ch
3972 Richard	14.4		29 May 1997	2C	1800(2)	1.39		s1	0.3605	-0.1805	0.0273		S
3976 Lise	11.6	0.06	27 May 1997	2C	1800(2)	1.44	m	s1	0.3552	0.1642	0.0443		X
3985 Raybatson	11.3		7 Feb 1995	2C	1800(2)	1.05		s2	0.4010	0.1548	0.0057		X
4001 Ptolemaeus	13.6		28 May 1997	2C	1800(2)	1.37		s1	0.2973	-0.1536	-0.0001		S
4036 1987 DW_5	12.5		8 Feb 1996	2C	1800(2)	1.16	m	s2	0.0049	0.1426	-0.1178		Cg
4037 Ikeya	12.5		8 Feb 1996	2C	1800(2)	1.16	m	s2	0.2795	-0.2028	-0.0180		Sk
4039 Souseki	13.0		8 Feb 1996	2C	1800(2)	1.04		s2	0.4217	-0.3830	-0.0142		S
4051 Hatanaka	12.4		11 Sep 1996	2C	1800(2)	1.33	h	s1	0.0564	-0.0941	0.0859		Sq
4082 Swann	12.9		11 Dec 1995	2C	1800(2)	1.10		s2	-0.0225	0.2574	-0.0730		Ch
4096 Kushiro	12.5		30 Mar 1994	2C	1800(2)	1.08	c	s3	0.7169	-0.2435	0.0586		Sl
4107 Rufino	11.6	0.29	9 Apr 1997	2C	1800(2)	1.10		s1	0.0737	0.1690	-0.0161		C
4116 Elachi	13.2		30 Mar 1994	2C	1200(2)	1.25	cm	s3	0.6572	-0.1836	0.0534		Sl
4124 Herriot	12.5	0.04	17 Oct 1996	2C	2700(3)	1.02		s2	-0.1484	0.2773	0.0259		B
4135 Svetlanov	12.1		15 Nov 1994	2C	1800(2)	1.26	cm	s1	-0.0487	0.3338	-0.0074		Ch
4142 Dersu-Uzala	13.6		6 Jan 1994	2C	1200(2)	1.03		s2	1.0608	-0.3041	0.0019		A
4156 1988 BE	12.1		24 Feb 1997	2C	1200(2)	1.13	cm	s2	-0.2504	0.2853	-0.1827		Cgh
			9 Apr 1997	2C	2700(3)	1.14		s1					
4157 Izu	11.9	0.07	8 Feb 1995	2C	1800(2)	1.14		s2	-0.2272	0.3407	-0.0127		Ch
4182 Mount Locke	12.2		16 Nov 1994	2C	1800(2)	1.23	m	s1	0.2945	-0.2795	0.0007		Sr
4188 Kitezh	12.7		8 Feb 1996	2C	1800(2)	1.16	m	s2	-0.0391	-0.5541	0.0006		V
4194 Sweitzer	12.0	0.08	1 Dec 1996	2C	1800(2)	1.10		s2	-0.0688	0.2299	0.0224		Cb
4200 Shizukagozen	13.5		16 Oct 1996	2C	2700(3)	1.09		s2	0.4306	-0.1552	-0.0229		S
			17 Oct 1996	2C	1800(2)	1.08		s2					
4205 David Hughes	14.7		6 Sep 1996	2C	2700(3)	1.12	h	s2	0.2392	0.1512	0.0188		Xe
4215 Kamo	12.4		8 Apr 1997	2C	2700(3)	1.77		s1	0.0374	-0.6283	0.0971		V
4222 Nancita	12.4	0.32	12 Feb 1995	2C	900(3)	1.05	hm	s2	0.3205	-0.2964	-0.0404		S
4261 Gokko	12.5		11 Sep 1996	2C	1800(2)	1.37	h	s1	0.1473	-0.0732	0.0496		Sq
4276 Clifford	14.3		1 Apr 1994	2C	1800(2)	1.14	m	s3	0.0977	0.3042	0.1018		Cb
4284 Kaho	12.5		5 Jan 1994	2C	1200(2)	1.12		s2	-0.1062	0.2655	-0.0771		Ch
			1 May 1996	2C	1350(3)	1.24		s1					
4287 Třísov	13.2		12 Oct 1996	2C	1800(2)	1.01		s1	0.6080	-0.2012	-0.0875		S
4292 Aoba	12.2	0.05	27 Apr 1996	2C	1800(2)	1.54	cm	s1	-0.0044	0.1668	0.0175		C
4299 1952 QX	13.1		12 Oct 1996	2C	1800(2)	1.05		s1	0.4638	-0.2508	-0.0645		S
4304 Gelchenko	13.6		20 Feb 1994	2C	1200(2)	1.07	m	s3	0.0631	0.2180	-0.0583		C
4305 Clapton	12.6		14 Nov 1994	2C	1800(2)	1.06	hm	s1	0.4416	-0.1639	0.0394		S
4327 Ries	12.3	0.07	5 Jan 1994	2C	1200(2)	1.02	c	s2	0.2787	-0.0988	0.0831		Sk
4332 Milton	11.9	0.23	20 Jan 1997	2C	1800(2)	1.21	m	s2	0.1056	0.2191	0.0872		Xe
4340 Dence	13.1		6 Apr 1997	2C	2700(3)	1.09	c	s1	0.3409	-0.1855	-0.0073		S
4342 Freud	12.1	0.08	14 May 1995	2C	1800(2)	1.17	m	s3	0.1312	0.1075	-0.0784		Xc
4343 Tetsuya	11.9	0.09	18 Oct 1996	2C	2700(3)	1.03		s2	-0.1337	0.3388	-0.0252		Ch
4352 Kyoto	11.7		8 Feb 1995	2C	1200(2)	1.01	cm	s2	0.4181	-0.2500	-0.0386		S
4353 Onizaki	12.4		15 May 1995	2C	1200(2)	1.60	m	s3	0.5738	-0.0187	0.0576		Xe

Asteroid	H	p_H	Observational circumstances					Spectral components			Classification	
			UT Date	*a*	*b*	*c*	*d* *e*	Slope	PC2'	PC3'	Old	New
4369 Seifert	11.9		8 Dec 1995	2C	1200(2)	1.01	m s2	0.4178	0.2322	0.0863		Xk
4372 Quincy	13.0		16 Nov 1994	2C	1800(2)	1.17	m s1	0.3874	-0.1745	-0.0712		S
4374 Tadamori	13.0		19 Jan 1997	2C	1800(2)	1.12	s2	0.4740	-0.2059	0.0040		S
4382 Stravinsky	12.3		20 Feb 1994	2C	1200(2)	1.03	cm s3	0.6237	-0.4044	-0.0102		Sa
4390 1976 GO_8	13.5		5 Jan 1994	2C	1200(2)	1.01	s2	0.1195	0.3481	-0.1469		Cgh
4396 Gressmann	13.9		9 Feb 1996	2C	2700(3)	1.18	c s2	-0.1408	0.2841	0.0562		B
4407 Taihaku	12.0		9 May 1995	2C	1800(2)	1.22	m s3	0.6645	-0.3384	-0.0727		Sa
4417 Lecar	11.5		10 Feb 1995	2C	1800(2)	1.09	c s3	0.5669	-0.3165	0.0091		S
4422 Jarre	12.6		17 Jan 1997	2C	1800(2)	1.05	hm s2	0.4941	-0.1864	-0.0240		S
4424 Arkhipova	11.5	0.07	15 May 1995	2C	1800(2)	1.21	m s3	0.3178	0.0453	-0.1245		Xk
4426 Roerich	12.3		15 May 1995	2C	1800(2)	1.52	m s3	0.7509	-0.1707	-0.0405		L
4434 Nikulin	13.2		6 Sep 1996	2C	1800(2)	1.45	h s2	-0.0808	-0.6478	0.0714		V
4435 Holt	13.2		15 Oct 1996	2C	1800(2)	1.14	c s2	0.4085	-0.2716	0.0126		S
4456 Mawson	13.4		7 Jan 1994	2C	1200(2)	1.04	s2	1.0236	0.0647	-0.0297		Ld
4461 Sayama	11.6		7 Feb 1995	2C	1800(2)	1.09	s2	0.2464	0.1682	0.0127		X
4479 1985 CP_1	12.7		9 May 1995	2C	1800(2)	1.43	s3	0.4200	-0.3044	-0.0665		S
4512 Sinuhe	11.9		15 May 1995	2C	1800(2)	1.24	m s3	0.6422	-0.3556	-0.0941		Sa
4516 Pugovkin	12.6		22 Feb 1994	2C	1800(2)	1.11	m s3	0.7283	-0.2668	-0.0357		Sa
4523 1981 DM_1	12.3		31 Mar 1994	2C	1800(2)	1.20	s3	-0.1425	0.2804	-0.0340		Ch
4534 Rimskij-Korsakov	12.3		16 Oct 1996	2C	2700(3)	1.01	s2	-0.1098	0.2726	0.0233		Cb
4536 1987 DA_6	13.3		14 Apr 1997	2C	1200(2)	1.41	s1	0.4186	-0.2099	-0.0294		S
4547 Massachusetts	11.0	0.10	24 Feb 1994	2C	1200(2)	1.31	cm s2	0.1250	0.2371	0.0199		X
			29 Nov 1996	2C	1200(2)	1.02	cm s2					
4558 Janesick	12.2		9 Feb 1996	2C	1800(2)	1.26	s2	0.3118	-0.2490	0.0328		S
4570 Runcorn	13.0		27 Feb 1997	2C	1800(3)	1.06	m s3	0.8207	-0.2424	-0.1007		Sa
4584 Akan	12.4		9 May 1995	2C	1800(2)	1.32	m s3	0.0171	0.2016	-0.0334		C
4611 Vulkaneifel	12.5		8 Feb 1996	2C	1800(2)	1.09	s2	0.4952	-0.3130	-0.0450		S
4619 Polyakhova	12.6		10 Dec 1995	2C	1800(2)	1.04	m s2	0.8124	-0.1169	-0.0329		L
4628 Laplace	11.0		9 Feb 1996	2C	1800(2)	1.03	c s2	0.5169	-0.2477	-0.0300		S
4649 Sumoto	11.6		27 Oct 1995	1C	2700(3)	1.03	s2	0.5224	-0.2991	0.0180		S
4701 Milani	13.0		11 Dec 1995	2C	1800(2)	1.04	m s2	0.3037	0.1943	0.0206		Xe
4702 1987 HW	12.2		15 Nov 1994	2C	1800(2)	1.04	cm s1	0.3677	-0.0967	0.0325		S
4713 Steel	12.8		27 Mar 1994	2C	1800(2)	1.04	s3	1.2143	-0.3011	0.0039		A
4719 Burnaby	12.0		29 Apr 1996	2C	2700(3)	1.40	cm s1	-0.1245	0.0888	0.0232		C
4726 Federer	12.8		9 Feb 1996	2C	2700(3)	1.02	s2	0.7503	-0.1549	-0.0235		L
4733 ORO	13.7		13 Oct 1996	2C	1800(2)	1.12	c s1	0.1767	-0.1539	0.0329		Sq
4737 Kiladze	12.8		13 Apr 1997	2C	2700(3)	1.18	s1	0.8308	-0.0255	-0.0488		L
4744 1988 RF_5	11.1		21 Apr 1996	1W	2700(3)	1.44	s1	0.8292	0.1983	0.1068		D
			23 Apr 1996	1C	1800(2)	1.44	s1					
4748 Tokiwagozen	11.7		28 Apr 1996	2C	1800(2)	1.09	m s1	0.4751	-0.3499	-0.0521		S
4750 Mukai	13.6		12 Oct 1996	2C	1800(2)	1.05	s1	0.2151	0.2000	0.0074		X
4767 1987 GC	12.8		27 Apr 1996	2C	1800(2)	1.25	c s1	0.5073	-0.2012	-0.0360		S
4774 Hobetsu	12.8		28 Nov 1996	2C	1800(2)	1.03	chm s2	0.4993	-0.1256	0.0243		S
4786 Tatianina	13.2		11 Feb 1995	2C	1800(2)	1.11	h s3	0.1723	0.0737	0.0198		Xc
4804 Pasteur	11.6		29 May 1997	2C	900(1)	1.64	c s1	0.0124	0.2198	0.0046		C
			30 May 1997	2C	1800(2)	1.72	s1					
4824 1986 WL_1	13.6		6 Sep 1996	2C	1800(2)	1.20	h s2	0.1861	-0.3636	0.1590		Sr
			8 Sep 1996	2C	1800(2)	1.20	s1					
4844 Matsuyama	12.4		11 Feb 1995	2C	1200(2)	1.15	hm s3	0.3952	-0.3093	-0.0150		S
4845 Tsubetsu	12.5		6 Sep 1996	2C	1800(2)	1.27	h s2	0.2154	0.1793	0.0527		X
			8 Sep 1996	2C	1800(2)	1.28	s1					
4853 1979 ML	12.6		10 May 1995	2C	1800(2)	1.28	s1	0.3494	-0.1469	0.0146		S
4884 1979 OK_{15}	14.3		12 Oct 1996	2C	1800(2)	1.09	s1	0.4088	-0.2228	-0.0415		S
4900 Maymelou	13.0		8 Sep 1996	2C	1800(2)	1.04	s2	0.0816	-0.6150	0.1127		V
4910 Kawasato	14.2		1 Apr 1994	2C	1800(2)	1.19	s3	0.5497	-0.2655	-0.0027		S
4917 Yurilvovia	12.9		12 Sep 1996	2C	1800(2)	1.06	h s2	1.1053	-0.0323	-0.0362		Ld

Asteroid	H	p_H	Observational circumstances						Spectral components			Classification	
			UT Date	a	b	c	d	e	Slope	PC2'	PC3'	Old	New
4923 Clarke	14.2		9 Apr 1997	2C	2700(3)	1.45		s1	0.4070	-0.2563	0.0201		S
4942 1987 DU_6	13.0		26 May 1997	2C	2700(3)	1.34		s1	0.2237	0.1450	0.0864		X
4944 Kozlovskij	12.8		15 Oct 1996	2C	2700(3)	1.19	c	s1	-0.0199	0.2148	0.0383		Cb
			16 Oct 1996	2C	1800(2)	1.18		s1					
4945 Ikenozenni	13.0		14 May 1995	2C	1800(2)	1.52	c	s3	0.5432	-0.3761	-0.0076		S
4950 House	11.5		11 Sep 1996	2C	2700(3)	1.27	h	s1	0.2659	-0.1952	0.0646		Sk
4951 Iwamoto	13.4		9 Apr 1997	2C	1800(2)	1.03		s1	0.4903	-0.3085	-0.0431		S
4968 Suzamur	12.7		13 Apr 1997	2C	1800(2)	1.36		s1	0.2061	-0.1529	0.0054		Sq
4969 Lawrence	12.6		11 Dec 1995	2C	1800(2)	1.36		s2	-0.1013	0.1528	0.0309		C
4982 Bartini	13.2		1 Dec 1996	2C	2700(3)	1.05		s2	0.5183	-0.4598	-0.2140		A
4993 1983 GR	13.0		22 Jan 1997	2C	1800(2)	1.04	m	s2	-0.0211	-0.5404	0.1039		V
4995 1984 QR	13.0		9 Dec 1995	2C	1800(2)	1.06	m	s2	0.3525	-0.1668	0.0132		S
4997 Ksana	11.9		15 Oct 1996	2C	1800(2)	1.06	c	s2	-0.1941	0.3050	0.0338		B
5008 Miyazawakenji	12.9		28 Nov 1996	2C	1800(2)	1.10	chm	s2	0.5067	-0.1362	-0.0192		S
5010 Amenemhêt	12.2		16 Oct 1996	2C	2700(3)	1.21		s2	0.2966	-0.1977	0.0313		S
5013 1964 VT_1	12.4		2 Dec 1996	2C	1800(2)	1.06		s2	0.6819	-0.1767	-0.0476		Sl
5038 1948 KF	14.1		9 Apr 1997	2C	1800(2)	1.11		s1	0.4931	-0.1252	-0.0188		S
5067 Occidental	12.2		21 Oct 1996	2C	2700(3)	1.04		s2	0.8871	-0.0756	0.0358		L
			30 Nov 1996	2C	1800(2)	1.05	m	s2					
5069 Tokeidai	13.2		14 Apr 1997	2C	1800(2)	1.12		s1	0.4895	-0.2321	-0.0287		S
5079 1975 DB	12.6	0.07	14 Dec 1995	2C	1800(2)	1.01	c	s2	-0.0437	0.2784	0.0908		B
5087 Emel'yanov	13.1		12 Sep 1996	2C	1800(2)	1.23	h	s2	0.2213	0.2231	-0.0124		X
5091 Isakovskij	12.1		10 Dec 1995	2C	2700(3)	1.19		s2	-0.0618	0.1637	-0.0150		C
5102 1986 RD_1	12.7	0.06	2 Dec 1996	2C	1800(2)	1.01		s2	-0.0924	0.2831	0.0997		B
5103 1986 RP_1	12.6		2 Dec 1996	2C	2700(3)	1.08		s2	0.1354	0.2659	0.0357		X
5133 Phillipadams	11.5	0.07	14 Apr 1997	2C	2700(3)	1.05		s1	-0.1509	0.2617	0.0444		B
5134 1990 SM_2	12.0		10 Apr 1997	2C	1800(2)	1.03		s1	0.7708	-0.1481	-0.0528		Sl
5142 Okutama	11.8		17 Nov 1994	2C	1200(2)	1.05	hm	s2	0.2588	-0.1965	0.0406		Sq
5159 Burbine	13.0		23 Feb 1994	2C	1900(2)	1.09	m	s3	0.4827	-0.2229	-0.0312		S
5195 Kaendler	13.8		30 May 1997	2C	1800(2)	1.54		s1	0.6469	-0.2944	-0.0499		Sa
5196 Bustelli	12.6		19 Jan 1997	2C	1800(2)	1.08	cm	s2	0.4894	-0.1918	-0.0231		S
5208 Royer	11.6		23 Feb 1997	2C	1800(2)	1.02	cm	s2	0.3853	-0.0578	-0.0005		S
5214 Oozora	13.5		6 Sep 1996	2C	1800(2)	1.28	h	s2	0.3764	-0.1783	-0.0031		S
5222 Ioffe	11.0	0.16	15 Nov 1994	2C	2700(3)	1.12	m	s1	-0.1883	0.3708	0.0672		B
5234 Sechenov	11.4		15 Nov 1994	2C	1800(2)	1.32		s1	-0.1337	0.3037	0.0445		B
5242 Kenreimonin	12.5		27 May 1997	2C	2700(3)	1.59		s1	0.1815	-0.1812	0.0529		Sq
5243 Clasien	12.9		10 May 1995	2C	1800(2)	1.24	m	s3	0.0783	0.1690	-0.0600		C
5253 1985 XB	13.7		15 Oct 1996	2C	1800(2)	1.11	c	s2	0.6193	-0.2829	-0.0299		S
5261 Eureka	16.1		16 Nov 1994	2C	3600(4)	1.13	m	s1	0.3320	-0.3913	-0.0877		Sr
5275 Zdislava	13.6		15 May 1995	2C	2700(3)	1.42	m	s3	0.6226	-0.5135	-0.0603		Sa
5294 Onnetoh	11.8		14 Apr 1997	2C	2700(3)	1.16		s1	0.1613	0.2101	0.0586		X
5329 1989 YP	12.4		8 Feb 1995	2C	1800(2)	1.11		s2	-0.0628	0.2476	0.0675		Cb
5330 Senrikyu	11.8	0.31	9 Feb 1995	2C	1800(2)	1.44		s2	-0.2380	0.3186	0.0970		B
5344 Ryabov	13.3		15 Oct 1996	2C	1800(2)	1.10	c	s2	-0.1493	0.2497	0.0158		B
5348 1988 BB	12.7		30 Nov 1996	2C	2700(3)	1.02	m	s2	-0.1599	0.3318	-0.0197		Ch
5349 Paulharris	12.7		6 Jan 1994	2C	1200(2)	1.04		s2	-0.0416	0.2639	0.0051		C
5364 1980 RC_1	12.9		20 Feb 1994	2C	1200(2)	1.19		s3	-0.0025	0.2122	-0.0260		C
5379 1991 HG	12.8		11 May 1995	2C	1800(2)	1.92	c	s1	-0.1117	-0.7321	0.1008		V
5392 Parker	12.7		26 Feb 1997	2C	1800(3)	1.04	m	s3	0.6551	-0.2368	-0.0849		Sl
5397 1988 VB_5	12.7		20 Feb 1994	2C	1200(2)	1.29	m	s3	0.6531	-0.1290	-0.0005		S
5401 Minamioda	11.8		17 Oct 1996	2C	1800(2)	1.28		s2	0.6189	-0.1520	-0.0148		S
5407 1992 AX	13.9		19 Jan 1997	2C	1800(2)	1.04	m	s2	0.2271	-0.0280	0.0124		Sk
5416 1978 VE_5	12.2		10 May 1995	2C	1800(2)	1.28	m	s4	-0.1068	0.1943	-0.0179		C
5438 Lorre	11.2		20 Jan 1997	2C	2700(3)	1.02	m	s2	0.2271	0.2182	-0.0484		C
5448 Siebold	13.0		20 Jan 1997	2C	1800(2)	1.03	cm	s2	0.5225	-0.2286	-0.0475		S
			27 Feb 1997	2C	1200(2)	1.04		s3					

Asteroid	H	p_H	Observational circumstances						Spectral components			Classification	
			UT Date	*a*	*b*	*c*	*d*	*e*	Slope	PC2'	PC3'	Old	New
5467 1988 AG	12.9		16 Oct 1996	2C	2700(3)	1.03	c	s2	0.4268	0.2419	0.0726		X
5482 1990 DX	12.9		22 Feb 1994	2C	1800(2)	1.22	m	s3	0.6792	-0.3630	-0.0472		Sa
5485 Kaula	13.2		17 Oct 1996	2C	2700(3)	1.08		s2	0.6367	-0.1496	0.0004		S
5492 Thoma	12.4		17 Oct 1996	2C	2700(3)	1.20		s2	0.7220	0.0629	0.0006		L
5510 1988 RF_7	13.9		1 Apr 1994	2C	1800(2)	1.35	m	s3	0.6165	-0.3177	-0.0071		S
5534 1941 UN	12.1		15 Oct 1996	2C	1800(2)	1.26	c	s2	0.4155	-0.1011	-0.0035		S
5552 1982 SJ_1	12.9		15 Oct 1996	2C	1200(2)	1.15	c	s2	0.3886	-0.1134	0.0170		S
5553 Chodas	13.0		2 Dec 1996	2C	2700(3)	1.15	m	s2	-0.0185	0.2660	-0.1085		Ch
5563 1991 VZ_1	11.7		19 Jan 1997	2C	1800(2)	1.02	cm	s2	0.3830	-0.1957	-0.0626		S
5565 Ukyounodaibu	11.8		20 Jan 1997	2C	1800(2)	1.08	m	s2	0.5981	-0.1042	-0.0005		S
5576 Albanese	12.2	0.06	30 Nov 1996	2C	2700(3)	1.06	m	s2	0.3584	0.1818	-0.0528		Xk
5585 Parks	13.7		15 Dec 1995	2C	1800(2)	1.10		s2	-0.0644	0.3653	0.0131		Ch
5588 1990 SW_3	11.9		14 Dec 1995	2C	1800(2)	1.06		s2	0.2318	0.2506	0.0953		X
5591 Koyo	12.5		27 Feb 1997	2C	1800(2)	1.17	m	s3	-0.0502	0.2460	0.0213		Cb
			7 Apr 1997	2C	2700(3)	1.16		s1					
5595 1991 PJ	12.5		21 Oct 1996	2C	1800(2)	1.21		s2	0.3650	-0.1954	-0.0181		S
5610 Balster	12.8		18 Oct 1996	2C	1800(2)	1.04		s2	0.3280	-0.1407	-0.0075		S
			21 Oct 1996	2C	1800(2)	1.03		s2					
5622 1990 TL_4	11.3		8 Dec 1995	2C	2700(3)	1.01	m	s2	0.2918	-0.2184	-0.0652		Sk
5632 Ingelehmann	11.5		25 Feb 1997	2C	900(1)	1.12	cm	s2	0.1359	0.0891	-0.0559		Xc
			9 Apr 1997	2C	1800(2)	1.04		s1					
5641 McCleese	11.7		13 May 1995	2C	1800(2)	1.01	m	s3	0.8533	-0.4087	-0.0744		A
5647 1990 TZ	11.3		8 Feb 1995	2C	1200(2)	1.16	cm	s2	0.3767	-0.2828	0.0242		S
5678 DuBridge	12.9	0.01	14 Nov 1994	2C	1800(2)	1.08	h	s1	-0.0893	0.2421	-0.0052		C
5685 1990 XA	11.7		14 Nov 1994	2C	2700(3)	1.04	hm	s1	0.4762	-0.1867	-0.0058		S
5690 1992 EU	12.5		27 Oct 1995	1C	2700(3)	1.09		s1	-0.3413	0.2708	0.0203		B
5817 1989 RZ	12.6		19 Feb 1994	2C	1200(2)	1.01	chm	s3	0.5106	-0.3445	0.0198		S
5840 1978 ON	12.2		10 May 1995	2C	2700(3)	1.21	m	s3	1.0081	-0.1981	-0.0039		Ld
5892 1981 YS_1	13.6		27 Feb 1997	2C	900(1)	1.17	m	s3	0.3508	-0.2375	-0.0376		S
			11 Apr 1997	2C	2700(3)	1.10		s1					
5956 d'Alembert	12.7		9 Dec 1995	2C	1800(2)	1.18	m	s2	0.0202	0.2073	0.0196		C
5965 1990 SV_{15}	12.4		27 Feb 1997	2C	1800(2)	1.08		s3	0.8333	-0.2391	-0.0201		Sa
6005 1989 BD	12.3		21 Oct 1996	2C	1800(2)	1.12	m	s2	-0.1936	0.2241	-0.0001		C
6071 1992 AS_1	11.8		10 Dec 1995	2C	1800(2)	1.17	m	s2	0.3235	-0.1969	0.0105		S
6077 1980 TM	12.6		29 Jan 1996	2C	1800(2)	1.03		s2	0.0817	-0.1616	-0.0072		Sq
6078 Burt	13.3		16 Nov 1994	2C	1800(2)	1.15	m	s1	0.3338	-0.2537	-0.0690		S
6086 1987 VU	12.4		17 Oct 1996	2C	1800(2)	1.08		s2	0.8577	-0.1275	-0.0317		Sl
6129 Demokritos	12.3	0.05	14 Apr 1997	2C	2700(3)	1.28		s1	-0.1148	0.3032	-0.0271		Ch
6146 Adamkrafft	13.0		11 Apr 1997	2C	2700(3)	1.19	c	s1	0.2623	-0.2024	-0.0063		Sq
6192 1990 KB_1	12.7	0.22	8 Apr 1997	2C	2700(3)	1.33		s1	0.4449	-0.2777	-0.0301		S
			29 May 1997	2C	1350(3)	1.34	c	s1					
6211 1991 DO	12.7		29 Apr 1996	2C	3600(4)	1.53	cm	s1	0.3534	-0.3787	0.0787		Sr
6230 1984 SG_1	13.1		14 Nov 1994	2C	1800(2)	1.03	h	s1	0.0581	0.2071	0.0599		C
6233 1986 CG	13.3		14 Nov 1994	2C	1800(2)	1.01	h	s1	-0.0188	0.2919	-0.0417		Ch
6249 Jennifer	12.4		30 May 1997	2C	1800(2)	1.08		s1	0.4044	0.1054	0.0519		Xe
6283 1980 VX_1	13.3		15 Nov 1994	2C	1800(2)	1.01	cm	s1	-0.2311	0.4308	0.0112		Ch
6364 1981 ET	12.3		17 Oct 1996	2C	1800(2)	1.20		s2	0.4714	-0.1622	-0.0074		S
6386 1989 NK_1	12.7		30 Nov 1996	2C	1800(2)	1.57	ch	s1	0.5220	-0.2065	0.0626		S
6410 1992 WO_4	12.2		18 Oct 1996	2C	2700(3)	1.56		s2	-0.1061	0.2618	-0.0654		Ch
6500 Kodaira	12.5		15 Oct 1996	2C	900(2)	1.33	c	s2	-0.2539	0.2873	0.0641		B
6509 1983 CQ_3	12.5		27 Feb 1997	2C	1800(2)	1.06		s3	-0.0013	0.2526	-0.1118		Ch
6582 1981 VS	12.7		9 Dec 1995	2C	1200(2)	1.14	m	s2	0.0100	0.3156	0.0165		Ch
6585 O'Keefe	14.3		27 Oct 1995	1C	2700(3)	1.02		s2	0.2748	-0.1635	-0.0163		Sk
6592 Goya	12.9		15 Dec 1995	2C	2700(3)	1.12	h	s2	0.2227	-0.2296	0.0566		Sq
6669 1994 JA_1	12.8		13 Apr 1997	2C	2700(3)	1.06		s1	0.3480	-0.2550	-0.0519		S
6704 1988 CJ	12.6		18 Jan 1997	2C	2700(3)	1.06		s2	0.3726	0.0300	0.0394		K

Asteroid	H	p_H	Observational circumstances						Spectral components			Classification	
			UT Date	a	b	c	d	e	Slope	PC2'	PC3'	Old	New
6716 1990 RO_1	12.8		11 Dec 1995	2C	1800(2)	1.13		s2	-0.0457	0.2310	0.0442		C
6782 1990 SU_{10}	12.5		11 Dec 1995	2C	1800(2)	1.04		s2	-0.0055	0.2677	0.0996		Cb
6847 1977 RL	13.7		28 Oct 1995	1C	2700(3)	1.20		s2	0.2590	-0.1005	0.0016		Sk
6906 1990 WC	12.7		14 Dec 1995	2C	1800(2)	1.03	cm	s2	0.0091	0.2453	-0.0635		C
6907 1990 WE	12.8		11 Dec 1995	2C	1800(2)	1.07	m	s2	-0.0435	0.2041	-0.0356		C
6908 1990 WB_3	12.6		11 Apr 1997	2C	2700(3)	1.20	ch	s1	0.3294	-0.1895	0.0457		S
7056 Kierkegaard	12.8		10 Apr 1997	2C	3600(4)	1.51	ch	s1	0.1427	-0.2810	0.0117		Sq
7081 1987 QF_7	12.8		16 Oct 1996	2C	2700(3)	1.32		s1	0.4675	0.0051	-0.0097		K
7110 1983 XH_1	12.5	0.06	10 May 1995	2C	1800(2)	1.38		s1	-0.2648	0.3396	0.0125		Ch
7170 1987 MK	13.3	0.14	18 Oct 1996	2C	1800(2)	1.16		s2	0.6408	-0.1918	-0.0437		S
7211 Xerxes	13.3		16 Oct 1996	2C	2700(3)	1.23		s1	0.3524	-0.1347	0.0400		S
7224 1982 TK_3	12.8		1 Dec 1996	2C	2700(3)	1.03		s2	0.1531	-0.2779	-0.0252		Sq
7225 1983 BH	13.3		2 Dec 1996	2C	1800(2)	1.04		s2	0.5660	-0.2549	-0.0904		S
7245 1991 RN_{10}	12.7		29 Nov 1996	2C	1800(2)	1.11	cm	s2	0.9069	-0.1593	-0.0797		L
7304 1994 AE_2	13.3		24 Feb 1994	2C	1600(2)	1.03	cm	s2	0.8737	-0.0029	0.1103		Ld
7397 1986 QS	12.5		29 Nov 1996	2C	2700(3)	1.09	cm	s2	0.6467	-0.1649	-0.0836		S
7402 1987 YH	13.1		29 Nov 1996	2C	2700(3)	1.12	cm	s2	-0.1833	0.3508	0.0070		Ch
7404 1988 AA_5	13.5		21 Oct 1996	2C	2700(3)	1.21	m	s2	-0.0979	0.2319	0.0572		Cb
7405 1988 FF	12.1		25 Feb 1997	2C	2700(3)	1.11	m	s2	-0.2324	0.3213	-0.0349		Ch
			8 Apr 1997	2C	2700(3)	1.02		s1					
7451 1978 PU_2	12.7		27 Apr 1996	2C	2700(3)	1.25	c	s1	0.3783	-0.2212	-0.0239		S
			28 Apr 1996	2C	1800(2)	1.25		s1					
7512 1983 CA_1	12.8		26 Feb 1997	2C	900(1)	1.10	cm	s3	-0.1002	0.3116	-0.0633		Ch
			7 Apr 1997	2C	2700(3)	1.11		s1					
7562 1986 WO_9	12.8		27 Feb 1997	2C	1800(2)	1.09		s3	1.2427	-0.0990	-0.1208		Ld
7564 1988 CA	12.2		18 Jan 1997	2C	2700(3)	1.11	m	s2	0.3782	-0.2568	0.0131		S
7604 1995 QY_2	13.7		15 Dec 1995	2C	1800(2)	1.96		s2	-0.0702	0.1184	0.0207		C
7728 1977 AW_2	12.5		14 Apr 1997	2C	2700(3)	1.47		s1	0.0551	-0.0932	0.0147		Sq
7763 1990 UT_5	12.3		11 Dec 1995	2C	1800(2)	1.03	m	s2	0.6853	-0.0801	-0.0371		L
7817 1988 RH_{10}	12.9		27 Apr 1996	2C	2700(3)	1.26	cm	s1	-0.0588	0.1228	-0.0670		C
8008 1988 TQ_4	12.9		7 Jan 1994	2C	1200(2)	1.04		s2	-0.0432	0.2544	-0.0344		C
8333 1982 VF	12.8		2 Dec 1996	2C	1800(2)	1.00		s2	0.2427	-0.1890	0.0141		Sq
8334 1984 CF	12.7		18 Oct 1996	2C	2700(3)	1.15		s2	0.3550	-0.1339	-0.0171		S
8450 1977 QL_1	12.9		2 Dec 1996	2C	1800(2)	1.00	m	s2	0.0780	0.2630	0.0277		C
8513 1991 PK_{11}	12.6		2 Dec 1996	2C	1800(2)	1.01		s2	0.8179	0.1775	0.0368		D
8516 1991 TW_1	13.1		2 Dec 1996	2C	1800(2)	1.03	m	s2	0.3742	-0.2548	-0.0178		S
1973 AW_3	12.0		11 Apr 1997	2C	900(1)	1.22	ch	s1	0.0710	0.1302	0.0418		Xc
			12 Apr 1997	2C	1800(2)	1.27		s1					
1981 EL_{21}	13.4		12 Sep 1996	2C	1800(2)	1.24	h	s2	0.5390	0.0371	-0.0680		K
1987 UF_5	13.0		17 Oct 1996	2C	2700(3)	1.22		s2	0.7224	-0.1558	-0.0620		Sl
1990 WA_5	13.0		10 Apr 1997	2C	2700(3)	1.27	c	s1	0.1538	0.2594	0.0071		X
1991 PE_{10}	13.8		18 Oct 1996	2C	1800(2)	1.01		s2	0.4556	-0.0945	0.0147		S
1992 AE_1	12.7		15 Apr 1997	2C	2700(3)	1.27		s1	0.2439	-0.2149	-0.0400		Sq
1992 ST_1	12.6		17 Oct 1996	2C	1800(2)	1.59		s2	-0.0744	0.2173	0.0987		Cb
			18 Oct 1996	2C	1800(2)	1.60		s2					
1995 BM_2	15.6		8 Feb 1995	2C	1800(2)	1.59	m	s2	0.2142	-0.2876	0.0184		Sq
1995 WQ_5	16.8		15 Dec 1995	2C	2700(3)	1.15	h	s2	-0.1551	0.3044	0.0162		Ch
1996 PW	14.1		8 Sep 1996	2C	2700(3)	1.60		s1	1.1516	0.0305	0.1010		Ld
1996 TE_{11}	16.0		18 Oct 1996	2C	2700(3)	1.69		s2	0.1238	0.1273	0.0015		Xc
1996 UK	15.9		1 Dec 1996	2C	2700(3)	1.13		s2	0.1050	-0.1516	0.0360		Sq
1996 VC	13.8		1 Dec 1996	2C	1200(2)	1.06		s2	0.3817	-0.1924	-0.0484		S
1997 CU_{26}	6.2		25 Feb 1997	2C	3600(4)	1.05	m	s2	1.0674	0.2513	0.0130		D
1997 CZ_5	13.6		25 Feb 1997	2C	900(1)	1.06		s2	0.3600	-0.2262	0.0029		S

Appendix B

Spectral plots for 1189 SMASSII asteroids

These plots represent the final reduced spectra for 1189 SMASSII asteroids. For each asteroid, this is the weighted mean of all observations listed in Appendix A, normalized to unity at 0.55 μm as described in Chapter 2. Each spectrum covers the maximum wavelength interval from 0.435 to 0.925 μm at a uniform dispersion of 0.0025 μm per channel, though points that were flagged as being discrepant during the reduction process are not shown. Error bars are plotted to represent the uncertainty for each channel of the combined spectrum, based on Poisson statistics.

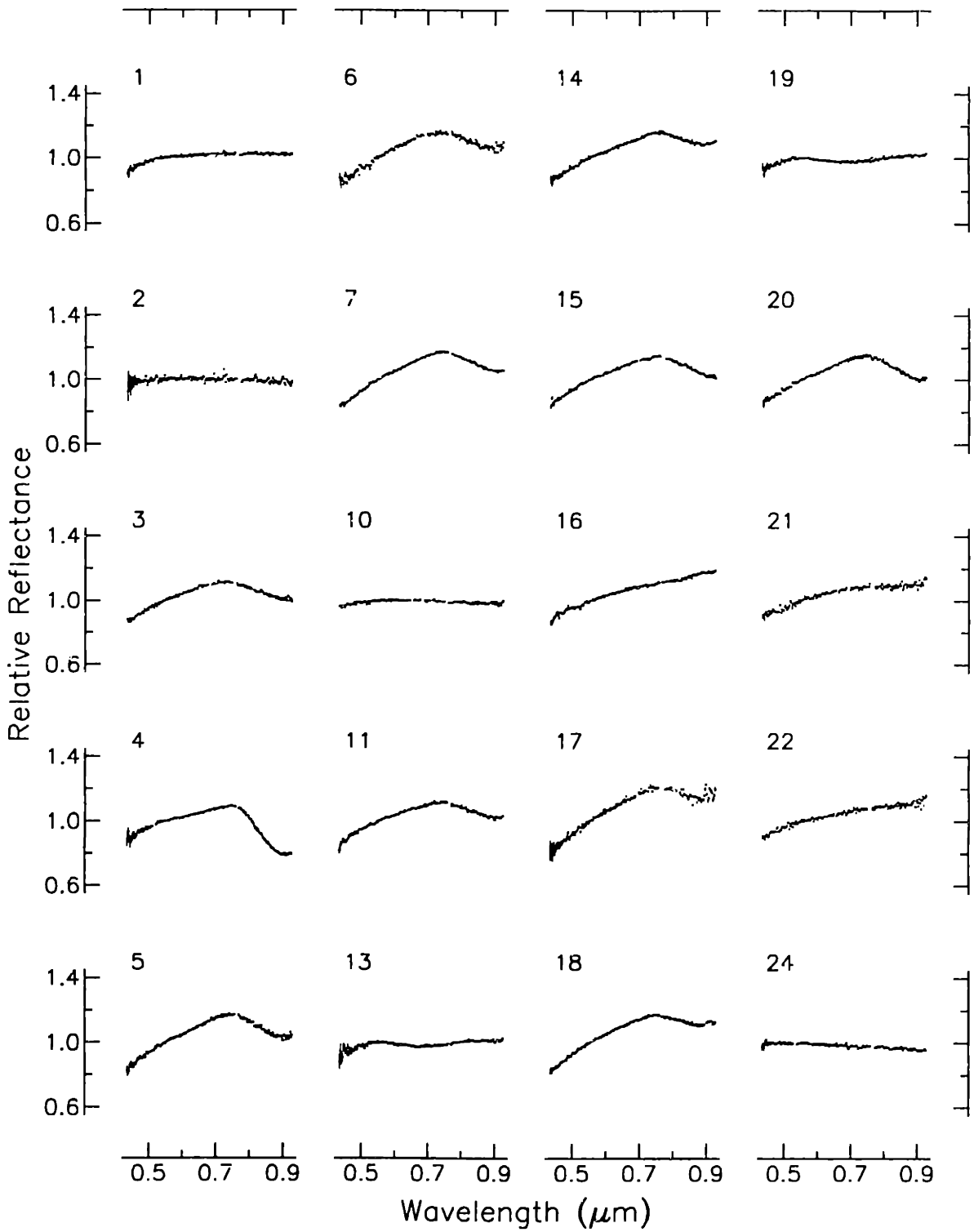
1
6
14
19
2
7
15
20
3
10
16
21
4
11
17
22
5
13
18
24
1.4
1.0
0.6
Relative Reflectance
0.5
0.7
0.9
Wavelength (μm)

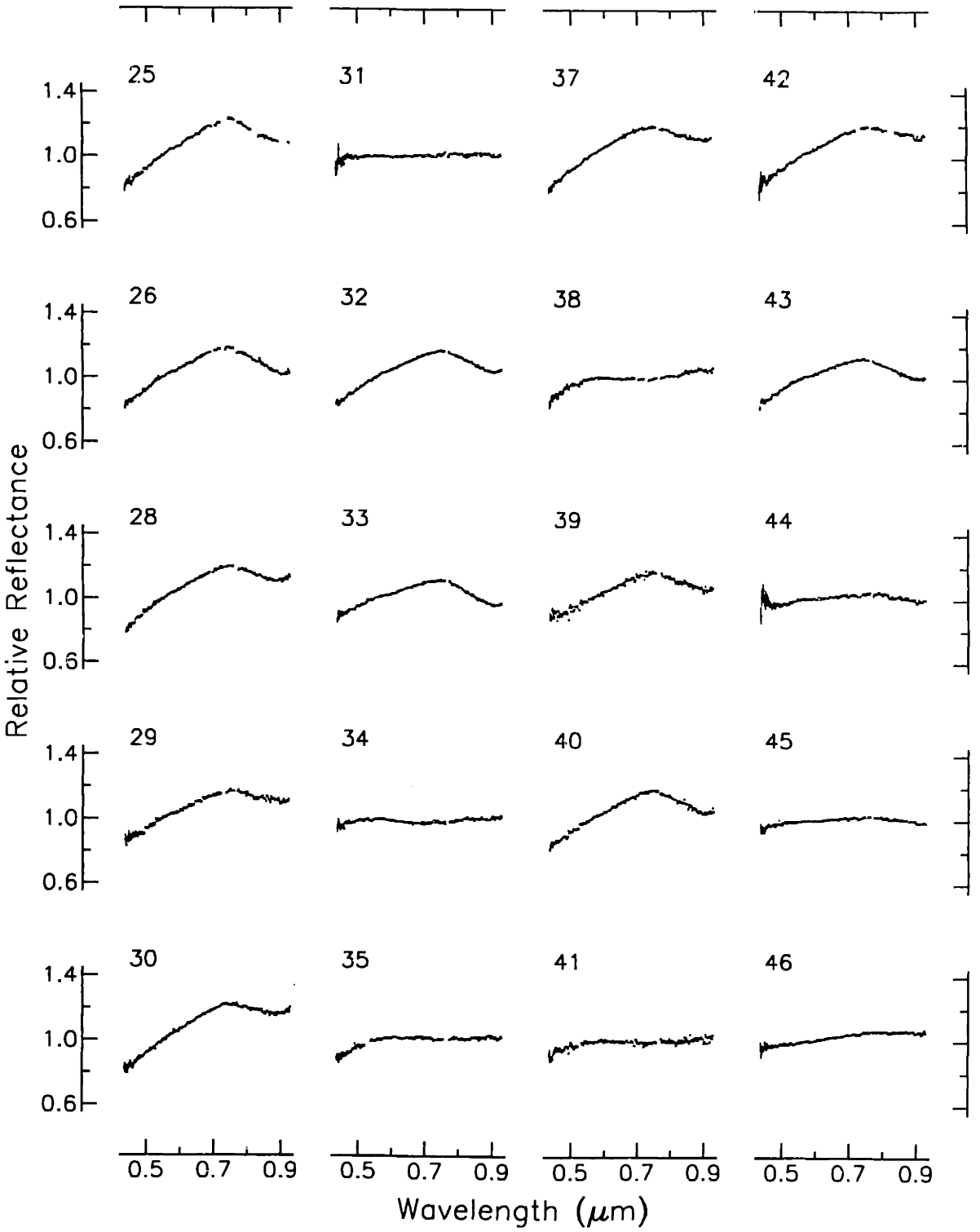
25
31
37
42
26
32
38
43
28
33
39
44
29
34
40
45
30
35
41
46
1.4
1.0
0.6
Relative Reflectance
0.5
0.7
0.9
Wavelength (μm)

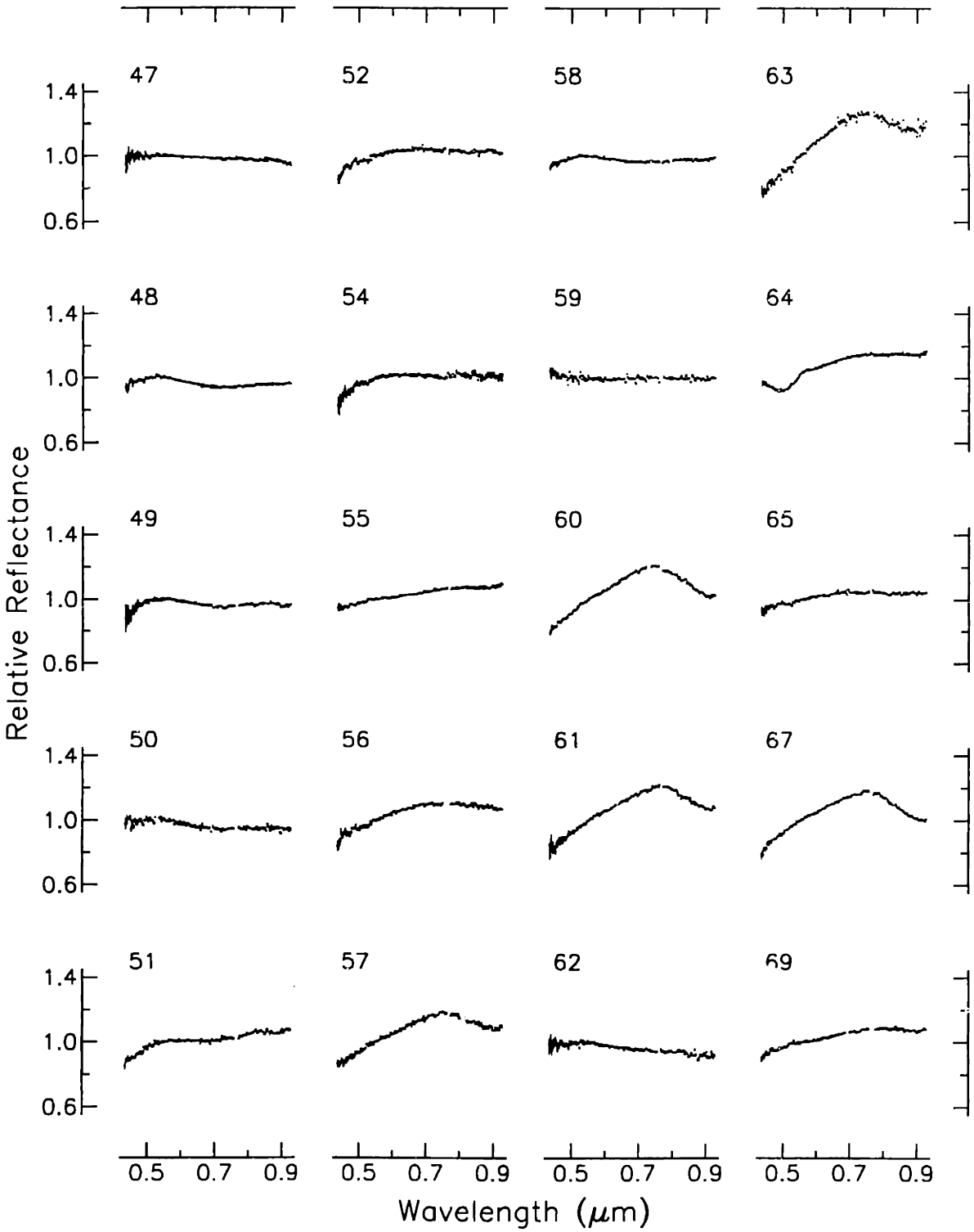
47
52
58
63
48
54
59
64
49
55
60
65
50
56
61
67
51
57
62
69
1.4
1.0
0.6
0.5
0.7
0.9
Relative Reflectance
Wavelength (μm)

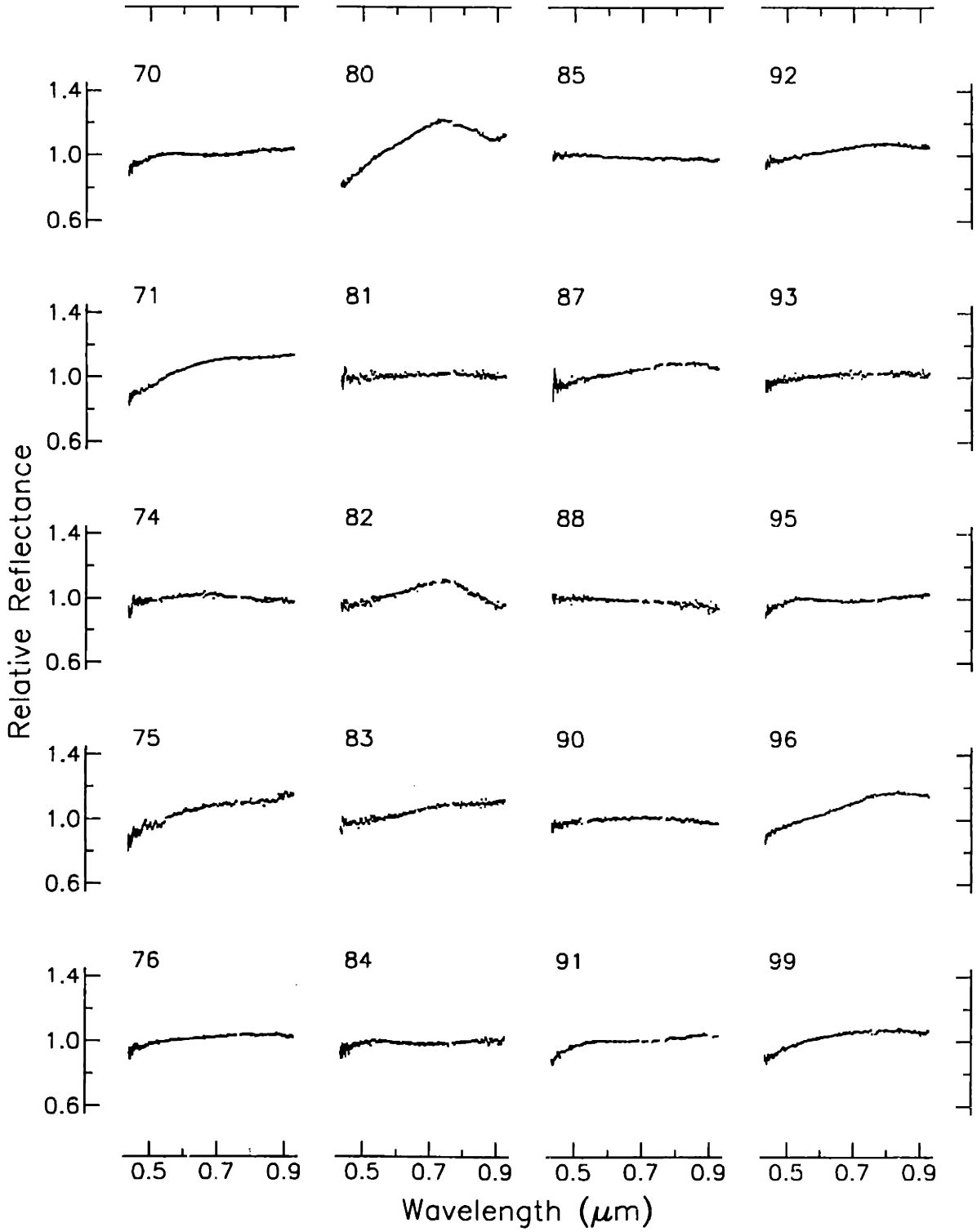
70
80
85
92
71
81
87
93
74
82
88
95
75
83
90
96
76
84
91
99
1.4
1.0
0.6
0.5
0.7
0.9
Relative Reflectance
Wavelength (μm)

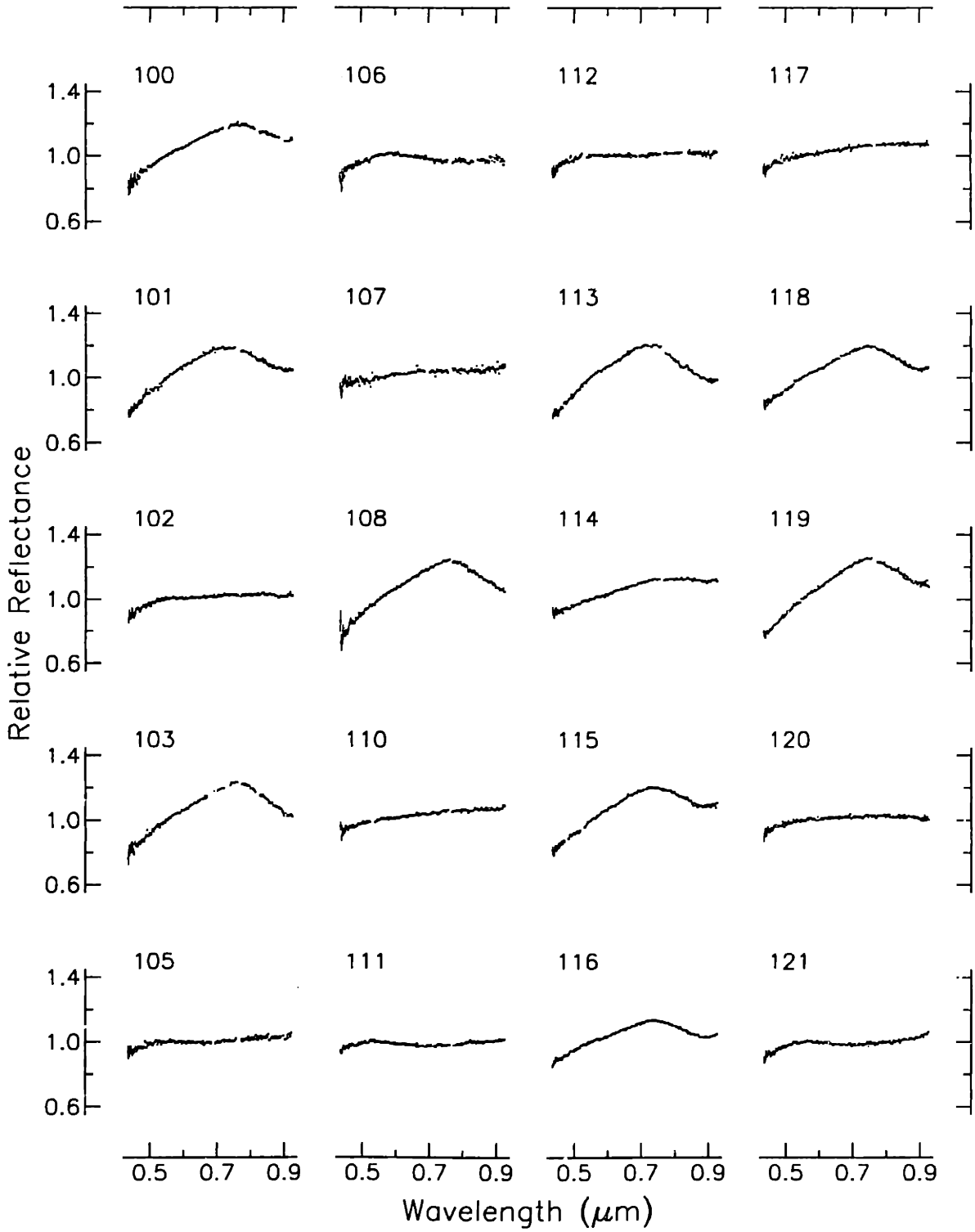
100
106
112
117
101
107
113
118
102
108
114
119
103
110
115
120
105
111
116
121
1.4
1.0
0.6
0.5
0.7
0.9
Relative Reflectance
Wavelength (μm)

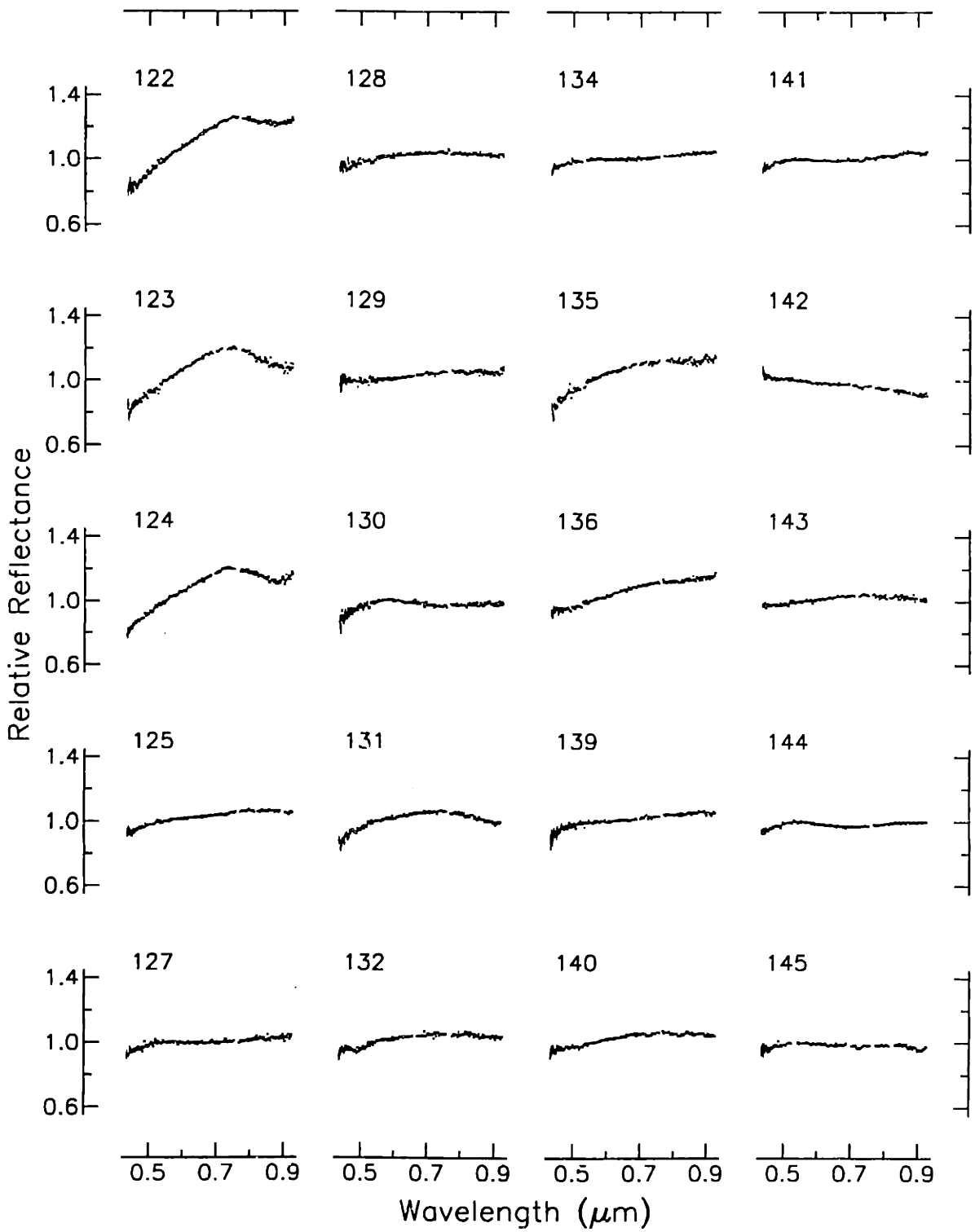
122
128
134
141
123
129
135
142
124
130
136
143
125
131
139
144
127
132
140
145
1.4
1.0
0.6
Relative Reflectance
0.5
0.7
0.9
Wavelength (μm)

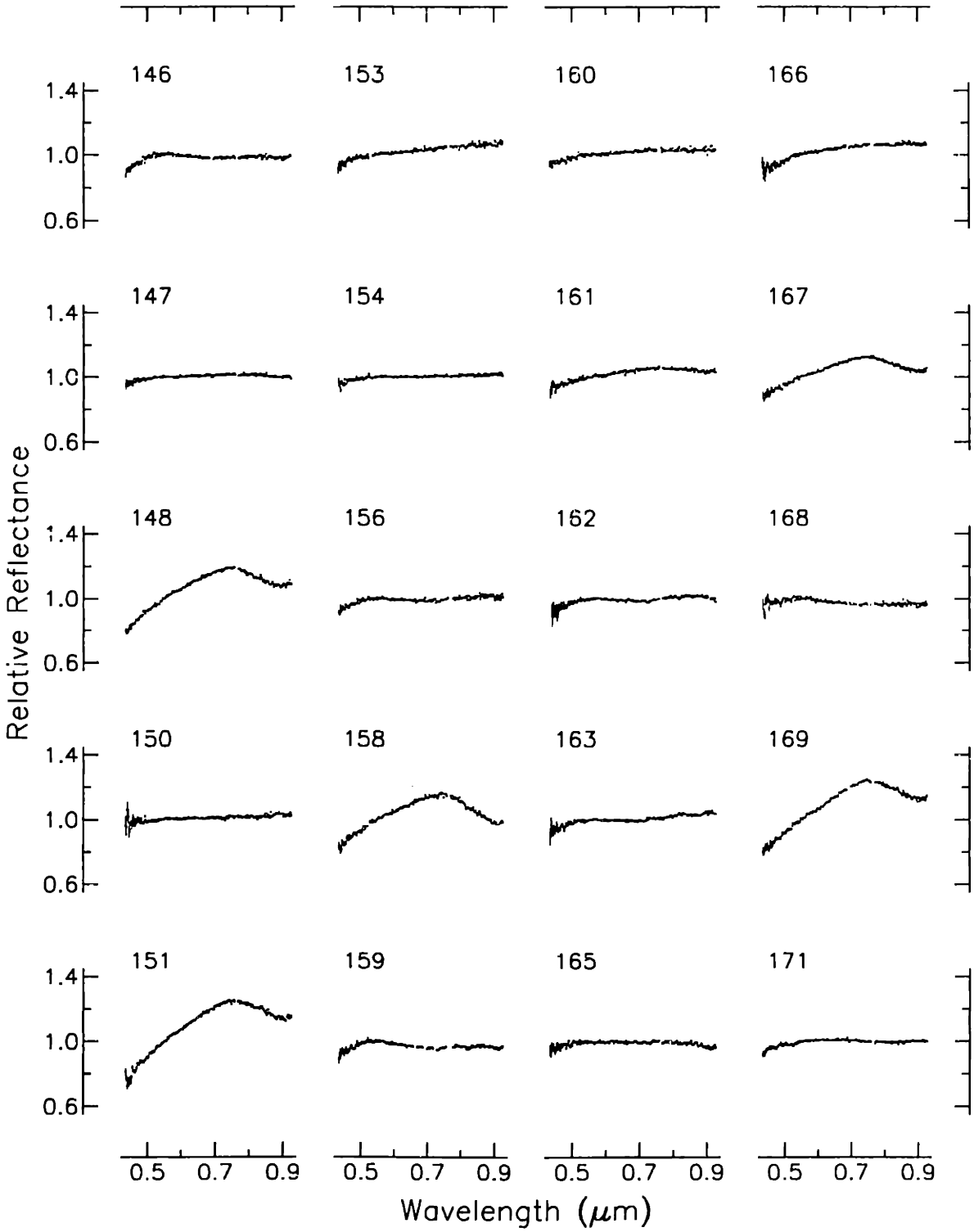
146
153
160
166
147
154
161
167
148
156
162
168
150
158
163
169
151
159
165
171
1.4
1.0
0.6
0.5
0.7
0.9
Relative Reflectance
Wavelength (μm)

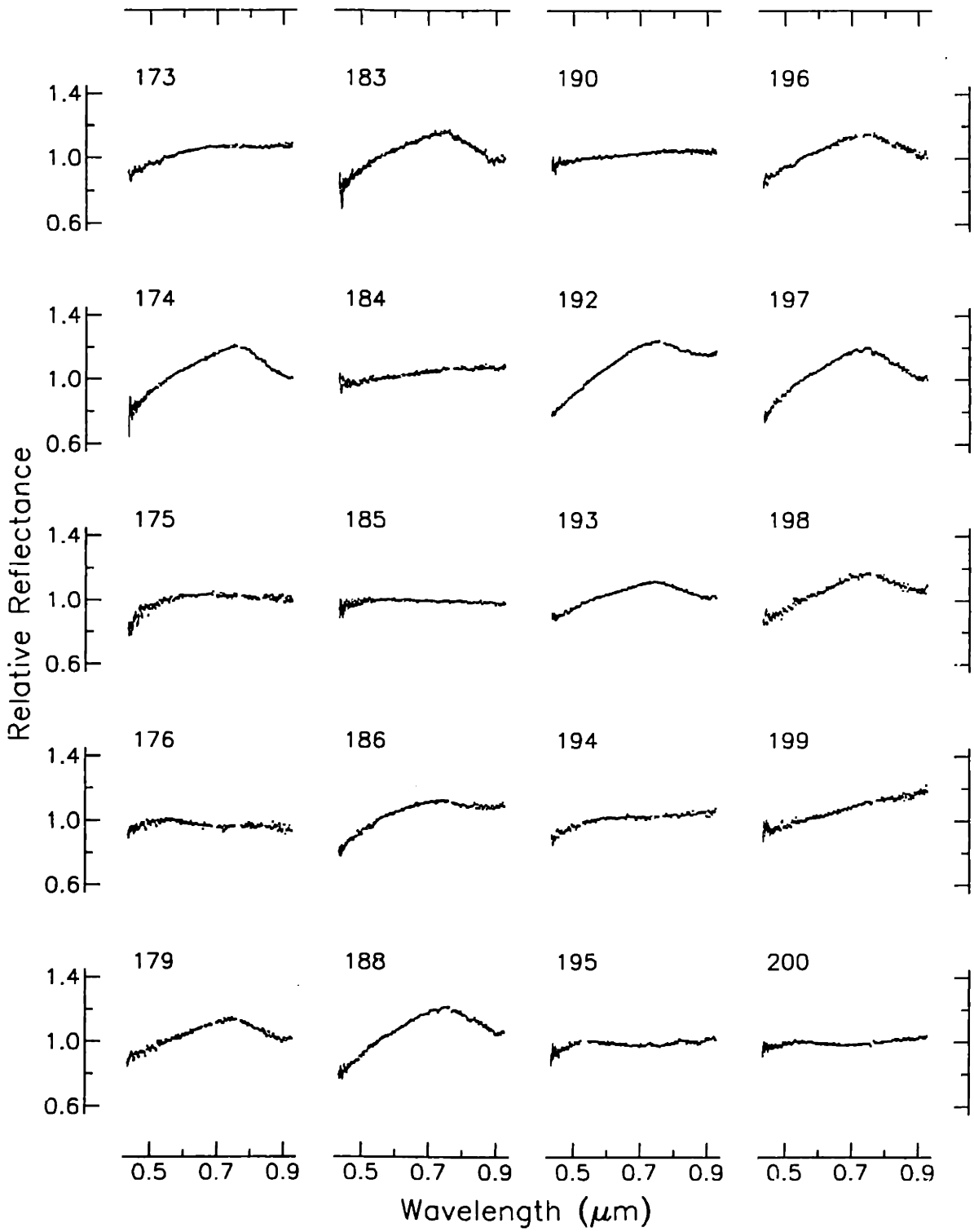
173
183
190
196
174
184
192
197
175
185
193
198
176
186
194
199
179
188
195
200
1.4
1.0
0.6
0.5
0.7
0.9
Relative Reflectance
Wavelength (μm)

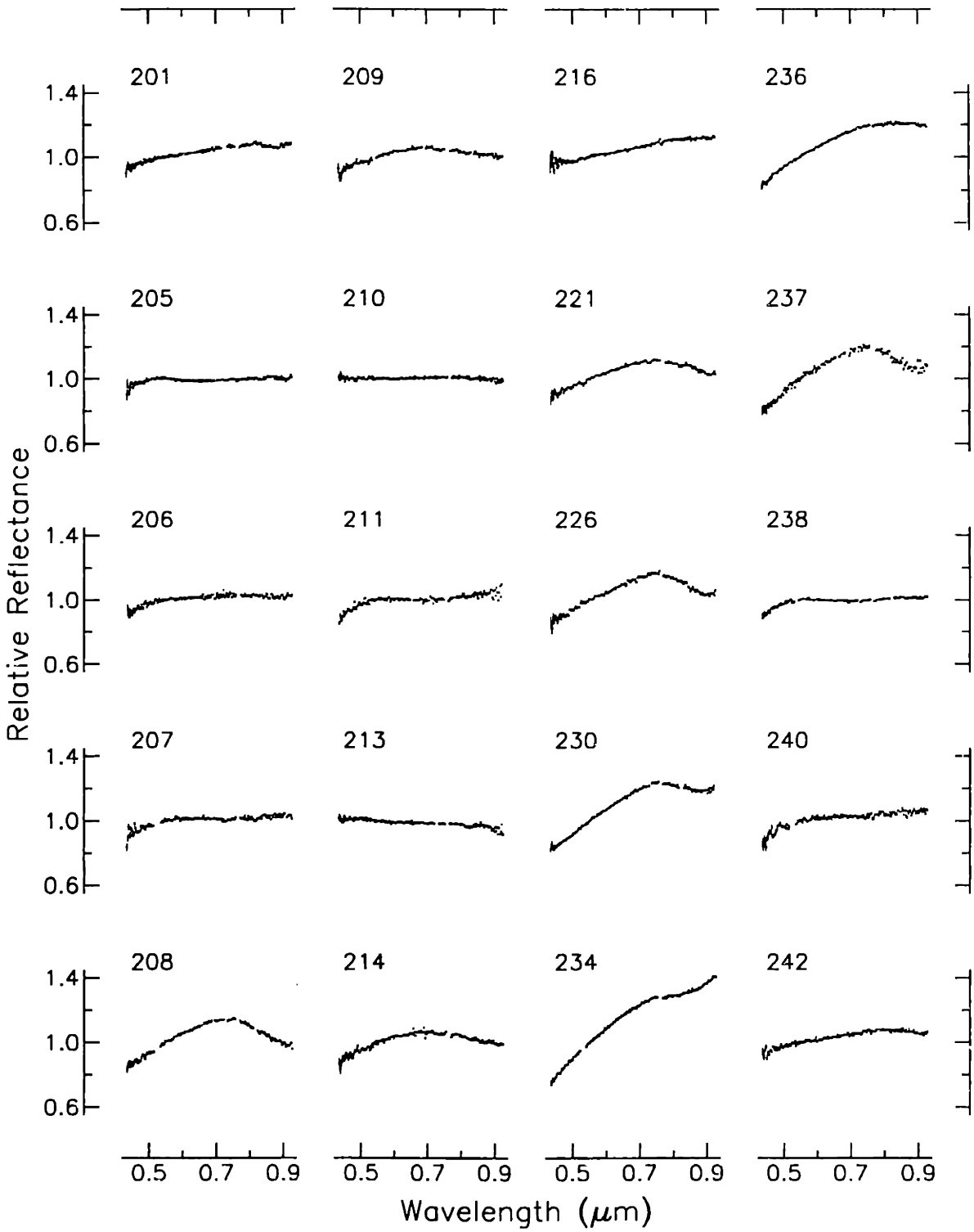
201
209
216
236
205
210
221
237
206
211
226
238
207
213
230
240
208
214
234
242
1.4
1.0
0.6
0.5
0.7
0.9
Relative Reflectance
Wavelength (μm)

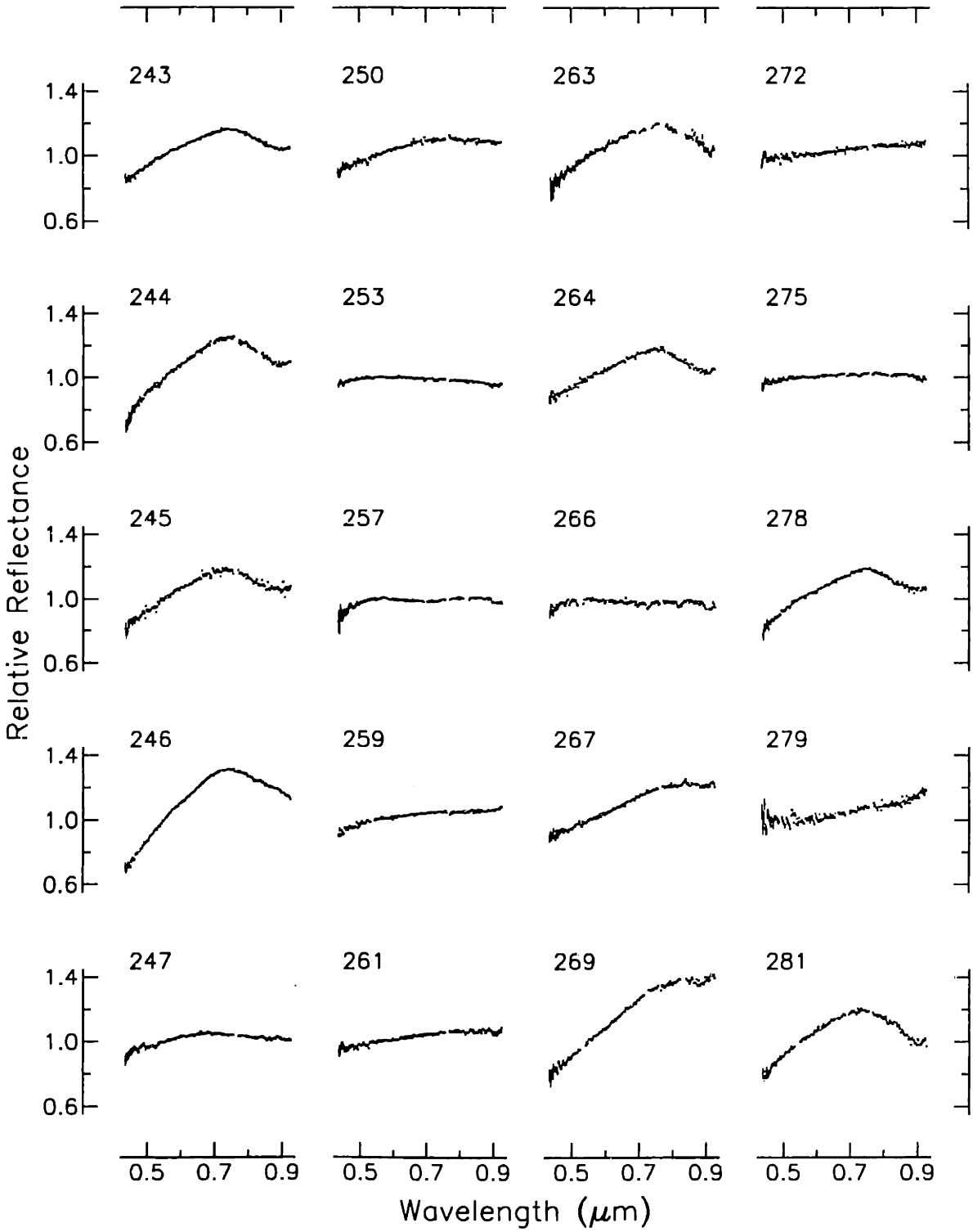
243
250
263
272
244
253
264
275
245
257
266
278
246
259
267
279
247
261
269
281
1.4
1.0
0.6
0.5
0.7
0.9
Relative Reflectance
Wavelength (μm)

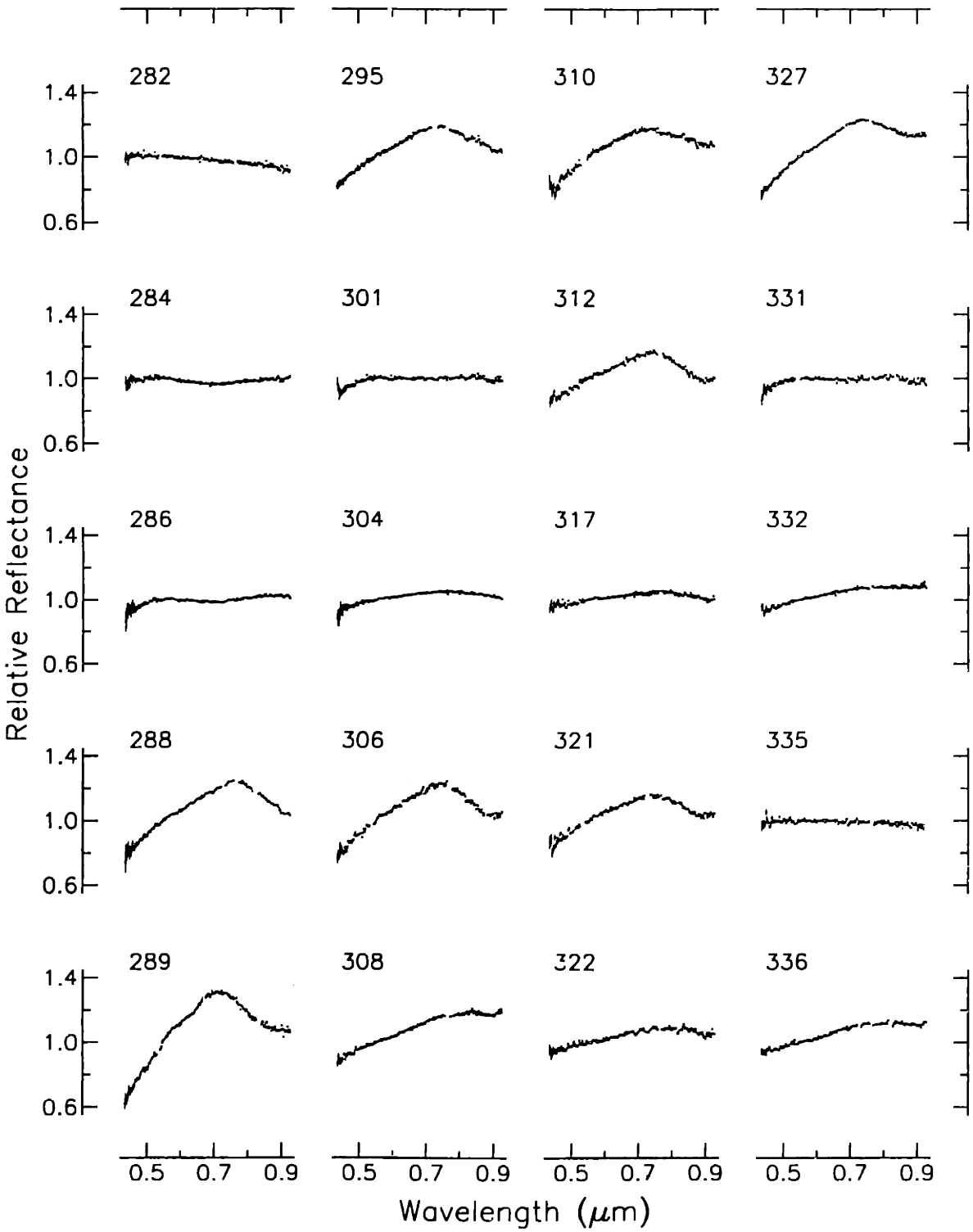
282
295
310
327
284
301
312
331
286
304
317
332
288
306
321
335
289
308
322
336
1.4
1.0
0.6
0.5
0.7
0.9
Relative Reflectance
Wavelength (μm)

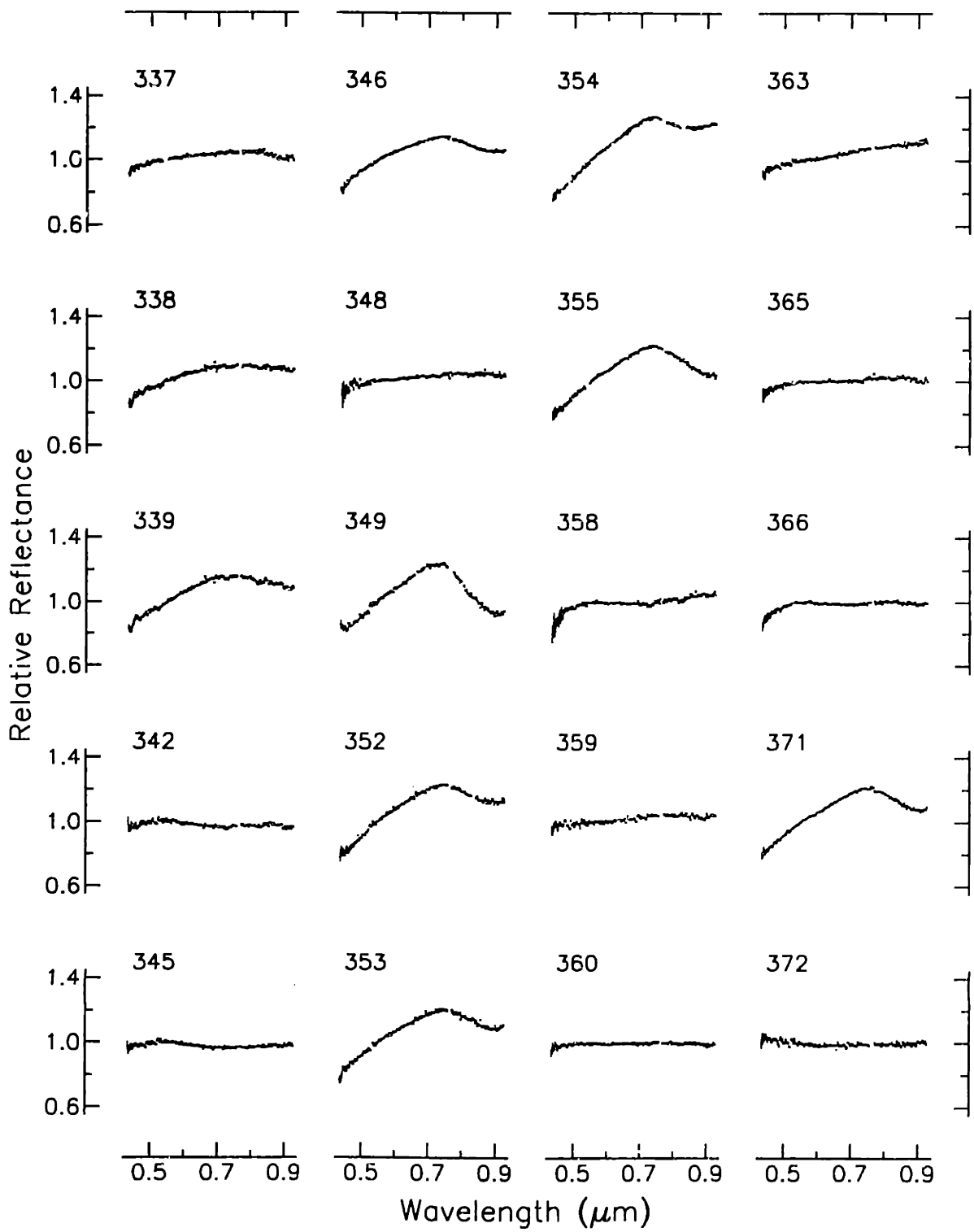
337
346
354
363
338
348
355
365
339
349
358
366
342
352
359
371
345
353
360
372
1.4
1.0
0.6
0.5
0.7
0.9
Relative Reflectance
Wavelength (μm)

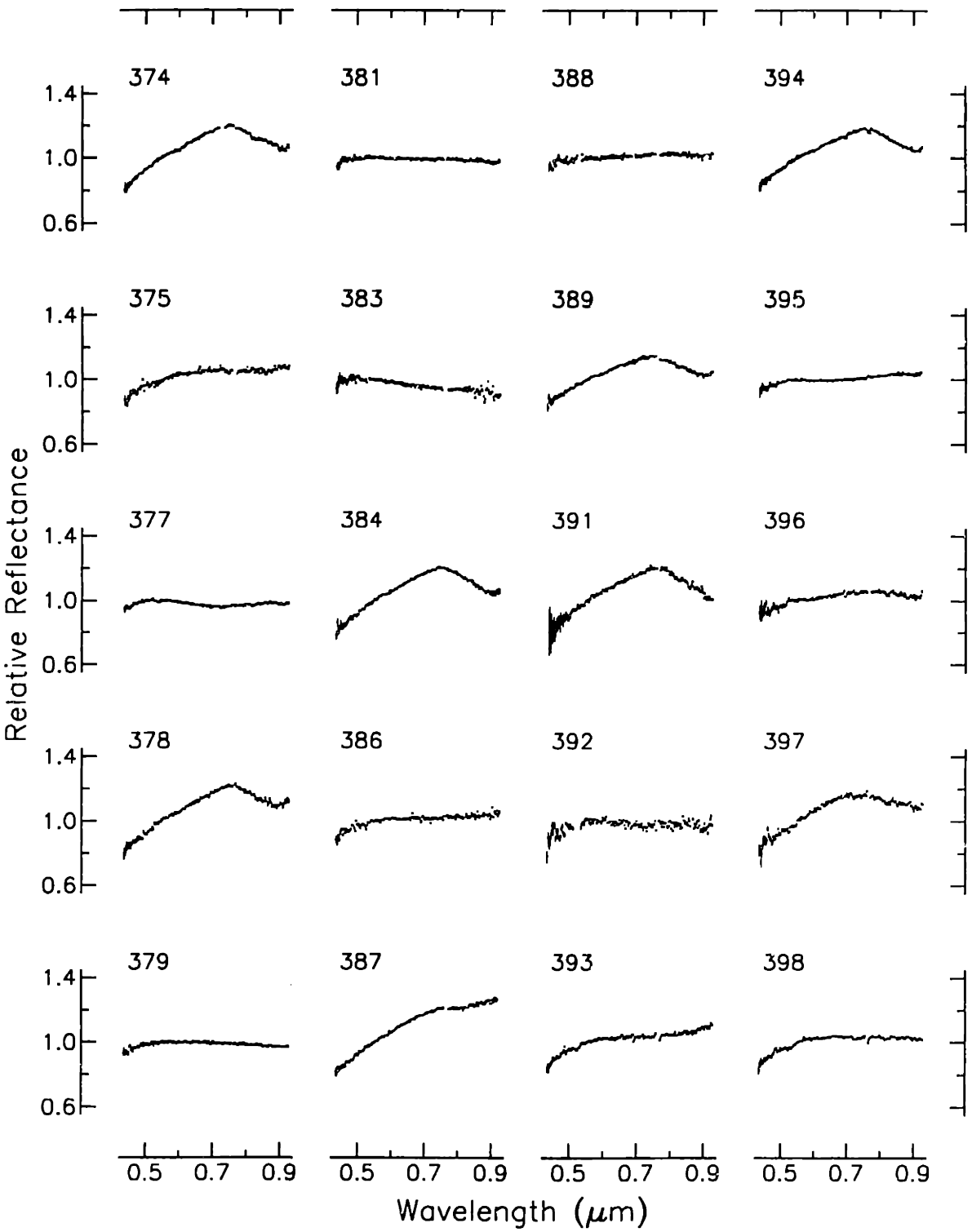
374
381
388
394
375
383
389
395
377
384
391
396
378
386
392
397
379
387
393
398
1.4
1.0
0.6
0.5
0.7
0.9
Relative Reflectance
Wavelength (μm)

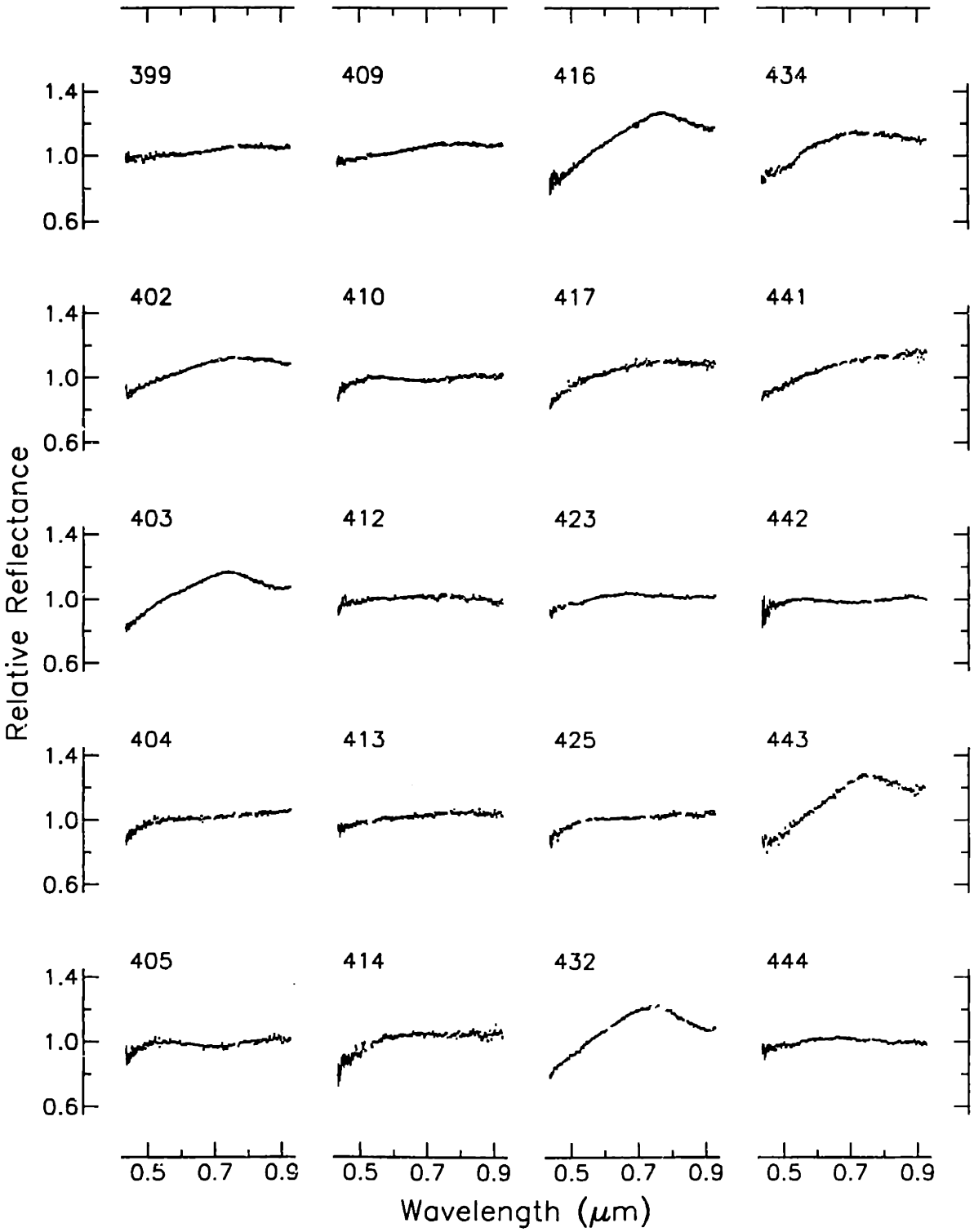
399
409
416
434
402
410
417
441
403
412
423
442
404
413
425
443
405
414
432
444
1.4
1.0
0.6
Relative Reflectance
0.5
0.7
0.9
Wavelength (μm)

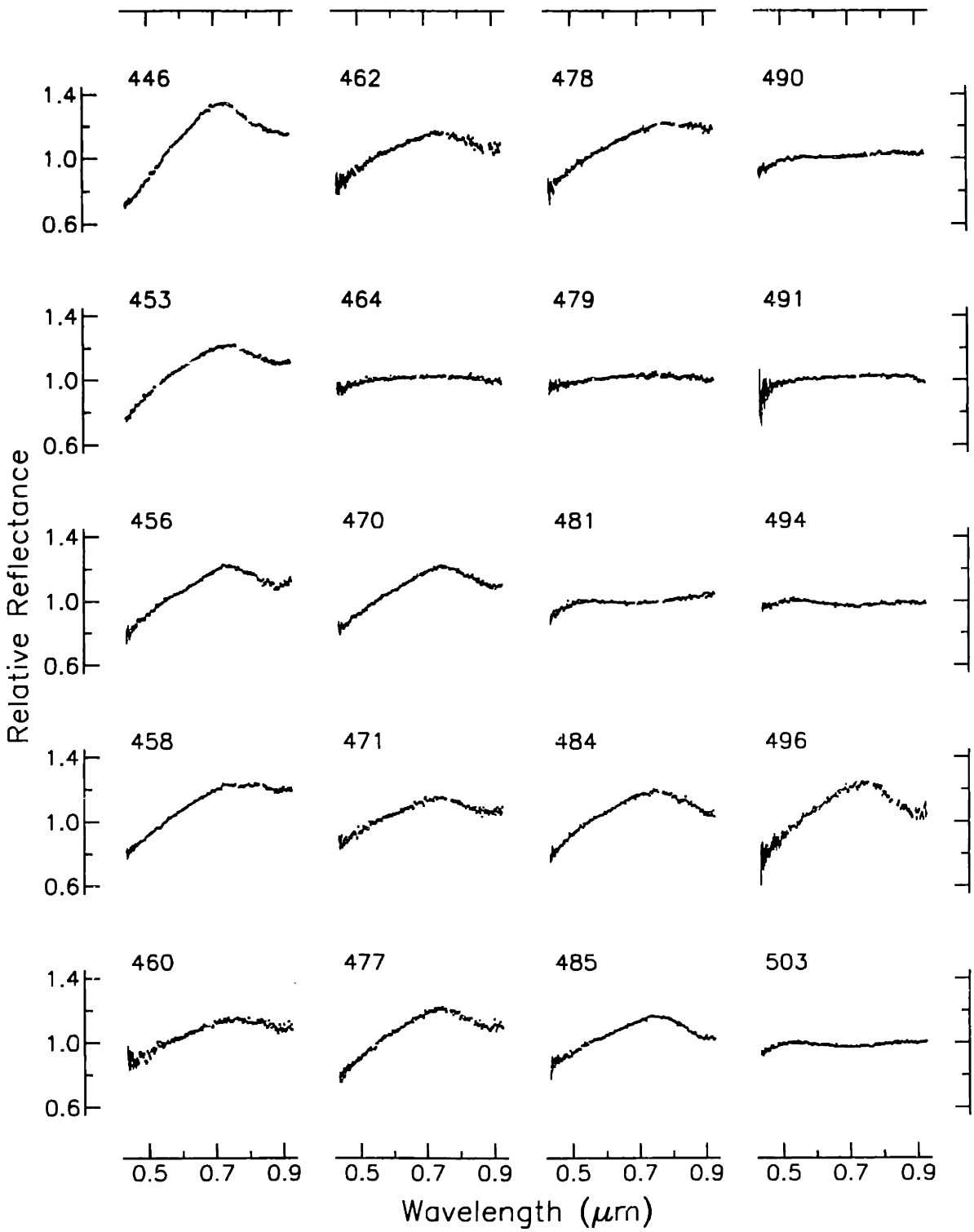
446
462
478
490
453
464
479
491
456
470
481
494
458
471
484
496
460
477
485
503
1.4
1.0
0.6
0.5
0.7
0.9
Relative Reflectance
Wavelength (μm)

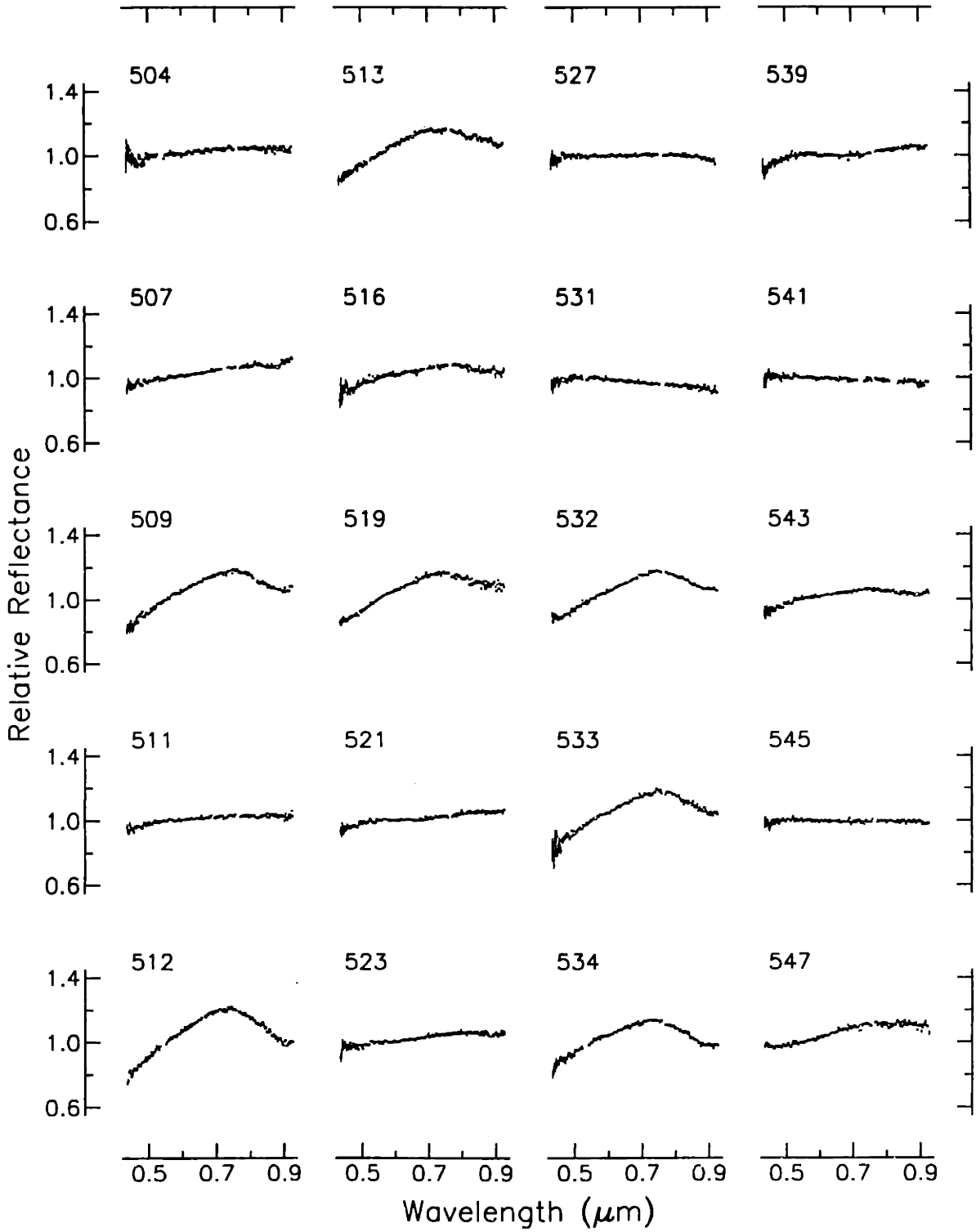
504
513
527
539
507
516
531
541
509
519
532
543
511
521
533
545
512
523
534
547
1.4
1.0
0.6
0.5
0.7
0.9
Relative Reflectance
Wavelength (μm)

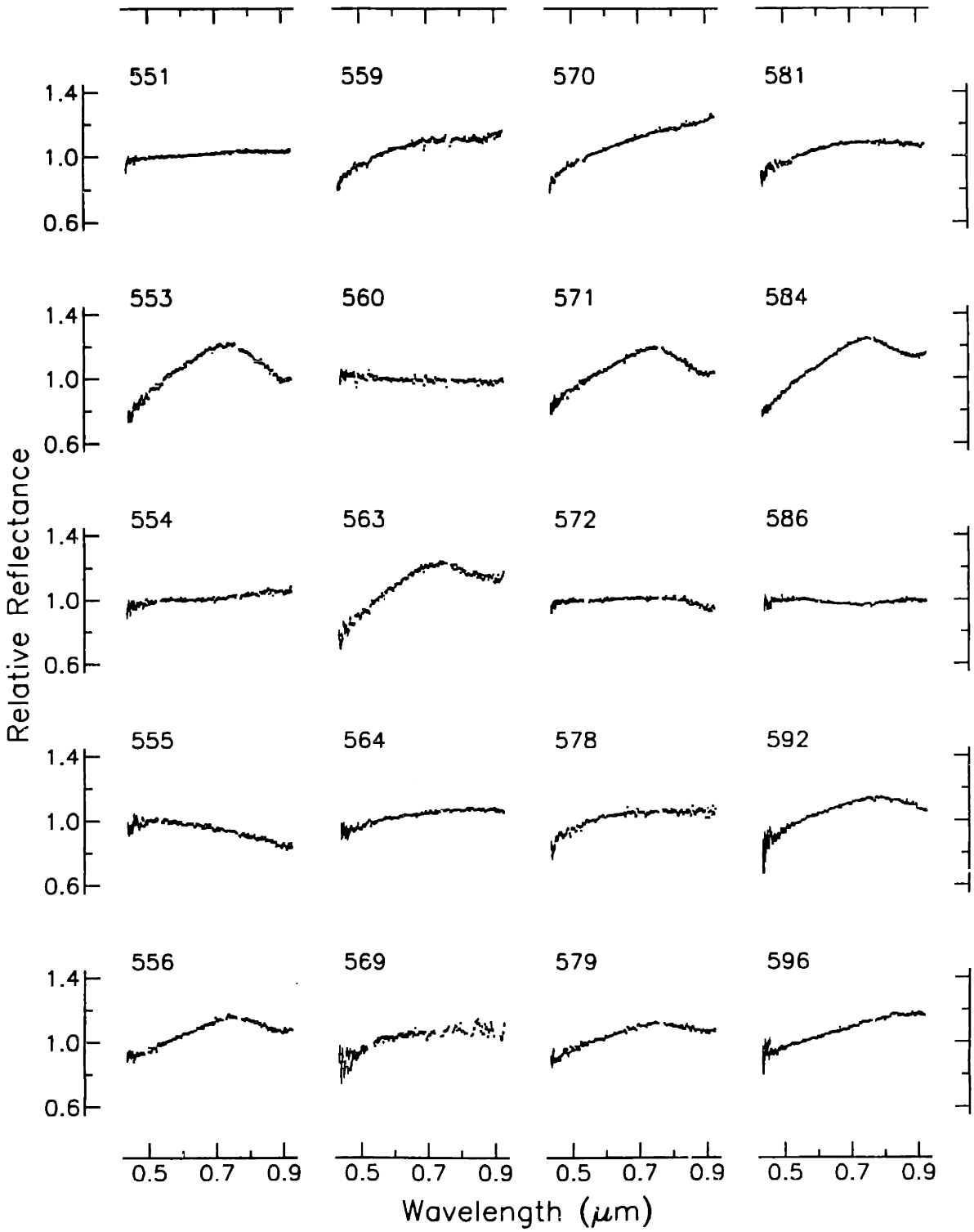
551
559
570
581
553
560
571
584
554
563
572
586
555
564
578
592
556
569
579
596
1.4
1.0
0.6
0.5
0.7
0.9
Relative Reflectance
Wavelength (μm)

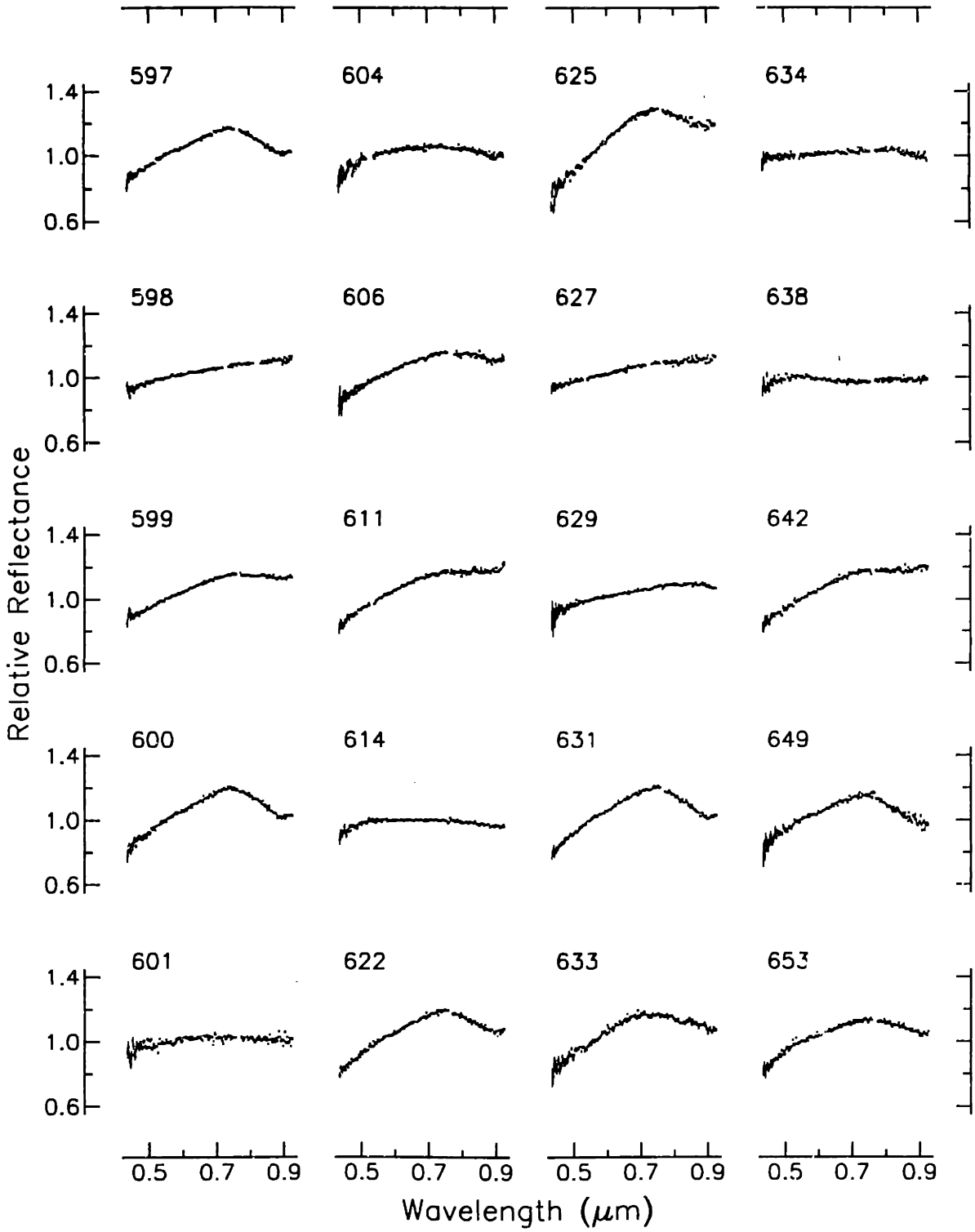
597
604
625
634
598
606
627
638
599
611
629
642
600
614
631
649
601
622
633
653
1.4
1.0
0.6
0.5
0.7
0.9
Relative Reflectance
Wavelength (μm)

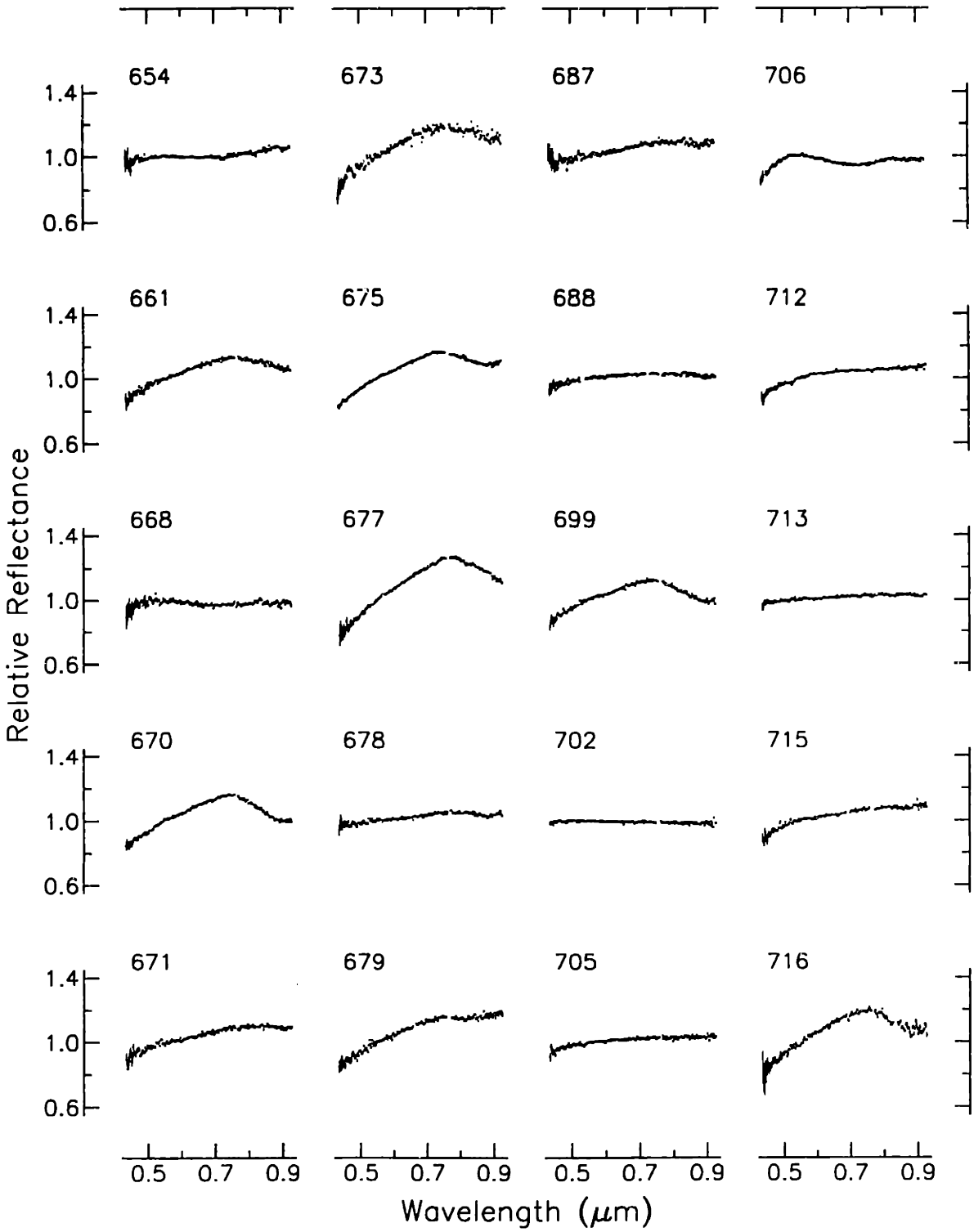
654
673
687
706
661
675
688
712
668
677
699
713
670
678
702
715
671
679
705
716
1.4
1.0
0.6
0.5
0.7
0.9
Relative Reflectance
Wavelength (μm)

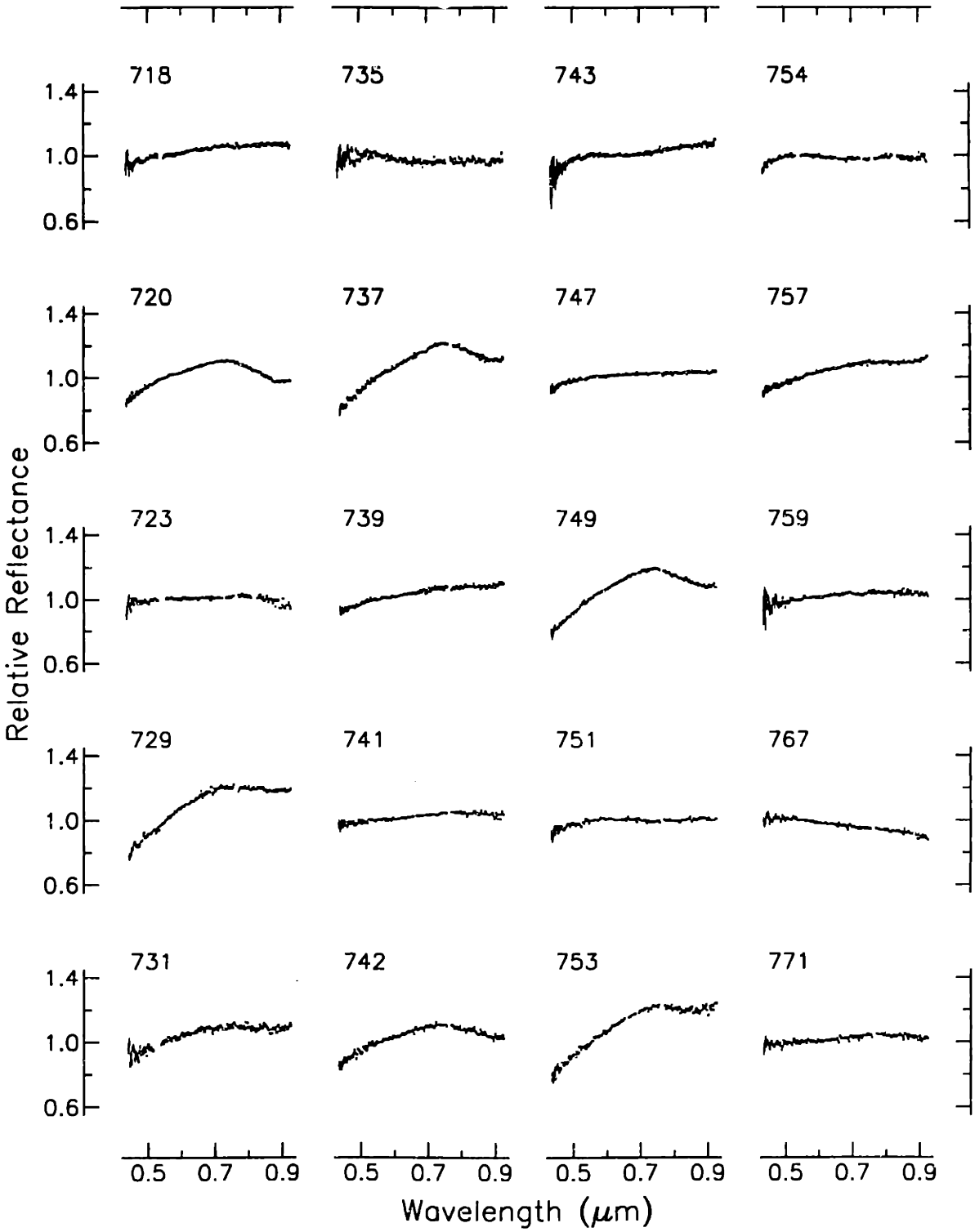
718
735
743
754
720
737
747
757
723
739
749
759
729
741
751
767
731
742
753
771
1.4
1.0
0.6
0.5
0.7
0.9
Relative Reflectance
Wavelength (μm)

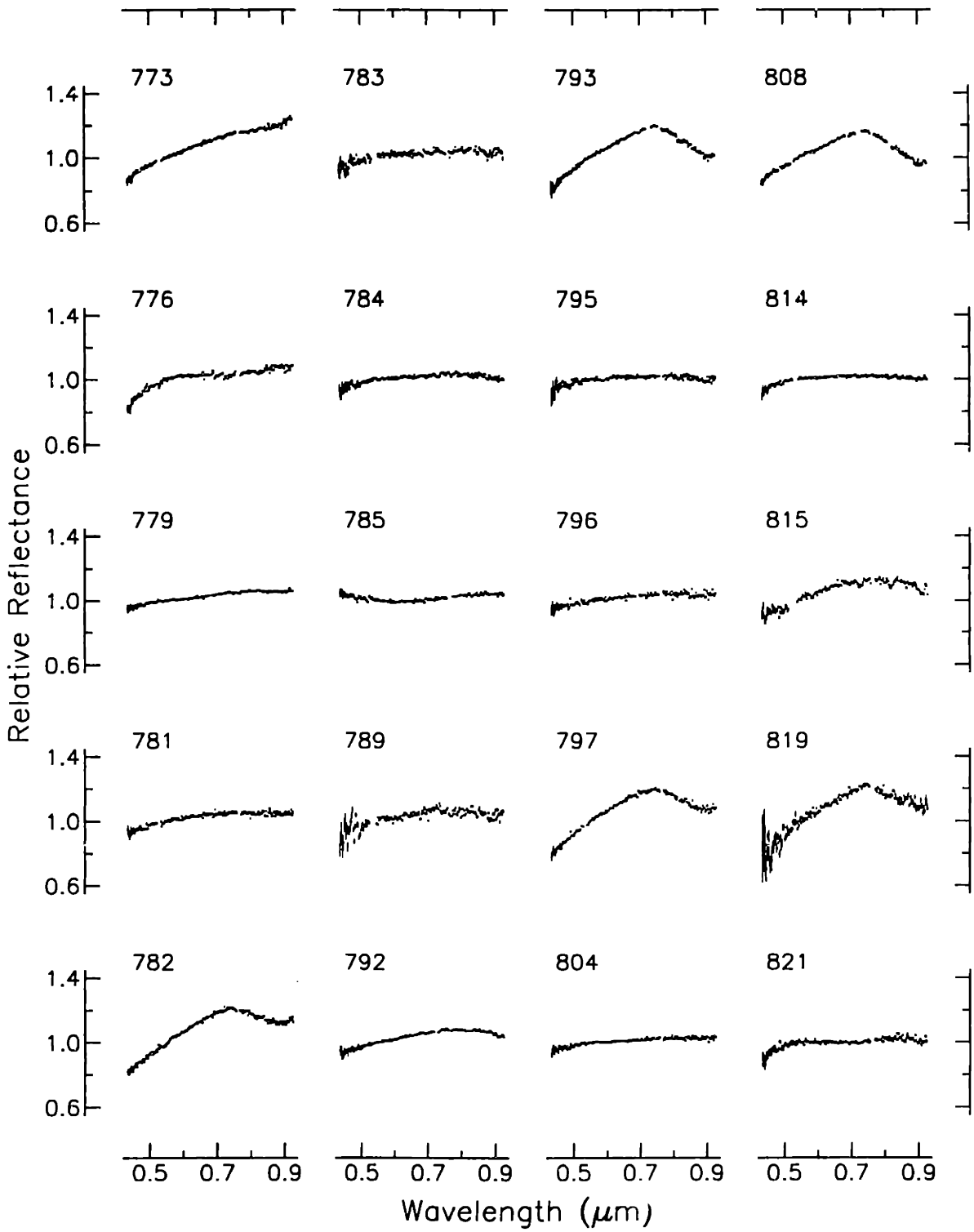
773
783
793
808
776
784
795
814
779
785
796
815
781
789
797
819
782
792
804
821
1.4
1.0
0.6
0.5
0.7
0.9
Relative Reflectance
Wavelength (μm)

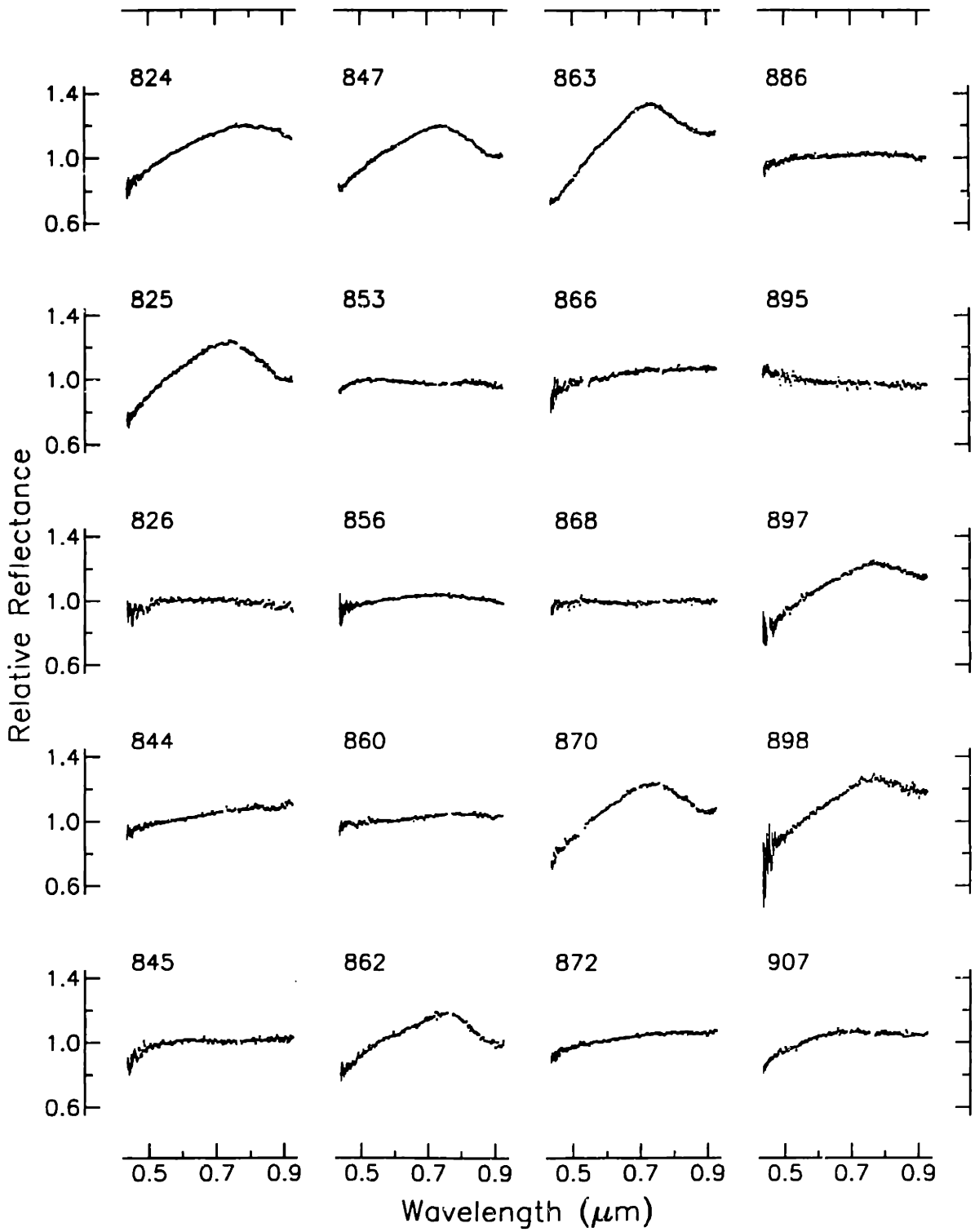
824
847
863
886
825
853
866
895
826
856
868
897
844
860
870
898
845
862
872
907
1.4
1.0
0.6
0.5
0.7
0.9
Relative Reflectance
Wavelength (μm)

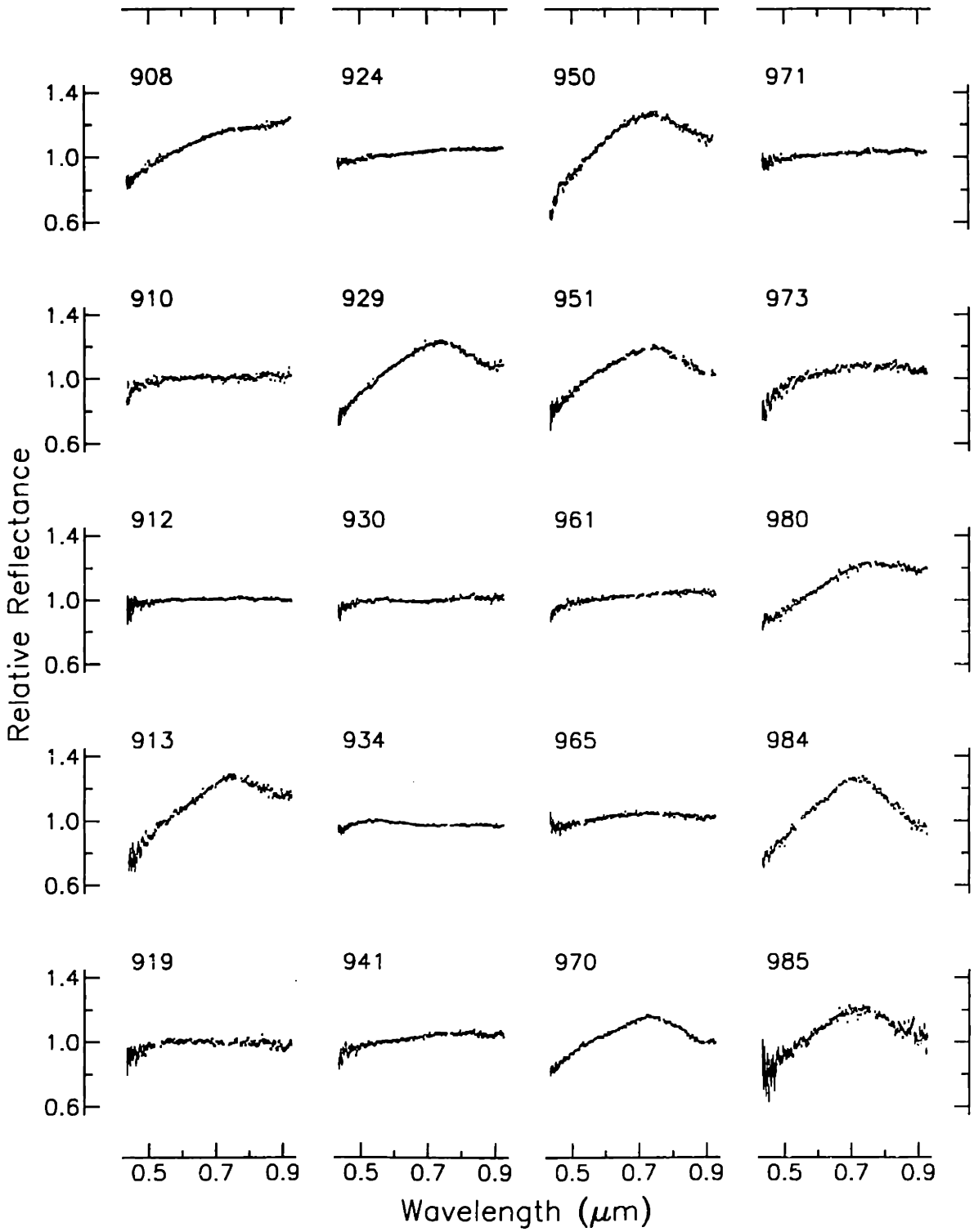
908
924
950
971
910
929
951
973
912
930
961
980
913
934
965
984
919
941
970
985
1.4
1.0
0.6
Relative Reflectance
0.5
0.7
0.9
Wavelength (μm)

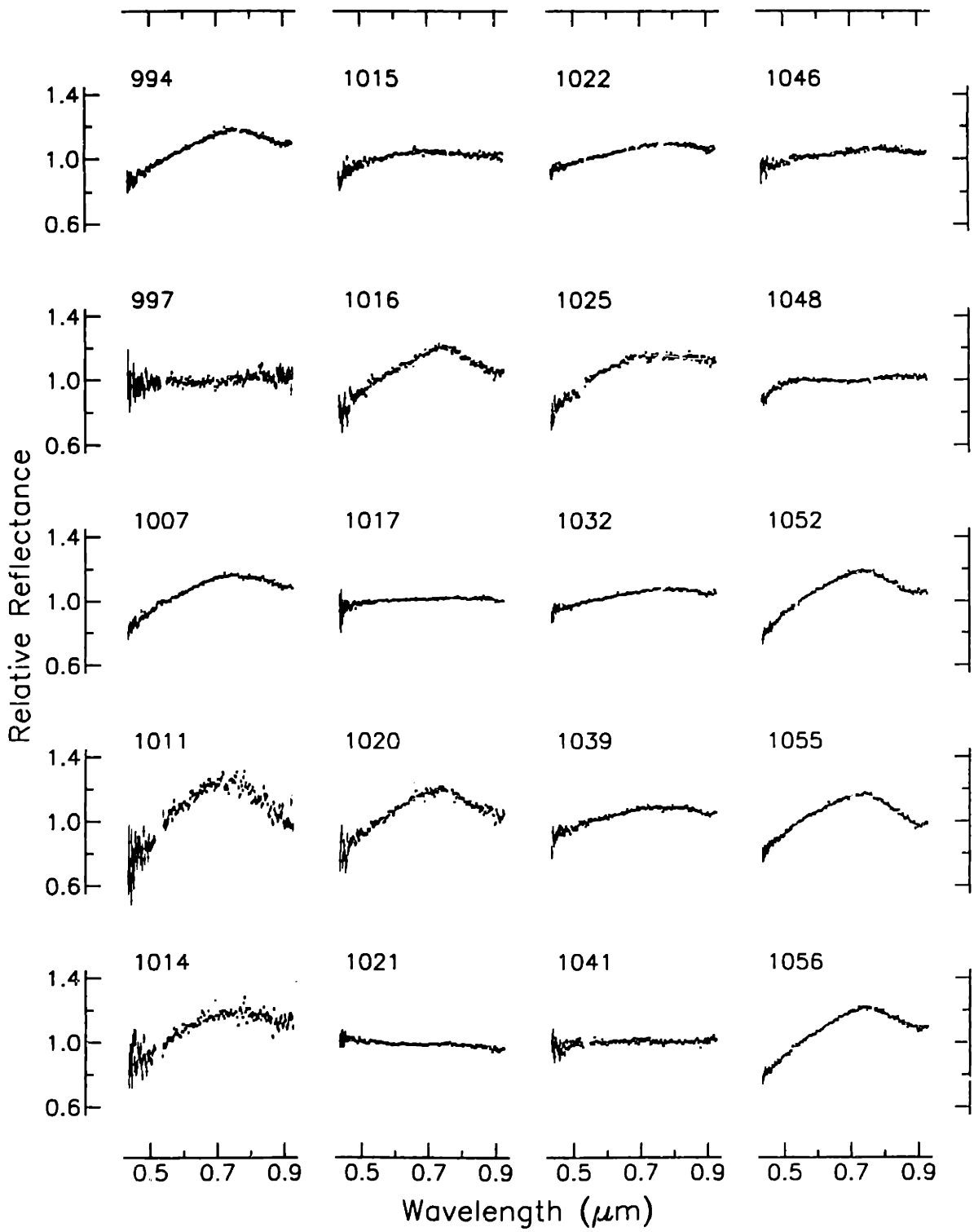
994
1015
1022
1046
997
1016
1025
1048
1007
1017
1032
1052
1011
1020
1039
1055
1014
1021
1041
1056
1.4
1.0
0.6
0.5
0.7
0.9
Relative Reflectance
Wavelength (μm)

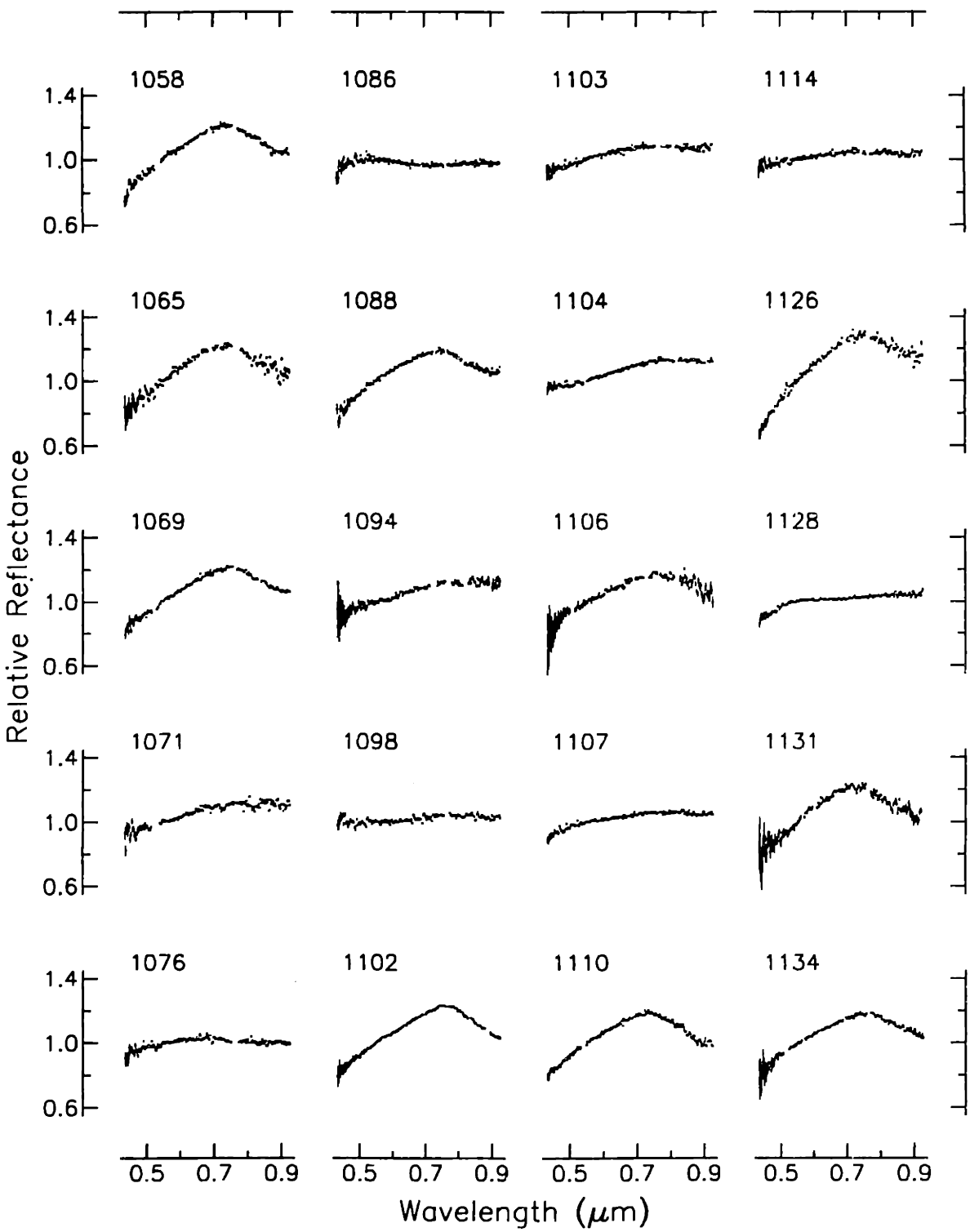
1058
1086
1103
1114
1065
1088
1104
1126
1069
1094
1106
1128
1071
1098
1107
1131
1076
1102
1110
1134
1.4
1.0
0.6
0.5
0.7
0.9
Relative Reflectance
Wavelength (μm)

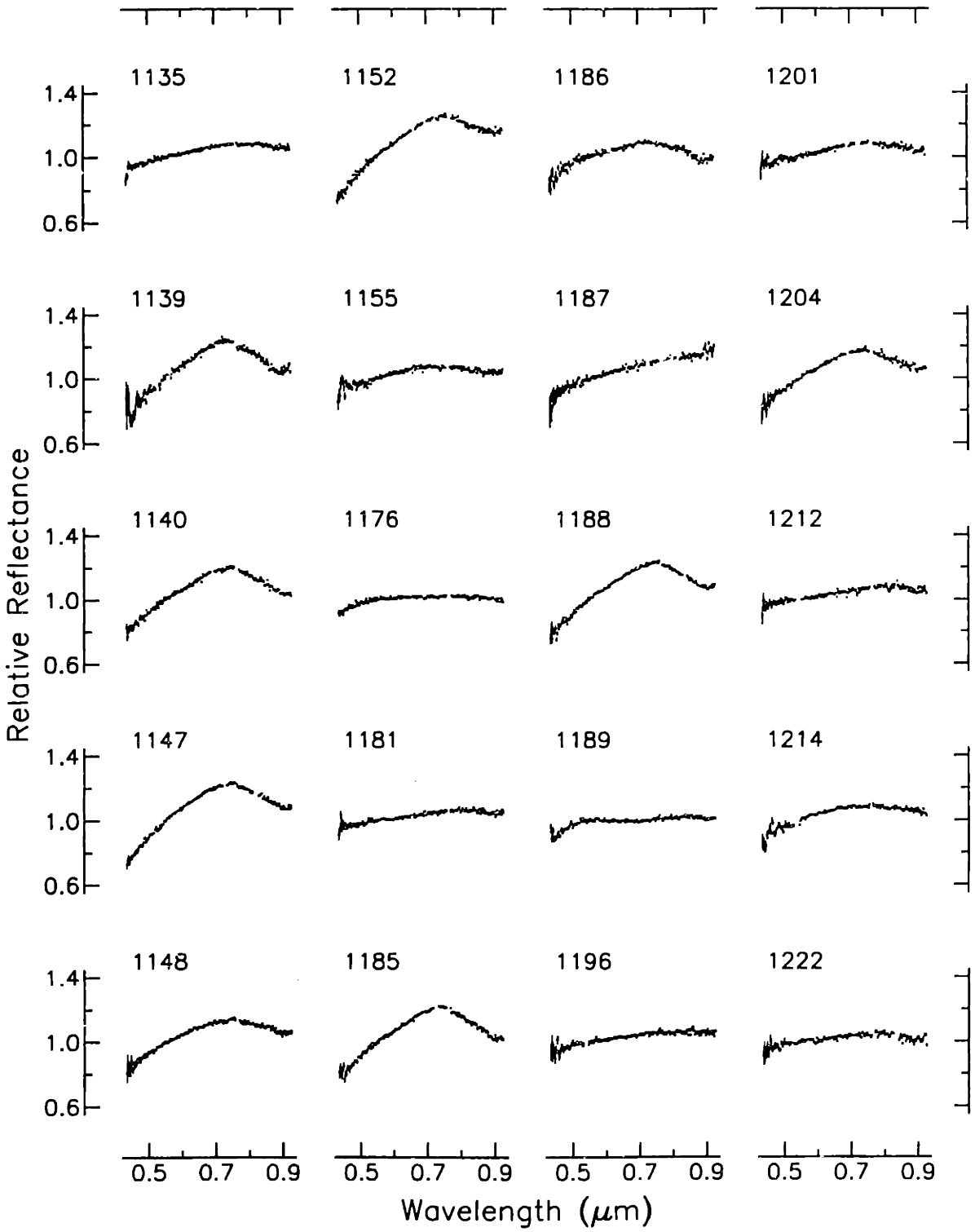
1135
1152
1186
1201
1139
1155
1187
1204
1140
1176
1188
1212
1147
1181
1189
1214
1148
1185
1196
1222
1.4
1.0
0.6
Relative Reflectance
0.5
0.7
0.9
Wavelength (μm)

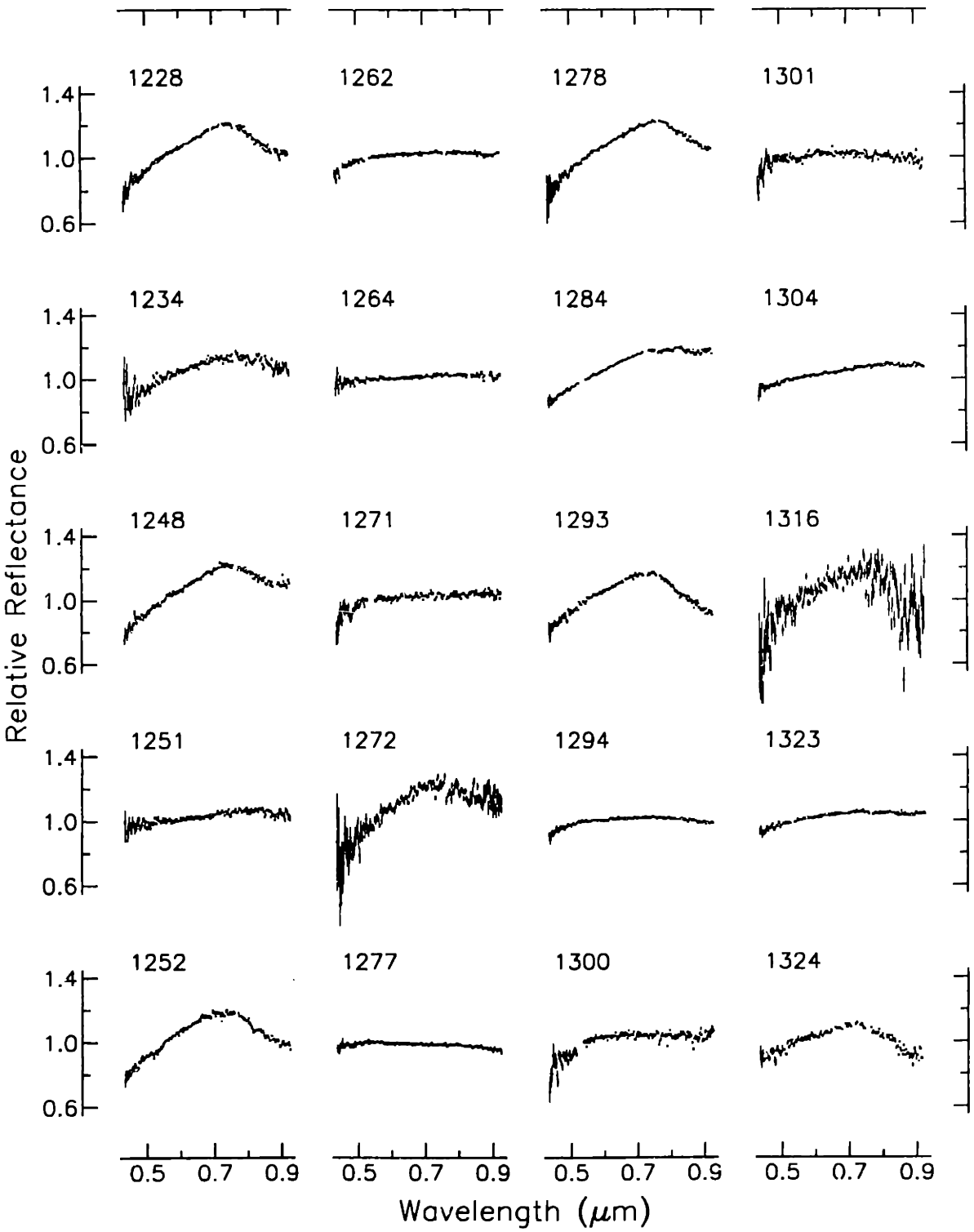
1228
1262
1278
1301
1234
1264
1284
1304
1248
1271
1293
1316
1251
1272
1294
1323
1252
1277
1300
1324
1.4
1.0
0.6
0.5
0.7
0.9
Relative Reflectance
Wavelength (μm)

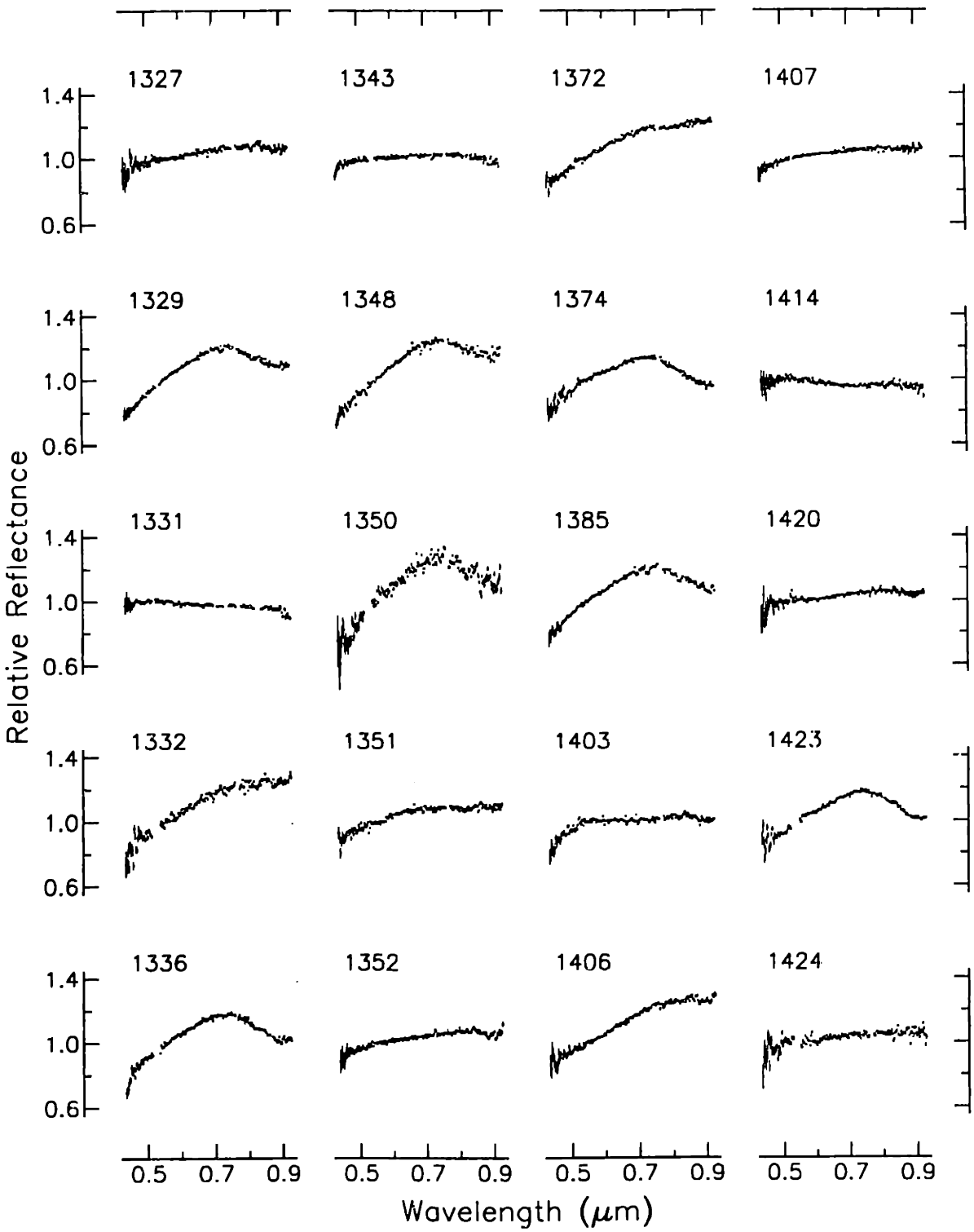
1327
1343
1372
1407
1329
1348
1374
1414
1331
1350
1385
1420
1332
1351
1403
1423
1336
1352
1406
1424
1.4
1.0
0.6
0.5
0.7
0.9
Relative Reflectance
Wavelength (μm)

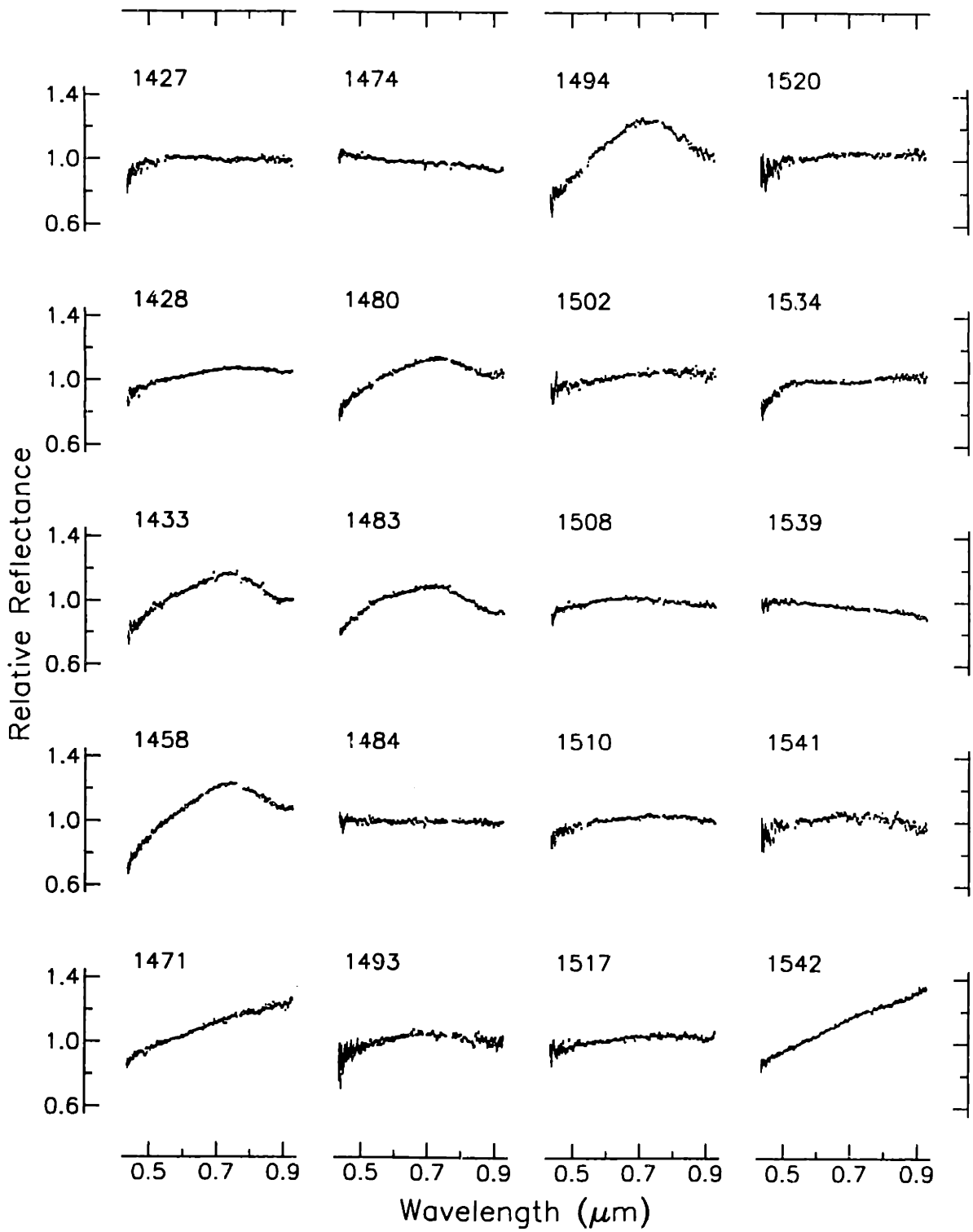
1427
1474
1494
1520
1428
1480
1502
1534
1433
1483
1508
1539
1458
1484
1510
1541
1471
1493
1517
1542
1.4
1.0
0.6
0.5
0.7
0.9
Relative Reflectance
Wavelength (μm)

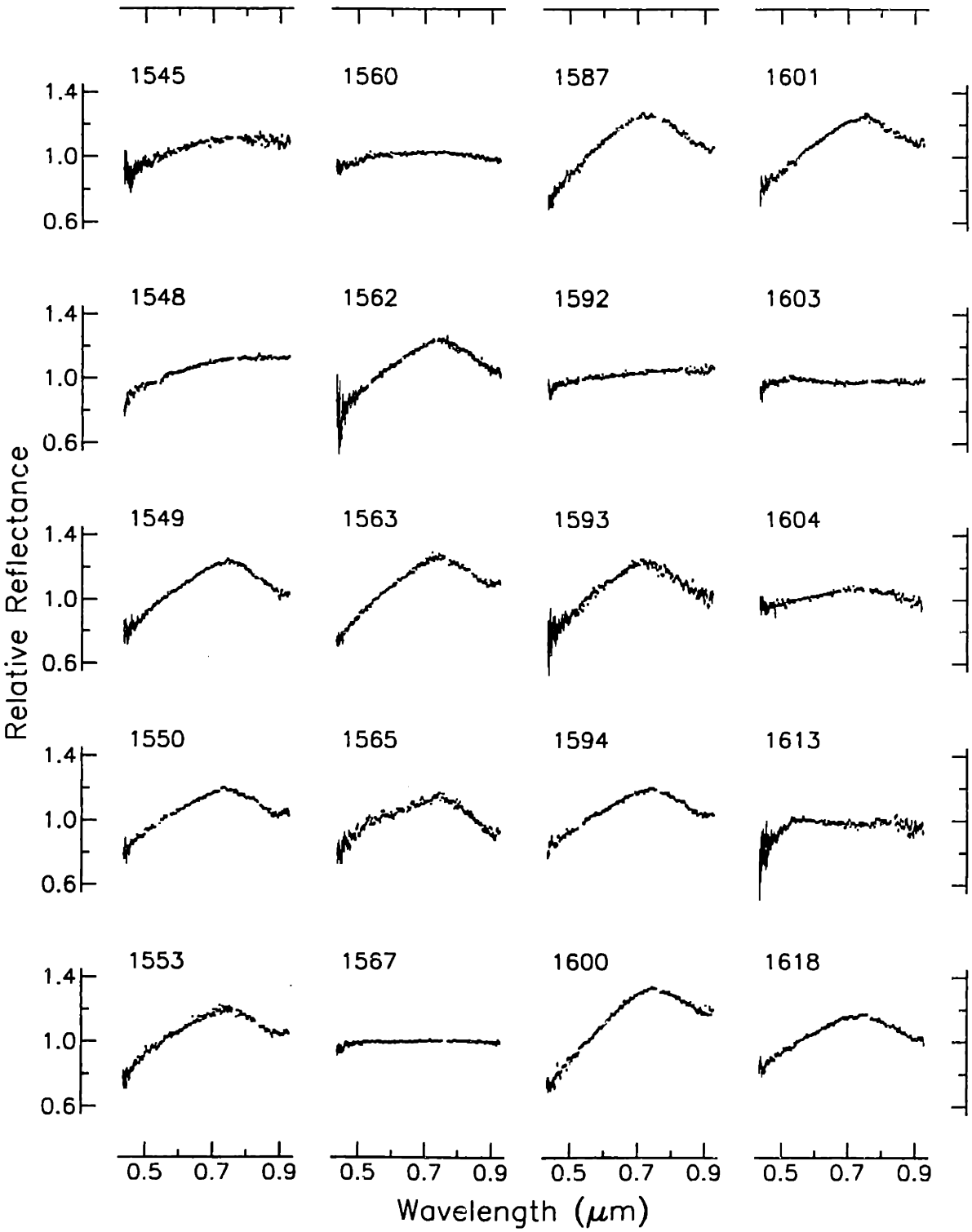
1545
1560
1587
1601
1548
1562
1592
1603
1549
1563
1593
1604
1550
1565
1594
1613
1553
1567
1600
1618
1.4
1.0
0.6
0.5
0.7
0.9
Relative Reflectance
Wavelength (μm)

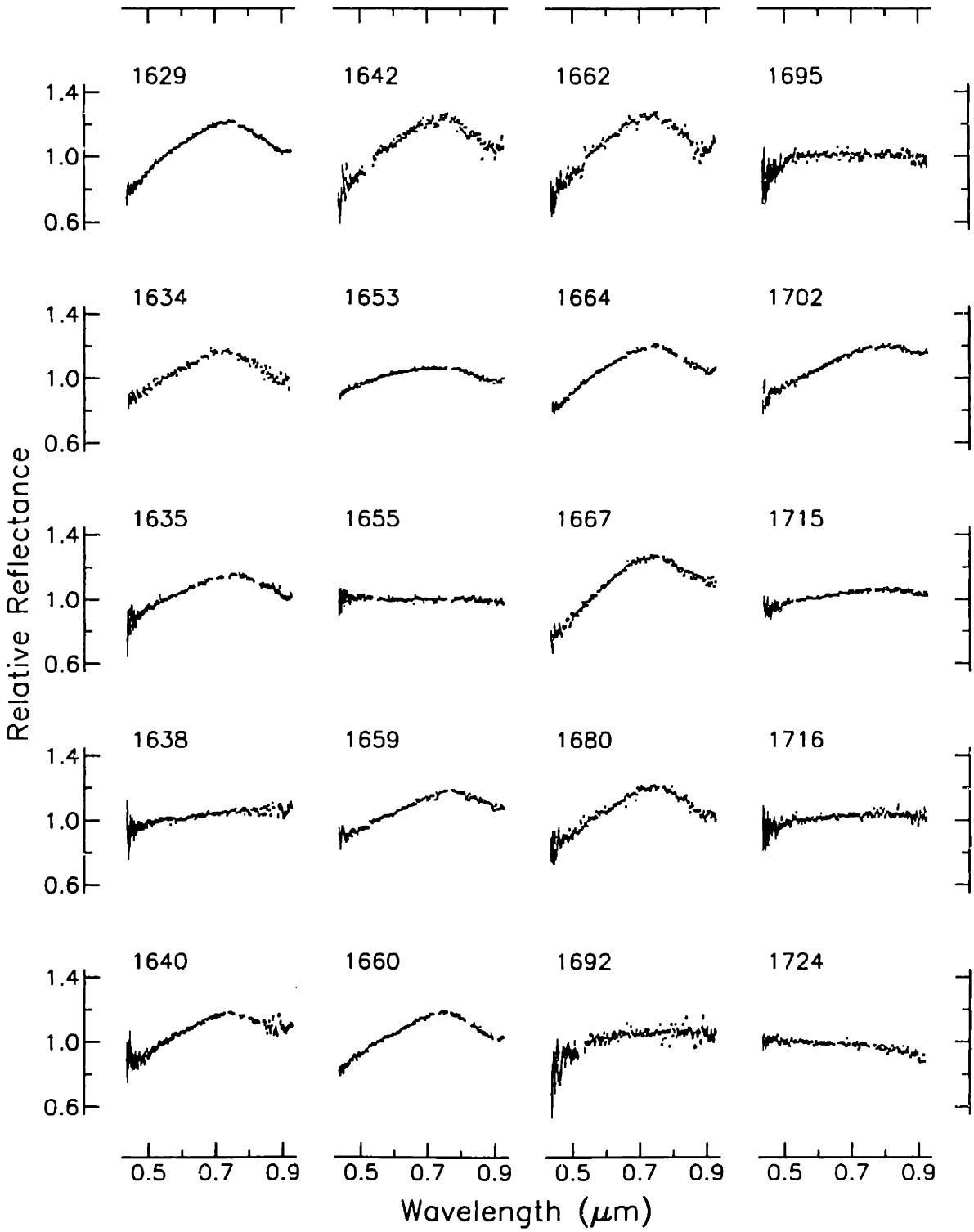
1629
1642
1662
1695
1634
1653
1664
1702
1635
1655
1667
1715
1638
1659
1680
1716
1640
1660
1692
1724
1.4
1.0
0.6
0.5
0.7
0.9
Relative Reflectance
Wavelength (μm)

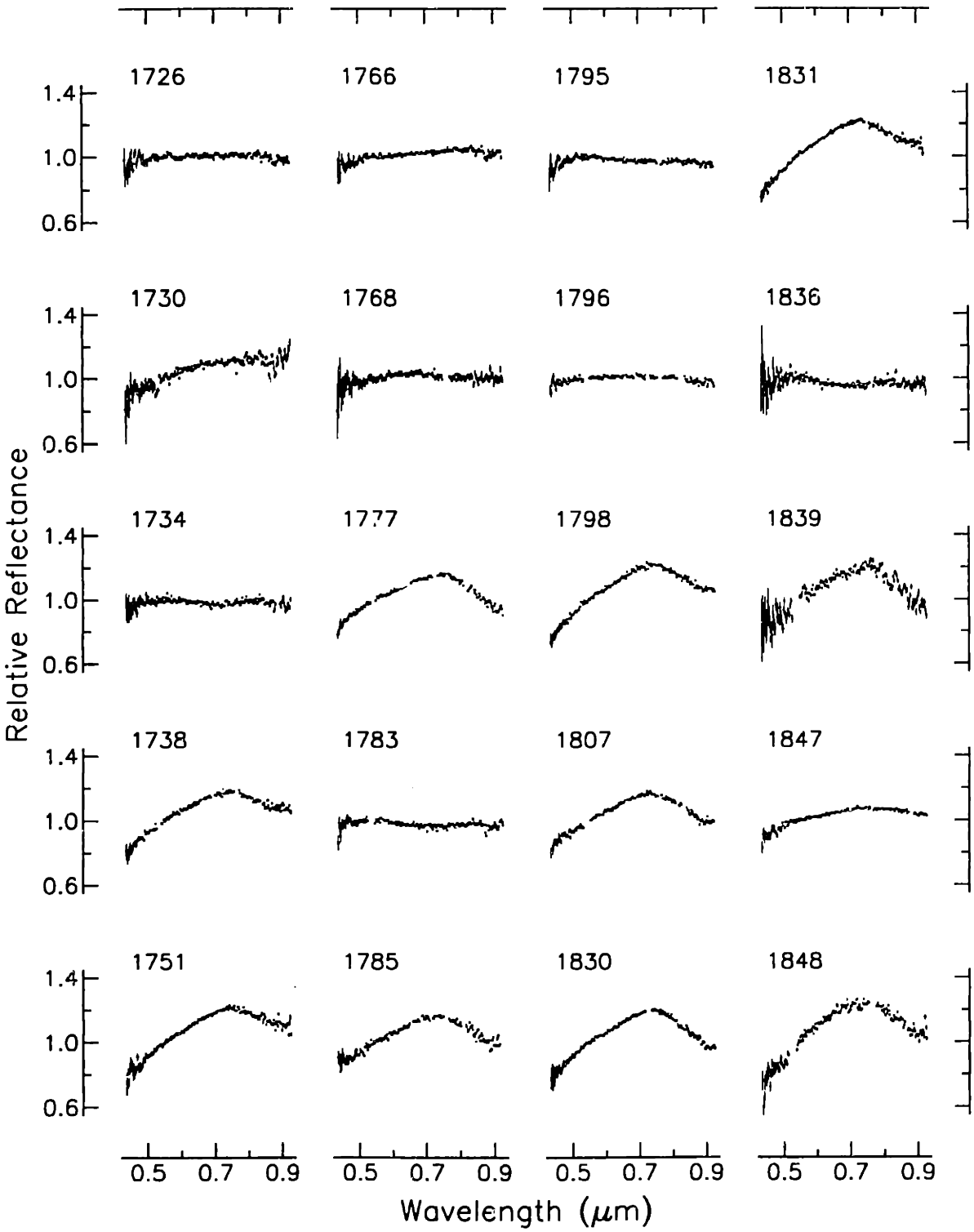
1726
1766
1795
1831
1730
1768
1796
1836
1734
1777
1798
1839
1738
1783
1807
1847
1751
1785
1830
1848
1.4
1.0
0.6
0.5
0.7
0.9
Relative Reflectance
Wavelength (μm)

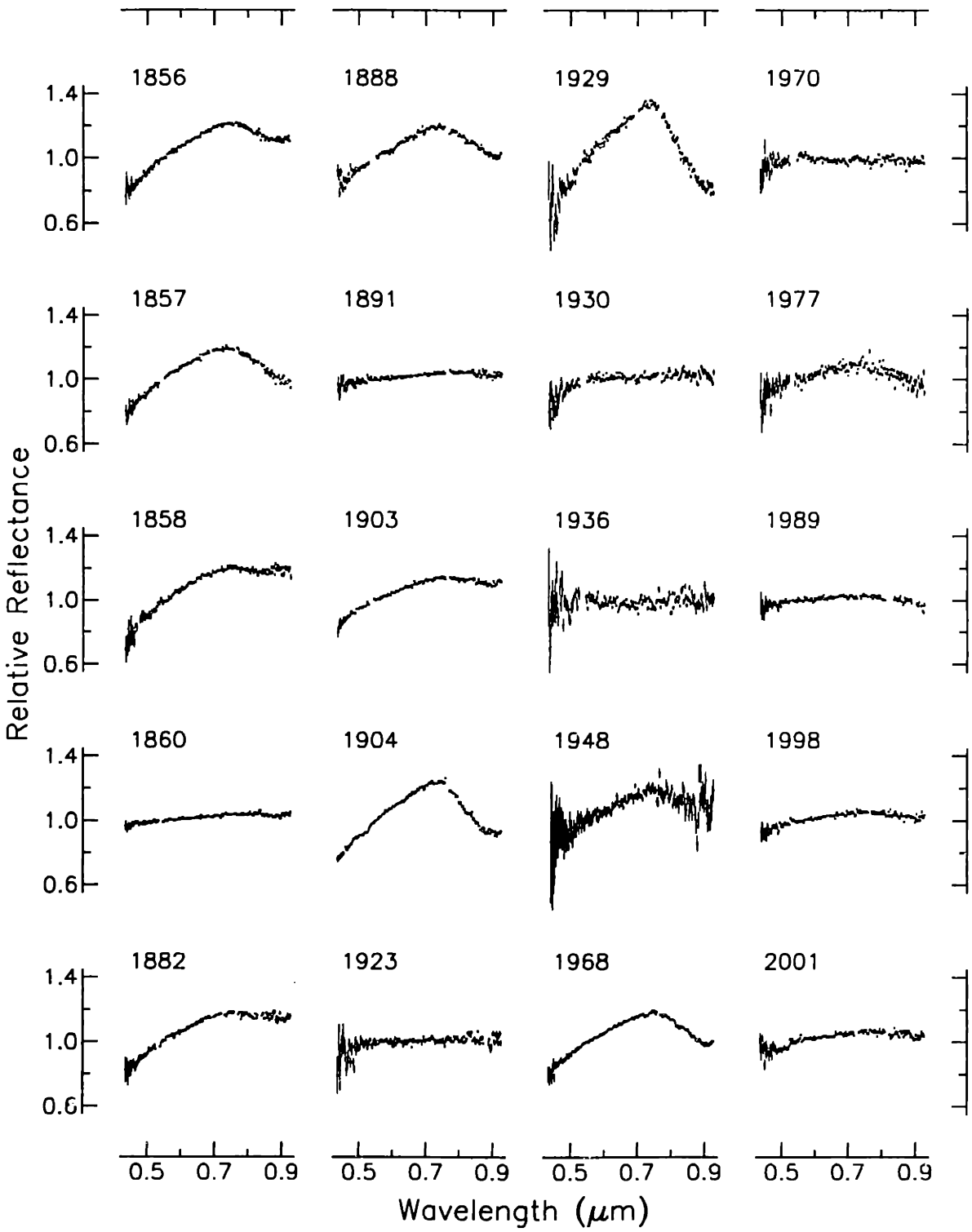
1856
1888
1929
1970
1857
1891
1930
1977
1858
1903
1936
1989
1860
1904
1948
1998
1882
1923
1968
2001
1.4
1.0
0.6
0.5
0.7
0.9
Relative Reflectance
Wavelength (μm)

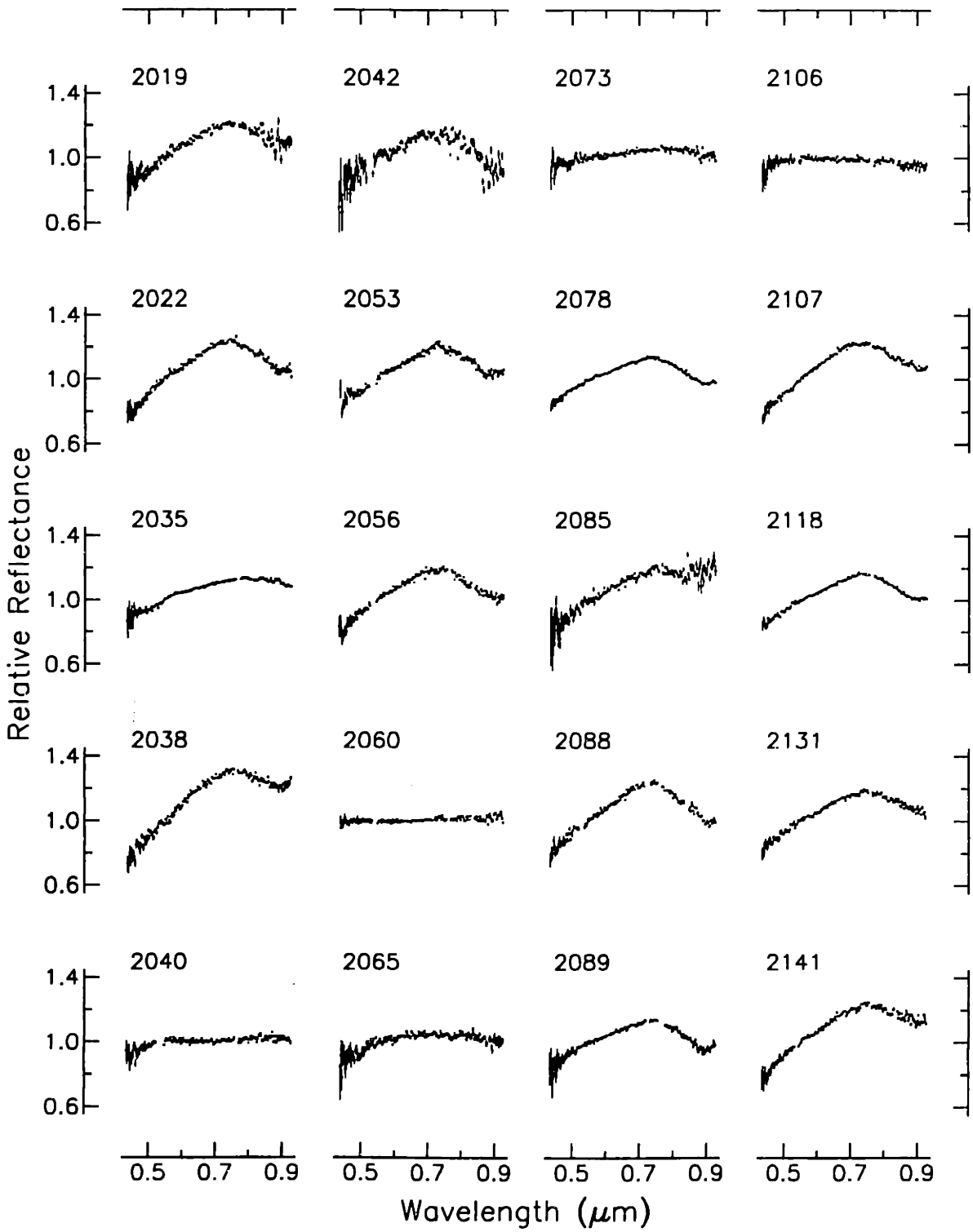
2019
2042
2073
2106
2022
2053
2078
2107
2035
2056
2085
2118
2038
2060
2088
2131
2040
2065
2089
2141
1.4
1.0
0.6
0.5
0.7
0.9
Relative Reflectance
Wavelength (μm)

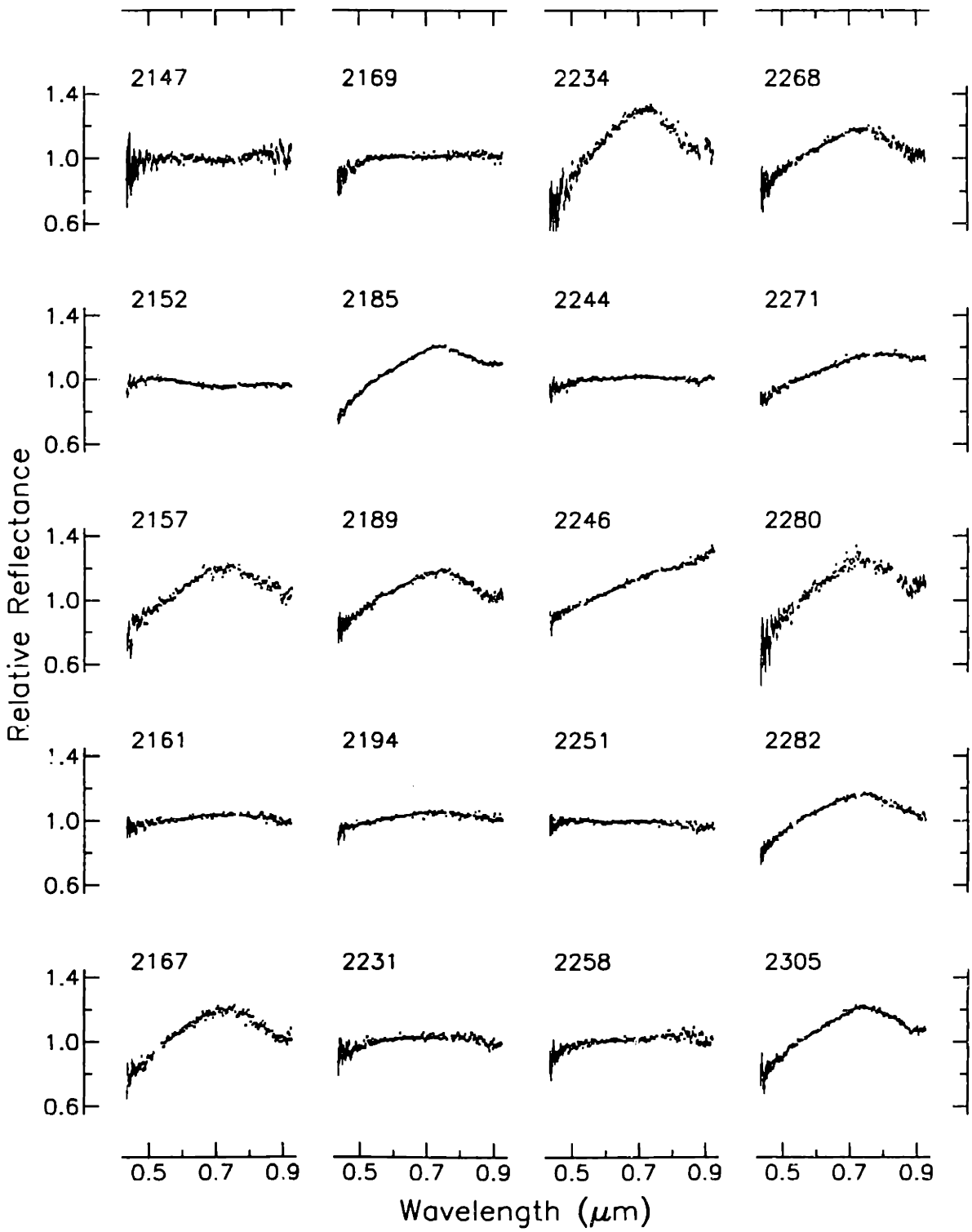
2147
2169
2234
2268
2152
2185
2244
2271
2157
2189
2246
2280
2161
2194
2251
2282
2167
2231
2258
2305
1.4
1.0
0.6
0.5
0.7
0.9
Relative Reflectance
Wavelength (μm)

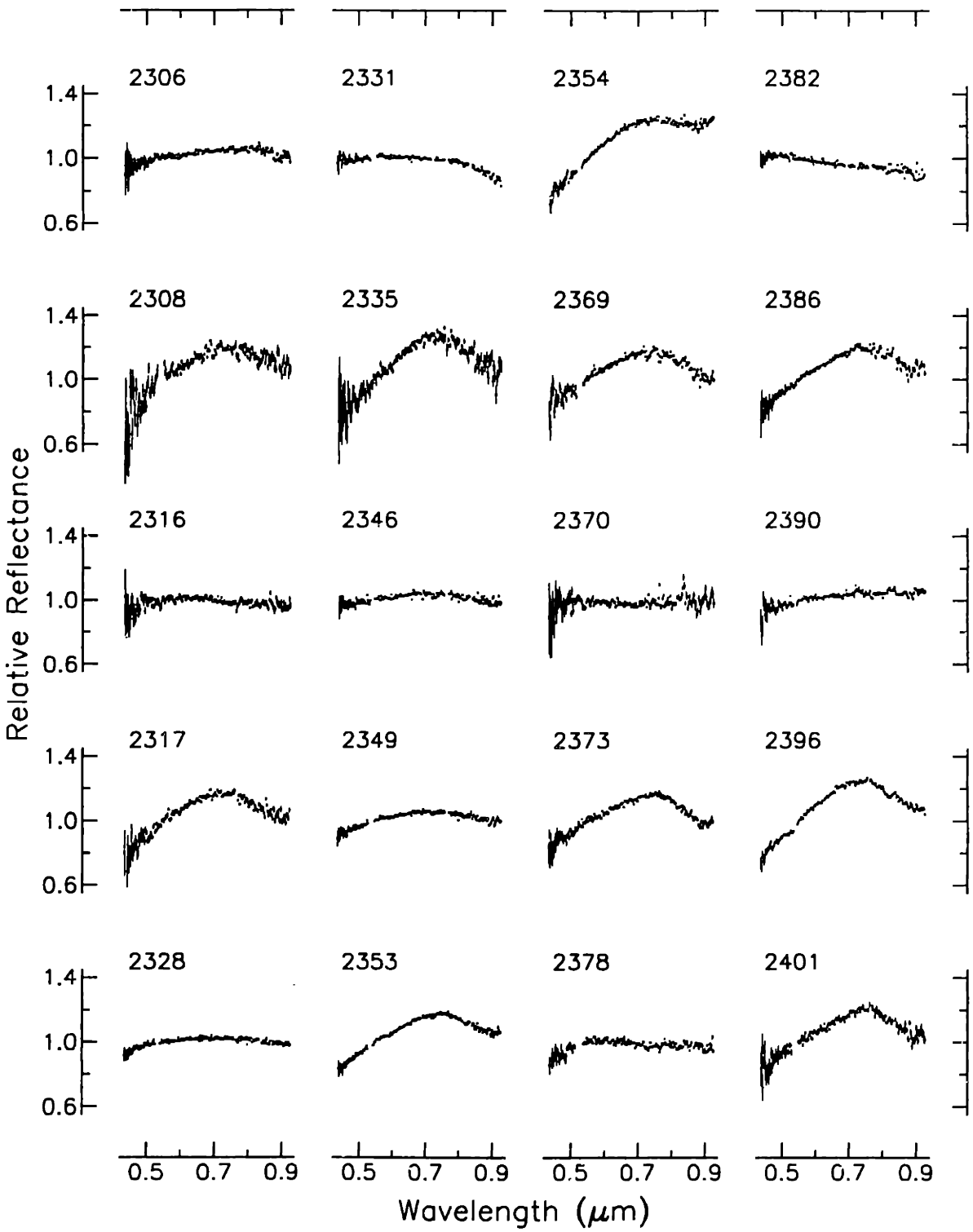
2306
2331
2354
2382
2308
2335
2369
2386
2316
2346
2370
2390
2317
2349
2373
2396
2328
2353
2378
2401
1.4
1.0
0.6
0.5
0.7
0.9
Relative Reflectance
Wavelength (μm)

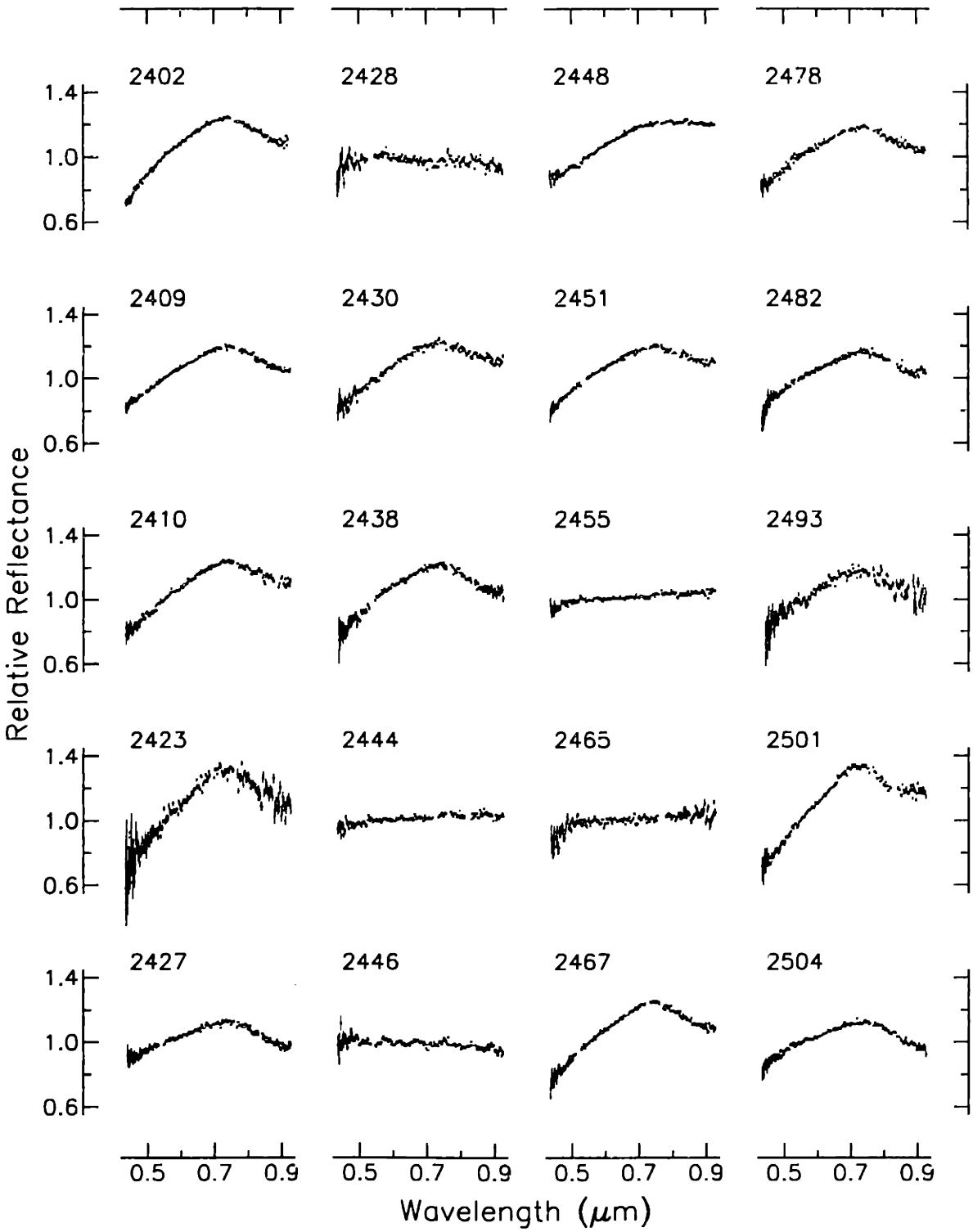
2402
2428
2448
2478
2409
2430
2451
2482
2410
2438
2455
2493
2423
2444
2465
2501
2427
2446
2467
2504
1.4
1.0
0.6
0.5
0.7
0.9
Relative Reflectance
Wavelength (μm)

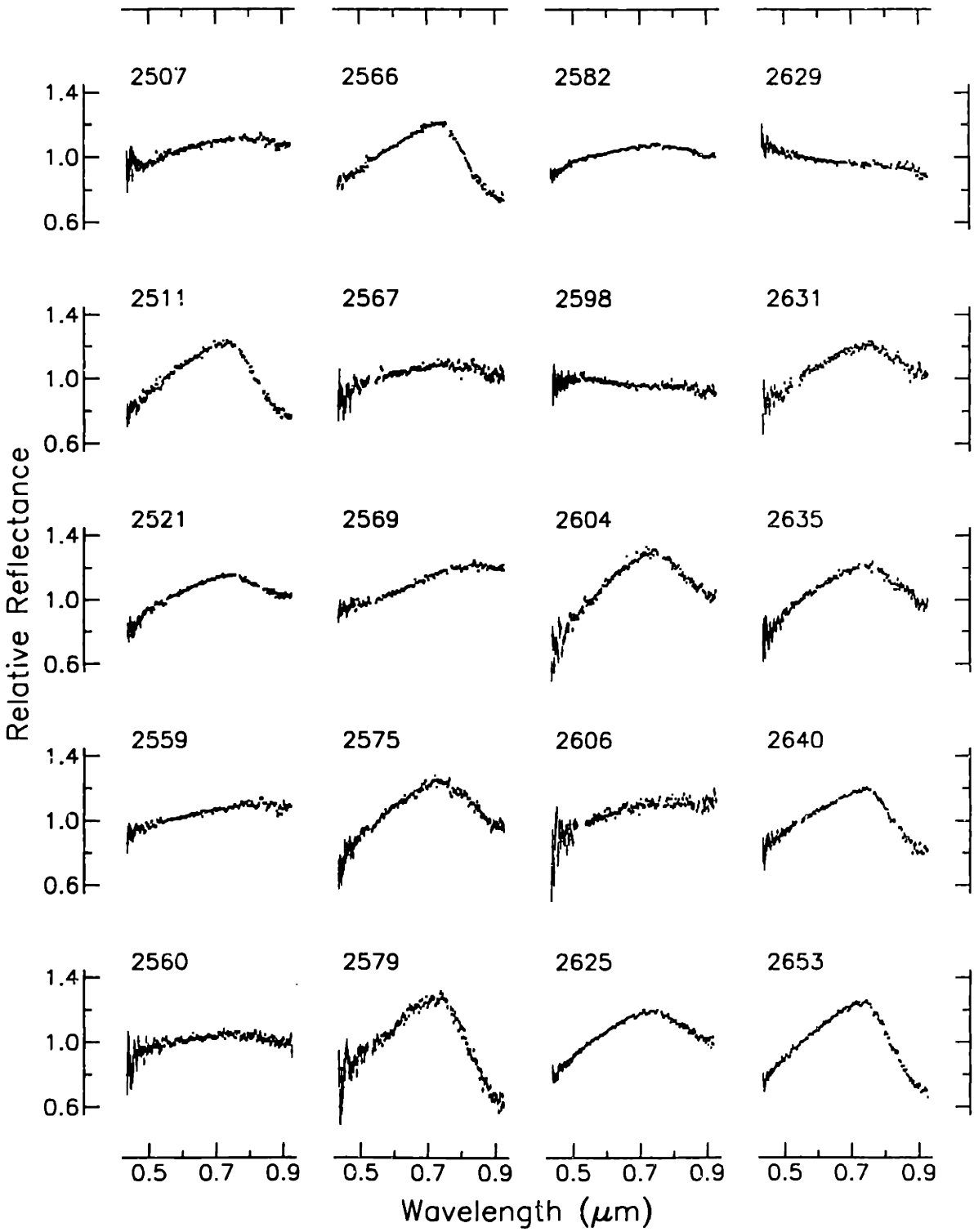
2507
2566
2582
2629
2511
2567
2598
2631
2521
2569
2604
2635
2559
2575
2606
2640
2560
2579
2625
2653
1.4
1.0
0.6
0.5
0.7
0.9
Relative Reflectance
Wavelength (μm)

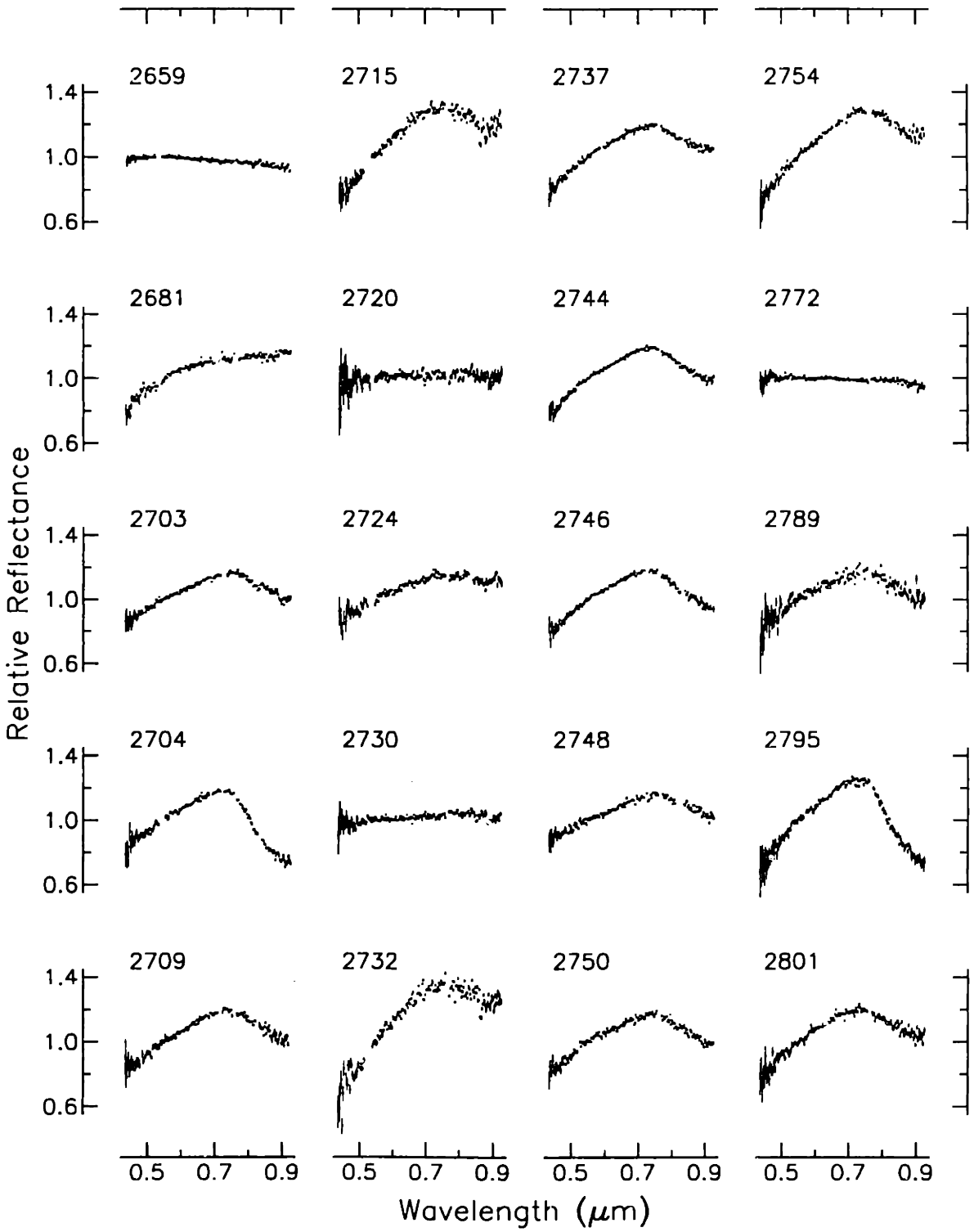
2659
2715
2737
2754
2681
2720
2744
2772
2703
2724
2746
2789
2704
2730
2748
2795
2709
2732
2750
2801
1.4
1.0
0.6
0.5
0.7
0.9
Relative Reflectance
Wavelength (μm)

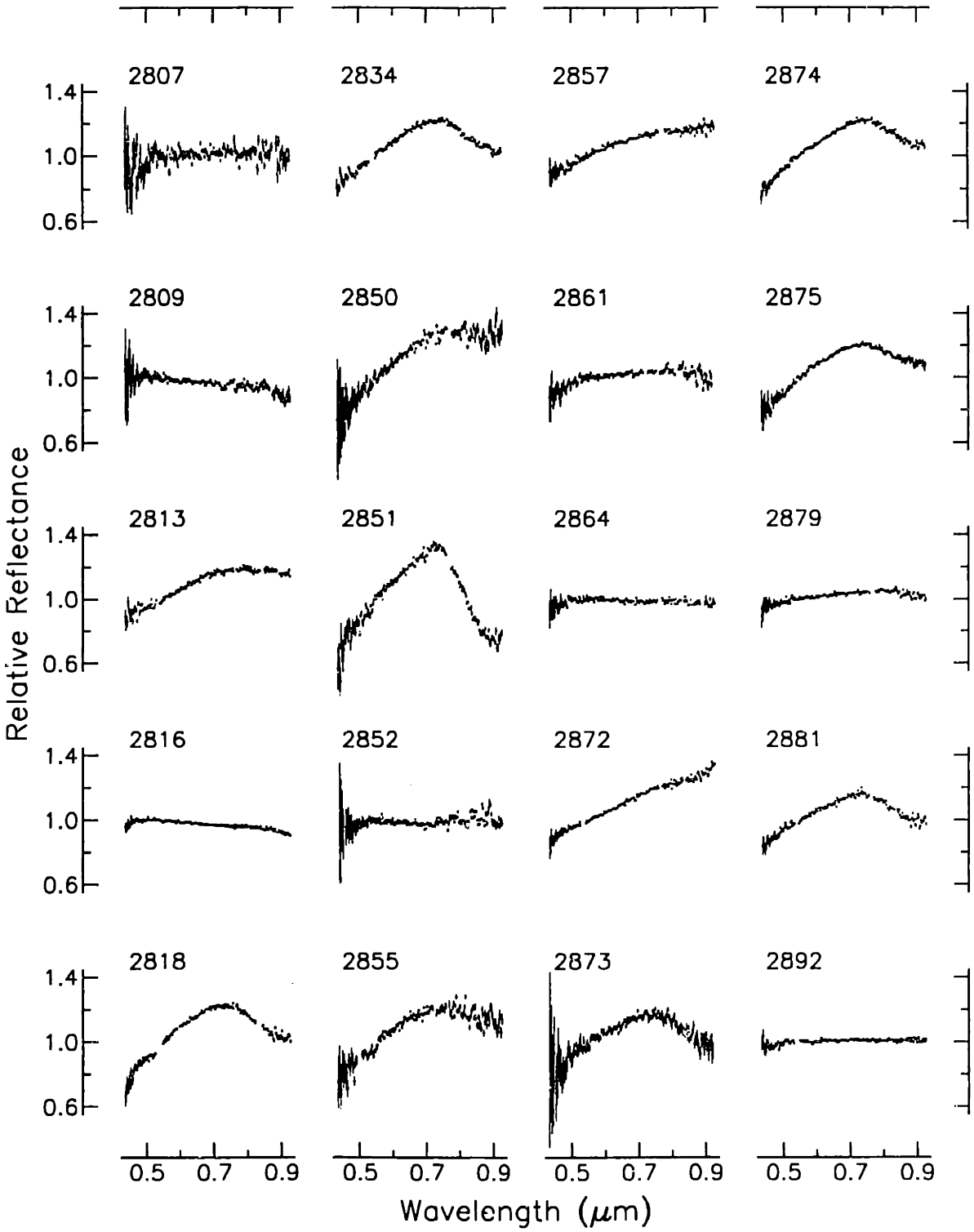
2807
2834
2857
2874
2809
2850
2861
2875
2813
2851
2864
2879
2816
2852
2872
2881
2818
2855
2873
2892
1.4
1.0
0.6
0.5
0.7
0.9
Relative Reflectance
Wavelength (μm)

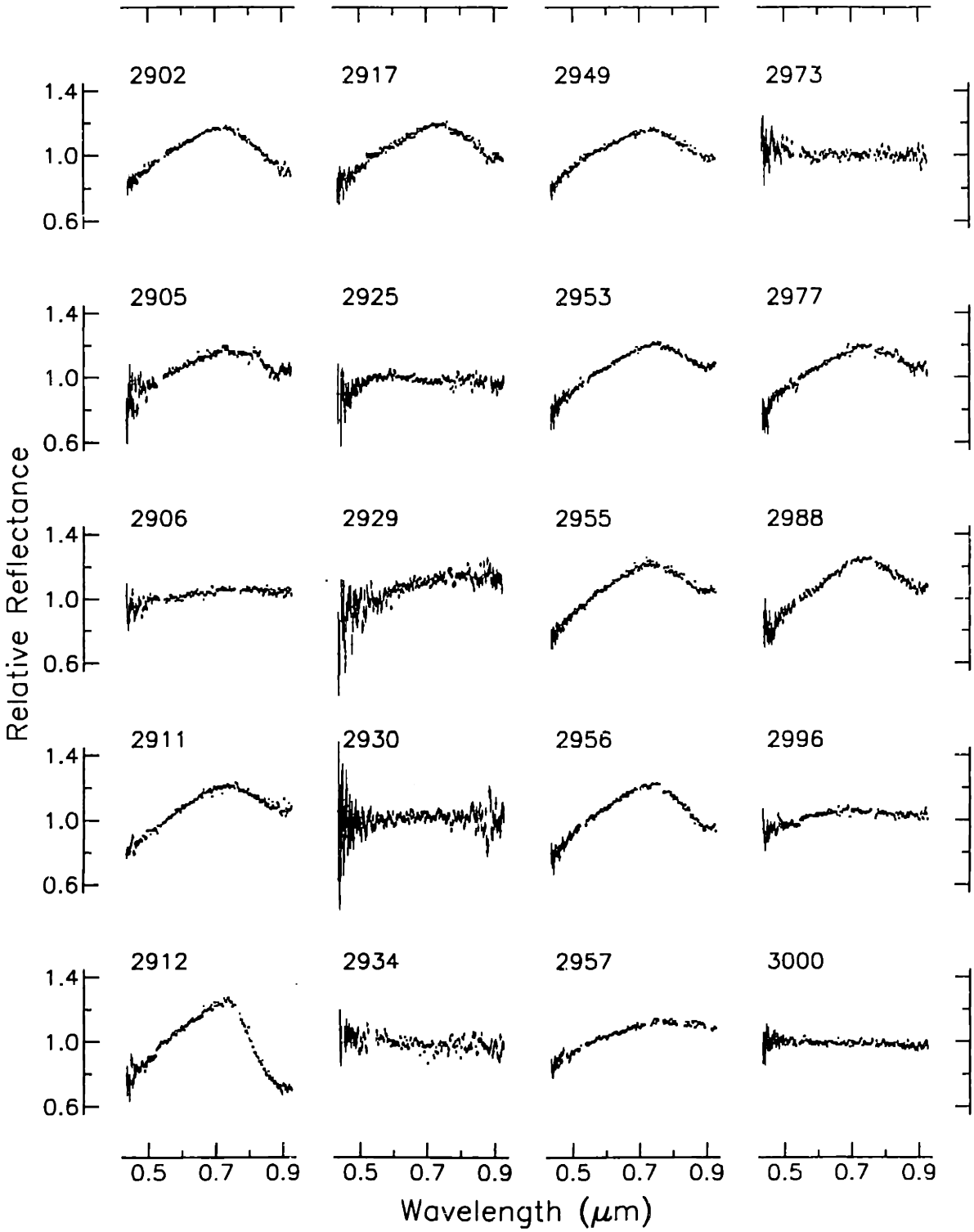
2902
2917
2949
2973
2905
2925
2953
2977
2906
2929
2955
2988
2911
2930
2956
2996
2912
2934
2957
3000
1.4
1.0
0.6
0.5
0.7
0.9
Relative Reflectance
Wavelength (μm)

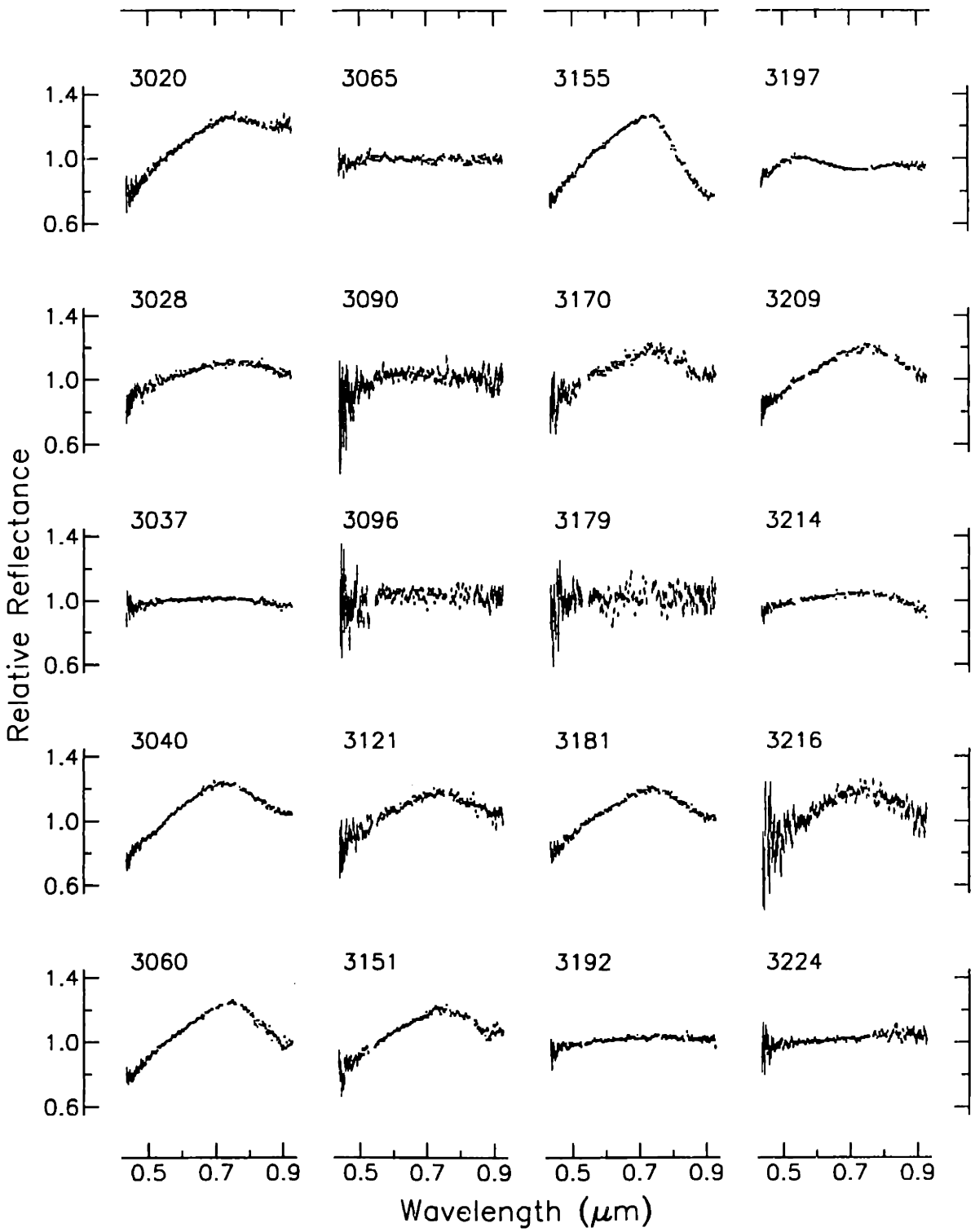
3020
3065
3155
3197
3028
3090
3170
3209
3037
3096
3179
3214
3040
3121
3181
3216
3060
3151
3192
3224
1.4
1.0
0.6
0.5
0.7
0.9
Relative Reflectance
Wavelength (μm)

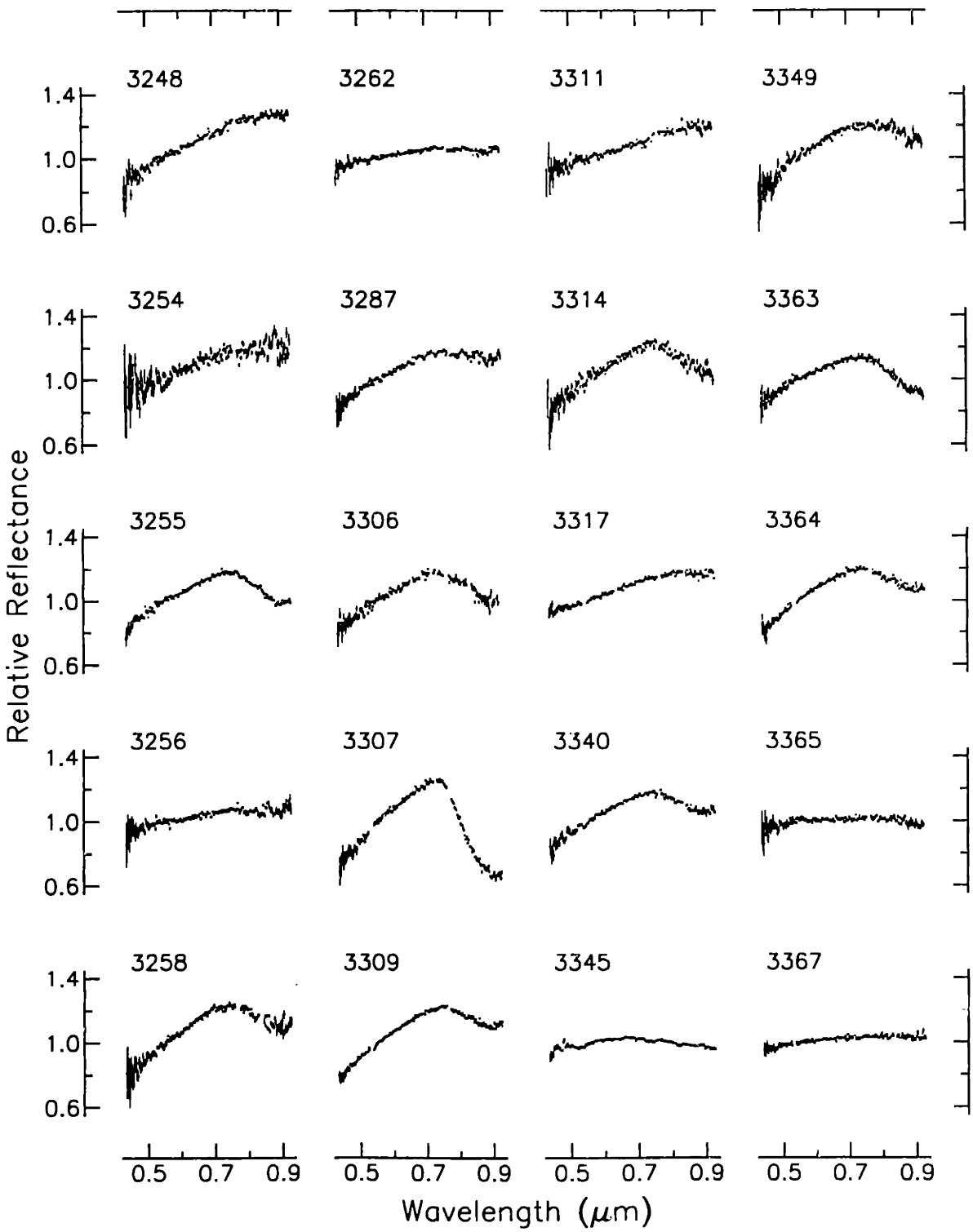
3248
3262
3311
3349
3254
3287
3314
3363
3255
3306
3317
3364
3256
3307
3340
3365
3258
3309
3345
3367
1.4
1.0
0.6
0.5
0.7
0.9
Relative Reflectance
Wavelength (μm)

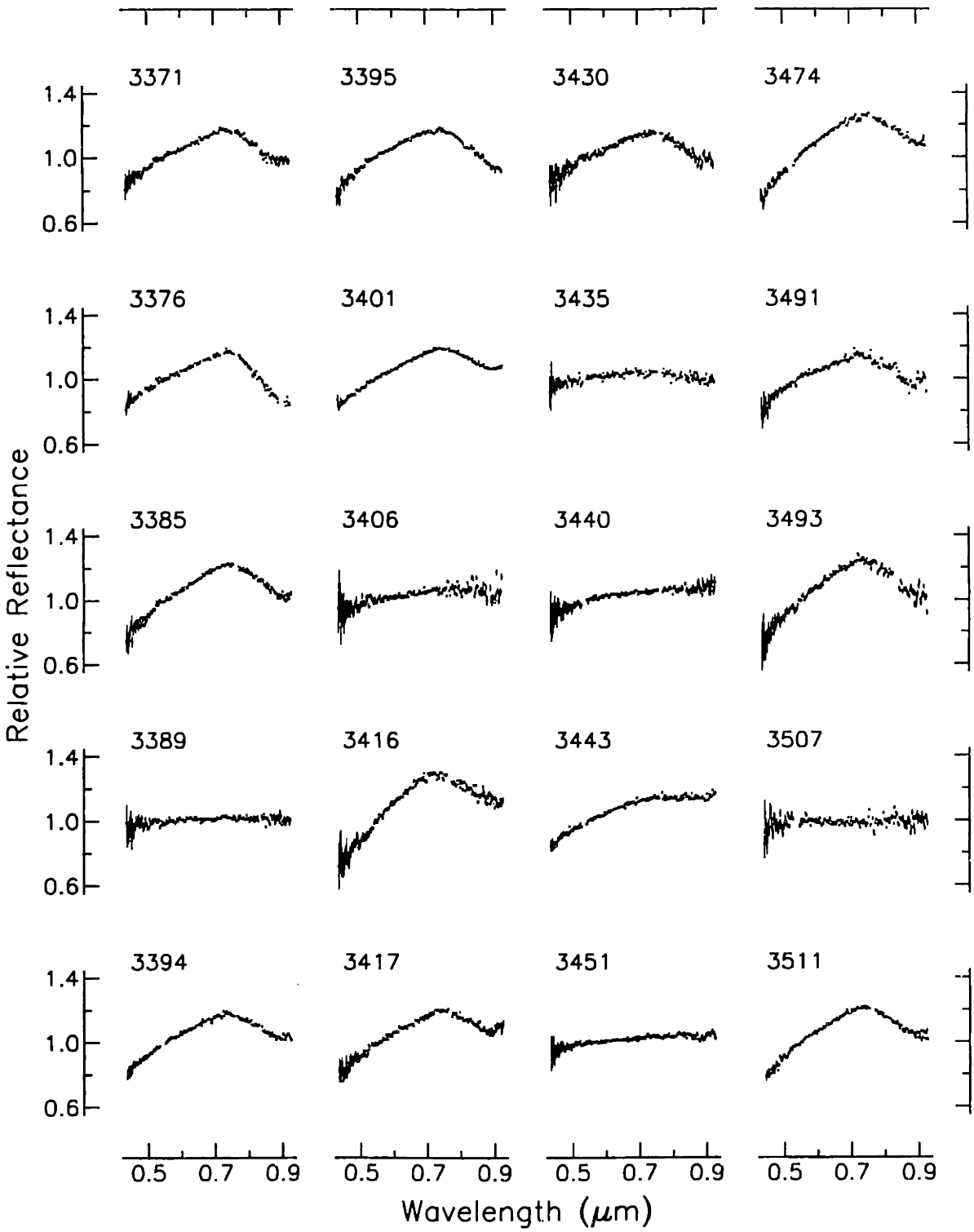
3371
3395
3430
3474
3376
3401
3435
3491
3385
3406
3440
3493
3389
3416
3443
3507
3394
3417
3451
3511
1.4
1.0
0.6
0.5
0.7
0.9
Relative Reflectance
Wavelength (μm)

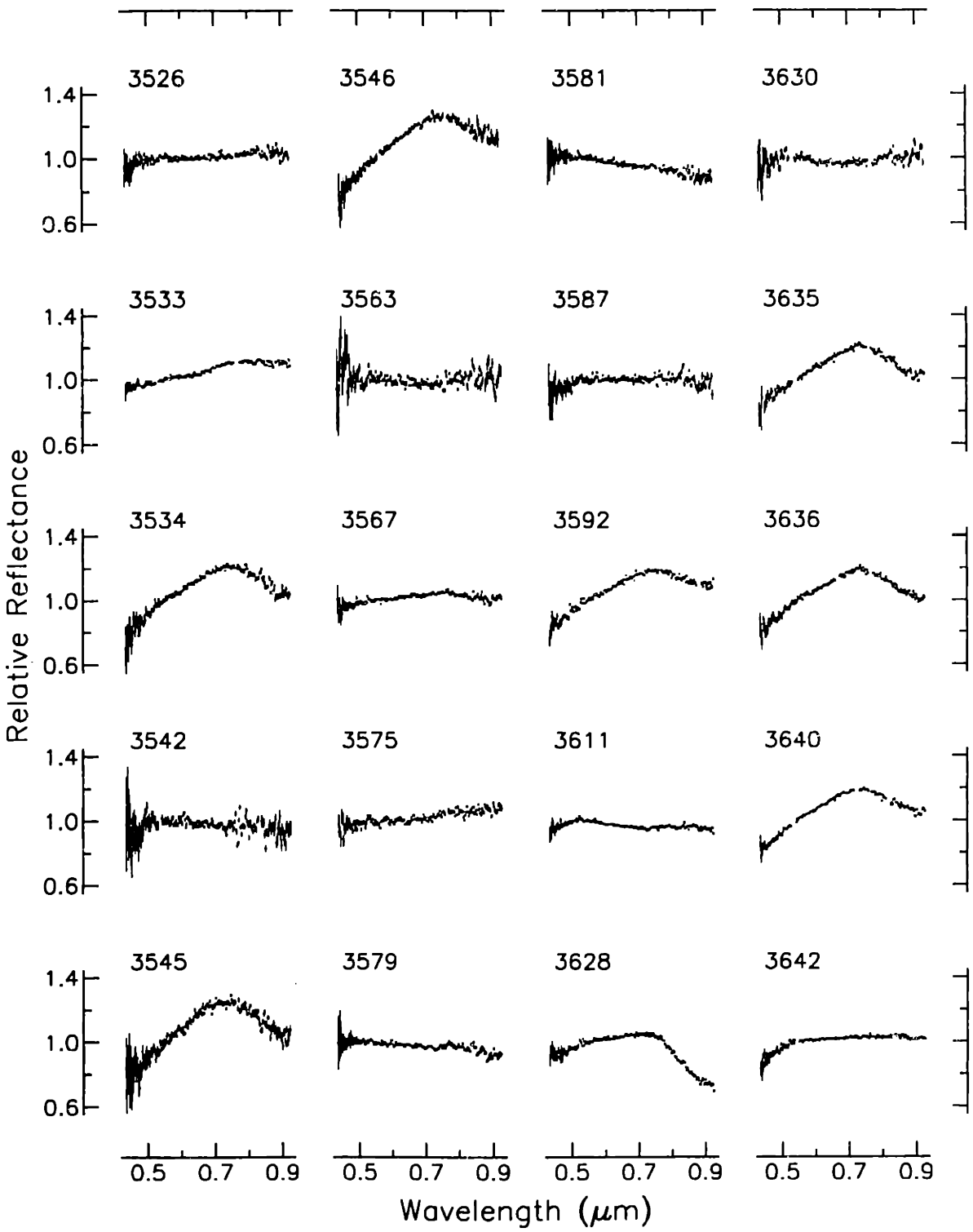
3526
3546
3581
3630
3533
3563
3587
3635
3534
3567
3592
3636
3542
3575
3611
3640
3545
3579
3628
3642
1.4
1.0
0.6
0.5
0.7
0.9
Relative Reflectance
Wavelength (μm)

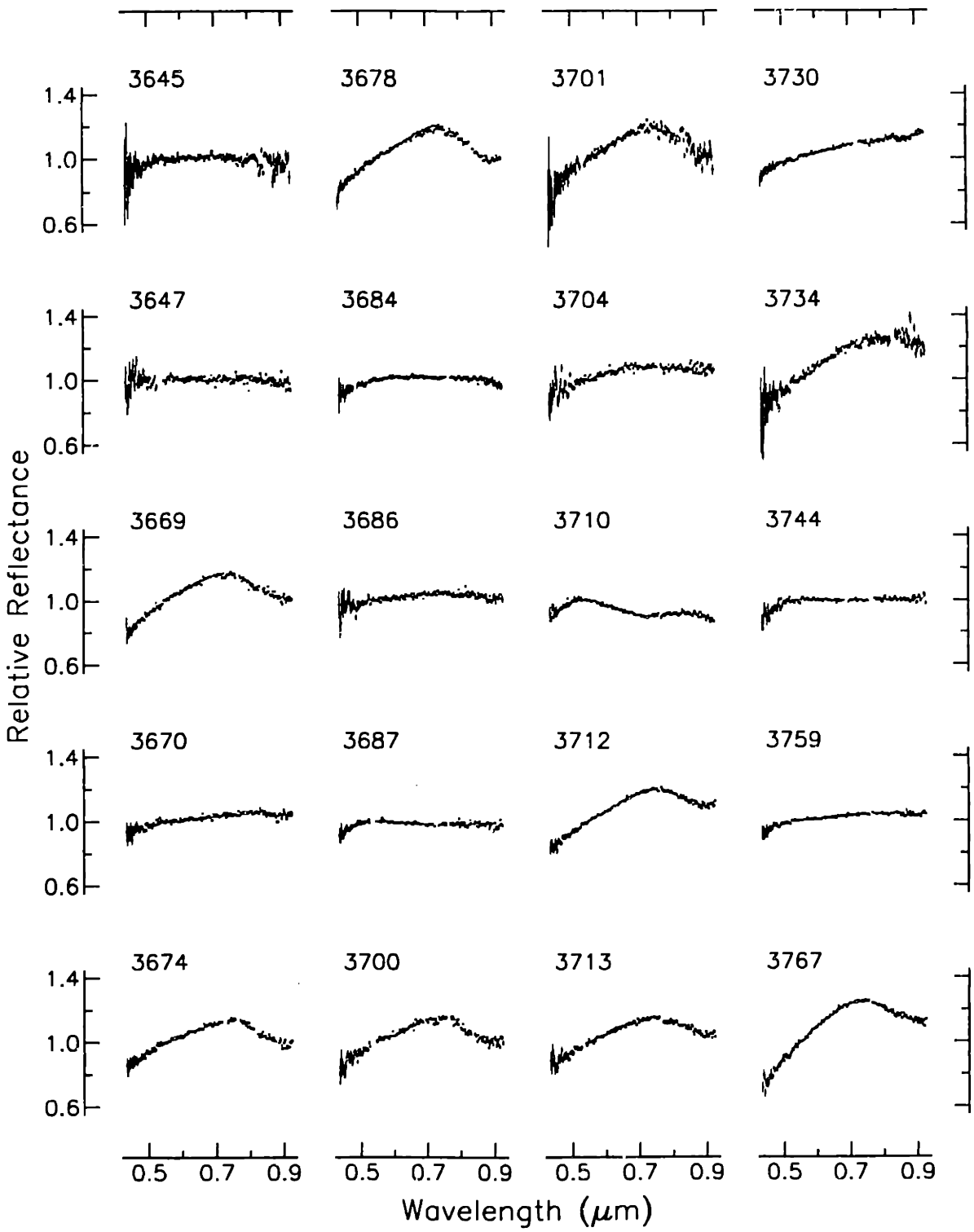
3645
3678
3701
3730
3647
3684
3704
3734
3669
3686
3710
3744
3670
3687
3712
3759
3674
3700
3713
3767
1.4
1.0
0.6
0.5
0.7
0.9
Relative Reflectance
Wavelength (μm)

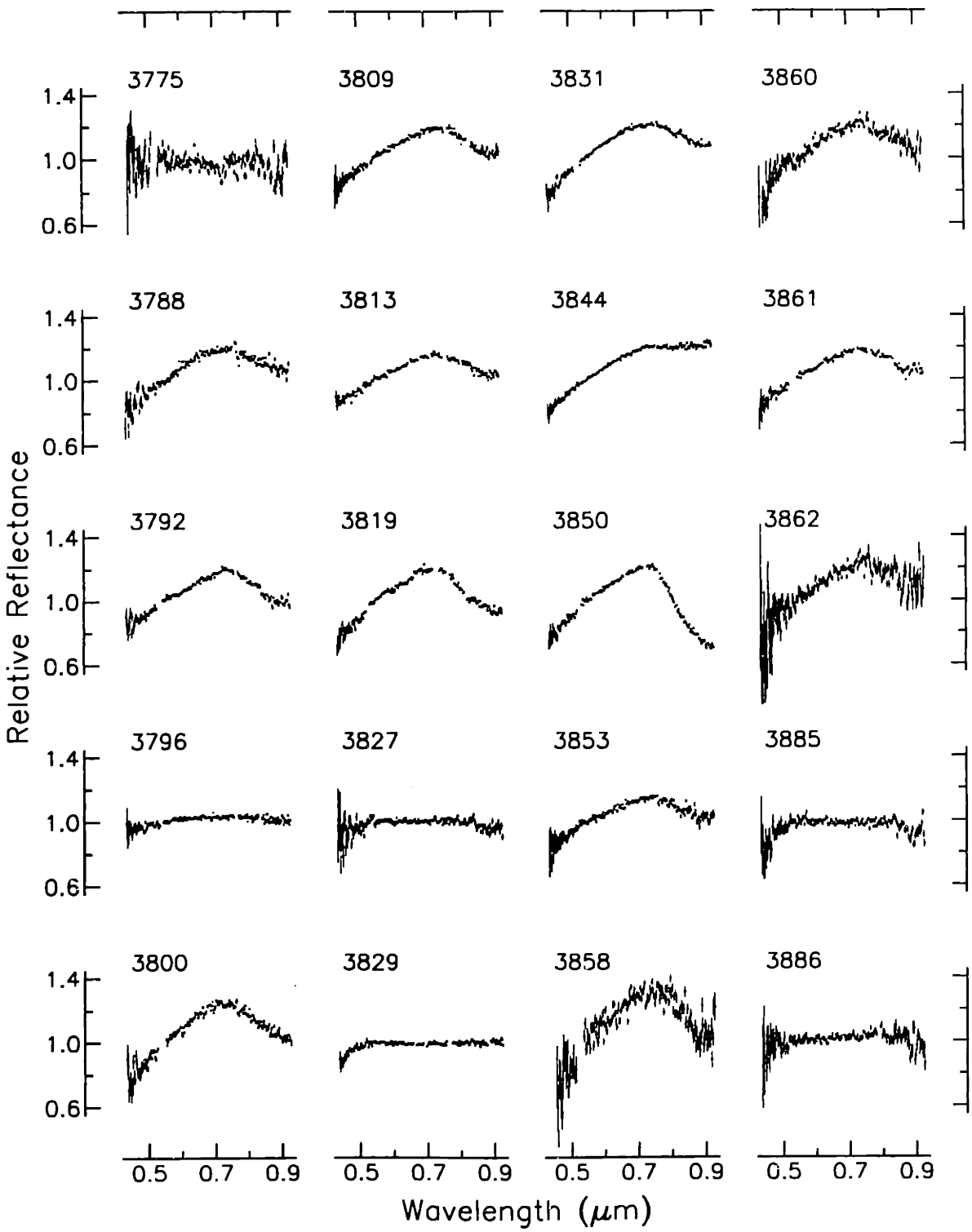
3775
3809
3831
3860
3788
3813
3844
3861
3792
3819
3850
3862
3796
3827
3853
3885
3800
3829
3858
3886
1.4
1.0
0.6
0.5
0.7
0.9
Relative Reflectance
Wavelength (μm)

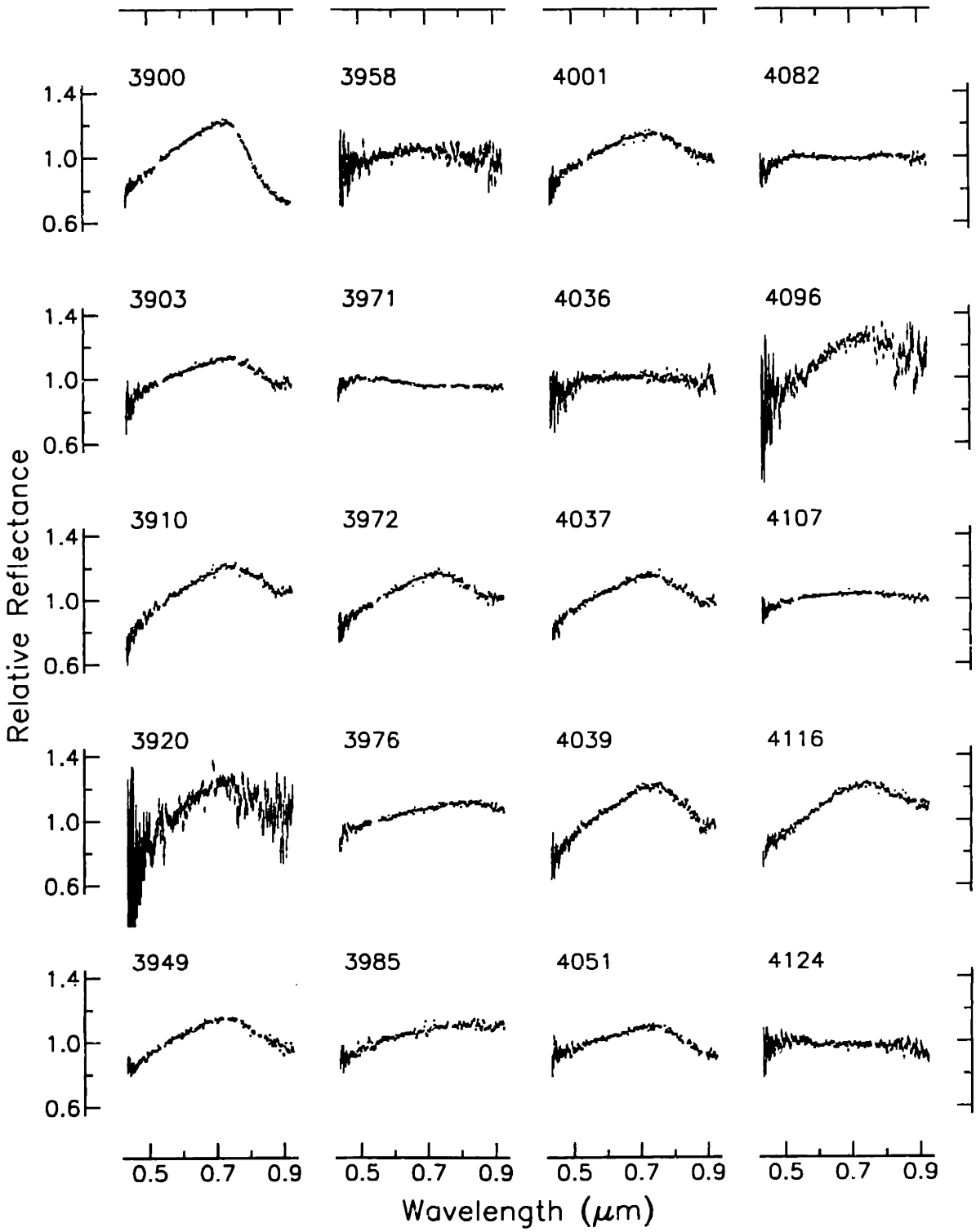
3900
3958
4001
4082
3903
3971
4036
4096
3910
3972
4037
4107
3920
3976
4039
4116
3949
3985
4051
4124
1.4
1.0
0.6
Relative Reflectance
0.5
0.7
0.9
Wavelength (μm)

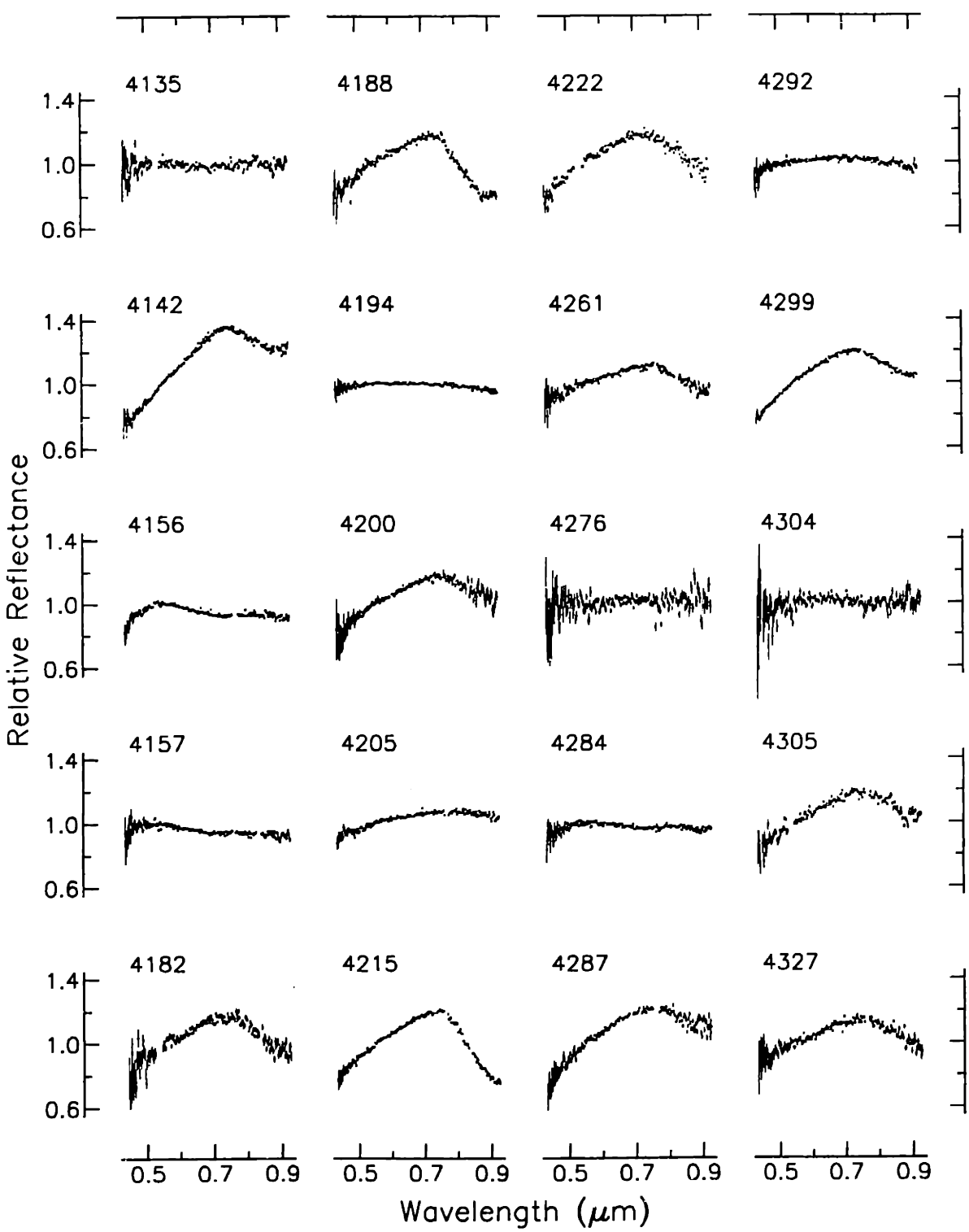
4135
4188
4222
4292
4142
4194
4261
4299
4156
4200
4276
4304
4157
4205
4284
4305
4182
4215
4287
4327
1.4
1.0
0.6
Relative Reflectance
0.5
0.7
0.9
Wavelength (μm)

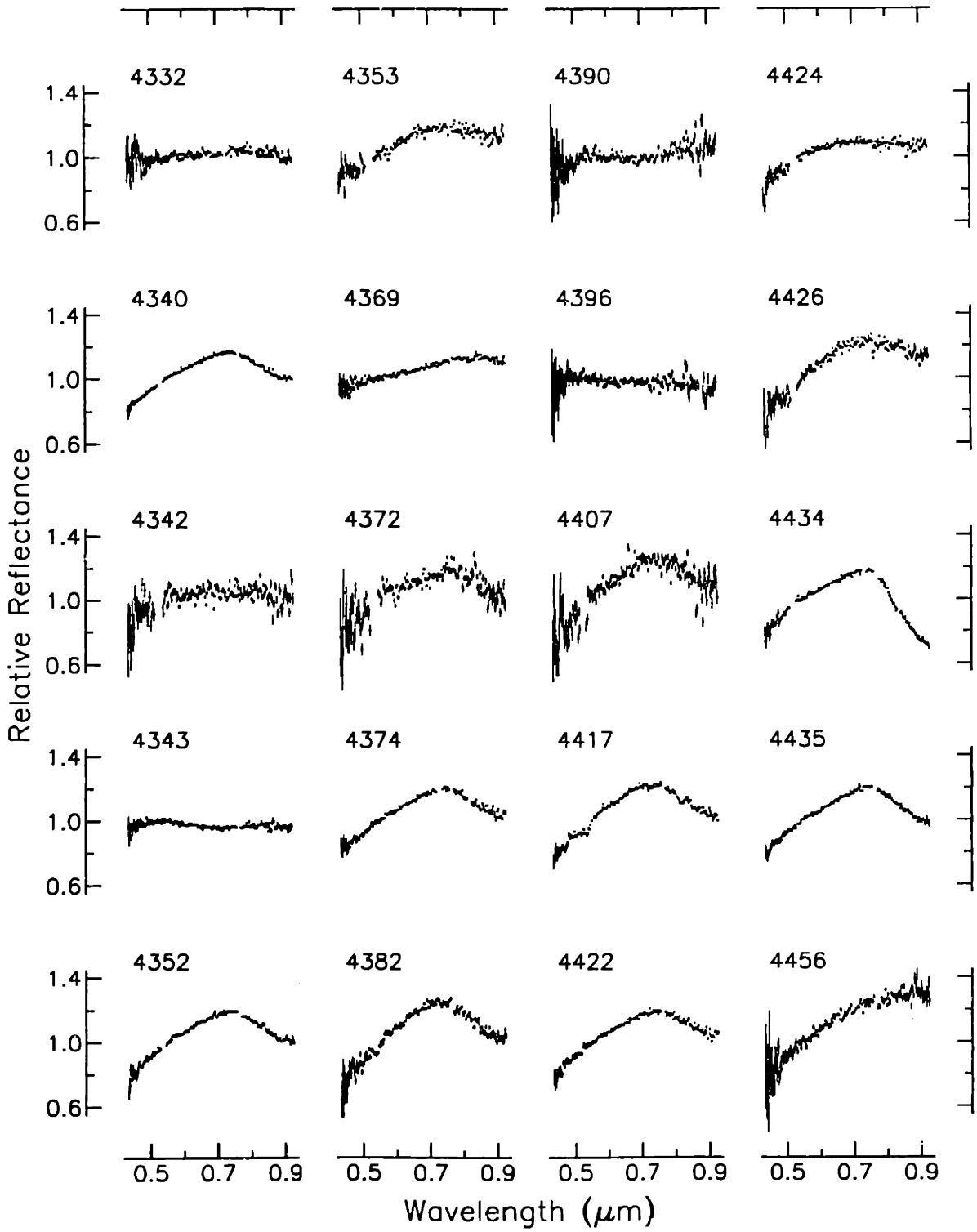
4332
4353
4390
4424
4340
4369
4396
4426
4342
4372
4407
4434
4343
4374
4417
4435
4352
4382
4422
4456
1.4
1.0
0.6
0.5
0.7
0.9
Relative Reflectance
Wavelength (μm)

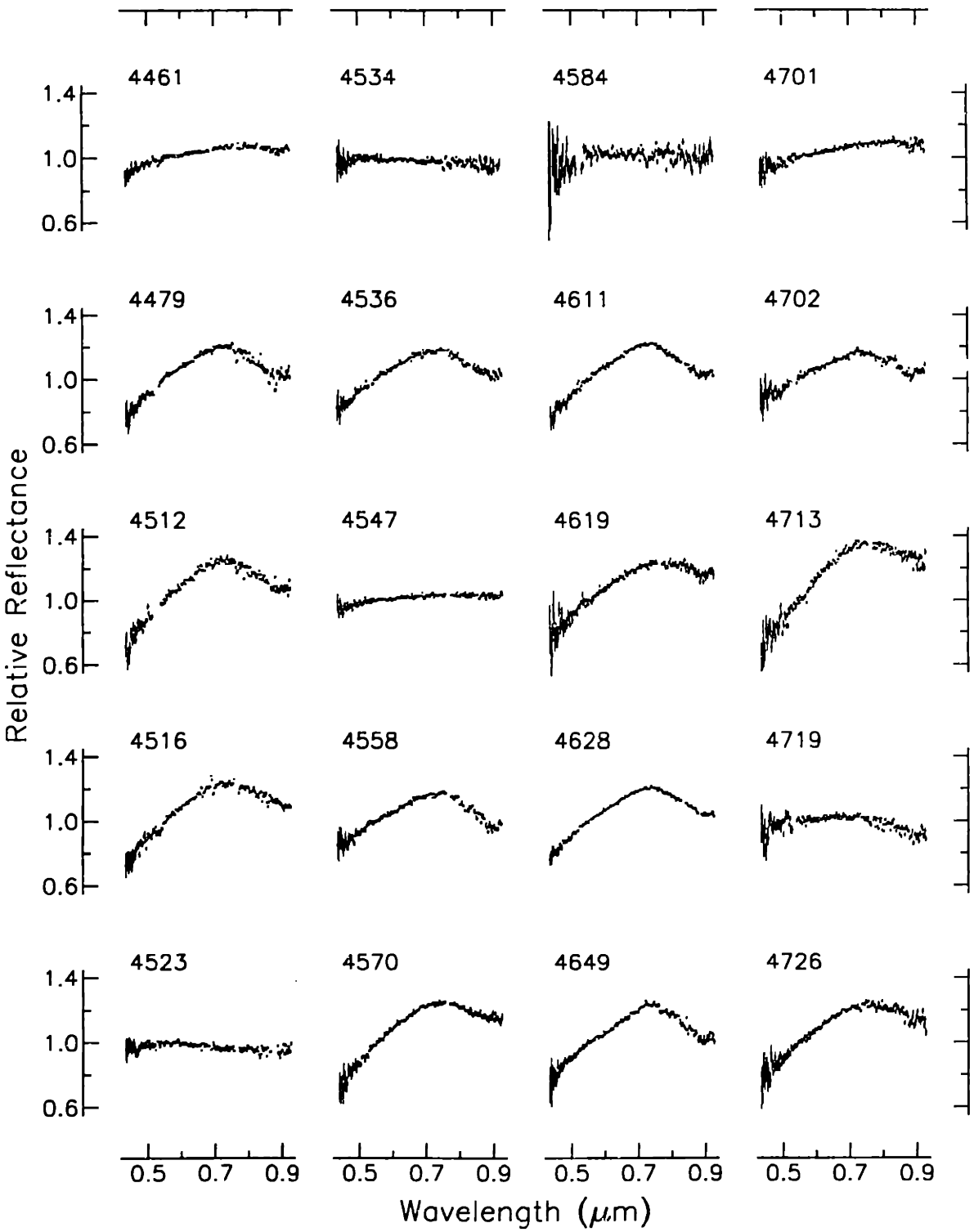
4461
4534
4584
4701
4479
4536
4611
4702
4512
4547
4619
4713
4516
4558
4628
4719
4523
4570
4649
4726
1.4
1.0
0.6
0.5
0.7
0.9
Relative Reflectance
Wavelength (μm)

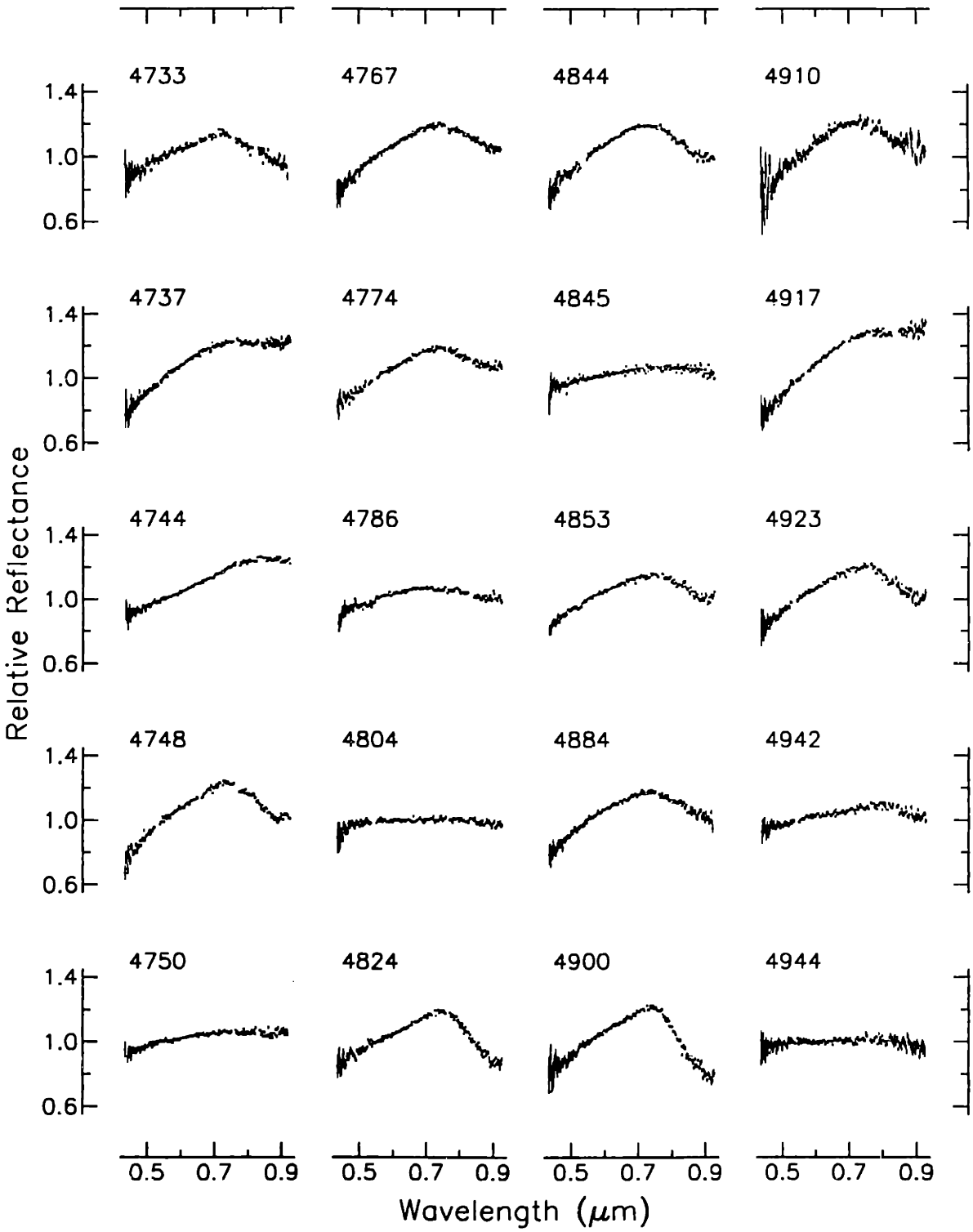
4733
4767
4844
4910
4737
4774
4845
4917
4744
4786
4853
4923
4748
4804
4884
4942
4750
4824
4900
4944
1.4
1.0
0.6
0.5
0.7
0.9
Relative Reflectance
Wavelength (μm)

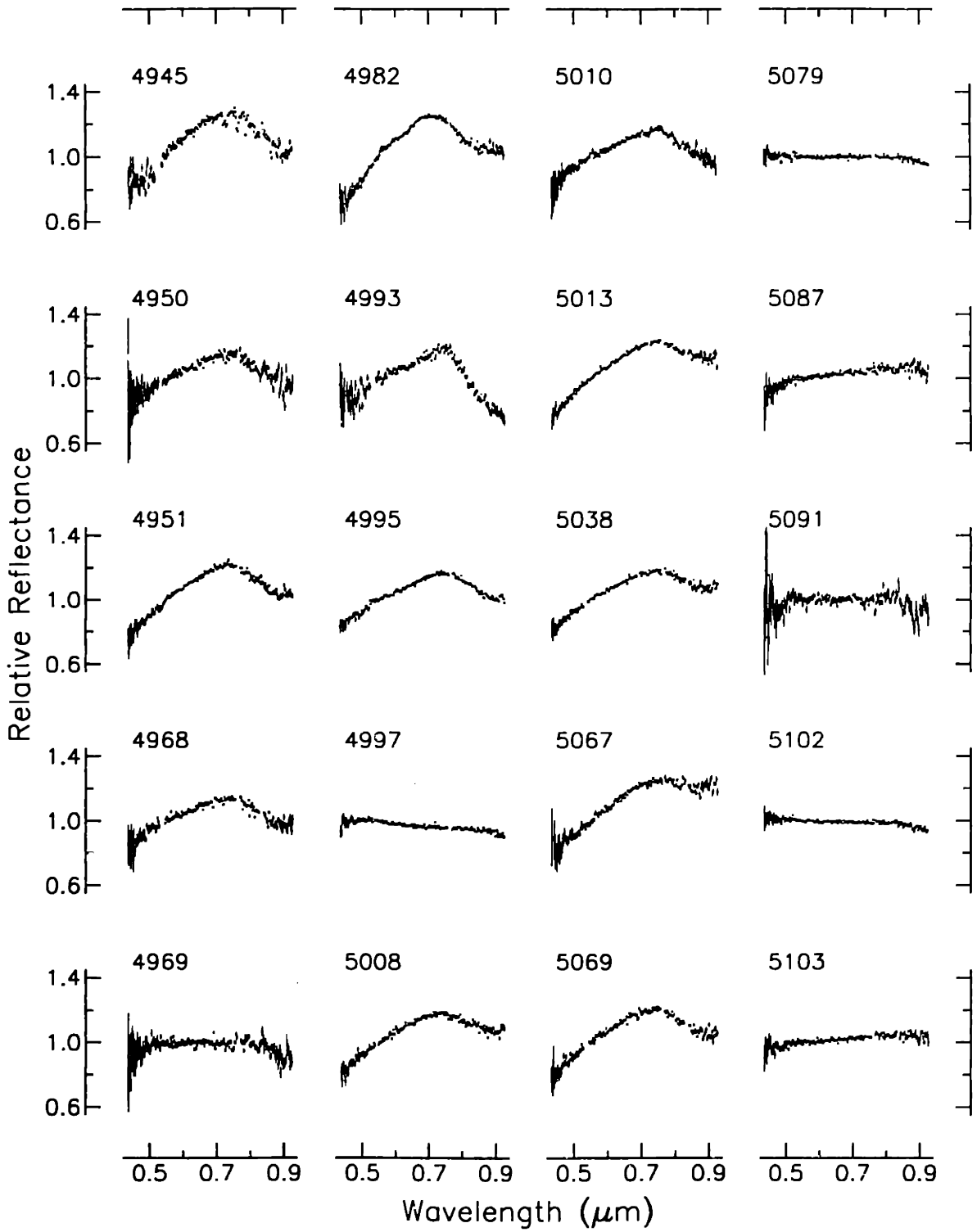
4945
4982
5010
5079
4950
4993
5013
5087
4951
4995
5038
5091
4968
4997
5067
5102
4969
5008
5069
5103
1.4
1.0
0.6
0.5
0.7
0.9
Relative Reflectance
Wavelength (μm)

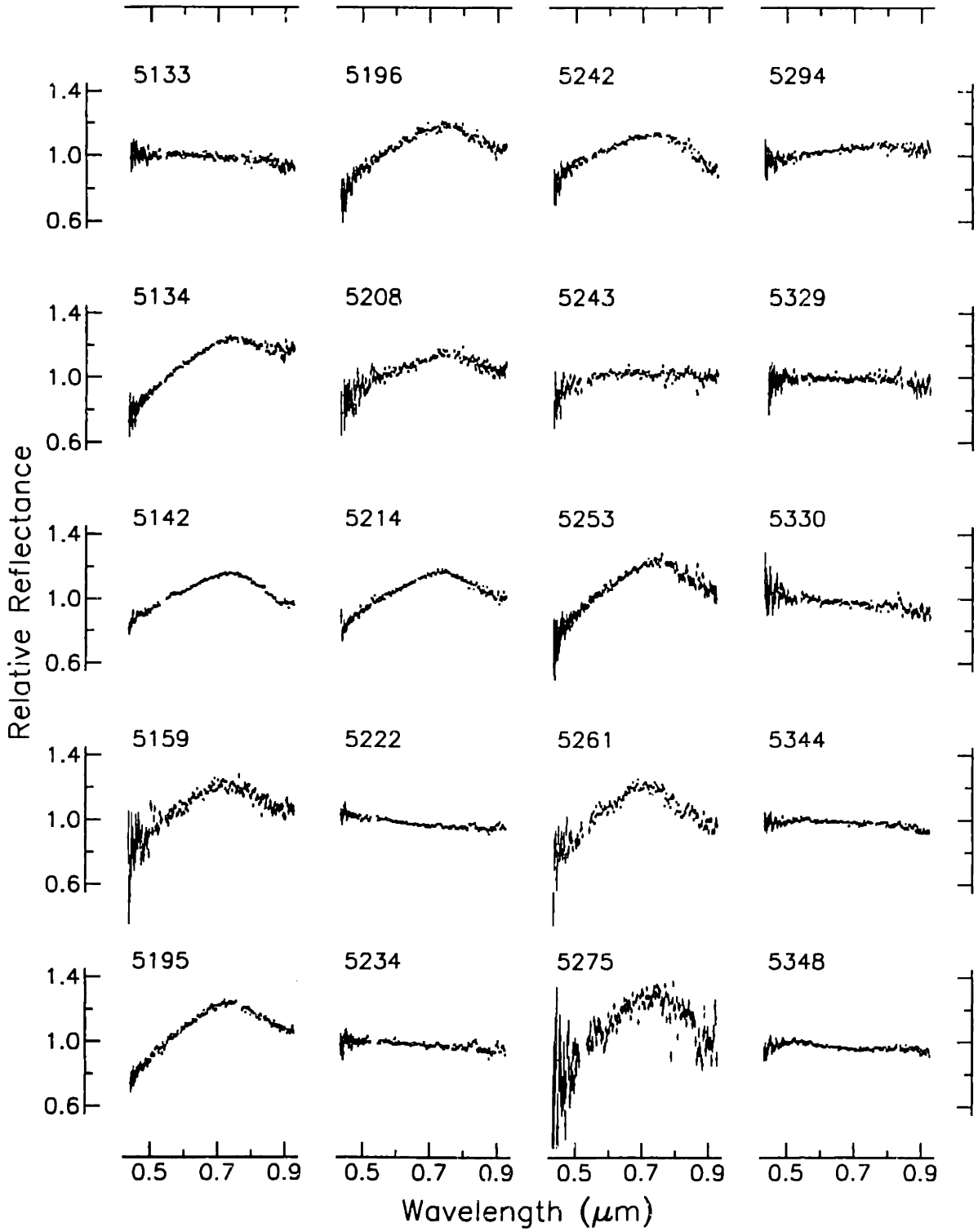
5133
5196
5242
5294
5134
5208
5243
5329
5142
5214
5253
5330
5159
5222
5261
5344
5195
5234
5275
5348
1.4
1.0
0.6
0.5
0.7
0.9
Relative Reflectance
Wavelength (μm)

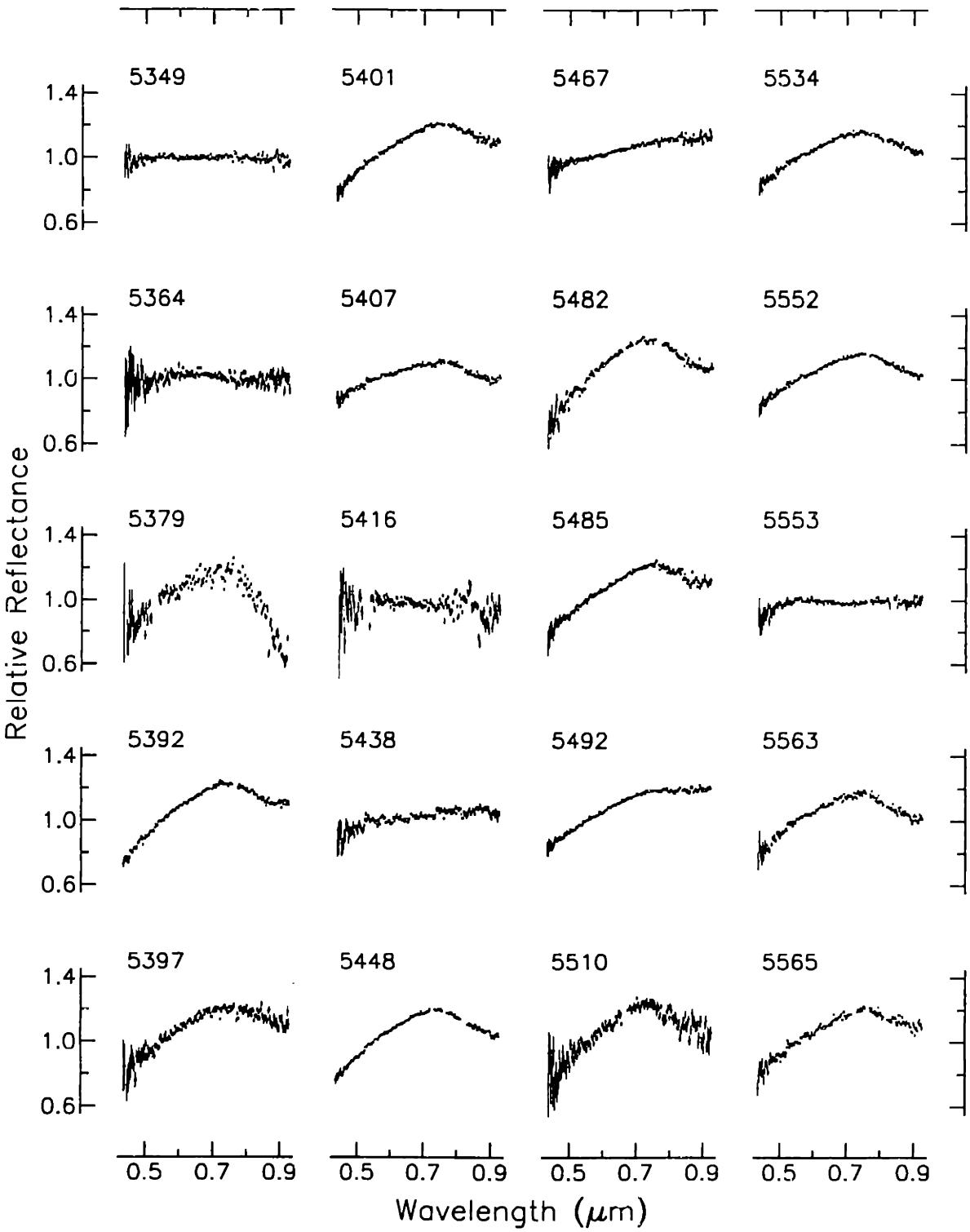
5349
5401
5467
5534
5364
5407
5482
5552
5379
5416
5485
5553
5392
5438
5492
5563
5397
5448
5510
5565
1.4
1.0
0.6
0.5
0.7
0.9
Relative Reflectance
Wavelength (μm)

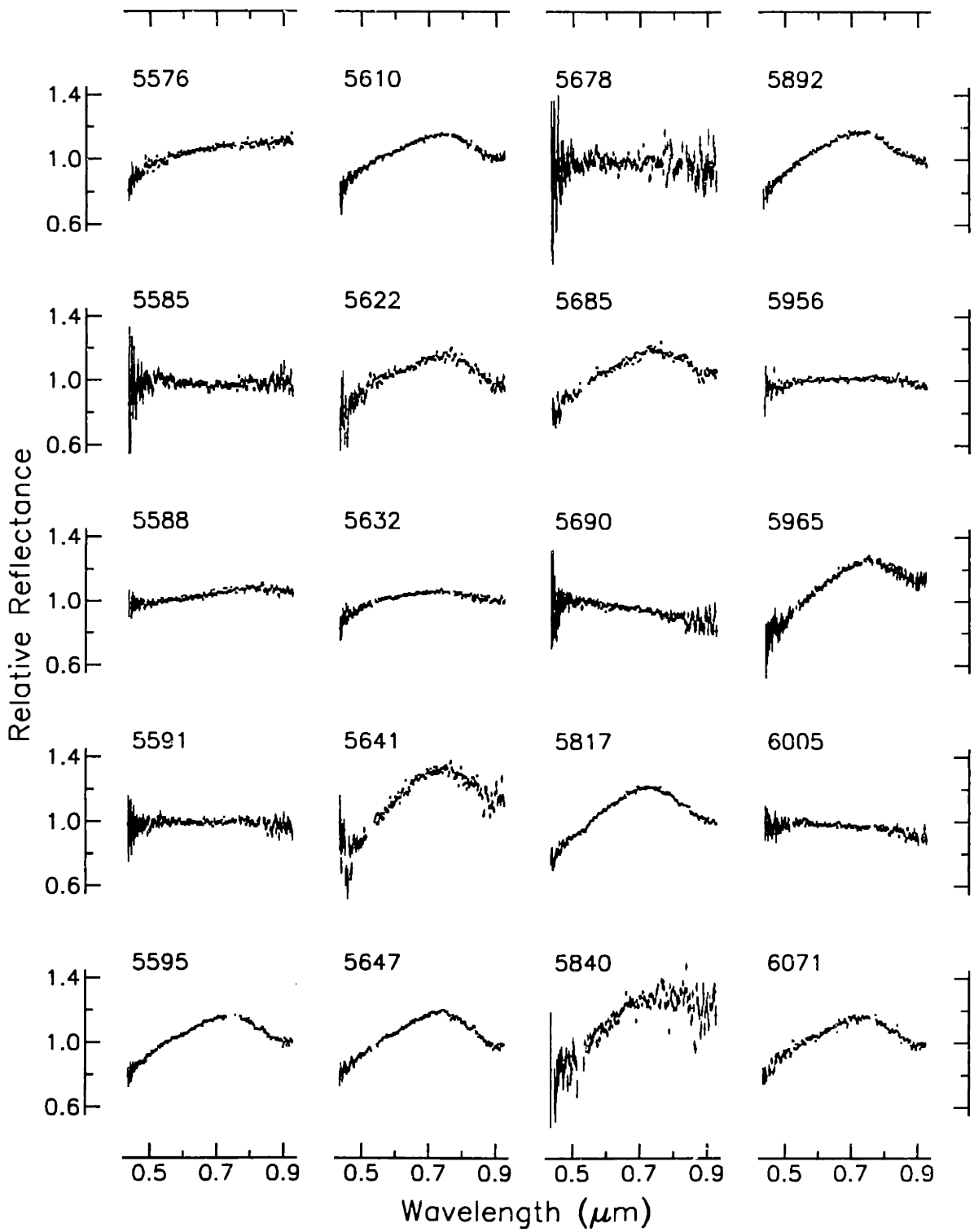
5576
5610
5678
5892
5585
5622
5685
5956
5588
5632
5690
5965
5591
5641
5817
6005
5595
5647
5840
6071
1.4
1.0
0.6
0.5
0.7
0.9
Relative Reflectance
Wavelength (μm)

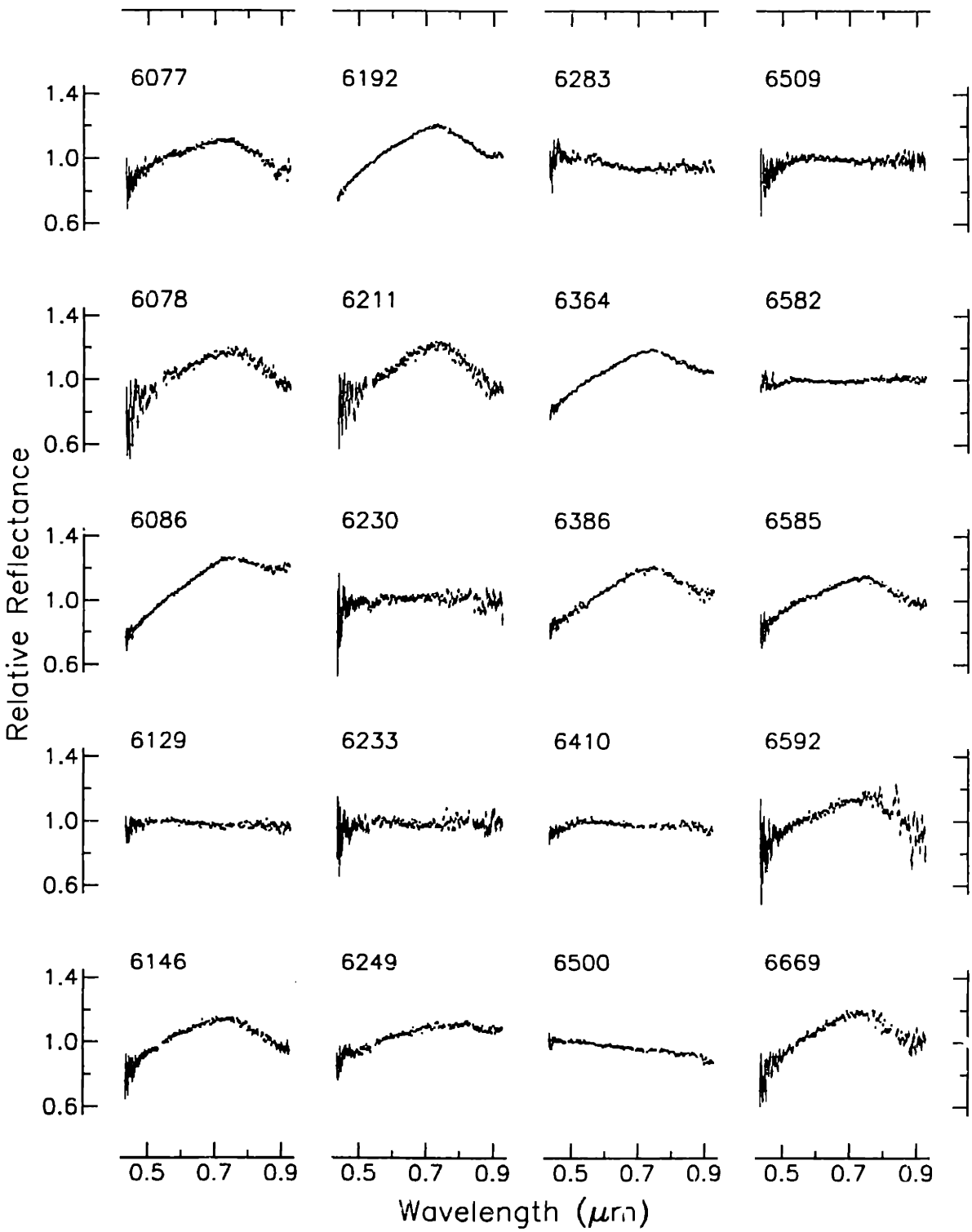
6077
6192
6283
6509
6078
6211
6364
6582
6086
6230
6386
6585
6129
6233
6410
6592
6146
6249
6500
6669
1.4
1.0
0.6
0.5
0.7
0.9
Relative Reflectance
Wavelength (μm)

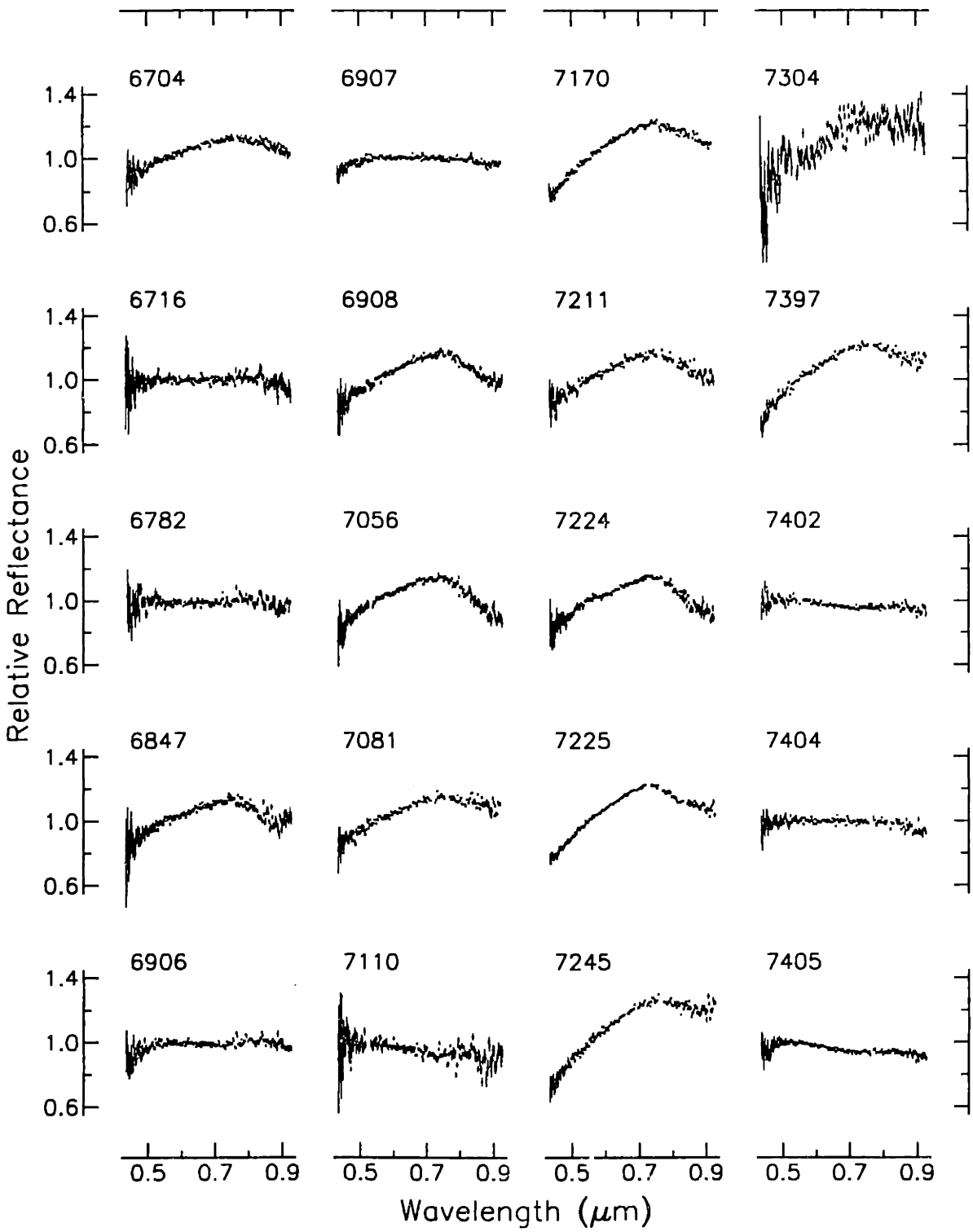
6704
6907
7170
7304
6716
6908
7211
7397
6782
7056
7224
7402
6847
7081
7225
7404
6906
7110
7245
7405
1.4
1.0
0.6
0.5
0.7
0.9
Relative Reflectance
Wavelength (μm)

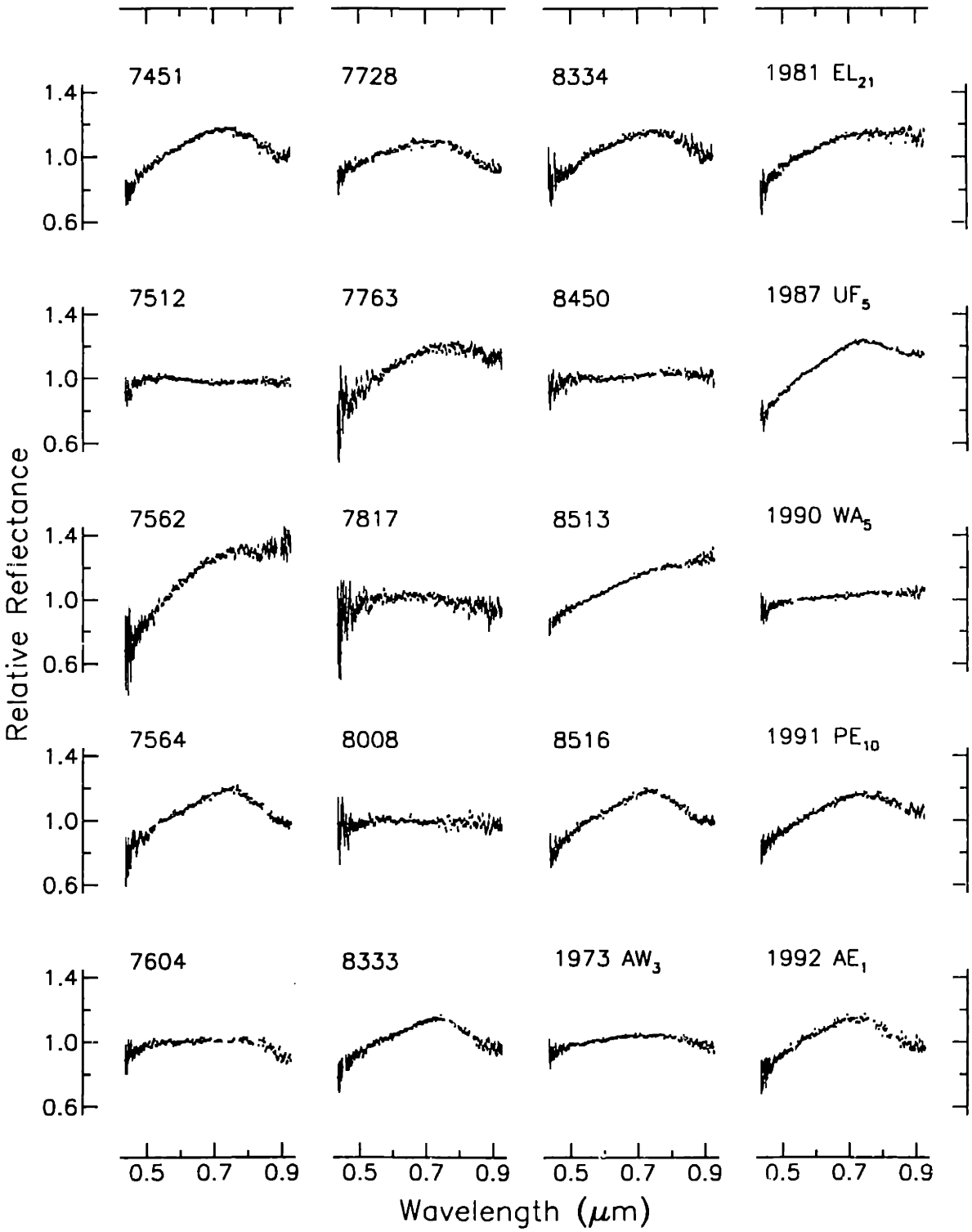
7451
7728
8334
1981 EL21
7512
7763
8450
1987 UF5
7562
7817
8513
1990 WA5
7564
8008
8516
1991 PE10
7604
8333
1973 AW3
1992 AE1
1.4
1.0
0.6
0.5
0.7
0.9
Relative Reflectance
Wavelength (μm)

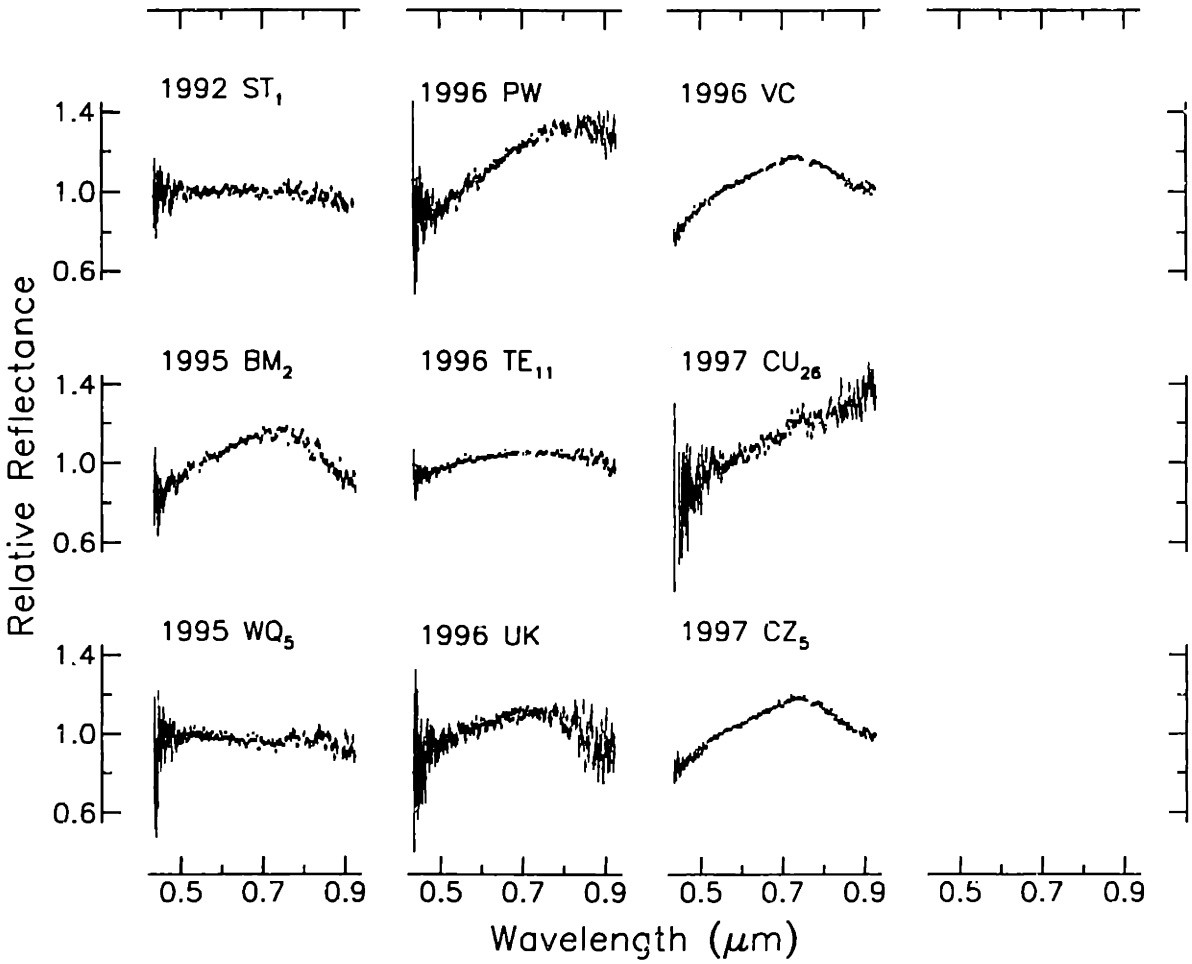
1992 ST1
1996 PW
1996 VC
1995 BM2
1996 TE11
1997 CU26
1995 WQ5
1996 UK
1997 CZ5
Relative Reflectance
1.4
1.0
0.6
0.5
0.7
0.9
Wavelength (μm)